

FLUORINATED NITROIMIDAZOLES AND THEIR RUTHENIUM COMPLEXES:
POTENTIAL HYPOXIA-IMAGING AGENTS

By

IAN ROBERT BAIRD

B.Sc., University of British Columbia, 1994

A THESIS SUBMITTED IN PARTIAL FULFILLMENT OF
THE REQUIREMENTS FOR THE DEGREE OF
DOCTOR OF PHILOSOPHY

in

THE FACULTY OF GRADUATE STUDIES

(Department of Chemistry)

We accept this thesis as conforming

to the required standard

THE UNIVERSITY OF BRITISH COLUMBIA

March 1999

© Ian Robert Baird, 1999

In presenting this thesis in partial fulfilment of the requirements for an advanced degree at the University of British Columbia, I agree that the Library shall make it freely available for reference and study. I further agree that permission for extensive copying of this thesis for scholarly purposes may be granted by the head of my department or by his or her representatives. It is understood that copying or publication of this thesis for financial gain shall not be allowed without my written permission.

Department of Chemistry

The University of British Columbia
Vancouver, Canada

Date May 13/1999

Abstract

With the goal of synthesizing nitroimidazole-based hypoxia imaging agents for the detection of cancerous tumours, the chemistry of halogen incorporation, especially fluorine, into the N1 side-chain of nitroimidazoles was investigated. The coordination of these nitroimidazoles and other methyl (Me)-substituted imidazoles to Ru(II) and Ru(III) centres was also investigated. The general objective was to combine the hypoxia-selective nature of the nitroimidazole moiety and the DNA-binding properties of Ru to deliver the active species selectively to its target.

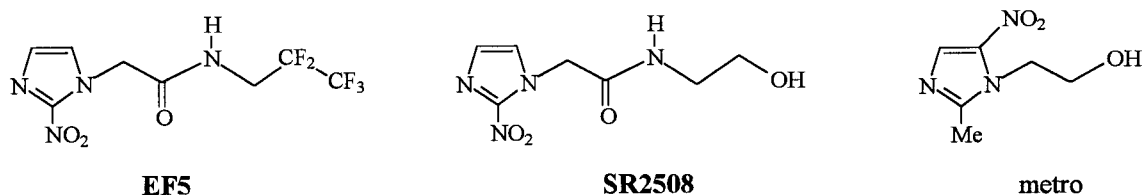
The nitroimidazole compounds and Ru complexes were characterized in general by a combination of NMR, IR and UV-Visible spectroscopies, as well as mass spectrometry, cyclic voltammetry, conductivity and elemental analysis; six nitroimidazoles and eleven Ru complexes were also characterized by X-ray crystallography.

The halogenated nitroimidazoles were synthesized using a standard amide coupling reaction; this was used for the synthesis of **EF5** [2-(2-nitro-1-H-imidazol-1-yl)-N-(2,2,3,3,3-pentafluoropropyl) acetamide], a known, sensitive probe for quantifying the amount of hypoxia within cells. Treatment of a desired acid with N-methylmorpholine and *iso*-butylchloroformate, followed by addition of the appropriate amine (either $\text{H}_2\text{NCH}_2\text{CX}_3$ or $\text{H}_2\text{NCH}_2\text{CX}_2\text{CX}_3$, where X= H, F, Cl and/or Br) led to formation of the halogenated nitroimidazole; 2-nitro- (2NO_2), 2-methyl-5-nitro- ($2\text{Me}5\text{NO}_2$) and 2-methyl-4-nitro- ($2\text{Me}4\text{NO}_2$) imidazole compounds were isolated in yields of 15 to 83 %.

The synthesis of **EF5** (typical yield 45 %) was improved by coupling iodoacetic acid with $\text{H}_2\text{NCH}_2\text{CF}_2\text{CF}_3$ to give $\text{ICH}_2\text{C}(\text{O})\text{NHCH}_2\text{CF}_2\text{CF}_3$ (**IF5**) which was subsequently reacted with $2\text{NO}_2\text{Im}$ and Cs_2CO_3 to yield the final product (78 %); this 2-step method circumvented the previously required 5-step synthesis. Other analogous compounds were less stable than **IF5**, especially those species containing a C-Br moiety, and they often decomposed in the presence of heat and/or light. Alteration of the associated side-chain on **EF5** by 'reversal' of its amide linkage was performed; however, the biological activity of the derivative was significantly less than that of **EF5**.

A nitroimidazole (NO_2Im) containing side-chain with a highly reactive terminal group, with the potential to exchange fluoride, was also sought. Attempts to isolate a

tosylated derivative of **SR2508** [2-(2-nitro-1-H-imidazol-1-yl)-N-(2-hydroxyethyl)acetamide] proved to be futile. The reaction with tosyl chloride led to the formation of a monochloro analogue of **SR2508**, presumably via the reactive tosylate intermediate, while reaction with triflic anhydride led to an intramolecular cyclization of the side-chain to give a compound whose X-ray structure was determined. The focus was then shifted to F-for-Br exchange; however, attempts to perform such a task revealed that the C-NO₂ bond of the Im ring was more labile than the C-Br bond, and this resulted in the formation of a 2-fluoroimidazole species. Further efforts to incorporate an F-atom into a nitroimidazole side-chain were unsuccessful.



[Ru(II)(L)₆]²⁺ complexes were synthesized from [Ru(DMF)₆][CF₃SO₃]₃; DMF = dimethylformamide, L = imidazole (Im), N-methylimidazole (NMeIm) and 5-methylimidazole (5MeIm). The 2-methylimidazole complex *trans*-[Ru(CO)(DMF)(2MeIm)₄][CF₃SO₃]₂ was synthesized via a reaction involving abstraction of CO from DMF; this complex loses CO reversibly at ambient temperature to form [Ru(DMF)(2MeIm)₄][CF₃SO₃]₂, and the DMF can be removed to generate [Ru(CF₃SO₃)_x(2MeIm)₄][CF₃SO₃]_y (x = 2, y = 0, or x = 1 = y). The X-ray structures of [Ru(Im)₆][CF₃SO₃]₂, [Ru(NMeIm)₆][CF₃SO₃]₂ and [Ru(5MeIm)₆][CF₃SO₃]₂ were obtained. Analogous [Ru(II)(L)_x]²⁺ nitroimidazole complexes (L = 2NO₂Im, x = 6; L = 4NO₂Im, x = 6; L = 2Me5NO₂Im, x = 5) were isolated from reaction with [Ru(DMF)₆][CF₃SO₃]₃. The reaction with **EF5** and **SR2508** in EtOH yielded the bis-substituted complexes [Ru(DMF)₂(EF5)₂(EtOH)₂][CF₃SO₃]₃ and [Ru(DMF)₄(SR2508)₂][CF₃SO₃]₃, respectively.

Ru(III) complexes of composition RuCl₃L₃ (L = 2NO₂Im, 4NO₂Im, 2Me5NO₂Im, metro) and RuCl₃L₂(EtOH) (L = **EF5**, **SR2508**) were synthesized directly from RuCl₃·3H₂O. Their ¹H NMR spectra were typically broad and sometimes signals were not observed; however, their paramagnetic, d⁵ low-spin composition was confirmed using the Evans method.

Some new Ru(II) and Ru(III) bis- β -diketonate (acac = acetylacetonate; hfac = 1,1,1,5,5,5-hexafluoroacetylacetonate) Im and NO₂Im complexes were synthesized. Reaction of two equiv. of an imidazole with *cis*-[Ru(acac)₂(MeCN)₂][CF₃SO₃] (synthesized from Ru(acac)₃ and CF₃SO₃H in MeCN) yielded Ru(III) complexes with composition [Ru(acac)₂(L)₂][CF₃SO₃] (L = Im, NMeIm, 2MeIm, 5MeIm, 2NO₂Im, metro, **EF5** and **SR2508**), the first four being structurally characterized by X-ray crystallography. The analogous Ru(II) hfac complexes were isolated from a reaction of *cis*-Ru(hfac)₂(MeCN)₂ (**71**) (synthesized from either Ru(hfac)₃ or Na[Ru(hfac)₃] and CF₃SO₃H in MeCN) with two equiv. of imidazole to yield Ru(hfac)₂(L)₂ (L = Im, NMeIm, 2MeIm, 4(5)MeIm, 2NO₂Im, **EF5** and **SR2508**). X-ray structures of **71** and Ru(hfac)₃ were obtained. Reaction of **71** with neat NMeIm gave [Ru(hfac)(NMeIm)₄][hfac]. The mixed ligand complex *cis*-Ru(hfac)(acac)(MeCN)₂ (X-ray) was synthesized from the new species Ru(hfac)₂(acac), which was isolated from a reaction of **71** with Hacac.

In vitro assays for toxicity and monoclonal antibody (MoAb) binding with SCCVII cells were used to evaluate the potential of selected nitroimidazoles as hypoxia-selective imaging agents. The toxicity, MoAb binding, cell accumulation and DNA-binding assays were used to test the utility of selected Ru complexes for transporting and/or localizing the coordinated nitroimidazoles within the cell. A preliminary radiosensitization study was also performed with two Ru complexes.

In general, the nitroimidazoles (NO₂Im)s and Ru complexes were non-toxic under both oxic and hypoxic conditions. The accumulation of the NO₂Im within the cell required hypoxic conditions, while the amount of NO₂Im bound within the hypoxic cells correlated with its one-electron reduction potential, the NO₂Im with the more positive reduction potentials giving the higher concentrations. The interaction of the fluorescently labeled MoAbs (ELK3-51 and ELK5-A8) with the NO₂Im depended on the length, size and composition of the halogenated side-chains. The Ru-NO₂Im complexes displayed relatively high cell accumulation and DNA-binding levels when compared to literature data for other Ru complexes. The most interesting result came from the MoAb assay in which the cells treated with [Ru(acac)₂(EF5)₂][CF₃SO₃] afforded a fluorescence signal four times greater than that seen for **EF5** itself.

Table of Contents

Abstract	ii
Table of Contents	v
List of Figures	xv
List of Schemes	xx
List of Tables	xxi
List of Abbreviations	xxvi
Key to Chemical Compound Numbers and Abbreviations	xxix
Acknowledgements	xxxv

Chapter 1 - Introduction

1.1 Introduction.....	1
1.2 Hypoxia.....	2
1.2.1 What is it?.....	2
1.2.1.1 Resistance to Treatment: Radioresistance.....	3
1.2.2 Hypoxia: The Aggressor?.....	5
1.3 Role of Nitroimidazoles in Cancer Therapy.....	6
1.3.1 Hypoxic Radiosensitizers.....	6
1.3.2 Chemistry of Nitroimidazoles in Biological Systems.....	7
1.4 Imaging of Hypoxic Tumours.....	10
1.4.1 Radiolabelling of Hypoxic Cells.....	11
1.4.2 Nuclear Medicine Techniques.....	11
1.4.3 Fluorescent Probes.....	12
1.4.4 Magnetic Resonance Imaging (MRI).....	14
1.4.5 Positron Emission Tomography (PET).....	14
1.5 Role of Metals in Cancer Therapy.....	16
1.6 Ruthenium Complexes.....	18
1.6.1 Chemical Properties Relevant to Tumour Treatment.....	18
1.6.2 DNA Binding.....	20

1.6.3 Tumouricidal Effects of Ru Complexes	22
1.7 Thesis Overview	24
1.8 References	26

Chapter 2 - General Experimental

2.1 Materials.....	33
2.1.1 Chemicals.....	33
2.1.1.1 Imidazoles.....	33
2.1.1.2 Amines.....	33
2.1.1.3 Miscellaneous Reagents.....	33
2.1.2 Solvents	34
2.2 Analytical Techniques	34
2.2.1 Nuclear Magnetic Resonance Spectroscopy.....	34
2.2.2 Infrared Spectroscopy	37
2.2.3 UV-Visible Spectroscopy	37
2.2.4 Mass Spectrometry	37
2.2.5 Gas Chromatography	38
2.2.6 Cyclic Voltammetry	38
2.2.7 Conductivity	39
2.2.8 X-Ray Analysis	40
2.2.9 Elemental Analysis	40
2.3 Compound Purification Techniques.....	40
2.3.1 Column Chromatography	40
2.3.2 Preparative Thin Layer Chromatography	41
2.3.3 Chromatotron	41
2.4 General Methodologies	41
2.4.1 Amide Coupling Reaction.....	41
2.5 Ruthenium Precursors.....	42
2.5.1 RuCl ₃ •3H ₂ O	42
2.5.2 [Ru(DMF) ₆][CF ₃ SO ₃] ₃	42

2.5.3 [Ru(DMF) ₆][CF ₃ SO ₃] ₂	43
2.5.4 <i>cis</i> -RuCl ₂ (DMSO)(DMSO) ₃	43
2.5.5 <i>trans</i> -RuCl ₂ (DMSO) ₄	44
2.5.6 <i>cis</i> -RuCl ₂ (TMSO) ₄	44
2.5.7 <i>mer</i> -RuCl ₃ (DMSO) ₃	44
2.5.8 [RuCl ₂ (COD)] _x	45
2.5.9 [RuCl ₂ (dppb)] ₂ (μ-dppb)	45
References	46

Chapter 3 - Synthesis and Characterization of New 2-, 4- and 5-Nitroimidazoles with Halogenated Side-Chains

3.1 Introduction	48
3.2 Experimental Section	49
3.2.1 Synthesis of Side-Chains	49
3.2.1.1 2-Iodo- <i>N</i> -(2,2,3,3,3-pentafluoropropyl)acetamide [IF5]	49
3.2.1.2 2-Iodo- <i>N</i> -(3-bromopropyl)acetamide [IBr]	49
3.2.1.3 2-Chloro- <i>N</i> -(2,2,3,3,3-pentafluoropropyl)acetamide [ClF5]	51
3.2.1.4 Reduction of IF5 to ICH ₂ CH ₂ NHCH ₂ CF ₂ CF ₃ (3)	52
3.2.1.5 3-Fluoropropylamine Hydrochloride (5)	52
3.2.2 2-Nitroimidazole Compounds	54
3.2.2.1 2-(2-Nitro-1-H-imidazol-1-yl)acetic acid (7)	54
3.2.2.2 2-(2-Nitro-1-H-imidazol-1-yl)- <i>N</i> -(2,2,3,3,3-pentafluoropropyl) acetamide [EF5]	56
3.2.2.3 2-(Imidazol-1-yl)- <i>N</i> -(2,2,3,3,3-pentafluoropropyl)acetamide [ImF5]	57
3.2.2.4 <i>N</i> -(2-nitro-1-H-imidazol-1-ethyl) pentafluoropropionamide [RevEF5]	58
3.2.2.5 2-(2-Nitro-1-H-imidazol-1-yl)- <i>N</i> -(3-bromo-2,2,3,3- tetrafluoropropyl) acetamide [EF4Br]	61

3.2.2.6 2-(2-Nitro-1-H-imidazol-1-yl)-N-(3,3,3-trifluoropropyl)acetamide [EF3]	62
3.2.2.7 2-(2-Nitro-1-H-imidazol-1-yl)-N-(2,2,2-trifluoroethyl)acetamide [EF3(-1)]	63
3.2.2.8 2-(2-Nitro-1-H-imidazol-1-yl)-N-(3-bromo-3,3-difluoropropyl)acetamide [EF2Br]	63
3.2.2.9 2-(2-Nitro-1-H-imidazol-1-yl)-N-(3,3-difluoropropylene)acetamide [E=F2]	64
3.2.2.10 2-(2-Nitro-1-H-imidazol-1-yl)-N-(3-fluoropropyl)acetamide [EF1]	65
3.2.2.11 2-(2-Nitro-1-H-imidazol-1-yl)-N-(2-fluoroethyl)acetamide [EF1(-1)]	67
3.2.2.12 2-(2-Nitro-1-H-imidazol-1-yl)-N-(3-chloropropyl)acetamide [EC11]	68
3.2.2.13 2-(2-Nitro-1-H-imidazol-1-yl)-N-(2-chloroethyl)acetamide [EC11(-1)]	69
3.2.2.14 2-(2-Nitro-1-H-imidazol-1-yl)-N-(3-bromopropyl)acetamide [EBr1]	70
3.2.2.15 2-(2-Nitro-1-H-imidazol-1-yl)-N-(2-bromoethyl)acetamide [EBr1(-1)]	71
3.2.2.16 2-(2-Nitro-1-H-imidazol-1-yl)-N-(propyl)acetamide [EPrA]	72
3.2.2.17 2-(2-Nitro-1-H-imidazol-1-yl)-N-(<i>iso</i> -amyl)acetamide [EIAA]	73
3.2.3 2-Methyl-5-Nitroimidazole Compounds	74
3.2.3.1 2-(2-Methyl-5-nitro-1 <i>H</i> -imidazol-1-yl)acetic acid (13)	74
3.2.3.2 2-(2-Methyl-5-nitro-1 <i>H</i> -imidazol-1-yl)-N-(2,2,3,3,3-pentafluoropropyl)acetamide [MF5]	74
3.2.3.3 2-(2-Methyl-5-nitro-1 <i>H</i> -imidazol-1-yl)-N-(2,2,2-trifluoroethyl)acetamide [MF3(-1)]	76

3.2.3.4 2-(2-Methyl-5-nitro-1 <i>H</i> -imidazol-1-yl)-N-(2-fluoroethyl)acetamide [MF1(-1)]	76
3.2.3.5 2-(2-Methyl-5-nitro-1 <i>H</i> -imidazol-1-yl)-N-(2-chloroethyl)acetamide [MCl1(-1)]	77
3.2.3.6 2-(2-Methyl-5-nitro-1 <i>H</i> -imidazol-1-yl)-N-(2-bromoethyl)acetamide [MBr1(-1)]	79
3.2.3.7 (2-Methyl-5-nitro-1 <i>H</i> -imidazol-1-yl)-N-(2-chloroethane) (16)	80
3.2.4 2-Methyl-4-Nitroimidazole Compounds	81
3.2.4.1 2-(2-Methyl-4-nitro-1- <i>H</i> -imidazol-1-yl)propionic acid (17)	81
3.2.4.2 3-(2-Methyl-4-nitro-1- <i>H</i> -imidazol-1-yl)-N-(2,2,3,3,3-pentafluoropropyl)propionamide [2M4NF5]	81
3.2.4.3 3-(2-Methyl-4-nitro-1- <i>H</i> -imidazol-1-yl)-N-(2,2,2-trifluoroethyl)propionamide [2M4NF3(-1)]	82
3.2.4.4 3-(2-Methyl-4-nitro-1- <i>H</i> -imidazol-1-yl)-N-(2-fluoroethyl)propionamide [2M4NF1(-1)]	83
3.2.4.5 3-(2-methyl-4-nitro-1- <i>H</i> -imidazol-1-yl)-N-(2-chloroethyl)propionamide [2M4NCl1(-1)]	84
3.2.4.6 2-(2-methyl-4-nitro-1- <i>H</i> -imidazol-1-yl)-N-(2-bromoethyl)propionamide [2M4NBr1(-1)]	85
3.2.5 Reactions of SR2508 with TiF_2O	85
3.2.5.1 2-(2-Nitro-1- <i>H</i> -imidazol-1-yl)-N-(ethylformate)acetamide (18)	85
3.2.5.2 CycF3 (19)	86
3.2.6 Reactions with RSU1111	87
3.2.6.1 Synthesis of (20), a pentafluorinated derivative of RSU1111	87
3.2.6.2 Synthesis of (21), a dibromo derivative of RSU1111	88
3.2.6.3 Synthesis of (22), a terminal nitrile derivative of RSU1111	88
3.2.7 Reactions of Nitroimidazoles with $\text{Bu}_4\text{NF}\cdot\text{H}_2\text{O}$	90
3.2.7.1 Reaction of EBr1 with $\text{Bu}_4\text{NF}\cdot\text{H}_2\text{O}$	90
3.2.7.2 Reaction of EBr1 with $\text{Bu}_4\text{NF}\cdot\text{H}_2\text{O}$ and $\text{CH}_3\text{CO}_2\text{H}$	91
3.2.7.3 Reaction of SR2508 with $\text{Bu}_4\text{NF}\cdot\text{H}_2\text{O}$	91

3.2.7.4 Reaction of $n\text{NO}_2\text{Im}$ ($n = 2, 4, 5$) with $\text{Bu}_4\text{NF}\cdot\text{H}_2\text{O}$	92
3.2.8 Cyclic Voltammetry of Nitroimidazoles	94
3.3 Results and Discussion	96
3.3.1 Synthesis of the Nitroimidazole Side-Chains	96
3.3.2 Nitroimidazoles	101
3.3.3 Electrochemistry of Nitroimidazoles	117
3.3.4 Incorporation of Fluorine into an Existing Side-chain	122
3.4 References	129

Chapter 4 - Synthesis and Characterization of Ru(II) and Ru(III) Imidazole Complexes

4.1 Introduction	134
4.2 Experimental Section	135
4.2.1 Complexes Synthesized from $[\text{Ru}(\text{DMF})_6][\text{CF}_3\text{SO}_3]_3$	135
4.2.1.1 $[\text{Ru}(\text{Im})_6][\text{CF}_3\text{SO}_3]_2$ (28)	135
4.2.1.2 $[\text{Ru}(\text{NMeIm})_6][\text{CF}_3\text{SO}_3]_2$ (29)	135
4.2.1.3 $[\text{Ru}(5\text{MeIm})_6][\text{CF}_3\text{SO}_3]_2$ (30)	136
4.2.1.4 <i>trans</i> - $[\text{Ru}(\text{CO})(\text{DMF})(2\text{MeIm})_4][\text{CF}_3\text{SO}_3]_2$ (31), $[\text{Ru}(\text{DMF})(2\text{MeIm})_4][\text{CF}_3\text{SO}_3]_2$ (32) and $[\text{Ru}(\text{CF}_3\text{SO}_3)_x$ $(2\text{MeIm})_4][\text{CF}_3\text{SO}_3]_y$ ($x=2, y=0$; or $x=1=y$) (33)	137
4.2.1.5 $[\text{Ru}(2\text{NO}_2\text{Im})_6][\text{CF}_3\text{SO}_3]_2$ (34)	138
4.2.1.6 $[\text{Ru}(5\text{NO}_2\text{Im})_6][\text{CF}_3\text{SO}_3]_2$ (35)	138
4.2.1.7 $[\text{Ru}(2\text{Me}5\text{NO}_2\text{Im})_5][\text{CF}_3\text{SO}_3]_2$ (36)	139
4.2.1.8 $[\text{Ru}(\text{DMF})_4(\text{SR}2508)_2][\text{CF}_3\text{SO}_3]_3$ (37)	140
4.2.1.9 $[\text{Ru}(\text{DMF})_2(\text{EF}5)_2(\text{EtOH})_2][\text{CF}_3\text{SO}_3]_3$ (38)	140
4.2.2 Complexes Synthesized from $\text{RuCl}_3\cdot 3\text{H}_2\text{O}$	141
4.2.2.1 <i>mer</i> - $\text{RuCl}_3(2\text{NO}_2\text{Im})_3$ (39)	141
4.2.2.2 <i>fac</i> - and <i>mer</i> - $\text{RuCl}_3(5\text{NO}_2\text{Im})_3$ (40)	142
4.2.2.3 " $\text{RuCl}_3(2\text{Me}5\text{NO}_2\text{Im})_3\cdot 3\text{CO}_2$ " (41)	143

4.2.2.4 RuCl ₃ (metro) ₃ (42).....	143
4.2.2.5 RuCl ₃ (SR2508) ₂ (EtOH) (43).....	144
4.2.2.6 RuCl ₃ (EF5) ₂ (EtOH) (44).....	145
4.2.2.7 RuCl ₂ (metro) ₄ (45).....	146
4.2.3 Complexes Synthesized from RuCl ₂ (DMSO) ₄	146
4.2.3.1 <i>cis</i> -RuCl ₂ (DMSO) ₂ (en) (46).....	146
4.2.3.2 <i>trans</i> -RuCl ₂ (DMSO) ₂ (en) (47).....	147
4.2.3.3 RuCl ₂ (DMSO) ₂ (EF5)(acetone) (48).....	148
4.2.4 Miscellaneous Complexes.....	148
4.2.4.1 [RuCl(dppb)(EF5)] ₂ (μ-Cl) ₂ (49).....	148
4.2.4.2 <i>cis</i> -RuCl ₂ (MeCN) ₄ (51) and <i>mer</i> -RuCl ₃ (MeCN) ₃ (52).....	149
4.2.4.3 Other Attempted Reactions.....	150
4.3 Results and Discussion.....	153
4.3.1 Complexes Synthesized from [Ru(DMF) ₆][CF ₃ SO ₃] ₃	153
4.3.1.1 Hexakis(imidazole) Ru(II) Complexes.....	153
4.3.1.2 Reaction of [Ru(DMF) ₆][CF ₃ SO ₃] ₃ with 2MeIm.....	158
4.3.1.3 Hexakis(nitroimidazole) Ru(II) Complexes, and some Ru(III) mixed DMF-SR2508 and -EF5 Complexes.....	160
4.3.2 Complexes Synthesized from RuCl ₃ •3H ₂ O.....	165
4.3.3 Complexes Synthesized from <i>cis/trans</i> -RuCl ₂ (DMSO) ₄	173
4.3.4 Miscellaneous Ru Complexes.....	175
4.4 References.....	182

Chapter 5 - Synthesis and Characterization of Ru(II) and Ru(III) β-Diketonate Imidazole Complexes

5.1 Introduction.....	187
5.2 Experimental.....	188
5.2.1 Ruthenium(III) Acetylacetonato Complexes.....	188
5.2.1.1 Ru(acac) ₃ (53).....	188

5.2.1.2 <i>cis</i> -[Ru(acac) ₂ (MeCN) ₂][CF ₃ SO ₃] (54).....	189
5.2.1.3 <i>cis</i> -[Ru(acac) ₂ (Im) ₂][CF ₃ SO ₃] (55).....	189
5.2.1.4 <i>cis</i> -[Ru(acac) ₂ (NMeIm) ₂][CF ₃ SO ₃] (58).....	190
5.2.1.5 <i>cis</i> -[Ru(acac) ₂ (2MeIm) ₂][CF ₃ SO ₃] (60).....	191
5.2.1.6 <i>cis</i> -[Ru(acac) ₂ (5MeIm) ₂][CF ₃ SO ₃] (62).....	192
5.2.1.7 [Ru(acac) ₂ (2NO ₂ Im) ₂][CF ₃ SO ₃] (64).....	193
5.2.1.8 [Ru(acac) ₂ (SR2508) ₂][CF ₃ SO ₃] (65).....	193
5.2.1.9 [Ru(acac) ₂ (EF5) ₂][CF ₃ SO ₃] (66).....	194
5.2.1.10 [Ru(acac) ₂ (metro) ₂][CF ₃ SO ₃] (67).....	195
5.2.1.11 Reaction of <i>cis</i> -[Ru(acac) ₂ (MeCN) ₂][CF ₃ SO ₃] (54) with EtOH	195
5.2.1.12 Reaction of <i>cis</i> -[Ru(acac) ₂ (MeCN) ₂][CF ₃ SO ₃] (54) with H ₂ O.....	196
5.2.2 Ruthenium(II) 1,1,1,5,5,5-Hexafluoroacetylacetonate Complexes..	197
5.2.2.1 [Na][Ru(hfac) ₃] (68) and [Ru(hfac)(EtOH) ₄][hfac] (69).....	197
5.2.2.2 Ru(hfac) ₃ (70).....	198
5.2.2.3 <i>cis</i> -Ru(hfac) ₂ (MeCN) ₂ (71).....	198
5.2.2.4 <i>cis</i> -Ru(hfac) ₂ (Im) ₂ (72).....	199
5.2.2.5 <i>cis</i> -Ru(hfac) ₂ (NMeIm) ₂ (74).....	200
5.2.2.6 [Ru(hfac)(NMeIm) ₄][PF ₆] (76).....	201
5.2.2.7 <i>cis</i> -Ru(hfac) ₂ (2MeIm) ₂ (77).....	202
5.2.2.8 <i>cis</i> -Ru(hfac) ₂ (4MeIm)(5MeIm) (80).....	203
5.2.2.9 Ru(hfac) ₂ (2NO ₂ Im) ₂ (82).....	203
5.2.2.10 Ru(hfac) ₂ (EF5) ₂ (83).....	204
5.2.2.11 Attempted Synthesis of Ru(hfac) ₂ (SR2508) ₂ (84).....	205
5.2.3 Ruthenium(II) and (III) acac/hfac Complexes.....	205
5.2.3.1 Ru(acac) ₂ (hfac) (85).....	205
5.2.3.2 [Na][Ru(hfac) ₂ (acac)] (86).....	206
5.2.3.3 Ru(hfac) ₂ (acac) (87).....	206
5.2.3.4 <i>cis</i> -Ru(acac)(hfac)(MeCN) ₂ (88).....	207

5.2.3.5 <i>cis</i> -Ru(acac)(hfac)(Im) ₂ (89).....	208
5.2.3.6 <i>cis</i> -Ru(acac)(hfac)(NMeIm) ₂ (90).....	208
5.2.4 Cyclic Voltammetry of Ru(II) and Ru(III) β-diketonato Complexes	209
5.3 Results and Discussion	211
5.3.1 Ruthenium tris(β-diketonato) complexes	211
5.3.2 Bis-MeCN Complexes.....	219
5.3.3 Bis-imidazole Complexes	227
5.3.3.1 Bis(acetylacetonato)bis(imidazole)ruthenium(III) complexes ..	227
5.3.3.2 Bis(1,1,1,5,5,5-hexafluoroacetylacetonato)bis(imidazole) ruthenium(II) complexes	238
5.3.3.3 Cyclic Voltammetric Results for the Bis-imidazole Complexes	245
5.4 References	248

Chapter 6 - *In Vitro* Evaluation of Selected Nitroimidazoles and Ruthenium Nitroimidazole Complexes

6.1 Introduction.....	252
6.2 Experimental.....	253
6.2.1 Materials and Methods	253
6.2.1.1 Media.....	253
6.2.1.2 General Solutions	253
6.2.1.3 Cell Handling	255
6.2.1.4 Preparation of Compound Solutions	255
6.2.1.5 Cell Incubation Procedures	256
6.2.2 Instrumentation	257
6.2.2.1 Atomic Absorption Spectroscopy (AAS).....	257
6.2.2.2 UV-Vis Spectroscopy.....	258
6.2.2.3 Flow Cytometry (FCM).....	258
6.2.2.4 Image Cytometry (ICM).....	258

6.2.3 Biological Assays	260
6.2.3.1 Toxicity Assays	260
6.2.3.2 Cell Accumulation (Uptake) Assay	260
6.2.3.3 DNA-binding Assay (Isolation of DNA from SCCVII Cells)...	261
6.2.3.4 Radiosensitizing Assays	261
6.2.3.5 Monoclonal Antibody Assay	263
6.3 Results and Discussion	265
6.3.1 Compound Solubility	265
6.3.2 Toxicity	266
6.3.2.1 Nitroimidazoles	266
6.3.2.2 Ruthenium Complexes	268
6.3.3 Cellular Accumulation of Ru Complexes	269
6.3.4 DNA-binding by Ru Complexes	272
6.3.5 Radiosensitization	274
6.3.6 Nitroimidazole Adduct Recognition using Monoclonal Antibodies.	276
6.3.6.1 Recognition of NO ₂ Im Adducts by ELK3-51	278
6.3.6.2 Recognition of NO ₂ Im Adducts by ELK5-A8	284
6.4 Refereneces	287

Chapter 7 - Conclusions and Recommendations for Future Work

7.1 General Remarks	291
7.2 Halogenated Nitroimidazoles (Chapter 3)	291
7.3 Ruthenium Imidazole Complexes (Chapter 4)	295
7.4 Ruthenium β -Diketonate Imidazole Complexes (Chapter 5)	297
7.5 <i>In Vitro</i> Evaluation of Nitroimidazoles and their Ru Complexes	298
7.6 References	301

Appendix I - X-ray data

Appendix I-1 X-ray data for EF5	302
Appendix I-2 X-ray data for EF2Br•0.5 H₂O	304
Appendix I-3 X-ray data for MF5	306
Appendix I-4 X-ray data for 2M4NF5	308
Appendix I-5 X-ray data for 2M4NF1(-1)	311
Appendix I-6 X-ray data for cycF3 (19)	313
Appendix I-7 X-ray data for [Ru(Im) ₆][CF ₃ SO ₃] ₂	316
Appendix I-8 X-ray data for [Ru(NMeIm) ₆][CF ₃ SO ₃] ₂	318
Appendix I-9 X-ray data for [Ru(5MeIm) ₆][CF ₃ SO ₃] ₂	320
Appendix I-10 X-ray data for <i>mer</i> -RuCl ₃ (MeCN) ₃ •CHCl ₃	322
Appendix I-11 X-ray data for Ru(hfac) ₃	324
Appendix I-12 X-ray data for Ru(hfac) ₂ (MeCN) ₂	327
Appendix I-13 X-ray data for Ru(acac)(hfac)(MeCN) ₂	330
Appendix I-14 X-ray data for [Ru(acac) ₂ (Im) ₂][CF ₃ SO ₃]•benzene.....	333
Appendix I-15 X-ray data for [Ru(acac) ₂ (NMeIm) ₂][CF ₃ SO ₃].....	335
Appendix I-16 X-ray data for [Ru(acac) ₂ (2MeIm) ₂][CF ₃ SO ₃]•0.5 hexane... 338	
Appendix I-17 X-ray data for [Ru(acac) ₂ (5MeIm) ₂][CF ₃ SO ₃].....	340

Appendix II - Miscellaneous Biological Data	343
--	-----

List of Figures

Figure i: Imidazole position numbering.....	xxviii
Figure 1-1: Oxygen gradient observed in a typical tumour (adapted from ref. 6).....	2
Figure 1-2: Typical results for X-ray irradiation of Chinese Hamster Ovary cells under aerobic (O ₂) or hypoxic (N ₂) conditions (adapted from ref. 6).....	3
Figure 1-3: Structures of metronidazole, misonidazole and etanidazole.....	7
Figure 1-4: Nitroimidazole reduction scheme (adapted from ref. 30).....	8
Figure 1-5: Ranges of reduction potentials for nitroimidazoles vs. NHE at pH 7.....	8

Figure 1-6: Nucleophilic addition of water to 1-methyl-2-nitrosoimidazole.....	9
Figure 1-7: Proposed reactions of 2-hydroxyaminoimidazole within the cell.....	10
Figure 1-8: Iodoazomycin arabinoside (IAZA).....	12
Figure 1-9: Indolizine-linked 2-nitroimidazole, fluorescent hypoxia probe.....	12
Figure 1-10: Structures of the hypoxia-selective fluorinated 2-nitroimidazoles CCI-103F and EF5.....	13
Figure 1-11: γ -ray production from positron emitting isotope [^{18}F].....	15
Figure 1-12: Chemical structures of antitumour agents cisplatin, carboplatin, JM216 and AMD473.....	17
Figure 1-13: Cisplatin/DNA interaction to form a GG intrastrand cross-link.....	21
Figure 2-1: Diagrammatic representation of a capillary (containing a solution of the complex) within a NMR tube (containing solvent only) used for the Evans method.....	36
Figure 2-2: Cyclic voltammetry cell (A) containing a Pt reference electrode.....	39
Figure 2-3: Cyclic voltammetry cell (B) containing an Ag reference electrode.....	39
Figure 3-1: TLC analysis of products obtained from 2-(2-Nitro-1-H-imidazol-1-yl)acetic acid (7) synthesis.....	55
Figure 3-2: TLC analysis of products obtained from EF1 synthesis.....	66
Figure 3-3: TLC analysis of MX1(-1) compounds (X =F, Cl, Br).....	79
Figure 3-4: ^1H NMR spectrum of EF1 in d_6 -acetone.....	111
Figure 3-5: ^1H NMR spectrum of EF1(-1) in d_6 -acetone.....	111
Figure 3-6: Typical IR spectrum of a 2-nitroimidazole, EF1	113
Figure 3-7: ORTEP view of EF5 ; 33 % probability thermal ellipsoids are shown.....	114
Figure 3-8: ORTEP view of MF5 ; 33 % probability thermal ellipsoids are shown.....	115
Figure 3-9: ORTEP view of 2M4NF5 ; 33 % probability thermal ellipsoids are shown..	116
Figure 3-10: ORTEP view of 2M4NF1(-1) ; 33 % probability thermal ellipsoids are shown.....	117
Figure 3-11: A lowering of pH levels in hypoxic cells due to increased [CO_2].....	118
Figure 3-12: Quasi-reversible CV plot for EF1 referenced to FeCp_2	120
Figure 3-13: CV plot for MC11(-1) referenced to FeCp_2	121

Figure 3-14: ORTEP view of 19 ; 33 % probability thermal ellipsoids are shown.	123
Figure 3-15: ORTEP view of EF2Br ; 33 % probability thermal ellipsoids are shown....	128
Figure 4-1: TLC analysis of products obtained from synthesis of 52	150
Figure 4-2: ORTEP view of $\text{Ru}(\text{Im})_6^{2+}$ (28); 50% probability thermal ellipsoids are shown.....	154
Figure 4-3: ORTEP view of $\text{Ru}(\text{NMeIm})_6^{2+}$ (29); 33% probability thermal ellipsoids are shown.	155
Figure 4-4: ORTEP view of $\text{Ru}(\text{5MeIm})_6^{2+}$ (30); 50% probability thermal ellipsoids are shown.	156
Figure 4-5: Proposed stepwise DMF displacement by $2\text{NO}_2\text{Im}$ for the synthesis of $[\text{Ru}(2\text{NO}_2\text{Im})_6][\text{CF}_3\text{SO}_3]_2$ (34).	161
Figure 4-6: In situ ^1H NMR spectrum in CD_3OD during the synthesis of 34	162
Figure 4-7: ^1H NMR spectrum for 39 in d_6 -dmso.	167
Figure 4-8: Geometrical isomerization of complex 40 in d_6 -dmso.	168
Figure 4-9: Possible configurations of a dimer formed from $2\text{Me5NO}_2\text{Im}$	168
Figure 4-10: IR spectrum for the isolated, orange complex 41	169
Figure 4-11: ^1H NMR spectra for complex 41 in CD_3OD (initial and after 6 d).	170
Figure 4-12: Successive aquation of 43 ($\text{L} = \text{SR2508}$) and 44 ($\text{L} = \text{EF5}$).	172
Figure 4-13: ^1H NMR (200 MHz) spectrum (Evans Method) of 43 (0.0032 g / mL D_2O , in a 0.1 mm capillary tube) referenced to the residual proton peak, HOD.	172
Figure 4-14: Isomerization of <i>cis</i> - $\text{RuCl}_2(\text{DMSO})_2(\text{en})$ from 46a to 46b	174
Figure 4-15: $^{31}\text{P}\{^1\text{H}\}$ NMR spectrum for complex 49 , with proposed structure.	176
Figure 4-16: $^{31}\text{P}\{^1\text{H}\}$ NMR spectrum for the proposed $[\text{RuCl}_2(\text{dppb})(\text{EF5})]_2(\mu\text{-dppb})$ (50).	177
Figure 4-17: $[\text{RuCl}_2(\text{diop})]_2(\mu\text{-diop})$ and the proposed structure for 50	178
Figure 4-18: ORTEP view of <i>mer</i> - $\text{RuCl}_3(\text{MeCN})_3$ (52); 50% probability thermal ellipsoids are shown.....	180
Figure 5-1: TLC analysis for the synthesis of 88 from 85	207
Figure 5-2: Resonance structures for acetylacetonate (<i>acac</i> $^-$).	211

Figure 5-3: ORTEP view of Ru(hfac) ₃ (70); 50 % probability thermal ellipsoids are shown.	213
Figure 5-4: ¹ H NMR spectrum of Ru(hfac) ₂ (acac) (87) in CDCl ₃ at r.t.	217
Figure 5-5: Relationship between E _{1/2} and Σ σ _m in 0.1 M TBAP at 25°C. --- ● ---, this work (CV data in MeCN); --- ■ ---, Patterson and Holm (polarographic data in DMF). ¹⁵	218
Figure 5-6: Proposed reaction mechanism for acid catalyzed displacement of acac (adapted from ref. 19).	220
Figure 5-7: ORTEP view of <i>cis</i> -Ru(hfac) ₂ (MeCN) ₂ (71); 50 % probability thermal ellipsoids are shown.	222
Figure 5-8: ORTEP view of <i>cis</i> -Ru(acac)(hfac)(MeCN) ₂ (88); 50 % probability thermal ellipsoids.	227
Figure 5-9: ¹ H NMR spectrum of <i>cis</i> -[Ru(acac) ₂ (Im) ₂][CF ₃ SO ₃] (55) in d ₆ -acetone.	230
Figure 5-10: ¹ H NMR spectrum of <i>cis</i> -[Ru(acac) ₂ (NMeIm) ₂][CF ₃ SO ₃] (58) in d ₆ -acetone.	232
Figure 5-11: ORTEP view of the cation of <i>cis</i> -[Ru(acac) ₂ (Im) ₂][Tf] (55); 50 % probability thermal ellipsoids are shown.	234
Figure 5-12: ORTEP view of <i>cis</i> -[Ru(acac) ₂ (NMeIm) ₂][Tf] (58); 50 % probability thermal ellipsoids.	235
Figure 5-13: ORTEP view of the cation of <i>cis</i> -[Ru(acac) ₂ (2MeIm) ₂][Tf] (60); 50 % probability thermal ellipsoids.	236
Figure 5-14: ORTEP view of the cation of <i>cis</i> -[Ru(acac) ₂ (5MeIm) ₂][Tf] (62); 50 % probability thermal ellipsoids.	237
Figure 5-15: ¹ H NMR spectra for complexes 72 and 73 in d ₆ -acetone.	241
Figure 5-16: Proton signals for the coordinated NMeIm ligands of 74 in d ₆ -acetone.	242
Figure 5-17: ¹ H NMR spectrum of [Ru(hfac)(NMeIm) ₄][PF ₆] (76) in d ₆ -acetone.	242
Figure 5-18: ¹ H NMR spectra of <i>cis</i> - and <i>trans</i> -Ru(hfac) ₂ (2MeIm) ₂ (77 and 79) in d ₆ -acetone.	243
Figure 5-19: ¹ H NMR of the mixed-ligand complex Ru(hfac) ₂ (4MeIm)(5MeIm) in d ₆ -acetone.	244

Figure 5-20: Cyclic voltammograms for <i>cis</i> - and <i>trans</i> -Ru(hfac) ₂ (2MeIm) ₂ in 0.1 M Bu ₄ NClO ₄ in MeCN.	247
Figure 6-1: Diagram of 'tox' vessel used for the accumulation and toxicity experiments.	257
Figure 6-2: Different types of SCCVII cells observed on microscope slides.	260
Figure 6-3: Setup used for irradiation of the "ducks" in the radiosensitization assay.	263
Figure 6-4: Pictorial summary of the <i>in vitro</i> MoAb assay.	264
Figure 6-5: Comparison of toxicity for selected compounds (at 100 μM except for TF5) in oxic and hypoxic SCCVII cells (incubated for 3 h); average of 2 or 3 experiments. (The plating efficiencies for the other 2NO ₂ Ims, which also show little oxic/hypoxic variability, reported in Table II-1, Appendix II.) ...	267
Figure 6-6: Accumulation data for RuCl ₃ (SR2508) ₂ (EtOH) in SCCVII cells after a 3 h incubation; reported as ng Ru/10 ⁶ cells (± 5 %).	272
Figure 6-7: DNA-binding data for RuCl ₃ (SR2508) ₂ (EtOH) in SCCVII cells after a 3 h incubation; reported as ng Ru/mg DNA (± 5 %).	274
Figure 6-8: Radiosensitization by SR2508 (600 μM) and EF5 (150 μM) and lack thereof by their Ru complexes RuCl ₃ (SR2508) ₂ (EtOH) (308 μM) and RuCl ₃ (EF5) ₂ (EtOH) (60.6 μM); after 3 h pre-incubation with hypoxic SCCVII cells. ...	275
Figure 6-9: The indocarbocyanine fluorescent dye Cy3.	276
Figure 6-10: Direct comparison of relative median fluorescence intensity and radioactive drug uptake for 9L cells incubated with 100 μM EF5 for 3 h at indicated oxygen partial pressures (adapted from ref. 13).	277
Figure 6-11: Relative mean fluorescence intensity for SCCVII cells incubated with 100μM drug for 3 h under N ₂ and then treated with ELK3-51 (Cy3); determined using flow cytometry (average of 2 or 3 expts.; ± 10 %). (The oxic data are reported in Table II-2, Appendix II.)	279
Figure 6-12: Log of mean fluorescence signal determined by flow cytometry versus the compound's reduction potential (determined by CV; chapter 3, Section 3.2.8). See Table II-3, Appendix II.	280

Figure 6-13: Relative mean fluorescence intensity for SCCVII cells incubated with 100μM drug for 3 h under N ₂ and then treated with ELK3-51; determined using image cytometry (data from 2 expts.; ± 10 %). (The oxic data are reported in Table II-4, Appendix II.)	281
Figure 6-14: Relative mean fluorescence intensity for SCCVII cells incubated with drug for 3 h under N ₂ and treated with ELK3-51; determined using flow cytometry (data for Ru complexes from 2 experiments; ± 10 %). All values are normalized for EF5 content (100 μM). The <i>cis</i> -PtCl ₂ (NH ₃)(EF5)(PtEF5) results were obtained from ref. 13.	283
Figure 6-15: Relative mean fluorescence intensity for SCCVII cells incubated with 100μM drug for 3 h under N ₂ and treated with ELK5-A8; determined using flow cytometry. (The oxic data are reported in Table II-5, Appendix II.)	285
Figure 6-16: Proposed recognition sites for the ELK5-A8 MoAb.	286
Figure 7-1: Proposed coordination geometry of [RuCl(PPh ₃) ₂ (2M4NF3(-1))][Cl].	296

List of Schemes

Scheme 2-1: Standard amide bond forming reaction.	42
Scheme 3-1: Synthesis of pentafluoropropylamine from perfluoropropionic acid. ³⁵	96
Scheme 3-2: Synthesis of IF5 , the precursor to EF5 .	97
Scheme 3-3: Formation of aziridine ring upon exposure of 3 to UV light.	98
Scheme 3-4: Cyclization of IBr in the presence of heat and/or UV-radiation.	98
Scheme 3-5: Synthesis of 3-fluoropropylamine reported by Pattison <i>et al.</i> ⁴⁵	99
Scheme 3-6: Reaction of 3-hydroxypropylamine with DAST.	100
Scheme 3-7: High yield Gabriel synthesis of 3-fluoropropylamine hydrochloride.	101
Scheme 3-8: Reaction mechanism for addition of side-chain via an amide linkage.	102
Scheme 3-9: Synthesis of 7 , via 8 from SR2508 .	102
Scheme 3-10: Oxidation of metronidazole with Jone's Reagent to yield the carboxylic acid derivative, 13 .	103
Scheme 3-11: Acid hydrolysis of 2-methyl-4-nitro-1-imidazolepropionitrile (abbreviated as	

RCN).	104
Scheme 3-12: New synthetic route to EF5 .	104
Scheme 3-13: Formation of the isobutylester (11) in the presence of H ₂ O.	106
Scheme 3-14: The 3-step synthesis of RevF5 from 2-bromoethylphthalamide.	107
Scheme 3-15: Stepwise reduction of 2-nitroimidazole to 2-aminoimidazole.	118
Scheme 3-16: Synthesis of EC11(-1) via the tosylate intermediate.	124
Scheme 3-17: Synthesis of fluoroetanidazole (EF1(-1)) via a tosylate intermediate. ⁷⁷	125
Scheme 3-18: Mechanism for reaction of SR2508 with DMF to yield the formate ester (18).	126
Scheme 4-1: Conversion of 31 → 32 → 33 , with suggested formulations (L= 2MeIm).	158
Scheme 5-1: Synthesis of Na[Ru(hfac) ₃] (68) from RuCl ₃ •3H ₂ O.	212
Scheme 5-2: Synthesis of <i>cis</i> -Ru(acac)(hfac)(MeCN) ₂ (88) from Ru(acac) ₂ (hfac) (85).	223
Scheme 5-3: Attempted synthesis of <i>cis</i> -Ru(acac)(hfac)(MeCN) ₂ (88) from Ru(hfac) ₂ (acac) (87).	224
Scheme 7-1: Proposed reduction of bis-CN compound (24) with BH ₃ •THF.	292
Scheme 7-2: Proposed synthesis of ligands containing two or three -CH ₂ CF ₂ CF ₃ units.	294
Scheme 7-3: Proposed synthesis of [¹⁸ F]- EF1 similar to that used by Tewson to synthesize [¹⁸ F]-fluoroetanidazole.	295
Scheme 7-4: Possible F ₂ addition to fluoroalkenes to yield EF4 and EF5 .	296

List of Tables

Table 3.1: Summary of the ¹ H NMR, ¹⁹ F{ ¹ H} NMR and UV-Vis data for <i>n</i> NO ₂ Im compounds and for their reaction with Bu ₄ NF•H ₂ O.	93
Table 3.2: Summary of reduction potentials for the 2-nitroimidazoles vs. SCE.	94
Table 3.3: Summary of reduction potentials for the 2-methyl-5-nitroimidazoles vs. SCE.	95
Table 3.4: Summary of reduction potentials for the 2-methyl-4-nitroimidazoles vs. SCE.	95
Table 4.1: Conductivity measurements versus time for 44 in H ₂ O.	146
Table 4.2: Summary of attempted reactions for which no pure product was isolated or characterized.	151
Table 5.1: Summary of Ru(III/II) reduction potentials vs. SCE.	210

Table 5.2: Summary of UV-Vis data for complexes 53 , 70 , 85 and 87 in MeOH	
$[\lambda_{\max} (\epsilon \times 10^{-3})]$	215
Table 5.3: ^1H and $^{19}\text{F}\{^1\text{H}\}$ NMR data for the Ru(III) tris(β -diketonato) complexes.....	216
Table 5.4: NMR data for the Im and MeIm complexes $[\text{Ru}(\text{acac})_2(\text{L})_2][\text{CF}_3\text{SO}_3]$ in	
d_6 -acetone at r.t.	231
Table 5.5 NMR data for the free imidazole ligands and their complexes $\text{Ru}(\text{hfac})_2(\text{L})_2$	
in d_6 -acetone at r.t.	240
Table 6.1: Actual drug concentrations used for <i>in vitro</i> experiments.	265
Table 6.2: Aerobic and hypoxic toxicity data (PE at 3 h) of Ru complexes in SCCVII	
cells. (See Table 6.1 for complex concentrations.).....	269
Table 6.3: Accumulation of Ru complexes (normalized to 100 μM) in SCCVII cells	
incubated for 3 h; expressed as ng Ru/ 10^6 cells ($\pm 5\%$).	270
Table 6.4: Amount of Ru bound to DNA extracted from SCCVII cells after 3 h exposure	
to complex (normalized to 100 μM ; ng Ru/mg DNA ($\pm 5\%$)).	273
Table 7-1: Summary of most significant <i>in vitro</i> assay results obtained during this thesis	
work.	300
Table I-1.1 Experimental details for EF5	A1
Table I-1.2 Atomic coordinates and $B_{\text{iso}}/B_{\text{eq}}$ for EF5	A2
Table I-1.3 Bond lengths (\AA) for EF5	A2
Table I-1.4 Bond angles ($^\circ$) for EF5	A2
Table I-2.1 Experimental details for EF2Br $\cdot 0.5 \text{H}_2\text{O}$	A3
Table I-2.2 Atomic coordinates and $B_{\text{iso}}/B_{\text{eq}}$ for EF2Br $\cdot 0.5 \text{H}_2\text{O}$	A4
Table I-2.3 Bond lengths (\AA) for EF2Br $\cdot 0.5 \text{H}_2\text{O}$	A4
Table I-2.4 Bond angles ($^\circ$) for EF2Br $\cdot 0.5 \text{H}_2\text{O}$	A4
Table I-3.1 Experimental details for MF5	A5
Table I-3.2 Atomic coordinates and $B_{\text{iso}}/B_{\text{eq}}$ for MF5	A6
Table I-3.3 Bond lengths (\AA) for MF5	A6
Table I-3.4 Bond angles ($^\circ$)for MF5	A6
Table I-4.1 Experimental details for 2M4NF5	A7

Table I-4.2 Atomic coordinates and $B_{\text{iso}}/B_{\text{eq}}$ for 2M4NF5	A8
Table I-4.3 Bond lengths (Å) for 2M4NF5	A8
Table I-4.4 Bond angles (°)for 2M4NF5	A9
Table I-5.1 Experimental details for 2M4NF1(-1)	A10
Table I-5.2 Atomic coordinates and $B_{\text{iso}}/B_{\text{eq}}$ for 2M4NF1(-1)	A11
Table I-5.3 Bond lengths (Å) for 2M4NF1(-1)	A11
Table I-5.4 Bond angles (°)for 2M4NF1(-1)	A11
Table I-6.1 Experimental details for cycF3	A12
Table I-6.2 Atomic coordinates and $B_{\text{iso}}/B_{\text{eq}}$ for cycF3	A13
Table I-6.3 Bond lengths (Å) for cycF3	A13
Table I-6.4 Bond angles (°) for cycF3	A14
Table I-7.1 Experimental details for $[\text{Ru}(\text{Im})_6][\text{CF}_3\text{SO}_3]_2$	A15
Table I-7.2 Atomic coordinates and $B_{\text{iso}}/B_{\text{eq}}$ for $[\text{Ru}(\text{Im})_6][\text{CF}_3\text{SO}_3]_2$	A16
Table I-7.3 Bond lengths (Å) for $[\text{Ru}(\text{Im})_6][\text{CF}_3\text{SO}_3]_2$	A16
Table I-7.4 Bond angles (°)for $[\text{Ru}(\text{Im})_6][\text{CF}_3\text{SO}_3]_2$	A16
Table I-8.1 Experimental details for $[\text{Ru}(\text{NMeIm})_6][\text{CF}_3\text{SO}_3]_2$	A17
Table I-8.2 Atomic coordinates and $B_{\text{iso}}/B_{\text{eq}}$ for $[\text{Ru}(\text{NMeIm})_6][\text{CF}_3\text{SO}_3]_2$	A18
Table I-8.3 Bond lengths (Å) for $[\text{Ru}(\text{NMeIm})_6][\text{CF}_3\text{SO}_3]_2$	A18
Table I-8.4 Bond angles (°)for $[\text{Ru}(\text{NMeIm})_6][\text{CF}_3\text{SO}_3]_2$	A18
Table I-9.1 Experimental details for $[\text{Ru}(\text{5MeIm})_6][\text{CF}_3\text{SO}_3]_2$	A19
Table I-9.2 Atomic coordinates and $B_{\text{iso}}/B_{\text{eq}}$ for $[\text{Ru}(\text{5MeIm})_6][\text{CF}_3\text{SO}_3]_2$	A20
Table I-9.3 Bond lengths (Å) for $[\text{Ru}(\text{5MeIm})_6][\text{CF}_3\text{SO}_3]_2$	A20
Table I-9.4 Bond angles (°)for $[\text{Ru}(\text{5MeIm})_6][\text{CF}_3\text{SO}_3]_2$	A20
Table I-10.1 Experimental details for <i>mer</i> - $\text{RuCl}_3(\text{MeCN})_3 \cdot \text{CHCl}_3$	A21
Table I-10.2 Atomic coordinates and $B_{\text{iso}}/B_{\text{eq}}$ for <i>mer</i> - $\text{RuCl}_3(\text{MeCN})_3 \cdot \text{CHCl}_3$	A22
Table I-10.3 Bond lengths (Å) for <i>mer</i> - $\text{RuCl}_3(\text{MeCN})_3 \cdot \text{CHCl}_3$	A22
Table I-10.4 Bond angles (°)for <i>mer</i> - $\text{RuCl}_3(\text{MeCN})_3 \cdot \text{CHCl}_3$	A22
Table I-11.1 Experimental details for $\text{Ru}(\text{hfac})_3$	A23
Table I-11.2 Atomic coordinates and $B_{\text{iso}}/B_{\text{eq}}$ for $\text{Ru}(\text{hfac})_3$	A24

Table I-11.3 Bond lengths (Å) for Ru(hfac) ₃	A24
Table I-11.4 Bond angles (°)for Ru(hfac) ₃	A25
Table I-12.1 Experimental details for Ru(hfac) ₂ (MeCN) ₂	A26
Table I-12.2 Atomic coordinates and B _{iso} /B _{eq} for Ru(hfac) ₂ (MeCN) ₂	A27
Table I-12.3 Bond lengths (Å) for Ru(hfac) ₂ (MeCN) ₂	A29
Table I-13.2 Atomic coordinates and B _{iso} /B _{eq} for Ru(acac)(hfac)(MeCN) ₂	A30
Table I-13.3 Bond lengths (Å) for Ru(acac)(hfac)(MeCN) ₂	A30
Table I-13.4 Bond angles (°) for Ru(acac)(hfac)(MeCN) ₂	A31
Table I-14.1 Experimental details for [Ru(acac) ₂ (Im) ₂][CF ₃ SO ₃]•benzene	A32
Table I-14.2 Atomic coordinates and B _{iso} /B _{eq} for [Ru(acac) ₂ (Im) ₂][CF ₃ SO ₃]•benzene..	A33
Table I-14.3 Bond lengths (Å) for [Ru(acac) ₂ (Im) ₂][CF ₃ SO ₃]•benzene.....	A33
Table I-14.4 Bond angles (°) for [Ru(acac) ₂ (Im) ₂][CF ₃ SO ₃]•benzene	A33
Table I-15.1 Experimental details for [Ru(acac) ₂ (NMeIm) ₂][CF ₃ SO ₃]	A34
Table I-15.2 Atomic coordinates and B _{iso} /B _{eq} for [Ru(acac) ₂ (NMeIm) ₂][CF ₃ SO ₃]	A35
Table I-15.3 Bond lengths (Å) for [Ru(acac) ₂ (NMeIm) ₂][CF ₃ SO ₃]	A35
Table I-15.4 Bond angles (°)for [Ru(acac) ₂ (NMeIm) ₂][CF ₃ SO ₃]	A36
Table I-16.1 Experimental details for [Ru(acac) ₂ (2MeIm) ₂][CF ₃ SO ₃]•0.5 hexane	A37
Table I-16.2 Atomic coordinates and B _{iso} /B _{eq} for [Ru(acac) ₂ (2MeIm) ₂][CF ₃ SO ₃]•0.5 hexane	A38
Table I-16.3 Bond lengths (Å) for [Ru(acac) ₂ (2MeIm) ₂][CF ₃ SO ₃]•0.5 hexane.....	A38
Table I-16.4 Bond angles (°) for [Ru(acac) ₂ (2MeIm) ₂][CF ₃ SO ₃]•0.5 hexane	A38
Table I-17.1 Experimental details for [Ru(acac) ₂ (5MeIm) ₂][CF ₃ SO ₃].....	A39
Table I-17.2 Atomic coordinates and B _{iso} /B _{eq} for [Ru(acac) ₂ (5MeIm) ₂][CF ₃ SO ₃]	A40
Table I-17.3 Bond lengths (Å) for [Ru(acac) ₂ (5MeIm) ₂][CF ₃ SO ₃]	A41
Table I-17.4 Bond angles (°) for [Ru(acac) ₂ (5MeIm) ₂][CF ₃ SO ₃].....	A41
Table II-1: Toxicity (PE ± 10 %) for selected compounds (at 100 µM) in oxic and hypoxic SCCVII cells (incubated for 3 h).	A42

Table II-2: Relative mean fluorescence intensity for SCCVII cells incubated with 100 μ M drug for 3 h under N ₂ and then treated with ELK3-51 (Cy3); determined using flow cytometry (average of 2 or 3 expts.; \pm 10 %).	A42
Table II-3: Log of mean fluorescence signal determined by flow cytometry and the compound reduction potential (determined by CV vs. SCE).	A42
Table II-4: Relative mean fluorescence intensity for SCCVII cells incubated with 100 μ M drug for 3 h under N ₂ and then treated with ELK3-51; determined using image cytometry (data from 2 expts.; \pm 10 %).	A43
Table II-5: Relative mean fluorescence intensity for SCCVII cells incubated with 100 μ M drug for 3 h under N ₂ and treated with ELK5-A8; determined using flow cytometry.	A43

List of Abbreviations

<u>Abbreviation</u>	<u>Meaning</u>
ϵ_r	relative permittivity
2D	2-dimensional
AAS	atomic absorption spectroscopy
Ab	antibody
acacH	acetylacetone
B.M.	Bohr magneton
b.p.	boiling point
BCCRC	British Columbia Cancer Research Centre
BSA	bovine serum albumin
BSO	buthionine sulfoximine
CCD	charge coupled device
CHO	chinese hamster ovary (cell line)
CNS	central nervous system
COSY	correlated spectroscopy
CTRON	chromatotron
CV	cyclic voltammetry
d	day
DAST	diethylaminosulfonyltrifluoride
DCC	dicyclohexylcarbodiimide
DCU	dicyclohexylurea
dd	doubly distilled
DEM	diethylmaleate
DMAD	dimethyladenine
DMF	N,N-dimethylformamide
dmsO	dimethylsulfoxide (solvent)
DMSO	dimethylsulfoxide coordinated through O-atom
DMSO	dimethylsulfoxide coordinated through S-atom
DNA	deoxyribonucleic acid
dppb	1,4 - bis(diphenylphosphino)butane
ELISA	enzyme-linked immunosorbent assay
ELK	Edith Lord Koch
en	1,2-diaminoethane (ethylenediamine)
EPR	electron paramagnetic resonance
equiv.	equivalent
FAB	fast atom bombardment
FCM	flow cytometry
FDG	fluorodeoxyglucose
GC	gas chromatography
GI	gastrointestinal
GSH	glutathione
Gy	gray

List of Abbreviations (cont.)

HEPES	N-2-hydroxyethylpiperazine-N'-2-ethane sulfonic acid
hfacH	1,1,1,6,6,6-hexafluoroacetylacetone
HR-MS	high resolution mass spectrometry
HSC	hypoxia selective cytotoxin
iBuClFrm	<i>iso</i> -butylchloroformate
ICM	image cytometry
Im	imidazole
IOI	integrated optical intensity
K _a	acid dissociation constant
LAH	lithium aluminum hydride
LET	linear energy transfer
lit.	literature reference
LMCT	ligand-to-metal charge transfer
LR-MS	low resolution mass spectrometry
LSIMS	low energy secondary ionization mass spectrometry
m.p.	melting point
MALDI	matrix assisted laser desorption ionization
MLCT	metal-to-ligand charge transfer
MO	molecular orbital
MoAb	monoclonal antibody
MRI	magnetic resonance imaging
MWCO	molecular weight cutoff
NBS	N-bromosuccinimide
NEM	N-ethyl maleimide
NHE	normal hydrogen electrode
NHS	N-hydroxysuccinimide
NMM	N-methylmorpholine
NO ₂	nitro
NO ₂ Im	nitroimidazole
NVIm	N-vinylimidazole
OD	optical density
ORTEP	Oakridge Thermal Ellipsoid Program
P	partition coefficient
PBS	phosphate buffered saline
PE	plating efficiency
PET	positron emission tomography
pF	paraformaldehyde
r.t.	room temperature
RBF	round-bottom flask
RF	radio-frequency
R _f	retention frequency
RNA	ribonucleic acid
RS	radiosensitizing

List of Abbreviations (cont.)

SCCVII	squamous cell carcinoma VII (cell line)
SCE	saturated calomel electrode
SDS	sodium dodecylsulphate
SER	sensitivity enhancement ratio
SF	surviving fraction
SR2508	etanidazole
SR4233	tirapazamine (1,2,4-benzotriazin-3-amine-1,4-di-N-oxide)
STMU•BF ₄	O-(N-succinimidyl)-N, N, N', N'-tetramethyl- uronium tetrafluoroborate
T/C	treated/control
TBAP	tetrabutylammonium perchlorate
TE	tris(hydroxymethyl)aminomethane + ethylenediamine- tetraacetic acid
Tf	triflate (CF ₃ SO ₃ ⁻)
Tf ₂ O	trifluorosulfonic anhydride
TF5	3-N-pentafluoropropylamido-1,2,4-benzotriazine-1,4-di-N- oxide
TLC	thin layer chromatography
TMSO	tetramethylenesulfoxide
TNE	TE + 150 mM NaCl
TsCl	<i>p</i> -toluenesulfonyl chloride
V	vinyl

Key to Chemical Compound Numbers and Abbreviations

The imidazole ring is numbered as shown in Figure i. The 1-position is typically referred to as the N-position at which various types of side-chains were added. For this work the 2-, 4- and 5-positions were usually substituted with either Me or NO₂ groups to give the corresponding imidazole compounds ($R_1 = R_2 = R_4 = R_5 = \text{H}$, **Im**; $R_2 = R_4 = R_5 = \text{H}$ and $R_1 = \text{Me}$, **NMeIm**; $R_1 = R_4 = R_5 = \text{H}$ and $R_2 = \text{Me}$, **2MeIm**; $R_1 = R_2 = R_{4/5} = \text{H}$ and $R_{4/5} = \text{Me}$, **4(5)MeIm**; $R_1 = R_4 = R_5 = \text{H}$ and $R_2 = \text{NO}_2$, **2NO₂Im**; $R_1 = R_2 = R_{4/5} = \text{H}$ and $R_{4/5} = \text{NO}_2$, **4(5)NO₂Im**; $R_1 = R_4 = \text{H}$ and $R_2 = \text{Me}$ and $R_5 = \text{NO}_2$, **2Me5NO₂Im**; $R_1 = R_5 = \text{H}$ and $R_2 = \text{Me}$ and $R_4 = \text{NO}_2$, **2Me4NO₂Im**).

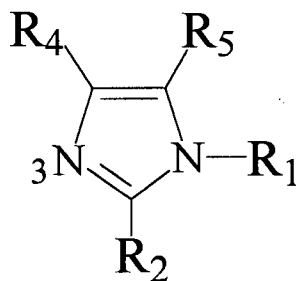
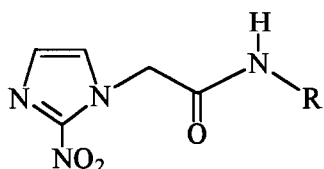


Figure i: Imidazole position numbering.

Numerous compounds were synthesized and used during the course of this thesis. The nitroimidazoles synthesized in chapter 3 were typically given names corresponding to the derivative from which they were synthesized (**E** = etanidazole (SR2508), **M** = metronidazole, **2M4N** = 2-methyl-4-nitro-) followed by the type and number of halogen atoms on the terminal propyl group attached to the amide N-atom of the N1 side-chain (*e.g.* **EF5** has a terminal -CF₂-CF₃ group, 5 F-atoms). A (-1) included at the end of the compound's name (*e.g.* **EF1(-1)**) corresponds to a terminal ethyl group (*i.e.* one -CH₂-group shorter). Other starting materials, side-products and incompletely characterized compounds are numbered 1 thru 27 in chapter 3. The Ru complexes reported in chapters 4 and 5 are numbered in the sequence in which they appear. It is suggested that the **Quick Reference** sheets on the following pages are used when reading the specific chapters.

Chapter 3 Quick Reference Compound Library

2NO₂Im compounds



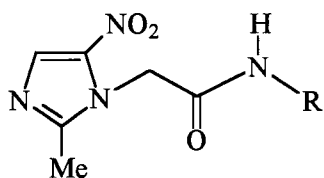
R

CH₂CF₂CF₃
 CH₂CF₂CF₂Br
 CH₂CH₂CF₃
 CH₂CF₃
 CH₂CH₂CF₂Br
 CH₂CH=CF₂
 CH₂CH₂CH₂F
 CH₂CH₂F
 CH₂CH₂CH₂Cl
 CH₂CH₂Cl
 CH₂CH₂CH₂Br
 CH₂CH₂Br
 CH₂CH₂CH₃
 CH₂CH(CH₃)₂

Compound

EF5
EF4Br
EF3
EF3(-1)
EF2Br
E=F2
EF1
EF1(-1)
EC11
EC11(-1)
EBr1
EBr1(-1)
EPrA
EIAA

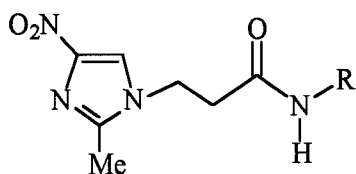
5NO₂Im compounds



CH₂CF₂CF₃
 CH₂CF₃
 CH₂CH₂F
 CH₂CH₂Cl
 CH₂CH₂Br

MF5
MF3(-1)
MF1(-1)
MC11(-1)
MBr1(-1)

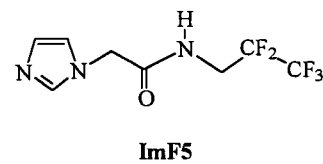
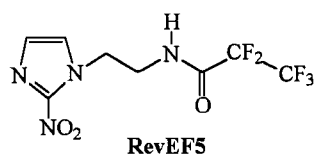
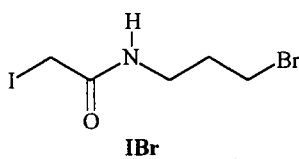
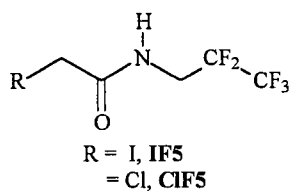
4NO₂Im compounds

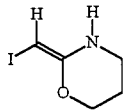
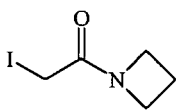
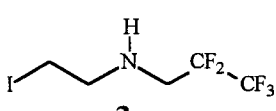
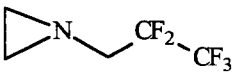

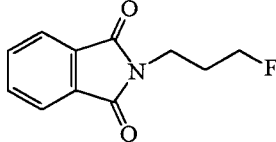
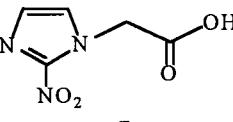
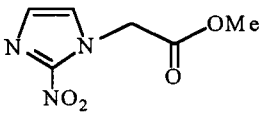
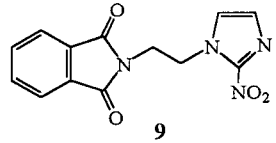
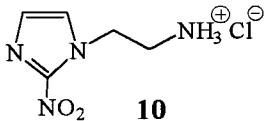
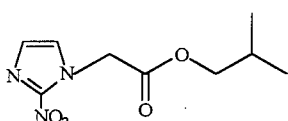
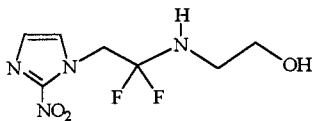
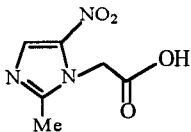
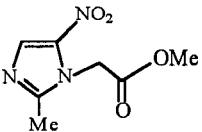
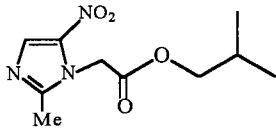
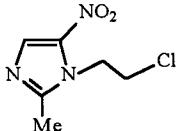
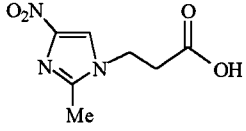
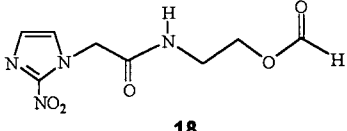
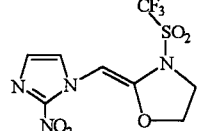
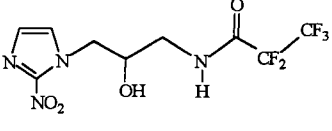
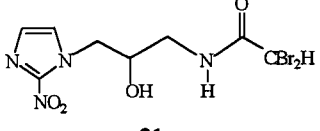
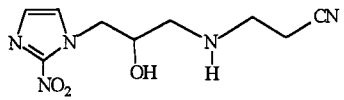
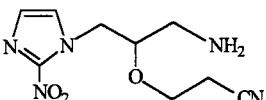
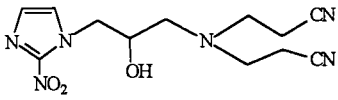
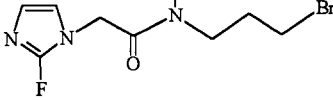
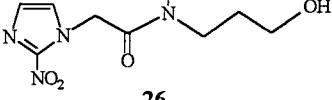
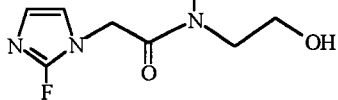


CH₂CF₂CF₃
 CH₂CF₃
 CH₂CH₂F
 CH₂CH₂Cl
 CH₂CH₂Br

2M4NF5
2M4NF3(-1)
2M4NF1(-1)
2M4NC11(-1)
2M4NBr1(-1)

Misc. Compounds



 1	 2	 3
 4	 5	 6
 7	 8	 9
 10	 11	 12
 13	 14	 15
 16	 17	 18
 19	 20	 21
 22	 23	 24
 25	 26	 27

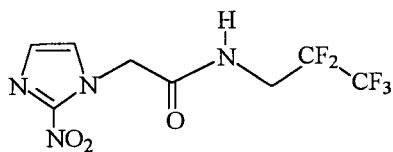
Chapter 4 Quick Reference Compound Library

Compound Number	Composition
28	$[\text{Ru}(\text{Im})_6][\text{CF}_3\text{SO}_3]_2$
29	$[\text{Ru}(\text{NMeIm})_6][\text{CF}_3\text{SO}_3]_2$
30	$[\text{Ru}(\text{5MeIm})_6][\text{CF}_3\text{SO}_3]_2$
31	<i>trans</i> - $[\text{Ru}(\text{CO})(\text{DMF})(2\text{MeIm})_4][\text{CF}_3\text{SO}_3]_2$
32	$[\text{Ru}(\text{DMF})(2\text{MeIm})_4][\text{CF}_3\text{SO}_3]_2$
33	$[\text{Ru}(\text{CF}_3\text{SO}_3)_x(2\text{MeIm})_4][\text{CF}_3\text{SO}_3]_y$ ($x=2$, $y=0$, or $x=1=y$)
34	$[\text{Ru}(2\text{NO}_2\text{Im})_6][\text{CF}_3\text{SO}_3]_2$
35	$[\text{Ru}(5\text{NO}_2\text{Im})_6][\text{CF}_3\text{SO}_3]_2$
36	$[\text{Ru}(2\text{Me5NO}_2\text{Im})_5][\text{CF}_3\text{SO}_3]_2$
37	$[\text{Ru}(\text{DMF})_4(\text{SR2508})_2][\text{CF}_3\text{SO}_3]_3$
38	$[\text{Ru}(\text{DMF})_2(\text{EF5})_2(\text{EtOH})_2][\text{CF}_3\text{SO}_3]_3$
39	<i>mer</i> - $\text{RuCl}_3(2\text{NO}_2\text{Im})_3$
40	<i>fac</i> - and <i>mer</i> - $\text{RuCl}_3(5\text{NO}_2\text{Im})_3$
41	" $\text{RuCl}_3(2\text{Me5NO}_2\text{Im})_3 \cdot 3\text{CO}_2$ "
42	$\text{RuCl}_3(\text{metro})_3$
43	$\text{RuCl}_3(\text{SR2508})_2(\text{EtOH})$
44	$\text{RuCl}_3(\text{EF5})_2(\text{EtOH})$
45	$\text{RuCl}_2(\text{metro})_4$
46	<i>cis</i> - $\text{RuCl}_2(\text{DMSO})_2(\text{en})$
47	<i>trans</i> - $\text{RuCl}_2(\text{DMSO})_2(\text{en})$
48	$\text{RuCl}_2(\text{DMSO})_2(\text{EF5})(\text{acetone})$
49	$[\text{RuCl}_2(\text{dppb})(\text{EF5})]_2(\mu\text{-Cl})_2$
50	$[\text{RuCl}_2(\text{dppb})\text{EF5}]_2(\mu\text{-dppb})$
51	<i>cis</i> - $\text{RuCl}_2(\text{MeCN})_4$
52	<i>mer</i> - $\text{RuCl}_3(\text{MeCN})_3$

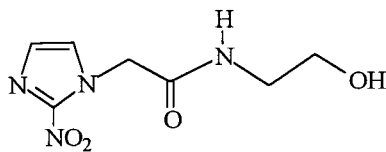
Chapter 5 Quick Reference Compound Library

Compound Number	Composition
53	$\text{Ru}(\text{acac})_3$
54	<i>cis</i> - $[\text{Ru}(\text{acac})_2(\text{MeCN})_2][\text{CF}_3\text{SO}_3]$
55	<i>cis</i> - $[\text{Ru}(\text{acac})_2(\text{Im})_2][\text{CF}_3\text{SO}_3]$
56	<i>trans</i> - $[\text{Ru}(\text{acac})_2(\text{Im})_2][\text{CF}_3\text{SO}_3]$
57	<i>cis</i> - $[\text{Ru}(\text{acac})_2(\text{MeCN})(\text{Im})][\text{CF}_3\text{SO}_3]$
58	<i>cis</i> - $[\text{Ru}(\text{acac})_2(\text{NMeIm})_2][\text{CF}_3\text{SO}_3]$
59	<i>cis</i> - $[\text{Ru}(\text{acac})_2(\text{MeCN})(\text{NMeIm})][\text{CF}_3\text{SO}_3]$
60	<i>cis</i> - $[\text{Ru}(\text{acac})_2(2\text{MeIm})_2][\text{CF}_3\text{SO}_3]$
61	<i>trans</i> - $[\text{Ru}(\text{acac})_2(2\text{MeIm})][\text{CF}_3\text{SO}_3]$
62	<i>cis</i> - $[\text{Ru}(\text{acac})_2(5\text{MeIm})_2][\text{CF}_3\text{SO}_3]$
63	<i>cis</i> - $[\text{Ru}(\text{acac})_2(4\text{MeIm})(5\text{MeIm})][\text{CF}_3\text{SO}_3]$
64	$[\text{Ru}(\text{acac})_2(2\text{NO}_2\text{Im})_2][\text{CF}_3\text{SO}_3]$
65	$[\text{Ru}(\text{acac})_2(\text{SR2508})_2][\text{CF}_3\text{SO}_3]$
66	$[\text{Ru}(\text{acac})_2(\text{EF5})_2][\text{CF}_3\text{SO}_3]$
67	$[\text{Ru}(\text{acac})_2(\text{metro})_2][\text{CF}_3\text{SO}_3]$
68	$[\text{Na}][\text{Ru}(\text{hfac})_3]$
69	$[\text{Ru}(\text{hfac})(\text{EtOH})_4][\text{hfac}]$
70	$\text{Ru}(\text{hfac})_3$
71	<i>cis</i> - $\text{Ru}(\text{hfac})_2(\text{MeCN})_2$
72	<i>cis</i> - $\text{Ru}(\text{hfac})_2(\text{Im})_2$
73	<i>cis</i> - $\text{Ru}(\text{hfac})_2(\text{Im})(\text{MeCN})$
74	<i>cis</i> - $\text{Ru}(\text{hfac})_2(\text{NMeIm})_2$
75	$[\text{Ru}(\text{hfac})(\text{NMeIm})_4][\text{hfac}]$
76	$[\text{Ru}(\text{hfac})(\text{NMeIm})_4][\text{PF}_6]$
77	<i>cis</i> - $\text{Ru}(\text{hfac})_2(2\text{MeIm})_2$
78	<i>cis</i> - $\text{Ru}(\text{hfac})_2(2\text{MeIm})(\text{MeCN})$

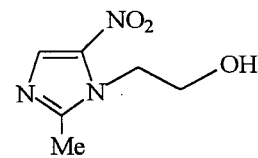
Compound Number	Composition
79	<i>trans</i> -Ru(hfac) ₂ (2MeIm) ₂
80	<i>cis</i> -Ru(hfac) ₂ (4MeIm)(5MeIm)
81	<i>trans</i> -Ru(hfac) ₂ (4MeIm)(5MeIm)
82	Ru(hfac) ₂ (2NO ₂ Im) ₂
83	Ru(hfac) ₂ (EF5) ₂
84	Ru(hfac) ₂ (SR2508) ₂
85	Ru(acac) ₂ (hfac)
86	[Na][Ru(hfac) ₂ (acac)]
87	Ru(hfac) ₂ (acac)
88	<i>cis</i> -Ru(acac)(hfac)(MeCN) ₂
89	<i>cis</i> -Ru(acac)(hfac)(Im) ₂
90	<i>cis</i> -Ru(acac)(hfac)(NMeIm) ₂
91	<i>cis</i> -Ru(acac)(hfac)(NMeIm)(MeCN)



EF5



SR2508



metro

Acknowledgements

I would like to thank my supervisors Brian James and Kirsten Skov for their guidance, encouragement, and support throughout the duration of this work. The low-key role they played was essential in helping me become a better scientist.

I would also like to thank the departmental services, especially Lianne Diarge, Marietta Austria, Peter Borda, Steve Rak, the late Steve Rettig, and the people at mass spectrometry for their support. From the BC Cancer Research Centre I am indebted to Hans Adomat, "the all-knowing-one," for help with essentially everything associated with the *in vitro* experiments. The help provided by Haibo Zhou and Jennifer Decker (thanks for staying late with me so many times) was also greatly appreciated. I must also give special thanks to Cameron Koch and Alex Kachur at the University of Pennsylvania and Mike Adam at TRIUMF for their collaboration on this project.

From BRJ's lab a special thanks must go to Jeff Posakony (Mr. Late Night) for being a great lab partner, running buddy, workout guru and diving mate. Never did I think that my second year TA would become my lab companion; thanks for waiting around Jeffy. Matt LePage (Pooch-Boy) must be commended for being the weirdest person in the lab BY FAR! Thanks for making sure things did not get too serious Matt. Other members of the James group past and present: Ken MacFarlane, Terrance Wong, Patric Meessen, Paul Cyr, Nathan Jones, Erin Ma, Elizabeth Cheu, Dave Kennedy (and all the rest) deserve honorable mention. Thanks to all for being my friend and also helping with the proofreading of parts of this thesis.

I must also thank Jeff and Katja for the fishing trips to rainbow country and Paul (my hunting buddy) and Helen for the many fantastic moose hunting trips up north. I am sure that it was these trips away from the city which helped me keep my sanity in an otherwise chaotic world.

Most importantly I must thank my beautiful wife, Kerry, for being the most caring, understanding and giving person I know. Without her encouragement throughout these past five years I surely would not have achieved this goal. I would also like to thank my parents and the rest of my family for all their love and support over the years.

Deluxe! Asta-lavista baby!

Chapter 1

Introduction

1.1 Introduction

Cancer is a complex family of diseases that is characterized by abnormal gene expression, resulting in uncontrolled growth and spread of abnormal cells. If the spread (metastases) of the cancer cells is not controlled it can ultimately lead to death. Approximately one in three people in North America will develop some form of cancer in their lifetime, and of these people approximately two-thirds will die of the disease. The most common cancers in the western world are lung, breast and colorectal cancer, which account for approximately 50 % of all cancer related deaths.¹

Although it is now possible to successfully treat ("cure") testicular cancer with cisplatin, most other cancers have limited response to chemotherapy and have only prolonged survival at best.² Hence, a major goal is to develop a system of cancer treatment which cures patients of their tumours while avoiding harmful side-effects to normal tissues. Our increased understanding of tumour biology and the cellular processes determining the behavior of cancer cells has allowed treatments to be directed specifically towards the tumour.³

The differences in tumour versus normal tissue stem from the rapid growth of cells within tumours which leads to formation of a tumour microenvironment. Typically, solid tumours contain areas of low extracellular pH and regions of low oxygen concentration (hypoxia). Exploitation of these properties, especially hypoxia, has been advantageous for the treatment of cancer using both organic compounds (*e.g.* radiosensitizers, hypoxic-selective cytotoxins) and metal complexes (*e.g.* antineoplastic and antimetastatic agents, see Section 1.6.3). However, the early detection of cancer using known imaging procedures (*i.e.* MRI, PET), prior to metastasis, is essential to ensuring patient survival. With early detection there would be approximately a 30 % increase in patient survival post treatment.¹

This chapter introduces the concept of hypoxia, how it develops in tumours, how it is measured/imaged and the postulation that hypoxia may make tumours more aggressive. The use of metal complexes in cancer therapy, focussing on Ru, is also briefly reviewed. These two topics are the major focus of this thesis and are reflected in the design and synthesis of the new compounds reported.

1.2 Hypoxia

1.2.1 What is it?

Hypoxic cells are those that are deficient in oxygen, yet remain viable, and are often found in tumours. Such cells may also exist in other living tissue; for example, both heart tissue damaged by cardiac arrest or a stroke and retinal tissue in the eye contain hypoxic cells.

The tissue in malignant tumours often outgrows its supply of oxygen and nutrients as the tumour enlarges. This is due to an inadequate production of a network of functioning blood vessels and capillaries. This poorly organized vasculature accounts for many of the environmental features unique to tumours.⁴ Although cells deprived of oxygen and nutrients ultimately die, at any given time a tumour may possess viable hypoxic cells.

There are currently two accepted mechanisms by which hypoxia may develop in tumours. First is the classical "chronic" diffusion-limited model of hypoxia.⁵ With chronic hypoxia, as oxygen diffuses from the blood, a gradient is formed where oxygen concentration decreases with increased distance from the vasculature (Figure 1-1).

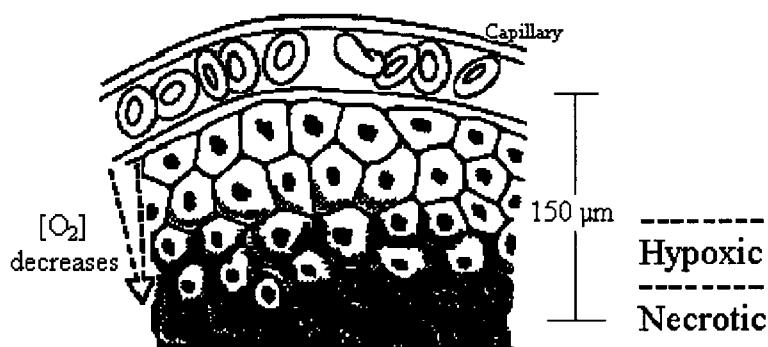


Figure 1-1: Oxygen gradient observed in a typical tumour (adapted from ref. 6).

Studies have determined the mean distance from the vasculature to the necrotic regions of a tumour to be 150 μm , consistent with the estimated diffusion range of oxygen.⁵ The cells just inside this distance, a layer of one to two cells thick, were proposed to be hypoxic.

The second mechanism is illustrated by the "acute" form of hypoxia which results from a localized pinching-off of blood vessels⁷ (*i.e.* when blood flow within the tumour vasculature fluctuates, resulting in a temporary cessation due to the transient opening and closing of vessels^{8,9}). The cells affected from acute hypoxia will, however, only be resistant to radiotherapy if the hypoxic environment lasts throughout the treatment (Section 1.2.1.1). The presence of viable hypoxic cells (both chronic and acute) has been observed in both animal^{9,10} and human tumours.¹¹

1.2.1.1 Resistance to Treatment: Radioresistance

Ionizing radiation is commonly used to kill tumour cells, however, it is not equally effective on each cell within a tumour. The fate of cells after radiation can be attributed to the biological effect of ionizing radiation which is greatly affected by the oxygen partial pressure within the cells (the "oxygen effect"). The ratio of hypoxic to oxic doses needed to achieve the same biological effect is referred to as the oxygen enhancement ratio (OER). For sparsely ionizing radiations, such as X- or γ -rays, the OER at high doses has a value between 2.5 and 3 (Figure 1-2). For densely ionizing radiation

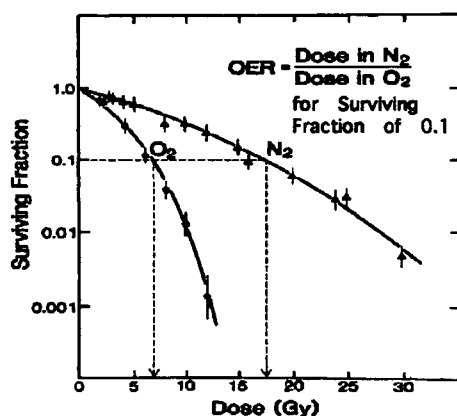


Figure 1-2: Typical results for X-ray irradiation of Chinese Hamster Ovary cells under aerobic (O₂) or hypoxic (N₂) conditions (adapted from ref. 6).

there is no oxygen effect. For the oxygen effect to be observed, oxygen must be present during the irradiation because the lifetime of the radicals produced by radiation via the indirect effect of low LET radiation is very short. The free radicals formed (typically from the hydrolysis of water) result in cleavage of chemical bonds leading to lesions which initiate the chain of events that results in the final expression of biological damage. The chemical damage produced by free radicals in DNA can be sometimes repaired under hypoxia, but the damage is "fixed", that is, made permanent and not infrequently irreparable if molecular oxygen is present.

The sensitivity of living cells to damage induced by radiation is due to a competition between oxygen and endogenous thiols (*e.g.* glutathione) for radiation induced radicals on the DNA.¹² The electron affinic oxygen reacts with the unpaired electrons produced on the DNA resulting in lesions which the cell has difficulty repairing, particularly the double-strand break.¹² At the same time, hydrogen atom donation to the unpaired electron from molecules such as glutathione yield lesions which are more readily repaired and it is this process which predominates in the absence of oxygen. To combat this effect various chemicals (DEM, NEM, diamide) which oxidize thiols have been tested against DNA repair with limited success. However, buthionine sulfoximine (BSO), a compound which selectively inhibits γ -glutamyl cysteine synthetase (the enzyme responsible for glutathione synthesis), exhibits some radiosensitization and has been shown to increase the effectiveness of other radiosensitizers (*e.g.* nitroimidazoles).^{13,14}

As a result of the radioresistance of hypoxic cells, a number of different methods have been employed to treat many tumours which might contain hypoxic regions. 1) Fractionated radiation treatment (2-2.5 Gy administered 5 days a week for 6 weeks) ensures that the treated cells could not accumulate and repair sublethal damage and the effect of increased cellular proliferation (repopulation) would be nullified. Moreover, the variation in the radiosensitivity of cells in different phases of the cell cycle and the ability of hypoxic cells to undergo reoxygenation would both be accounted for; 2) hyperbaric oxygen could be used to increase oxygen concentration within the blood in hopes of increasing the oxygen concentration in the tumour; 3) hypoxic-selective radiosensitizers (Section 1.3.1), many of which are oxygen mimetic, are useful. Like oxygen, these species

are highly electron affinic, but unlike oxygen they are not metabolized as they diffuse through the tissue and so actually reach and hence accumulate within the hypoxic cells; and 4) the use of bioreductive cytotoxins, which selectively target and directly kill hypoxic cells, can be beneficial. Methods 2-4 (all containing selectivity for hypoxia) provide a therapeutic advantage over other treatments because hypoxic cells are rare in normal tissue while they occur frequently in tumour tissue.

1.2.2 Hypoxia: The Aggressor?

Over the past 60 years there has been increasing evidence that hypoxia is prevalent in certain tumours and it poses a major problem in the treatment of cancer with either radiotherapy or chemotherapy.^{5,15,16} A meta analysis reporting all hypoxic sensitizer studies (>10,000 patients), including those agents now known to be ineffective, showed only a 14 % improvement in outcome.^{17,18} There is clearly an urgent need to find better methods of detection, and to select those patients who would benefit from adjuvant therapy such as a sensitizer or hypoxic cytotoxin.

There is compelling evidence that hypoxia in the tumour has far greater implications than the response to treatment of the primary tumour itself. Direct evidence for this comes from the assessment of hypoxia in patients containing carcinomas of the uterine cervix, using an Eppendorf electrode to determine oxygen concentration prior to treatment.^{19,20} The treatment of patients with radiation during this study showed a direct correlation between tumour inhibition and low hypoxic fractions. More importantly though, is that hypoxia was prognostic for outcome (curability) after surgery. For patients containing either cervix carcinomas²¹ or soft tissue sarcomas,²² the result was significantly better in those whose tumours were relatively well oxygenated and were treated with surgery, implying that tumours with hypoxia are more aggressive. Indirect evidence for hypoxia as an aggressor includes reports that hypoxia promotes genomic instability, a potential factor in tumour heterogeneity and progression.²³ The report that the expression of the p53 gene (which encodes a tumour suppressor protein important in chemical and viral carcinogenesis, apoptosis and cell cycle drug resistance) is induced by hypoxia and that cells exposed to hypoxia die by p53-mediated apoptosis is essential to our

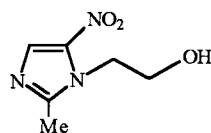
understanding of hypoxia. Hypoxic regions were shown to correlate spatially with highly apoptotic regions of tumours.²⁴ However, cells lacking intact p53 were resistant to low oxygen concentrations; hence hypoxia selects for mutant p53, and these cells survive. Hypoxia was also shown to be present in metastases which affected the cell's response to radiation; this may potentially increase the metastatic potential of a tumour.

The above findings which suggest that hypoxia makes a tumour more "aggressive" (or vice-versa), greatly increase the importance of determining which patients have hypoxia-containing tumours (not all tumours contain hypoxia). Finding treatments which will not only eradicate the hypoxic cells in the primary tumour, but also be directed towards the metastatic disease accompanying the aggressiveness caused by hypoxia, is also imperative.

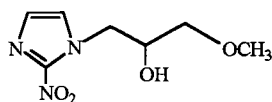
1.3 Role of Nitroimidazoles in Cancer Therapy

1.3.1 Hypoxic Radiosensitizers

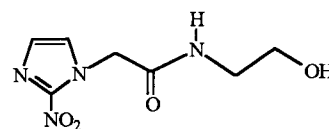
In the early 1970s nitroimidazoles were first proposed as radiosensitizers because of the high electron affinity of the nitro group. The 5-nitroimidazole, metronidazole (Figure 1-3), demonstrated radiosensitization in a variety of murine tumour systems²⁵ and its low toxicity and long biological half-life made it a good candidate for clinical testing. The drug at high doses, however, resulted in severe gastrointestinal (GI) intolerance which led to the search for a more effective, less toxic radiosensitizer. A number of 2-nitroimidazoles (2NO₂Im) were investigated due to their higher electron affinity (more positive $E_{1/2}$ value) and were shown to be more active than their 5-nitroimidazole analogues *in vitro*. The leading compound of this series was misonidazole (Figure 1-3) which showed marked activity in many different tumour models *in vivo* using several different assays.²⁵ Initial clinical trials with misonidazole using single doses appeared promising, with a decrease in GI intolerance from that of metronidazole. Notwithstanding, when multiple doses were administered patients developed neurological complications,²⁶ limiting the doses required to produce significant hypoxic cell sensitization.²⁷



Metronidazole (flagyl)



Misonidazole (Ro 07-0582)



Etanidazole (SR2508)

Figure 1-3: Structures of metronidazole, misonidazole and etanidazole.

Investigations of the mechanism of neural toxicity observed for misonidazole and other related compounds have revealed that toxicity is related to lipophilicity of the compounds.²⁸ This study revealed that lowering the partition coefficient (lipid:water) of a 2-nitroimidazole, via alteration of side-chain substituents on N1 of the imidazole ring, decreased the penetration of drug across the blood-brain barrier. The reduction of lipophilicity also led to poorer absorption of the drug into the blood from the peritoneal cavity. This problem was overcome by using intravenous injection. These studies also revealed that the partition coefficient of a 2NO₂Im could be lower than that of misonidazole by a factor of up to 20 without compromising tumour penetration or the radiosensitizing effectiveness. The 2NO₂Im, etanidazole (Figure 1-3), exhibited a greatly reduced lipophilicity compared to misonidazole (0.046 compared to 0.43) resulting in more rapid plasma clearance and less penetration into neural tissue, while maintaining the potency of misonidazole *in vivo*.²⁹ Clinical trials of etanidazole demonstrated that patients could tolerate a total dose of three times that of misonidazole without significant side-effects; however, etanidazole did result in nausea, vomiting and peripheral neuropathies which limited its use.²⁹

1.3.2 Chemistry of Nitroimidazoles in Biological Systems

The importance of using nitro-containing compounds (*e.g.* nitroimidazoles) for treatment and/or detection of hypoxia stems from the reducibility of the nitro group at physiological pH. A mechanism involving the reduction of the nitro group has been proposed (Figure 1-4).³⁰ Under hypoxic conditions the nitro group is reduced (it has been suggested that cytochrome P450 reductase is the dominant enzyme for the reduction of 2NO₂Im³¹) through a number of reactive intermediates, one or more of which is

presumed to be toxic to the cells.³² The selectivity towards hypoxic cells is because the reverse oxidation to the parent nitroimidazole is effectively reduced in the presence of low oxygen concentrations. In aerobic cells the reverse oxidation results in futile cycling of the nitro group with concomitant production of the superoxide radical and hydrogen peroxide.³³ A direct correlation between the sensitizing efficiency and electron affinity has been supported by various pulse radiolysis studies on one-electron transfer reactions between known radiosensitizers.³⁴

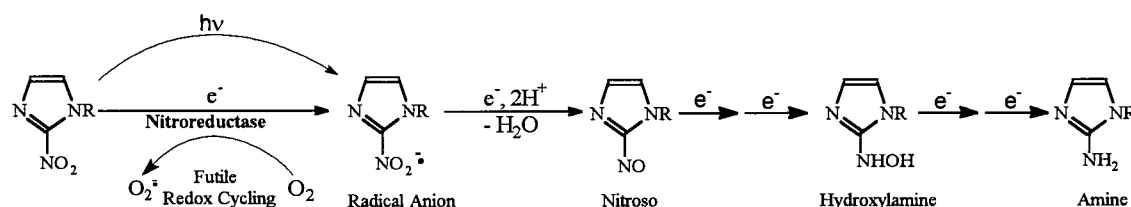


Figure 1-4: Nitroimidazole reduction scheme (adapted from ref. 30).

The position of the nitro group on the imidazole ring is also of marked importance to the effectiveness of the nitroimidazole as a sensitizer. The electron affinity of the nitro group is measured by the one-electron reduction potential of the nitroimidazole; the more positive the $E_{1/2}$ value the easier the reduction to the radical nitro anion. The reduction potentials for 2-, 4-, and 5-nitroimidazoles fall in typical ranges (Figure 1-5), with those of the 2NO₂Im's being the most positive.³²

		$E_{1/2}$ (mV)
	2-nitroimidazole	-360 to -400
	5-nitroimidazole	-510 to -545
	4-nitroimidazole	-540 to -685

Figure 1-5: Ranges of reduction potentials for nitroimidazoles vs. NHE at pH 7.

In the nitroimidazole reduction scheme, focussing on 2-nitroimidazoles, three products are expected from reduction in two-electron jumps. 2-Aminoimidazoles can be prepared as stable compounds by chemical methods and have been detected as metabolites of 2-nitroimidazoles.³⁵ However, the amines lack significant biological activity, leading to the consensus that one of the intermediate reaction products, either the 2-hydroxylaminoimidazole or the 2-nitrosoimidazole, is involved in adduct formation within the cell.³⁶

The nitrosoimidazole, 1-methyl-2-nitrosoimidazole, has been isolated in the solid state, but was found to be unstable in aqueous solution with a maximum half-life of 10 h at neutral pH. The product in acidic conditions, typical of hypoxic regions, has been identified, and results from the nucleophilic addition of water to the imidazole ring (Figure 1-6).³⁷ Products at neutral pH are more complex, but appear to arise from ring opening reactions of the hydrolyzed species. Reactions have also been observed with phosphines and aromatic amines, but the products have not yet been identified. 2-Nitrosoimidazole is more electron affinic than oxygen, can cause strand breaks in DNA and its half-life in cells with [GSH] > 0.1 mM is estimated to be less than one second. The rapid redox reaction with GSH is thought to be the major mode of activity for the nitrosoimidazole, leading to the formation of hydroxylaminoimidazole.³⁷

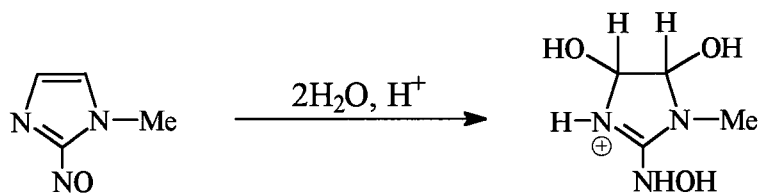


Figure 1-6: Nucleophilic addition of water to 1-methyl-2-nitrosoimidazole.

The 2-hydroxylaminoimidazoles have a longer half-life (~3-5 min) than the 2-nitrosoimidazoles and form stable species in acid.³⁷ Products of further reaction have been identified as the dihydrodihydroxyimidazolium ions resulting from the N-O bond heterolysis of the hydroxylamine that yields the nitrenium ion, which subsequently reacts with two equivalents of water. In the presence of other nucleophiles, the chemistry is modified such that the nucleophile competes with water for the nitrenium ion intermediate, and nucleophile-incorporated products are formed (Figure 1-7). These products include

covalent binding with GSH and other protein thiols,³⁸ guanine (DNA), phosphates (DNA) and other biological amines.^{37,39}

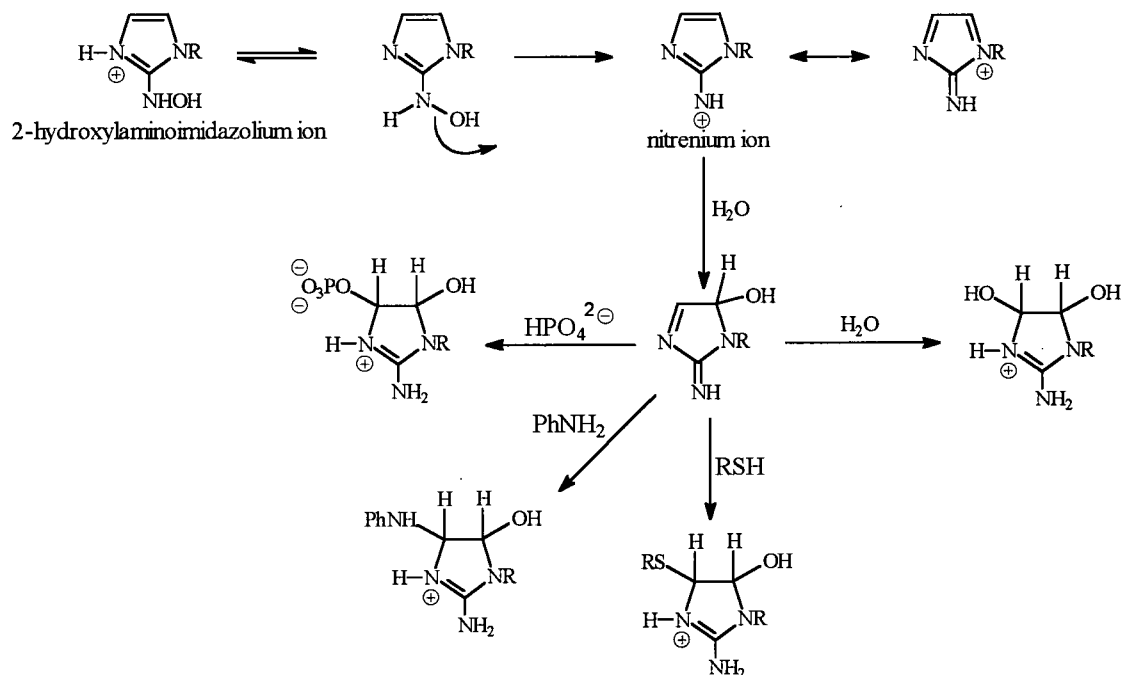


Figure 1-7: Proposed reactions of 2-hydroxyaminoimidazole within the cell.

1.4 Imaging of Hypoxic Tumours

The ideal marker of tissue oxygenation should: 1) have a large ratio of absolute binding between hypoxic tissue and aerobic tissue (large dynamic range); 2) exhibit an oxygen dependency that is similar to that of cellular radiosensitivity; 3) have a partition coefficient which facilitates its rapid diffusion into both well-perfused and poorly-perfused tissues; 4) contain a probe which can be accurately measured by invasive and/or non-invasive procedures; and 5) have no toxicity at its optimum concentration for this diagnostic use.³⁰ Many techniques have been used in an attempt to meet these requirements, a few of which are summarized in the following subsections.

1.4.1 Radiolabelling of Hypoxic Cells

By taking advantage of the selective bioreduction and subsequent binding of nitroimidazoles under conditions of low oxygen concentration, it was proposed that incorporation of ^3H or ^{14}C into the imidazole would allow for detection of hypoxia by radioactivity. For ^{14}C -misonidazole, for example, it was determined using this technique that the binding to cellular molecules within hypoxia was proportional to the square root of the drug concentration.⁴⁰ Detection methods are liquid scintillation techniques, immunochemical techniques or through autoradiography of histological sections depending on the label attached to the nitroimidazole. This last mentioned technique was used for patients with different metastatic lesions and, although there was a large tumour to plasma ratio of radiolabelled nitroimidazole, the high dose of radiolabels required made this approach unsuitable as a predictive assay of tumour hypoxia.⁴¹

1.4.2 Nuclear Medicine Techniques

Similar to the technique described above, this approach uses high energy γ -emitting radionuclides as labels on nitroimidazoles. The ^{82}Br -labelled 4-bromo-misonidazole compound was one of the first compounds developed in an attempt to quantify the amount of hypoxia in a tumour.⁴² Biodistribution and blood clearance studies revealed that the label was retained on the compound *in vitro* and *in vivo* and that the tumour and normal tissue distribution kinetics were similar or superior, from the perspective of imaging, to those of the parent compound, misonidazole. There was also higher uptake in the tumour for the bromo derivative, likely resulting from the significantly higher partition coefficient when compared to that of misonidazole (2.9 vs. 0.43). Moreover, this property also led to increased toxicity, presumably due to CNS toxicity. Hence, the usefulness of this compound as a hypoxia imaging agent was abandoned.

More recently, a series of 2-nitroimidazoles linked to iodinated sugars has been developed. These ^{123}I -radioiodinated azomycin ($2\text{NO}_2\text{Im}$) nucleosides show promise for use in the detection of tumour hypoxia while avoiding the toxicity of previously developed compounds. The leading compound in this series is iodoazomycin arabinoside (IAZA, Figure 1-8) and was shown to undergo hypoxia-dependent binding in murine tumour

models *in vitro*.⁴³ Tumour to blood ratios of 5-10 at 8 h post injection were observed indicating areas of hypoxia *in vivo* for EMT-6 tumours in BALB/c mice. These promising results led to the clinical study investigating ¹²³I-IAZA as a potential non-invasive marker of hypoxia which is currently under consideration.⁴⁴

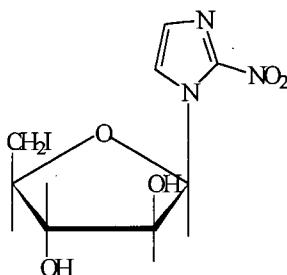


Figure 1-8: Iodoazomycin arabinoside (IAZA).

1.4.3 Fluorescent Probes

Analogous to the methods used to develop radiolabelled compounds for the detection of hypoxia, the addition of a fluorophore chemically linked to the side-chain of the 2-nitroimidazole moiety was pursued in hopes of utilizing the selective binding of the nitro species in hypoxia. Provided that the chain linking the 2-nitroimidazole moiety does not suffer metabolic cleavage from the fluorophore, the fluorescence should be “fixed” within the hypoxic cells. The best compound developed using this technique was an indolizine-linked 2-nitroimidazole species (Figure 1-9) which yielded a maximum fluorescence differential between oxic and hypoxic cells of 12.5:1 when tested *in vitro*. Unfortunately, when this probe was tested *in vivo* there was no observable difference between oxic and hypoxic cells, presumably due to an insufficient concentration of compound remaining in the cells.⁴⁵

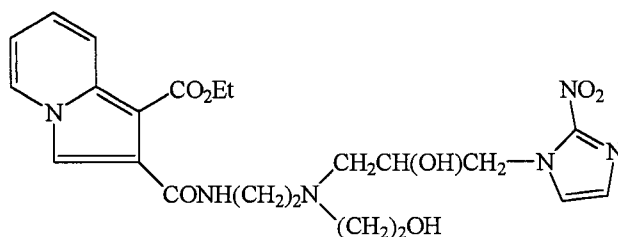


Figure 1-9: Indolizine-linked 2-nitroimidazole, fluorescent hypoxia probe.

1.4.4 Magnetic Resonance Imaging (MRI)

MRI is a biological multi-slice imaging technique utilizing the effect of atoms on an applied magnetic field, and is able to access specific areas of the body. The application of a magnetic field results in the orientation of nuclear spins, usually parallel to the magnetic field. For MRI, the patient is subjected to energy in the form of radiowaves via an RF (radio-frequency) pulse. This energy causes some of the low energy atoms (P, H, or F) to flip to their high energy (anti-parallel) state. A two-dimensional Fourier transform then manipulates the signal into an output which allows a computer to transform it into a signal strength versus intensity picture.

MRI has been used as a non-invasive diagnostic method for detecting tumour hypoxia for molecules containing ^{31}P , ^1H and ^{19}F . ^{31}P -MRI makes use of the fact that compounds associated with cellular energetics contain phosphorus atoms (especially ATP). In animal tumours these spectra were shown to correlate with changes in oxygen concentration as measured by microelectrodes, but there was too much scatter in the data to be clinically useful.⁵⁰ ^1H -MRI makes use of the high rate of glycolytic metabolism found in tumours resulting from lactate production. However, interference from other cellular signals make conclusive measurement difficult.⁵¹

The incorporation of ^{19}F atoms into known hypoxia-selective agents like 2-nitroimidazoles has also been investigated.^{52,53} The hexafluorinated 2-nitroimidazole CCI-103F was shown to lose the hexafluoropropyl substituent from its side-chain *in vivo*, but the trifluorinated hypoxia probe SR4554 was shown to remain intact upon enzymatic reduction *in vivo*, displaying selective uptake into the tumour in preliminary MRI studies.⁵³ MRI studies with EF5, which revealed a dynamic range of at least 50 using immunohistochemical techniques (as above), are currently underway in hopes of producing a clinically useful MRI hypoxia probe.⁵⁴

1.4.5 Positron Emission Tomography (PET)

PET is a biological imaging technique that allows one to measure in microscopic detail the function and/or metabolism of a labelled compound in specific areas throughout the body. This technique uses short-lived, neutron-poor, positron-emitting isotopes

produced by a cyclotron such as ^{15}O (half-life of 2 min), ^{13}N (10 min), ^{11}C (20 min) and ^{18}F (110 min) which are incorporated into biological substrates, substrate analogues or drugs. PET, like MRI, allows for multi-slice imaging. The most attractive candidate radionuclide is ^{18}F due to its sufficiently long half-life which allows for complex or multistep organic synthesis. The decay of ^{18}F is predominantly by positron emission (97 %) and the positron is of relatively low energy (0.635 MeV maximum) and thus has a short mean range (2.39 mm in water).⁵⁵ When the positron meets an electron they annihilate each other. All that remains is energy in the form of two γ -rays, of equal intensity, going in opposite directions (Figure 1-11). The γ -rays are then registered by detectors within the PET camera to generate a useful image.

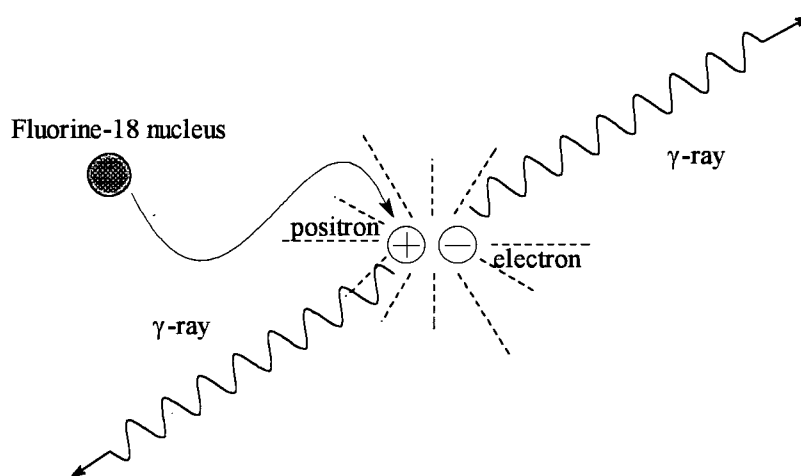


Figure 1-11: γ -ray production from positron-emitting isotope [^{18}F].

Fluorine is an interesting substituent in medicinal chemistry with a long and successful history of F-incorporation into organic pharmaceuticals. Fluorine is small (atomic radius, 0.57 Å) and exhibits high C-F bond energies (~ 106 kcal/mol). Fluorine is also extremely electronegative ($\chi = 3.98$) and its substitution into a molecule can often produce large changes in physiochemical and biological properties. A good example of this is the differences observed between **SR2508** (no F-atoms) and **EF5** (5 F-atoms). The most widely used PET agent to date, fluorodeoxyglucose (FDG), incorporates an ^{18}F atom into the ring of D-glucose and is used for imaging in both cancerous and non-cancerous tissues.⁵⁶

In order to provide a non-invasive detection method for hypoxia, ^{18}F was incorporated into a proven, hypoxia-selective 2-nitroimidazole. The first and most investigated compound of this type was [^{18}F]-fluoromisonidazole;⁵⁷ however, this compound is not ideal due to its hypoxia-independent tissue retention.⁵⁸ More recently, syntheses of [^{18}F]-fluoroetanidazole⁵⁹ and [^{18}F]-EF1⁶⁰ were reported, both showing promising hypoxia imaging results in cells and small animals. These findings indicate that the introduction of a non-invasive hypoxia imaging agent into the clinic is not far off.

1.5 Role of Metals in Cancer Therapy

Initially the use of metals and metal complexes as antitumour agents was not considered by most scientists due to the fact that numerous cases of poisoning, especially with heavy metals, had been documented. Researchers did not assume that such metals could be used to synthesize effective therapeutic agents when introduced to different ligand environments.⁶¹ Systematic studies into the relationship between chemical structure and efficacy or toxicity of metal compounds began only about sixty-five years ago. Collier and Krauss in 1931 described the first metal complex tumour-inhibiting study and developed a theory, which remains valid: "the effect of a heavy metal on experimental murine cancer is not only due to the metal alone, but also the structure of the compounds and the type of compound."⁶² Nevertheless, it was not until 34 years later (1965) when the first metal-containing anticancer drug was discovered, somewhat serendipitously by Rosenberg *et al.*,⁶³ that the field of metal complexes in cancer therapy escalated.

Rosenberg's new platinum "wonder-drug" was initially generated as an electrolysis product formed by the association of dissolved platinum (from a Pt electrode) with the ammonium cation from a culture medium containing *E. coli* bacteria.^{63,64} The resultant product was identified as $(\text{NH}_4)_2[\text{PtCl}_6]$ which converted to *cis*- $[\text{PtCl}_4(\text{NH}_3)_2]$ via a photochemical reaction. Similar neutral, *cis*-amine Pt species were synthesized and the series was tested for possible antitumour activity against the mouse tumour, Sarcoma 180. All of the compounds reduced tumour growth, but the most promising complex was *cis*- $[\text{PtCl}_2(\text{NH}_3)_2]$ (now known as cisplatin, Figure 1-12),⁶⁵ which entered clinical trials in 1971 and was approved by the US Food and Drug Administration in 1978 for treatment of

testicular and ovarian cancer.² Due to the severe toxic side-effects associated with cisplatin therapy, in particular nausea and vomiting, neuropathy, ototoxicity and most significantly, nephrotoxicity, the search for metal complexes having similar activity but with decreased side-effects was initiated.

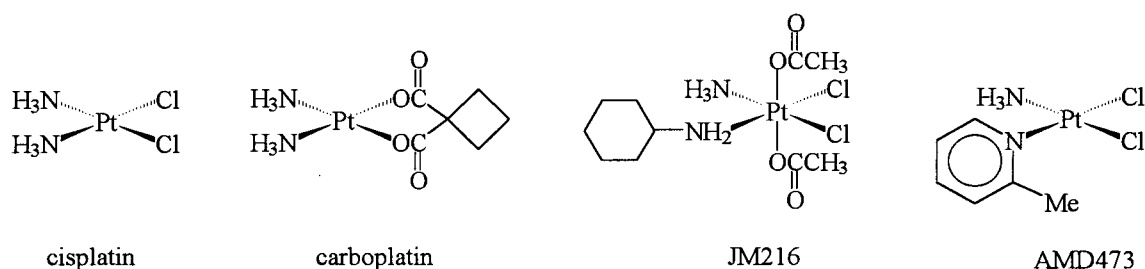


Figure 1-12: Chemical structures of antitumour agents cisplatin, carboplatin, JM216 and AMD473.

A less toxic analogue of cisplatin, carboplatin (Figure 1-12), was introduced into clinical practice in 1981, but disappointingly the two drugs were effective against the same population of tumours and thus shared cross-resistance with one another.^{66,67} A novel class of platinum (IV) dicarboxylates which demonstrated promising oral activity against a number of murine tumour models was discovered within the past ten years.⁶⁸ In preclinical studies, one such compound (bis-acetatoammine(dichloro)cyclohexylamineplatinum (IV)) (JM216, Figure 1-12) provided a structural lead to platinum complexes which may circumvent transport-determined resistance to cisplatin,^{69,70} this complex contains toxicological properties reminiscent of carboplatin rather than cisplatin.⁷¹ More recently, the sterically hindered Pt(II) complex AMD473 has entered clinical trials because of its circumvention of cisplatin resistance.⁷²

Since the discovery of cisplatin, a myriad of different metal complexes (Ti, V, Mo, Tc, Fe, Ru, Co, Rh, Ni, Pd, Cu, Au, Ga, Ge, Sn and Bi) have been synthesized and tested for their antitumour activity both *in vitro* and *in vivo* in hopes of discovering drugs which have activity against Pt resistant tumours. A few examples are Au(I) auranofin which displays irreversible inhibition of DNA synthesis in HeLa cells⁷³; Rh(II) carboxylates which act to inhibit murine ascitic tumours⁷⁴; and Ti(IV) titanocene dichloride which

demonstrates a reduced growth of solid animal tumour systems and in some cases this effect was more pronounced than that of cisplatin.⁷⁵ For the most part these complexes do not have the chemical properties required for an antitumour agent (see below). Most metal complexes have dose-limiting side-effects and are not tumour specific, restricting their possible use in the clinic. For example, Ga(III) nitrate was shown to inhibit tumour growth by greater than 90 % in 6 of 8 solid tumours transplanted subcutaneously,⁷⁶ but the gallium concentration was 130 times higher in the kidney than in the tumour.⁷⁷ The lack of selectivity likely explains this drug's poor clinical effect.

It is important, when considering the utility of a potential metal-containing antitumour agent, to take into account its kinetic characteristics. If too labile, the complex is likely to interact with physiological nucleophiles before reaching its site of action in the tumour and, if too inert, the complex may not interact with its biomolecular target as required to produce the antitumour effect.⁷⁸ In this regard, many metals form complexes that would be deemed too labile. However, the Pt group metals (Ru, Os, Rh, Ir, Pd, Pt) are capable of forming many relatively inert complexes whose kinetic properties can be tailored by variation of the ligands about the metal centre.

Although the main focus over the past 30 years has been on Pt antitumour complexes, the biological effects of Ru complexes, with the possibility of producing Ru-based drugs active in the treatment of human malignancies, have also been widely investigated.⁷⁹⁻⁸⁵ The Ru complexes differ from cisplatin, particularly when tumour sensitivity and the effects of tumour reduction on host survival time are concerned. This suggests that Ru complexes (the focus of this thesis work) have a select place in cancer therapy, opening further directions in the development of a new generation of anticancer agents.⁷⁹

1.6 Ruthenium Complexes

1.6.1 Chemical Properties Relevant to Tumour Treatment

As antitumour drugs are generally cytotoxic, the development of drugs which selectively target the tumour to ensure a selective cell kill is essential. The use of Ru over Pt is one approach to avoid the problems associated with Pt drug therapy.

There are two significant differences between Ru- and most of the Pt-based antitumour drugs which make their prospective mechanism of action advantageous: 1) the usually six-coordinate, octahedral geometry of Ru complexes (versus square planar Pt (II)) may allow for new modes of binding to nucleic acids, and 2) the ease with which electron-transfer takes place for the Ru^{II/III} couple because of a small activation barrier (see below).⁸³

The most stable complexes in aqueous solution are generally Ru^{II} and Ru^{III} and these are usually readily interconverted via oxidation/reduction within biological systems. The Ru^{III} ion (d⁵, low-spin) usually accepts π -electron density into its partially filled d π -orbital and thus has a strong attraction for halides and anionic oxygen ligands; a low-spin, d⁶ Ru^{II} ion has little affinity for π -donors, but readily binds π -acceptor ligands. This is due to further extended d π orbitals which lead to better π -orbital overlap.⁸⁶ The Ru^{III} reduction potentials can be tuned by changing the type of coordinated ligand.⁸⁷ For example, the reduction potential for [L(NH₃)₅Ru^{III}] varies from -0.08 V (L = OH) to 1.1 V (L = N₂). In general, anionic σ -donor ligands lower the reduction potential, while neutral or cationic, π -acceptor ligands raise it. As the Franck-Condon barrier to electron transfer is low for Ru^{II/III} couples, owing to small bond distortions between these two ions, redox reactions are often rapid.⁸⁸

The reduction of Ru^{III} to Ru^{II} allows for the use of Ru^{III} complexes as "prodrugs" for Ru^{II} species which have an elevated propensity to coordinate to biomolecules. In particular, the binding of Ru^{II} with the imine N of imidazole rings on histidine and purines^{89,90} predominates where reducing power is relatively high and oxygen, which can reoxidize Ru^{II} back to Ru^{III}, is virtually non-existent. Such an environment occurs in many tumours^{91,92} which are hypoxic due to their higher metabolism and diffusion limited oxygen supply.^{93,94} Tumours also typically have a lower pH which favours pH-dependent reduction of some complexes.⁹⁵ Consequently, the Ru^{II}/Ru^{III} ratio should be higher in most types of tumours than in other tissues leading to increased binding and hence localized cytotoxicity. And so, the treatment of tumours with Ru^{II} complexes (potentially toxic for all tissues) should be avoided in favour of the more inert Ru^{III} prodrugs.

The accumulation of Ru ions within tumour tissues is not only due to reduction of Ru^{III} , but is also significantly increased by coupling with transferrin.^{96,97} This phenomenon is due to the similarities between Ru^{III} and Fe^{III} , which both have a high affinity for phenolate ligands^{98,99} which are integral in complexing Fe^{III} in transferrin for transport through the blood to the tissues. Release of Ru^{III} from transferrin (like Fe^{III}) may be facilitated by lower pH or reduction to Ru^{II} ,¹⁰⁰ which has little affinity for phenolate.

1.6.2 DNA Binding

Antitumour agents are expected to block the DNA activity of tumour cells in order to be effective, and accordingly DNA is thought to be the major target for most antitumour drugs. Ru complexes are no exception. The bulk of evidence suggests that DNA binding is possible, and in some instances is as frequent and effective as with cisplatin, for which a DNA interaction has been well documented using X-ray crystallography.¹⁰¹

Cisplatin (*cis*-DDP) is believed to result mainly from the 1,2 (GG) and 1,3 (GXG) intrastrand cross-links within DNA which *trans*-DDP cannot form. The 1,2 cross-link involves binding of Pt to N7 of adjacent deoxyguanosines along the same strand of DNA to form a 17-membered chelate ring (Figure 1-13).¹⁰² This intrastrand adduct can be removed by nucleotide excision repair (an entire oligomer containing the adduct is excised¹⁰³), but some results suggest that the repair of a GG intrastrand cross-link is significantly impaired when compared with that for monofunctional adducts.¹⁰⁴ The intrastrand cross-link also results in a bending of the DNA double helix (a 33° kink) which promotes binding of a specific class of damage-recognition proteins.¹⁰⁵ It has been postulated that these proteins may be important in cisplatin toxicity by blocking access of repair enzymes to damaged DNA.¹⁰⁶ The *trans* isomer of cisplatin (*trans*platin) was determined to be much less active likely due to its steric inability to form the major intrastrand cross-links.

Ru complexes, and more importantly Ru^{II} complexes, were shown to be capable of strong interaction with oligonucleotides (e.g. with calf thymus DNA)⁸⁹ for which preferential N-N adduct formation between two adjacent guanines, identical to that of

cisplatin, was observed.⁹⁰ However, Clarke reports that the GG cross-link formation with

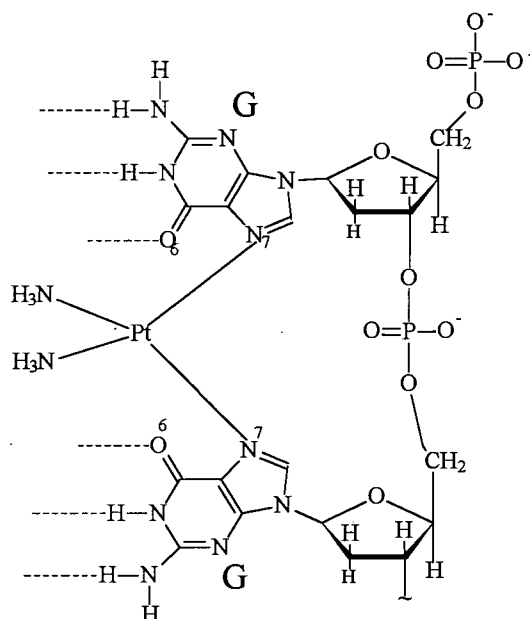


Figure 1-13: Cisplatin/DNA interaction to form a GG intrastrand cross-link.

DNA is not essential for antitumour activity, with, for example, pentaammine-Ru complexes as it is for the platinum drugs.⁸³ The N7 of guanine is relatively exposed in the major groove of B-DNA and the metal complexes, typically positively charged species (*e.g.* $[\text{Ru}(\text{NH}_3)_5(\text{H}_2\text{O})]^{2+}$), undergo a fairly strong electrostatic attraction for the polyanionic DNA. Once bound to the DNA the Ru complex is also thought to induce localized denaturation of the DNA which makes the interior sites (N6 of adenine and N4 of cytosine) available for Ru^{II} interaction.¹⁰⁷ Interestingly, a comparison of DNA binding for *cis*- and *trans*- $\text{RuCl}_2(\text{DMSO})_4$ reveals that the *trans* isomer covalently binds at a markedly higher reaction rate (behaviour opposite to that of *cis*- and *trans*-DDP) and protects G-rich sequences from cutting by specific restriction endonucleases, indicating a preferential interaction with adjacent guanines.⁹⁰

DNA-bound Ru was also found after *in vivo* treatment with antitumour doses of either Ru^{II} or Ru^{III} complexes; this was measured by atomic absorption spectroscopy, in samples of DNA extracted from tumour cells and from cells of lung, internal mucous, liver

and spleen tissue. These data displayed unequal distribution of DNA-bound Ru, which was more concentrated (selective localization) in the lung and tumour tissue than in the spleen or liver.¹⁰⁸

1.6.3 Tumouricidal Effects of Ru Complexes

The selectivity of Ru complexes for tumours makes them highly appropriate for investigation in antitumour research. As none of the existing antitumour drugs are devoid of severe and dose-limiting side-effects, the search for novel non-toxic compounds continues. Preliminary studies have revealed that "Ru complexes may help to overcome the dose-limiting complication, and it would be hypothesized that new derivatives could find a place in therapy as new-generation target-specific anticancer drugs."⁷⁹

There is a myriad of newly synthesized Ru complexes reported in the literature each year, but those which exhibit antitumour activity can be grouped into three categories. The first is the Ru-ammine complexes, the first series of Ru complexes to undergo screening for antitumour activity. The compound, *fac*-RuCl₃(NH₃)₃ exhibited excellent activity in several tumour screens (up to T/C of 190 %); however, its poor solubility impedes it from adequate formulation as a drug.⁸⁰ Keppler and co-workers synthesized a number of similar complexes, yielding species which were more soluble in aqueous media due to their anionic charge. For example, *cis*-[RuCl₂(NH₃)₄]Cl (with T/C values up to 160 %) is active against P388 leukemia, a highly sensitive platinum tumour model used to compare Ru drug performance to cisplatin.^{109,110}

The second group of complexes is that characterized by the presence of DMSO, which, as a ligand, facilitates transport through, and penetration into membranes, increases complex water solubility and is significantly labile to undergo displacement by stronger binding nitrogenous DNA bases (especially N7 of guanine). Both *cis*- and *trans*-RuCl₂(DMSO)₄ exhibit interesting antitumour properties, with the *trans* isomer exhibiting significantly higher toxicity than the *cis* isomer. More importantly, both exhibit antimetastatic activity greater than cisplatin.⁸²

The third group (the focus of this thesis) is comprised of Ru complexes containing one or two heterocyclic ligands such as imidazole, pyrazole, indazole and their

methyl substituted derivatives. Generally, these complexes exhibit significant antitumour activity.⁸¹ For example, the water soluble, bis-imidazole complex $[\text{ImH}][\text{RuCl}_4(\text{Im})_2]$ showed a T/C value of about 200 % against the P388 leukemia (*cf.* cisplatin, T/C 175 %).¹¹¹ The complex also possessed potent and selective antitumour activity in a carcinogen-induced colorectal tumour of the rat.

Assessment of cytotoxicity with all three classes of Ru antitumour complexes generally revealed a low *in vitro* effectiveness.⁷⁹ This is not the case for all Ru complexes, but it is clearly evident that most of them, despite being capable of reducing *in vivo* tumours and/or increasing the lifespan of tumour-bearing animals, are essentially void of any capacity to reduce cell viability when tested *in vitro*.⁷⁹ This implies that if the new Ru complexes are initially screened using *in vitro* assays, the result might be misleading and hence fail to unmask the real effectiveness of these complexes against cancer growth. The development of Ru complexes by examining the general effect of tumour growth, or by examining tumour size variation with solid tumours, may also limit the scope of these complexes as potential antitumour agents. It is clear that each Ru complex must be used at a maximum tolerated dose to significantly reduce primary tumours, while the reduction of solid tumour metastases is achievable at doses with undetectable cytotoxic side-effects for the hosts.¹¹²

The development of antimetastatic drugs for the treatment of solid tumours is essential in combating cancer which can readily disseminate throughout the host. Tumour metastases behave quite differently from their primary neoplasms due to differences in drug sensitivity, antigenicity and clonogenic capacity.¹¹³ The drugs available for the management of human tumours are usually only active on primary lesions. Therefore, if the tumour has metastasized, the antimetastatic drug becomes equally as important in prevention of tumour growth. The first compound capable of selective activity against metastatic tumours (*trans*- $\text{Na}[\text{RuCl}_4(\text{DMSO})(\text{Im})]$) was developed by Sava *et al.* and showed a significant advantage for the postsurgical prognosis when associated with ablation of primary tumours.¹¹⁴ The mechanism of action of this complex is, however, poorly understood and so obtaining a full understanding of this process is essential to the

preparation of complexes which will circumvent the actual limits of *trans*-Na[RuCl₄(DMSO)(Im)].

1.7 Thesis Overview

At the onset of this thesis work the major goal was to synthesize, characterize and assess in mamalian cells *in vitro* new Ru nitroimidazole complexes for use as potential non-toxic radiosensitizers. However, because of the development of **EF5** (a pentafluorinated 2NO₂Im) and a highly selective monoclonal antibody to **EF5** (ELK3-51),^{47,49} the focus shifted to the synthesis and characterization of new 2-, 4- and 5-nitroimidazoles with halogenated side-chains (Chapter 3). Alteration of the side-chain and position of the nitro group on the imidazole ring provides valuable information on the interaction of the monoclonal antibody with the drug (Chapter 6).

This thesis consists of seven chapters plus appendices of 17 X-ray structures. Chapter 2 describes the general experimental procedures used in the characterization of the newly synthesized complexes, including the synthetic procedures for all the Ru starting complexes used in Chapter 4. Each of Chapters 3, 4 and 5 contains its own experimental and results and discussion sections. Chapter 3 contains the synthesis and complete characterization of nearly 30 new 2-, 4-, and 5-nitroimidazoles, containing N1-halogenated side-chains, including their reduction potentials as determined by cyclic voltammetry (CV). Chapter 4 describes the synthesis and characterization of many Ru complexes obtained from the reaction of imidazoles and nitroimidazoles with different Ru precursors (*e.g.* [Ru(DMF)₆][CF₃SO₃]₃, RuCl₃•3H₂O, *cis/trans*-RuCl₂(DMSO)₄). Many of these complexes were paramagnetic Ru(III) species which made their characterization by NMR more difficult. Chapter 5 is comprised of the synthesis and characterization of Ru(II) and Ru(III) bis-acetylacetonate (acac), bis-1,1,1,6,6,6-hexafluoroacetylacetonate (hfac) and mixed acac/hfac complexes with imidazole and nitroimidazole ligands. A comprehensive study of the reduction potentials of these complexes, as determined by CV, suggests the capability of synthesizing a complex with a reduction potential in the desired biological range by altering the substituents on the chelating β-diketonato ligands. Chapter 6 focuses on the *in vitro* testing of selected nitroimidazoles and Ru

imidazole/nitroimidazole complexes. The toxicity and monoclonal antibody recognition (using both MoAbs ELK3-51 and ELK5-A8) of some of the nitroimidazoles from Chapter 3 are evaluated in SCCVII cells. The Ru complexes are tested for their toxicities and abilities to accumulate within the cell and to coordinate to DNA, and a preliminary radiosensitization study of two of these complexes is included. Conclusions and suggestions for future experiments, including a report on the studies that are currently underway to answer some of the chemical and biological questions generated from this thesis work, are reported in Chapter 7.

1.8 References

- 1 Cook, A. R. The New Cancer Source Book, Health Reference Series, Vol. 12; Omnigraphics, Inc., Detroit, 1996, p. 3.
- 2 Fricker, S. P. *In* Metal Compounds in Cancer Therapy; S. P. Fricker, Ed.; Chapman and Hall, London, 1994, p.3.
- 3 Ruddon, R. W. Cancer Biology; Oxford University Press, New York, 1995, p. 3.
- 4 Jain, R. K. *J. Natl. Cancer Inst.* **1989**, *81*, 570.
- 5 Thomlinson, R. H.; Gray, L. H. *Br. J. Cancer* **1955**, *9*, 539.
- 6 Farrell, N. *In* Transition Metal Complexes as Drugs and Chemotherapeutic Agents; R. Ugo and B. R. James, Eds.; Kluwer Academic, Dordrecht, 1989, p. 183.
- 7 Brown, J. M. *Br. J. Radiol.* **1979**, *52*, 650.
- 8 Dudar, T. E.; Jain, R. K. *Cancer Res.* **1984**, *44*, 605.
- 9 Chaplin, D. J.; Durand, R. E.; Olive, P. L. *Int. J. Radiat. Oncol. Biol. Phys.* **1986**, *12*, 1279.
- 10 Moulder, J. E.; Rockwell, S. *Int. J. Radiat. Oncol. Biol. Phys.* **1984**, *10*, 695.
- 11 Vaupel, P.; Kallinowski, F.; Okunieff, P. *Cancer Res.* **1989**, *49*, 6449.
- 12 Ward, J. F. *In* Radioprotectors and Anticarcinogens; O. F. Nygaard and M. G. Simic, Eds.; Academic Press, New York, 1983, p. 73.
- 13 Bump, E. A.; Yu, N. Y.; Brown, J. M. *Pharmac. Ther.* **1990**, *47*, 117.
- 14 Koch, C. J.; Skov, K. A. *Int. J. Radiat. Oncol. Biol. Phys.* **1994**, *29*, 345.
- 15 Bush, R. S.; Jenkin, R. D. T.; Allt, W. E. C.; Beale, F. A.; Bean, H. A.; Dembo, A. J.; Pringle, J. F. *Br. J. Cancer* **1978**, *37*, 255.
- 16 Teicher, B. A.; Laxo, J. S.; Sartorelli, A. C. *Cancer Res.* **1981**, *41*, 73.
- 17 Coleman, C. N. *Br. J. Cancer* **1996**, *74*, S297.
- 18 Overgaard, J. *Conference Summary - clinical. 9th Int. Conf. on Chem. Modifiers of Cancer Treatment*, Oxford, U. K., Aug. 22-26, 1995.
- 19 Vaupel, P.; Schlenger, K.; Knoop, C.; Höckel, M. *Cancer Res.* **1991**, *51*, 3316.
- 20 Höckel, M.; Schlenger, K.; Knoop, C.; Vaupel, P. *Cancer Res.* **1991**, *51*, 6098.

- 21 Höckel, M.; Schlenger, K.; Aral, B.; Mitze, M.; Schäffer, U.; Vaupel, P. *Cancer Res.* **1996**, *56*, 4509.
- 22 Brizel, D. M.; Scully, S. P.; Harrelson, J. M.; Layfield, L. J.; Bean, J. M.; Prosnitz, L. R.; Dewhirst, M. W. *Cancer Res.* **1996**, *56*, 941.
- 23 Paquette, B.; Little, J. B. *Cancer Res.* **1994**, *54*, 3173.
- 24 Graeber, T. G.; Osmanian, C.; Jacks, T.; Housman, D. E.; Koch, C. J.; Lowe, S. W.; Giaccia, A. J. *Nature* **1996**, *379*, 88.
- 25 Fowler, J. F.; Denekamp, J. *Pharmacol. Therapeut.* **1979**, *7*, 413.
- 26 Dische, S. *Int. J. Radiat. Oncol. Biol. Phys.* **1991**, *20*, 147.
- 27 Brown, J. M. *Int. J. Radiat. Oncol. Biol. Phys.* **1984**, *52*, 650.
- 28 Brown, J. M.; Workman, P. *Radiat. Res.* **1980**, *82*, 171.
- 29 Brown, J. M.; Yu, N. Y.; Brown, D. M.; Lee, W. W. *Int. J. Radiat. Oncol. Biol. Phys.* **1981**, *7*, 695.
- 30 Chapman, J. D.; Lee, J.; Meeker, B. E. *In* Selective Activation of Drugs by Redox Processes; G. E. Adams, A. Breccia, E. M. Fielden, P. Wardman, Eds.; Plenum Press, New York, 1990, p. 316.
- 31 Joseph, P.; Jaiswal, A. K.; Stobbe, C. C.; Chapman, J. D. *Int. J. Radiat. Oncol. Biol. Phys.* **1994**, *29*, 351.
- 32 Adams, G. E.; Flockhart, I. R.; Smither, C. E.; Stratford, I. J.; Wardman, P.; Watts, M. E. *Radiat. Res.* **1976**, *67*, 9.
- 33 Biaglow, J.; Varnes, M.; Roizen-Towle, L.; Clarke, E.; Epp, E.; Astor, M.; Hall, E. *Biochem. Pharmacol.* **1986**, *35*, 77.
- 34 Adams, G. E.; Cooke, M. S. *Int. J. Radiat. Biol.* **1969**, *15*, 457.
- 35 Walton, M. I.; Workman, P. *Biochem. Pharmacol.* **1987**, *36*, 887.
- 36 Palcic, B.; Josephy, D.; Skov, K.; Skarsgard, L. D. *Proceedings of a Conference Sponsored by the Radiosensitizer/Radioprotector Working Group DCT/NCI*, 1979, p. 16.

- 37 McClelland, R. A. *In Selective Activation of Drugs by Redox Processes*; G. E. Adams, A. Breccia, E. M. Fielden, P. Wardman, Eds.; Plenum Press, New York, 1990, p. 125.
- 38 Raleigh, J. A.; Koch, C. J. *Biochem. Pharmacol.* **1990**, *40*, 2457.
- 39 McClelland, R. A.; Panicucci, R.; Rauth, A. M. *J. Am. Chem. Soc.* **1987**, *109*, 4308.
- 40 Koch, C. J.; Stobbe, C. C.; Baer, K. A. *Int. J. Radiat. Oncol. Biol. Phys.* **1984**, *10*, 1327.
- 41 Urtasun, R. C.; Chapman, J. D.; Raleigh, J. A.; Franko, A. J.; Koch, C. J. *Int. J. Radiat. Oncol. Biol. Phys.* **1986**, *12*, 1263.
- 42 Rasey, J. S.; Krohn, K. A.; Freauuff, S. *Radiat. Res.* **1982**, *91*, 555.
- 43 Mannan, R. H.; Somayaji, V. V.; Lee, J.; Mercer, J. R.; Chapman, J. D.; Wiebe, L. I. *J. Nucl. Med.* **1991**, *32*, 1764.
- 44 Parliament, M. B.; Chapman, J. D.; Urtasun, R. C.; McEwan, A. J.; Goldberg, L.; Mercer, J. R.; Mannan, R. H.; Wiebe, L. I. *Br. J. Cancer* **1992**, *65*, 90.
- 45 Parrick, J.; Hodgkiss, R. J.; Jones, G. W.; Middleton, R. W.; Rami, H. K.; Wardman, P. *In Selective Activation of Drugs by Redox Processes*; G. E. Adams, A. Breccia, E. M. Fielden, P. Wardman, Eds.; Plenum Press, New York, 1990, p. 249.
- 46 Raleigh, J. A.; Miller, G. G.; Franko, A. J.; Koch, C. J.; Fuciarelli, A. F.; Kelly, D. A. *Br. J. Cancer* **1987**, *56*, 395.
- 47 Koch, C. J.; Evans, S. M.; Lord, E. M. *Br. J. Cancer* **1995**, *72*, 869.
- 48 Matthews, J.; Adomat, H.; Farrell, N.; King, P.; Koch, C.; Lord, E.; Palcic, B.; Poulin, N.; Sangulin, J.; Skov, K. *Br. J. Cancer* **1996**, *74*, S200.
- 49 Evans, S. M.; Joiner, B.; Jenkins, W. T.; Laughlin, K. M.; Lord, E. M.; Koch, C. J. *Br. J. Cancer* **1995**, *72*, 875.
- 50 Fu, K. K.; Wendland, M. F.; Iyer, S. B.; Lam, K. N.; Eugeseth, H.; James, T. L. *Int. J. Radiat. Oncol. Biol. Phys.* **1990**, *18*, 1341.
- 51 Stone, H. B.; Brown, J. M.; Philips, T. L.; Sutherland, R. M. *Radiat. Res.* **1993**, *136*, 422.

-
- 52 Raleigh, J. A.; Franko, A. J.; Treiber, E. O.; Lunt, J. A.; Allen, P. S. *Int. J. Radiat. Oncol. Biol. Phys.* **1986**, *12*, 1243.
- 53 Aboagye, E. O.; Kelson, A. B.; Workman, P. *Anti-cancer Drug Design* **1998**, *13*, 703.
- 54 Siemann, D. W.; Inglis, B. A.; Cranston, B. A.; Lord, E. M.; Koch, C. J. *10th International Conference on Chemical Modifiers of Cancer Treatment*, Jan. 28-31, 1998, Clearwater, Florida, Abstract p. 43.
- 55 Kilbourn, M. R. *Nucl. Med. (Nuclear Science Series)*; National Academy Press, Washington, D. C., 1990, p. 1.
- 56 Brennan, M. B. *Chemical and Engineering News* **1996**, *2*, 26.
- 57 Grierson, J. R.; Link, J. M.; Mathis, C. A.; Rasey, J. S.; Krohn, K. A. *J. Nucl. Med.* **1989**, *30*, 343.
- 58 Rasey, J. S.; Nelson, N. J.; Chin, L.; Evans, M. L.; Grunbaum, Z. *Radiat. Res.* **1990**, *122*, 301.
- 59 Tewson, T. J. *Nucl. Med. Biol.* **1997**, *24*, 755.
- 60 Kachur, A. V.; Evans, S. M.; Shiue, C.-Y.; Dolbier, Jr., W. R.; Li, A.-R.; Roche, A.; Skov, K. A.; Baird, I. R.; James, B. R.; Koch, C. J. *Appl. Rad. Isot.* (submitted Oct., 1998).
- 61 Keppler, B. K. *In Metal Complexes In Cancer Chemotherapy*; B. K. Keppler, Ed.; VCH, Weinheim, 1993, p.3.
- 62 Source of information, ref. 61.
- 63 Rosenberg, B.; Van Camp, L.; Krigas, T. *Nature* **1965**, *205*, 698.
- 64 Rosenberg, B.; Van Camp, L.; Grimely, E. B.; Thomson, A. J. *J. Biol. Chem.* **1967**, *242*, 1347.
- 65 Rosenberg, B.; Van Camp, L.; Trosko, J. E.; Mansour, V. H. *Nature* **1969**, *222*, 385.
- 66 Gore, M.; Fryatt, I.; Wiltshaw, E.; Dawson, T.; Robinson, B. A.; Calvert, A. H. *Br. J. Cancer* **1989**, *60*, 767.

-
- 67 Eisenhauer, E.; Swerton, K.; Sturgeon, J. et al. *In Carboplatin: Current Perspectives and Future Directions*; P. Burn, R. Caretta, R. Ozols, M. Rozencweig, Eds.; W. B. Saunders Company, Philadelphia, 1990, p. 133.
- 68 Harrap, K. R.; Murrer, B. A.; Giandomenico, C. *In Platinum and Other Metal Coordination Compounds in Cancer Chemotherapy*; S. B. Howell, Ed.; Plenum Press, New York, 1991, p. 391.
- 69 Kelland, L. R.; Mistry, P.; Abel, G.; Freidlos, F.; Loh, S. Y.; Roberts, J. J.; Harrap, K. R. *Cancer Res.* **1992**, *52*, 1710.
- 70 Kelland, L. R.; Jones, M.; Abel, G.; Harrap, K. R. *Cancer Chemother. Pharmacol.* **1992**, *30*, 43.
- 71 McKeage, K. J.; Morgan, S. E.; Boxall, F. E.; Murrer, B. A.; Hard, G. C.; Harrap, K. R. *Proc. Am. Assoc. Cancer Res.* **1992**, *33*, A3197.
- 72 Holford, J.; Sharp, S. Y.; Murrer, B. A.; Abrams, M.; Kelland, L. R. *Br. J. Cancer* **1998**, *77*, 366.
- 73 Simon, T. M.; Kunishima, D. H.; Vilbert, G. J.; Lorber, A. *Cancer* **1979**, *44*, 1965.
- 74 Howard, R. A.; Sherwood, E.; Erck, A.; Kimball, A. P.; Bear, J. L. *J. Med. Chem.* **1977**, *20*, 943.
- 75 Köpf-Maier, P.; Köpf, H. *Arzneim.-Forsch./Drug Res.* **1987**, *70*, 103.
- 76 Adamson, R. H.; Canellos, G. P.; Sieber, S. M. *Cancer Chemother. Rep.* **1975**, *59*, 599.
- 77 Hall, S. W.; Yeung, K.; Benjamin, R. S. *Clin. Pharmacol. Ther.* **1979**, *25*, 82.
- 78 Buckley, R. G. *In Metal Compounds in Cancer Therapy*; S. P. Fricker, Ed.; Chapman and Hall, London, 1994, p. 92.
- 79 Sava, G. *In Metal Compounds in Cancer Therapy*; S. P. Fricker, Ed.; Chapman and Hall, London, 1994, p. 65.
- 80 Clarke, M. J. *In Progress in Clinical Biochemistry and Medicine*; Springer-Verlag, Berlin, 1989, Vol. 10, p. 26.

-
- 81 Keppler, B. K.; Hern, M.; Juhl, U. M.; Berger, M. R.; Niebl, R.; Wagner, F. E. *In* Progress in Clinical Biochemistry and Medicine; Springer-Verlag, Berlin, 1989, Vol. 10, p. 41.
- 82 Mestroni, G.; Alessio, E.; Calligaris, M.; Attia, W. M.; Quadrifoglio, F.; Cauci, S.; Sava, G.; Zorzet, S.; Pacor, S.; Monti-Bragadin, C.; Tamaro, M.; Dolzani, L. *In* Progress in Clinical Biochemistry and Medicine; Springer-Verlag, Berlin, 1989, Vol. 10, p. 71.
- 83 Clarke, M. J. *In* Metal Complexes in Cancer Chemotherapy; B. K. Keppler, Ed.; VCH, Weinheim, 1993, p. 129.
- 84 Mestroni, G.; Alessio, E.; Sava, G.; Pacor, S.; Coluccia, M. *In* Metal Complexes in Cancer Chemotherapy; B. K. Keppler, Ed.; VCH, Weinheim, 1993, p. 157.
- 85 Keppler, B. K.; Lipponer, K.-G.; Stenzel, B.; Kratz, F. *In* Metal Complexes in Cancer Chemotherapy; B. K. Keppler, Ed.; VCH, Weinheim, 1993, p. 188.
- 86 Wishart, J. F.; Bino, A.; Taube, H. *Inorg. Chem.* **1986**, 25, 3318.
- 87 See Chapter 5, Table 5.1.
- 88 Chou, M.; Creutz, C.; Sutin, N. J. *J. Am. Chem. Soc.* **1977**, 99, 5615.
- 89 Kelly, J. M.; Feeney, M. M.; Tosi, A. B.; Lecomte, J. P.; Kirsch-De Mesmaeker, A. *Anticancer Drug Des.* **1990**, 5, 69.
- 90 Loseto, F.; Mestroni, G.; Lacidogna, G.; Nassi, A.; Giordano, D.; Coluccia, M. *Anticancer Res.* **1991**, 11, 1549.
- 91 Palmer, B. D.; Wilson, W. R.; Pullen, S. M. *J. Med. Chem.* **1990**, 33, 112.
- 92 Luk, C. K.; Veinot-Drebot, L.; Tjan, E. *J. Natl. Canc. Inst.* **1990**, 82, 684.
- 93 Vaupel, P.; Kallinowski, F.; Okunleff, P. *Cancer Res.* **1989**, 49, 6449.
- 94 Sasai, K.; Ono, K.; Hiraoko, M. *Int. J. Radiat. Oncol. Biol. Phys.* **1989**, 16, 1477.
- 95 Herman, T. S.; Teicher, B. A.; Holden, S. A. *Cancer Res.* **1989**, 49, 3338.
- 96 Som, P.; Oster, Z. H.; Matsui, K.; Gugliemi, G.; Persson, B. R.; Pellettieri, M. L.; Srivastava, S. C.; Richards, P.; Atkins, H. L.; Brill, A. B. *Eur. J. Med.* **1983**, 8, 491.

-
- 97 Srivastava, S. C.; Mausner, L. F.; Clarke, M. J. *In Ruthenium and other Non-Platinum Metal Complexes in Cancer Chemotherapy*; M. J. Clarke, Ed.; Springer-Verlag, Heidelberg, 1989, Vol.10, p. 11.
- 98 Snetsinger, P. A.; Chasteen, N. D.; van Willigen, H. J. *J. Am. Chem. Soc.* **1990**, *112*, 8155.
- 99 Pell, S. J.; Salmousen, R.; Abelliera, A.; Clarke, M. J. *Inorg. Chem.* **1984**, *23*, 385.
- 100 Bomford, A.; Young, S. P.; Williams, R. *Biochem.* **1985**, *24*, 3472.
- 101 Takahara, P. M.; Frederick, C. A.; Lippard, S. J. *J. Am. Chem. Soc.* **1996**, *118*, 12309.
- 102 Fichtinger-Schepman, A. M. J.; van der Veer, J. L.; den Hartog, J. H. J.; Lohman, P. H. M.; Reedijk, J. *Biochem.* **1985**, *24*, 707.
- 103 Beck, D. J.; Popoff, S.; Sancar, A.; Rupp, W. D. *Nucleic Acid Res.* **1985**, *13*, 7395.
- 104 Page, J. D.; Husain, I.; Sancar, A.; Chaney, S. G. *Biochem.* **1990**, *29*, 1016.
- 105 Hughes, E. N.; Engelsberg, B. N.; Billings, P. C. *J. Biol. Chem.* **1992**, *267*, 13520.
- 106 Donahue, B. A.; Augot, M.; Bellon, S. F.; Treiber, D. K.; Toney, J. H.; Lippard, S. J.; Essigmann, J. M. *Biochem.* **1990**, *29*, 5872.
- 107 Clarke, M. J.; Buchbinder, M.; Kelman, A. D. *Inorg. Chim. Acta* **1978**, *27*, L87.
- 108 Sava, G. Unpublished results, from ref. 18.
- 109 Keppler, B. K.; Wehe, D.; Endres, H.; Rupp, W. *Inorg. Chem.* **1987**, *26*, 844.
- 110 Keppler, B. K.; Wehe, D.; Endres, H.; Rupp, W. *Inorg. Chem.* **1987**, *26*, 4366.
- 111 Keppler, B. K.; Rupp, W.; Juhl, U. M.; Endres, H.; Niebl, R.; Balzer, W. *Inorg. Chem.* **1987**, *26*, 4366.
- 112 Sava, G.; Pacor, S.; Mestroni, G.; Alessio, E. *Anti-Cancer Drugs* **1992**, *3*, 25.
- 113 Talmadge, J. E. *Cancer Metast. Rev.* **1983**, *2*, 25.
- 114 Sava, G.; Pacor, S.; Coluccia, M.; Mariggio, M.; Cocchietto, M.; Alessio, E.; Mestroni, G. *Drug Invest.* **1994**, *8*, 150.

Chapter 2

General Experimental

2.1 Materials

2.1.1 Chemicals

2.1.1.1 Imidazoles

Im, 2MeIm and 4MeIm (from Aldrich) and NMeIm (from Merck) were used as received. 2NO₂Im was synthesized according to literature procedures¹ or purchased from Aldrich. Other nitroimidazoles purchased from Aldrich included: 4(5)NO₂Im, 2Me5NO₂Im, 2-methyl-4-nitro-1-imidazolepropionitrile and 2-methyl-4-nitro-1-imidazolepropionic acid. **SR2508** was kindly donated by Dr. C. Koch (Univ. of Penn.), while metronidazole and **RSU1111** were donated from the laboratory of Dr. M. Naylor (MRC - Chilton).

2.1.1.2 Amines

The following amines were synthesized and kindly donated from Prof. W. Dolbier's group (Univ. of Florida): H₂NCH₂CF₂CF₃•HCl, H₂NCH₂CF₂CF₂Br•HCl, H₂NCH₂CH₂CF₃•HCl, H₂NCH₂CH₂CF₂Br•HCl, H₂NCH₂CH₂CH₂F•HF. All other amines used throughout this work were purchased from Aldrich and generally used without further purification. Et₃N was distilled prior to use.

2.1.1.3 Miscellaneous Reagents

RuCl₃•3H₂O was supplied on loan from both Johnson Matthey Ltd. and Colonial Metals, Inc. with a Ru composition of 39 to 41 %. N-methylmorpholine (NMM) and *iso*-butylchloroformate (iBuClFrm) were purchased from Aldrich and were vacuum distilled prior to use. All other commercial chemicals were used as purchased, unless otherwise indicated, from Aldrich Chemical Co., Fisher Scientific Co., Strem, Sigma Chemical Co., BDH Chemicals, Merck and Co., Inc. or Mallinckrodt Chemical Works. NBS and TsCl

were recrystallized before use. All gases (N_2 , H_2 and CO ; minimum purity 99.99 %) were purchased from Linde (Union Carbide, Inc.) and used as received.

2.1.2 Solvents

Reagent grade DMF (Fisher) and dmsO (Fisher) were distilled and dried over molecular sieves, and MeCN and EtOAc (anhydrous, Aldrich) were used as received. Other solvents were dried using the appropriate drying agent and distilled prior to use: MeOH (Mg), EtOH (Mg), THF (Na-K alloy), Et_2O (Na), hexanes (Na), pentane (CaH_2), acetone (K_2CO_3) and CH_2Cl_2 (CaH_2). Deuterated solvents (d_6 -acetone, d_6 -dmsO, CD_3OD , CDCl_3 , CD_3CN , D_2O) were supplied by MSD Isotopes or Isotech Inc. and used immediately upon opening of an ampule (except for D_2O) to ensure dryness. Please note that throughout this thesis dmsO is used to indicate solvent while DMSO is used to indicate a coordinated ligand.

2.2 Analytical Techniques

2.2.1 Nuclear Magnetic Resonance Spectroscopy

^1H (200 MHz), ^2H (46.1 MHz), $^{13}\text{C}\{^1\text{H}\}$ (50.3 MHz) and $^{19}\text{F}\{^1\text{H}\}$ (188.2 MHz) NMR spectra were recorded on a Bruker AC200F spectrometer. ^{19}F NMR (282.2 MHz) spectra requiring larger sweep widths (SW up to 100,000) were recorded on a Varian XL300 spectrometer, while large sweep width ^1H NMR spectra were recorded on either the Varian XL300 (300.0 MHz) or the Bruker WH400 (400.0 MHz) spectrometers. $^{31}\text{P}\{^1\text{H}\}$ (121.5 MHz) and $^{13}\text{C}\{^1\text{H}\}$ (75.4 MHz) NMR spectra were recorded on a Varian XL300 spectrometer. The ^1H NMR chemical shifts were referenced to the residual proton signal of the internal deuterated solvent (δ 7.24 for CDCl_3 , 4.78 for D_2O , 3.30 for CD_3OD , 2.50 for $(\text{CD}_3)_2\text{SO}$, 2.20 for $(\text{CD}_3)_2\text{CO}$; all are reported relative to the external standard of tetramethylsilane (δ 0.00)) while the $^{13}\text{C}\{^1\text{H}\}$ NMR chemical shifts were also referenced to the shift from the solvent (δ 29.8 for Me of acetone). The $^{19}\text{F}\{^1\text{H}\}$ NMR chemical shifts were referenced to trifluoroacetic acid in D_2O (external reference) and the $^{31}\text{P}\{^1\text{H}\}$ NMR chemical shifts were reported relative to 85 % H_3PO_4 (external reference) with the downfield shifts observed as positive. All spectra were recorded at r.t.

The peak multiplicities are reported as observed in a given spectrum (s = singlet; d = doublet; t = triplet; q = quartet; p = pentet; sex = sextet; spt = septet; br = broad, vbr = very broad, including a combination of these symbols, for example, qt = quartet of triplets). For those signals where peak coincidences have altered the peak multiplicity for a specific set of protons, the expected multiplicity is reported in brackets (e.g. for -NH-CH₂-CH₂- one would expect to observe a doublet of triplets; however, a quartet is observed and so is recorded as q (dt)). The J values are reported for those nitroimidazole compounds containing F atom(s) on their side-chain and those Ru complexes containing more than two P-bound ligands.

The computer program MestRe-C (Magnetic Resonance Companion, Version 1.5.0) was used to expand various spectra obtained on the AC200F NMR spectrometer. This program was especially useful for observing the F-F coupling in the ¹⁹F{¹H} NMR spectra which could not be observed with the resolution of the standard HP plotter.

Determination of the μ_{eff} and number of unpaired electrons for selected paramagnetic Ru(III) complexes (in chapter 4) was performed at room temperature (r.t.) using the Evans method.² Two resonance lines were obtained from the residual solvent protons in two solutions owing to the difference in their volume susceptibilities, with the line from the more paramagnetic solution lying at higher frequencies. Typically the solution of the complex (of known concentration) is outside and the solvent only is placed within the capillary tube; however, because of problems with overlap of peaks of the complex with those of the residual solvent this was reversed (Figure 2-1). The $\Delta\delta$ values were determined using both the 200 and 300 MHz NMR machines and the μ_{eff} calculated for each case. The μ_{eff} values agreed within ± 0.1 . Of note, the Evans method measurements were made for a compound dissolved in the same deuterated solvent as reported for the ¹H NMR unless otherwise stated.

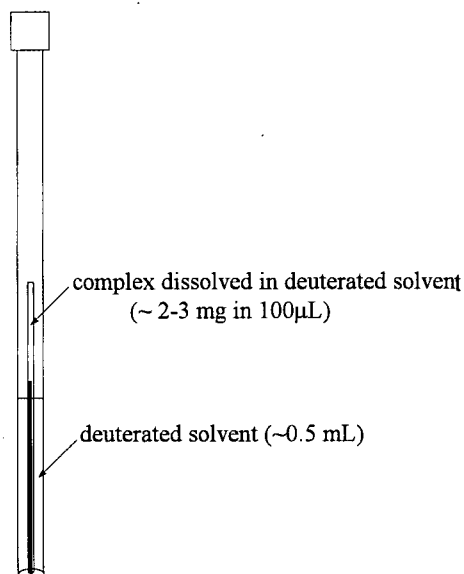


Figure 2-1: Diagrammatic representation of a capillary (containing a solution of the complex) within a NMR tube (containing solvent only) used for the Evans method.

The following equations used to calculate μ_{eff} were obtained from various literature sources.²⁻⁴ The equations are listed in the order in which they were used.

$$\chi_g = \frac{3\Delta f}{4\pi f m} + \chi_o$$

m = concentration of sample (g/mL)

Δf = frequency separation between two lines (Hz)

f = frequency at which proton resonances are studied (Hz)

χ_o = mass susceptibility of solvent (cm^3/g)

$$\chi_M = \chi_g M$$

M = compound molecular weight (g/mol)

$$\chi_M' = \chi_M - \sum \chi_L - \chi_m$$

χ_M' = molar susceptibility of metal ion (cm^3/mol)

χ_L = diamagnetic correction for ligand (cm^3/mol)

χ_m = diamagnetic correction for metal (cm^3/mol)

$$\mu_{\text{eff}} = 2.83 \sqrt{\chi_M' T} = \sqrt{n(n+2)} \quad T = \text{absolute temperature (K)}$$

n = number of unpaired electrons on metal ion

The diamagnetic correction values for the ligands (χ_L) were calculated from a table of Pascal's constants⁵ ($\chi_L = 34, 34, 46, 74, 91$ and 115 ($\times 10^{-6} \text{ cm}^3/\text{mol}$) for $2\text{NO}_2\text{Im}$, $4\text{NO}_2\text{Im}$, $2\text{Me}_5\text{NO}_2\text{Im}$, metronidazole, **SR2508** and **EF5**, respectively).

2.2.2 Infrared Spectroscopy

IR spectra were recorded on an ATI Mattson Genesis FTIR spectrophotometer using either KBr (by compression to 17,000 psi of a mixture of finely ground KBr and the compound, $\sim 100:3$ ratio) or a thin film on a KBr disc (from slow evaporation of a solution of a compound on the surface of a 0.5 mm KBr disc). Only the major bands in the spectra (transmittance $<70\%$) are reported. Only select bands are assigned (stretching frequencies unless otherwise indicated) according to references from standard IR texts.⁶⁻⁸ Values are given in cm^{-1} ($\pm 4 \text{ cm}^{-1}$).

2.2.3 UV-Visible Spectroscopy

UV-Vis absorption spectra were recorded on an HP 8452A diode array spectrophotometer and are given as λ_{max} ($\pm 2 \text{ nm}$), [$\epsilon_{\text{max}} \times 10^{-3} (\text{M}^{-1}\text{cm}^{-1})$], sh=shoulder.

2.2.4 Mass Spectrometry

The mass spectra for selected compounds were obtained from the Mass Spectrometry (MS) lab at UBC (under the supervision of Dr. G. Eigendorf). The following spectrometers were used: KRATOS MS80 (DCI), KRATOS Concept IIIHQ (LSIMS) and KRATOS MS50 (EI). For the most part, the most valuable MS technique used for determination of the composition of the nitroimidazoles was DCI+ MS. For those nitroimidazoles which did not yield acceptable elemental analyses, a high resolution determination of the exact elemental composition of the parent peak was performed. The Ru complexes were all run using +LSIMS, but unfortunately only a small number of the Ru-nitroimidazole complexes displayed acceptable MS spectra using this technique. For the nitroimidazole complexes other MS techniques were used in addition to LSIMS; these

included MALDI, Electrospray and EI mass spectrometries; however, none of these techniques yielded acceptable/useful MS data.

2.2.5 Gas Chromatography

GC Analysis was done on an HP 5890A instrument using a 30 kPa He flow at 75 °C with an HP-17 50% phenyl, 50% methyl, polysiloxane intermediate polarity column, using a flame ionization detector and an HP 3392A Integrator.

2.2.6 Cyclic Voltammetry

Electrochemistry was performed on 10^{-3} M solutions of selected compounds with 0.1 M TBAP in dry, degassed MeCN under Ar or N₂ in the cells illustrated in Figures 2.2 and 2.3; the potential was scanned down at 100 mV/s. The potentiometer was a Pine Biopotentiostat Model AFCBP1 attached to a 80MHz computer using Pine Chem (Version 2.00) cyclic voltammetry software. The working and counter electrodes for cell A (Figure 2-2) were Pt plates (6 mm²) and the reference electrode was a Pt wire, while the working and counter electrodes for cell B (Figure 2-3) were Pt wire, and the reference electrode was Ag wire. For each sample, an initial run was performed to determine the potential range required to observe all of the expected reductions; a fresh solution of the compound and electrolyte was then prepared and the scan performed again. If necessary, further solutions were prepared and analyzed until the values were in good agreement ($\Delta E_{1/2} < \pm 5$ mV). The reduction potentials ($E_{1/2}$) were obtained from the average of the potentials of the reduction and oxidation peaks $[(E_{p.c.} + E_{p.a.})/2]$ and the reported $E_{1/2}$ value (± 3 mV) is the average of the combined runs. Because of the irreproducibility of the reduction potential of the ferrocene/ferrocenium couple for both of the cells, ferrocene was added as an internal standard to the solution of each compound measured. The ferrocene/ferrocenium couple in MeCN vs. the SCE is reported as 424 mV;⁹ hence the conversion factor used to report the selected compound's $E_{1/2}$ vs. the SCE was $424 - E_{1/2}(\text{FeCp}_2)$.

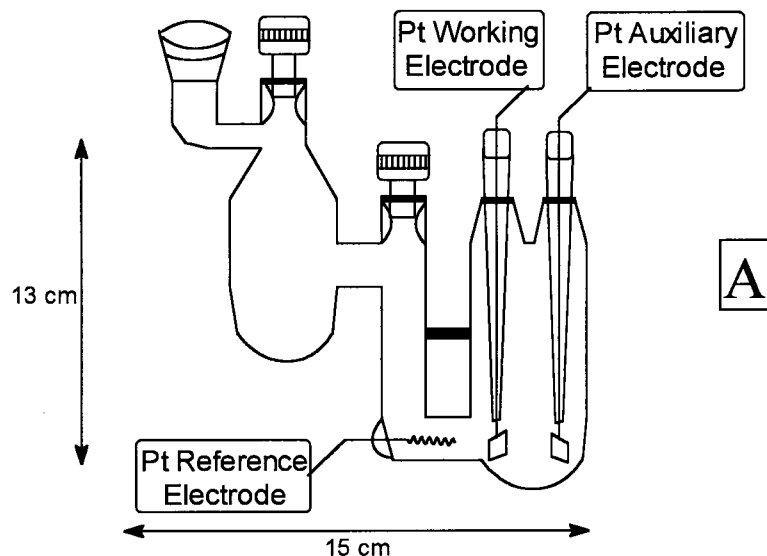


Figure 2-2: Cyclic voltammetry cell (A) containing a Pt reference electrode.

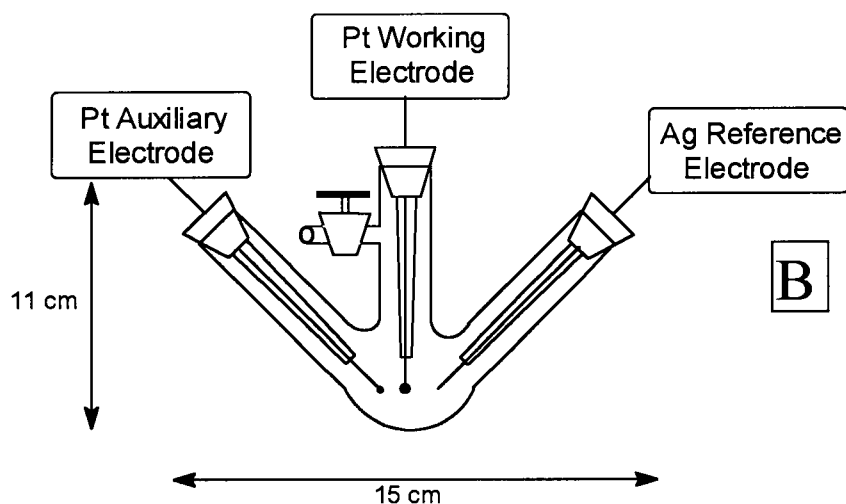


Figure 2-3: Cyclic voltammetry cell (B) containing an Ag reference electrode.

2.2.7 Conductivity

Conductivity measurements were made on a 10^{-3} M solution of the selected complex at room temperature (r.t.) using a Serfass conductance bridge model RCM15B1 (Arthur H. Thomas Co. Ltd.) connected to a Yellow Springs Instrument Co. 3404 cell (cell constant = 1.016), and are reported as $\Lambda_M (\pm 0.5 \text{ ohm}^{-1} \text{ mol}^{-1} \text{ cm}^2)$.

2.2.8 X-Ray Analysis

All single crystal X-ray diffraction studies were performed by the late Dr. S. J. Rettig of the UBC chemistry department on a Rigaku/ADSC CCD area detector or a Rigaku AFC6S diffractometer, both of which use graphite monochromated Cu-K α radiation.

2.2.9 Elemental Analysis

Elemental analyses were performed in the UBC chemistry department by Mr. P. Borda using either a Carlo Erba (Model 1106) or a Fisons Instruments (Model EA 1108) CHN-O elemental analyzer. The results reported have an absolute accuracy of $\pm 0.3\%$.

2.3 Compound Purification Techniques

In general, the visualization of nitroimidazoles on TLC plates was achieved with the aid of a UV lamp (Mineralight® Lamp Model UVG-54 short wave UV-254 nm), but imidazoles and other non-UV absorbing compounds were visualized by exposing the developed TLCs to I₂ or Br₂. For each chromatographic technique used, the solvent combination, including the ratio, follows in brackets (*e.g.* solvent A : solvent B, 10:1) and in specific cases where the eluent strength was altered an arrow is included (*e.g.* 10:1 \rightarrow 5:1).

2.3.1 Column Chromatography

Column chromatography was performed using Merck silica gel (230-400 mesh). The eluent was added to the silica gel in a large Erlenmeyer flask; the contents were stirred with a glass rod for 1 min and then poured into the column on a 45° angle to ensure that no air-bubbles were introduced. (If air-bubbles were present the column was tapped gently to agitate them to the surface of the silica gel.) The silica gel was packed using a pressurized air-flow adapter and then eluted to the edge of the silica gel. The compound was introduced onto the silica gel two ways: 1) by dissolving the compound in a minimum volume of the eluent and then loading onto the silica gel, making sure not to

disturb the top of the gel layer; 2) by adding silica gel to a solution of the mixture to be purified, followed by removal of the solvent under vacuum and then addition of the silica gel (with the compound) to the top of the column. For this technique the solvent must be slightly above the gel layer. The solvent (containing a mixture of compounds) was eluted to the gel front, sea sand (~2 cm) was then added, and the column eluted dropwise, unless otherwise stated. The R_f values of the pure compounds were measured on Merck silica gel 60F₂₅₄ TLC Al sheets.

2.3.2 Preparative Thin Layer Chromatography

Preparative TLCs of the Ru complexes were performed with Merck silica gel 60, 0.5 mm plates (without indicator) and for nitroimidazoles and other organic compounds, preparative TLCs were performed with silica gel 60 F₂₅₄, 1.0 mm plates. All plates used for preparative TLC had dimensions of 20cm x 20cm.

2.3.3 Chromatotron

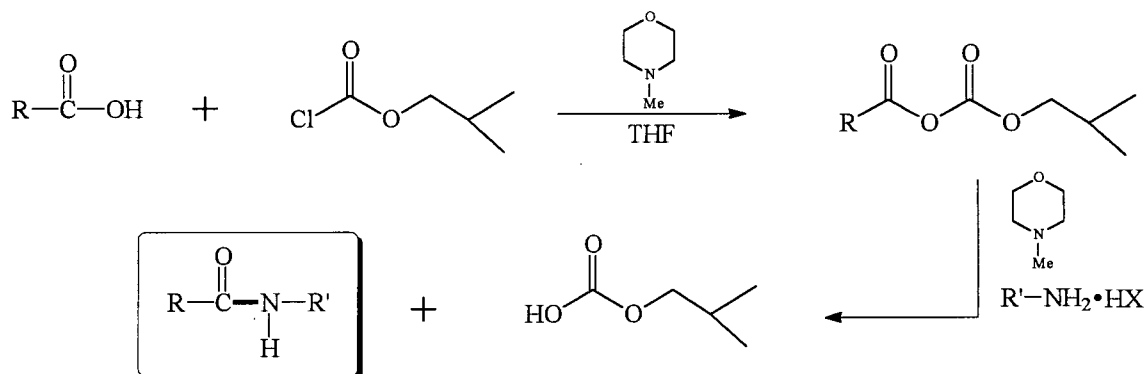
Some products were purified on a Harrison Research model 7924T Chromatotron (a rotating disc TLC) using silica as the stationary phase and an eluent flow rate of ~3 mL/min. The thickness of the plate used (1.0 mm or 2.0 mm) was dependent on the amount of compound used for purification (up to 250 mg or 750 mg, respectively). This technique was extremely useful for compounds which had similar R_f values as the band separation could be observed during the elution using a UV lamp, and hence the amount of compound overlap in the collected fractions could be reduced to a minimum.

2.4 General Methodologies

2.4.1 Amide Coupling Reaction

The synthesis of most of the nitroimidazole compounds was performed using a standard amide coupling technique (Scheme 2-1)^{10,11} in which a carboxylic acid and an amine are coupled to form an amide linkage. The N-methylmorpholine (NMM) deprotonates the acid group, making it a better nucleophile, which attacks the acyl carbonyl group of *iso*-butylchloroformate (iBuClFrm); this displaces the chlorine as Cl⁻

and gives formation of the mixed anhydride species. Addition of $R'-NH_2 \cdot HX$ and another equivalent of NMM (to mop up HX) leads to attack at the activated carbonyl nearest the nitroimidazole ring by the amine N-atom to yield an amide bond. In the presence of any H_2O , the *iso*-butylcarbonate hydrolyzes to form CO_2 and *iso*-butanol, which can then react with the activated anhydride; hence extremely anhydrous conditions are pertinent to the success of this reaction.



Scheme 2-1: Standard amide bond forming reaction.

2.5 Ruthenium Precursors

2.5.1 $RuCl_3 \cdot 3H_2O$

This starting material, for which the oxidation state of the metal (possibly a mixture of Ru^{III} and Ru^{IV} oxidation states) and degree of hydration of the compound are ill-defined,^{12,13} was kindly donated from both Johnson Matthey Ltd. and Colonial Metals, Inc. The formulation of the chloride for the purpose of estimating a known number of millimoles was taken as $RuCl_3 \cdot 3H_2O$.

2.5.2 $[Ru(DMF)_6][CF_3SO_3]_3$ ¹⁴

In a 2-neck flask, $RuCl_3 \cdot 3H_2O$ (2.00 g, 8.13 mmol) was dissolved in DMF (120 mL) and then Sn metal (7.00 g, 58.9 mmol) was added. The mixture was stirred at r.t. for 1 h, the colour changing from orange-brown to green to blue. To the blue solution, $Pb(CF_3SO_3)_2$ (6.51 g, 12.9 mmol; synthesized from $Pb(CO_3)$ and reagent grade CF_3SO_3H ,

1:2) were added and the mixture was heated to 50 °C for 2 h (the colour changed to red-brown). The mixture was gravity filtered and then the volume was reduced to ~25 mL before the addition of CH₂Cl₂ (300 mL). The mixture instantly formed a dark brown slurry which was stirred for 12 h at r.t. The brown solid was filtered off and the filtrate's volume was reduced to ~30 mL. The addition of 1,2-dichloroethane (100 mL) to the solution at 0 °C led to the formation of a yellow precipitate. After 1 h at 0 °C the yellow solid was collected via suction filtration and washed with 1,2-dichloroethane (3 x 10 mL). This crude solid was recrystallized from CH₂Cl₂:pentane to yield a yellow microcrystalline solid (4.85 g, 56%). Anal. calc for C₂₁H₄₂N₆O₁₅S₃F₉Ru: C, 25.56; H, 4.29; N, 8.52; found: C, 25.43; H, 4.30; 8.54. UV-Vis (DMF): 254 (1.72), 273 (6.95), 342 (5.80). IR (KBr): 1642 (C=O_{coord.} DMF) (*cf.* 1673 for C=O_{free} DMF). ¹H NMR (300 MHz, d₆-dmsO): δ 22.50 (br s, -Me₁), 19.80 (br s, -Me₂); the lower-field Me resonance has been assigned to the Me group *cis* to the carbonyl oxygen atom. These data agree well with those reported in the literature.¹⁵

2.5.3 [Ru(DMF)₆][CF₃SO₃]₂¹⁴

In a Schlenk tube, [Ru(DMF)₆][CF₃SO₃]₃ (0.237 g, 0.240 mmol) was dissolved in 5 mL DMF (purged with N₂ for 10 min) to give a yellow solution. A trace amount (<1 mg) of Pt black (Adam's catalyst) was added and the mixture was stirred at 50 °C for 1.5 h under H₂ bubbling. The Pt black was filtered off and the red-orange filtrate's volume was reduced to ~1 mL prior to the addition of n-pentanol (5 mL). Vigorous stirring for 20 min at 0 °C yielded an orange solid that was washed with Et₂O (3 x 5 mL) and dried *in vacuo* (0.207 g, 87 %). UV-Vis (DMF): 494 (0.182). IR (KBr): 1635 (C=O_{coord.} DMF). ¹H NMR (200 MHz, d₆-dmsO): δ 7.50 (s, -CHO), 3.10 (s, 3H, -Me₁), 2.89 (s, 3H, -Me₂). These data agree well with those reported in the literature.¹⁵

2.5.4 *cis*-RuCl₂(DMSO)(DMSO)₃¹⁶

In a 50 mL flask RuCl₃•3H₂O (1.00 g, 4.06 mmol) was dissolved in 10 mL dmsO, and the mixture was refluxed for 30 min in air. The reaction mixture was cooled to r.t. and addition of acetone (20 mL) led to the accumulation of a yellow precipitate. The yellow

solid was collected, washed with acetone (3 x 10 mL) and dried *in vacuo* at 78 °C for 24 h (1.32 g, 84 %). Anal. calc for $C_8H_{24}Cl_2O_4S_4Ru$: C, 19.38; H, 4.99; found: C, 19.23; H, 4.81. UV-Vis ($CHCl_3$): 305 (0.74), 355 (1.05). IR (KBr): 1116 ($S=O$), 963 ($S=O$). 1H NMR (200 MHz, $CDCl_3$): δ 3.55, 3.51, 3.45, 3.44 (S-bonded DMSO); 2.76 (O-bonded DMSO); 2.59 (free DMSO). The spectroscopic data agree well with those previously reported.^{16,17}

2.5.5 *trans*- $RuCl_2(DMSO)_4$ ¹⁸

In a 25 mL flask, $RuCl_3 \cdot 3H_2O$ (0.500 g, 2.03 mmol) was dissolved in 3 mL dmso, and the mixture was heated to 70 °C and stirred for 15 min in air. The resulting red solution was cooled to room temperature and acetone (15 mL) was added slowly with continuous stirring. A red solid precipitated which was collected, washed with acetone (3 x 10 mL) and dried *in vacuo* at 78 °C for 24 h (0.525 g, 67 %). Anal. calc for $C_8H_{24}Cl_2O_4S_4Ru$: C, 19.38; H, 4.99; found: C, 19.53; H, 5.16. UV-Vis ($CHCl_3$): 440 (0.22). IR (KBr): 1086 ($S=O$). 1H NMR (200 MHz, $CDCl_3$): δ 3.41 (s, S-bonded CH_3), 2.59 (free DMSO). The spectroscopic data agree well with those previously reported.^{17,18}

2.5.6 *cis* $_2(TMSO)_4$ ¹⁹

In a 100 mL RBF, $RuCl_3 \cdot 3H_2O$ (2.00 g, 8.13 mmol) was refluxed in MeOH (40 mL) under H_2 for 4 h when the colour of the solution turned from brown-orange through a green intermediate to finally become dark blue. TMSO (8 mL, 89.1 mmol) was added and refluxing under H_2 was continued for an additional 4 h, generating a yellow-green precipitate. The solid was collected, washed with Et_2O (3 x 10 mL) and dried *in vacuo* at 78 °C for 24 h (4.02 g, 84 %). Anal. calc for $C_{16}H_{32}Cl_2O_4S_4Ru$: C, 32.60; H, 5.44; found: C, 32.29; H, 5.19. UV-Vis ($CHCl_3$): 355 (1.07), 300 (0.58). IR (KBr): 1121, 1086 ($S=O$). 1H NMR (200 MHz, $CDCl_3$): δ 4.15, 3.47 (m, 2H each, $-CH_2-S(O)-CH_2-$), 2.26 (m, 4H, $-CH_2-CH_2-$). The spectroscopic data agree well with those previously reported.¹⁹

2.5.7 *mer*- $RuCl_3(DMSO)_3$ ²⁰

In a large RBF, $[(DMSO)_2H][Ru(DMSO)_2Cl_4]$ (1.12 g, 2.13 mmol; kindly donated by E. Cheu of this group) was suspended in acetone (80 mL), and then dmso (0.5

mL, 7 mmol) was added. The mixture was refluxed with vigorous stirring. To the refluxing mixture, a AgBF_4 solution (0.400 g, 2.05 mmol, dissolved in 20 mL acetone) was added dropwise to give a bright orange solution which becomes turbid over time (due to formation of AgCl). The AgCl was filtered off (whilst the mixture was hot) and then the volume of the filtrate was reduced to ~ 10 mL before the addition of 5 mL Et_2O . Storage at 4°C for 12 h yielded a fine, microcrystalline red solid that was collected, washed with Et_2O and dried *in vacuo* at 78°C for 24 h (0.297 g, 34 %). UV-Vis (CH_2Cl_2): 446 (1.28), 382 (3.54), 268 (sh) (6.43). IR (KBr): 1123, 1105 ($\text{S}=\text{O}$); 910 ($\text{S}=\text{O}$). ^1H NMR (300 MHz, CDCl_3): δ 9.45 (br s, DMSO), 2.62 (free DMSO), -15.35 (br s, DMSO). The spectroscopic data agree well with those previously reported.²⁰

2.5.8 $[\text{RuCl}_2(\text{COD})]_x$ ²¹

In a Schlenk tube $\text{RuCl}_3 \cdot 3\text{H}_2\text{O}$ (2.0 g, 8.13 mmol) was dissolved in EtOH (80 mL), and 1,5-cyclooctadiene (7.5 mL, 61.0 mmol) was added under N_2 to the resulting solution. The orange mixture was heated at reflux for 3 d, at which point the solution was pale yellow after a brown product had precipitated. The brown solid was collected, washed with EtOH (3 x 10 mL) and dried *in vacuo* (2.01 g, 86 %). Anal. calc for $[\text{C}_8\text{H}_{12}\text{Cl}_2\text{Ru}]_x$: C, 34.30; H, 4.32; found: C, 34.49; H, 4.58.

2.5.9 $[\text{RuCl}_2(\text{dppb})]_2(\mu\text{-dppb})$ ^{22,23}

This complex was kindly donated by Dr. K. S. MacFarlane, formerly of this group. The physical and spectroscopic data of this precursor agree with those previously reported.^{22,23}

2.6 References

- 1 Davis, D. P.; Kirk, K. L.; Cohen, L. A. *J. Heterocyclic Chem.* **1982**, *19*, 253.
- 2 Evans, D. F. *J. Chem. Soc.* **1959**, 2003.
- 3 Live, D. H.; Chan, S. I. *Anal. Chem.* **1970**, *42*, 791.
- 4 Crawford, T. H.; Swanson, J. J. *Chem. Educ.* **1971**, *48*, 382.
- 5 Figgis, B. N.; Lewis, J. *In Modern Coordination Chemistry*; J. Lewis and R. G. Wilkins, Eds.; Interscience Publishers, Inc., London, 1960, p. 402.
- 6 Silverstein, R. M.; Bassler, G. C.; Morrill, T. C. *Spectrometric Identification of Organic Compounds*; John Wiley and Sons, Inc., Toronto, 1991.
- 7 Nakamoto, K.; McCarthy, P. J. *Spectroscopy and Structure of Metal Chelate Compounds*; John Wiley and Sons, Inc., New York, 1968.
- 8 Nakamoto, K. *Infrared Spectra of Inorganic and Coordination Compounds*, 2nd Ed.; Wiley-Interscience, Toronto, 1970.
- 9 Connelly, N. G.; Geiger, W. E. *Chem. Rev.* **1996**, *96*, 877.
- 10 Bock, M. G.; DiPardo, R. M.; Evans, B. E.; Rittle, K. E.; Veber, D. F.; Freidinger, R. M. *Tetrahedron Lett.* **1987**, *28*, 939.
- 11 Holzapfel, C. W.; Pettit, G. R. *J. Org. Chem.* **1985**, *50*, 2323.
- 12 Seddon, E. A.; Seddon, K. R. *The Chemistry of Ruthenium*; Elsevier, Amsterdam, **1984**.
- 13 Hui, B. C.; James, B. R. *Can. J. Chem.* **1974**, *52*, 348.
- 14 Cao, R. M.Sc. Thesis, University of Bern, 1992.
- 15 Judd, R. J.; Cao, R.; Biner, M.; Armbruster, T.; Bürgi, H.-B.; Merbach, A. E.; Ludi, A. *Inorg. Chem.* **1995**, *34*, 5080.
- 16 Evans, I. P.; Spencer, A.; Wilkinson, G. *J. Chem. Soc., Dalton Trans.* **1973**, 204.
- 17 Alessio, E.; Milani, B.; Mestroni, G.; Calligaris, M.; Faleschini, P.; Attia, W. M. *Inorg. Chim. Acta* **1990**, *177*, 255.
- 18 Jaswal, J.; Rettig, S. J.; James, B. R. *Can. J. Chem.* **1990**, *68*, 1808.
- 19 Yapp, D. T. T. Ph. D. Thesis, University of British Columbia, 1993.

- 20 Alessio, E.; Balducci, G.; Calligaris, M.; Costa, G.; Attia, W. M. *Inorg. Chem.* **1991**, *30*, 609.
- 21 Genêt, J. P.; Pinel, C.; Ratovelomanana-Vidal, V.; Mallart, S.; Pfister, X.; Caño De Andrade, M. C.; Laffitte, J. A. *Tetrahedron: Asymmetry* **1994**, *5*, 665.
- 22 Joshi, A. M. Ph. D. Thesis, University of British Columbia, 1990.
- 23 Bressan, M.; Rigo, P. *Inorg. Chem.* **1975**, *14*, 2286.

Chapter 3

Synthesis and Characterization of New 2-, 4- and 5-Nitroimidazoles with Halogenated Side-Chains

3.1 Introduction

The use of nitroimidazoles provides a sensitive technique for the detection of hypoxia in human cancers; as a result of hypoxia-dependent bio-reduction of nitroimidazoles by cellular nitroreductases, they can be used to determine the variation of oxygen concentration within a tumour based on the amount of reduction product that forms adducts with cellular macromolecules.¹ Recently, a monoclonal antibody (ELK3-51) was raised against the bio-reduction adduct of a fluorine-containing analogue of etanidazole, named **EF5** [2-(2-nitro-1-H-imidazol-1-yl)-N-(2,2,3,3,3-pentafluoropropyl)acetamide],^{2,3} and the amount of binding in tumour cells was determined based on the fluorescence of a fluorophore called Cy3⁴ that was chemically coupled to the antibody.⁵ This technique has been used to assess hypoxia *in vitro* and in various animal tumour models.^{6,7} The detection and quantification of hypoxia in tumours should provide better insight into which patients would most likely benefit from hypoxia-targeted therapies. The National Cancer Institute (US) has approved clinical trials on **EF5** through support of large scale synthesis, formulation and toxicology.

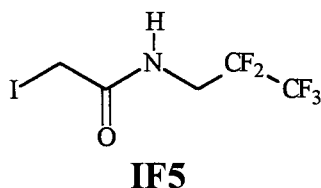
In this chapter we report the synthesis and characterization of various halogenated nitroimidazole compounds, including their one-electron reduction potentials. The major goal was to expand this area of chemistry in hopes of developing a nitroimidazole compound that was more biologically active than **EF5**. The preliminary studies for the development of a new PET imaging agent are also reported.

3.2 Experimental Section

3.2.1 Synthesis of Side-Chains

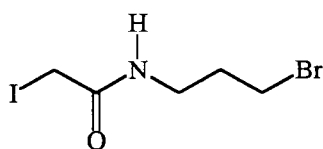
3.2.1.1 2-Iodo-*N*-(2,2,3,3,3-pentafluoropropyl)acetamide [**IF5**]

Iodoacetic acid (0.224 g, 1.20 mmol) was dissolved in THF (15 mL) at 0°C (ice-bath) under a constant N₂-flow. NMM (140 µL, 1.28 mmol) was added, and the mixture was stirred for 10 min after which *i*BuClFrm (195 µL, 1.50 mmol) was added. The mixture was further stirred for 30 min during which a slurry was formed. The ice-bath was removed, and H₂NCH₂CF₂CF₃•HCl (0.249 g, 1.45 mmol) and NMM (165 µL, 1.51 mmol) were added. Stirring was continued for 20 h at r.t. after which the resulting yellow-orange precipitate was filtered off and washed with dry THF. The dark orange washings were combined and eluted through a silica gel column (CH₂Cl₂:MeOH, 10:1); a purple band (I₂) appeared, followed by a yellow band that was analyzed using TLC and found to contain two products. The yellow band was eluted off and, after removal of the solvents, the residue was placed in a sublimation apparatus and heated to 110 °C under vacuum, when pure **IF5** sublimed as a pale yellow solid (0.202 g, 53%); mp 90-93 °C. Anal. calc. for C₅H₅NOF₅I: C, 18.94; H, 1.59; N, 4.42; found: C, 18.76; H, 1.67; N, 4.61. IR (ν, cm⁻¹): 3305 (N-H); 3088 (C-H_{im}); 2963, 2858 (C-H); 1658 (C=O); 1204, 1185, 1141, 1067, 1036. ¹H NMR (300 MHz, d₆-acetone): δ 8.06 (s, 1H, N-H), 4.05 (td, 2H, ³J_{HF} = 6.5 Hz, ³J_{HH} = 0.9 Hz, -CH₂-CF₂-), 3.81 (s, 2H, I-CH₂-). ¹⁹F{¹H} NMR (188 MHz, d₆-acetone): δ -8.18 (t, -CF₃), -45.34 (q, -CF₂-).

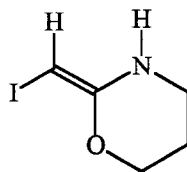


3.2.1.2 2-Iodo-*N*-(3-bromopropyl)acetamide [**IBr**]

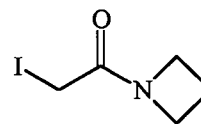
A similar procedure to that for the synthesis of **IF5** was used (see above). Iodoacetic acid (0.979 g, 5.27 mmol) and NMM (576 μ L, 5.27 mmol) were dissolved in THF (20 mL), and *i*BuClFrm (752 μ L, 5.78 mmol) was added. After 40 min, $\text{H}_2\text{NCH}_2\text{CH}_2\text{CH}_2\text{Br}\cdot\text{HBr}$ (1.26 g, 5.79 mmol) and NMM (639 μ L, 5.85 mmol) were then added, the mixture giving a yellow slurry. Stirring was continued for 4 h at r.t. during which the colour changed to a red/brown and a yellow precipitate was formed. This was filtered off and washed with THF (3 x 15 mL). The washings were combined and the solvent was removed by rotoevaporation yielding a dark red oil; subsequent TLC analysis revealed several products. Purification of the desired product was achieved via column chromatography (CH_2Cl_2 :MeOH, 20:1). The first band (yellow, low concentration) was followed by a minor red band after which the product band (bright orange) emerged; TLC analysis of the orange band revealed a single species. Subsequent removal of solvent afforded an orange oil (0.978 g, 61 %). LR-MS [DCI(+)]: 306 (M^+), 255 (I_2), 227 ($\text{M}^+ - \text{Br}$), 180 ($\text{M}^+ - \text{I}$), 169 ($\text{M}^+ - \text{NHCH}_2\text{CH}_2\text{CH}_2\text{Br}$), 128 (I). ^1H NMR (300 MHz, d_6 -acetone): δ 7.90 (s, 1H, N-H), 3.77 (s, 2H, I- CH_2 -), 3.52 (t, 2H, - CH_2 -Br), 3.36 (dt, 2H, -NH- CH_2 -), 2.07 (m, 2H, -NH- CH_2 - CH_2 -, partially overlapped with residual acetone peak). (These chemical shifts are comparable to those seen for compounds of similar composition, e.g. **IF5** and **EBr1** (Section 3.2.2.14)). Unlike with **IF5**, purification of **IBr** by sublimation (at 70°C) was unsuccessful due to thermal instability as evidenced by NMR spectroscopy (see Discussion, p. 98). Of note, mass spectrometric analysis of **IBr** after such a sublimation procedure revealed the presence of species attributable to compounds containing cyclic rings, such as **1** and **2** of the same molecular weight (see Scheme 3-4, section 3.3.1, p. 98). LR-MS [DCI(+)]: 226 (M^+), 128 (I), 99 ($\text{M}^+ - \text{I}$). ^1H NMR, including 2D-cosy (200 MHz, d_6 -acetone): (**1**) δ 4.81 (t, 2H, O- CH_2 -), 4.12 (s, 1H, I-CH=), 3.74 (t, 2H, -NH- CH_2 -), 2.51 (s, 1H, -NH-), 2.37 (p, 2H, - CH_2 - CH_2 - CH_2 -); (**2**) δ 4.82 (s, 2H, I- CH_2 -), 3.55 (t, 2H, -N- CH_2 -), 3.32 (t, 2H, -N- CH_2 -), 2.03 (m, 2H, - CH_2 - CH_2 -). Of note, partial formation of **1** and **2** was observed when neat **IBr** was exposed to UV radiation (TLC lamp) at r.t. for 2 d.



IBr



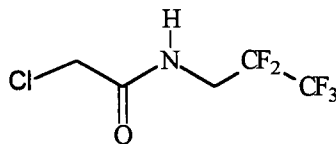
1



2

3.2.1.3 2-Chloro-*N*-(2,2,3,3,3-pentafluoropropyl)acetamide [CIF5]

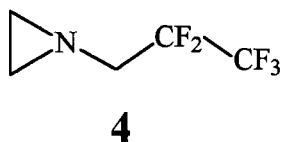
Chloroacetic acid (0.101 g, 1.08 mmol) was dissolved in THF (10 mL) under 1 atm N₂. NMM (120 μ L, 1.08 mmol) was then added, and the reaction mixture was stirred at 0 °C for 10 min. Afterwards, *i*BuClFrm (151 μ L, 1.16 mmol) was added and a white precipitate was formed instantaneously. Stirring was continued for 30 min after which the ice-bath was removed, and H₂NCH₂CF₂CF₃•HCl (0.189 g, 1.10 mmol) and NMM (128 μ L, 1.17 mmol) were added. The final mixture was stirred at r.t. for 8 h before the white solid was collected and washed with THF. The solvent was subsequently removed giving a pale yellow oil whose TLC analysis revealed two products, one visible under UV light and the other appearing after development using I₂/hexanes. The mixture was sublimed at 60 °C under vacuum, and a crystalline white solid was obtained (the remaining non-sublimed product was a dark yellow oil). TLC analysis revealed a single species, not visible under UV light (0.148 g, 61 %); mp 44-45 °C. LR-MS [DCI(+)]: 225 (M⁺), 190 (M⁺ - Cl), 176 (M⁺ - CH₂Cl). HR-MS [DCI(+)] calc. for C₅H₅NO³⁵ClF₅: 224.99799; found 224.99782. IR (ν , cm⁻¹): 3324 (N-H); 3106 (C-H_{im}); 2966, 2872 (C-H); 1653 (C=O); 1206, 1180, 1146, 1067, 1037. ¹H NMR (300 MHz, d₆-acetone): δ 8.12 (s, 1H, N-H), 4.24 (s, 2H, Cl-CH₂-), 4.17 (td, 2H, ³J_{HF} = 6.7 Hz, ³J_{HH} = 2.2 Hz, -CH₂-CF₂-). ¹⁹F{¹H} NMR (188 MHz, d₆-acetone): δ -8.21 (t, -CF₃), -45.26 (q, -CF₂-).



CIF5

3.2.1.4 Reduction of IF5 to ICH₂CH₂NHCH₂CF₂CF₃ (3)

IF5 (0.040 g, 0.126 mmol) was placed in a 25 mL two-neck flask and THF (5 mL) was added. To the resulting pale yellow solution was added BH₃•THF (1.0 M, 290 μL, 0.290 mmol), when the reaction mixture turned bright yellow within 1 min. After 15 min the colour reverted to pale yellow; additional BH₃•THF (50 μL) was added and the solution became colourless. A condenser was attached and the solution was refluxed at 80 °C for 1 h to ensure completion of the reaction. The reaction mixture was then cooled to r.t. and MeOH (10 mL) was added to decompose unreacted BH₃. The solvent was then removed to give a yellow oil; TLC revealed the presence of one major and several minor products. The major product was purified via preparative TLC (CH₂Cl₂:MeOH, 50:1) as a yellow oil, **3** (0.028 g, 73 %). Note: the product spot on the TLC plate, on exposure to UV light, turned yellow, a phenomenon not seen for IF5. ¹H NMR (300 MHz, d₆-acetone): δ 7.75 (br s, 1H, -NH-), 4.02 (td, 2H, ³J_{HF} = 10 Hz, ³J_{HH} = 2 Hz, -CH₂-CF₂), 3.59 (t, 2H, I-CH₂-), 3.31 (dt, 2H, -CH₂-NH-). ¹⁹F{¹H} NMR (188 MHz, d₆-acetone): δ -8.13 (t, -CF₃), -45.27 (q, -CF₂-). After exposure to UV light the solution became dark red/brown and a new species (**4**) formed. ¹H NMR (300 MHz, d₆-acetone): δ 4.02 (t, 2H, ³J_{HF} = 10 Hz, ³J_{HH} = 1.6 Hz, -CH₂-CF₂), 3.62 (m, 2H, -CH_{eq}-), 2.05 (m, 2H, -CH_{ax}-). ¹⁹F{¹H} NMR (188 MHz, d₆-acetone): δ -8.16 (t, -CF₃), -45.19 (q, -CF₂-). Two of the minor bands, one yellow and one red, were determined by UV-Vis spectrophotometric analysis to be I₃⁻ and I₂, respectively.⁸ UV-Vis (CH₂Cl₂): [band 2] 292, 362; [band 3] 502.



3.2.1.5 3-Fluoropropylamine Hydrochloride (5)

The parent amine for this compound was previously synthesized by Pattison *et al.* from 3-fluoropropionic acid (see Scheme 3-5, p. 99),⁹ but the yield was low. Here other possible routes to the HCl salt of 3-fluoropropylamine were investigated.¹⁰

Synthesis 1 (Scheme 3-6, p. 100)

The use of dialkylaminosulfur fluorides as effective fluorinating agents has been reported previously; the hydroxyl group in alcohols can be replaced with fluorine atoms, and high yields are obtained for the non-rearranged fluoro compound.^{11,12} In a 25 mL two-neck flask at 0°C under a constant flow of N₂ was added DAST (1 mL) to 5 mL CH₂Cl₂ to give a pale yellow solution. 3-Hydroxypropylamine (500 µL) was then added dropwise, when the mixture turned orange and then quickly brown. The mixture was stirred for 1 h at 0 °C, and then frozen using liquid N₂. The volatile components were then vacuum transferred to another flask as a pale yellow solution through which HCl_(g) was bubbled for 5 min. A white solid was formed, and Et₂O (10 mL) was added to complete the precipitation before the solid was isolated via suction filtration. (N.B. This compound is extremely hygroscopic and is best handled in an inert atmosphere.) ¹H NMR spectroscopic analysis of the solid revealed that **5** was formed, but only as a minor product. The major product was Et₂NH•HCl and according to spectral integration was present in a six-fold excess over **5**. ¹H NMR (300 MHz, d₆-dmso): (**5**) δ 8.09 (br s, 2H, -NH-), 4.52 (dt, 2H, ²J_{HF} = 44 Hz, ³J_{HH} = 4.8 Hz, -CH₂F), 2.91 (peak overlaps with H₂O peak, -NH-CH₂-), 2.00 (dp (dtt), 2H, ³J_{HF} = 20 Hz, ³J_{HH} = 4.7 Hz, -CH₂-CH₂F); (Et₂NH•HCl) δ 8.80 (br s, 1H, -NH), 2.91 (m, 2H, NH-CH₂), 1.20 (t, 3H, CH₃-CH₂-). ¹⁹F NMR (282 MHz, d₆-dmso): (**5**) δ -144.94 (spt (tt), ²J_{HF} = 47.4 Hz, ³J_{HF} = 24.0 Hz, -CH₂F). Separation of these two products was extremely difficult and was not further pursued.

Synthesis 2 (Scheme 3-7, p. 101)

This procedure was adapted from that reported by Gibson and Bradshaw on the Gabriel synthesis of primary amines.¹³ In a Schlenk tube under 1 atm N₂ was added 10 mL DMF to potassium phthalamide (0.500 g, 2.70 mmol) to produce a white slurry. 1-Bromo-3-fluoropropane (225 µL, 2.45 mmol) was then added, and the reaction mixture was stirred at 70 °C for 24 h. Afterwards, the mixture was filtered and the filtrate was chromatographed using preparative TLC (CH₂Cl₂:acetone, 20:1); the major band (R_f = 0.85) was isolated as a colourless oil which when cooled yielded a white crystalline solid

(0.334 g, 66 %), N-3-fluoropropylphthalamide (**6**). LR-MS [DCI(+)]: 207 (M^+), 187 ($M^+ - F$), 160 ($M^+ - CH_2CH_2F$). HR-MS [DCI(+)] calc. for $C_{11}H_{10}NO_2F$ 207.06955; found 207.06938. 1H NMR (300 MHz, d_6 -acetone): δ 7.85 (s, 4H, $-CH_{Bz}-$), 4.56 (dt, 2H, $^2J_{HF} = 51$ Hz, $^3J_{HH} = 6.2$ Hz, $-CH_2F$), 3.80 (t, 2H, $^3J_{HH} = 6.8$ Hz, $-N-CH_2-$), 2.10 (dp (dtt), 2H, $^3J_{HF} = 27$ Hz, $^3J_{HH} = 5.6$ Hz, $-CH_2-CH_2F$). ^{19}F NMR (282 MHz, d_6 -acetone): -142.08 (spt (tt), $^2J_{HF} = 49.4$ Hz, $^3J_{HF} = 24.0$ Hz, $-CH_2F$).

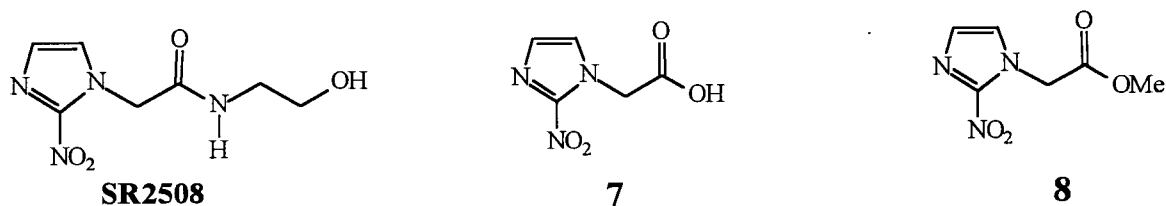
The hydrazinolysis of **6** was adapted from a procedure described by Sheehan and Ryan.¹⁴ **6** (0.120 g, 0.579 mmol) was suspended in 10 mL EtOH and the mixture was heated to 50 °C to facilitate dissolution. Hydrazine monohydrate (40 μ L) was then added and the mixture was refluxed for 2.5 h and then was stirred for 16 h at r.t.; the initially colourless solution became a white slurry. The volume was reduced to ~5 mL, 6M HCl (10 mL) added, and the mixture stirred at 80 °C for 1 h. The resulting white precipitate was filtered and extracted with warm H_2O (3 x 10 mL). The solvent volume was then reduced resulting in the re-formation of the white precipitate which was filtered off. The rotoevaporation/filtration procedure was then repeated to obtain additional product. The final filtrate was taken to dryness to recover the remaining product (0.060 g, 91 %). The 1H NMR spectrum revealed only the presence of **5**. Analysis calc. for C_3H_9NCIF : C, 31.72; H, 7.93; N, 12.33; found C, 31.56; H, 8.20; N, 11.83.¹⁵ LR-MS [DCI(+)]: 78 (M^+), 59 ($M^+ - F$), 30 (H_2NCH_2-). HR-MS [DCI(+)] calc. for C_3H_9NF 78.07190; found 78.07158.

3.2.2 2-Nitroimidazole Compounds

3.2.2.1 2-(2-Nitro-1-H-imidazol-1-yl)acetic acid (**7**) (see Scheme 3-9, p. 102)

In a 250 mL RBF, **SR2508** (3.70 g, 0.0173 mol) was dissolved in MeOH (100 mL) to give a clear, colourless solution. Dowex 50-X8(H^+) (40.3g, previously washed with equiv. amounts (50 mL) of 0.1M HCl, dd H_2O and MeOH) was then added followed by an additional 50 mL MeOH. The mixture was refluxed for 24 h when amide bond cleavage occurs to form the intermediate methyl ester, **8**, as shown by TLC analysis; the reaction mixture was then filtered and the filtrate was rotary evaporated to dryness

yielding an orange oil (the accompanying orange colour comes from the cation exchange resin and, if the methyl ester is purified via column chromatography at this stage, **8** can be isolated as a white solid). The oil was dissolved in 100 mL 0.1M NaOH and the mixture stirred at 100 °C for 45 min to hydrolyze the ester (monitored by TLC). The mixture was cooled to r.t. and 2M HCl added dropwise until the pH was ~ 4. Saturated NaCl solution (50 mL) was added and the product was extracted with EtOAc (10 x 100 mL). The organic extracts were combined and dried with MgSO₄; the mixture was filtered and the solvent removed to give a pale yellow solid (0.805 g, 27%). UV-Vis (MeOH): (**7**) 316 (7.7); (**8**) 316 (7.7). ¹H NMR (200 MHz, d₆-dmsO): (**7**) δ 13.42 (s, 1H, -OH), 7.63 (s, 1H, Im-H₅), 7.22 (s, 1H, Im-H₄), 5.20 (s, 2H, -CH₂-); (**8**) δ 7.64 (s, 1H, Im-H₅), 7.22 (s, 1H, Im-H₄), 5.33 (s, 2H, -CH₂-), 3.72 (s, 3H, -CH₃). Data are in agreement with those previously reported.¹⁶



The aqueous layers were also combined and rotovapped to dryness. The resulting yellow solid was then dissolved in MeOH (40 mL) and the solution was filtered; removal of the solvent from the filtrate gave a bright yellow solid (1.35 g). TLC analysis (shown below) showed the presence of large amounts of **7** that was not extracted with EtOAc.

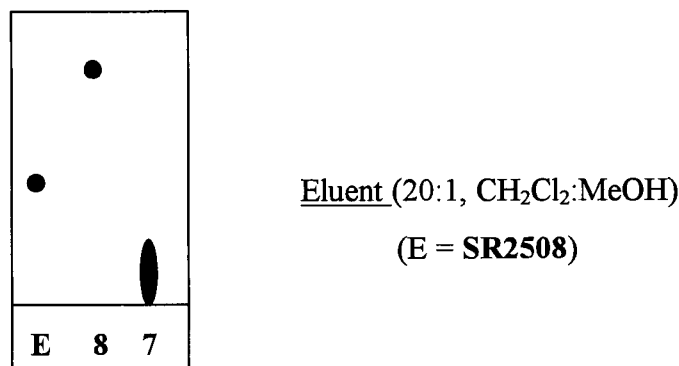


Figure 3-1: TLC analysis of products obtained from 2-(2-Nitro-1-H-imidazol-1-yl)acetic acid (**7**) synthesis.

3.2.2.2 2-(2-Nitro-1-H-imidazol-1-yl)-N-(2,2,3,3,3-pentafluoropropyl) acetamide [EF5]

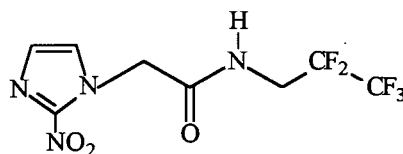
Synthesis 1 (*cf.* Scheme 3-8, p.102)

7 (0.200 g, 1.16 mmol) was dissolved in THF (25 mL) at 0°C under N₂. NMM (130 µL, 1.18 mmol) was then added and the colourless mixture was stirred for 10 min. *i*BuClFrm (167 µL, 1.28 mmol) was added and the mixture was stirred for 30 min during which a white slurry was formed. The ice-bath was removed, and H₂NCH₂CF₂CF₃•HCl (0.241 g, 1.41 mmol) and NMM (142 µL, 1.30 mmol) were added. The reaction slurry was stirred at r.t. for 4.5 h and the resulting white precipitate was filtered off and washed with THF (3 x 5 mL). The yellow filtrate was rotovapped to dryness yielding a pale yellow oil that was purified via column chromatography (CH₂Cl₂:acetone, 10:1 → 5:2). The major band (colourless) followed a minor yellow band and the combined fractions were rotovapped to dryness to yield EF5. Recrystallization from EtOAc/hexanes yielded a white microcrystalline solid (0.116 g, 33%).

Synthesis 2¹⁷

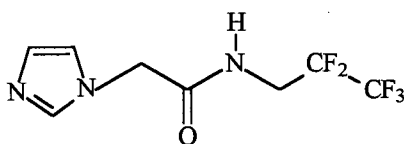
2NO₂Im (0.0257 g, 0.227 mmol) was dissolved in DMF (10 mL) at r.t. under N₂, and powdered Cs₂CO₃ (0.0720 g, 0.221 mmol) was added to give a white slurry. The mixture was heated to 50 °C when a pale yellow solution resulted; after 30 min a white precipitate was formed. The slurry was stirred for 2 h and IF5 (0.0724 g, 0.229 mmol) was then added, and the mixture stirred for 3 h at 50 °C. The resulting pale yellow precipitate was filtered off and washed with DMF (3 x 5 mL); the filtrate was then worked up as described in Synthesis 1 (0.0535 g, 78%); mp 136-137 °C. X-ray quality crystals were obtained by slow evaporation of a concentrated MeOH solution of EF5. Anal. calc. for C₈H₇N₄O₃F₅: C, 31.80; H, 2.34; N, 18.54; found: C, 31.96; H, 2.24; N, 18.37. LR-MS [DCI(+)]: 303 (M⁺), 256 (M⁺ -NO₂). IR (ν, cm⁻¹): 3317 (N-H); 3086 (C-H_{Im}); 2921, 2850 (C-H); 1689 (C=O); 1490 (N-O_{asym}); 1367 (N-O_{sym}). UV-Vis (H₂O): 323 (6.8). ¹H NMR (obtained in d₆-dmso and in CD₃OD to show the effect that H/D exchange of the N-H proton has on the -CH₂-CF₂- signal): (300 MHz, CD₃OD) δ 7.47 (s, 1H, Im-H₅), 7.20 (s,

1H, Im-*H*₄), 5.25 (s, 2H, -CH₂-CO-), 4.01 (t, 2H, ³J_{HF} = 15 Hz, -CH₂-CF₂-); (200 MHz, d₆-dmsO) δ 9.05 (t, 1H, N-*H*), 7.66 (s, 1H, Im-*H*₅), 7.21 (s, 1H, Im-*H*₄), 5.24 (s, 2H, -CH₂-CO-), 4.06 (td, 2H, ³J_{HF} = 15 Hz, ³J_{HH} = 1.5 Hz, -CH₂-CF₂-). ¹⁹F{¹H} NMR (188 MHz, CD₃OD): δ -10.66 (t, -CF₃), -47.24 (q, -CF₂-); (188 MHz, d₆-dmsO) δ -4.34 (t, -CF₃), -41.31 (q, -CF₂-).

**EF5**

3.2.2.3 2-(Imidazol-1-yl)-N-(2,2,3,3,3-pentafluoropropyl)acetamide [ImF5]

Sodium imidazolate (0.0312 g, 0.344 mmol) was added in DMF (5 mL) at r.t. under N₂ to give a yellow slurry. **IF5** (0.117 g, 0.366 mmol) was then added and the mixture was stirred for 4 h at 70 °C. The volume was reduced under vacuum to yield a yellow oil that was subsequently loaded onto a preparative TLC plate (CH₂Cl₂:MeOH, 20:1). (Two major bands with similar R_f values were visible only after development using I₂.) The isolated brown solid from the two bands was heated to 120 °C under vacuum in a sublimation apparatus when a yellow oil deposited onto a cold finger maintained at 5 °C (0.0365 g, 41%). Of note, exposure of the oil to air caused a colour change to dark purple while re-dissolution and exposure to air in acetone generated a bright yellow colour; removal of the acetone regenerated the dark purple colour. LR-MS [EI]: 257 (M⁺), 81 (M⁺ - CONHCH₂CF₂CF₃). HR-MS [EI] calc. for C₈H₈N₃OF₅: 257.05875; found 257.05903. ¹H NMR (300 MHz, d₆-acetone): δ 7.96 (br. s, 1H, N-*H*), 7.65 (s, 1H, Im-*H*₂), 7.16 (s, 1H, Im-*H*₅), 6.97 (s, 1H, Im-*H*₄), 4.92 (s, 2H, -CH₂-CO-), 4.10 (td, 2H, ³J_{HF} = 17 Hz, ³J_{HH} = 6.4 Hz, -CH₂-CF₂-). ¹⁹F{¹H} NMR (188 MHz, d₆-acetone): δ -8.16 (t, -CF₃), -44.87 (q, -CF₂-).

**ImF5****3.2.2.4 N-(2-nitro-1-H-imidazol-1-ethyl) pentafluoropropionamide [RevEF5]****Synthesis 1** (see Scheme 3-14, p. 107)**Step 1**

In a 250 mL 2-neck flask, 2NO₂Im (0.870 g, 7.70 mmol) was dissolved in 50 mL DMF under a constant flow of N₂. Cs₂CO₃ (2.75 g, 8.47 mmol) was then added and the resulting yellow slurry was stirred at 90 °C for 3 h when dissolution was completed. Bromoethylphthalamide (3.96 g, 15.6 mmol) was added and the resulting yellow slurry was stirred for 15 h during which a white solid appeared. The solid was filtered off and the filtrate was reduced in volume to 2 mL before MeOH (20 mL) was added to precipitate a white solid (**9**). The solid was filtered, washed with hot MeOH (3 x 25 mL) and dried *in vacuo* at 80 °C for 3 d (1.95 g, 99 %). LR-MS [DCI(+)]: 287 (M⁺ + H), 240 (M⁺ - NO₂), 160 (M⁺ - 2NO₂ImCH₂). HR-MS [DCI(+)] calc. for C₁₃H₁₁N₄O₄: 287.07803; found 287.07810. ¹H NMR (300 MHz, d₆-acetone): δ 7.78 & 7.73 (overlapping multiplets, 4H, Bz-H), 7.01 (s, 1H, Im-H₅), 6.89 (s, 1H, Im-H₄), 4.70 (t, 2H, -CH₂-Phth), 4.18 (t, 2H, -CH₂-CH₂-Phth).

Step 2

In a 25 mL RBF, **9** (0.0705 g, 0.273 mmol) was suspended in 10 mL EtOH. H₂NNH₂•H₂O (35 μL, 0.721 mmol) was then added via syringe and the mixture was stirred at 80 °C for 18 h during which a clear, colourless solution was formed; TLC analysis revealed that **9** had completely reacted. 6 M HCl (10 mL) was added to the reaction mixture and the EtOH was then removed to yield a white slurry. The solid [LR-MS DCI(+): 162 (M⁺), 132 (M⁺ - N₂H₂), 104 (M⁺ - CO - N₂H₂), 76 (M⁺ - 2CO - N₂H₂).] was isolated and washed with copious amounts of H₂O. The solvent was removed from the pale yellow filtrate to yield an extremely hygroscopic, cream coloured

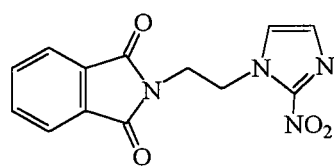
solid (**10**) (0.0565 g, 90 %). LR-MS [DCI(+)]: 157 ($M^+ + H$), 110 ($M^+ - NO_2$). [Only the parent cation is observed with DCI (+), so it is unclear whether 1 or 2 mol of HCl is associated with the compound.] 1H NMR (300 MHz, D_2O): δ 7.48 (d, 1H, Im- H_5), 7.18 (d, 1H, Im- H_4), 4.75 (t, 2H, Im- CH_2 -), 3.51 (t, 2H, - CH_2 - NH_2).

Step 3a

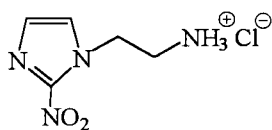
In a 3-neck 50 mL flask, DCC (0.182 g, 0.880 mmol) and NHS (0.101 g, 0.880 mmol) were dissolved in 4 mL DMF under N_2 to give a clear, colourless solution. $CF_3CF_2CO_2H$ (92 μ L, 0.870 mmol) was added and a white microcrystalline precipitate was immediately formed. The mixture was stirred for 1 h at r.t. before a DMF solution (3 mL) of **10** (0.206 g, 0.900 mmol) and NMM (198 μ L, 1.80 mmol), was added. Stirring was continued for 4 h after which TLC analysis revealed that **10** had completely reacted. The white precipitate [DCU according to LR-MS [DCI(+)]: 225 (M^+), 143 ($M^+ - C_6H_5$), 99 (C_6H_5 - NH -)] was isolated and washed with DMF; the filtrate was reduced in volume to ~ 1 mL before being loaded onto a preparative TLC plate (CH_2Cl_2 :MeOH, 18:1). The product band ($R_f = 0.45$) was isolated to yield **RevEF5** as an off-white solid (0.0757 g, 29 %).

Step 3b

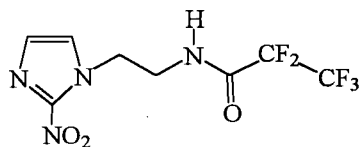
This reaction was continued from Step 2 prior to the addition of HCl (same amount of **9** used for this synthesis). The colourless EtOH solution was taken to dryness to yield an oily, white film which was subsequently taken up in $CHCl_3$ (10 mL) to give a white slurry. NMM (1 equiv.) was added and the mixture stirred for 30 min at r.t. Upon addition of $(CF_3CF_2CO)_2O$ (1 equiv.) the mixture became a clear solution which slowly deposited a white residue on the walls of the flask over 5 h. Addition of EtOH led to the formation of a white precipitate which was filtered off and washed with EtOH (3 x 5 mL). TLC analysis of the filtrate revealed two major products which were separated using preparative TLC (CH_2Cl_2 :MeOH, 20:1). The band corresponding to **RevEF5** was identified by comparison of the R_f value with that of an authentic sample of the compound. The isolated **RevEF5** was reprecipitated from an EtOAc/hexanes mixture to yield a white solid (0.0265 g, 32%).



9



10



RevEF5

Synthesis 2

Reaction conditions similar to those used for synthesis 1 of **EF5** (section 3.2.2.2) were used: $\text{CF}_3\text{CF}_2\text{CO}_2\text{H}$ (25 μL , 0.238 mmol) was dissolved in THF (10 mL) after which NMM (25 μL , 0.238 mmol) and $i\text{BuClFrm}$ (36 μL , 0.276 mmol) were added giving a white slurry. **10** (0.0605 g, 0.262 mmol) and NMM (60 μL , 0.571 mmol) were then added and the mixture was stirred at r.t. for 4 h. The white precipitate that formed was filtered off and washed with THF (3 x 5 mL); the crude product (filtrate) was then purified using preparative TLC (CH_2Cl_2 :MeOH, 20:1). Four bands were observed and the minor band with $R_f = 0.37$ was isolated to yield **RevEF5** (0.0115 g, 16 %). Anal. calc. for $\text{C}_8\text{H}_7\text{N}_4\text{O}_3\text{F}_5$: C, 31.80; H, 2.34; N, 18.54; found: C, 31.85; H, 2.33; N, 18.59. LR-MS [DCI(+)]: 320 ($\text{M}^+ + \text{NH}_4^+$), 303 ($\text{M}^+ + \text{H}$), 287 ($\text{M}^+ - \text{O}$), 273 ($\text{M}^+ - \text{NO}$), 256 ($\text{M}^+ - \text{NO}_2$). HR-MS [DCI(+)] calc. for $\text{C}_8\text{H}_8\text{N}_4\text{O}_3\text{F}_5$: 303.05164; found 303.05137. IR (ν , cm^{-1}): 3327 (N-H); 2965, 2932, 2866 (C-H); 1613 (C=O); 1457 (N- O_{asym}); 1383 (N- O_{sym}). UV-Vis (MeOH): 316 (6.2). ^1H NMR (300 MHz, d_6 -acetone): δ 8.89 (br s, 1H, -NH-), 7.41 (s, 1H, Im- H_5), 7.05 (s, 1H, Im- H_4), 4.68 (t, 2H, Im- CH_2 -), 3.86 (q (dt), 2H, - CH_2 -NH-). $^{19}\text{F}\{^1\text{H}\}$ NMR (188 MHz, d_6 -acetone): δ -6.79 (t, - CF_3), -46.43 (q, - CF_2 -).

Synthesis 3

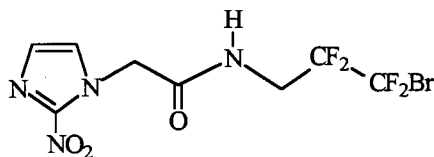
Based on published peptide-coupling techniques,^{18,19} $\text{CF}_3\text{CF}_2\text{CO}_2\text{H}$ (30 μL , 0.286 mmol) and Et_3N (1 equiv.) were dissolved in DMF (2 mL) and $\text{STMU}\cdot\text{BF}_4$ (0.0941 g, 0.313 mmol), a reagent used to produce the -NHS esters was then added. The clear mixture was then stirred for 18 h at r.t. after which TLC analysis (CH_2Cl_2 :MeOH, 20:1) indicated the presence of a new product in high yield, presumed to be the activated succinimidyl ester. **7** (0.0652 g, 0.288 mmol) and Et_3N (2 equiv.) were subsequently added, and the mixture, now cloudy, was stirred for 24 h when TLC analysis indicated the

presence of two major products. The solvent was removed under reduced pressure, and the residue was chromatographed using preparative TLC (CH_2Cl_2 :MeOH, 25:1) to give two pale yellow oils; comparison of TLC data with those of an authentic sample of **RevEF5** revealed that neither oil contained the desired product. A minor band with the same R_f as **RevEF5** was observed but the product was not isolated due to low concentrations (<1%).

3.2.2.5 2-(2-Nitro-1-H-imidazol-1-yl)-N-(3-bromo-2,2,3,3-tetrafluoropropyl) acetamide [EF4Br]

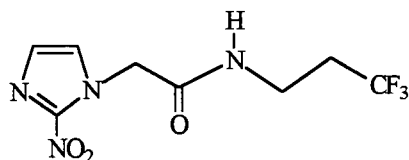
Reaction conditions similar to those used for the synthesis of **EF5** (synthesis 1) were employed: **7** (0.0760 g, 0.442 mmol) was dissolved in THF (15 mL) and NMM (50 μL , 0.458 mmol) and $i\text{BuClFrm}$ (63 μL , 0.483 mmol) were added. To the resulting pale yellow slurry, $\text{H}_2\text{NCH}_2\text{CF}_2\text{CF}_2\text{Br}\cdot\text{HCl}$ (0.120 g, 0.487 mmol) and NMM (53 μL , 0.485 mmol) were added, and the mixture was then stirred at r.t. for 5 h. The white precipitate that formed was filtered off and washed with THF (3 x 5 mL). The filtrate was taken to dryness to give a yellow oil that was purified via preparative TLC (CH_2Cl_2 :MeOH, 20:1). The isolated product band appeared to have two species present (with almost identical R_f values) and so a second preparative TLC was performed (CH_2Cl_2 :MeOH, 12:1). The major band separated from the minor band; however, when isolated and eluted with acetone the eluate was taken to dryness to give back the original oil. The oil was dissolved in 1 mL EtOAc followed by addition of hexanes (15 mL) which resulted in formation of a white precipitate. The fine white solid was isolated via suction filtration, washed with Et_2O (3 x 5 mL) and dried *in vacuo* (0.0425 g, 27%). Anal. calc. for $\text{C}_8\text{H}_7\text{N}_4\text{O}_3\text{F}_4\text{Br}\cdot 0.15 \text{ Et}_2\text{O}$: C, 27.61; H, 2.29; N, 14.97; found C, 27.76; H, 2.13; N, 14.94. LR-MS [DCI(+)]: 365, 363 ($\text{M}^+ + \text{H}$), 335, 333 ($\text{M}^+ - \text{NO}$), 318, 316 ($\text{M}^+ - \text{NO}_2$), 283 ($\text{M}^+ - \text{Br}$). HR-MS [DCI(+)] calc. for $\text{C}_8\text{H}_8\text{O}_3\text{N}_4\text{F}_4^{81}\text{Br}$ ($\text{C}_8\text{H}_8\text{O}_3\text{N}_4\text{F}_4^{79}\text{Br}$): 364.96954 (362.97163); found 364.96834 (362.97100). IR (ν , cm^{-1}): 3310 (N-H); 3076 (C- H_{Im}); 2960, 2851 (C-H); 1697 (C=O); 1493 (N- O_{asym}); 1370 (N- O_{sym}). UV-Vis (MeOH): 316 (6.9), 232 (3.5). ^1H NMR (300 MHz, d_6 -acetone): δ 8.18 (br s, 1H, -NH-), 7.49 (s, 1H, Im- H_5), 7.20 (s, 1H, Im- H_4), 5.31

(s, 2H, $-\text{CH}_2\text{-CO-}$), 4.10 (td, 2H, $^3J_{\text{H-F}} = 15.6$ Hz, $-\text{NH-CH}_2\text{-CF}_2\text{-}$). $^{19}\text{F}\{^1\text{H}\}$ NMR (188 MHz, $\text{d}_6\text{-acetone}$): δ 10.04 (t, $-\text{CF}_2\text{Br}$), -38.75 (t, $-\text{CH}_2\text{-CF}_2\text{-}$).



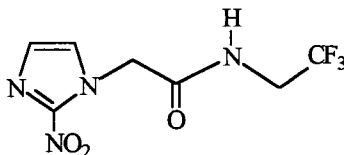
3.2.2.6 2-(2-Nitro-1-H-imidazol-1-yl)-N-(3,3,3-trifluoropropyl)acetamide [EF3]

Compound 7 (0.150 g, 0.873 mmol) was dissolved in THF (20 mL) at 0°C under N_2 . NMM (96 μL , 0.873 mmol) was then added and the clear, colourless mixture was stirred for 10 min. $i\text{BuClFrm}$ (125 μL , 0.961 mmol) was added and the solution was stirred for 30 min during which the mixture became a white slurry. The ice-bath was removed and $\text{H}_2\text{NCH}_2\text{CH}_2\text{CF}_3 \cdot \text{HCl}$ (0.199 g, 0.961 mmol) and NMM (105 μL , 0.961 mmol) were added. Stirring was continued for 5.5 h at r.t. before the white precipitate that formed was filtered off and washed with THF (3 x 5 mL); the yellow filtrate was taken to dryness to yield a yellow solid that was subsequently recrystallized from EtOAc/hexanes to give white microcrystalline needles (0.193 g, 83 %). Anal. calc. for $\text{C}_8\text{H}_9\text{N}_4\text{O}_3\text{F}_3$: C, 36.10; H, 3.41; N, 21.05; found: C, 36.35; H, 3.35; N, 21.05. IR (ν , cm^{-1}): 3312 (N-H), 3026, 2923, 2851 (C-H), 1669 (C=O), 1493 (N- O_{asym}), 1370 (N- O_{sym}). UV-Vis (dmso): 328 (9.4); (MeCN) 322 (4940). ^1H NMR (300 MHz, $\text{d}_6\text{-acetone}$): δ 7.81 (br s, 1H, -NH-), 7.50 (s, 1H, Im- H_5), 7.15 (s, 1H, Im- H_4), 5.25 (s, 2H, $-\text{CH}_2\text{-CO-}$), 3.50 (q, 2H, $-\text{NH-CH}_2\text{-}$), 2.50 (qt, 2H, $^3J_{\text{H-F}} = 11$ Hz, $-\text{CH}_2\text{CF}_3$), $^{19}\text{F}\{^1\text{H}\}$ NMR (188 MHz, $\text{d}_6\text{-acetone}$): δ 10.84 (s, $-\text{CF}_3$).



3.2.2.7 2-(2-Nitro-1-H-imidazol-1-yl)-N-(2,2,2-trifluoroethyl)acetamide [EF3(-1)]

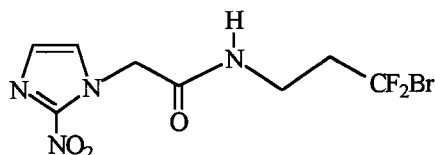
Reaction conditions similar to those used for the synthesis of **EF3** were employed: **7** (0.172 g, 0.998 mmol) was dissolved in THF (17 mL) and NMM (109 μ L, 0.996 mmol) and *i*BuClFrm (142 μ L, 1.09 mmol) were added. To the resulting pale yellow slurry, $\text{H}_2\text{NCH}_2\text{CF}_3 \cdot \text{HCl}$ (0.149 g, 1.10 mmol) and NMM (120 μ L, 1.10 mmol) were added, and the mixture was then stirred at r.t. for 4 h. The white precipitate that formed was filtered off and washed with Et_2O (3 x 5 mL); the filtrate was taken to dryness to give a yellow oil that was purified using a CTRON (THF:acetone, 10:1). The fourth, most concentrated band was isolated to yield a white solid (0.208 g, 83%). Anal. calc. for $\text{C}_7\text{H}_7\text{N}_4\text{O}_3\text{F}_3 \cdot 0.15$ acetone: C, 34.40; H, 3.08; N, 21.39; found C, 34.25; H, 2.86; N, 21.31. IR (ν , cm^{-1}): 3299 (N-H); 3117 (C-H_{Im}); 2923, 2851 (C-H); 1685 (C=O); 1489 (N-O_{asym}); 1374 (N-O_{sym}). UV-Vis (MeOH): 316 (8.5). ^1H NMR (300 MHz, d_6 -acetone): δ 8.21 (br s, 1H, -NH-), 7.53 (s, 1H, Im-H_5), 7.15 (s, 1H, Im-H_4), 5.36 (s, 2H, $-\text{CH}_2-\text{CO}-$), 4.06 (qd, 2H, $^3J_{\text{H-F}} = 9.4$ Hz, $-\text{CH}_2-\text{CF}_3$). $^{19}\text{F}\{^1\text{H}\}$ NMR (188 MHz, d_6 -acetone): δ 4.30 (s, $-\text{CF}_3$).



3.2.2.8 2-(2-Nitro-1-H-imidazol-1-yl)-N-(3-bromo-3,3-difluoropropyl) acetamide [EF2Br]

Reaction conditions similar to those in the synthesis of **EF3** were used: **7** (0.206 g, 1.20 mmol) was dissolved in THF (20 mL) and NMM (131 μ L, 1.20 mmol) and *i*BuClFrm (172 μ L, 1.32 mmol) were added. To the resulting pale orange slurry were added $\text{H}_2\text{NCH}_2\text{CH}_2\text{CF}_2\text{Br} \cdot \text{HCl}$ (0.273 g, 1.30 mmol) and NMM (142 μ L, 1.30 mmol). The mixture was then stirred at r.t. for 6 h. The white precipitate that formed was filtered off and washed with THF (3 x 5 mL). The filtrate was taken to dryness to give an orange oil that was purified via CTRON (Et_2O :acetone, 10:0 \rightarrow 10:3). An orange band eluted

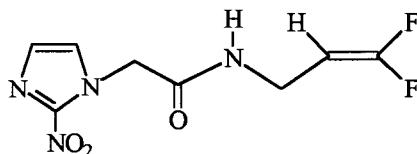
from the plate first using Et₂O; the product band was then eluted using acetone which when taken to dryness yielded an off-white solid (0.242 g, 62%). Crystals suitable for X-ray analysis were obtained from slow evaporation of a concentrated MeOH solution. Anal. calc. for C₈H₉N₄O₃F₂Br: C, 29.38; H, 2.77; N, 17.13; found C, 29.35; H, 2.87; N, 17.22. LR-MS [DCI(+)]: 346, 344 (M⁺ + NH₄⁺), 329, 327 (M⁺ + H), 299, 297 (M⁺ - NO), 282, 280 (M⁺ - NO₂), 247 (M⁺ - Br). HR-MS [DCI(+)] calc. for C₈H₁₀O₃N₄⁸¹Br (C₈H₁₀O₃N₄⁷⁹Br): 328.98838 (326.99047); found 328.98733 (326.99038). IR (ν, cm⁻¹): 3287 (N-H); 3120 (C-H_{Im}); 3062, 2963 (C-H); 1671 (C=O); 1494 (N-O_{asym}); 1371 (N-O_{sym}). UV-Vis (MeCN): 328 (6.6). ¹H NMR (300 MHz, d₆-acetone): δ 7.86 (br s, 1H, -NH-), 7.50 (s, 1H, Im-H₅), 7.14 (s, 1H, Im-H₄), 5.25 (s, 2H, -CH₂-CO-), 3.55 (q, 2H, -NH-CH₂-), 2.73 (tt, 2H, ³J_{H-F} = 17 Hz, -CH₂-CF₂Br). ¹⁹F{¹H} NMR (188 MHz, d₆-acetone): δ 32.71 (s, -CF₂Br).



3.2.2.9 2-(2-Nitro-1-H-imidazol-1-yl)-N-(3,3-difluoropropyl)acetamide [E=F2]

An attempt to synthesize **EF3** from **EF2Br** using a standard halogen exchange procedure (Br for F) led mainly to the “-HBr elimination product” **E=F2**; no **EF3** was observed according to ¹⁹F{¹H} NMR. Addition of **EF2Br** (0.0401 g, 0.122 mmol) to Bu₄NF·H₂O (0.0684 g, 0.245 mmol) in 2 mL MeCN led to formation of a bright yellow solution. Stirring was continued at r.t. for 10 h before the solvent was removed and the major product isolated as a yellow oil via preparative TLC (CH₂Cl₂:MeOH, 25:1). The oil was dissolved in EtOAc, and hexanes were added to precipitate a white solid, which was filtered off and dried *in vacuo* (0.0132 g, 44 %). Anal. calc. for C₈H₈N₄O₃F₂: C, 39.03; H, 3.28; N, 22.76; found C, 39.12; H, 3.20; N, 22.55. IR (ν, cm⁻¹): 3311 (N-H); 3104(C-H_{Im}); 2923, 2851 (C-H); 1668 (C=O); 1487 (N-O_{asym}); 1375 (N-O_{sym}). UV-Vis (MeCN): 320 (3.9). ¹H NMR (300 MHz, d₆-acetone): δ 7.75 (br s, 1H, -NH-), 7.50 (s, 1H, Im-H₅), 7.12 (s, 1H, Im-H₄), 5.22 (s, 2H, -CH₂-CO-), 4.55 (dtd, 1H, ³J_{HF(trans)} = 25

Hz, $^3J_{\text{HH}} = 7.7$ Hz, $^3J_{\text{HF(cis)}} = 2.2$ Hz, $-\text{CH}=\text{CF}_2$), 3.85 (dddd, 2H, $^2J_{\text{HH}} = 9.2$ Hz, $^3J_{\text{HH}} = 7.1$ Hz, $^4J_{\text{HF(trans)}} = 2.1$ Hz, $^4J_{\text{HF(cis)}} = 1.4$ Hz, $-\text{CH}_2-\text{CH}=\text{}$). $^{19}\text{F}\{^1\text{H}\}$ NMR (188 MHz, d_6 -acetone): δ -12.78 (d, $^2J_{\text{FF}} = 26.3$ Hz, $=\text{C}-\text{F}_{\text{cis}}$), -13.82 (d, $^2J_{\text{FF}} = 26.3$ Hz, $=\text{C}-\text{F}_{\text{trans}}$).

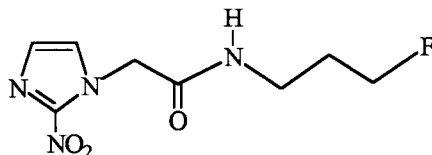


3.2.2.10 2-(2-Nitro-1-H-imidazol-1-yl)-N-(3-fluoropropyl)acetamide [EF1]

Reaction conditions similar to those in the synthesis of EF3 were used: **7** (0.124 g, 0.722 mmol) was dissolved in THF (15 mL) and NMM (79 μL , 0.717 mmol) and *i*BuClFrm (103 μL , 0.789 mmol) were added. To the resulting white slurry were added $\text{H}_2\text{NCH}_2\text{CH}_2\text{CH}_2\text{F}\cdot\text{HF}$ (0.241 g, 1.41 mmol) and NMM (142 μL , 1.30 mmol). The mixture was stirred at r.t. for 4.5 h before the white precipitate that formed was filtered off and washed with THF (3 x 5 mL). The filtrate was taken to dryness to give a yellow oil that was purified using preparative TLC (CH_2Cl_2 :MeOH, 20:1); the major band isolated yielded a creamy white solid (0.0146 g, 9 %).

The hydrochloride salt of 3-fluoropropylamine (**5**) was used in order to eliminate problems caused by the presence of HF in the hydrofluoride salt. Identical reaction conditions were used as described above, but using 0.264 g (1.41 mmol) of the hydrochloride, and a white solid was isolated (0.0249 g, 15 %). Anal. calc. for $\text{C}_8\text{H}_{11}\text{N}_4\text{O}_3\text{F}$: C, 41.74; H, 4.82; N, 24.34; found C, 40.69; H, 4.62; N, 21.34. LR-MS [DCI(+)]: 231 ($\text{M}^+ + \text{H}$), 184 ($\text{M}^+ - \text{NO}_2$). HR-MS [DCI(+)] calc. for $\text{C}_8\text{H}_{12}\text{O}_3\text{N}_4\text{F}$: 231.08933; found 231.08881. IR (ν , cm^{-1}): 3284 (N-H); 3124 ($\text{C}-\text{H}_{\text{im}}$); 2926, 2851 (C-H); 1660 (C=O); 1492 ($\text{N}-\text{O}_{\text{asym}}$); 1369 ($\text{N}-\text{O}_{\text{sym}}$). UV-Vis (MeOH): 316 (6.7), 210 (5.2). ^1H NMR (300 MHz, d_6 -acetone): δ 7.64 (br s, 1H, $-\text{NH}-$), 7.52 (s, 1H, $\text{Im}-\text{H}_5$), 7.18 (s, 1H, $\text{Im}-\text{H}_4$), 5.22 (s, 2H, $-\text{CH}_2-\text{CO}-$), 4.51 (dt, 2H, $^2J_{\text{H-F}} = 66$ Hz, $^3J_{\text{H-H}} = 9.4$ Hz, $-\text{CH}_2\text{F}$), 3.38 (q (dt), 2H, $-\text{NH}-\text{CH}_2-$), 1.91 (dp (dtt), 2H, $^3J_{\text{H-F}} = 42$ Hz, $^3J_{\text{H-H}} = 9.7$ Hz, $-\text{CH}_2-\text{CH}_2\text{F}$).

^{19}F NMR (282 MHz, d_6 -acetone): δ -142.50 (spt (tt), $^2J_{\text{H-F}} = 49.1$ Hz, $^3J_{\text{H-F}} = 25.1$ Hz, $-\text{CH}_2\text{F}$).



Comparison of the TLCs obtained from the above reactions shows that both gave two other major products having higher R_f values than that of **EF1**; a small amount of unreacted **7** ($R_f = 0$) was also observed (Figure 3-2). The difference in yield of **EF1** (9% vs. 15%) between the two reactions probably indicates that the presence of HF does not limit the reaction yield.

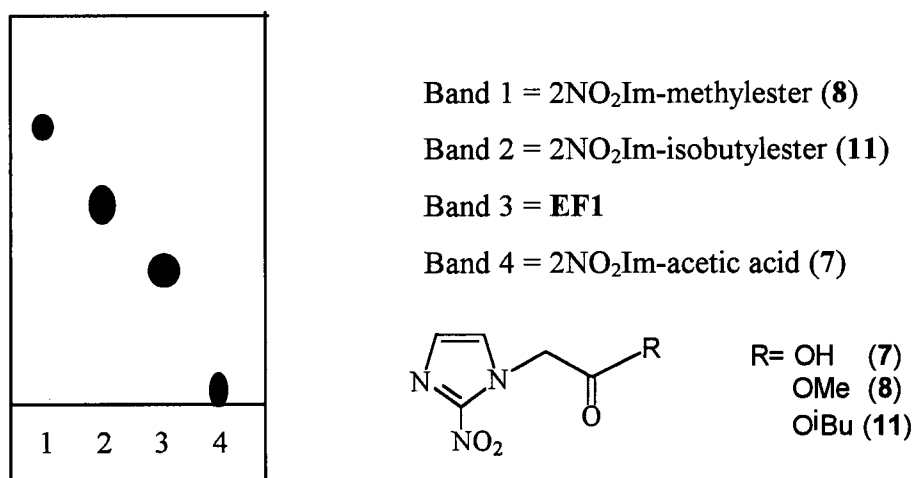


Figure 3-2: TLC analysis of products obtained from **EF1** synthesis.

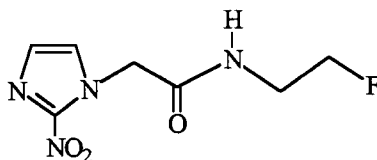
Bands 1 and 2 were also isolated and characterized in order to determine the identities of the side-products responsible for the low yields of **EF1**. The pale yellow solid isolated from band 1 was identified as **8** as evidenced by ^1H NMR spectroscopy (p. 55). This species is likely formed from reaction of the acyl carbonate with MeOH during preparative TLC separation. The species isolated from band 2 was more difficult to identify; the ^1H NMR spectrum shows signals corresponding to the isobutyl protons and

IR revealed the presence of a ν_{CO} band. MS analysis definitely showed that the species is the isobutylester (**11**) (see Scheme 3-13, p.106). LR-MS [DCI(+)]: 228 (M^+), 182 ($\text{M}^+ - \text{NO}_2$). IR (ν , cm^{-1}): 3125 (C-H_{Im}); 2964, 2876 (C-H); 1751 (C=O); 1490 (N-O_{asym}); 1369 (N-O_{sym}). ^1H NMR (200 MHz, d_6 -acetone): δ 7.59 (s, 1H, Im- H_5), 7.19 (s, 1H, Im- H_4), 5.40 (s, 2H, $-\text{CH}_2\text{-CO-}$), 4.01 (d, 2H, $\text{O-CH}_2\text{-CH-}$), 1.92 (m, 1H, $-\text{CH-}(\text{CH}_3)_2$), 0.87 (d, 6H, $-\text{CH-}(\text{CH}_3)_2$).

3.2.2.11 2-(2-Nitro-1-H-imidazol-1-yl)-N-(2-fluoroethyl)acetamide [EF1(-1)]

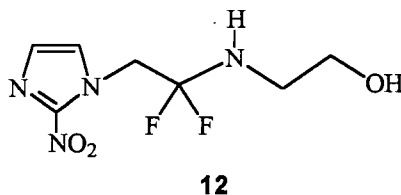
Synthesis 1

Reaction conditions similar to those in the synthesis of **EF3** were used: **7** (0.154 g, 0.891 mmol) was dissolved in THF (10 mL), and NMM (105 μL , 0.953 mmol) and *i*BuClFrm (140 μL , 1.07 mmol) were added. To the resulting pale yellow slurry were added $\text{H}_2\text{NCH}_2\text{CH}_2\text{F}\cdot\text{HCl}$ (0.132 g, 1.33 mmol) and NMM (120 μL , 1.10 mmol). The mixture was stirred at r.t. for 6 h before the white precipitate that formed was filtered off and washed with THF (3 x 5 mL). The filtrate and washings were taken to dryness to give a yellow oil that was chromatographed using CTRON (CH_2Cl_2 :THF, 10:3). A white solid was isolated from the fourth band and was recrystallized from acetone/ Et_2O (1:1) (0.124 g, 64%). Anal. calc. for $\text{C}_7\text{H}_9\text{N}_4\text{O}_3\text{F}$: C, 38.89; H, 4.20; N, 25.92; found C, 38.88; H, 4.25; N, 25.77. IR (ν , cm^{-1}): 3296 (N-H); 3120 (C-H_{Im}); 2926, 2851 (C-H); 1669 (C=O); 1488 (N-O_{asym}); 1372 (N-O_{sym}). UV-Vis (MeOH): 316 (6.2), 212 (4.7). ^1H NMR (300 MHz, d_6 -acetone): δ 7.87 (br s, 1H, $-\text{NH-}$), 7.50 (s, 1H, Im- H_5), 7.14 (s, 1H, Im- H_4), 5.26 (s, 2H, $-\text{CH}_2\text{-CO-}$), 4.48 (dt, 2H, $^2J_{\text{H-F}} = 48$ Hz, $^3J_{\text{H-H}} = 6.5$ Hz, $-\text{CH}_2\text{F}$), 3.55 (dq (dtd), 2H, $^3J_{\text{H-F}} = 30$ Hz, $^3J_{\text{HH}} = 6.2$ Hz, $-\text{NH-CH}_2\text{-}$). ^{19}F NMR (282 MHz, d_6 -acetone): δ -144.94 (spt (tt), $^2J_{\text{H-F}} = 49.1$ Hz, $^3J_{\text{H-F}} = 26.2$ Hz, $-\text{CH}_2\text{F}$). ^{13}C NMR (50 MHz, d_6 -acetone): δ 166.89 ($-\text{CO-}$), 130.92 and 129.92 (Im- C_4 and C_5), 84.70 (d, $^1J_{\text{CF}} = 166.5$ Hz, $-\text{CH}_2\text{F}$), 54.33 ($-\text{CH}_2\text{-CO-}$), 42.89 (d, $^2J_{\text{CF}} = 21$ Hz, $-\text{NH-CH}_2\text{-}$).



Synthesis 2

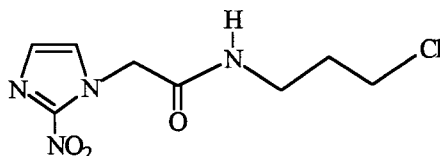
In a N₂-flushed 50 mL, 2-neck flask at -78 °C, CH₂Cl₂ (10 mL) was added to **SR2508** (0.100 g, 0.466 mmol) to give a white slurry; DAST (80 µL, 0.606 mmol) was then added dropwise and the mixture was stirred for 3 h at r.t. The resulting yellow/orange solution was chromatographed using CTRON (Et₂O → THF), but neither of the two products was the desired **EF1(-1)**. A wafer-like, crystalline, white solid was isolated from the second band (*R_f* = 0.40 with THF) (~ 10 mg). ¹H NMR (300 MHz, d₆-acetone): δ 7.59 (s, 1H, Im-*H*₅), 7.38 (dd, 1H, -CF₂-NH-), 7.13 (s, 1H, Im-*H*₄), 5.34 (q, 2H, -CH₂-CF₂-), 4.38 (dt, 2H, -NH-CH₂), 3.71 (t, 2H, -CH₂OH). ¹⁹F{¹H} NMR (188 MHz, d₆-acetone): δ -6.22 (s, -CF₂-NH-). NMR data indicate fluorine substitution at the carbonyl group (**12**) rather than at the OH group, and so this reaction procedure was pursued no further.



3.2.2.12 2-(2-Nitro-1-H-imidazol-1-yl)-N-(3-chloropropyl)acetamide [EC11]

Reaction conditions similar to those for the synthesis of **EF3** were used: **7** (0.103 g, 0.596 mmol) was dissolved in THF (15 mL) and NMM (64 µL, 0.581 mmol) and iBuClFrm (83 µL, 0.636 mmol) were added. To the resulting pale yellow slurry were added H₂NCH₂CH₂CH₂Cl·HCl (0.0871 g, 0.700 mmol) and NMM (71 µL, 0.650 mmol). The mixture was then stirred at r.t. for 3.5 h after which the yellow precipitate that formed was filtered off and washed with THF (3 x 5 mL). The filtrate and washings were taken to dryness and the resulting yellow oil was chromatographed using preparative TLC (CH₂Cl₂:MeOH, 20:1). The major band yielded a white solid (0.0945 g, 64%). Anal. calc. for C₈H₁₁N₄O₃Cl: C, 38.96; H, 4.50; N, 22.71; found: C, 39.36; H, 4.64; N, 22.70. IR (ν, cm⁻¹): 3287 (N-H); 3099 (C-H_{im}); 2946, 2868 (C-H); 1657 (C=O); 1484 (N-O_{asym}); 1368 (N-O_{sym}). UV-VIS (MeOH): 316 (6.1), 216 (3.4). ¹H NMR (300 MHz, d₆-acetone): δ

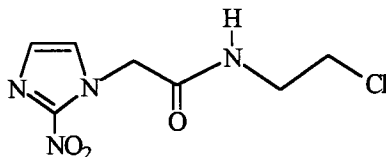
7.70 (br s, 1H, -NH-), 7.49 (s, 1H, Im- H_5), 7.14 (s, 1H, Im- H_4), 5.23 (s, 2H, -CH₂-CO-), 3.66 (t, 2H, -CH₂Cl), 3.39 (q (dt), 2H, -NH-CH₂-), 1.98 (p (tt), 2H, -CH₂-CH₂-).



3.2.2.13 2-(2-Nitro-1-H-imidazol-1-yl)-N-(2-chloroethyl)acetamide [EC11(-1)]

Synthesis 1

Reaction conditions similar to those for the synthesis of **EF3** were used: **7** (0.100 g, 0.585 mmol) dissolved in THF (15 mL) and NMM (65 μ L, 0.590 mmol) and *i*BuClFrm (84 μ L, 0.644 mmol) were added. To the resulting yellow slurry were added H₂NCH₂CH₂Cl·HCl (0.0746 g, 0.644 mmol) and NMM (72 μ L, 0.659 mmol). The mixture was then stirred at r.t. for 4.5 h before the white precipitate that formed was filtered off and washed with THF (3 x 5 mL). The filtrate and washings were taken to dryness to give a yellow oil which was chromatographed using preparative TLC (CH₂Cl₂:MeOH, 20:1); the major band yielded a white solid (0.0939 g, 69%). Anal. calc. for C₇H₉N₄O₃Cl: C, 36.14; H, 3.90; N, 24.08; found: C, 36.17; H, 3.92; N, 24.04. LR-MS [EI(+)]: 233 (M⁺), 196 (M⁺ - Cl), 186 (M⁺ - NO₂). IR (ν , cm⁻¹): 3292 (N-H); 3117 (C-H_{Im}); 2926, 2851 (C-H); 1665 (C=O); 1489 (N-O_{asym}); 1373 (N-O_{sym}). UV-Vis (MeOH): 316 (5.8), 218 (3.7). ¹H NMR (300 MHz, d₆-dmso) δ 8.64 (br t, 1H, -NH-), 7.53 (s, 1H, Im- H_5), 7.20 (s, 1H, Im- H_4), 5.15 (s, 2H, -CH₂-CO-), 3.61 (t, 2H, -CH₂Cl), 3.44 (q (dt), 2H, -NH-CH₂-). ¹³C NMR (50 MHz, d₆-acetone): δ 166.17 (-CO-), 128.90 and 127.58 (Im- $C_{4 \text{ and } 5}$), 51.63 (-CH₂-CO-), 43.46 (-CH₂Cl), 40.90 (-NH-CH₂-).



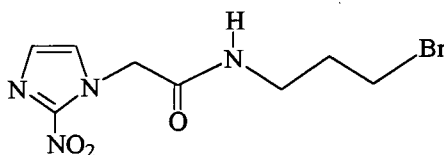
Synthesis 2 (see Scheme 3-16, p. 124)

In a flask equipped with a reflux condenser, CHCl_3 (10 mL) was added to **SR2508** (0.403 g, 1.88 mmol) at 0 °C to yield a white slurry. DMF (3 mL) was then added, resulting in a clear, colourless solution. TsCl (0.553 g, 2.90 mmol) and py (350 μL , 4.34 mmol) were added (together), and the reaction mixture was stirred for 0.5 h. The ice-bath was then removed and the reaction mixture was allowed to warm to r.t. Et_2O was then added dropwise (~ 30 mL) and the white precipitate that formed was isolated via suction filtration. (From ^1H NMR, this solid was found to be a mixture of pyridinium hydrochloride and pyridinium tosylate.) The filtrate was taken to dryness and the resulting residue was dissolved in minimal acetone before being loaded onto a column. The column was then eluted with 5% acetone in CH_2Cl_2 and two major bands were isolated. The first band yielded unreacted TsCl, while the second band gave **ECH(-1)** (0.207 g, 47 %).

3.2.2.14 2-(2-Nitro-1-H-imidazol-1-yl)-N-(3-bromopropyl)acetamide [EBr1]

Reaction conditions similar to those for the synthesis of **EF3** were used: **7** (0.100 g, 0.585 mmol) was dissolved in THF (15 mL), and NMM (65 μL , 0.590 mmol) and $i\text{BuClFrm}$ (84 μL , 0.644 mmol) were added. To the resulting pale yellow slurry were added $\text{H}_2\text{NCH}_2\text{CH}_2\text{CH}_2\text{Br}\cdot\text{HBr}$ (0.141 g, 0.644 mmol) and NMM (72 μL , 0.659 mmol). The mixture was then stirred at r.t. for 4 h before the white precipitate that formed was filtered off and washed with THF (3 x 5 mL). The filtrate and washings were reduced in volume and subsequently loaded onto a column and eluted dropwise (CH_2Cl_2 :THF, 5:1). The first 200 mL of eluate was discarded and the first band was collected in 3 x 50 mL fractions. The eluent strength was increased (using 50% THF) and after 150 mL of eluate, the second band emerged containing the desired product. Eight 50 mL fractions were collected (the purity of the product being confirmed by TLC analysis) and combined before being taken to dryness to give a pale yellow solid (0.113 g, 67%). Anal. calc. for $\text{C}_8\text{H}_{11}\text{N}_4\text{O}_3\text{Br}$: C, 33.04 ; H, 3.83; N, 19.22; found: C, 32.19; H, 3.68; N, 18.57. LR-MS [DCI(+)] : 293, 291 ($\text{M}^+ + \text{H}$), 246, 244 ($\text{M}^+ - \text{NO}_2$). HR-MS [DCI(+)] calc. for $\text{C}_8\text{H}_{12}\text{O}_3\text{N}_4^{81}\text{Br}$ ($\text{C}_8\text{H}_{12}\text{O}_3\text{N}_4^{79}\text{Br}$): 293.00723 (291.00932); found 293.00732 (291.00932).

IR (ν , cm^{-1}): 3286 (N-H); 3100 (C-H_{Im}); 2929 (C-H); 1656 (C=O); 1484 (N-O_{asym}); 1366 (N-O_{sym}). UV-Vis (MeOH): 316 (6.2), 212 (3.7). ^1H NMR (300 MHz, d_6 -acetone): δ 7.70 (br s, 1H, -NH-), 7.51 (s, 1H, Im- H_5), 7.08 (s, 1H, Im- H_4), 5.21 (s, 2H, $-\text{CH}_2\text{-CO-}$), 3.50 (t, 2H, $-\text{CH}_2\text{Br}$), 3.39 (q (dt), 2H, $-\text{NH-CH}_2\text{-}$), 2.01 (m (tt), 2H, $-\text{CH}_2\text{-CH}_2\text{Br}$).

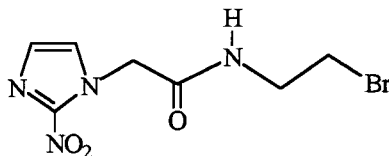


3.2.2.15 2-(2-Nitro-1-H-imidazol-1-yl)-N-(2-bromoethyl)acetamide [EBr1(-1)]

Synthesis 1

Reaction conditions similar to those for the synthesis of **EF3** were used: **7** (0.237 g, 1.37 mmol) was dissolved in THF (25 mL), and NMM (154 μL , 1.40 mmol) and *i*BuClFrm (196 μL , 1.50 mmol) were added. To the resulting pale yellow slurry were added $\text{H}_2\text{NCH}_2\text{CH}_2\text{Br}\cdot\text{HBr}$ (0.312 g, 1.53 mmol) and NMM (167 μL , 1.53 mmol). The mixture was then stirred at r.t. for 4 h before the white precipitate was filtered off and washed with Et_2O (3 x 5 mL). The pale yellow filtrate and washings were taken to dryness and the residue was chromatographed on a silica gel column. The desired product was collected in the first 3 fractions as its R_f was higher than those of the side-products and unreacted starting material. The purity of these fractions was confirmed by TLC analysis; the combined fractions were taken to dryness to give a pale yellow solid (0.269 g, 71%). Anal. calc. for $\text{C}_7\text{H}_9\text{N}_4\text{O}_3\text{Br}\cdot(0.5 \text{ THF})$: C, 35.90 ; H, 3.63 ; N, 17.53; found: C, 36.04 ; H, 3.92 ; N, 17.60. IR (ν , cm^{-1}): 3293 (N-H); 3108 (C-H_{Im}); 2923, 2854 (C-H); 1668 (C=O); 1488 (N-O_{asym}); 1370 (N-O_{sym}). UV-Vis (MeOH): 316 (6.4), 214 (3.5). ^1H NMR (300 MHz, CD_3OD): δ 7.41 (s, 1H, Im- H_5), 7.15 (s, 1H, Im- H_4), 5.13 (s, 2H, $-\text{CH}_2\text{-CO-}$), 3.58 (t, 2H, $-\text{NH-CH}_2\text{-}$), 3.43 (t, 2H, $-\text{CH}_2\text{Br}$); (300 MHz, d_6 -acetone) 7.99 (br s, 1H, $-\text{NH-CH}_2\text{-}$), 7.53 (s, 1H, Im- H_5), 7.17 (s, 1H, Im- H_4), 5.28 (s, 2H, $-\text{CH}_2\text{-CO-}$), 3.64 (q (dt), 2H, $-\text{NH-CH}_2\text{-}$), 3.52 (t, 2H, $-\text{CH}_2\text{Br}$). [The analysis in d_6 -acetone permitted identification of the triplet $-\text{NH-CH}_2\text{-}$ (methylene) signals found in the CD_3OD spectrum.]

^{13}C NMR (50 MHz, d_6 -acetone): δ 172.75 (-CO-), 134.84 and 134.26 (Im- C_4 and 5), 58.60 (- CH_2 -CO-), 48.24 (-NH- CH_2 -), 37.88 (- CH_2Br).



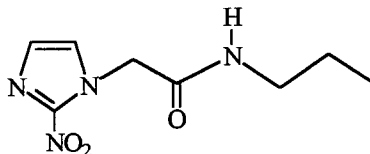
Synthesis 2

In a Schlenk tube under a flow of N_2 , **SR2508** (0.114 g, 0.533 mmol) was dissolved in DMF (6 mL). The solution was then acidified using $\text{HBr}_{(\text{g})}$ (pH acidity tests were accomplished using pH paper, the DMF sample first being added to H_2O ; the $\text{HBr}_{(\text{g})}$ line was flushed with N_2 prior to use as this reduces fuming that results from the presence of H_2O .) The N_2 -flow was resumed and PBr_3 (62.5 μL , 0.659 mmol) was added via syringe. The reaction was monitored by TLC and, after 3 h MeOH (10 mL) was added to quench unreacted PBr_3 . The mixture was then stirred for 5 min after which Et_3N was added until the mixture was strongly basic. Excess Et_3N and DMF were removed under vacuum and the remaining residue was chromatographed (CH_2Cl_2 :MeOH, 10:1). The eluate was collected in fractions, each analyzed using TLC; the fractions containing the product were combined and taken to dryness to yield a pale yellow solid (0.0177 g, 12 %).

3.2.2.16 2-(2-Nitro-1-H-imidazol-1-yl)-N-(propyl)acetamide [EPrA]

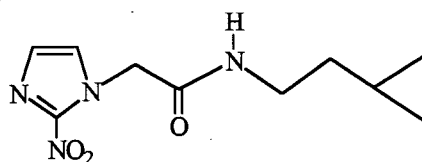
Reaction conditions similar to those for the synthesis of **EF3** were used: **7** (0.0808 g, 0.469 mmol) was dissolved in THF (10 mL), and NMM (50 μL , 0.467 mmol) and $i\text{BuClFrm}$ (70 μL , 0.536 mmol) were added. To the resulting yellow slurry were added $\text{H}_2\text{NCH}_2\text{CH}_2\text{CH}_3\cdot\text{HCl}$ (0.0466 g, 0.488 mmol) and NMM (56 μL , 0.513 mmol). The mixture was then stirred at r.t. for 4.5 h before the white precipitate was filtered off and washed with THF (3 x 5 mL). The filtrate and washings were taken to dryness and the desired product was isolated using preparative TLC (CH_2Cl_2 :MeOH, 10:1) to give a white solid (0.0301 g, 30 %). Anal. calc. for $\text{C}_8\text{H}_{12}\text{N}_4\text{O}_3$: C, 45.28 ; H, 5.70 ; N, 26.40; found: C, 45.21 ; H, 5.58 ; N, 26.27. IR (ν , cm^{-1}): 3290 (N-H); 3113 (C- H_{Im}); 2969, 2878 (C-H) 1662 (C=O); 1490 (N- O_{asym}); 1361 (N- O_{sym}). UV-Vis (MeOH): 316 (5.6), 228 (3.1). ^1H

NMR (300 MHz, d_6 -acetone): δ 7.52 (br s, 1H, -NH-CH₂-, overlapping with peak at 7.50), 7.50 (s, 1H, Im-*H*₅), 7.13 (s, 1H, Im-*H*₄), 5.20 (s, 2H, -CH₂-CO-), 3.20 (q (dt), 2H, -NH-CH₂-), 1.52 (sex (qt), 1H, -NHCH₂CH₂-), 0.89 (t, 3H, -CH₂-CH₃).



3.2.2.17 2-(2-Nitro-1-H-imidazol-1-yl)-N-(*iso*-amyl)acetamide [EIAA]

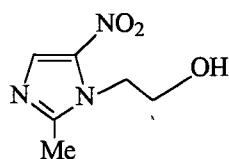
Reaction conditions similar to those for the synthesis of **EF3** were used: **7** (0.0812 g, 0.472 mmol) dissolved in THF (10 mL), and NMM (50 μ L, 0.467 mmol) and *i*BuClFrm (70 μ L, 0.536 mmol) were added. To the resulting yellow slurry was added H₂NCH₂CH₂CH(CH₃)₂ (59 μ L, 0.508 mmol). The mixture was then stirred at r.t. for 4 h before the white precipitate was filtered off and washed with THF (3 x 5 mL). The filtrate and washings were taken to dryness and the desired product was isolated using preparative TLC (CH₂Cl₂:MeOH, 20:1) to give a white solid (0.0773 g, 68%). Anal. calc. for C₁₀H₁₆N₄O₃: C, 49.99 ; H, 6.71 ; N, 23.32; found: C, 49.64 ; H, 6.56 ; N, 22.98. IR (ν , cm⁻¹): 3267 (N-H); 3127 (C-H_{Im}); 2958, 2875 (C-H); 1656 (C=O); 1490 (N-O_{asym}); 1374 (N-O_{sym}). UV-Vis (MeOH): 316 (7.1), 228 (4.0). ¹H NMR (300 MHz, d_6 -acetone): δ 7.52 (br s, 1H, -NH-CH₂-, overlapping with peak at 7.50), 7.50 (s, 1H, Im-*H*₅), 7.11 (s, 1H, Im-*H*₄), 5.20 (s, 2H, -CH₂-CO-), 3.27 (q (dt), 2H, -NH-CH₂-), 1.65 (m, 1H, -CH-(CH₃)₂), 1.38 (q (dt), 2H, -NHCH₂CH₂-), 0.88 (d, 6H, -CH(CH₃)₂).



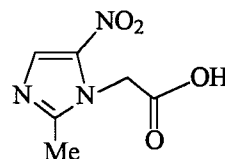
3.2.3 2-Methyl-5-Nitroimidazole Compounds

3.2.3.1 2-(2-Methyl-5-nitro-1*H*-imidazol-1-yl)acetic acid (**13**)

A slightly modified literature synthetic procedure was used.²⁰ In a 3-neck flask, metronidazole (3.33 g, 19.5 mmol) was dissolved in acetone (120 mL) under N₂. To the resulting white slurry was added Jones' Reagent (20 mL of {7g CrO₃ + 50 mL H₂O + 6.1 mL H₂SO₄}) dropwise via a pressure-equalized addition funnel, when a clear, dark orange solution resulted; this was then stirred at r.t. for 24 h to ensure complete oxidation of the alcohol to the corresponding acid. [After 3 h, TLC analysis revealed the presence of three compounds, the unreacted metronidazole, trace aldehyde and the acid ($R_{f(\text{aldehyde})} > R_{f(\text{alcohol})} > R_{f(\text{acid})}$).] The final mixture was now dark green and a green, oily deposit was observed. The mixture was filtered twice through a plug of Celite to remove the green oil, and the clear, pale yellow filtrate was rotovapped to dryness. The resulting residue was then dissolved in H₂O (50 mL) and the solution was transferred to a separatory funnel and washed with EtOAc (5 x 80 mL). The organic fractions were combined and dried over MgSO₄ (10 min) before filtration and rotary evaporation yielded a pale yellow solid (3.61g, 55 %); mp 176-178 °C (lit.²¹ mp 179-180 °C). ¹H NMR (200 MHz, D₂O): δ 8.00 (s, 1H, Im-*H*₄), 4.85 (s, 2H, -CH₂-), 2.40 (s, 3H, Im-CH₃). The NMR data are in agreement with previously reported values.²⁰



Metronidazole

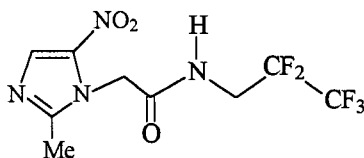


13

3.2.3.2 2-(2-Methyl-5-nitro-1*H*-imidazol-1-yl)-*N*-(2,2,3,3,3) pentafluoropropyl) acetamide [MF5]

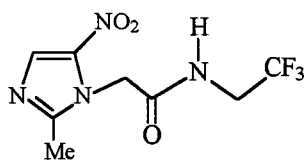
Compound **13** (0.130 g, 0.70 mmol) was dissolved in a 5:1 mixture of THF (25 mL) and DMF (5 mL) at 0°C under N₂ [**13** is sparingly soluble in neat THF].

NMM (80 μ L, 0.73 mmol) was then added and the clear, colourless mixture was stirred for 10 min before *i*BuClFrm (130 μ L, 1.00 mmol) was added. Stirring was continued for 30 min during which the reaction mixture became a pale yellow slurry. The ice-bath was removed, and $\text{H}_2\text{NCH}_2\text{CF}_2\text{CF}_3 \cdot \text{HCl}$ (0.149 g, 0.87 mmol) and NMM (95 μ L, 0.87 mmol) were added. The reaction slurry was then stirred at r.t. for 3 h when TLC analysis confirmed the presence of a single product. The creamy white precipitate that formed was filtered off and washed with THF (3 x 5 mL). The pale yellow filtrate was taken to dryness to give a yellow oil that was purified via column chromatography using THF as the eluent. Two bands were observed: the first, a pale yellow band and the second, a colourless one containing **MF5**. The second band was collected in several fractions and these were combined and taken to dryness to yield a white solid (0.117 g, 53 %). X-ray quality crystals were grown by slow evaporation of a concentrated MeOH solution of **MF5**. Anal. calc. for $\text{C}_9\text{H}_9\text{N}_4\text{O}_3\text{F}_5$: C, 34.19; H, 2.87; N, 17.53; found: C, 34.25; H, 2.99; N, 17.53. IR (ν , cm^{-1}): 3212 (N-H); 3028 (C-H_{Im}); 2921, 2851 (C-H); 1670 (C=O); 1473 (N-O_{asym}); 1368 (N-O_{sym}). UV-Vis (MeOH): 310 (8.1), 230 (3.7), 212 (3.9). ^1H NMR (300 MHz, CD_3OD): δ 8.07 (s, 1H, Im- H_4), 5.24 (s, 2H, $-\text{CH}_2\text{-CO-}$), 4.08 (t, 2H, $-\text{CH}_2\text{CF}_2-$), 2.54 (s, 3H, Im- CH_3); (300 MHz, CDCl_3) δ 7.93 (s, 1H, Im- H_4), 6.28 (br s, 1H, $-\text{NH-}$), 4.93 (s, 2H, $-\text{CH}_2\text{-CO-}$), 3.97 (dt, 2H, $-\text{CH}_2\text{CF}_2-$), 2.47 (s, 3H, Im- CH_3). $^{19}\text{F}\{^1\text{H}\}$ NMR (188 MHz, CD_3OD): δ -7.56 (t, $-\text{CF}_3$), -44.63 (q, $-\text{CF}_2-$); (188 MHz, CDCl_3) δ -8.17 (t, $-\text{CF}_3$), -45.79 (q, $-\text{CF}_2-$).



3.2.3.3 2-(2-Methyl-5-nitro-1*H*-imidazol-1-yl)-*N*-(2,2,2-trifluoroethyl) acetamide [MF3(-1)]

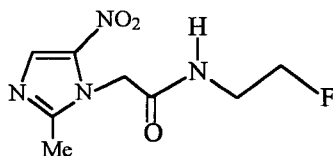
Reaction conditions similar to those for the synthesis of **MF5** were employed: **13** (0.252 g, 1.359 mmol) was added to THF (15 mL) and NMM (150 μ L, 1.361 mmol) and *i*BuClFrm (192 μ L, 1.472 mmol) were added (**13** is not completely soluble in THF but the subsequent addition of base increases solubility). The resulting off-white slurry was then stirred at 0°C before H₂NCH₂CF₃•HCl (0.202 g, 1.490 mmol) and NMM (164 μ L, 1.489 mmol) were added. The mixture was then warmed to r.t. and stirred for 4.5 h. The precipitate that formed was filtered off and the filtrate taken to dryness. Purification of the desired product from the residue was achieved via column chromatography (THF). It was imperative to elute dropwise (slowly) to ensure the separation of the desired product from a number of side-products (as seen from TLC analysis). **MF3(-1)** was the third and most concentrated band to elute from the column. The fractions from this band were combined and taken to dryness to give an off-white solid (0.291 g, 80 %). Anal. calc. for C₈H₉N₄O₃F₃: C, 36.10; H, 3.41; N, 21.05; found: C, 36.24; H, 3.25; N, 20.01. IR (ν , cm⁻¹): 3304 (N-H); 3117 (C-H_{Im}); 2960, 2871 (C-H); 1678 (C=O); 1471 (N-O_{asym}); 1373 (N-O_{sym}). UV-Vis (MeOH): 310 (8.6), 230 (3.5), 210 (4.0). ¹H NMR (300 MHz, d₆-acetone): δ 8.26 (br s, 1H, -NH-), 7.92 (s, 1H, Im-*H*₄), 5.25 (s, 2H, -CH₂-CO-), 4.05 (qd, 2H, -CH₂CF₃), 2.43 (s, 3H, Im-CH₃). ¹⁹F{¹H} NMR (188 MHz, d₆-acetone): δ 4.76 (s, -CF₃).



3.2.3.4 2-(2-Methyl-5-nitro-1*H*-imidazol-1-yl)-*N*-(2-fluoroethyl)acetamide [MF1(-1)]

Reaction conditions similar to those for the synthesis of **MF3(-1)** were used: **13** (0.251 g, 1.359 mmol) was dissolved in THF (15 mL), and NMM (150 μ L, 1.361 mmol)

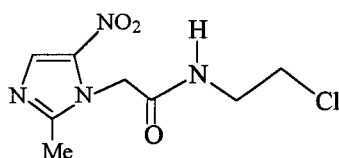
and *i*BuClFrm (192 μ L, 1.472 mmol) were added. To the resulting white slurry at 0°C were added $\text{H}_2\text{NCH}_2\text{CH}_2\text{F}\cdot\text{HCl}$ (0.155 g, 1.560 mmol) and NMM (164 μ L, 1.489 mmol). The mixture was warmed to r.t. and stirred for 4.5 h before the precipitate formed was filtered off. The filtrate was taken to dryness and the residue purified via column chromatography (THF); dropwise (slow) elution yielded **MF1(-1)** (fourth and most concentrated band) as several fractions from the column. These fractions were combined and taken to dryness to yield a pale yellow solid (0.207 g, 66 %). Anal. calc. for $\text{C}_8\text{H}_{11}\text{N}_4\text{O}_3\text{F}$: C, 41.74; H, 4.82; N, 24.34; found: C, 41.85; H, 4.80; N, 24.11. IR (ν , cm^{-1}): 3288 (N-H); 3110 (C-H_{Im}); 2956, 2874 (C-H); 1668 (C=O); 1463 (N-O_{asym}); 1367 (N-O_{sym}). UV-Vis (MeOH): 310 (9.2), 226 (4.7), 210 (5.4). ^1H NMR (300 MHz, d_6 -acetone) δ 7.80 (br s, 2H, -NH- + Im- H_4), 5.16 (s, 2H, -CH₂-CO-), 4.50 (dt, 2H, -CH₂F, $^2J_{\text{HF}}$ = 42 Hz), 3.55 (dq (ddt), 2H, -NH-CH₂-, $^3J_{\text{HF}}$ = 26 Hz), 2.45 (s, 3H, Im-CH₃). ^{19}F NMR (282 MHz, d_6 -acetone) δ -144.91 (spt (tt), $^2J_{\text{HF}}$ = 50.5 Hz, $^3J_{\text{HF}}$ = 25.7 Hz, -CH₂F).



3.2.3.5 2-(2-Methyl-5-nitro-1*H*-imidazol-1-yl)-*N*-(2-chloroethyl)acetamide [MC11(-1)]

Reaction conditions similar to those for the synthesis of **MF1(-1)** were used: **13** (0.301 g, 1.62 mmol) was dissolved in THF (20 mL), and NMM (165 μ L, 1.62 mmol) and *i*BuClFrm (220 μ L, 1.73 mmol) were added. To the resulting white slurry at 0°C were added $\text{H}_2\text{NCH}_2\text{CH}_2\text{Cl}\cdot\text{HCl}$ (0.200 g, 1.73 mmol) and NMM (184 μ L, 1.73 mmol). The mixture was warmed to r.t. and stirred for 5.5 h. The precipitate formed was removed via filtration and the pink filtrate was taken to dryness to yield an orange-pink oil that was purified using preparative TLC (CH_2Cl_2 :MeOH, 10:1). The major band (lowest R_f) was isolated to give a white, microcrystalline solid (0.190 g, 47 %). Anal. calc. for

$C_8H_{11}N_4O_3Cl$: C, 38.96; H, 4.50; N, 22.71; found: C, 37.28; H, 4.68; N, 20.89. LR-MS [DCI(+)]: 249, 247 ($M^+ + H$), 202, 200 ($M^+ - NO_2$). HR-MS [DCI(+)] calc. for $C_8H_{11}N_4O_3^{37}Cl$ ($C_8H_{11}N_4O_3^{35}Cl$): 249.05684 (247.05980); found 249.05725 (247.05896). IR (ν , cm^{-1}): 3312 (N-H); 3028 (C-H_{Im}); 2921, 2851 (C-H); 1670 (C=O); 1473 (N-O_{asym}); 1368 (N-O_{sym}). UV-Vis (MeOH): 310 (6.9), 232 (2.9), 210 (3.7). 1H NMR (300 MHz, d_6 -acetone) δ 7.94 (br s, 2H, -NH- + Im- H_4), 5.16 (s, 2H, -CH₂-CO-), 3.69 (t, 2H, -CH₂Cl), 3.61 (q (dt), 2H, -NH-CH₂-), 2.46 (s, 3H, Im-CH₃).



Of note, this reaction was not as clean when compared to those for the preparation of **MF3(-1)** and **MF1(-1)**. TLC analysis reveals the presence of two other major products having R_f values higher than that of **MCI1(-1)**; a small amount of unreacted **13** ($R_f = 0$) was also observed. Comparison of the TLC for authentic samples of **MF1(-1)** and **MBr1(-1)** with the reaction mixture facilitated identification of the desired product (Figure 3-3).

1H NMR spectroscopic analysis of band 1 revealed the presence of the methyl ester (**14**), probably formed from the reaction of acyl carbonate with MeOH on the preparative TLC plate [1H NMR (300 MHz, d_6 -acetone): δ 7.99 (s, 1H, Im- H_4), 5.11 (s, 2H, -CH₂-), 3.72 (s, 3H, -CH₃), 2.42 (s, 3H, Im-CH₃)]. For band 2, the isolated white crystalline solid (in relatively high concentration) was determined to be the isobutyl ester side-product (**15**) (analogous to **11**, Scheme 3-13, p. 106). This finding suggests that H₂O was present during the reaction, likely coming from the extremely hygroscopic amine hydrochloride. 1H NMR (300 MHz, d_6 -acetone): δ 7.96 (s, 1H, Im- H_4), 5.26 (s, 2H, -CH₂-CO-), 3.97 (d, 2H, O-CH₂-), 2.49 (s, 3H, Im-CH₃), 1.93 (m, 1H, -CH-(CH₃)₂), 0.91 (d, 6H, -CH-(CH₃)₂).

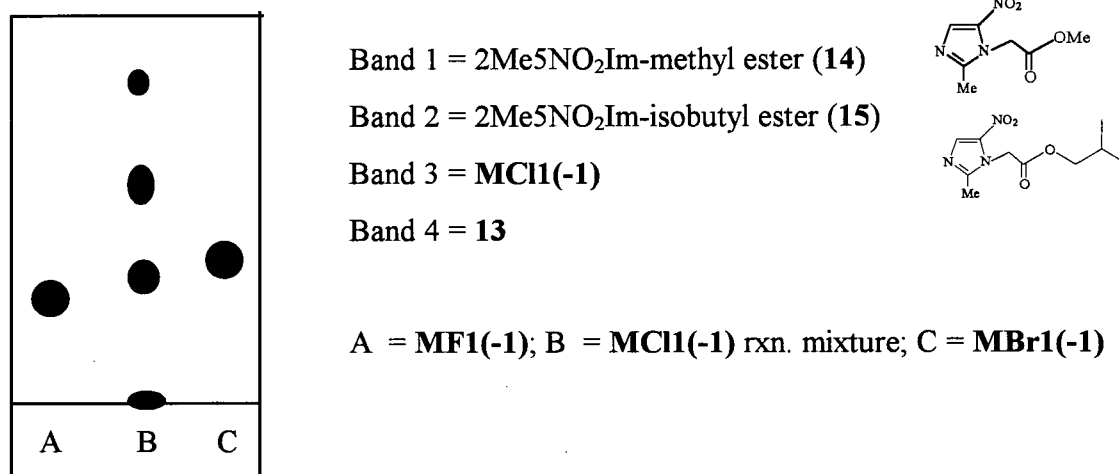
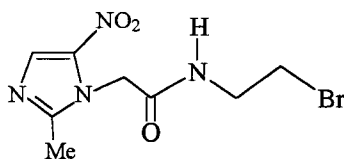


Figure 3-3: TLC analysis of **MX1(-1)** compounds (X = F, Cl, Br).

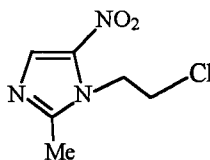
3.2.3.6 2-(2-Methyl-5-nitro-1*H*-imidazol-1-yl)-N-(2-bromoethyl)acetamide [**MBr1(-1)**]

Reaction conditions similar to those for the synthesis of **MF1(-1)** were used: **13** (0.108 g, 0.586 mmol) was dissolved in THF (10 mL) and NMM (65 μ L, 0.590 mmol) and *i*BuClFrm (83 μ L, 0.636 mmol) were added. To the resulting white slurry at 0°C were added H₂NCH₂CH₂Br•HBr (0.135 g, 0.660 mmol) and NMM (73 μ L, 0.663 mmol). The mixture was warmed to r.t. and stirred for 5 h. The precipitate was filtered off and the filtrate was taken to dryness. The resulting residue was chromatographed using preparative TLC (CH₂Cl₂:MeOH, 20:1), and the major band was isolated to yield an off-white solid (0.137 g, 80 %). Anal. calc. for C₈H₁₁N₄O₃Br: C, 33.01; H, 3.81; N, 19.25 [with 0.1 mol acetone C, 33.58; H, 3.94; N 18.87]; found: C, 33.69; H, 3.75; N, 18.66. IR (ν , cm⁻¹): 3295 (N-H); 3100 (C-H_{Im}); 2926, 2854 (C-H); 1661 (C=O); 1458 (N-O_{asym}); 1372 (N-O_{sym}). UV-Vis (MeOH): 310 (8.9), 228 (3.7), 210 (4.8). ¹H NMR (300 MHz, d₆-acetone) δ 7.91 (br s, 2H, -NH- + Im-H₄), 5.16 (s, 2H, -CH₂-CO-), 3.65 (q (dt), 2H, -NH-CH₂-), 3.53 (t, 2H, -CH₂Br), 2.45 (s, 3H, Im-CH₃).



3.2.3.7 (2-Methyl-5-nitro-1H-imidazol-1-yl)-N-(2-chloroethane) (16)

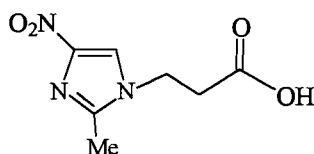
Reaction conditions similar to those described for the synthesis of **EC11(-1)** were used (see synthesis 2, p. 70). In a flask equipped with a reflux condenser, CHCl_3 (10 mL) was added to metronidazole (0.434 g, 2.54 mmol) at 0 °C to give a white slurry. TsCl (0.672 g, 3.53 mmol) and py (380 μL , 4.71 mmol) were then added simultaneously, and the reaction mixture was stirred for 0.5 h. The ice-bath was removed and the mixture was permitted to warm to r.t. over ~2 h. In attempts to isolate both the tosylated intermediate and the chlorinated metronidazole at this stage, the mixture was taken to dryness and the residue was column chromatographed. CH_2Cl_2 was first used to elute unreacted TsCl . Afterwards, the eluent strength was then increased to 5% MeOH and a pale yellow band emerged followed by a colourless band. These were identified to contain the desired product (**16**) and the unreacted metronidazole, respectively. No evidence for the presence of the tosylate was seen. The yellow fractions were combined and taken to dryness. A small amount of py present, as evidenced by TLC analysis, was removed under vacuum. The final product was isolated as a yellow, microcrystalline solid (0.125 g, 26%). Anal. calc. for $\text{C}_6\text{H}_8\text{N}_3\text{O}_2\text{Cl}$: C, 38.01; H, 4.25; N, 22.16; found: C, 37.79; H, 3.96; N, 22.56. LR-MS $[\text{DCI}(+)]$: 190 (M^+). HR-MS $[\text{DCI}(+)]$ calc. for $\text{C}_6\text{H}_8\text{N}_3\text{O}_2^{37}\text{Cl}$ ($\text{C}_6\text{H}_8\text{N}_3\text{O}_2^{35}\text{Cl}$): 192.03539 (190.03833); found 192.03610 (190.03792). ^1H NMR (300 MHz, d_6 -acetone) δ 7.96 (s, 1H, Im- H_4), 4.80 (t, 2H, $-\text{CH}_2\text{-Cl}$), 4.09 (t, 2H, Im- CH_2 -), 2.60 (s, 3H, Im- CH_3).

**16**

3.2.4 2-Methyl-4-Nitroimidazole Compounds

3.2.4.1 2-(2-Methyl-4-nitro-1-H-imidazol-1-yl)propionic acid (17)

This synthesis was adapted from the nitrile hydrolysis procedure reported by Mann and Porter.²² 2-Methyl-4-nitro-1-imidazolepropionitrile (2.709 g, 15.0 mmol) and NaNO₂ (1.384 g, 20.1 mmol) were refluxed in aqueous 40% H₂SO₄ solution (25 mL). TLC analysis revealed that the reaction was complete after 2.5 d. The solution was neutralized with 6M NaOH and then the pH adjusted to 3.23 using 0.1 M HCl and 0.1 M NaOH. The resulting 17 precipitate was collected, washed with H₂O (2 x 25 mL) and dried *in vacuo* to yield a white powder (2.287g, 76 %). The purity of the compound was confirmed by melting point (mp: found 223-225 °C, reported 221-225°C (Aldrich)) and ¹H NMR (200 MHz, d₆-dmsO) δ 8.32 (s, 1H, Im-H₅), 4.18 (t, 2H, -CH₂-CO-), 2.84 (t, 2H, Im-CH₂-), 2.39 (s, 3H, Im-CH₃).

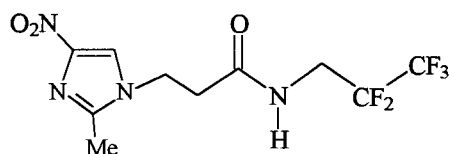


17

3.2.4.2 3-(2-Methyl-4-nitro-1-H-imidazol-1-yl)-N-(2,2,3,3,3-pentafluoropropyl)propionamide [2M4NF5]

17 (0.305 g, 1.53 mmol) was placed in a 25 mL two-neck flask under N₂, and THF (10 mL) was added. To the resulting white slurry was added DMF dropwise (~3 mL) until a clear, colourless solution was obtained. NMM (169 µL, 1.53 mmol) was then added and the mixture stirred for 10 min at 0°C before iBuClFrm (215 µL, 1.65 mmol) was next added. Stirring was continued for 30 min during which a pale yellow slurry formed. The ice-bath was removed, H₂NCH₂CF₂CF₃•HCl (0.311 g, 1.82 mmol) and NMM (200 µL, 1.83 mmol) were added and the slurry was stirred at r.t. for 4 h. The white precipitate that formed was filtered off and washed with dry THF (3 x 5 mL). The filtrate was reduced in volume to ~5 mL before Et₂O was added slowly. A resulting pale yellow

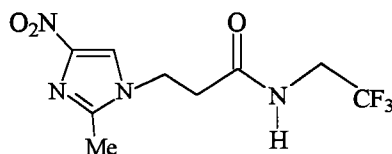
precipitate was isolated via filtration, but TLC analysis revealed later that this precipitate was not **2M4NF5**. The filtrate was stored at 0°C overnight, resulting in the formation of clear, pale yellow crystals which were isolated via filtration (0.403 g, 83%). X-ray quality crystals were obtained from slow evaporation of a concentrated MeOH solution of **2M4NF5**. Anal. calc. for C₁₀H₁₁N₄O₃F₅: C, 36.37; H, 3.36; N, 16.97; found: C, 36.67; H, 3.45; N, 16.69. IR (ν , cm⁻¹): 3260 (N-H); 3128 (C-H_{Im}); 3079, 2921 (C-H); 1674 (C=O); 1506 (N-O_{asym}); 1400 (N-O_{sym}). UV-Vis (MeOH): 300 (6.2), 224 (3.6), 210 (4.2). ¹H NMR (300 MHz, d₆-dmso) δ 8.69 (t, 1H, -NH-), 8.22 (s, 1H, Im-H₅), 4.23 (t, 2H, -CH₂-CO-), 3.96 (td, 2H, ³J_{HF} = 16.5 Hz, -CH₂-CF₂-), 2.78 (t, 2H, Im-CH₂-), 2.38 (s, 3H, Im-CH₃). ¹⁹F{¹H} NMR (188 MHz, d₆-dmso) δ -7.06 (t, -CF₃), -43.99 (q, -CF₂-).



3.2.4.3 3-(2-Methyl-4-nitro-1-H-imidazol-1-yl)-N-(2,2,2-trifluoroethyl)propionamide [**2M4NF3(-1)**]

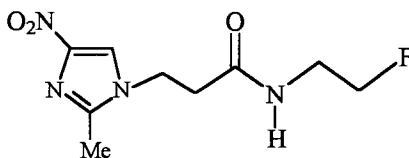
Reaction conditions similar to those for the synthesis of **2M4NF5** were used: **17** (0.308 g, 1.55 mmol) was dissolved in THF (10 mL) and DMF (~3 mL), and NMM (170 μ L, 1.55 mmol) and iBuClFrm (220 μ L, 1.68 mmol) were added. To the resulting yellow/pink slurry were added H₂NCH₂CF₃•HCl (0.234 g, 1.73 mmol) and NMM (190 μ L, 1.74 mmol). The mixture was stirred at r.t. for 4 h before the white solid was filtered off and washed with THF (3 x 5 mL). The THF volume was reduced to ~5 mL under vacuum and then Et₂O was added until a cloudy white mixture persisted. This mixture was stored at 0°C for 16 h to yield a white, microcrystalline solid (0.377 g, 87%). Anal. calc. for C₉H₁₁N₄O₃F₃: C, 38.58; H, 3.96; N, 19.99; found: C, 38.79; H, 3.93; N, 19.78. IR (ν , cm⁻¹): 3263 (N-H); 3122 (C-H_{Im}); 3076, 2946 (C-H); 1675 (C=O); 1506 (N-O_{asym}); 1400 (N-O_{sym}). UV-Vis (MeOH): 300 (6.3), 224 (3.8), 212 (3.9). ¹H NMR (300 MHz,

d_6 -dmsO) δ 8.70 (t, 1H, -NH-), 8.21 (s, 1H, Im- H_5), 4.20 (t, 2H, -CH₂-CO-), 3.90 (sex (qd), 2H, -CH₂-CF₃), 2.73 (t, 2H, Im-CH₂-), 2.37 (s, 3H, Im-CH₃). $^{19}\text{F}\{^1\text{H}\}$ NMR (188 MHz, d_6 -dmsO) δ 5.63 (s, -CF₃).



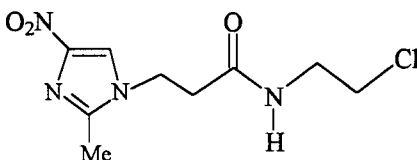
3.2.4.4 3-(2-Methyl-4-nitro-1-H-imidazol-1-yl)-N-(2-fluoroethyl) propionamide [2M4NF1(-1)]

Reaction conditions similar to those for the synthesis of **2M4NF5** were used: **17** (0.308 g, 1.55 mmol) was dissolved in THF (10 mL) and DMF (~3 mL), and NMM (170 μL , 1.55 mmol) and *i*BuClFrm (220 μL , 1.68 mmol) were added. To the resulting yellow/pink slurry was added H₂NCH₂CH₂F•HCl (0.174 g, 1.74 mmol) and NMM (190 μL , 1.74 mmol). The mixture was stirred at r.t. for 5 h before the white solid was filtered off and washed with THF (3 x 5 mL). The volume of the pink filtrate was reduced to ~3 mL under vacuum, followed by the addition of Et₂O until a cloudy white mixture persisted. Sonication of the mixture for 5 min at 5 °C and then filtration yielded a white microcrystalline solid (0.290 g, 77%). X-ray quality crystals were grown from slow evaporation of a concentrated MeOH solution of **2M4NF1(-1)**. Anal. calc. for C₉H₁₃N₄O₃F: C, 44.25; H, 5.37; N, 22.94; found: C, 44.38; H, 5.34; N, 22.75. IR (ν , cm⁻¹): 3298 (N-H); 3110 (C-H_{Im}); 3073, 2947 (C-H); 1668 (C=O); 1504 (N-O_{asym}); 1396 (N-O_{sym}). UV-Vis (MeOH): 300 (9.1), 210 (7.0). ^1H NMR (300 MHz, d_6 -dmsO) δ 8.28 (t, 1H, -NH-), 8.23 (s, 1H, Im- H_5), 4.37 (dt, 2H, -CH₂F, $^2J_{\text{HF}}$ = 56 Hz), 4.19 (t, 2H, -CH₂-CO-), 3.31 (dq (ddt), 2H, -CH₂-CH₂F, $^3J_{\text{HF}}$ = 28 Hz), 2.69 (t, 2H, Im-CH₂-), 2.38 (s, 3H, Im-CH₃). ^{19}F NMR (282 MHz, d_6 -dmsO) δ -142.64 (spt (tt), $^2J_{\text{HF}}$ = 49.2 Hz, $^3J_{\text{HF}}$ = 24.2 Hz).



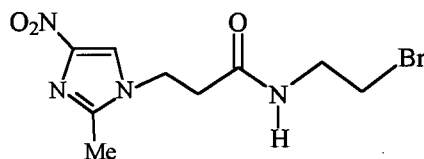
3.2.4.5 3-(2-methyl-4-nitro-1-H-imidazol-1-yl)-N-(2-chloroethyl)propionamide [2M4NCl1(-1)]

Reaction conditions similar to those for the synthesis of **2M4NF5** were used: **17** (0.306 g, 1.54 mmol) was dissolved in THF (10 mL) and DMF (~3 mL), and NMM (169 μ L, 1.54 mmol) and *i*BuClFrm (220 μ L, 1.68 mmol) were added. To the resulting yellow/pink slurry were added $\text{H}_2\text{NCH}_2\text{CH}_2\text{Cl}\cdot\text{HCl}$ (0.195 g, 1.69 mmol) and NMM (188 μ L, 1.69 mmol). The mixture was stirred at r.t. for 4 h before the white solid was filtered off and washed with THF (3 x 5 mL). The colourless filtrate was taken to dryness to give an oily white residue; TLC analysis indicated several side-products. The residue was chromatographed using preparative TLC (CH_2Cl_2 :MeOH, 20:1); the major band yielded a colourless oil. Addition of a small volume (~3 mL) of MeOH to the oil, followed by addition of Et_2O (15 mL) led to a cloudy white mixture. The white slurry was stored at r.t. for 2 h, before sonication (5 min at 5 $^\circ\text{C}$) and then filtration gave a white, microcrystalline solid (0.315 g, 79%). Anal. calc. for $\text{C}_9\text{H}_{13}\text{N}_4\text{O}_3\text{Cl}$: C, 41.47; H, 5.03; N, 21.49; found: C, 41.83; H, 4.81; N, 20.64. IR (ν , cm^{-1}): 3258 (N-H); 3119 (C-H_{Im}); 3079, 2923 (C-H); 1666 (C=O); 1499 (N-O_{asym}); 1384 (N-O_{sym}). UV-Vis (MeOH): 302 (6.7), 226 (3.9), 212 (4.3). ^1H NMR (300 MHz, d_6 -acetone) δ 8.03 (s, 1H, Im- H_5), 7.60 (br s, 1H, -NH-), 4.38 (t, 2H, - CH_2 -CO-) 3.60 (t, 2H, - CH_2Cl), 3.51(q (dt), 2H, - CH_2 - CH_2Cl), 2.84 (t, 2H, Im- CH_2 -), 2.44 (s, 3H, Im- CH_3).



3.2.4.6 2-(2-methyl-4-nitro-1-H-imidazol-1-yl)-N-(2-bromoethyl)propionamide [2M4NBr1(-1)]

Reaction conditions similar to those for the synthesis of **2M4NF5** were used: **17** (0.307 g, 1.54 mmol) was dissolved in THF (10 mL) and DMF (~3 mL), and NMM (169 μ L, 1.54 mmol) and *i*BuClFrm (220 μ L, 1.68 mmol) were added. To the resulting pale yellow slurry were added $\text{H}_2\text{NCH}_2\text{CH}_2\text{Br}\cdot\text{HBr}$ (0.347 g, 1.70 mmol) and NMM (189 μ L, 1.70 mmol). The mixture was stirred at r.t. for 6 h. A workup identical to that used for **2M4NCl1(-1)** yielded clear, colourless crystals (0.098 g, 21%). Anal. calc. for $\text{C}_9\text{H}_{13}\text{N}_4\text{O}_3\text{Br}$: C, 35.43; H, 4.29; N, 18.36; found: C, 35.62; H, 4.28; N, 18.65. IR (ν , cm^{-1}): 3259 (N-H); 3115 (C-H_{Im}); 3072, 2918 (C-H); 1660 (C=O); 1499 (N-O_{asym}); 1399 (N-O_{sym}). UV-Vis (MeOH): 300 (7.4), 226 (4.4), 210 (5.6). ^1H NMR (300 MHz, d_6 -acetone) δ 8.03 (s, 1H, Im-*H*₅), 7.67 (br s, 1H, -NH-), 4.36 (t, 2H, -CH₂-CO-), 3.56 (q (dt), 2H, -CH₂-CH₂Br), 3.44 (t, 2H, -CH₂Br), 2.83 (t, 2H, Im-CH₂-), 2.42 (s, 3H, Im-CH₃).

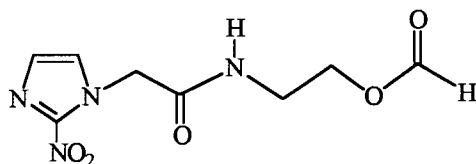


3.2.5 Reactions of SR2508 with Tf₂O

3.2.5.1 2-(2-Nitro-1-H-imidazol-1-yl)-N-(ethylformate)acetamide (18)

This reaction was carried out in an attempt to synthesize the triflate analogue of **SR2508**; however, the presumed triflate was too reactive as demonstrated by the results from the attempted synthesis. In a Schlenk tube under 1 atm N₂, CH₂Cl₂ (15 mL) and DMF (3 mL) were added to **SR2508** (0.303 g, 1.14 mmol) to give a clear, colourless solution; this was then stirred at 0 °C for 30 min before py (320 μ L, 3.95 mmol) and subsequently (CF₃SO₂)₂O (342 μ L, 3.95 mmol) were added dropwise. The ice-bath was removed and the dark orange reaction mixture was stirred for 3 h at r.t. TLC analysis

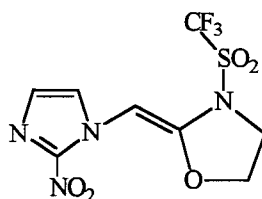
(using THF) revealed the presence of three products characterized by a bright yellow band ($R_f = 0.95$, **19**), a colourless band ($R_f = 0.65$, **18**) and another colourless band ($R_f = 0.10$, unidentified). The solvent was removed (under high vacuum) and **18** was isolated using column chromatography (THF); further purification via sublimation (at 130 °C under vacuum) yielded a white solid (0.703 g, 67 %). Anal. calc. for $C_8H_{10}N_4O_5$: C, 39.67; H, 4.16; N, 23.13; found: C, 39.90; H, 4.15; N, 23.03. LR-MS [EI(+)] : 243 (M^+), 196 ($M^+ - NO_2$). IR (ν , cm^{-1}): 3275 (N-H); 3096 (C-H_{Im}); 2940 (C-H); 1716 (C=O_{ald}); 1655 (C=O_{amide}); 1487 (N-O_{asym}); 1362 (N-O_{sym}). 1H NMR (300 MHz, d_6 -acetone): δ 8.13 (s, 1H, -CHO), 7.80 (br. s, 1H, -NH-), 7.50 (s, 1H, Im-H₅), 7.14 (s, 1H, Im-H₄), 5.25 (s, 2H, -CH₂-CO-), 4.21 (t, 2H, -CH₂-O), 3.55 (q (dt), 2H, -NH-CH₂-). ^{13}C NMR (75 MHz, d_6 -acetone): δ 166.7 (-CO-NH-), 161.8 (-CHO), 128.7 and 128.2 (Im-C₄ and ₅), 62.8 (-CH₂-CO-), 52.5 (-NH-CH₂-), 39.0 (-CH₂-O).

**18**

3.2.5.2 CycF3 (**19**)

Conditions similar to those for the synthesis of **18** were used, except that DMF was not used. Following addition of $(CF_3SO_2)_2O$, the slurry became a clear, bright yellow solution; stirring was continued for 1 h at 0 °C and 2 h at r.t. during which a yellow slurry was formed. The mixture was filtered and the filtrate was reduced in volume to ~5 mL. before Et₂O (25 mL) was added to yield a white precipitate. The solid was filtered off and the yellow filtrate was reduced in volume to ~2 mL before being column chromatographed ($CH_2Cl_2 \rightarrow CH_2Cl_2$:acetone, 4:1). The first eluted band ($R_f = 0.85$, yellow) yielded **19**, a brilliant yellow powder (0.135 g, 36 %). Crystals suitable for X-ray analysis were obtained from slow evaporation of a solution of the compound in a 1:1 mixture of CH_2Cl_2 :acetone. Anal. calc. for $C_8H_7N_4O_5SF_3$: C, 29.28; H, 2.15; N, 17.07; found: C, 29.15; H, 2.22; N,

17.42. LR-MS [DCI(+)]: 329 ($M^+ + H$). IR (ν , cm^{-1}): 3155 ($\text{C-H}_{\text{alkene}}$); 2980 (C-H_{Im}); 2918 (C-H); 1710 (C-O); 1485 (N-O_{asym}); 1362 (N-O_{sym}); 1203 (S=O). UV-Vis (MeOH): 314 (4.3). ^1H NMR (300 MHz, d_6 -acetone): δ 7.58 (d, 1H, Im- H_5), 7.17 (d, 1H, Im- H_4), 6.78 (s, $-\text{CH}=\text{C}-$), 4.64 (t, 2H, $-\text{CH}_2\text{-O}-$), 4.36 (t, 2H, $-\text{N-CH}_2-$). ^{13}C NMR (75 MHz, d_6 -acetone): δ 146.5 ($-\text{CH}=\text{C}-$), 128.6 and 127.8 (Im- C_4 and C_5), 120.9 (q, $-\text{CF}_3$), 89.0 ($-\text{CH}=\text{C}-$), 68.8 ($-\text{CH}_2\text{-O}-$), 49.9 ($-\text{N-CH}_2-$). $^{19}\text{F}\{^1\text{H}\}$ NMR (188 MHz, d_6 -acetone): δ 0.88 (s, $-\text{CF}_3$).

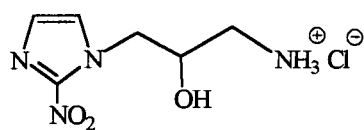


19

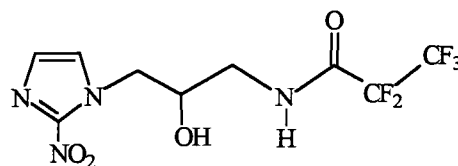
3.2.6 Reactions with RSU1111

3.2.6.1 Synthesis of (20), a pentafluorinated derivative of RSU1111

The same reaction procedure to synthesize **RevEF5** (synthesis 3) was used to synthesize **20**. $\text{CF}_3\text{CF}_2\text{CO}_2\text{H}$ (105 μL , 1.00 mmol) was dissolved in THF (15 mL) and NMM (110 μL , 1.05 mmol) and $i\text{BuClFrm}$ (150 μL , 1.15 mmol) were added. To the resulting white slurry were added **RSU1111** (0.206 g, 1.07 mmol) and NMM (125 μL , 1.19 mmol). Stirring was continued at r.t. for 20 h before the yellow precipitate that formed was filtered off, washed with THF (3 x 5 mL) and the filtrate purified via column chromatography (CH_2Cl_2 :acetone, 20:1). Two bands eluted, and the minor band with $R_f = 0.60$ was isolated to yield **20** as a colourless oil (0.0155 g, 5 %). LR-MS [DCI(+)]: 350 ($M^+ + \text{NH}_4$), 333 ($M^+ + H$). HR-MS [DCI(+)] calc. for $\text{C}_9\text{H}_{10}\text{O}_4\text{N}_4\text{F}_5$: 333.06221; found 333.06198. ^1H NMR (300 MHz, d_6 -acetone): δ 8.76 (br. s, 1H, $-\text{NH}-$), 7.54 (s, 1H, Im- H_5), 7.09 (s, 1H, Im- H_4), 4.90 (d, 1H, $-\text{OH}$), 4.78 (dd, 1H, Im- $\text{CH}(\text{H})-$), 4.38 (dd, 1H, Im- $\text{CH}(\text{H})-$), 4.22 (m, 1H, $-\text{CH}(\text{OH})-$), 3.50 (m, 2H, $-\text{CH}_2\text{-NH}-$). $^{19}\text{F}\{^1\text{H}\}$ NMR (188 MHz, d_6 -acetone): δ -6.77 (t, $-\text{CF}_3$), -46.35 (q, $-\text{CF}_2-$).



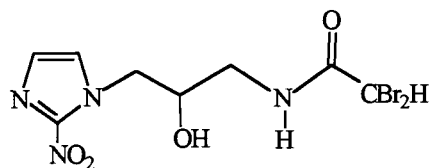
RSU1111



20

3.2.6.2 Synthesis of (21), a dibromo derivative of RSU1111

Reaction conditions including stoichiometries identical to those for the synthesis of compound **20** were used except $\text{CBr}_3\text{CO}_2\text{H}$ was used instead of $\text{CF}_3\text{CF}_2\text{CO}_2\text{H}$. The white precipitate that formed was filtered off, washed with THF (3×5 mL) and the filtrate was purified using the CTRON (Et_2O :acetone, 1:1). Two bands eluted and the second band ($R_f = 0.65$) gave a yellow oil. Addition of Et_2O yielded a white precipitate that was isolated via filtration and dried *in vacuo* (0.0184 g, 5 %). Anal. calc. for $\text{C}_8\text{H}_{10}\text{N}_4\text{O}_4\text{Br}_2$: C, 24.89; H, 2.61; N, 14.51; found: C, 25.60; H, 2.65; N, 13.54. LR-MS $[\text{EI}(+)]$: 387 ($\text{M}+1$), 340 ($\text{M}^+ - \text{NO}_2$), 156 ($\text{M}^+ - \text{CH}_2\text{NHCOCBr}_2\text{H}$), 114 ($2\text{NO}_2\text{Im}$), 80 (Br). HR-MS $[\text{EI}(+)]$ calc. for $\text{C}_8\text{H}_{10}\text{O}_4\text{N}_4^{81}\text{Br}_2$ ($\text{C}_8\text{H}_{10}\text{O}_4\text{N}_4^{81}\text{Br}^{79}\text{Br}$) [$\text{C}_8\text{H}_{10}\text{O}_4\text{N}_4^{79}\text{Br}_2$]: 388.91061 (386.91266) [384.91470]; found 388.91604 (386.91227) [384.91401]. ^1H NMR (300 MHz, CD_3OD): δ 7.46 (s, 1H, Im- H_5), 7.13 (s, 1H, Im- H_4), 6.21 (s, 1H, $-\text{CBr}_2\text{H}$), 4.67 (dd, 1H, Im- $\text{CH}(\text{H})-$), 4.29 (dd, 1H, Im- $\text{CH}(\text{H})-$), 4.05 (m, 1H, $-\text{CH}(\text{OH})-$), 3.38 (dd, 2H, $-\text{CH}_2-\text{NH}-$). ^{13}C NMR (75 MHz, CD_3OD): δ 151.7 ($-\text{C}=\text{O}$), 129.1 and 128.2 (Im- C_4 and 5), 66.9 ($-\text{CH}(\text{OH})-$), 54.3 ($-\text{CH}_2-\text{NH}-$), 44.8 (Im- CH_2-), 37.2 ($-\text{CBr}_2\text{H}$).



21

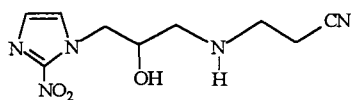
3.2.6.3 Synthesis of (22), a terminal nitrile derivative of RSU1111

This procedure was adapted from a synthesis reported by Fortier and McAuley describing the synthesis of a chelating ligand from an amine and an acrylonitrile.^{23,24} In a

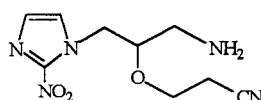
50 mL flask, CH_2Cl_2 (5 mL) was added to **RSU1111** (0.102 g, 0.531 mmol) to give a slurry. Acrylonitrile (5 mL, excess) and K_2CO_3 (0.150 g) were then added and the reaction mixture was refluxed for 24 h. TLC analysis revealed the presence of numerous products (~ 19). The two major bands observed were isolated via preparative TLC (band 1 (**22**), $R_f = 0.33$; band 2 (**23**), $R_f = 0.55$ for CH_2Cl_2 :MeOH, 20:1) to yield colourless oils (0.0136 g and 0.0334 g, respectively). IR (**22**, ν , cm^{-1}): 3376 (OH); 3139 (C-H_{Im}); 2929, 2847 (C-H); 2247 (C \equiv N); 1631 (C-OH); 1487 (N-O_{asym}); 1363 (N-O_{sym}). ^1H NMR (200 MHz, d_6 -acetone, **22**): δ 7.49 (s, 1H, Im- H_5), 7.09 (s, 1H, Im- H_4), 4.73 (dd, 1H, Im-CH(H)-), 4.46 (dd, 1H, Im-CH(H)-), 4.10 (m, 1H, -CH(OH)-), 2.93 (td, 2H, -NH-CH₂-), 2.80 (dd, 1H, -CH(H)-NH-), 2.71 (dd, 1H, -CH(H)-NH-), 2.64 (t, 2H, -CH₂-CN); integrations support the addition of only 1 mol acrylonitrile per **RSU1111**, while peak assignments were made with the aid of 2D COSY; (d_6 -acetone, **23**): δ 7.52 (s, 1H, Im- H_5), 7.11 (s, 1H, Im- H_4), 4.83 (dd, 1H, Im-CH(H)-), 4.60 (dd, 1H, Im-CH(H)-), 3.98 (m, 1H, -CH(O-CH₂-)), 3.81 (dt, 1H, -O-CH(H)-), 3.60 (dt, 1H, -O-CH(H)-), 2.80 (dd, 1H, -CH(H)-NH₂-), 2.76 (dd, 1H, -CH(H)-NH₂-), 2.64 (dd, 2H, -CH₂-CN). ^{13}C NMR (75 MHz, d_6 -acetone, **22**): δ 128.5 and 127.9 (Im- C_4 and C_5), 100.6 (-CN), 69.7 (-CH(OH)-), 53.9 (-CH₂-NH-), 52.8 (-NH-CH₂-), 46.0 (Im-CH₂-), 18.8 (-CH₂-CN).

The reaction was repeated as described above, except Et_3N (165 μL) was substituted for K_2CO_3 and the reaction was performed in neat acrylonitrile; the resulting white slurry became an orange solution after 24 h at reflux. The solvent was then removed and acetone was added to the residual oil to generate a tan-coloured, microcrystalline solid that was filtered off. The filtrate was taken to dryness to give a yellow-brown oil; TLC revealed 2 major bands, one of which was **22**, that was purified via column chromatography (CH_2Cl_2 :MeOH, 20:1). Two colourless oils corresponding to **22** (0.0409 g) and a new product (**24**) (0.0196 g) were isolated. LR-MS [DCI(+)]: 283 ($M + \text{NH}_4 - \text{CN}$), 267 ($M + \text{H} - \text{CN}$), 240 ($M - 2\text{CN}$). ^1H NMR (300 MHz, d_6 -acetone): δ 7.50 (s, 1H, Im- H_5), 7.09 (s, 1H, Im- H_4), 4.81 (dd, 1H, Im-CH(H)-), 4.44 (dd, 1H, Im-CH(H)-), 4.19 (m, 1H, -CH(OH)-), 3.00 (t, 4H, -N-CH₂-), 2.86 (m, 1H, -CH₂-N-), 2.71 (t, 4H, -CH₂-CN); integrations support the addition of 2 mol acrylonitrile per

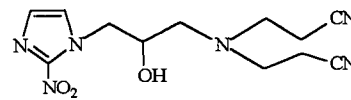
RSU1111, while peak assignments made with the aid of 2D COSY. ^{13}C NMR (75 MHz, d_6 -acetone): δ 128.4 and 127.9 (Im- C_4 and 5), 100.7 (-CN), 69.2 (-CH(OH)-), 58.0 (-CH₂-N-), 54.1 (-N-CH₂-), 50.7 (Im-CH₂-), 16.6 (-CH₂-CN).



22



23



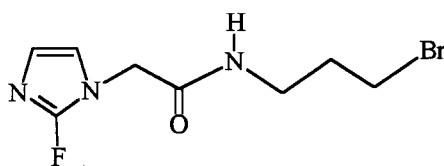
24

3.2.7 Reactions of Nitroimidazoles with $\text{Bu}_4\text{NF}\cdot\text{H}_2\text{O}$

The syntheses of fluorinated nitroimidazoles via exchange of F^- with other halogens on the side-chain were attempted, with the goal being to develop a useful procedure for obtaining fluorinated PET precursors.

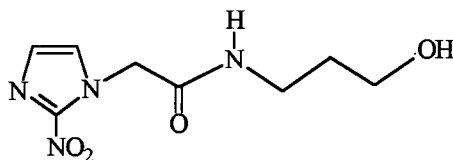
3.2.7.1 Reaction of **EBr1** with $\text{Bu}_4\text{NF}\cdot\text{H}_2\text{O}$

EBr1 (10 mg) and $\text{Bu}_4\text{NF}\cdot\text{H}_2\text{O}$ (40 mg, 4.2 equiv.; this compound must be handled quickly in air as it is extremely hygroscopic) were added to a Schlenk tube and the system was evacuated at r.t. (~1 h). Dry d_6 -dmso (1 mL) was added via syringe and the mixture was stirred for 3 h; within 1 min the initially colourless solution immediately changed to blue, then green, green-brown, orange and finally to yellow-orange. TLC analysis revealed the formation of a new product that was isolated via preparative TLC (CH_2Cl_2 :MeOH, 20:1) as a colourless oil (**25**). UV-Vis (dmso): 372, 264 nm. ^1H NMR (200 MHz, d_6 -dmso): 7.58 (s, Im- H_5), 7.01 (s, Im- H_4), 5.11 (s, -CH₂-CO-), 4.15 (t, -CH₂Br), 3.46 (t, -NH-CH₂-), 2.11 (m, -CH₂-CH₂Br). ^{19}F NMR (188 MHz, d_6 -dmso): δ -69.85 (s). Identical observations were made when the nitroimidazole used was **EBr1(-1)**; however, when the fluoride source used was KF/2,2,2-Kryptofix with either **EBr1** or **EBr1(-1)** there was no blue intermediate observed.

**25**

3.2.7.2 Reaction of EBr1 with Bu₄NF•H₂O and CH₃CO₂H

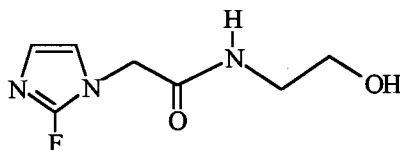
The above procedure (see 3.2.7.1) was repeated except acetic acid (1.2 equiv.) was also used, its function being to perhaps stabilize the nitroimidazole ring and hence promote fluoride exchange on the side-chain (C-Br bond).²⁵ Again, the final solution was yellow, and TLC analysis revealed two bands that were isolated via preparative TLC (CH₂Cl₂:MeOH, 20:1). Band 1 (**26**, R_f = 0.15) was isolated to yield a white solid, while band 2 (R_f = 0.55) was a colourless oil, its analytical data matching those of compound **25**. Data for **26**: LR-MS [EI]: 229 (M⁺ + H), 211 (M⁺ - OH), 182 (M⁺ - NO₂). ¹H NMR (200 MHz, d₆-acetone): δ 7.62 (br s, 1H, -NH-), 7.40 (s, 1H, Im-H₅), 7.00 (s, 1H, Im-H₄), 5.11 (s, 2H, -CH₂-CO-), 3.60 (t, 1H, -OH), 3.46 (q, 2H, -CH₂OH), 3.23 (q (dt), 2H, -NH-CH₂-), 1.54 (p, 2H, -CH₂-CH₂OH); peak assignments made with the aid of 2D COSY. These data suggest that the presence of acetic acid leads to hydrolysis of the C-Br bond.

**26**

3.2.7.3 Reaction of SR2508 with Bu₄NF•H₂O

Reaction conditions identical to those for the reaction of fluoride with EBr1 (section 3.2.7.1) were used, except the solvent was MeCN. The major band observed for TLC analysis was isolated to give a yellow oil that was purified using the CTRON (CH₂Cl₂:MeOH, 10:1) to yield a colourless oil (**27**) (0.0252 g, 27 %). LR-MS[EI(+)]: 185

($M^+ - H$), 167 ($M^+ - F$), 137 ($M^+ - F - CH_2OH$), 123 ($M^+ - F - CH_2CH_2OH$), 108 (Im- CH_2CO^-). IR (ν , cm^{-1}): 3403 (N-H); 2924, 2851 (C-H); 1735 (C=O); 1588, 1377, 1331, 1059; no ν_{NO} bands were observed. UV-Vis (dmso): 370 (ϵ was $\sim 70\%$ of that for **SR2508**). 1H NMR (200 MHz, d_6 -acetone): δ 7.00 (d, 1H, Im- H_5), 6.73 (s, 1H, Im- H_4), 4.77 (br s, 1H, -NH-), 4.56 (s, 2H, - CH_2-CO -), 3.83 (m, 4H, - CH_2OH + -NH- CH_2 -), 3.52 (t, 1H, -OH). ^{19}F NMR (188 MHz, d_6 -acetone): δ -74.72 (s).



27

3.2.7.4 Reaction of nNO_2Im ($n = 2, 4, 5$) with $Bu_4NF \cdot H_2O$

The title reaction was carried out in d_6 -dmso and the analytical data are summarized in Table 3.1. The results from this study were all obtained from the *in situ* reaction mixtures, and are used for the qualitative comparison of the data obtained from the reactions with fluoride in the previous sections (3.2.7.1-3). For the reaction with 2Me5NO₂Im, the major band from the TLC analysis was isolated [IR (ν , cm^{-1}): 3406 (N-H); 2959, 2872 (C-H); 1523, 1460, 1376, 1254, 1206, 1028, 878; no ν_{NO} bands at 1501 and 1380 cm^{-1} were observed.]

Table 3.1: Summary of the ^1H NMR, $^{19}\text{F}\{^1\text{H}\}$ NMR and UV-Vis data for $n\text{NO}_2\text{Im}$ compounds and for their reaction with $\text{Bu}_4\text{NF}\cdot\text{H}_2\text{O}$

Sample	^1H NMR (δ)				$^{19}\text{F}\{^1\text{H}\}$ NMR ^a (δ)	UV-Vis (nm)
	Imidazole Positions					
	1 ^b	2	4	5		
2NO ₂ Im	14.40	--	7.35	7.35	--	328
2NO ₂ Im + F ⁻	--	--	6.70	6.70	-68.95	374
4NO ₂ Im	13.25	8.32	--	7.84	--	302
4NO ₂ Im + F ⁻	--	7.70	--	7.04	-67.94	364
2Me5NO ₂ Im	12.95	2.32	8.20	--	--	314
2Me5NO ₂ Im + F ⁻	--	2.15	7.60	--	-67.80	376

^a The ^{19}F signal observed in each spectrum is rather broad.

^b The N-H signal is not observed in the ^1H NMR spectrum of the reaction mixture because of the addition of H_2O with the fluoride source ($\text{Bu}_4\text{NF}\cdot\text{H}_2\text{O}$) which leads to rapid proton exchange with the N-H proton.

3.2.8 Cyclic Voltammetry of Nitroimidazoles

The cyclic voltammograms for the nitroimidazoles were obtained using the procedure described in Chapter 2 (Section 2.2.6) using the cell depicted in Figure 2-2 which contains the Ag reference electrode. The reduction potentials of the one-electron reduction of the nitro group are reported in Tables 3.2-3.4 versus the SCE, the standard reference used to report these values in the literature. The listed conversion factor is detailed in Chapter 2, Section 2.2.6.

Table 3.2: Summary of reduction potentials for the 2-nitroimidazoles vs. SCE

Compound	FeCp ₂ E _{1/2} (avg.) vs. Ag	E _{pc} , E _{pa} : E _{1/2} (avg.) vs. Ag	Conversion Factor ²⁶ (424 - E _{1/2} FeCp ₂)	E _{1/2} vs. SCE (mV)
SR2508	479	-953, -1088; -1021	-56	-1077
EF5	408	-933, -1053; -993	+16	-977
EF3	336	-1060, -1163; -1112	+88	-1024
EF3(-1)	474	-910, -1020; -965	-50	-1015
EF2Br	471	-905, -1045; -975	-47	-1022
E=F2	520	-843, -1027; -935	-96	-1031
EF1	507	-899, -1009; -954	-83	-1037
EF1(-1)	620	-857, -981; -919	-196	-1115
ECH	565	-836, -954; -895	-141	-1036
ECH(-1)	595	-883, -1013; -948	-171	-1119
EBr1	489	-893, -1053; -973	-65	-1038
EBr1(-1)	650	-815, -965; -890	-226	-1116

Table 3.3: Summary of reduction potentials for the 2-methyl-5-nitroimidazoles vs. SCE

Compound	FeCp ₂ E _{1/2} (avg.) vs. Ag	E _{pc} , E _{pa} : E _{1/2} (avg.) vs. Ag	Conversion Factor ²⁶ (424 - E _{1/2} FeCp ₂)	E _{1/2} vs. SCE (mV)
Metronidazole	393	-1039, -1207; -1123	+31	-1092
MF5	363	-1031, -1225; -1128	+60	-1068
MF3(-1)	379	-1026, -1212; -1119	+45	-1074
MF1(-1)	338	-1139, -1331; -1235	+85	-1150
MCl1(-1)	504	-999, -1167; -1083	-80	-1163
MBr1(-1)	649	-856, -1008; -932	-225	-1157

Table 3.4: Summary of reduction potentials for the 2-methyl-4-nitroimidazoles vs. SCE

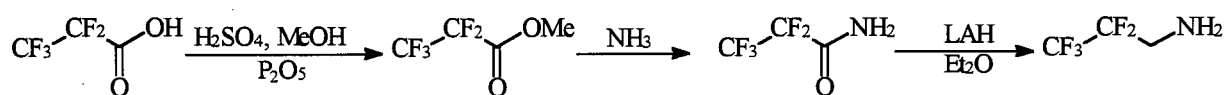
Compound	FeCp ₂ E _{1/2} (avg.) vs. Ag	E _{pc} , E _{pa} : E _{1/2} (avg.) vs. Ag	Conversion Factor ²⁶ (424 - E _{1/2} FeCp ₂)	E _{1/2} vs. SCE (mV)
2M4NF5	575	-1078, -1220; -1149	-151	-1300
2M4NF3(-1)	628	-1060, -1220; -1140	-204	-1344
2M4NF1(-1)	629	-1134, -1286; -1210	-205	-1415
2M4NCl1(-1)	660	-1090, -1216; -1153	-236	-1389
2M4NBr1(-1)	707	-1029, -1201; -1115	-283	-1398

3.3 Results and Discussion

3.3.1 Synthesis of the Nitroimidazole Side-Chains

Nitroimidazoles themselves have been shown to exhibit some activity in biological systems (*e.g.* 2NO₂Im or azomycin is a natural antibiotic and antiprotozoal agent).²⁷ However, because of their relatively low solubility in aqueous systems their use is limited. Various groups have reported the addition of numerous side-chains onto the N1 position of the nitroimidazole ring^{16,28-31} and the efficacy of such derivatives as hypoxia-selective cytotoxins or radiosensitizers seems to depend on the partition coefficient (P); as P increases the lipophilicity increases and thus the compound's ability to cross the cell membrane also increases.³² The major problem with most of these nitroimidazole compounds is that addition of the side-chain leads to increased cytotoxicity, specifically neurotoxicity which is the major factor that limits clinical dose.^{33,34} A relatively new compound with a pentafluorinated side-chain (**EF5**) seems to be one of the best candidates for use as a hypoxia-selective species.^{2,5} The original synthesis of **EF5** (Section 3.2.2.2, synthesis 1) required a number of reaction steps that resulted in a relatively low yield (33 %), so a new method was developed in which the side-chain could be added in a single, high-yield step.

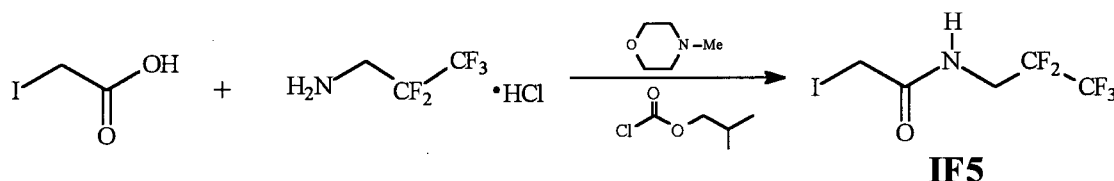
The perfluoropropylamine side-chain for **EF5** (section 3.2.2.2, synthesis 1) was originally synthesized via a 3-step reaction from perfluoropropionic acid (Scheme 3-1).^{35,36} The synthesis of compound **7** required two steps (see Scheme 3-9, p. 102) while the coupling of **7** and pentafluoropropylamine to form the amide linkage took place in the final



Scheme 3-1: Synthesis of pentafluoropropylamine from perfluoropropionic acid.³⁵

step (total of six steps). In the present work, linking the amine with iodoacetic acid to form **IF5** (Scheme 3-2), two of the steps are eliminated which gives a higher overall yield

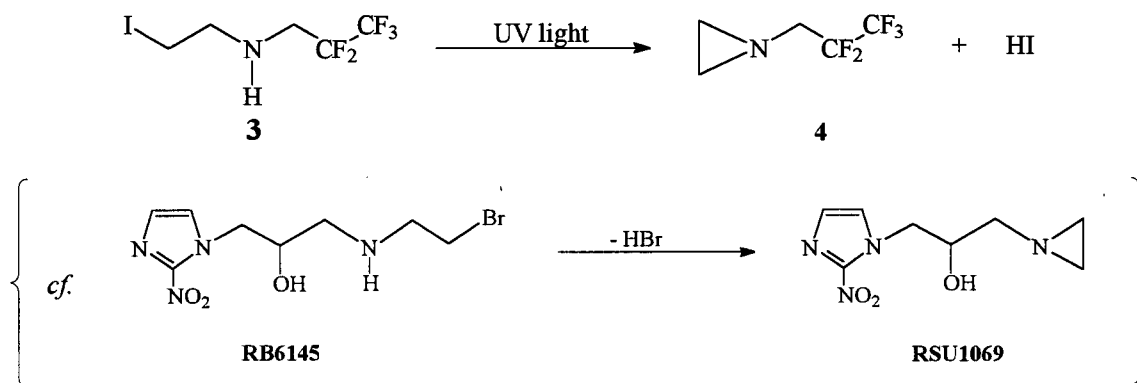
of **EF5**.¹⁷ **IF5** is easily purified via sublimation, however the C-I bond is mildly reactive



Scheme 3-2: Synthesis of **IF5**, the precursor to **EF5**.

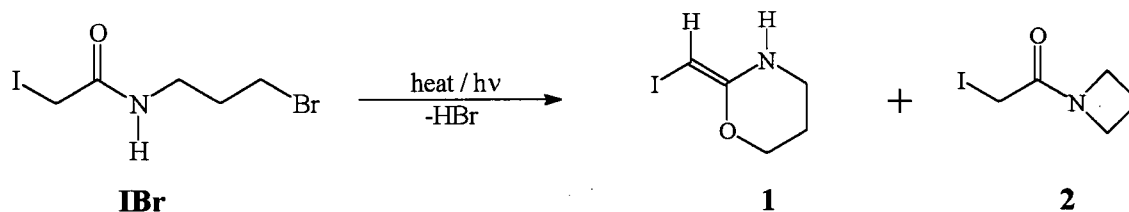
and if the compound is not stored in the absence of light, it will slowly decompose. Changing the halogen from iodine to chlorine produces a more stable side-chain (**ClF5**), as the C-Cl bond is more resistant to cleavage by UV radiation.³⁷ An interesting feature of **ClF5** is that it is only visible on the TLC plate in the presence of UV light, behaviour opposite to that of **IF5**. The use of **ClF5**, although stable upon exposure to UV light (as monitored by ¹H NMR spectroscopy) did not, however, give a higher yield for the synthesis of **EF5**. Therefore, from a practical sense, **ClF5** may be more useful than **IF5**. Kagiya and others²⁸⁻³⁰ have investigated reduction of the amide side-chain to the amine using the relatively mild reducing agent borane-THF which selectively reduces the amide^{38,39} without affecting the nitro moiety. The reduction of **IF5** using BH₃·THF was successful in forming the corresponding amine (**3**) (see Scheme 3-3), but its stability was much lower than that of **IF5**. An NMR sample of the initially pale yellow solution of **3**, stored at r.t. under ambient light, turned dark red-brown over a period of several days. ¹H NMR spectra recorded every 2 d revealed a decrease in the intensities of the signals for **3** and the appearance of new signals. Chromatographic separation of a 10-day old NMR sample (via preparative TLC) gave three bands with the first one assigned as compound **4**; this was initially colourless but became yellow on the TLC plate upon exposure to UV light. Analysis of the ¹H NMR data indicated that **3** underwent cyclization to form compound **4** (Scheme 3-3). The instability of **3** is in accordance with the weak C-I bond; the loss of iodine is confirmed from the UV-Vis data which show that both I₂ and I₃⁻ are formed (presumably by the photolysis of HI). The liberation of I₂ from HI in the presence of UV light is well known.^{8,37} Of note, **4** has an aziridine ring analogous to that in RSU

1069 (formed from the bromoethylamino derivative RB 6145).⁴⁰ RSU 1069 is used as a DNA alkylating agent, suggesting that **4** may also serve the same purpose; however, because there is no nitroimidazole moiety attached **4** will not be hypoxia-selective.



Scheme 3-3: Formation of aziridine ring upon exposure of **3** to UV light.

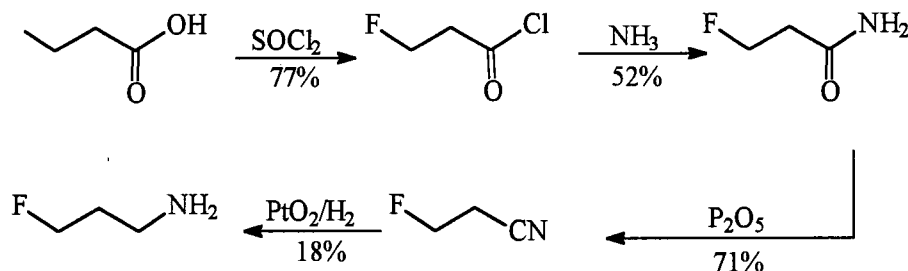
Because of the interest in using halogen exchange reactions to form radiolabelled species for use in PET imaging of hypoxia,⁴¹ a monobromo derivate of **IF5** was synthesized (**IBr**) (see Scheme 3-4). This compound is extremely reactive as it contains two reactive C-X (X = Br, I) bonds. **IBr** was only stable at < 10 °C in the dark, while exposure to heat and/or UV light resulted in decomposition to two new species (Scheme 3-4). The decomposition was monitored by ¹H NMR spectroscopy. The peak at δ 7.90 for **IBr**, typical of NH amides, disappears and a new peak appears at δ 2.51, in the range typical for cyclic amine NH protons.⁴² The other signals at δ 4.81 (a methylene triplet shifted slightly downfield due to the proximity of the CH₂ to an O atom), δ 3.74 (a



Scheme 3-4: Cyclization of **IBr** in the presence of heat and/or UV-radiation.

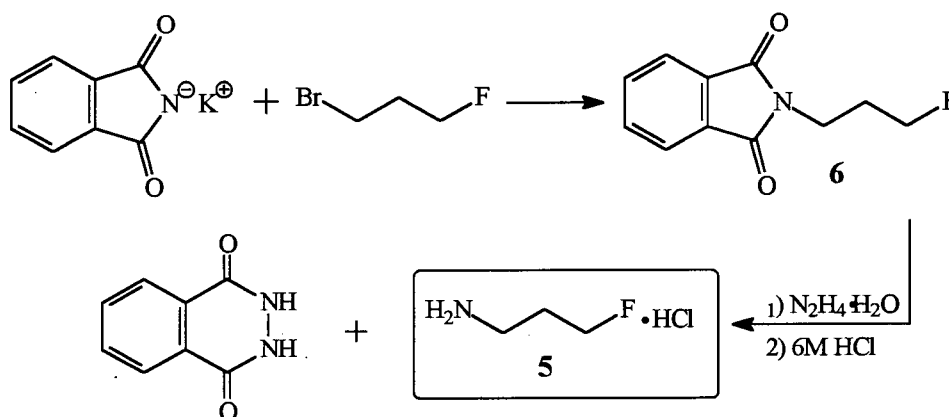
triplet adjacent to the amine NH, showing no coupling to the NH proton) and δ 2.37 (a pentet, presumably resulting from an overlapping triplet of triplets) together support the formation of a cyclic species with the proposed structure **1**. Analogous cyclization products have been suggested in the literature, but no spectroscopic data has been reported to support these hypotheses.^{43,44} For the reaction of **SR2508** with TiF_2O a similar cyclized product was observed in this thesis work, as confirmed by an X-ray structure (Figure 3-14, p. 123). The H-atoms adjacent to an amide linkage are more acidic (activated) because the amide exists in two tautomeric forms, while removal of electron density from the C-H bonds also increases their acidity. Although the bond energy of C-I is lower than that of C-Br, reactivity of the C-I appears to be limited by its proximity to the amide moiety. This prevents the formation of any cyclization products resulting from the cleavage of the C-I bond. The formation of a species corresponding to **2** (Scheme 3-4) is also supported by the ^1H NMR spectrum. Because the four-membered ring is torsionally strained this species is short-lived and eventually rearranges to **1**.

Most of the "side-chain compounds" were either purchased from Aldrich or received as kind donations from Prof. W. Dolbier at the University of Florida. The only fluorinated amine side-chain synthesized was 3-fluoropropylamine hydrochloride (**5**), the precursor for the synthesis of **EF1**. Obtaining **5** was imperative for comparison of the reaction products from the halogen exchange reaction between **EBr1** and F^- , and the authentic **EF1** compound. A previously reported synthesis required four steps to obtain the parent amine of **5**, and the yield was necessarily small (Scheme 3-5).^{45,46} For this thesis



Scheme 3-5: Synthesis of 3-fluoropropylamine reported by Pattison *et al.*⁴⁵

reaction is that the amine can be easily separated by extraction with HCl from the phthaloyl hydrazide formed during the hydrazinolysis. In this case, the hydrochloride salt was actually the desired product, **5** (Scheme 3-7). One other synthesis of **5** exists in which the reaction intermediate is the azide species,¹⁰ although the yield is much lower than via the chemistry illustrated in Scheme 3-7.



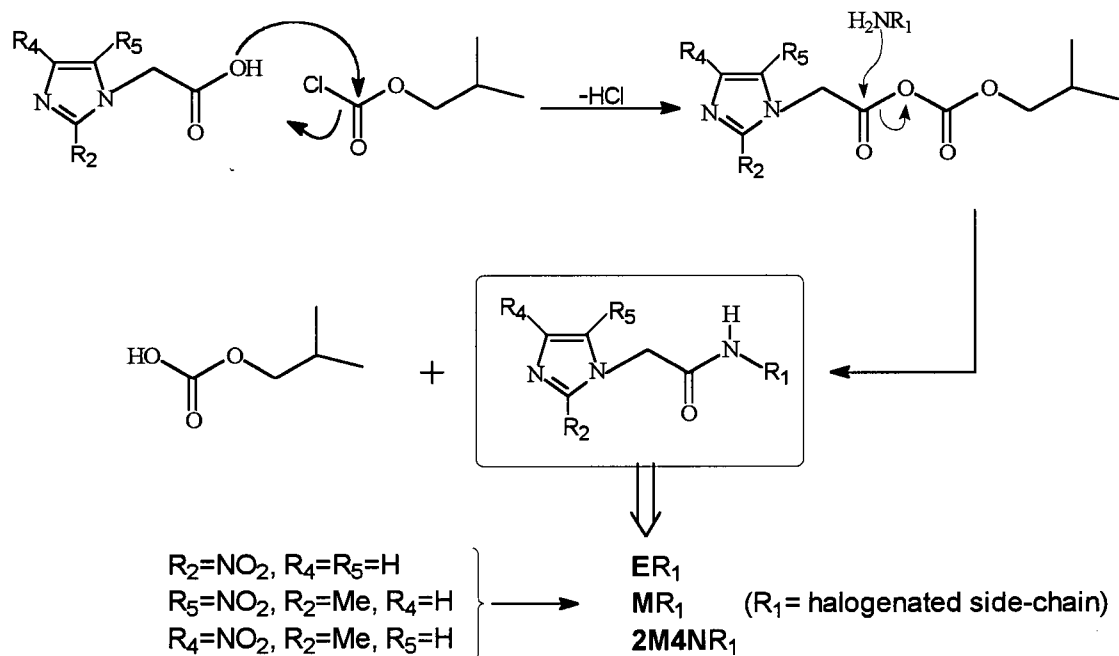
Scheme 3-7: High yield Gabriel synthesis of 3-fluoropropylamine hydrochloride.

3.3.2 Nitroimidazoles

Nitroimidazoles are useful compounds for targeting the hypoxic regions of cancerous tumours; the nitro moiety is readily reduced in the presence of nitroreductases within the cells to form macromolecular adducts. Various nitroimidazoles (2, 4 and 5NO₂ derivatives) have been synthesized previously for use as radiosensitizers⁵⁰⁻⁵² and their efficacy was up to three times greater in areas of hypoxia. Because the nitroimidazole, **EF5**, was found to be non-toxic when compared to other compounds of similar composition,² the focus of this thesis work was on variation of the fluorinated side-chain and the position of the nitro group about the imidazole ring.

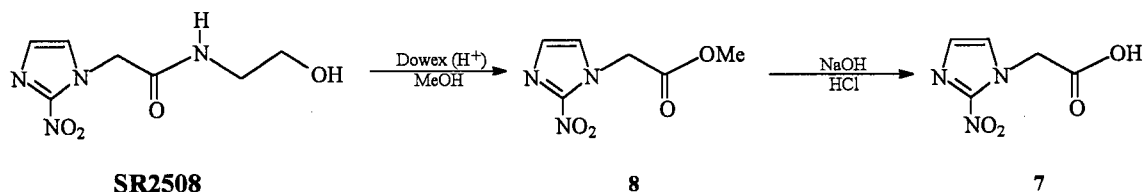
Most of the nitroimidazoles were synthesized via the mixed anhydride species generated from reaction of an acid moiety with isobutylchloroformate (Scheme 3-8). The carbonyl group nearest the imidazole is the more reactive of the two, the isobutyl carbonate being the better leaving group on reaction with an appropriate R₁NH₂ amine,

this leading to formation of an amide bond. N-Methylmorpholine (NMM) was used to "mop up" free H^+ in solution (Scheme 3-8).



Scheme 3-8: Reaction mechanism for addition of side-chain via an amide linkage.

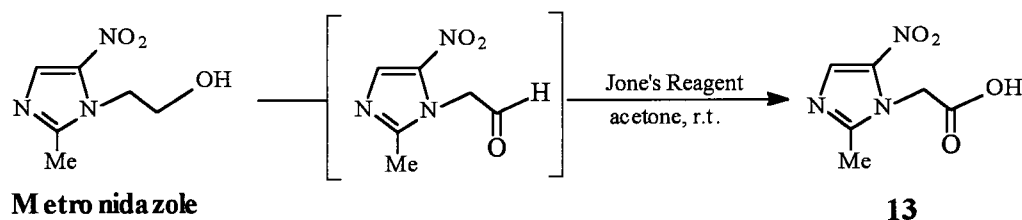
Synthesis of the nitroimidazole acetic acid derivatives was achieved by chemically altering existing nitroimidazoles. For 2-nitroimidazole derivatives, the hypoxia selective radiosensitizer **SR2508**, obtainable in large amounts from Dr. C. Koch (Univ. of Penn.), was treated with $H^+/MeOH$. This treatment cleaved the amide bond to yield the methyl ester (**8**) which was subsequently worked up with $NaOH/HCl$ to yield the corresponding acid (**7**) (Scheme 3-9). The major problem with this procedure is that



Scheme 3-9: Synthesis of **7**, via **8** from **SR2508**.

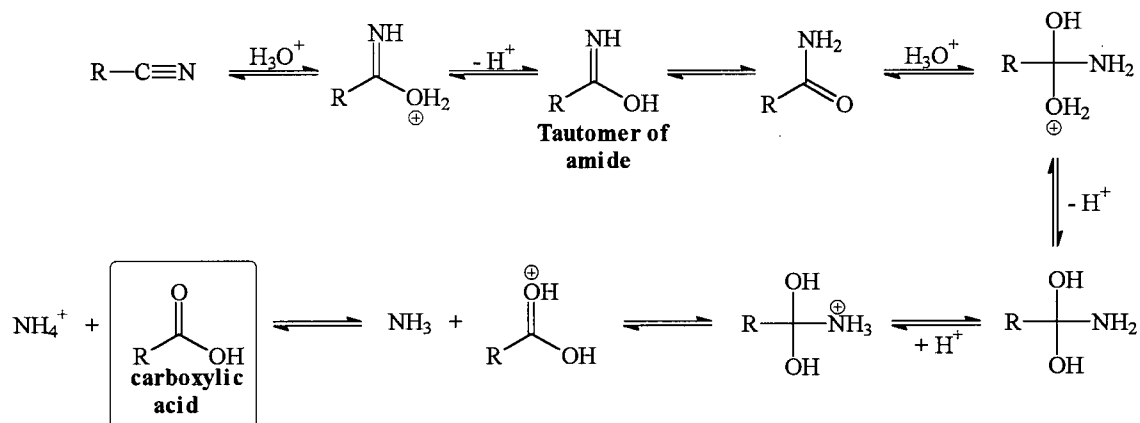
increasing the acidity of the solution (with HCl) to a pH of ~4, to ensure the formation of **7**, results in concomitant protonation of the imidazole ring at N3. Subsequent extraction with EtOAc thus produced **7** in significantly low yield because most of it remained in the aqueous layer as the hydrochloride salt (as judged by TLC and ^1H NMR spectroscopy). The protonated species proved to be useable for the synthesis of the desired halogenated nitroimidazoles, the procedure (Scheme 3-8) requiring an additional equivalent of NMM; however, the yields were typically half of those obtained when the pure acid was used.

For the $2\text{Me}5\text{NO}_2\text{Im}$ compounds, the hypoxia-selective cytotoxin metronidazole, which is used in the treatment of anaerobic bacterial infections,⁵³ was oxidized with Jones' reagent converting the alcohol to the acid functional group (Scheme 3-10). The yield obtained was slightly higher than reported²⁰ and, according to TLC, some of the metronidazole was only partially oxidized to the aldehyde species. Of particular note, when additional Jones' reagent was added to convert the remaining aldehyde to the acid, a lower yield was obtained.



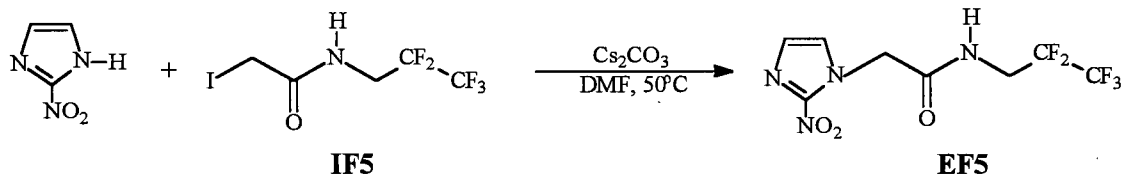
Scheme 3-10: Oxidation of metronidazole with Jones Reagent to yield the carboxylic acid derivative, **13**.

For the $2\text{Me}4\text{NO}_2\text{Im}$ compounds, the acid species had an extra methylene in the link between the imidazole ring and the acid functional group. Treatment of 2-methyl-4-nitro-1-imidazolepropionitrile (Aldrich) with sulfuric acid resulted in hydrolysis of the nitrile to the carboxylic acid after several days at high temperature. Formation of the amide is facile, nevertheless, further hydrolysis to the acid requires relatively harsh conditions, mainly because of the extra resonance capability of the nitrogen lone-pair (Scheme 3-11).



Scheme 3-11: Acid hydrolysis of 2-methyl-4-nitro-1-imidazolepropionitrile (abbreviated as RCN).

The title compound (**EF5**) on which most of this work was based on has been approved for clinical trials by the National Cancer Institute (US) through support of large scale synthesis, formulation and toxicological studies. The improved synthesis (Scheme 3-12)¹⁷ of **EF5** from **IF5** will be useful, especially if the compound is approved for use in



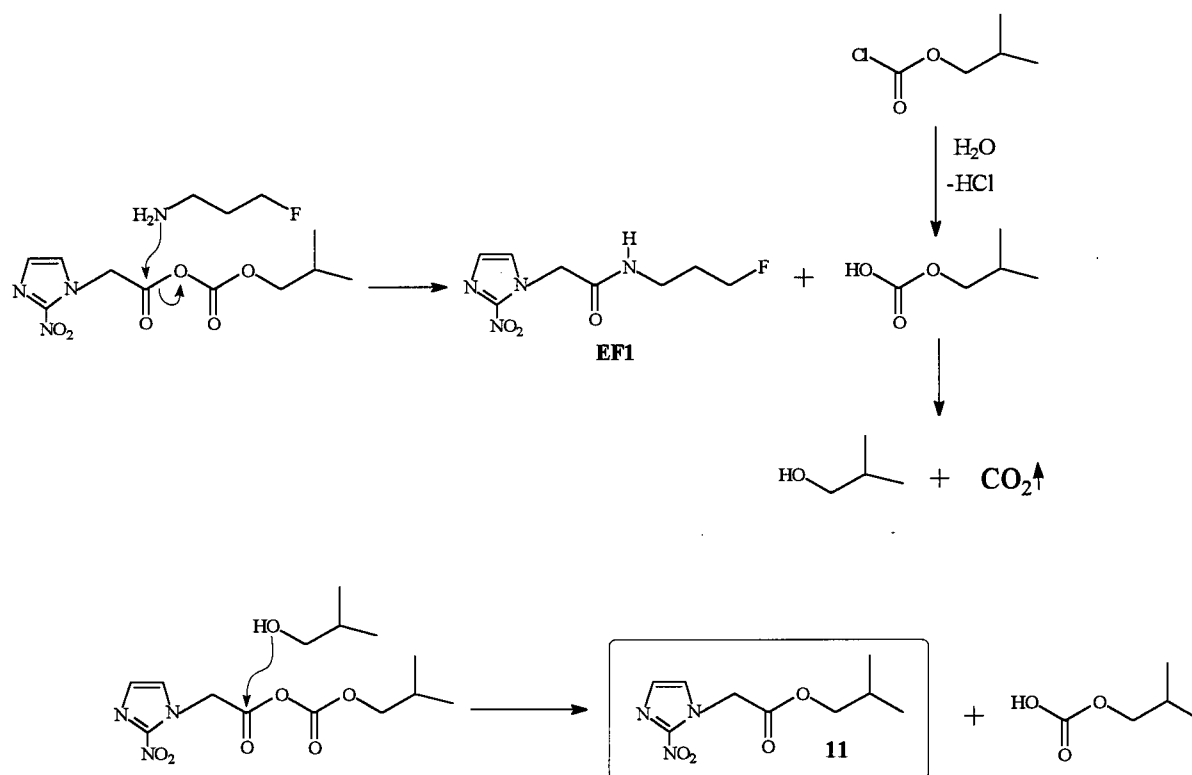
Scheme 3-12: New synthetic route to **EF5**.

humans as either a radiosensitizer or a hypoxia-selective imaging agent. Other 2-nitroimidazole compounds in this series (**EF4Br**, **EF3**, **EF3(-1)**, **EF2Br**, **EF1(-1)**, **EC11**, **EC11(-1)**, **EBr1**, **EBr1(-1)**, **EIAA**, **EPrA**) were all isolated in relatively high yield (up to 83 %) and could be synthesized via the alternate route (*i.e.* synthesis of the complete side-chain via reaction of the appropriate amine with iodoacetic acid, followed by coupling with 2NO₂Im, see Scheme 3-2 and Scheme 3-12) with the exception of the bromo derivatives which are too reactive (see Section 3.2.1.2). The high reactivity of the bromo derivatives is also indicated by their poor elemental analyses as the C-Br bond is readily hydrolyzed by H₂O (in the air).

The monofluorinated species (**EF1**, see Scheme 3-13) was the only 2-nitroimidazole compound in the series that could not be isolated in a yield higher than 15 %. The required monofluoropropylamine hydrochloride (or hydrofluoride) reagent was extremely hygroscopic which may explain why 2-nitro-1-H-imidazol-1-yl-ethyl isobutanoate (**11**) is the major product (Scheme 3-13). The presence of H₂O in this reaction could result in the formation of isobutylcarbonate via reaction with isobutylchloroformate. The isobutylcarbonate would also be formed as a co-product of the reaction between 3-fluoropropylamine and isobutylmethyylimidazoylcarbonate. The isobutylcarbonate could lose CO₂ to form isobutanol, which is the next strongest nucleophile present after the amine. Because of the formation of HCl the amine would remain as its hydrochloride salt, thus decreasing its nucleophilicity and therefore allowing the isobutanol to react with the acyl carbonate group to form **11**.

The synthesis of **EC11(-1)** via reaction of TsCl with **SR2508** was unexpected. The desired product was the tosylate species that could be used as a reactive intermediate for the formation of **EF1(-1)** (Section 3.2.7). Unfortunately, the tosylate could not be isolated because the chloride ions readily react to form the monochloro species **EC11(-1)**. The reaction of phenylmethanesulfonyl fluoride using the same reaction conditions did not yield the sulfonate intermediate and consequently the desired **EF1(-1)** species was not formed. The highly reactive tosylate intermediate was also exploited for the synthesis of compound **16**, the chlorinated derivative of metronidazole (Section 3.2.3.7).

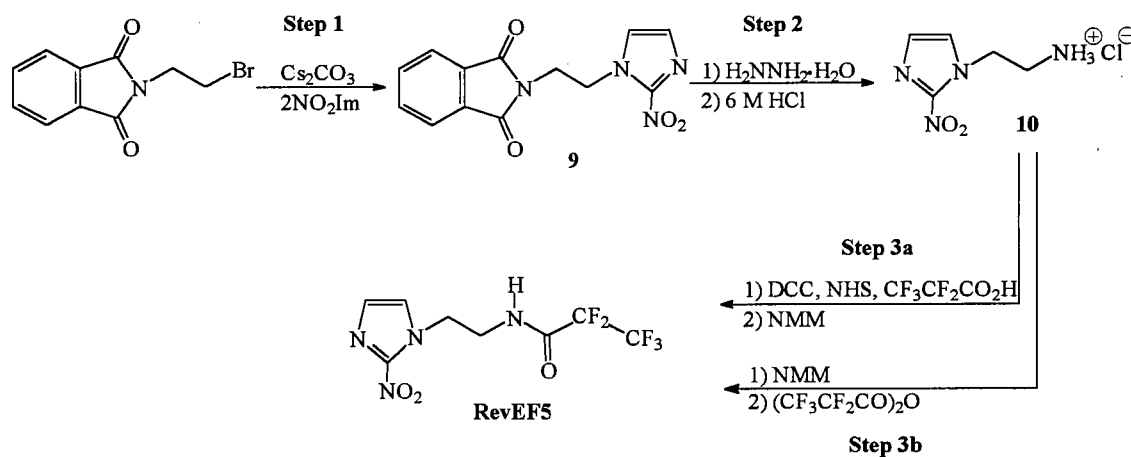
The ability to alter the biological activity of a compound by changing the composition of an associated side-chain prompted the attempted synthesis of a pentafluoro species analogous to **EF5**, but with the amide linkage reversed (Scheme 3-14). Because of the difficulty in forming the reverse amide linkage for **RevEF5**, three different syntheses were attempted. Synthesis 2 uses conditions identical to those of synthesis 1 for **EF5** (Scheme 3-8), the major difference being that the pentafluoro group is introduced as pentafluoropropionic acid. This acid species is highly reactive with H₂O from the air, as apparent from substantial fuming when the sample bottle is opened, but does readily react



Scheme 3-13: Formation of the isobutylester (11) in the presence of H₂O.

with *iso*-butylchloroformate to form the mixed anhydride. The problem with this reaction arises when **10** (the 2-nitroimidazole ethylamine product from synthesis 1, step 2) is added to the reaction mixture. The amine preferentially reacts with the carbonyl group associated with the isobutylformate to yield a species similar to **11** as the major product (as shown by ¹H NMR), analogous to that formed during the synthesis of **EF1** (see Scheme 3-13), although a different mechanism must be involved. This result can be explained accordingly: the electron-withdrawing fluorine atoms stabilize the negative charge of the pentafluoropropionate, making it a better leaving group than isobutylcarbonate. To avoid the problem encountered in synthesis 2, the peptide coupling agent STMU•BF₄ was reacted with pentafluoropropionic acid (synthesis 3). Addition of base (Et₃N) in the first step leads to formation of tetramethylurea and (N-succinimidyl)-pentafluoropropionate (according to TLC data). Once again, addition of **10** results in a reaction; however, neither of the major products was **RevEF5**, which was observed in low

concentration via TLC. Synthesis 1 allowed the isolation of **RevEF5** in high yield using two different synthetic approaches for the third step of the reaction (steps 3a and 3b). The first route, a well known procedure for the formation of an amide bond using DCC (synthesis 1, step 3a) was employed, leading to the formation of a reaction intermediate analogous to that in synthesis 3. This reaction (29 % yield), however, was more successful than synthesis 3 (< 1% yield), and may be attributed to the greater stability of the side-product formed, dicyclohexylurea (DCU). The presence of BF_4^- in synthesis 3 may also hinder the reaction although it is not obvious how. An advantage of synthesis 1 (step 3a) is that the DCU (because of its low solubility in DMF) can be readily separated from the product mixture via filtration. For the second route (step 3b), the amine on the side-chain of **10** (nucleophilic) was reacted with the highly reactive perfluoroanhydride $(\text{CF}_3\text{CF}_2\text{CO})_2\text{O}$ to give **RevEF5** in a somewhat higher yield (32 %).



Scheme 3-14: The 3-step synthesis of **RevF5** from 2-bromoethylphthalamide.

Another 2-nitroimidazole species with a side-chain terminating with an amino group is **RSU1111**. This compound contains a side-chain one methylene unit longer than in **10**, and also contains a secondary hydroxyl group similar to that of the radiosensitizer misonidazole.⁵⁴ Analogous to synthesis 2 of **RevEF5**, the major product formed was the isobutylformate-linked amide species, while **20** was isolated in low yield (5 %). The incorporation of the pentafluoropropyl acyl group is confirmed by HR-MS and more importantly, by $^{19}\text{F}\{^1\text{H}\}$ NMR spectroscopy, which gives signals at δ -6.77 and -46.35

corresponding to the CF_3 and CF_2 groups, respectively (*cf.* **RevEF5**: δ -6.79 and -46.43). In the ^1H NMR spectrum the protons on the methylene groups adjacent to the chiral $-\text{CH}(\text{OH})-$ centre are all magnetically inequivalent (diastereotopic protons). An interesting aspect of this spectrum is that the $-\text{CH}_2-\text{NH}-$ protons have essentially the same chemical shift while the $\text{Im}-\text{CH}_2-$ proton chemical shifts are well separated ($\Delta\delta$ 0.40). This may suggest that the OH group on the adjacent carbon is interacting with one of the protons of the methylene group nearest the nitroimidazole. The same chemical shift distribution is seen in the ^1H NMR spectrum of **21**; the $\text{Im}-\text{CH}_2-$ proton chemical shifts have nearly the same separation as above ($\Delta\delta$ 0.38). The observation of a signal at δ 6.21 is in accordance with the HR-MS results which suggest that one of the Br-atoms of the $\text{CBr}_3\text{CO}_2\text{H}$ precursor has been displaced by a hydrogen. The anticipated product was the tribromo species, but presumably because of the bulkiness of the Br-atoms and the relatively weak C-Br bond, the dibromo species is isolated. The ^{13}C NMR spectrum of **21**, compared with that of **RSU1111**, has extra signals at δ 151.7 and 37.2, confirming the presence of $-\text{C}=\text{O}$ and $-\text{CBr}_2\text{H}$ units.

The coordination chemistry of nitroimidazoles is also of interest because these do not typically form strong interactions with the metal centres of interest (*e.g.* Pt, Ru), unlike imidazoles which form more stable species.^{55,56} The metal complexes may be used as nitroimidazole delivery agents to the DNA by coordinating to the DNA's nitrogen bases, hence bringing the nitroimidazoles in close proximity to the site of action.⁵⁷ Synthesis of a nitroimidazole with a side-chain containing a chelating moiety would ensure stronger interaction with the metal centre, while maintaining the functionality of the hypoxia active nitroimidazole. Reaction of acrylonitrile with an amine is a useful method for adding two $\text{CH}_2\text{CH}_2\text{CN}$ groups to the existing amine, followed by reduction of the nitriles to yield the tridentate species $\text{RN}(\text{CH}_2\text{CH}_2\text{CH}_2\text{NH}_2)_2$.^{23,24} Addition of acrylonitrile to **RSU1111** proved to be much more difficult than anticipated. Even when the reaction was done in neat acrylonitrile, the major product was the mono-substituted species **22**, while the bis-substituted species (**24**) was formed only half as much. A small quantity of a compound corresponding to the addition of acrylonitrile at the hydroxyl group (**23**) was

also isolated and characterized by ^1H NMR spectroscopy. An interesting property of compounds **22** and **23** is that not only do they exhibit inequivalent methylene ^1H signals for the CH_2 bound to the $2\text{NO}_2\text{Im}$ moiety, but they also have inequivalent methylene proton signals for a CH_2 bound to the NH and NH_2 group, respectively. This is not observed for compound **24**. The difference between the chemical shifts of the two protons is not as pronounced for the methylene group bound to either the NH or NH_2 groups (*e.g.* δ 2.80 and 2.71 for **22** vs. δ 4.73 and 4.46 for the $2\text{NO}_2\text{Im-CH}_2$ - protons), suggesting a weaker intramolecular interaction. This finding is puzzling and tends to suggest that the newly added propynitrile arm in **22** has a conformation which interacts with one of the methylene protons nearest to the NH group, consequently inducing magnetic inequivalence. The presence of the two pendant arms in **24** possibly makes the species bulky enough to prevent such an interaction. Reduction of the nitrile groups of **24** was unsuccessful using a number of different reducing agents (*e.g.* LAH , NaH , H_2) including B_2H_6 , which has been reported to reduce CN groups in the presence of an NO_2 group.²⁹ In all cases, the nitro group was reduced, either partially or completely, making further pursuit of this chelating compound futile.

Comparison of the ^1H NMR spectra for the 2-nitroimidazole compounds with variation in number and type of halogen atoms present reveals some interesting results. For the most part, for each of these compounds the chemical shifts of the protons of the $2\text{NO}_2\text{Im-CH}_2$ - entity fall in the same range, displaying that the composition of the side-chain has little effect on this component of the molecule (Im-H_5 : δ 7.49 \rightarrow 7.66; Im-H_4 : δ 7.08 \rightarrow 7.21; CH_2CO : δ 5.15 \rightarrow 5.36). There is a larger variation for the chemical shift of the NH proton (δ 7.52 \rightarrow 9.05) as its position shifts with changes in concentration of H_2O in the NMR solvent due to proton exchange between the two species.⁴² Removal of the NO_2 -group, however, does effect the chemical shifts of the imidazole protons and CH_2 bound to the imidazole at N1. For **ImF5**, the compound identical to **EF5** less the nitro group, the chemical shifts are significantly upfield of those for **EF5** (*e.g.* Im-H_5 : δ 7.66 (**EF5**) \rightarrow 7.16 (**ImF5**)). The electron-withdrawing NO_2 -group decreases electron density within the imidazole ring. The ^1H NMR signals for the CH_2 adjacent to the CF_2CF_3 group

for these two compounds are not effected by the presence or absence of the NO₂-group on the imidazole ring.

The chemical shift(s) of the CH₂ group(s) in the side-chain bound to the amide NH are dependent on the atoms on either side of them. For instance, the chemical shift for the CH₂ of **EF5** (bound to NH and CF₂) is 4.06 ppm, which matches exactly that of **EF3(-1)** whose only difference is that the CF₂ group is now CF₃. Comparison of the δ values for **EF5** versus **EF3** and **EF1** shows an upfield shift for the -NH-CH₂- moiety (δ 4.06 \rightarrow 3.50 \rightarrow 3.38, respectively), exhibiting the effect of the proximity and number of electronegative F-atoms. The absence of halogen atoms on the side-chain (*e.g.* as in **EPrA**) results in a δ of 3.20, even further upfield. The most pronounced effect of the fluorine atom can be seen for **EF1** (Figure 3-4) and **EF1(-1)** (Figure 3-5) as the protons for CH₂F are shifted downfield to $\delta \sim 4.50$. This group is also easily identified in the ¹H NMR spectrum as a doublet of triplets due to the large ²J_{HF} value (66 Hz and 48 Hz, respectively). The adjacent CH₂ also has a strong interaction with the fluorine atom, as indicated by ³J_{HF} values (42 Hz and 30 Hz, respectively). The NH signal for **EF1** is not observable at the magnification presented in Figure 3-4; however, the signal is present at δ 7.64 if the vertical scale is expanded. The NH signal is more pronounced for the **EF1(-1)** spectrum at δ 7.87 (Figure 3-5) and may be related to the increased amount of H₂O evident in this spectrum; the broad signal is a result of slow exchange of the NH proton, and the electrical quadrupole moment of the nitrogen nucleus that induces moderately efficient spin relaxation.⁴²

Comparison of the compounds with identical composition, except for variation in the halogen atom terminating the side-chain, demonstrates the direct correlation between electronegativity and chemical shift. The δ values for the CH₂X protons (**EF1**: δ 4.51; **EC11**: δ 3.66; **EB11**: δ 3.50) decrease almost proportionally to the decrease in electronegativity (EN) of the X atom (EN for F, Cl and Br is 4.0, 3.0 and 2.8, respectively); the trend is as expected. The same effect is observed for the **EX1(-1)** compounds. Analysis of the ¹³C NMR spectra for these compounds for the C atom

directly bound to X also exhibits the dependence of δ on EN (**EF1(-1)**: δ 84.70; **EC11(-1)**: δ 43.46; **EBr1(-1)**: δ 37.88).

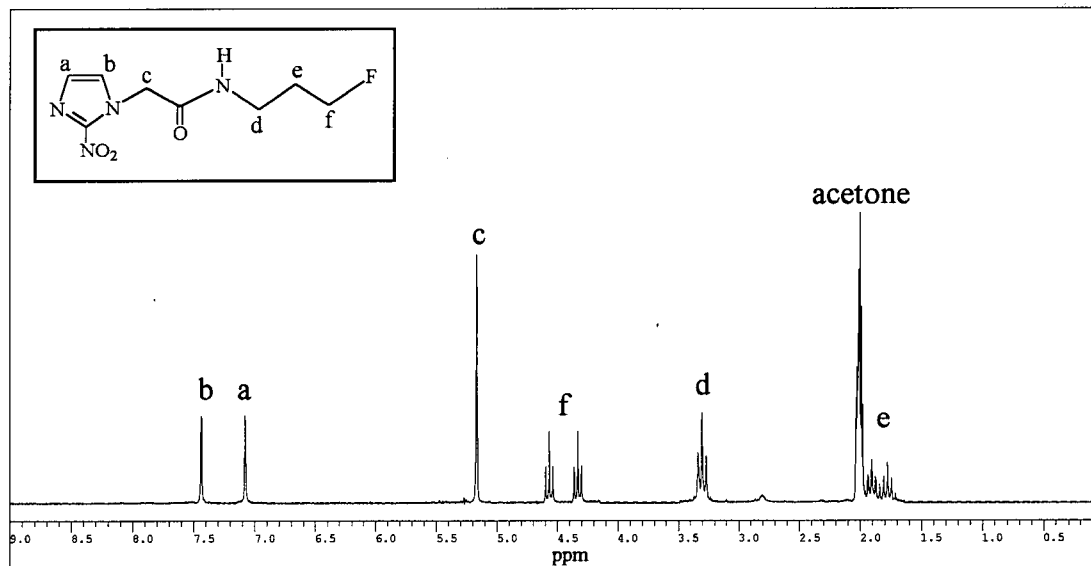


Figure 3-4: ^1H NMR spectrum of **EF1** in d_6 -acetone.

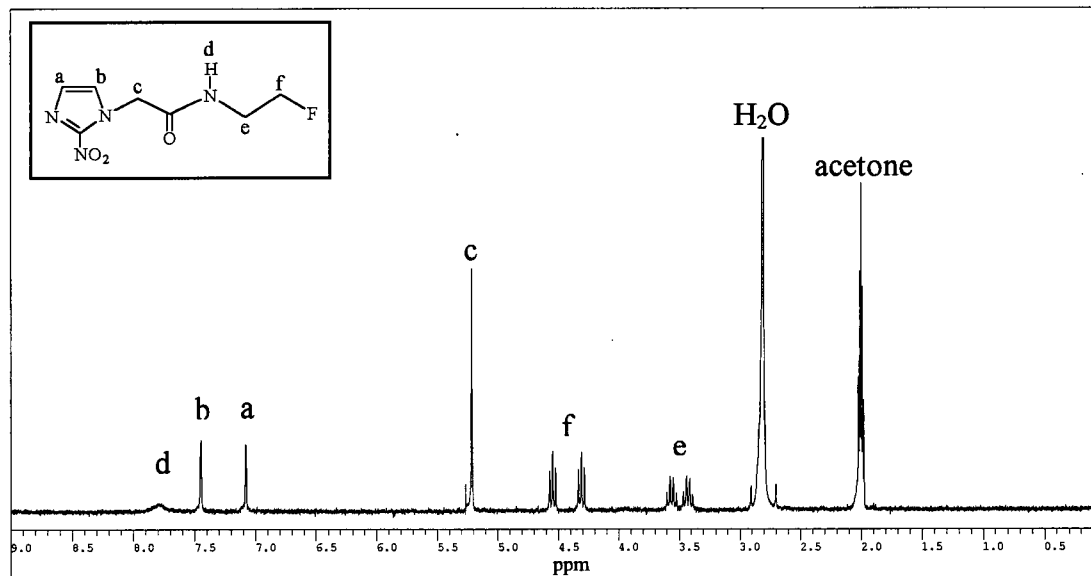


Figure 3-5: ^1H NMR spectrum of **EF1(-1)** in d_6 -acetone.

Analysis of the ^{19}F NMR spectra for the fluorinated compounds reveals some interesting and unpredictable results. For example, comparison of the chemical shifts of

the CF₃ groups of **EF5** and **EF3**, δ -4.34 and 10.84 respectively, shows results opposite to those expected. The signal for **EF5**, which has an electron-withdrawing CF₂-group adjacent to the CF₃, is further upfield than for **EF3** which has a CH₂ bound to the CF₃. Also surprising is the downfield shift of the fluorine signal for **EF2Br** (δ 32.71) when compared to that for **EF3**. The two compounds are identical with the exception of substitution of one of the F atoms by Br. The lower electronegativity of Br should have shifted the signal further upfield; however, the opposite is true. The CF₂ of **EF5** comes at δ -41.31 while the CH₂F has a signal at δ -142.50 showing that as the number of F-atoms on a single carbon decreases the signal is shifted further upfield, following the expected electronegativity trend.

Examination of the ¹H and ¹⁹F NMR spectra for the 4-nitro- and 5-nitroimidazole compounds reveals the same trends observed for the 2-nitroimidazole species. In the ¹H NMR spectra, the closer proximity of the nitro group to the imidazole proton leads to a downfield shift of the signal (e.g. **MF5**: Im-*H*₄ δ 7.93 vs. **EF5**: Im-*H*₄ δ 7.21). For both **MX1(-1)** and **2M4NX1(-1)** (where X= F, Cl and Br), chemical shift differences are observed analogous to those for the **EX1(-1)** compounds, following the trend that increased EN leads to a downfield shift in the CH₂X proton signal.

Other analytical techniques used to characterize these compounds included mass spectrometry, and UV-Vis and IR spectroscopies. The UV-Vis spectra did not reveal much information other than the presence of a nitro group on the imidazole ring (the energy band of the major chromophore was very distinctive of the nitro group position; 316, 310 and 300 nm for 2NO₂, 5NO₂, and 4NO₂, respectively). Mass spectrometry was used to characterize the compounds for which acceptable elemental analysis results were not obtainable. For the most part, the compounds with the brominated side-chains were problematic due to their highly reactive C-Br bond. The MS spectra typically contained a very weak parent peak and a base peak which corresponded to M⁺ - NO₂, suggesting that the bond between the imidazole ring and the nitro group is easily cleaved. IR spectroscopy, next to NMR spectroscopy, was the most diagnostic tool for characterizing the nitroimidazole compounds. The major bands of interest were the stretching bands for

the N-H and C=O groups of the side-chain and the N-O of the NO₂-group associated with the imidazole ring. A comparison of the IR data for these compounds shows that there is some electronic influence, albeit weak, from the substituents of the side-chain on the N-H and C=O stretching frequencies. For the most part the NO₂-group was too far removed from the substituents on the end of the side-chain to be affected. The asymmetric and symmetric ν_{NO} values were two of the more dominant bands observed in the spectrum of each nitroimidazole and typically spanned the ranges, ν_{NOasym} (1484 - 1506 cm⁻¹) and ν_{NOsym} (1361 - 1400 cm⁻¹). The 4NO₂ group had bands at slightly higher wavenumbers than those of the 2NO₂ group, while the values of the 5NO₂ group were lower. These findings may result from the proximity of the NO₂-group to the side-chain. The 4NO₂ group is the furthest removed and therefore the possibility of interaction with the side-chain via H-bonding is limited. A comparison of the 2NO₂Im compounds **EF1**, **EC11** and **EBr1** (each with -C(O)-NH-(CH₂)₂CH₂X moieties) reveals virtually no change in ν_{NH} or ν_{CO} with variation in X. When two CH₂-groups (vs. three) separate the halogen from the amide functionality, ν_{NH} and ν_{CO} both are shifted to higher values (e.g. **EF1(-1)**: ν_{CO} 1669 cm⁻¹ vs. **EF1**: ν_{CO} 1660 cm⁻¹; see Figure 3-6).

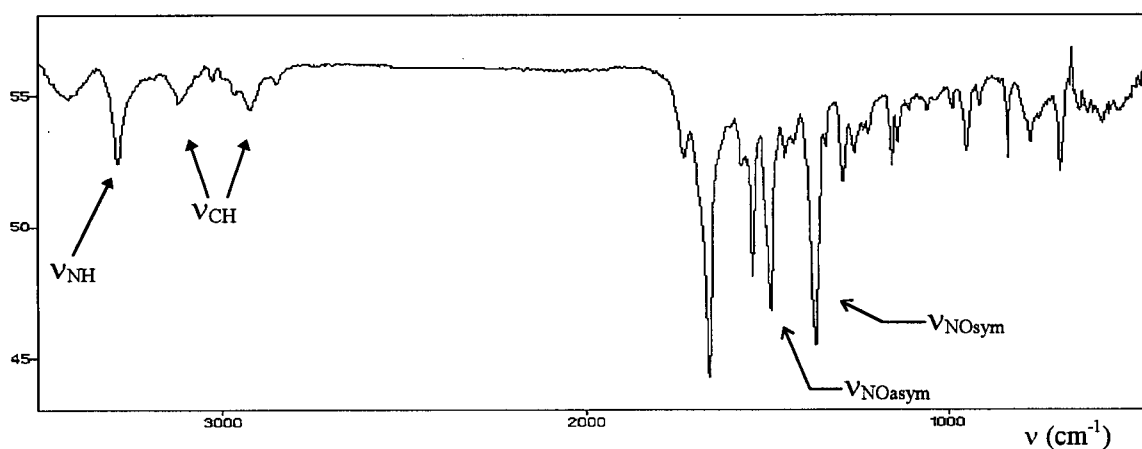


Figure 3-6: Typical IR spectrum of a 2-nitroimidazole, **EF1**.

For the three pentafluorinated compounds **EF5**, **MF5** and **2M4NF5**, X-ray structures were obtained (Figures 3-7 to 3-9, respectively). These structures may prove useful for modelling the active binding site of the MoAb used for the imaging of hypoxia

(see Chapter 6). **EF5** crystallized in the primitive monoclinic space group Pc , and all bond lengths and bond angles within the structure are in the normally expected ranges (Appendix I-1).⁵⁸ The packing of the **EF5** molecules within the unit cell results in a layered effect with inter- and intramolecular H-bonding stabilizing the lattice. The intermolecular interactions include H-bonding between H(1) and O(1), and N(2) with either F(5) or H(7), alternating every second molecule. The intramolecular interactions are stronger than the intermolecular interactions (~ 2.8 Å vs. 3.0-3.3 Å), and are observed between H(5) and O(2), involving the nitro group, and H(6) and O(1).

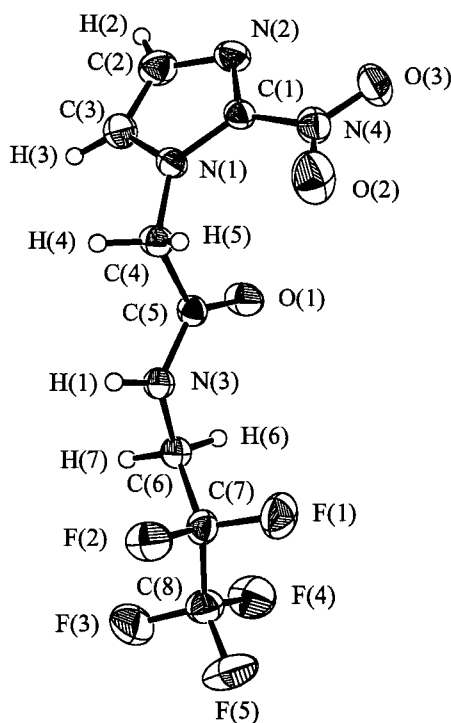


Figure 3-7: ORTEP view of **EF5**; 33 % probability thermal ellipsoids are shown.

MF5 crystallized in the primitive monoclinic space group $P2_1/c$ and the bond lengths and bond angles (Appendix I-3) were similar to those observed for **EF5**. Also,

similar to **EF5**, intramolecular H-bonding interactions are observed between H(6) and O(2) and H(9) and O(1) (2.49 and 2.39 Å, respectively). The intermolecular interactions, however, are much stronger and are observed at different points between the molecules, H(1) and N(3) and H(7) and O(1) (2.11 and 2.46 Å, respectively).

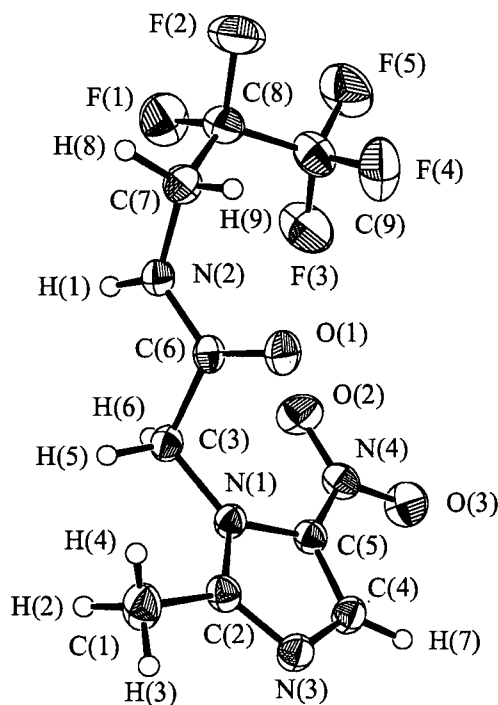


Figure 3-8: ORTEP view of **MF5**; 33 % probability thermal ellipsoids are shown.

2M4NF5 crystallized in the primitive monoclinic space group $P2_1/n$, and the bond lengths and bond angles (Appendix I-4) were also comparable to those of **EF5**⁵⁸. Disorder was observed for the CF_2 and CF_3 groups. For this molecule only a single intramolecular interaction is observed between H(10) and O(1), similar to those found in both **EF5** and **MF5**. The nitro group is at the 4-position on the imidazole ring and is far enough removed from the side-chain that no H-bonding interaction is observed for the

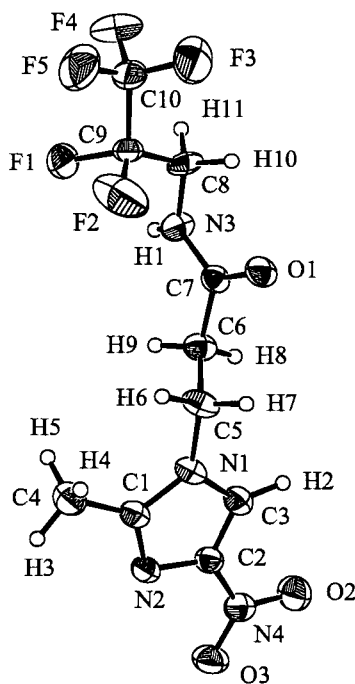


Figure 3-9: ORTEP view of **2M4NF5**; 33 % probability thermal ellipsoids are shown.

nitro moiety. Intermolecular H-bonding is observed once again between H(1) and N(2), and a new interaction between H(3) of the methyl group and F(1) is integral in the arrangement of the **2M4NF5** molecules within the lattice.

2M4NF1(-1) (Figure 3-10) crystallized in the same space group as **2M4NF5**. The F(1) atom for **2M4NF1(-1)** falls in the same position as F(1) of the CF₂ group of **2M4NF5** and again undergoes intermolecular H-bonding with the methyl group on the imidazole ring (Appendix I-5).

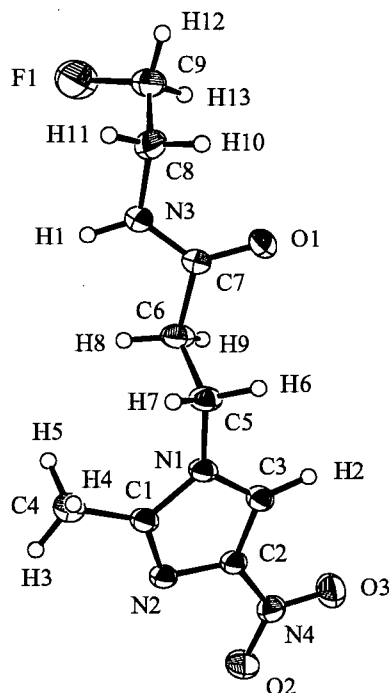
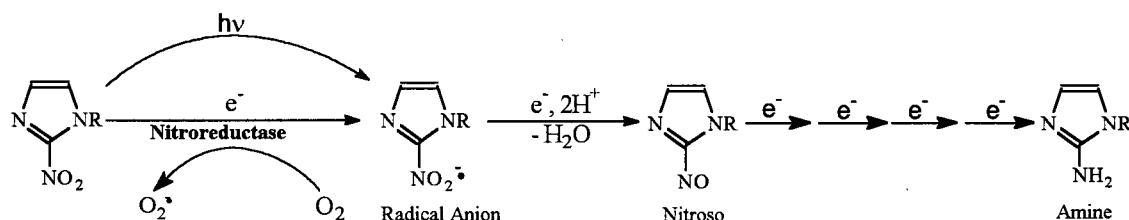


Figure 3-10: ORTEP view of **2M4NF1(-1)**; 33 % probability thermal ellipsoids are shown.

3.3.3 Electrochemistry of Nitroimidazoles

The investigation of the use of nitroimidazoles as radiosensitizers and hypoxia-selective cytotoxins has clearly verified the correlation between the efficacy of these compounds and the one-electron reduction potential of the nitro moiety.⁵⁹⁻⁶² The nitro group undergoes a series of one-electron reduction steps to finally yield the amine (Scheme 3-15). The extent to which the nitro group is reduced within a given biological system will be determined by the nature of its enzymatic activation.⁶³ The initial steps in



Scheme 3-15: Stepwise reduction of 2-nitroimidazole to 2-aminoimidazole.

the reductive metabolism of 2-nitroimidazoles are mainly catalyzed by cytochrome P₄₅₀ reductase and to a lesser extent by cytochrome P₄₅₀, both of which are found in the endoplasmic reticulum.^{64,65} The stability of the radical anion depends on the prototropic properties of the compound and pH; as the pH level decreases below physiological values the amount of DNA damage observed during radiation increases.⁶⁶ Because the hypoxic cells are low in oxygen concentration, the pH is lowered slightly because of the increased concentration of CO₂ from cellular respiration (Figure 3-11).

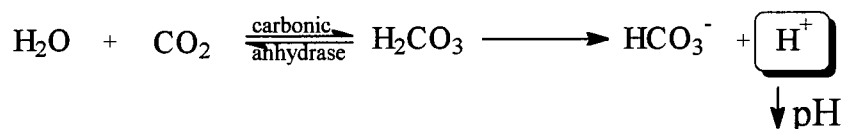


Figure 3-11: A lowering of pH levels in hypoxic cells due to increased [CO₂].

Nitroimidazoles can enter most cells of a living organism where the nitro group is reduced enzymatically. In oxic cells (high [O₂]), the reduced radical anion species is readily oxidized back to the NO₂ moiety as the reduction potential of O₂ is higher (more positive) than that of the nitroimidazole, this resulting in a futile cycle (at least for effective radiosensitization).⁶⁷ Hypoxic cells, however, have significantly reduced [O₂] and lead to binding of the reduced species to macromolecules within the vicinity of the metabolism site. Importantly, there is evidence to suggest that the reactive metabolites do not migrate out of the cells.⁶⁸

Prediction of the efficacy of nitroimidazoles as radiosensitizers or as HSCs is done in part by measuring the one-electron reduction potential, the so-called " E_7^1 ", of the nitro moiety by pulse radiolysis in neutral, buffered, aqueous media.⁶⁹ This initial reduction step activates the molecule and is the key to initiation of its action within hypoxia, although the active species may be one of the subsequently reduced species.⁶² For nitroimidazoles, the ideal reduction potential for the first reduction step falls in the range E_7^1 -300 to -450 mV vs. NHE.⁶⁹ The reduction potentials measured by cyclic voltammetry in MeCN ($E_{1/2}$) cannot be compared directly to E_7^1 values, but a linear correlation has been observed between the two and can be used to approximately convert from $E_{1/2}$ to E_7^1 and vice-versa ($E_7^1 \approx E_{1/2} - 241$ mV).^{70,71}

The electrode system used to measure the one-electron reduction potential of the nitroimidazoles from this thesis work included a Pt working and counter electrode and Ag wire (Ag/AgO) as the reference electrode. The amount of oxide deposited on the Ag wire varies from one run to the other as demonstrated by the inconsistent measurements for the ferrocene/ferrocenium redox couple (range: 330 to 660 mV vs Ag, Tables 3.2 to 3.4). To compensate for this problem, FeCp₂ was added as an internal standard for the measurement of the cyclic voltammogram of each nitroimidazole (there is a large separation between the waveforms for FeCp₂ and NO₂Im; see Figure 3-12). The measured $E_{1/2}$ value was then converted to a potential versus the SCE. Analysis of three separate solutions of the same nitroimidazole produced $E_{1/2}$ values within ± 3 mV, confirming the accuracy of this technique. Of note, the reduction potentials are measured in MeCN and so do not correlate with those reported in aqueous solution. Values can be compared to those of the known 2-NO₂Im, **SR2508**, whose reduction potential is known in aqueous solution ($E_7^1 = -388$ mV, vs. NHE)⁶⁹ and in MeCN ($E_{1/2} = -1077$ mV vs. SCE, this thesis work, Table 3.2).

There is significant variation between the CV plots for the different nitroimidazoles. For the most part, the nitroimidazole redox couple is quasi-reversible as the peaks shift further apart with increasing scan rate. The cathodic peak current is

typically not equal to the anodic peak current (Figure 3-12), a requirement of electrochemical reversibility, implying that the electron transfer to the nitroimidazole and

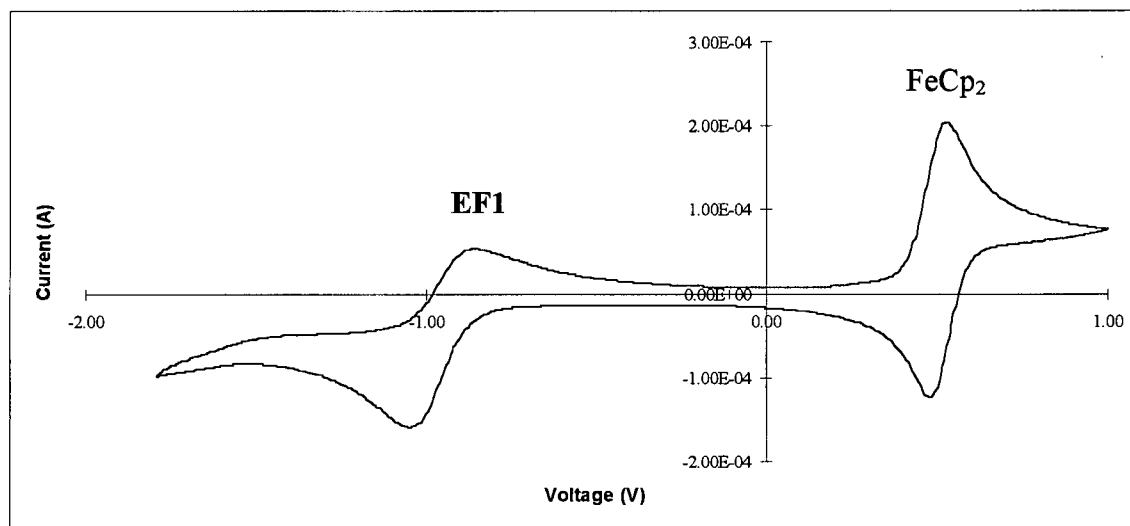


Figure 3-12: Quasi-reversible CV plot for **EF1** referenced to FeCp_2 .

back to the electrode is not completely reversible. The potential difference between the cathodic (E_{pc}) and anodic (E_{pa}) peaks was considerably higher than 59 mV, also suggesting the absence of reversibility. The $4\text{NO}_2\text{Im}$ and $5\text{NO}_2\text{Im}$ compounds exhibit even less reversible behaviour as the E_{pc} and E_{pa} peaks are further separated from one another (although a slower scan rate has little effect on the separation) and the difference between the peak currents is even more pronounced than in the $2\text{NO}_2\text{Im}$ systems (Figure 3-13).

Analysis of the reduction potentials of the nitroimidazoles (Tables 3.2 to 3.4) leads to a number of conclusions. Most importantly, the $E_{1/2}$ value decreases noticeably as the position of the nitro group is changed from 2NO_2 (-977 to -1116 mV) to 5NO_2 (-1068 to -1163 mV) to 4NO_2 (-1300 to -1415 mV) on the imidazole ring, that is, the electron affinity decreases as the nitro group changes from the $2 \rightarrow 5 \rightarrow 4$ positions. This trend is, for example, readily apparent for the pentafluorinated species **EF5**, **MF5** and **2M4NF5** which have $E_{1/2}$ values of -977, -1068 and -1300 mV, respectively. A literature example of

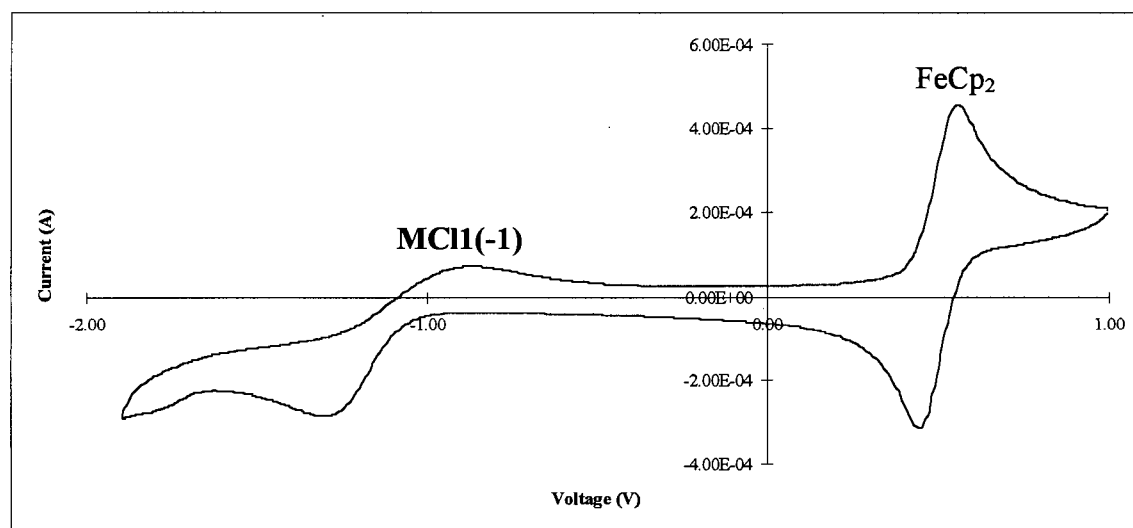


Figure 3-13: CV plot for **MCl1(-1)** referenced to **FeCp₂**.

this effect is seen with the comparison of the reduction potentials of the isomeric nitroimidazoles **RGW-601** (**2NO₂ImR**), **nimorazole** (**5NO₂ImR**) and **RGW-611** (**4NO₂ImR**, where **R** = -CH₂CH₂N(CH₂CH₂)₂O) (*E*₇¹ values of -390, -457 and -554 mV, respectively).⁵² Adams *et al.* reported that a comparison of *E*_{1/2} values within a given group reveals that the constitution of the side-chain has only a small effect on the reduction potential of the nitro group; the electron-withdrawing groups are sufficiently distant from the imidazole ring that little inductive effect is incurred on the nitro group.⁵² However, for **EF5** and the other nitroimidazoles containing more than one F-atom in their side-chains this suggestion appears to be false as there appears to be an influence on the *E*_{1/2} values (*cf.* *E*_{1/2} for **SR2508**, -1077 mV). **EF5** has the highest reduction potential at -977 mV, as expected, while successive removal of fluorine atoms leads to more negative *E*_{1/2} values (*e.g.* **EF3**, -1024 mV). Surprisingly, for the monohalogenated compounds (**EX1** and **EX1(-1)**, where **X** = F, Cl and Br) the reduction potential is significantly decreased (by ~ 80 mV) when one methylene is removed. The CV data imply that pursuit of **2NO₂Im** compounds with longer side-chains and more fluorine atoms (*i.e.* **EF5**) for use as hypoxia-selective bioreductive agents will be most advantageous.

3.3.4 Incorporation of Fluorine into an Existing Side-chain

The imaging and, more importantly, quantification of hypoxia using nitroimidazoles have been demonstrated recently using a fluorescently labeled monoclonal antibody which recognizes a bio-reduction adduct of a F-containing nitroimidazole, in this case **EF5**, within hypoxic cells.^{5,72} The problem with this technique is that it is invasive, requiring a biopsy to obtain samples of the cancerous tissues. Therefore, utilization of a technique for which hypoxia can be imaged non-invasively would be extremely advantageous. A non-invasive technique, known as positron emission tomography (PET), does exist and is used to study, for example, metabolism of dopamine (labeled with the positron-emitting isotope ^{18}F) within the heart.⁷³ Consequently, if the chemistry can be developed to incorporate ^{18}F into one of the existing nitroimidazoles synthesized in this thesis work, the new species could be used to image areas of hypoxia non-invasively. The limiting factor for this chemistry is the time taken to introduce the F-atom into the nitroimidazole and subsequently isolate the product, because the half-life of ^{18}F is only 109.8 min.

There are many potential precursor ($2\text{NO}_2\text{Im}$) compounds presented in this thesis, but the most obvious choice was **SR2508** as it contains a primary hydroxyl group. The conversion of an alcohol to a sulfonate ester is an excellent method for labeling compounds with fluorine,^{74,75} provided that these esters can be isolated. The most reactive of the sulfonate esters are the triflates which are used in the synthesis of ^{18}F -labeled sugars; the best example is 3- ^{18}F FDG,⁷⁶ the most frequently used radiolabeled imaging compound since its discovery in 1975.

The attempted synthesis of the triflate analogue of **SR2508** by its reaction with triflic anhydride was not successful (Section 3.2.5). The X-ray structure of the isolated yellow product (**19**, Figure 3-14, see Appendix I-6) revealed surprisingly a $2\text{NO}_2\text{Im}$ species containing a "cyclic" side-chain; the C(4)-C(5) bond length of 1.312 Å is consistent with the exocyclic methylene functionality. The $^{19}\text{F}\{^1\text{H}\}$ NMR spectrum displays a singlet at δ 0.88 that results from the triflate bonded at the side-chain N-atom. The ^1H NMR spectrum is consistent with the solid state structure, and shows shifts

downfield from those of the precursor **SR2508** side-chain. The signal for the methylene group between the carbonyl and the imidazole ring of **SR2508** (δ 5.21) is replaced by one

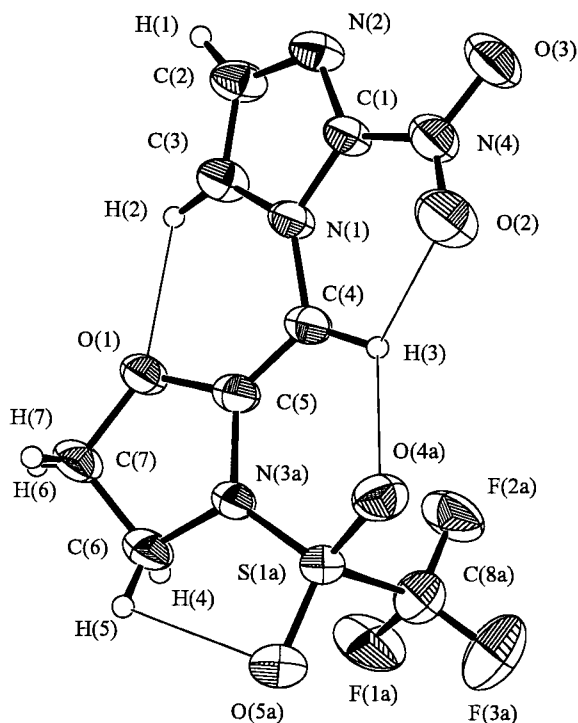
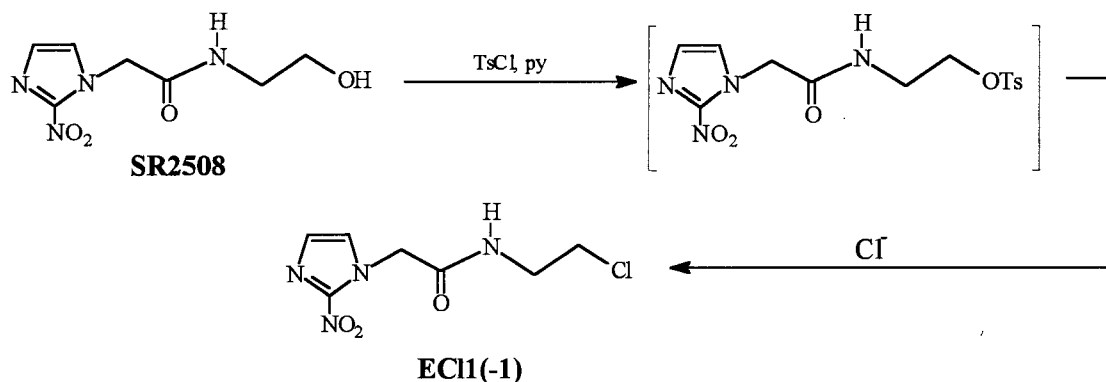


Figure 3-14: ORTEP view of **19**; 33 % probability thermal ellipsoids are shown.

at δ 6.78 corresponding to a single, olefinic proton. The H-bonding interactions, involving the oxygens of the NO₂ group (H(3)-O(2) 2.35 Å) and the SO₂CF₃ group (H(3)-O(4a) 2.50 Å) (both electron-withdrawing groups), also have a marked effect on δ value of the CH proton. The ¹H NMR signals corresponding to the two other methylene groups on the **SR2508** side-chain are also shifted significantly downfield (δ 3.59 to 4.36, and 3.34 to 4.64, for N-CH₂- and -CH₂-O, respectively) due to the intramolecular cyclization. The shift observed for the N-CH₂- protons may be because of their proximity to, and H-bonding interaction (H(5)-O(5a) 2.47 Å) with, the SO₂CF₃ group. This intramolecular

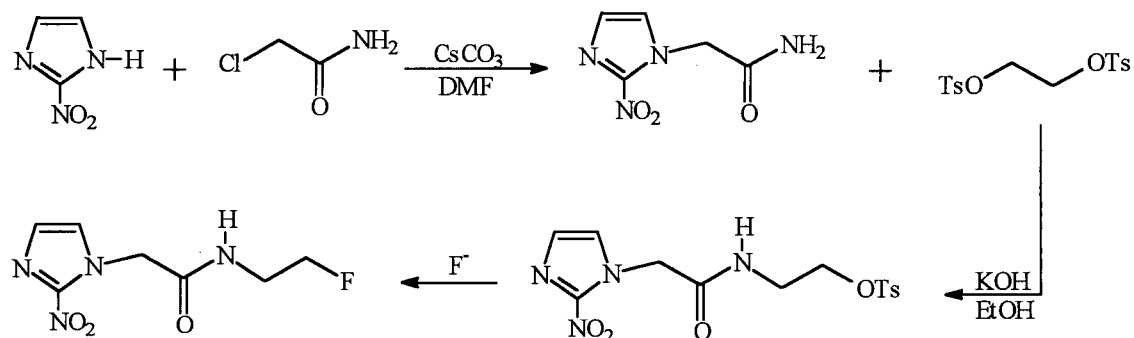
cyclization has been previously suggested,^{44,75} but no evidence was presented in either report.

The synthesis of the tosylate derivative of **SR2508** was also attempted using TsCl, but the isolated product was **EC11(-1)** formed via a presumed tosylate intermediate (Scheme 3-16). These results suggest that formation of a sulfonate ester from **SR2508** is not a viable route to the incorporation of fluorine into the side-chain via introduction of an active F-containing species. Lim and Berridge reported the isolation of the tosylated



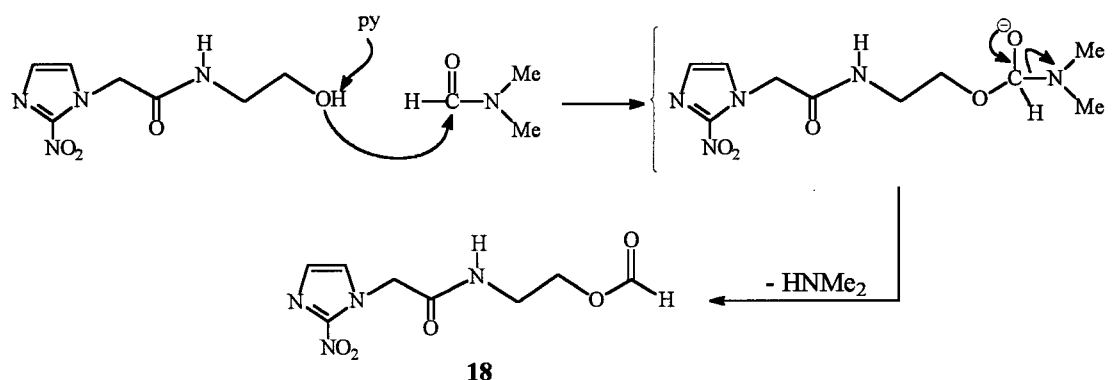
Scheme 3-16: Synthesis of **EC11(-1)** via the tosylate intermediate.

SR2508 compound via an alternate route (Scheme 3-17) and subsequent reaction with fluoride gave an acceptable yield (40 %) of **EF1(-1)**.⁷⁷ However, Tewson later reported that reaction of fluoride (¹⁸F or ¹⁹F) with the isolated tosylate gave no sign of any fluorinated product.⁴⁴ Johnstrom and Stone-Elander have reported the synthesis of the fluorinated alkylating agent 2,2,2-trifluoroethyl triflate⁷⁸ which in theory could be coupled to a nitroimidazole containing the composition required (for example, the 2-nitroimidazolacetamide in Scheme 3-17) to yield a desired product (in this case, **EF3(-1)**). This coupling would avoid unwanted side-reactions (such as nitro group displacement (to be discussed below) and cyclization chemistry) incurred by doing chemistry on the nitroimidazole itself.



Scheme 3-17: Synthesis of fluoroetanidazole (**EF1(-1)**) via a tosylate intermediate.⁷⁷

An interesting and unexpected finding during the attempted synthesis of the triflated **SR2508** was the isolation of the formate ester, compound **18** (Scheme 3-18). Originally, DMF was added to the reaction mixture to solubilize the **SR2508** in CH_2Cl_2 , and reaction of triflic anhydride under basic conditions yielded compound **19** as a minor product, but mainly **18**. The $^{19}\text{F}\{^1\text{H}\}$ NMR spectrum indicated the absence of triflate, while ^1H NMR data unveiled a new proton signal at δ 8.13 and a shifted signal for the original $\text{CH}_2\text{-O}$ protons of **SR2508** (from δ 3.34 to 4.21). These results indicated the presence of an aldehydic proton on the terminal end of the side-chain. The possibility of the new signal corresponding to a carboxylic acid functionality was nullified when the compound did not react with a fluorinated amine (using NMM and $i\text{BuClFrm}$). Further evidence supporting formation of an aldehyde is observed in the IR spectrum which displays two ν_{CO} bands at 1716 and 1655 cm^{-1} corresponding to $\text{CO}_{\text{aldehyde}}$ and CO_{amide} , respectively. Interestingly, formation of the aldehyde implies that the **SR2508** alcohol preferentially reacts with DMF over the triflic anhydride. The carbonyl C-atom of DMF is apparently more electrophilic than the S-atoms of the Tf_2O , and this leads to formation of the formate (**18**) (Scheme 3-18). This result is contrary to the expected reaction of the alcohol with Tf_2O which should be more active because of the presence of the strongly electron-withdrawing CF_3 group.⁷⁹



Scheme 3-18: Mechanism for reaction of **SR2508** with DMF to yield the formate ester (**18**).

The unsuccessful formation of a sulfonate ester of **SR2508** led to a different approach to incorporate fluorine into the side-chain. The halide substitution reaction is widely used for the synthesis of ¹⁸F-containing compounds.⁷⁶ In general, the yields of substitution products are higher with fluorine displacements of Br and I, although there is one successful synthesis which utilized ¹⁸F-for-Cl exchange.⁸⁰ According to other reactions investigated in this work (*e.g.* reactivity of **3** (Section 3.2.1.4, also see Scheme 3-3) and **IBr** (Section 3.2.1.2, also see Scheme 3-4)) the terminal C-I and C-Br bonds are quite reactive and lead to formation of intramolecular cyclization products analogous to **19**. The synthesis of an **EI1(-1)** species was unsuccessful as a cyclized product forms instantaneously, and so the **EBr1(-1)** species was used as a precursor in the exchange reactions.

The introduction of fluorine as a nucleophile requires the use of the fluoride ion; however, fluoride salts (like KF) have low solubility in organic solvents. The enhancement of K⁺ solubility in organic solvents is obtained through use of crown ethers (*e.g.* 18-crown-6) or aminopolyethers (*e.g.* 2,2,2-Kryptofix) which in turn solubilize the fluoride anion. Tetraalkylammonium fluoride salts can also be used as the cation is readily soluble in dipolar, aprotic solvents (*e.g.* MeCN, DMF and dmsO) which are the preferred solvents for the exchange reaction. Because the nucleophilicity of the fluoride ion is decreased in

the presence of H₂O (truly anhydrous fluoride has never been achieved), the use of dry solvents and a dry atmosphere is essential.

The reaction of Bu₄NF•H₂O with **EBr1** (section 3.2.7.1) did not yield the desired **EF1** product, but data suggest that the fluoride was incorporated into the isolated product. UV-Vis analysis revealed a split in the major chromophore of the precursor **EBr1** at 328 nm, two bands at 264 and 372 nm being seen. IR analysis revealed the disappearance of the ν_{NO} bands of **EBr1** at 1484 and 1386 cm⁻¹ which indicates nucleophilic displacement of the NO₂-group.^{81,82} The ¹H NMR spectrum revealed no change in the splitting pattern for the methylene groups on the side-chain, while incorporation of a F-atom would lead to two doublet of triplets. The ¹⁹F{¹H} NMR spectrum, however, does show that F is present (δ -69.85). As no H-F coupling is observed in the ¹H NMR spectrum, the F atom is assumed to be at the 2-position of the imidazole ring and the product is formulated as **25**; no peak is observed at δ -142.50 for **EF1**. The nucleophilic displacement of the NO₂-group appears to be quite facile,⁸³ and occurs independently of the position of the NO₂-group in the imidazole ring (see Section 3.2.7.4, p.92). This reaction is actually used as a method for incorporation of ¹⁸F into N-methylspiroperidol, a PET agent used for investigating dopamine receptors.⁸⁴ Investigation of the reaction of **EBr1** with an ¹⁸F fluoride source gave up to a 2 % radiochemical yield of [¹⁸F]-**EF1**¹⁰, implying that γ -ray detection is a more sensitive technique than NMR for detection of the fluorinated nitroimidazole.

The synthesis of **EF2Br** (Section 3.2.2.8) was intended to increase the electrophilicity of the C-Br carbon to the point where fluoride would preferentially react at the C-Br to displace the bromine (and generate **EF3**), rather than at the 2-position of the imidazole ring to displace the NO₂ group. The X-ray structure of **EF2Br** (Figure 3-15, see Appendix I-2) shows that the C(8)-Br(1) bond (1.936(3) Å) is much longer than either of the C(8)-F(1 or 2) bonds (average = 1.353(4) Å). Unfortunately, the fluorine atoms on **EF2Br** apparently increase the acidity of the protons on the CH₂ group adjacent to CF₂Br, and reaction of **EF2Br** with Bu₄NF•H₂O resulted in the elimination of HBr to form the difluoroalkene, **E=F2**. ¹⁹F{¹H} NMR analysis of the reaction mixture before **E=F2** was

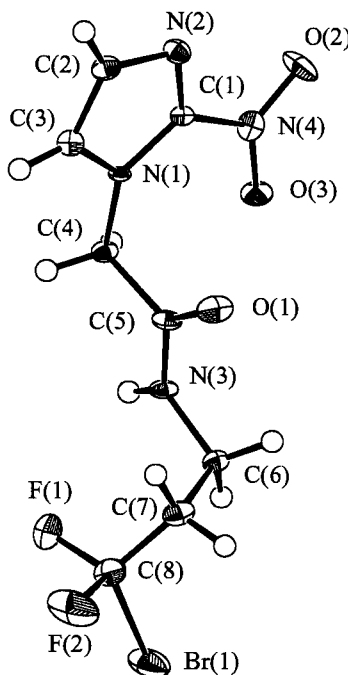


Figure 3-15: ORTEP view of **EF2Br**; 33 % probability thermal ellipsoids are shown.

isolated indicated that there was some NO₂-group displacement, but no signals corresponding to **EF3** were observed. In order to prevent the elimination of HBr, **EF4Br** was synthesized (Section 3.2.2.5) that in which the β-H atoms of **EF2Br** were replaced by F-atoms. **EF4Br**, however, was totally inert and did not react with fluoride, even at high [F⁻] and high temperatures (and a small amount of the nitro displacement product was detected using ¹⁹F{¹H} NMR).⁸⁵ These results suggest that the chemistry of the side-chain needs to be investigated further before a high yield exchange reaction can be accomplished.

3.4 References

- 1 Urtasun, R. C.; Chapman, J. D.; Raleigh, J. A.; Franko, A. J.; Koch, C. J. *Int. J. Radiat. Oncol. Biol. Phys.* **1986**, *12*, 1263.
- 2 Lord, E. M.; Harwell, L.; Koch, C. J. *Cancer Res.* **1993**, *53*, 5271.
- 3 Woods, M. L.; Koch, C. J.; Lord, E. M. *Int. J. Rad. Oncol. Biol. Phys.* **1996**, *34*, 93.
- 4 Southwick, P. L.; Ernst, L. A.; Tauriello, E. W.; Parker, S. R.; Mujumdar, R. B.; Mujumdar, S. R.; Clever, H. A.; Waggoner, A. S. *Cytometry* **1990**, *11*, 418.
- 5 Koch, C. J.; Evans, S. M.; Lord, E. M. *Br. J. Cancer* **1995**, *72*, 869.
- 6 Evans, S. M.; Jenkins, W. T.; Joiner, B.; Lord, E. M.; Koch, C. J. *Cancer Res.* **1996**, *56*, 405.
- 7 Evans, S. M.; Joiner, B.; Jenkins, W. T.; Laughlin, K. M.; Lord, E. M.; Koch, C. J. *Br. J. Cancer* **1995**, *72*, 875.
- 8 Wong, T. Y. H. Ph.D. Thesis, University of British Columbia, 1996.
- 9 Pattison, F. L. M.; Howell, W. C.; White, R. W. *J. Am. Chem. Soc.* **1956**, *78*, 3487.
- 10 Kachur, A. V.; Evans, S. M.; Shiue, C. -Y.; Dolbier, Jr., W. R.; Li A. -R.; Roche, A.; Skov, K. A.; Baird, I. R.; James, B. R.; Koch, C. J. *Appl. Rad. Isot.* submitted.
- 11 Middleton, W. J. *J. Org. Chem.* **1975**, *40*, 574.
- 12 Markovskij, L. N.; Pashinnik, V. E.; Kirsanov, A. V. *Synthesis* **1973**, 787.
- 13 Gibson, M. S.; Bradshaw, R. W. *Angew. Chem. Int. Ed. Engl.* **1968**, *7*, 919.
- 14 Sheehan, J. C.; Ryan, J. J. *J. Am. Chem. Soc.* **1951**, *73*, 1204.
- 15 Elemental analysis data obtained in collaboration with Dr. A. Kachur (Univ. of Penn.).
- 16 Beaman, A. G.; Duschinsky, R.; Tautz, W. P. U.S. Patent #3679698 (**1972**).
- 17 This work, performed during the course of my Ph. D., was recently published: Baird, I. R.; Rettig, S. J.; James, B. R.; Skov, K. A. *Synth. Commun.* **1998**, *28*, 3701.
- 18 Knorr, R.; Trzeciak, A.; Bannwarth, W.; Gillessen, D. *Tetrahedron Lett.* **1989**, *30*, 1927.
- 19 Bannwarth, W.; Schmidt, D.; Stallard, R. L.; Hormung, C.; Knorr, R.; Müller, F. *Helv. Chim. Acta* **1988**, *71*, 2085.

- 20 Hay, M. P.; Wilson, W. R.; Moselen, J. W.; Palmer, B. D.; Denny, W. A. *J. Med. Chem.* **1994**, 37, 381.
- 21 Kajfez, F.; Sunjic, V.; Kolbah, D.; Fajdiga, T.; Oklodziga, M. *J. Med. Chem.* **1968**, 11, 167.
- 22 Mann, F. G.; Porter, J. W. G. *J. Chem. Soc.* **1945**, 751.
- 23 Fortier, D. G.; McAuley, A. *Inorg. Chem.* **1989**, 28, 655.
- 24 Fortier, D. G.; McAuley, A. *J. Am. Chem. Soc.* **1990**, 112, 2640.
- 25 Koch, C. Private communication, Univ. of Penn.
- 26 Connelly, N. G.; Geiger, W. E. *Chem. Rev.* **1996**, 96, 877.
- 27 Jenkins, T. C. *In The Chemistry of Antitumour Agents*; D. E. V. Wilman, Ed.; Blackie and Son Ltd., Glasgow, 1990, p. 354.
- 28 Kagiya, T.; Abe, M.; Nishimoto, S.; Shibamoto, Y.; Shimokawa, K.; Hisanaga, Y.; Nakada, T.; Yoshizawa, T. U.S. Patent #4927941 (1990).
- 29 Kagiya, T.; Abe, M.; Nishimoto, S.; Shibamoto, Y.; Otomo, K.; Tanami, T.; Shimokawa, K.; Yoshizawa, Y. U.S. Patent #4977273 (1990).
- 30 Kagiya, T.; Abe, M.; Nishimoto, S.; Shibamoto, Y.; Shimokawa, K.; Hisanaga, Y.; Nakada, T.; Yoshizawa, T. U.S. Patent #5304654 (1994).
- 31 Tracy, M.; Kelson, A. B.; Workman, P.; Lewis, A. D.; Aboagye, E.O. International Patent: PCT/US95/09611 (1996).
- 32 Adams, G. E.; Clarke, E. D.; Flockhart, I. R.; Jacobs, R. S.; Sehmi, D. S.; Stratford, I. J.; Wardman, P.; Watts, M. E. *Int. J. Radiat. Biol.* **1979**, 35, 133.
- 33 Urtasan, R. C.; Band, P.; Chapman, J. D.; Rabin, H. R.; Wilson, A. F.; Fryer, C. G. *Radiology* **1977**, 122, 801.
- 34 Coleman, C. N.; Urtasan, R. C.; Wasserman, T. H.; Hancock, S.; Harris, J. W.; Halsey, J.; Hirst, K. V. *Int. J. Radiat. Oncol. Biol. Phys.* **1984**, 10, 1749.
- 35 Husted, D. R.; Ahlbrecht, A. H. *J. Am. Chem. Soc.* **1953**, 75, 1605.
- 36 Haszeldine, R. N.; Leedham, K. *J. Chem. Soc.* **1953**, 1548.

-
- 37 Calvert, J. G.; Pitts, Jr., J. N. *Photochemistry*; John Wiley and Sons, New York, 1966, p. 522.
- 38 Threadgill, M. D.; Webb, P. *Synth. Commun.* **1990**, *20*, 2319.
- 39 Brown, H. C.; Heim, P. *J. Org. Chem.* **1973**, *38*, 912.
- 40 Jenkins, T. C.; Naylor, M. A.; O'Neill, P.; Threadgill, M. D.; Cole, S.; Stratford, I. J.; Adams, G. E.; Fielded, M.; Suto, M. J.; Stier, M. A. *J. Med. Chem.* **1990**, *33*, 2603.
- 41 Koh, W.-J.; Rasey, J. S.; Evans, M. L.; Grierson, J. R.; Lewellen, T. K.; Graham, M. M.; Krohn, K. A.; Griffin, T. W. *Int. J. Radiat. Oncol. Biol. Phys.* **1992**, *22*, 199.
- 42 Silverstein, R. M.; Bassler, G. C.; Morrill, T. C. *Spectrometric Identification of Organic Compounds*, 5th edn.; John Wiley and Sons, Toronto, 1991, p. 185.
- 43 Chi, D. Y.; Kilbourn, M. R.; Katzenellenbogen, J. A.; Welch, M. J. *J. Org. Chem.* **1987**, *52*, 658.
- 44 Tewson, T. J. *Nucl. Med. Biol.* **1997**, *24*, 755.
- 45 Pattison, F. L. M.; Cott, W. J.; Howell, W. C.; White, R. W. *J. Am. Chem. Soc.* **1956**, *78*, 3484.
- 46 Pattison, F. L. M.; Howell, W. C.; White, R. W. *J. Am. Chem. Soc.* **1956**, *78*, 3487.
- 47 Middleton, W. J. *J. Org. Chem.* **1975**, *40*, 574.
- 48 Olah, G. A.; Nojima, M.; Kerekes, I. *Synthesis* **1973**, 786.
- 49 Olah, G. A.; Nojima, M.; Kerekes, I. *J. Am. Chem. Soc.* **1974**, *96*, 925.
- 50 Wilson, R. L.; Cramp, W. A.; Ings, R. M. J. *Int. J. Radiat. Biol.* **1974**, *26*, 557.
- 51 Denny, W. A.; Roberts, P. B.; Anderson, R. F.; Brown, J. M.; Wilson, W. R. *Int. J. Radiat. Biol. Oncol. Phys.* **1992**, *22*, 553.
- 52 Adams, G. E.; Clarke, E. D.; Flockhart, I. R.; Jacobs, R. S.; Sehmi, D. S.; Stratford, I. J.; Wardman, P.; Watts, M. E.; Parrick, J.; Wallace, R. G.; Smithen, C. E. *Int. J. Radiat. Biol.* **1979**, *35*, 133.
- 53 Edwards, D. I.; Dye, M.; Carne, H. *J. Gen. Microbiol.* **1973**, *76*, 135.
- 54 Franko, A. J. *Int. J. Radiat. Oncol. Biol. Phys.* **1986**, *12*, 1195.
- 55 Anderson, C.; Beauchamp, A. L. *Inorg. Chem.* **1995**, *34*, 6065.

- 56 Anderson, C.; Beauchamp, A. L. *Inorg. Chim. Acta* **1995**, 233, 33.
- 57 Clarke, M. J. *In Progress in Clinical Biochemistry*; Springer-Verlag, Berlin, 1989, Vol. 10, p.25.
- 58 Orpen, G. A.; Brammer, L.; Allen, F. H.; Kennard, O.; Watson, D. G.; Taylor, R. J. *Chem. Soc., Dalton Trans.* **1989**, S31.
- 59 Adams, G. E.; Stratford, I. J.; Wallace, R. G.; Wardman, P.; Watts, M. E. *J. Natl. Cancer Inst.* **1980**, 64, 555.
- 60 Adams, G. E.; Flockhart, I. R.; Smithen, C. E.; Stratford, I. J.; Wardman, P.; Watts, M. E. *Radiat. Res.* **1976**, 67, 9.
- 61 Denny, W. A.; Wilson, W. R. *J. Med. Chem.* **1986**, 29, 879.
- 62 Denny, W. A.; Wilson, W. R.; Hay, M. P. *Br. J. Cancer* **1996**, 74, S32.
- 63 Joseph, P.; Jaiswal, A. K.; Stobbe, C. C.; Chapman, J. D. *Int. J. Radiat. Oncol. Biol. Phys.* **1994**, 29, 351.
- 64 McManus, M. E.; Lang, M. A.; Stuart, K.; Strong, J. *Biochem. Pharmacol.* **1982**, 31, 547.
- 65 Walton, M. I.; Workman, P. *Biochem. Pharmacol.* **1987**, 36, 887.
- 66 Edwards, D. I.; Knight, R. C.; Zahoor, A. *Int. J. Radiat. Oncol. Biol. Phys.* **1986**, 12, 1207.
- 67 Wardman, P.; Clarke, E. D. *Biochem. Biophys. Res. Commun.* **1976**, 69, 942.
- 68 Aboagye, E. O.; Lewis, A. D.; Johnson, A.; Workman, P.; Tracy, M.; Huxham, I. M. *Br. J. Cancer* **1995**, 73, 312.
- 69 Wardman, P. *Environ. Health Perspec.* **1985**, 64, 309.
- 70 Breccia, A.; Berrilli, G. Roffia, S. *Int. J. Radiat. Biol.* **1979**, 36, 85.
- 71 Tercel, M.; Wilson, W. R.; Denny, W. A. *J. Med. Chem.* **1993**, 36, 2578.
- 72 Evans, S. M.; Joiner, B.; Jenkins, W. T.; Laughlin, K. M.; Lord, E. M.; Koch, C. J. *Br. J. Cancer* **1995**, 72, 875.
- 73 Brennan, M. B. *Chemical and Engineering News* **1996**, 2, 26.

- 74 Kiesewetter, D. O.; Kilbourn, M. R.; Landvatter, S. W.; Heiman, D. F.; Katzenellenbogen, J. A.; Welch, M. J. *J. Nucl. Med.* **1984**, *25*, 1212.
- 75 Chi, D. Y.; Kilbourn, M. R.; Katzenellenbogen, J. A.; Welch, M. J. *J. Org. Chem.* **1987**, *52*, 658.
- 76 Kilbourn, M. R. Fluorine-18 Labeling of Radiopharmaceuticals, *Nucl. Med.* (Nuclear Science Series), National Academy Press, Washington, D. C., 1990, p. 49.
- 77 Lim, J. -L.; Berridge, M. S. *J. Nucl. Med. 41st Annual Meeting*, 1994, section 6P, No.13.
- 78 Johnstrom, P.; Stone-Elander, S. *J. Labelled Compd. Radiopharm.* **1995**, *36*, 537.
- 79 McBee, E. T.; Battershell, R. D.; Braendlin, H. P. *J. Chem. Soc.* **1962**, 3157.
- 80 Luxen, A.; Barrio, J. R.; Satyamurthy, N.; Bida, G. T.; Phelps, M. E. *J. Fluorine Chem.* **1987**, *36*, 83.
- 81 Beck, J. R. *Tetrahedron* **1978**, *34*, 2057.
- 82 Bartoli, G.; Todesco, P. E. *Acc. Chem. Res.* **1977**, *10*, 125.
- 83 Beck, J. R. *Tetrahedron* **1978**, *34*, 2057.
- 84 Arnett, C. D.; Wolf, A. P.; Shiue, C. -Y.; Fowler, J. S.; MacGregor, R. R.; Christman, D. R.; Smith, M. R. *J. Nucl. Med.* **1986**, *27*, 1878.
- 85 Kachur, A.; Koch, C. Unpublished results (Univ. of Penn.).

Chapter 4

Synthesis and Characterization of Ru(II) and Ru(III) Imidazole Complexes

4.1 Introduction

Ruthenium imidazole complexes as chemotherapeutic agents show less cytotoxicity than their platinum counterparts.^{1,2} These Ru complexes are of interest for their antitumour activity,³ for their ability to ligate radiosensitizing agents to DNA,⁴ as models for the bonding of Ru to nucleic acids (occurring most frequently on the imidazole ring of guanine),^{5,6} and as a new class of compounds that, in the low nanomolar range, specifically inhibit the proliferation of human T-lymphocytes *in vitro*.^{2,7} The interaction of Ru complexes with biomolecules has been studied extensively,^{8,9} and the form of the complex surviving to coordinate the biomolecules usually differs from that originally introduced into the organism. This is especially true for Ru(III) complexes which are transformed by an *in vivo* reduction to Ru(II), a more active species toward DNA binding, as reduction accelerates substitution reactions at the metal center.¹⁰

This chapter reports the synthesis of some new Ru(II) and Ru(III) imidazole and nitroimidazole complexes which may have potential biological implications. Several different starting materials (see Chapter 2) were used, and the product complexes were characterized using NMR, UV-Vis, IR, MS, elemental analysis, conductivity and magnetic moment (Evans method) measurements, while X-ray analysis was only performed on the Ru(II) hexakis(imidazole) complexes and *mer*-RuCl₃(MeCN)₃.

4.2 Experimental Section

4.2.1 Complexes Synthesized from $[\text{Ru}(\text{DMF})_6][\text{CF}_3\text{SO}_3]_3$

4.2.1.1 $[\text{Ru}(\text{Im})_6][\text{CF}_3\text{SO}_3]_2$ (**28**)

In a 100 mL Schlenk tube, $[\text{Ru}(\text{DMF})_6][\text{CF}_3\text{SO}_3]_3$ (0.362 g, 0.367 mmol) was dissolved in MeOH (20 mL) under N_2 to yield a bright yellow solution. Finely ground Im (0.189 g, 2.78 mmol), dissolved in hot MeOH (5 mL), was then added. The mixture was stirred at 70 °C for 5 h over which time the solution became orange and then dark green; however, the reaction remained incomplete according to TLC (CH_2Cl_2 :MeOH, 20:1). The solution was thus stirred at 40 °C for an additional 8 h. The MeOH was removed *in vacuo* leaving a dark green gum that contained DMF. Acetone (5 mL) was then added, followed by CH_2Cl_2 (~30 mL) which resulted in a green, microcrystalline precipitate. This was collected, washed with warm CH_2Cl_2 (6 x 5 mL, to ensure removal of excess Im) and dried *in vacuo* at 80 °C for 2 days (yield 0.236 g, 80%). Dark green, X-ray quality crystals resulted from slow evaporation of a MeOH solution of **28**. Anal. calc. for $\text{C}_{20}\text{H}_{24}\text{N}_{12}\text{F}_6\text{S}_2\text{O}_6\text{Ru}$: C, 29.74; H, 3.00; N, 20.81; found C, 29.87; H, 2.87; N, 20.45. IR (ν , cm^{-1}): 3329 (N-H); 3145, 2966, 2864 (C-H); 1253, 1226(sh), 1173, 1068, 1027, 766, 636. UV-Vis (MeOH): 218 (12.3), 288 (7.6), 642 (0.033); for free Im, 216 (1.6). ^1H NMR (200 MHz, d_6 -dmso): δ 12.47 (s, 1H, Im- H_1), 7.23 (s, 1H, Im- H_5), 6.88 (br s, 1H, Im- H_2), 6.22 (s, 1H, Im- H_4). $^{19}\text{F}\{^1\text{H}\}$ NMR (188 MHz, d_6 -dmso): δ -1.20 (s, CF_3SO_3^-). $E_{1/2} = 246$ mV.

4.2.1.2 $[\text{Ru}(\text{NMeIm})_6][\text{CF}_3\text{SO}_3]_2$ (**29**)

In a 2-neck, 25 mL flask, equipped with a reflux condenser, $[\text{Ru}(\text{DMF})_6][\text{CF}_3\text{SO}_3]_3$ (0.088 g, 0.089 mmol) was dissolved in neat NMeIm (8 mL) under N_2 to give a bright yellow solution. The mixture was stirred at 70 °C. After 2 h the solution became pale green and slowly became darker with time. After 20 h, at which time the solution had become orange-brown, the mixture was immersed in an ice-bath; addition of toluene (10 mL) resulted in a creamy white precipitate, that was collected, washed with Et_2O (4 x 5

mL) and dried *in vacuo* at 80 °C for 3 days (yield 0.0691 g, 87%). Bright yellow crystals suitable for X-ray analysis formed from slow cooling of a hot MeOH solution of **29**. Anal. calc. for $C_{26}H_{36}N_{12}F_6S_2O_6Ru$: C, 35.02; H, 4.07; N, 18.85; found C, 35.13; H, 3.95; N, 18.93. IR (ν , cm^{-1}): 3131, 2967, 2926 (C-H); 1533, 1270, 1226(sh), 1151, 1094, 1033, 637. UV-Vis (MeOH): 224 (12.1), 298 (10.2); for free NMeIm, 220 (1.3). 1H NMR (200 MHz, d_6 -dmsO): δ 7.28 (s, 1H, Im- H_5), 7.20 (s, 1H, Im- H_2), 6.31 (s, 1H, Im- H_4), 3.68 (s, 3H, Im- NMe). $^{19}F\{^1H\}$ NMR (188 MHz, d_6 -dmsO): δ -1.21 (s, $CF_3SO_3^-$). $E_{1/2} = 271$ mV.

4.2.1.3 $[Ru(5MeIm)_6][CF_3SO_3]_2$ (**30**)

In a 100 mL Schlenk tube, $[Ru(DMF)_6][CF_3SO_3]_3$ (0.352 g, 0.357 mmol) was dissolved in MeOH (15 mL) under N_2 to give a bright yellow solution. 4(5)MeIm (0.240 g, 2.92 mmol) dissolved in hot MeOH (5 mL) was then added, when the solution became orange. After being stirred at 70 °C for 4 h, the solution became dark brown-green. The MeOH was removed *in vacuo* leaving a dark brown gum. Acetone and CH_2Cl_2 were added (~5 mL each) to yield a brown-green solution which upon addition of Et_2O gave a yellow precipitate (yield 0.210 g, 66%). Bright yellow crystals suitable for X-ray diffraction formed from slow cooling of a hot MeOH solution of **30**. Anal. calc. for $C_{26}H_{36}N_{12}F_6S_2O_6Ru$: C, 35.02; H, 4.07; N, 18.85; found C, 35.07; H, 4.09; N, 18.77. IR (ν , cm^{-1}): 3267 (N-H); 3187, 3016, 2903 (C-H); 1599, 1263, 1225(sh), 1170, 1099, 1030, 820, 637. UV-Vis (MeOH): 228 (12.1), 292 (5.6), 366 (sh); for free 4(5)MeIm, 220 (2.7). 1H NMR (200 MHz, d_6 -dmsO, for isolated crystals): δ 12.09 (br s, 1H, Im- H_1), 6.85 (s, 1H, Im- H_2), 6.03 (s, 1H, Im- H_4), 2.40 (s, 3H, Im-5Me); (for yellow precipitate) δ 12.10 (br s, 12H, Im- H_1), 6.95 and 6.85 (overlapping singlets, 12H, Im- H_2), 6.60 (s, 1H, Im- H_5), 6.28 (s, 5H, Im- H_4), 6.03 (s, 6H, Im- H_4), 2.40 (s, 36H, Im-5Me + Im-4Me). $^{19}F\{^1H\}$ NMR (188 MHz, d_6 -dmsO): δ -1.22 (s, $CF_3SO_3^-$). $E_{1/2} = 174$ mV.

Pure complexes **28** - **30** were also synthesized from $[Ru(DMF)_6][CF_3SO_3]_2$ and the appropriate imidazole in MeOH. The reaction times were considerably shorter (2 h maximum) than those described in the above syntheses, and the yields were similar to those from the Ru(III) precursor.

4.2.1.4 *trans*-[Ru(CO)(DMF)(2MeIm)₄][CF₃SO₃]₂ (**31**),
 [Ru(DMF)(2MeIm)₄][CF₃SO₃]₂ (**32**) and
 [Ru(CF₃SO₃)_x(2MeIm)₄][CF₃SO₃]_y (x=2, y=0; or x=1=y) (**33**)

The procedure used was identical to that used for the synthesis of **28**, but using [Ru(DMF)₆][CF₃SO₃]₃ (0.208 g, 0.211 mmol) and 2MeIm (0.123 g, 1.49 mmol); colour changes similar to those noted for the Im system were seen. For the work-up procedure, the MeOH volume was reduced to ~5 mL and then Et₂O (20 mL) was added slowly. The green solution became cloudy, and storage at 0 °C for 16 h resulted in a green, crystalline solid (**31**), which was collected, washed with Et₂O (3 x 5 mL) and dried *in vacuo* at r.t. During pumping, the green solid started to turn brown and after 4 h was a dark brown solid formulated as [Ru(DMF)(2MeIm)₄][CF₃SO₃]₂ (**32**). ¹H NMR (200 MHz, d₆-acetone) (**32**): δ 11.91 (br s, 4H, Im-*H*₁), 8.40 (s, 1H, DMF-*H*), 6.77 (s, 4H, Im-*H*₅), 6.61 (s, 4H, Im-*H*₄), 3.22 (s, 3H, DMF-*Me*), 3.10 (s, 3H, DMF-*Me*), 2.45 (s, 12H, Im-2*Me*). ¹⁹F{¹H} NMR (188 MHz, d₆-acetone): δ -1.21 (s, CF₃SO₃⁻). If acetone is added to the NMR sample, a new peak appears at δ 2.14 (s, coord. Me₂C=O), slightly downfield of the free acetone peak (δ 2.04). If the brown solid was pumped on at 80 °C, it turned black, being converted to [Ru(CF₃SO₃)_x(2MeIm)₄][CF₃SO₃]_y (**33**). ¹H NMR (200 MHz, d₆-dmsO): δ 12.11 (br s, 1H, Im-*H*₁), 7.24 (s, 1H, Im-*H*₅), 7.03 (s, 1H, Im-*H*₄), 2.07 (s, 3H, Im-2*Me*). ¹⁹F{¹H} NMR (188 MHz, d₆-dmsO): δ -1.21 (s, CF₃SO₃⁻). Anal. calc. for C₁₈H₂₄N₈F₆S₂O₆Ru (**33**): C, 29.71; H, 3.32; N, 15.40; (for C₁₈H₂₄N₈F₆S₂O₆Ru•H₂O (and **33** was extremely hygroscopic): C, 29.00; H, 3.51; N, 15.03); found C, 29.05; H, 3.52; N, 14.73. IR (ν, cm⁻¹): (**31**) 3257, 3134, 2933, 2861, 2103 (C≡O), 1654 (C=O_{DMF}), 1572, 1283, 1249, 1167, 1030, 749, 638; (**32**) 3256, 3129, 2929, 2857, 1648 (C=O_{DMF}), 1572, 1284, 1248, 1167, 1030, 749, 638; (**33**) 3249, 3127, 2926, 2850, 1572, 1280, 1251, 1169, 1031, 754, 639. Conductivity of **33** (MeOH): Λ_M 115 (1 min) [1:1 electrolyte], becoming 165 after 3 h [2:1 electrolyte]. GC data: retention times for MeOH (5.26 min) and dry dimethylamine (5.06 min) match those found in the headspace of the sealed reaction vessel used for the synthesis of **31** (5.29 and 5.05 min).

4.2.1.5 [Ru(2NO₂Im)₆][CF₃SO₃]₂ (**34**)

In a Schlenk tube, [Ru(DMF)₆][CF₃SO₃]₃ (0.0715 g, 0.0724 mmol) was dissolved in MeOH (10 mL) under N₂ to give a bright yellow solution. 2NO₂Im (0.0513 g, 0.454 mmol) dissolved in hot MeOH (5 mL) was then added. The solution initially became green after stirring at 70 °C for 1 h, and then slowly became darker, yielding a navy blue mixture after 18 h. A small amount of blue precipitate was present on the walls of the reaction vessel, however, upon sonication of the mixture the solid dissolved. The addition of Et₂O (25 mL) to the reaction mixture led to the formation of a dark blue precipitate which was collected and then washed with Et₂O (3 x 5 mL) followed by hot MeOH, until there was no evidence (using TLC) of unreacted 2NO₂Im in the filtrate. The isolated solid was dried *in vacuo* for 3 d at 80 °C to yield 0.0209 g (27 %). Once isolated as a powdered solid, **34** was insoluble in all solvents tested (MeOH, EtOH, THF, H₂O, DMF, acetone, CH₂Cl₂, toluene) except for dmso; however, the complex only dissolved in dmso at >150 °C and the solution was no longer blue, suggesting decomposition of **34**. Anal. calc. for C₂₀H₁₈N₁₈F₆S₂O₁₈Ru·2H₂O: C, 21.57; H, 1.99; N, 22.64; found C, 21.62; H, 1.75; N, 22.57. IR (ν, cm⁻¹): 3405 (H₂O); 3253, 2912, 2854 (C-H); 1477 (N-O_{asym.}); 1360 (N-O_{sym.}), 1326, 1256, 1153, 1029, 975, 803, 642. UV-Vis (MeOH, *in situ*): 340, 596, 746; for free 2NO₂Im, 314. ¹H NMR (300 MHz, d₆-dmso; *in situ*): δ 6.22 (br s, overlapping proton signals of coordinated 2NO₂Im ligands). ¹⁹F{¹H} NMR (188 MHz, d₆-dmso, *in situ*): -1.38 (s, CF₃SO₃⁻). Of note, the NMR data were obtained by removing the MeOH from the reaction mixture and then adding d₆-dmso to yield a dark blue solution.

4.2.1.6 [Ru(5NO₂Im)₆][CF₃SO₃]₂ (**35**)

In a Schlenk tube, [Ru(DMF)₆][CF₃SO₃]₃ (0.0553 g, 0.0560 mmol) was dissolved in MeOH (15 mL) under N₂ to give a bright yellow solution. 4(5)NO₂Im (0.0444 g, 0.392 mmol) was then added and the yellow-white slurry was stirred at 75 °C (4(5)NO₂Im is sparingly soluble in the hot MeOH, and slowly dissolves during the reaction). After 5 min the solution was dark green and then became dark blue after 45 min.

The mixture was then stirred for an additional 15 h to ensure complete substitution of all the DMF ligands. The solvent was removed from the resulting blue-black mixture and then EtOH was added to the residue, and the mixture was sonicated to yield a blue-black suspension. The solid was collected and washed with hot EtOH (5 x 10 mL). TLC analysis (toluene:MeOH, 15:1) of the solid revealed the presence of a single blue spot ($R_f=0$) on the baseline and a faint band corresponding to free 4(5)NO₂Im ($R_f=0.65$). The solid was then washed with boiling MeOH until no free 4(5)NO₂Im was detected in the filtrate according to TLC. The solid was dried *in vacuo* for 3 d to yield 0.0345 g (58 %). Anal. calc. for C₂₀H₁₈N₁₈F₆S₂O₁₈Ru•3H₂O: C, 21.22; H, 2.14; N, 22.27; found C, 21.06; H, 2.30; N, 22.02. IR (ν, cm⁻¹): 3458 (H₂O); 3133, 2924, 2852 (C-H); 1654; 1509 (N-O_{asym}); 1458; 1377 (N-O_{sym}); 1245, 1189, 1091, 994, 645. UV-Vis (MeOH, *in situ*): 344, 672; for free 4(5)NO₂Im, 286. ¹H NMR (300 MHz, CD₃OD, *in situ*): δ 8.06 (s, Im-H₂), 7.76 (s, Im-H₄), 2.69; (D₂O) δ 8.12 (s, Im-H₂), 7.76 (s, Im-H₄). ¹⁹F{¹H} NMR (188 MHz, CD₃OD, *in situ*): -1.34 (s, CF₃SO₃⁻).

4.2.1.7 [Ru(2Me5NO₂Im)₅][CF₃SO₃]₂ (36)

In a Schlenk tube, [Ru(DMF)₆][CF₃SO₃]₃ (0.149 g, 0.151 mmol) and 2Me5NO₂Im (0.118 g, 0.928 mmol) were dissolved in MeOH (20 mL) under N₂ to give a yellow solution. The mixture was stirred at 75 °C for 5 h over which time the colour changed from yellow to orange to green and finally blue. The temperature was decreased to 50 °C and the mixture was stirred for an additional 12 h. The solvent was removed *in vacuo* to yield a blue-black residue which according to TLC contained three new products and some unreacted 2Me5NO₂Im. The isolated solid was purified using column chromatography (THF:MeOH, 100:1 → 2:1). The unreacted nitroimidazole eluted from the column first, followed by a turquoise band once the polarity of the eluent had been increased. The turquoise band was taken to dryness and then THF was added to the blue residue. After sonication (5 min) the blue solid was isolated via suction filtration and washed with THF until the filtrate revealed no further presence of free nitroimidazole according to TLC. The solid was dried *in vacuo* for 3 d to yield 0.0204 g (13 %). Anal. calc. for C₂₂H₂₅N₁₅F₆S₂O₁₆Ru•6H₂O: C, 23.12; H, 3.26; N, 17.38; found C, 23.41; H,

3.34; N, 17.43. IR (ν , cm^{-1}): 3478 (H_2O); 3158, 3046, 2894 (CH); 1569; 1504 ($\text{N-O}_{\text{asym.}}$); 1464; 1380 ($\text{N-O}_{\text{sym.}}$); 1280, 1099, 1029, 815. UV-Vis (MeOH): 356, 606, 710; for free 2Me5NO₂Im, 300. ^1H NMR (300 MHz, CD_3OD): δ 7.97 (s, Im- H_4), 2.69, 2.40 (s, Im-2Me); (300 MHz, d_6 -dmso) δ 12.86 (vbr s, Im- H_1), 8.24 (s, Im- H_4), 2.34 (s, Im-2Me). $^{19}\text{F}\{^1\text{H}\}$ NMR (188 MHz, d_6 -acetone): -1.28 (s, CF_3SO_3^-).

4.2.1.8 $[\text{Ru}(\text{DMF})_4(\text{SR2508})_2][\text{CF}_3\text{SO}_3]_3$ (37)

In a Schlenk tube, $[\text{Ru}(\text{DMF})_6][\text{CF}_3\text{SO}_3]_3$ (0.149 g, 0.151 mmol) and **SR2508** were dissolved in 5 mL EtOH under air to yield a yellow solution. The mixture was stirred for 24 h at 55 °C over which time the yellow mixture changed colour from orange to green to blue to purple, finally yielding a pink-purple solution. The volume of the mixture was reduced under vacuum to ~2 mL and then Et₂O (30 mL) was added. The mixture slowly, over a period of 2 h, deposited a dark purple film on the inside of the flask. Sonication for 5 min released the precipitate from the walls of the flask. The solid was collected and washed with CH_2Cl_2 (4 x 10 mL). TLC analysis revealed the presence of two minor species which were separated following a second precipitation of the purple solid with acetone:Et₂O (1:20). The purple solid was dried *in vacuo* at 50 °C for 3 d (0.0842 g, 48%). Anal. calc. for $\text{C}_{29}\text{H}_{48}\text{N}_{12}\text{O}_{21}\text{S}_3\text{F}_9\text{Ru}$: C, 27.45; H, 3.81; N, 13.25; found C, 27.25; H, 3.50; N, 13.13. IR (ν , cm^{-1}): 3337 (N-H); 3142, 2982, 2945 (CH); 1647 ($\text{C}=\text{O}_{\text{DMF}}$; $\text{C}=\text{O}_{\text{SR2508}}$ buried within this band); 1561; 1503 ($\text{N-O}_{\text{asym.}}$), 1432; 1360 ($\text{N-O}_{\text{sym.}}$); 1281, 1251, 1167, 1064, 1029, 638. UV-Vis (MeOH): 352, 546; for free **SR2508**, 316. ^1H NMR (300 MHz, d_6 -dmso): 22.46 (br s, 12H, DMF- Me_1), 19.75 (br s, 12H, DMF- Me_2), 8.35 (br t, 2H, -NH-), 7.62 (s, 2H, Im- H_5), 7.17 (s, 2H, Im- H_4), 5.20 (s, 4H, Im- CH_2 -), 3.42 (t, 4H, CH_2 -OH), 3.16 (q, 4H, -NH- CH_2 -). $^{19}\text{F}\{^1\text{H}\}$ NMR (188 MHz, d_6 -acetone): -1.53 (s, CF_3SO_3^-).

4.2.1.9 $[\text{Ru}(\text{DMF})_2(\text{EF5})_2(\text{EtOH})_2][\text{CF}_3\text{SO}_3]_3$ (38)

In a Schlenk tube, **EF5** (0.0352 g, 0.117 mmol) was dissolved in 10 mL EtOH to give a colourless solution to which $[\text{Ru}(\text{DMF})_6][\text{CF}_3\text{SO}_3]_3$ (0.0506 g, 0.0513 mmol) was added. The tube was sealed under 1 atm air and the yellow solution was stirred at 50

°C for 24 h over which time the mixture became a pink-purple solution. The volume was reduced to ~1 mL and Et₂O (10 mL) was added. After 1 h at r.t. a purple precipitate had formed on the inside of the flask. The solvent was decanted from the flask and the volume reduced to ~1 mL followed by addition of Et₂O (this procedure was repeated several times until purple solid ceased to precipitate from the solution). The combined purple solids were dissolved in MeOH, transferred to a RBF and taken to dryness to yield a microcrystalline, dark purple solid. TLC analysis of this solid revealed two minor products (pink) both with $R_f > 0$, with $R_f = 0$ for the purple band; hence the purple solid was loaded onto a fine frit and washed with warm CH₂Cl₂ until the pink colour was absent in the filtrate. The pure, purple solid was dried *in vacuo* for 3 d at r.t. (0.0269 g, 38%). Anal. calc. for C₂₉H₄₀N₁₀F₁₉S₃O₁₉Ru: C, 25.04; H, 2.90; N, 10.07; found C, 24.99; H, 2.99; N, 9.92. IR (ν, cm⁻¹): 3411 (N-H); 3061, 2929 (CH); 1686 (C=O_{EF5}); 1645 (C=O_{DMF}); 1562; 1491 (N-O_{asym.}); 1429; 1352 (N-O_{sym.}); 1251, 1199, 1160, 1030, 639. UV-Vis (MeOH): 344, 550; for free EF5, 316. ¹H NMR (300 MHz, d₆-acetone): δ 22.16 (s, DMF-*Me*₁), 19.88 (s, DMF-*Me*₂), 8.20 (vbr s, Im-*H*_{4&5}), 5.61 (s, -CO-CH₂-), 4.16 (br s, -CH₂-CF₂-), 3.40 (q, CH₃CH₂OH), 1.14 (t, CH₃CH₂OH). ¹⁹F{¹H} NMR (188 MHz, d₆-acetone): -1.74 (s, CF₃SO₃⁻), -8.13 (s, -CF₃), -45.23 (s, -CF₂-).

4.2.2 Complexes Synthesized from RuCl₃•3H₂O

4.2.2.1 *mer*-RuCl₃(2NO₂Im)₃ (39)

In a Schlenk tube, 2NO₂Im (0.202 g, 1.78 mmol) was dissolved in 7 mL EtOH and then the mixture was heated to 75 °C to produce a colourless solution. RuCl₃•3H₂O (0.154 g, 0.595 mmol) was subsequently added with an additional 5 mL EtOH, and the tube was sealed under air and the mixture was stirred at reflux for 5 h. During the course of the reaction the original orange mixture became green-blue and finished as a dark blue-black solution. After 5 h, TLC analysis revealed the increased formation of side-products other than the desired dark blue band ($R_f = 0$). The EtOH was removed to give a blue-black solid which was treated with 15 mL EtOAc and the mixture was sonicated with stirring for 1 h. The mixture was filtered, and the resulting solid (still containing unreacted

2NO₂Im according to TLC) was washed with hot EtOAc until no free 2NO₂Im was detectable by TLC in the filtrate. The solid was washed through the frit with MeOH and the MeOH was then removed *in vacuo* to yield a blue-black solid (0.0870 g, 27 %). Anal. calc. for C₉H₉N₉O₆Cl₃Ru•4H₂O: C, 17.47; H, 2.77; N, 17.19; found C, 17.75; H, 2.97; N, 17.24. IR (ν, cm⁻¹): 3415 (H₂O); 3135, 2923, 2856 (C-H); 1707; 1660; 1508 (N-O_{asym.}); 1370 (N-O_{sym.}); 1326, 1224, 1149, 1066, 965, 697. UV-Vis (MeOH): 210, 268, 368. ¹H NMR (300 MHz, d₆-dmsO): δ 14.40 (br s, 3H, -NH-), 7.88 (s, 1H, Im-H₅, *trans* to Cl), 7.82 (s, 2H, Im-H₅, *trans* to 2NO₂Im), 7.64 (s, 1H, Im-H₄, *trans* to Cl), 7.37 (s, 2H, Im-H₄, *trans* to 2NO₂Im).

4.2.2.2 *fac*- and *mer*-RuCl₃(5NO₂Im)₃ (40)

In a Schlenk tube, RuCl₃•3H₂O (0.0973 g, 0.406 mmol) was dissolved in 10 mL EtOH, followed by the addition of 4(5)NO₂Im (finely ground, 0.212 g, 1.88 mmol). The tube was sealed, evacuated and then purged with N₂. The mixture was stirred at 70 °C for 16 h. Initially the mixture was a slurry due to the low solubility of 4NO₂Im and, when the temperature was reduced to ambient, some unreacted 4(5)NO₂Im precipitated. The solid was removed via filtration using Schlenk techniques and then Et₂O was added dropwise to the filtrate, resulting in formation of an orange precipitate. This was isolated, washed with Et₂O (3 x 5 mL) and dried *in vacuo* at r.t. (0.0765 g, 34 %). After 1 month, the sealed filtrate revealed formation of small orange crystals which were isolated via filtration; attempts at removing solvent under vacuum resulted in the crystals becoming opaque, suggesting the presence of solvent within the crystal lattice. Anal. calc. for C₉H₉N₉O₆Cl₃Ru•0.5EtOH•H₂O: C, 20.44; H, 2.40; N, 21.45; found C, 20.42; H, 2.31; N, 21.28. LR-MS [-lsims]: 547 (M⁺ - H), 441 (M⁺ - 3Cl), 435 (M⁺ - 4(5)NO₂Im). IR (ν, cm⁻¹): 3148, 2972, 2875 (C-H); 1559; 1525 (N-O_{asym.}); 1480; 1379 (N-O_{sym.}); 1228, 1090, 814, 643. UV-Vis (MeOH): 288, 350(sh). ¹H NMR (300 MHz, d₆-dmsO): [ppt., *fac*] δ 13.24 (br s, Im-H₂ and 4), 3.39 (q, CH₃CH₂OH), 1.05 (t, CH₃CH₂OH); [crystals, *mer*] δ 4.71 (br s, 2H, 5NO₂Im *trans* to Cl), 3.35 (q, CH₃CH₂OH), 1.03 (t, CH₃CH₂OH), -14.15 (vbr s, 4H, 5NO₂Im *trans* to one another). μ_{eff} = 1.5 B.M. at 20 °C.

4.2.2.3 “RuCl₃(2Me5NO₂Im)₃•3CO₂” (41)

In a Schlenk tube, RuCl₃•3H₂O (0.319 g, 1.23 mmol) was dissolved in 25 mL EtOH followed by addition of 2Me5NO₂Im (1.43 g, 11.2 mmol). The tube was sealed, evacuated and then purged with N₂. The mixture was stirred at 70 °C for 5 h, when the orange-brown solution was taken to dryness. TLC analysis revealed a series of products and so the mixture was purified using column chromatography (THF). The bands eluted in the following order: band 1 (colourless), band 2 (yellow), band 3 (orange), band 4 (colourless, unreacted 2Me5NO₂Im). Analysis of band 3 revealed the presence of 2Me5NO₂Im, and so this band was purified further using preparative TLC (THF). Of note, the use of preparative TLC for compound purification from the initial product mixture was also successful. The dark orange solid (41) (0.132 g, 18 %) was air-sensitive, becoming brown-black after exposure to air for > 3 h.

Band 1: LR-MS [DCI(+)]: 270 (M⁺ (for C₈H₈N₆O₄) + NH₄⁺), 253 (M⁺ + H), 238 (M⁺ - Me), 220, 206 (M⁺ - NO₂). UV-Vis (MeOH): 218, 238, 278; for free 2Me5NO₂Im, 300. ¹H NMR (200 MHz, CDCl₃): δ 7.02 (s, 14.4, Im-*H*₄), 5.05 (s, 6.2, unassigned), 2.31 (s, 19.5, Im-2*Me*), 1.47 (s, 172.1, unassigned).

Band 3: Anal. calc. for C₁₂H₁₅N₉O₆Cl₃Ru (41): C, 24.48; H, 2.57; N, 21.41 (with •3CO₂: C, 25.00; H, 2.10; N, 17.49); found C, 24.93; H, 2.02; N, 17.76. IR (ν, cm⁻¹): 3411 (N-H); 3153, 2921, 2848 (C-H); 2370, 2337 (CO₂); 1625; 1508 (N-O_{asym}), 1476; 1380 (N-O_{sym}); 1210, 1136. UV-Vis (MeOH): 212, 234, 358. ¹H NMR (300 MHz, CD₃OD): [initial spectrum] δ 17.25 (br s, Im-*H*₄, 1H), -3.95 (br s, Im-2*Me*, 6H), -5.05 (br s, Im-2*Me*, 3H), -7.90 (vbr s, Im-*H*₄, 2H); [spectrum after 6 d] δ -3.85 (br s, Im-*H*₄, 3H), -8.65 (vbr s, Im-2*Me*, 9H). μ_{eff} = 1.7 B.M. at 20 °C.

4.2.2.4 RuCl₃(metro)₃ (42)

In a Schlenk tube, RuCl₃•3H₂O (0.0872 g, 0.364 mmol) and metronidazole (metro) (0.278 g, 1.62 mmol) were dissolved in 15 mL EtOH; the partially soluble metro dissolved on heating the mixture to 65 °C. After 10 min, the initial brown solution turned

orange and an orange precipitate began to form, and after 3 h, a bright orange slurry was present. The tube was then submersed in an ice-bath for 30 min. The orange solid was collected and then washed with warm EtOH (5 x 10 mL). According to TLC analysis the orange solid ($R_f=0.70$) contained two minor side-products with lower R_f values. The orange solid was dissolved in minimal MeOH and the solution then loaded onto a silica gel column (THF:MeOH, 20:1). The pure orange band (the 2nd to elute) was collected in a number of fractions which were combined and taken to dryness to yield an orange solid (0.0993 g, 38%). Anal. calc. for $C_{18}H_{27}N_9O_9Cl_3Ru \cdot 2H_2O$: C, 28.56; H, 4.13; N, 16.65; found C, 28.73; H, 3.99; N, 15.96. UV-Vis (MeOH): 298, 476; for free metro, 312. 1H NMR (400 MHz, d_6 -acetone): δ 12.05 (vbr s, 1H, Im- H_4), 10.20 (br s, 2H, - CH_2 -), 8.25 (br s, 2H, - CH_2 -), 4.85 (s, 3H, Im-2Me), 4.55 (br s, 2H, -OH), 4.35 (s, 6H, Im-2Me), 3.55 (br s, 1H, -OH), -1.20 (br s, 4H, - CH_2 -), -3.10 (br s, 4H, - CH_2 -), -9.21 (vbr s, 2H, Im- H_4); peak assignments are tentative and are based on the integration ratios and trends observed for complexes **40** and **41**, of similar composition and geometry. $\mu_{eff} = 1.8$ B.M. at 20 °C.

4.2.2.5 $RuCl_3(SR2508)_2(EtOH)$ (**43**)

In a Schlenk tube, $RuCl_3 \cdot 3H_2O$ (0.0829 g, 0.346 mmol) and **SR2508** were dissolved in 10 mL EtOH to yield an orange-brown solution. The mixture was stirred under 1 atm N_2 at 75 °C for 2 h over which time the mixture turned green and then finally dark blue, including the formation of a blue-black precipitate. The solid was collected, washed with EtOH (3 x 10 mL) and dried *in vacuo* at r.t. for 3 d (0.136 g, 62%). Anal. calc. for $C_{16}H_{26}N_8O_9Cl_3Ru \cdot 3H_2O$: C, 26.11; H, 4.38; N, 15.23; found: C, 26.07; H, 3.91; N, 14.84. IR (ν , cm^{-1}): 3327 (br, $H_2O + N-H$); 3124, 2944, 2878 (CH); 1761; 1677 (C=O); 1627; 1506 (N- $O_{asym.}$), 1421, 1351 (N- $O_{sym.}$), 1064, 766, 509. UV-Vis (H_2O): 326, 522, 760. 1H NMR (300 MHz, d_6 -dmso): no peaks observed other than those corresponding to free EtOH. The UV-Vis spectrum in water changed with time, showing shifts of the λ_{max} values to 322 and 518 nm, and the band at 760 nm remained unchanged. After 8 h at r.t., the solution was taken to dryness to yield a purple solid which was dried *in vacuo* at r.t. Anal. calc. for $C_{14}H_{22}N_8O_9Cl_3Ru \cdot 2H_2O [RuCl_3(SR2508)_2(H_2O) \cdot 2H_2O]$: C, 24.38; H, 3.80; N, 16.24; found C, 24.45; H, 3.62; N, 16.06. IR (ν , cm^{-1}): 3319 (br, H_2O

+ N-H); 3108, 2938 (C-H); 1672 (C=O); 1631; 1494 (N-O_{asym.}); 1358 (N-O_{sym.}); 1189, 1110, 1059. $\mu_{\text{eff}} = 1.9$ B.M. at 20 °C. Conductivity of **43** (H₂O): Λ_{M} increased over ~48 h from ~35 to 372 ohm⁻¹mol⁻¹cm² (blue → purple → burgundy); implying a final 3:1 electrolyte.

4.2.2.6 RuCl₃(EF5)₂(EtOH) (**44**)

In a 100 mL RBF, RuCl₃•3H₂O (0.0296 g, 0.114 mmol) and **EF5** (0.101 g, 0.334 mmol) were dissolved in 15 mL EtOH. The brown-orange mixture was stirred at 60 °C under 1 atm N₂ for 2 h. A small aliquot was then removed and diluted with EtOH in a 1 cm cuvette. The UV-Vis spectrum of the resulting pale purple solution revealed an absorption band at 530 nm. The mixture was then diluted by addition of 35 mL EtOH and stirred in air at reflux for 6 h. The final dark purple solution contained some unreacted **EF5** and a single product ($R_f=0$) according to TLC analysis. The volume was reduced to ~5 mL under vacuum and the solution then transferred to a dialysis bag (MWCO = 1000). The bag was sealed and submersed in EtOH (1 L); stirring for 16 h resulted in a pink external EtOH solution and a purple-black internal EtOH solution which, according to TLC, contained no free **EF5**. The EtOH was removed from the internal solution to yield a purple solid (0.045 g, 49 %). Anal. calc. for C₁₈H₂₀N₈O₇F₁₀Cl₃Ru•3H₂O: C, 23.71; H, 2.87; N, 12.29; found C, 24.09; H, 2.65; N, 11.68. LR-MS [-LSIMS]: 910 (M⁺ + 3H₂O), 892 (M⁺ + 2H₂O), 876 (M⁺ + H₂O), 301 (**EF5**). IR (ν , cm⁻¹): 3318 (H₂O + N-H); 3117, 2984 (C-H); 1762; 1686 (C=O); 1555; 1492 (N-O_{asym.}); 1346 (N-O_{sym.}); 1195, 1155, 1104, 1023. UV-Vis (MeOH): 308, 530. ¹H NMR (300 MHz, CD₃OD): δ trace signals due to free **EF5**. $\mu_{\text{eff}} = 1.9$ B.M. at 20 °C (d₆-acetone). Drying the purple solid at 80 °C *in vacuo* resulted in a green solid. (Anal. calc. for C₁₆H₁₄N₈O₆F₁₀Cl₃Ru [RuCl₃(EF5)₂]: C, 23.67; H, 1.74; N, 13.80; found C, 23.86; H, 1.99; N, 13.48.) Dissolution of the green solid in EtOH revealed no 530 nm peak, but after ~1 h the solution became purple with a peak at 530 nm. Dissolution of the green solid in H₂O eventually led to formation of a pink solution with an increase in conductivity to that of a 3:1 electrolyte (Table 4.1).

Table 4.1: Conductivity measurements versus time for **44** in H₂O.

Time (h)	Conductivity (ohm ⁻¹ mol ⁻¹ cm ²)
0.1	10.5
8	142.4
18	280.6
24	317.7
31	337.7
120	365.8

4.2.2.7 RuCl₂(metro)₄ (45)

In a Schlenk tube, RuCl₃•3H₂O (0.106 g, 0.441 mmol) was dissolved in 10 mL MeOH and the resulting brown solution was stirred under a steady stream of H₂ at 65 °C. The mixture went from brown to orange to green and after 3 h a navy blue colour persisted. Metro (0.308 g, 1.80 mmol) was then added; after 20 min the mixture became yellow-green and then brown after 1 h. Stirring for 14 h under 1 atm H₂ resulted in the formation of a red-brown solution and a purple precipitate. The solid was isolated, washed with MeOH (3 x 10 mL) and dried *in vacuo* (0.0469 g, 26 %). Anal. calc. for C₂₄H₃₂N₁₂O₁₂Cl₂Ru•H₂O: C, 33.11; H, 3.94; N, 19.31; found C, 33.09; H, 4.21; N, 18.97. IR (ν, cm⁻¹): 3385 (H₂O); 3151, 3112, 3028, 2930, 2882 (C-H); 1738; 1647 (C-OH); 1544; 1472 (N-O_{asym.}); 1425; 1345 (N-O_{sym.}); 1259, 1179, 1146, 1056, 866, 828, 740. UV-Vis (MeOH): 304, 494; (acetone): 556. ¹H NMR (200 MHz, d₆-acetone): δ 7.91 (s, Im-H₄), 4.23 (br s, -CH₂-), 3.91 (br s, OH), 3.60 (br s, -CH₂-), 2.05 (s, Im-2Me).

4.2.3 Complexes Synthesized from RuCl₂(DMSO)₄**4.2.3.1 cis-RuCl₂(DMSO)₂(en) (46)**

In a 25 mL RBF, *cis*-RuCl₂(DMSO)(DMSO)₃ (0.208 g, 0.430 mmol) and en (29 μL, 0.430 mmol) were dissolved in CHCl₃ (10 mL) and the solution stirred at reflux for 45 min to yield a bright yellow solution. TLC analysis revealed a single product. The

solution was cooled to r.t. and then Et₂O (10 mL) was added to form a yellow precipitate, which was isolated and then rinsed through the frit with MeOH into a RBF. The solvent was removed under vacuum to give a yellow-orange film on the inside of the flask. The flask was heated to 120 °C under vacuum, and after 4 h the yellow-orange solid (**46a**) was isolated (0.0443 g, 27%). Anal. calc. for C₆H₂₀N₂O₂S₂Cl₂Ru: C, 18.56; H, 5.19; N, 7.21; found C, 18.41; H, 5.37; N, 7.61. IR (ν, cm⁻¹): 3243 (N-H); 3146, 3003, 2919 (C-H); 1578, 1417, 1313; 1051, 1012 (S-O); 421. UV-Vis (CH₂Cl₂): 306, 366. ¹H NMR (200 MHz, CDCl₃): δ 3.65 (s, 2H, -NH₂), 3.47 (s, 2H, -CH₂-NH₂), 3.28 (s, 12H, Me₂S=O), 3.04 (s, 2H, -NH₂), 2.61 (s, 2H, -CH₂-NH₂).

The same reaction described above was repeated, but using a refluxing time of 15 h. The product yellow solution was taken to dryness and CH₂Cl₂ was added to give a yellow precipitate which was removed via filtration. To the resulting pale yellow filtrate, Et₂O was added to yield a yellow precipitate (**46b**) which was isolated, washed with Et₂O (2 x 5 mL) and dried *in vacuo* at 80 °C for 2 d (0.0953 g, 57%). Anal. calc. for C₆H₂₀N₂O₂S₂Cl₂Ru·0.5DMSO: C, 19.67; H, 5.42; N, 6.55; found: C, 19.52; H, 5.41; N, 6.69. IR (ν, cm⁻¹): 3238 (N-H); 3149, 2922 (C-H); 1581, 1418, 1310; 1054, 1012 (S-O); 683, 425. UV-Vis (CH₂Cl₂): 302, 414. ¹H NMR (200 MHz, CDCl₃): δ 3.60 (s, 4H, -NH₂), 3.25 (s, 12H, Me₂S=O), 3.00 (s, 4H, -CH₂-NH₂), 2.52 (s, 2H, free Me₂S=O).

4.2.3.2 *trans*-RuCl₂(DMSO)₂(en) (**47**)

In a 25 mL RBF, *trans*-RuCl₂(DMSO)₄ (0.0532 g, 0.110 mmol) and en (15 μL, 0.225 mmol) were dissolved in CHCl₃ (10 mL) and the solution stirred at reflux for 30 min; the mixture became cloudy due to the formation of an insoluble, yellow solid. The solid was isolated, washed with Et₂O (3 x 5 mL) and dried *in vacuo* at 80 °C for 24 h (0.0427 g, 54%). Anal. calc. for C₆H₂₀N₂O₂S₂Cl₂Ru: C, 18.56; H, 5.19; N, 7.21; found C, 18.69; H, 5.12; N, 7.04. IR (ν, cm⁻¹): 3310, 3245 (N-H); 3144, 2916 (CH); 1602, 1575, 1415, 1292; 1075, 1059, 1008 (SO); 719, 684, 426. UV-Vis (CH₂Cl₂): 300, 418. ¹H NMR (200 MHz, CD₃OD): δ 4.20 (s, 4H, -NH₂), 3.25 (s, 12H, Me₂S=O), 2.90 (s, 4H, -CH₂-NH₂).

4.2.3.3 $\text{RuCl}_2(\text{DMSO})_2(\text{EF5})(\text{acetone})$ (48)

In a Schlenk tube, *cis*- $\text{RuCl}_2(\text{DMSO})(\text{DMSO})_3$ (0.0874 g, 0.180 mmol) and **EF5** (0.0540 g, 0.180 mmol) were dissolved in a 1:1 mixture of acetone: CH_2Cl_2 (10 mL) to give a yellow solution. Over 2.5 h the mixture, stirred at r.t., went from yellow through green to blue. TLC analysis revealed unreacted starting compounds, so the mixture was then heated to 65 °C for an additional 15 h. The final dark blue solution contained five products according to TLC, and some unreacted **EF5**. The solution volume was reduced (to ~3 mL) under vacuum and then loaded onto a preparative TLC plate (CH_2Cl_2 :MeOH, 10:1). The major blue band was scraped from the plate, eluted from the silica gel with acetone and the eluate taken to dryness to a dark blue solid (0.0188 g, 15%). Of note, drying the solid at 80 °C resulted in melting of the complex (m.p. 62–65 °C). Anal. calc. for $\text{C}_{12}\text{H}_{19}\text{N}_4\text{O}_5\text{Cl}_2\text{F}_5\text{S}_2\text{Ru}$: C, 22.86; H, 3.04; N, 8.89 (with 1 mol acetone: C, 26.17; H, 3.66; N, 8.14); found C, 26.24; H, 3.70; N, 8.46. IR (v, cm^{-1}): 3286 (N-H); 3076, 3011, 2957, 2925, 2854 (C-H); 1706, 1703 (sh) (C=O); 1538; 1493 (N-O_{asym.}); 1421; 1370 (N-O_{sym.}); 1193, 1156 (C-F); 1108, 1020 (S-O); 981, 841, 778, 728, 679, 452. UV-Vis (MeOH): 312, 366(sh). ^1H NMR (200 MHz, d_6 -acetone): δ 8.42 (s, Im- H_5), 8.20 (s, Im- H_4), 5.67 (s, -CO- CH_2 -), 4.18 (td, - CH_2 - CF_2 -), 3.60–3.35 (~ 5 peaks, DMSO Me groups), 2.05 (s, acetone). $^{19}\text{F}\{^1\text{H}\}$ NMR (188 MHz, d_6 -acetone): -8.06 (s, - CF_3), -45.17 (s, - CF_2 -).

4.2.4 Miscellaneous Complexes

4.2.4.1 $[\text{RuCl}(\text{dppb})(\text{EF5})]_2(\mu\text{-Cl})_2$ (49)

$[\text{RuCl}_2(\text{dppb})]_2(\mu\text{-dppb})$ (0.0614 g, 0.0378 mmol) and **EF5** (0.0321 g, 0.106 mmol) were placed in a Schlenk tube, which was then evacuated and filled with Ar. CH_2Cl_2 (5 mL) was added via syringe and the mixture was stirred at r.t. After 2 h, the original dark green suspension had become a brilliant blue solution. After an additional 24 h, the volume was decreased under vacuum to ~2 mL and then Et_2O (20 mL) was added to yield a blue precipitate which was isolated via suction filtration. TLC and ^{31}P NMR analyses revealed the presence of $\text{dppb}(\text{O})_2$, so the solid was purified via preparative TLC

(CH₂Cl₂:MeOH, 20:1) to yield a pure blue solid which was dried *in vacuo* for 24 h at 80 °C (0.0147 g, 22%). Anal. calc. for C₇₂H₇₀N₈O₆Cl₄F₁₀P₄Ru₂: C, 48.01; H, 3.92; N, 6.22; found C, 47.98; H, 3.89; N, 5.99. IR (ν, cm⁻¹): 3253 (N-H); 3061, 2928, 2859 (C-H); 1714(sh); 1709 (C=O); 1508(sh) (N-O_{asym.}); 1479, 1434; 1366(sh) (N-O_{sym.}); 1195, 1156, 1096, 744, 697. UV-Vis (CH₂Cl₂): 236 (14.4), 336 (3.14), 694 (1.97). ¹H NMR (300 MHz, CDCl₃): δ 8.35-6.90 (many overlapping peaks corresponding to Im and Ph H-atoms), 5.13 (s, -CO-CH₂-), 3.89 (t, -CH₂-CF₂-), 2.26, 1.72, 0.55-0.15 (dppb CH₂'s). ³¹P{¹H} NMR (121 MHz, CDCl₃): δ 47.00 (d, ²J_{AB} = 42.0 Hz, P_A), 45.20 (d, ²J_{AB} = 41.8 Hz, P_B), 39.94 (d, ²J_{CD} = 39.3 Hz, P_C), 34.41 (d, ²J_{CD} = 39.3 Hz, P_D). [A purple band (**50**) was also isolated from the preparative TLC, but the complex was not characterized; ³¹P{¹H} NMR (121 MHz, CDCl₃): δ 20.89 (dd, ²J_{AX} = 33.2 Hz, ²J_{BX} = 30.6 Hz), 12.83 (dd, ²J_{AB} = 270 Hz, ²J_{AX} = 33.2 Hz), 3.39 (dd, ²J_{AB} = 270 Hz, ²J_{BX} = 30.6).]

4.2.4.2 *cis*-RuCl₂(MeCN)₄ (**51**) and *mer*-RuCl₃(MeCN)₃ (**52**)

The procedure reported by Fogg¹¹ for the synthesis of *trans*-RuCl₂(MeCN)₄ was followed; however, two different species, one Ru(II) and one Ru(III) were isolated. An orange-brown suspension of RuCl₃·3H₂O (0.585 g, 2.26 mmol) and PtO₂ (0.00592 g) in MeCN (8 mL) was sealed under 1.1 atm H₂, and stirred at r.t. for 24 h, over which time a deep orange solution formed with a small amount of yellow-orange precipitate. The precipitate was collected using Schlenk techniques and washed with Et₂O (2 x 10 mL). Addition of Et₂O to the resulting orange filtrate yielded an orange precipitate that was collected and dried at r.t. (0.216 g, 29%). TLC analysis (CH₂Cl₂:MeOH, 20:1) revealed that the precipitate was a single species (**52**), while the filtrate predominantly contained another orange product (**51**) and a small amount of **52**. Both species are air-sensitive and become black on the TLC plate after ~24 h.

The filtrate's volume was reduced under vacuum to ~5 mL and the solution loaded onto a silica gel column containing CH₂Cl₂. The first 100 mL eluted was CH₂Cl₂ and then 5% MeOH was added which eluted the first orange band as pure **52**. The second orange band (**51**) followed quickly, N₂ being flushed through the collection flask to reduce the exposure of **51** to air, and the fraction was taken to dryness to yield a dark orange

solid which was dried *in vacuo* at r.t. (0.0723 g). **51** and **52** are thermally unstable and decompose to black solids at 80 °C *in vacuo*. Bright orange, X-ray quality crystals of **52** were obtained from a MeOH/CH₂Cl₂ solution stored in an NMR tube for 2 weeks.

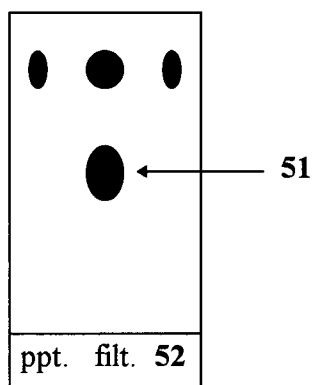


Figure 4-1: TLC analysis of products obtained from synthesis of **52**.

Data for **51**: IR (ν , cm⁻¹): 2976, 2918 (CH); 2322, 2296 (C \equiv N); 1623, 1414, 1365, 1028, 455. UV-Vis (CH₂Cl₂): 392 (2.09), 412 (2.12), 444 (1.27). ¹H NMR (300 MHz, CDCl₃): δ 2.19 (s, 6H, MeCN trans to Cl), 2.05 (s, 6H, MeCN trans to MeCN).

Data for **52**: Anal. calc. for C₆H₉N₃Cl₃Ru•CHCl₃ (crystals): C, 18.69; H, 2.24; N, 9.34; found C, 18.42; H, 2.20; N, 8.61. IR (ν , cm⁻¹): 2977, 2918 (CH); 2325, 2297, 2235 (C \equiv N); 1631, 1413, 1029, 922, 727, 454. UV-Vis (CH₂Cl₂): 292 (1.15), 414 (3.83), 482 (1.02). ¹H NMR (300 MHz, CDCl₃): [initial] δ 46.95 (br s, 3H, MeCN trans to Cl), -15.24 (s, 6H, MeCN trans to MeCN); [1 week] δ 3.11 (br s), 2.04 (s), -15.47 (br s).

4.2.4.3 Other Attempted Reactions

The synthesis of several other complexes was attempted from numerous different Ru(II) and Ru(III) precursors. These reactions are summarized in Table 4.2 on the following two pages.

Table 4.2: Summary of attempted reactions for which no pure product was isolated or characterized.

Ru complex (g, mmol)	Ligand (g, mmol)	Solvent (mL)	Atm.	Temp (°C)	Time (h)	Initial Colour	Final Colour	NOTES
[RuCl ₂ (COD)] _x (0.144, 0.370)	2Melm (0.122, 1.46)	EtOH (15)	Air	75	6	brown	orange	¹ H NMR and UV-Vis (λ_{max} = 360) spectra suggest 2Me Im coord.; poor EA
[RuCl ₂ (COD)] _x (0.0920, 0.237)	2Me5NO ₂ Im (0.124, 0.974)	EtOH (15)	N ₂	60	15	brown	yellow/ orange	UV-Vis (λ_{max} = 364 nm); poor EA
[RuCl ₂ (COD)] _x (0.0538, 0.138)	2NO ₂ Im (0.0645, 0.570)	EtOH (15)	Air	75	5	brown	green	UV-Vis (λ_{max} = 332, 718 nm); >5 products according to TLC
<i>cis</i> -RuCl ₂ (DMSO) ₄ (0.0725, 0.150)	SR2508 (0.116, 0.542)	MeOH (15)	Air	65	4	yellow	blue/ purple	UV-Vis (λ_{max} = 436, 656 (blue); 352, 400, 588 (purple) nm); 2 products according to TLC; light sensitive
<i>cis</i> -RuCl ₂ (DMSO) ₄ (0.0427, 0.0882)	Metro (0.0318, 0.186)	MeOH (10)	N ₂	65	4	yellow	orange/ brown	unstable in air; >5 products according to TLC
<i>cis</i> -RuCl ₂ (TMSO) ₄ ^a (0.0240, 0.0407)	EF5 (0.0129, 0.0427)	MeOH (4)	N ₂	70	12	yellow	blue	UV-Vis (λ_{max} = 318 (blue); 352, 574 (purple) nm); EF5 ligands readily dissociate in coord. solvents

^a Using conditions identical to those reported by D.T.T. Yapp for the synthesis of RuCl₂(TMSO)₂(SR2508)•2H₂O.

Table 4-2: (continued)

Ru complex (g, mmol)	Ligand (g, mmol)	Solvent (mL)	Atm.	Temp (°C)	Time (h)	Initial Colour	Final Colour	NOTES
<i>mer</i> -RuCl ₃ (DMSO) ₃ (0.105, 0.238)	2NO ₂ Im (0.0806, 0.713)	acetone (10)	N ₂	55	12	orange	dark orange	UV-Vis (λ_{max} = 388, 488 nm); IR 1491 and 1384 cm ⁻¹ (ν_{NO}); ¹ H NMR peaks range from +8 to -25 ppm (\therefore Ru ³⁺)
<i>mer</i> -RuCl ₃ (DMSO) ₃ (0.0401, 0.0908)	4NO ₂ Im (0.0312, 0.276)	MeOH (5)	N ₂	65	8	orange	orange	No reaction according to TLC
<i>mer</i> -RuCl ₃ (DMSO) ₃ (0.105, 0.238)	SR2508 (0.204, 0.952)	MeOH (10)	N ₂	65	8	orange	blue	UV-Vis (λ_{max} = 420, 608 (blue); 350, 552 (purple) nm); SR2508 ligand(s) readily dissociate in coord. solvents
RuCl ₃ •3H ₂ O (Ru Blue) (0.0127, 0.0529)	MF5 (0.0435, 0.138)	MeOH (10)	H ₂	60	8	blue	green	UV-Vis (λ_{max} = 296 nm); single, pure product isolated according to TLC; poor EA
RuCl ₃ •3H ₂ O (Ru Blue) (0.0127, 0.0529)	2M4NFS (0.0435, 0.138)	EtOH (10)	Air	65	24	brown	green	¹⁹ F NMR suggests coordination of ligand for isolated species; poor EA
[Ru(DMF) ₆][CF ₃ SO ₃] ₃ (0.0368, 0.0373)	Metro (0.0583, 0.341)	MeOH (20)	Air	65	5	yellow	red	UV-Vis (λ_{max} = 322, 420, 516 nm); >8 products according to TLC

4.3 Results and Discussion

4.3.1 Complexes Synthesized from $[\text{Ru}(\text{DMF})_6][\text{CF}_3\text{SO}_3]_3$

Ruthenium(III) imidazole complexes such as $[\text{ImH}]_2[\text{RuCl}_5(\text{Im})]^{12}$ and *trans*- $[\text{ImH}][\text{RuCl}_4(\text{Im})_2]^{13-16}$ have been synthesized and characterized, and their solution chemistry and antitumour activity thoroughly investigated. Ruthenium(II) imidazole complexes, however, are less common and, during studies of such species in this work, the two homoleptic species $[\text{Ru}(\text{Im})_6]\text{CO}_3 \cdot 5\text{H}_2\text{O}^{15}$ and $[\text{Ru}(\text{NMeIm})_6]\text{Cl}_2 \cdot 2\text{H}_2\text{O}^{17}$ were reported; X-ray structures were presented but no spectroscopic data, and indeed no synthetic procedures for these complexes, have been reported, at least in the open literature. Several Ru(II)-imidazole species have been reported to show immunosuppression activity¹⁸ while Ru(II)-nitroimidazole complexes have been reported to exhibit increased radiosensitizing activity.^{19,20}

4.3.1.1 Hexakis(imidazole) Ru(II) Complexes

Availability of the starting complexes $[\text{Ru}(\text{DMF})_6][\text{CF}_3\text{SO}_3]_x$, where $x = 2$ or 3 ,²¹ provides a useful general method for access to the homoleptic hexa-coordinate Ru(II) imidazole complexes $[\text{Ru}(\text{L})_6][\text{CF}_3\text{SO}_3]_2$ ($\text{L} = \text{Im}$ (**28**), NMeIm (**29**) and 5MeIm (**30**)). The DMF-containing precursors provide a useful alternative to the commercially available $\text{RuCl}_3 \cdot 3\text{H}_2\text{O}$ which is of variable composition. The cations of **28** and **29** have been previously reported with X-ray structural data, but with CO_3^{2-} and $[\text{Cl}]_2$ as their respective anions^{15,17} and no other characterization data were reported for $[\text{Ru}(\text{Im})_6][\text{CO}_3] \cdot 5\text{H}_2\text{O}$, which was insoluble in common solvents,¹⁵ or $[\text{Ru}(\text{NMeIm})_6]\text{Cl}_2 \cdot 2\text{H}_2\text{O}$;¹⁷ CV data have been given for $[\text{Ru}(\text{Im})_6][\text{ClO}_4]_3$ and $[\text{Ru}(\text{NMeIm})_6][\text{PF}_6]_3$.¹⁷

Complexes **28** - **30**, which contain no waters of crystallization, can be obtained by simple exchange of the DMF ligands of $[\text{Ru}(\text{DMF})_6]^{2+}$ by the imidazole. However, this Ru(II) precursor is moderately air-sensitive and it is more convenient to use the air-stable $[\text{Ru}(\text{DMF})_6][\text{CF}_3\text{SO}_3]_3$ precursor, although longer reaction times are needed, presumably (at least in part) because of the reduction of Ru(III) to Ru(II). There is literature

precedence for both MeOH²² and imidazoles^{15,23,24} acting as reductants of transition metal species, including those of Ru(III) which have been observed in analogous nitroimidazole systems (see Section 4.3.1.3). Substitution reactions at Ru(II) centres are typically faster than those at corresponding Ru(III) centres,²⁵ and the longer Ru-O bond in [Ru(DMF)₆]²⁺ vs. [Ru(DMF)₆]³⁺ is consistent with such a reactivity trend.²¹

Structural data on the cations within **28** and **29** have been reported previously within the structures of [Ru(Im)₆]CO₃•5H₂O (**28'**)¹⁵ and [Ru(NMeIm)₆]Cl₂•2H₂O (**29'**),¹⁷ respectively. The corresponding pairs of crystal structures, however, are quite different. Complex **28** crystallizes in the triclinic space group $P\bar{1}$ with the Ru atom situated on an inversion centre with the three unique Ru-N distances averaging 2.099(2) Å (Figure 4-2)

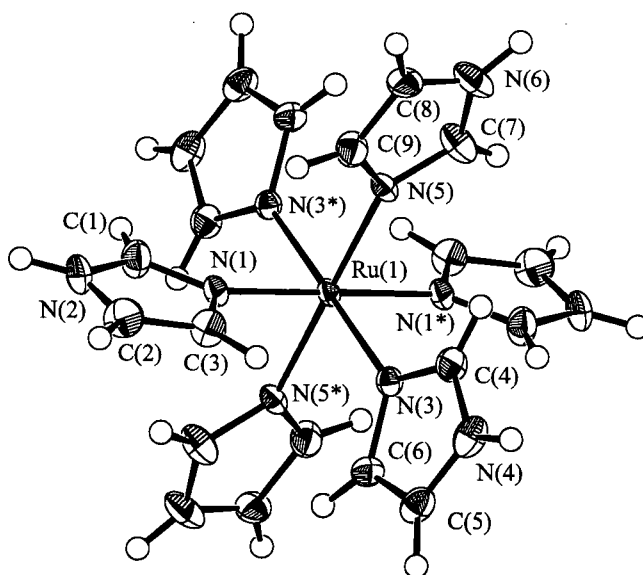


Figure 4-2: ORTEP view of Ru(Im)₆²⁺ (**28**); 50% probability thermal ellipsoids are shown.

(see Appendix I-7); crystals of **28'** are hexagonal with the Ru atom located at a point of S_6 symmetry with six equivalent Ru-N bonds of 2.102(2) Å. Complex **29** crystallizes in a trigonal space group with (like **28'**) the Ru atom at a point of S_6 symmetry and Ru-N bond lengths of 2.100(2) Å (Figure 4-3, Appendix I-8), while **29'** forms monoclinic crystals in which the Ru atom lies on a centre of symmetry (like **28**) with the three independent Ru-N distances averaging 2.106(8) Å. Complex **30**, the (5MeIm)₆ species, is similar to **29** in being trigonal, with the Ru being at an S_6 site and the Ru-N length being 2.093(2) Å (Figure 4-4, Appendix I-9). The Ru-N distances are significantly less than that reported for Ru(NH₃)₆²⁺, 2.144(4) Å,²⁶ this could result from a combination of some degree of π -backbonding from the Ru(II) to the imidazole ligands, and σ -hybridization effects (a

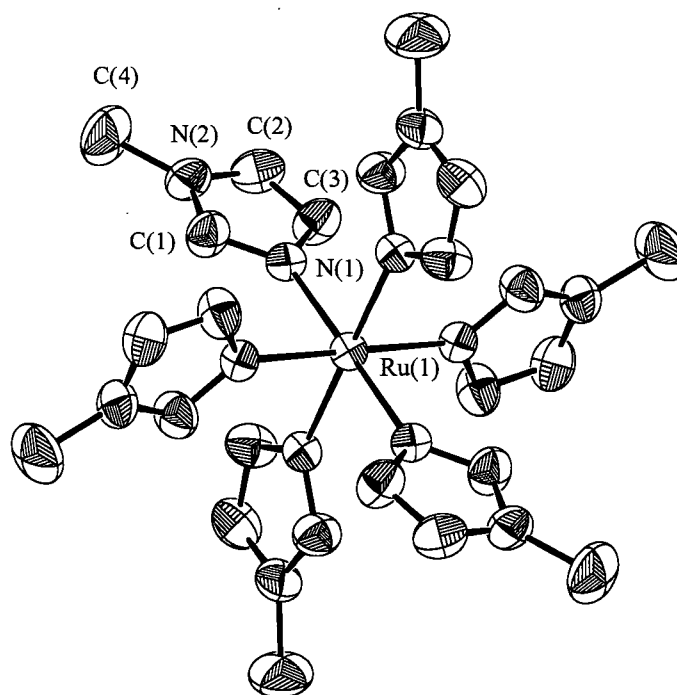


Figure 4-3: ORTEP view of Ru(NMeIm)₆²⁺ (**29**); 33% probability thermal ellipsoids are shown.

trigonal planar nitrogen has a slightly shorter bond radius than a tetrahedral nitrogen). Clarke *et al.* have misquoted this $\text{Ru}^{\text{II}}\text{-NH}_3$ bond length as 2.114(4) Å, and reached a different conclusion.¹⁷ The N-Ru-N angles for all of the complexes mentioned above are essentially orthogonal, and the basic geometries of the imidazoles (Im, NMeIm, 5MeIm) are very similar. H-bonding is evident between the triflate oxygens and the H-atoms of the non-bonded N-atoms of the coordinated imidazoles (e.g. in Figure 4-4, $\text{N}(2)\cdots\text{O}(1) = 2.885(3)$ Å, with $\text{N}(2)\text{-H}\cdots\text{O}(1) = 163.5^\circ$).

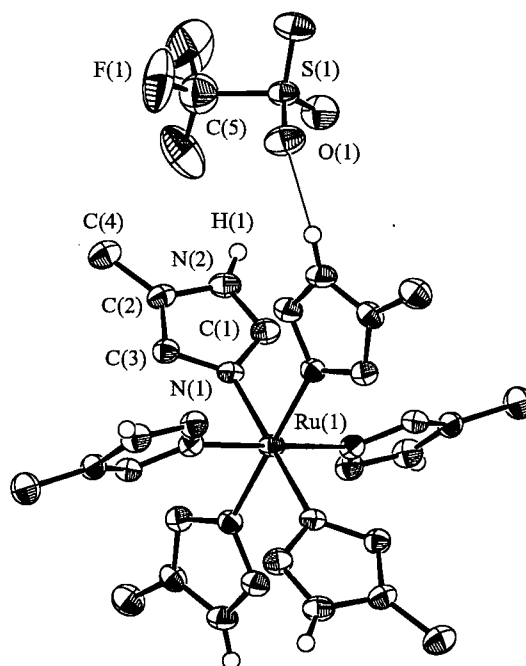


Figure 4-4: ORTEP view of $\text{Ru}(\text{5MeIm})_6^{2+}$ (**30**); 50% probability thermal ellipsoids are shown.

The ^1H NMR spectra for **28** - **30** reveal sharp, well defined peaks with δ values near those of the free ligands, consistent with imidazoles bonded to a diamagnetic $\text{Ru}(\text{II})$ centre; in d_6 -dmso, the N-H_1 signal is readily detected. Paramagnetic shifts diagnostic of

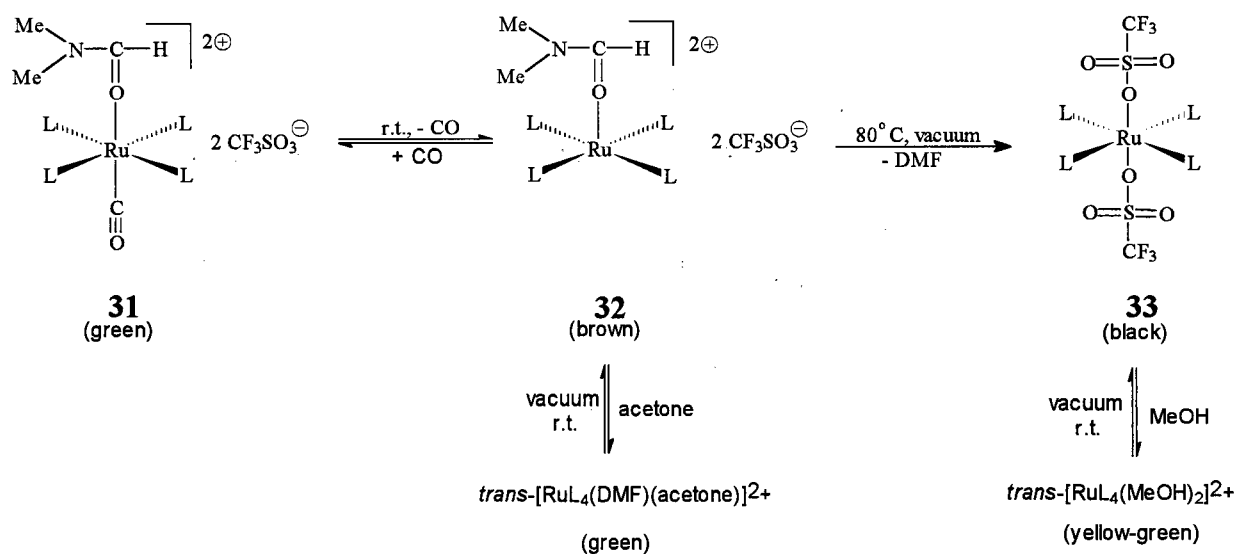
analogous Ru(III) complexes^{15,17, 27} are not seen (see also chapter 5, Sections 5.2.1.3-6). Free Im has signals at δ 12.02 (H_1), 7.63 (H_2) and 7.00 (H_4 and H_5 , these being equivalent due to tautomerization in solution); within complex **28**, H_1 shifts downfield to δ 12.47, H_2 upfield to δ 6.88, and H_4 and H_5 split into separate resonances at 6.22 and 7.23, respectively. The proximity of the H to Ru(II), a strong π -donor, determines whether the signal will be shifted upfield (as for H_2 and H_4), or downfield (as for H_5 and H_1). The 1H spectrum for **29** shows the same trend, with H_5 shifting from δ 7.08 to 7.28, and H_2 and H_4 shifting upfield from δ 7.60 and 6.92 to 7.20 and 6.31, respectively; the N-Me signal shifts slightly downfield from δ 3.61 to 3.68. The solution proton resonances of the X-ray sample of **30** also follow the same trend: H_1 (δ 11.89 \rightarrow 12.09), H_2 (δ 7.51 \rightarrow 6.85), H_4 (δ 6.69 \rightarrow 6.03) and 5Me (δ 2.16 \rightarrow 2.40). Of note, the 1H NMR data for the initially precipitated **30** (overlapping resonances for H_4 , H_5 and H_2 , as well as overlapping Me resonances) most likely imply the presence of a 1:1 mixture of $[Ru(5MeIm)_6]^{2+}$ and $[Ru(5MeIm)_5(4MeIm)]^{2+}$ species; the X-ray data show that $[Ru(5MeIm)_6]^{2+}$ preferentially crystallizes out. Clarke *et al.* have noted, similarly, formation of complexes $[Ru(NH_3)_5(5MeIm)]Cl_3$ and $[Ru(NH_3)_5(4MeIm)]Cl_3$ in a 20:1 ratio from reaction of $[Ru(NH_3)_5(H_2O)]Cl_2$ with 4(5)MeIm in air.¹⁷ The results also imply that there is a preference for formation of the less sterically demanding species, $[Ru(5MeIm)_6]^{2+}$.

Complexes **28-30** in MeOH show two UV bands: the higher energy absorbances come at 218, 224 and 228 nm, respectively, slightly higher wavelengths than those of the $\pi \rightarrow \pi^*$ transitions of the free ligands, but the ϵ values within the complexes are an order of magnitude greater than those of the free ligands. The lower energy UV maxima in **28 - 30** have ϵ values of $(5.6 - 10.2) \times 10^3 M^{-1}cm^{-1}$ and presumably correspond to an LMCT band.^{28,29} Only **28** (which has a crystallographic centre of symmetry) has a band in the visible region (642 nm, $\epsilon = 33$) typical of a d-d transition which is formally Laporte-forbidden for an octahedral complex; however, in the presence of unsymmetrical vibrations the centre of symmetry can be destroyed and vibronic transitions can be observed.²⁸ Solutions of **29** and **30** (which have crystallographic S_6 symmetry) do not exhibit an absorption maximum in the visible region.

The CV data for the Ru(III/II) reduction potentials for **28** ($E_{1/2} = 246$ mV vs, Ag/AgCl) and **29** ($E_{1/2} = 271$ mV) in MeCN/TBAP compare with the values of 295 and 283 mV reported by Clarke *et al.* for the Ru(III) salts $[\text{Ru}(\text{Im})_6][\text{ClO}_4]_3$ and $[\text{Ru}(\text{NMeIm})_6][\text{PF}_6]_3$, respectively, in aqueous chloride media.¹⁷ The $E_{1/2}$ value of 174 mV for **30**, the $(5\text{MeIm})_6$ species, shows a relative stabilization of the Ru(III) state for this system.

4.3.1.2 Reaction of $[\text{Ru}(\text{DMF})_6][\text{CF}_3\text{SO}_3]_3$ with 2MeIm

The reaction of 2MeIm, a more sterically demanding ligand than Im, NMeIm and 5MeIm, with $[\text{Ru}(\text{DMF})_6][\text{CF}_3\text{SO}_3]_3$ led to the isolation of a green solid (**31**), similar in appearance to complex **28**. However, **31** is formulated as *trans*- $[\text{Ru}(\text{CO})(\text{DMF})(2\text{MeIm})_4][\text{CF}_3\text{SO}_3]_2$. The CO results from the decarbonylation of DMF, and the required co-product, dimethylamine, was detected by GC analysis. Such decarbonylation of DMF to generate metal carbonyls is well documented.³⁰ It has not been possible to obtain good elemental analysis or definitive NMR data for **31** because during attempts to remove associated DMF by pumping, the CO is removed to generate the brown complex $[\text{Ru}(\text{DMF})(2\text{MeIm})_4][\text{CF}_3\text{SO}_3]_2$ (**32**) and, of note, **31** can be regenerated by exposing solid **32** to 1 atm CO (Scheme 4-1).



Scheme 4-1: Conversion of **31** → **32** → **33**, with suggested formulations (L = 2MeIm).

Complex **31** shows ν_{CO} bands in the IR at 2103 and 1654 cm^{-1} attributed to the CO and DMF ligands, respectively (for free CO and DMF, these bands appear at 2143 and 1673 cm^{-1}). More typically, ν_{CO} values for Ru(II)-N donor systems are in the range 2010 - 1920 cm^{-1} ,^{31,32} and it should be recalled that the ν_{CO} value is dependent on the medium used for measurement (for example, ν_{CO} values for $[\text{Ru}(\text{NH}_3)_5\text{CO}]^{2+}$ vary from 1993 - 1923 cm^{-1} depending on the associated anion and the medium).³¹ A ν_{CO} value of 2008 cm^{-1} is seen for a *trans*-Ru(porp)(CO)₂ species; the mutually *trans*- π -acceptor carbonyls expectedly lead to a high ν_{CO} and a relatively labile CO ligand.³² For *tcc*-RuCl₂(CO)₂(PPh₃)₂, the *cis*-carbonyls are each trans to the π -acceptor phosphines and ν_{CO} values of 2059 and 1995 cm^{-1} are recorded.³³ The π -electron density available from the Ru(II) for backbonding to the CO of **31** must be minimal, resulting in the remarkably high ν_{CO} value of 2103 cm^{-1} , a weak Ru-CO bond, and high lability of the CO. The 2103 cm^{-1} band could result from 'occluded' rather than coordinated CO, but there is no experimental evidence for this. The ν_{CO} value for the DMF in **31** is some 20 cm^{-1} below that of free DMF (ν_{CO} 1673 cm^{-1}), while that for Ru(DMF)₆²⁺ is 1635 cm^{-1} . The IR spectrum of **32** is essentially identical to that of **31**, except the ν_{CO} for the CO has disappeared and ν_{CO} (DMF) has shifted to 1648 cm^{-1} , consistent with somewhat more π -backbonding available from Ru(II) to the carbonyl of DMF.

An analytically pure sample of **32** was not isolated as its generation from **31** always leads to contamination by $[\text{Ru}(\text{CF}_3\text{SO}_3)_x(2\text{MeIm})_4][\text{CF}_3\text{SO}_3]_y$ (**33**) (see below) which is formed from **32** by removing the coordinated DMF under vacuum (Scheme 4-1). Nevertheless, ¹H NMR data for samples of **32** reveal the existence of one coordinated DMF with inequivalent Me resonances at δ 3.22 and 3.10, and the formyl proton seen at δ 8.40 (these signals are downfield from those of free DMF and are comparable to those found for $[\text{Ru}(\text{DMF})_6]^{2+}$).²¹ The brown **32** reacts with acetone to give a green solution, and a singlet at δ 2.14 (downfield from that of free acetone, δ 2.04) is assigned to coordinated acetone; the acetone can be removed *in vacuo* to regenerate **32** (Scheme 4-1).

Complex **33** (Scheme 4-1) is obtained as an analytically pure solid; the black colour is unusual and the complex was originally thought to be $[\text{Ru}(2\text{MeIm})_4][\text{CF}_3\text{SO}_3]_2$

containing tetrahedrally coordinated Ru. However, the NMR data and an Evans method³⁴ magnetic moment measurement illustrate the diamagnetic character of **33**. On dissolution in MeOH, species **33** shows an immediate conductivity corresponding to a 1:1 electrolyte, but this increases over 3 h to a maximum Λ_M typical of a 2:1 electrolyte;³⁵ during the conductivity measurements, the original black solution fades to a final yellow-green colouration, presumably due to *trans*-[Ru(2MeIm)₄(MeOH)₂]²⁺. The data cannot distinguish between (i) **33** being a neutral, six-coordinate species with *trans*-triflate ligands, which on dissolution in MeOH immediately dissociates one triflate ligand and then the second one is slowly displaced, and (ii) **33** being a five-coordinate species [Ru(CF₃SO₃)(2MeIm)₄][CF₃SO₃] that in MeOH slowly loses the coordinated triflate. Of note, the measured ν_{SO} values for the triflate anion within [Ru(DMF)₆][CF₃SO₃]₃ and complexes **28** - **30** are seen at 1255, 1253, 1270 and 1263 cm⁻¹, respectively; in **33**, two IR bands are seen at 1280 and 1251 cm⁻¹ and such splitting could be consistent with the presence of coordinated triflate.^{36,37} Contrary to such reasoning, however, complexes **31** and **32** also show 'split' bands in this region of the IR spectrum (1283 and 1249, and 1284 and 1248 cm⁻¹, respectively). Complex **32** could be reformulated as the six-coordinate species [Ru(CF₃SO₃)(DMF)(2MeIm)₄][CF₃SO₃], but **31** cannot contain coordinated triflate. The measured ν_{CF_3} values for **28** - **30** are seen at 1173, 1151, and 1170 cm⁻¹, while those for **31** - **33** were observed at 1167, 1167 and 1169 cm⁻¹, respectively, suggesting this IR band cannot be used as a diagnostic tool for the presence or absence of coordinated triflate. More definite evidence is needed to unambiguously identify species **31** - **33**. The incorporation of the sterically hindered 2MeIm ligand certainly enriches the chemistry of these Ru(II)-imidazole species.

4.3.1.3 Hexakis(nitroimidazole) Ru(II) Complexes, and some Ru(III) mixed DMF-SR2508 and -EF5 Complexes

Analogous to the results obtained for the imidazole complexes, the nitroimidazole species were also isolated in the Ru(II) oxidation state, resulting from the *in situ* reduction of the Ru(III) precursor. Unlike free imidazoles which can show reductive properties,^{15,23,24} the nitroimidazoles are typically oxidants, readily accepting

electrons which makes them useful as radiosensitizers.³⁸ Reaction of excess nitroimidazole with $[\text{Ru}(\text{DMF})_6][\text{CF}_3\text{SO}_3]_3$ in refluxing MeOH (under an inert atmosphere) appears to be a sufficient reducing environment²² for a Ru(III) to Ru(II) reduction, recalling that RuCl_3 in refluxing MeOH is reduced to an ill-defined "Ru blue" solution.³⁹

The reaction of $2\text{NO}_2\text{Im}$ with $[\text{Ru}(\text{DMF})_6][\text{CF}_3\text{SO}_3]_3$ was monitored using ^1H NMR spectroscopy in CD_3OD which appears to show successive displacement of the DMF ligands by $2\text{NO}_2\text{Im}$, as new peaks appear possibly corresponding to the substituted

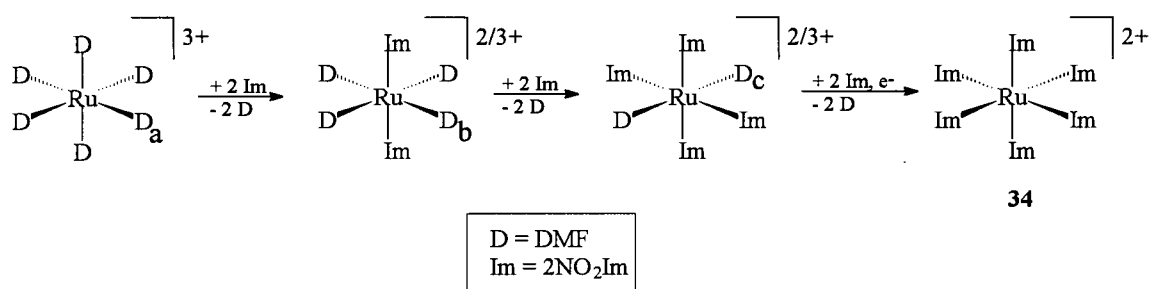


Figure 4-5: Proposed stepwise DMF displacement by $2\text{NO}_2\text{Im}$ for the synthesis of $[\text{Ru}(2\text{NO}_2\text{Im})_6][\text{CF}_3\text{SO}_3]_2$ (**34**).

complexes $[\text{Ru}(\text{DMF})_{6-x}(2\text{NO}_2\text{Im})_x][\text{CF}_3\text{SO}_3]_3$, where $x = 2, 4, 6$ (see Figure 4-5). A coordinated $2\text{NO}_2\text{Im}$ ligand exhibits a strong *trans* effect due to the electron-withdrawing properties of the nitro group,²⁷ and the peak pattern observed in the ^1H NMR spectrum (Figure 4-6) suggests that the DMF ligands are effectively displaced two at a time. The upfield shift of the Me signals of the remaining DMF ligands which occurs upon substitution is not understood; however, all Ru(III) imidazole^{13,15,40} and nitroimidazole²⁷ complexes display signals in the upfield region (δ -5 to -20); hence, successive addition of nitroimidazoles to give **34** might lead to this upfield shift ($a \rightarrow b \rightarrow c$, see Figures 4-4 and 4-5). The Ru is probably reduced to the 2+ oxidation state after complete substitution of the DMF ligands, as the *in situ* NMR data show paramagnetic isotropic shifts for each species observed. The observation of very broad peaks in the upfield region of the

spectrum (δ -14 to -23) also supports the formation of a Ru(III) 2NO₂Im complex prior to reduction to Ru(II).

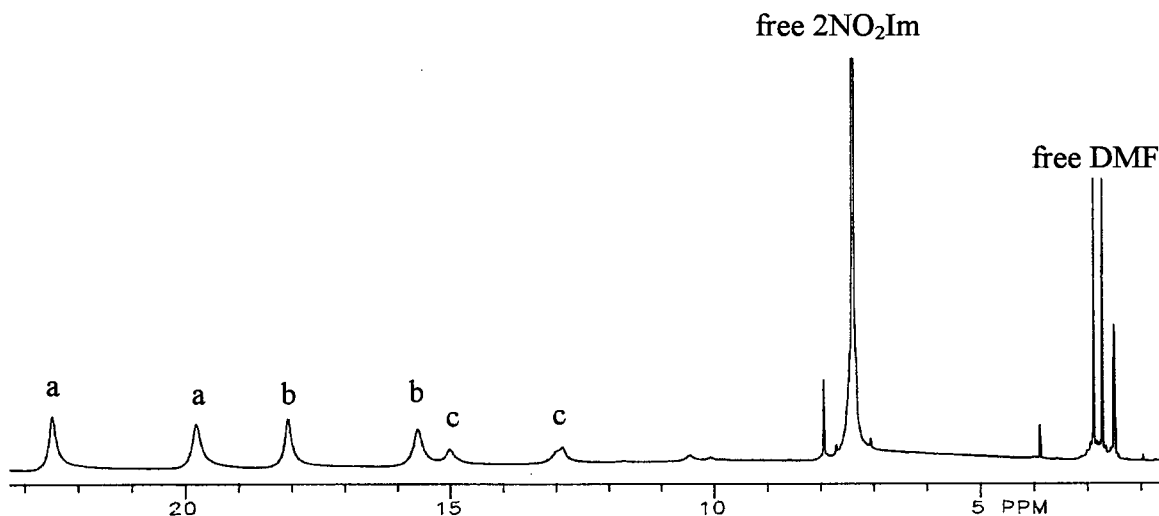


Figure 4-6: In situ ¹H NMR spectrum in CD₃OD during the synthesis of **34**.

The isolated **34** was insoluble in all common solvents, and its ¹H NMR spectrum, obtained by removing MeOH from the reaction mixture and then dissolving the residue in d₆-dmsO, showed one broad singlet (δ 6.22) presumably corresponding to 6 equivalent 2NO₂Im ligands, the signals of the H₄ and H₅ Im protons overlapping (free 2NO₂Im was also observed in the *in situ* spectrum at δ 7.35). The upfield shift of both of the proton signals upon coordination of the 2NO₂Im to Ru(II) follow a different trend to that observed for the imidazole complexes, where H₅ shifts downfield and H₄ shifts upfield (Section 4.3.1.1); the coordination removes the degeneracy of H₄ and H₅ (which are equivalent in the free ligand due to tautomerization), but only one broad singlet is observed. The broadening is apparently an electronic effect incurred by the presence of the nitro group at the 2-position on the imidazole ring, as this phenomenon is not observed with, for example, the Ru(II)-2MeIm complexes (Section 4.2.1.4). Of note, there is no peak observed for C2 of free 2-nitroimidazoles (see Chapter 3) in their ¹³C NMR spectra because of the electron-withdrawing ability of the nitro group.⁴¹

$[\text{Ru}(\text{5NO}_2\text{Im})_6][\text{CF}_3\text{SO}_3]_2$ (**35**) was also insoluble in all solvents except D_2O , while **36**, the $2\text{Me5NO}_2\text{Im}$ analogue, was sparingly soluble in MeOH and in dmso . Coordination of $5\text{NO}_2\text{Im}$ and $2\text{Me5NO}_2\text{Im}$ to $\text{Ru}(\text{II})$ leads to an upfield shift in the proton signals as a result of the π -donor ability of $\text{Ru}(\text{II})$. For **35**, the peaks for H_2 and H_4 were observed at δ 8.06 and 7.76 in CD_3OD , respectively (*cf.* δ 8.35 and 7.85 for the free ligand). For **36**, the upfield shift of H_4 in d_6 - dmso is less pronounced (from δ 8.28 to 8.24), while the shift of the 2Me group from δ_{free} 2.36 to δ_{complex} 2.34 is essentially negligible. For **35** and **36**, an 'extra' unidentified peak appears at δ 2.69 for the *in situ* and isolated solid spectra, respectively, in CD_3OD .

The elemental analysis for **34** supports a hexacoordinated $2\text{NO}_2\text{Im}$ formulation with 2 solvate H_2O molecules. The presence of H_2O was supported by solid state IR data ($\nu_{\text{O-H}}$ at 3405 cm^{-1}) and was commonly observed for many of the nitroimidazole complexes throughout this thesis work (complexes **35** and **36** contain 3 and 6 moles of H_2O , respectively). Initially, a hexa-substituted $2\text{NO}_2\text{Im}$ species was not expected because the nitro group is in the sterically demanding position of the imidazole ring. Others have reported that reactions with Ru which occur for NMe- and 5MeIm do not occur with 2MeIm or $1,2\text{-Me}_2\text{Im}$ using the same conditions;^{14,27,42} this is also observed for the reaction of 2MeIm with $[\text{Ru}(\text{DMF})_6][\text{CF}_3\text{SO}_3]_3$ (Section 4.2.1.4). A ChemDraw SymApps model revealed that the size of the Me and NO_2 groups are quite similar; however, presumably due to the planarity of the NO_2 the coordinated nitroimidazoles must adopt a configuration which permits coordination of six $2\text{NO}_2\text{Im}$ ligands to the $\text{Ru}(\text{II})$ in **34**. For **36**, the steric demand of the 2Me position is reinforced as only five coordinated $2\text{Me5NO}_2\text{Im}$ ligands are permitted, as determined from elemental analysis data. For **35** the coordinated nitroimidazole is assumed to involve the less sterically hindered 5NO_2 tautomer, analogous to the situation found in the structurally characterized **30**. Previous NMR studies have shown that complexes containing 4MeIm can exist,¹⁷ albeit in significantly smaller quantities than the 5MeIm geometric isomer (see also the data for **30** in Section 4.3.1.1).

A comparison of the the UV-Vis spectra for complexes **34**, **35** and **36** reveals some similarities and differences. Each spectrum exhibits a high intensity band (as judged by the high absorbance for a dilute solution) in the range 340-360 nm which conceivably corresponds to a ligand $\pi \rightarrow \pi^*$ transition or the $t_2(\text{Ru}) \rightarrow \pi^*(\text{L})$ transition (MLCT).⁴³ Complexes **34** and **36** each contain two other bands (**34**: 596 and 746 nm; **36**: 606 and 710 nm); the more intense band at higher energy is believed to be the spin-allowed singlet-singlet transition while the weaker band at lower energy could be the corresponding singlet-triplet transition allowed by the strong spin-orbit coupling in ruthenium.^{44,45} Complex **35** contains a single band at 672 nm and, as judged by the ratio of the band absorbancies, is presumably a d-d transition.

The IR spectra for **34** - **36** reveal that coordination of the nitroimidazole to Ru(II) shifts both the asymmetric and symmetric ν_{NO} bands, to slightly lower energies.^{19,46} For example, in **34**, ν_{NOasym} and ν_{NOsym} are shifted 8 and 10 cm^{-1} lower, respectively, than the values observed for the free ligand (1485 and 1370 cm^{-1}). That the ν_{NOasym} and ν_{NOsym} bands for **35** (1509 and 1377 cm^{-1}) are similar to those found for **36** (1504 and 1380 cm^{-1}), a 2Me5NO₂Im complex, implies that the 5NO₂ tautomer predominates in **35**. The 4NO₂ tautomer would be expected to have ν_{NO} values at higher energy, in agreement with the difference observed between those for free **MF5** (1473 and 1368 cm^{-1} , a 2Me5NO₂Im) and those for free **2M4NF5** (1506 and 1400 cm^{-1} , a 2Me4NO₂Im) (see chapter 3).

The hexakis(nitroimidazole) complexes **34** - **36** were found to be insoluble in most common solvents and except for **35** were also insoluble in aqueous media. In hopes of synthesizing water-soluble complexes that could be used for *in vitro* testing, only 2 equivalents of **SR2508** and **EF5** were reacted with $[\text{Ru}(\text{DMF})_6][\text{CF}_3\text{SO}_3]_3$. In both cases the isolated product was a Ru(III) species, suggesting that the *in situ* reduction observed during syntheses of the hexakis-imidazole and -nitroimidazole complexes was dependent on the number of coordinated (nitro)imidazole ligands.

The composition of **37** was $[\text{Ru}(\text{DMF})_4(\text{SR2508})_2][\text{CF}_3\text{SO}_3]_3$, but for **38**, the **EF5** analogue, two of the DMF ligands of the precursor had been displaced by EtOH, the reaction solvent. The ¹H NMR spectrum of **37** contains peaks at δ 22.46 and 19.75 for the Me groups of DMF coordinated to Ru(III)²¹ and the peaks corresponding to the protons

of **SR2508** display no significant isotropic shifts which have been observed for nitroimidazoles (and imidazoles) within anionic Ru(III) chloro complexes.¹⁵⁻¹⁷ The IR spectrum contains $\nu_{C=O}$ for coordinated DMF at 1647 cm^{-1} (*cf.* $\nu_{C=O}$ of 1673 cm^{-1} for free DMF), while $\nu_{C=O}$ for **SR2508** is considered to be buried within the DMF band ($\nu_{C=O}$ is 1667 cm^{-1} for free **SR2508**). The presence of bands at 3337 and 3142 cm^{-1} (attributed to ν_{NH} and ν_{CH} , respectively) and at 1503 and 1360 cm^{-1} ($\nu_{NO_{asym}}$ and $\nu_{NO_{sym}}$; *cf.* 1487 and 1365 cm^{-1} for free ligand) proves the presence of the **SR2508** ligand. The 1H NMR spectrum of **38** reveals the presence of **EF5**, EtOH and DMF, but surprisingly only the shifts for the coordinated DMF Me-groups are paramagnetically shifted (δ 22.16, 19.88). The peaks of **EF5** and EtOH are broadened and shifted downfield from those of the free ligands, as to be expected upon coordination to an electron deficient metal like Ru(III). The $^{19}F\{^1H\}$ NMR spectrum, with peaks at δ -8.13 and -45.23 (*cf.* δ -8.10 and -45.19 for free **EF5** in d_6 -acetone), may also support coordination of **EF5**. The IR spectrum for **38** revealed $\nu_{C=O}$ bands for both coordinated DMF and **EF5** at 1645 and 1686 cm^{-1} (*cf.* 1689 cm^{-1} for free **EF5**), respectively. Attempts at obtaining a mass spectrum for **38** proved to be futile. Complexes **37** and **38** have similar electronic spectra, with bands appearing at around 350 nm and 548 nm.

4.3.2 Complexes Synthesized from $RuCl_3 \cdot 3H_2O$

The synthesis of Ru(III) imidazole complexes has been thoroughly investigated for the isolation of both neutral⁴⁷ and anionic^{12-16,40} complexes. The synthesis of Ru(III) nitroimidazole complexes, however, is a relatively new area. The only Ru(III) nitroimidazole complex reported to date is $[4NO_2ImH][RuCl_4(5NO_2Im)_2]$ which appeared in the literature in 1995.²⁷ Attempts by Anderson and Beauchamp were also made to synthesize the analogous $2Me5NO_2Im$ complex, but pure products could not be obtained. Advantages of synthesizing chloride-containing nitroimidazole complexes are: (i) they undergo solvolysis in aqueous media;^{13,16} (ii) the solvolysis product can bind to the nitrogen bases of DNA^{48,49} (also see chapter 6, Section 6.3.5) and histidines in serum proteins;^{50,51} and (iii) coordinated nitroimidazoles (to Pt, Ru and Rh) are useful radiosensitizers.⁵²⁻⁵⁴ In Ru(III) complexes, the Ru-N bonds are substitution inert^{15,55} and

thus the species generally remain intact prior to reduction at neutral pH,¹⁰ although exceptions are known.⁵⁶ Antitumour-active Ru(III) complexes are likely prodrugs that are transformed by *in vivo* reduction into more active DNA-binding Ru(II) complexes.^{10,57}

The synthesis of imidazole complexes from $\text{RuCl}_3 \cdot 3\text{H}_2\text{O}$ has been reported previously,⁴⁷ but no nitroimidazole work was presented. The reaction of various imidazoles with $\text{RuCl}_3 \cdot 3\text{H}_2\text{O}$ in EtOH led to the formation of Ru(III,III) dimers $[\text{Ru}_2\text{L}_4\text{Cl}_6] \cdot 2\text{H}_2\text{O}$, $[\text{Ru}_2\text{L}'_4\text{Cl}_6] \cdot 4\text{H}_2\text{O}$ and $[\text{Ru}_2\text{L}''_3(\text{H}_2\text{O})\text{Cl}_6]$, where $\text{L} = \text{NVIIm}$ or 4MeIm ; $\text{L}' = \text{Im}$ or $2\text{Et}4(5)\text{MeIm}$; $\text{L}'' = \text{NMeIm}$ or 2MeIm ; the more sterically demanding 2MeI VIIm gave a monomer $[\text{mer-RuCl}_3(2\text{MeI VIIm})_3] \cdot \text{H}_2\text{O}$. Monomeric Ru-Im complexes such as $\text{RuCl}_3(\text{NMeIm})_2(\text{DMSO})$,⁵⁸ $\text{RuCl}_3(\text{Im})_2(\text{DMAD})$,¹⁵ and $\text{RuCl}_3(\text{Im})_3$ ⁵⁹ have also been isolated in the *mer* configuration. In this thesis work, the reaction with nitroimidazoles appears to form Ru(III) monomers according to elemental analysis and spectroscopic data; however, a dimer formulation cannot be totally ruled out in some cases.

Similar to the hexakis(nitroimidazole) complexes, **39** and **40** contain waters of hydration, as observed for many of the imidazole complexes.⁴⁷ For **39**, the IR spectrum revealed a strong ν_{OH} band at 3415 cm^{-1} and also weak bands at 1707 and 1660 cm^{-1} which could also be due to the presence of H_2O . The ^1H NMR spectrum also contained a H_2O peak, significantly more intense than for the blank, but the amount of H_2O could not be quantified by integration. Of interest, the $2\text{NO}_2\text{Im}$ proton signals were not significantly shifted from those of the free ligands, a phenomenon common to all Ru(III)- $2\text{NO}_2\text{Im}$ complexes synthesized during this work. Complex **39** has two sets of two peaks which integrate to $\sim 2:1$ ratio (Figure 4-7). Coordination of $2\text{NO}_2\text{Im}$ removes the ability of the ligand to tautomerize and results in separate signals for H_4 and H_5 , and thus the $2:1$ ratio implies a *mer*-geometry. The peak assignments for **39** are based on proximity of the H atom to the Ru(III), and electronegativity arguments where the protons of the ligand *trans* to Cl are likely further downfield than those of the mutually *trans* $2\text{NO}_2\text{Im}$ ligands; the lower intensity peaks must correspond to the protons of the $2\text{NO}_2\text{Im}$ *trans* to the Cl.

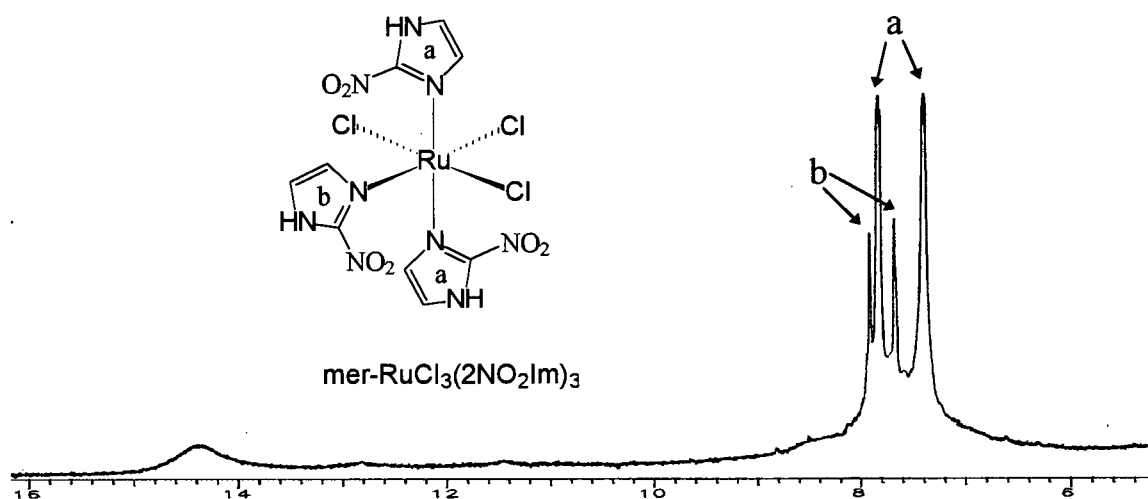


Figure 4-7: ^1H NMR spectrum for **39** in d_6 -dmso.

The pale orange **40** was the first non-blue nitroimidazole complex isolated. In air, **40** slowly (over ~2 h) decomposes to a black tar, and inert atmosphere techniques are needed to isolate the pure solid. Drying the solid at ~80 °C also resulted in its decomposition, so **40** could only be dried at r.t., which likely explains the presence of EtOH. The ^1H NMR spectrum contains one broad peak at δ 13.24 for the unresolved contributions from the H_2 and H_4 protons of three equivalent, coordinated $5\text{NO}_2\text{Im}$ ligands implying *fac* geometry. After one month, the spectrum changes to two broad peaks at δ 4.71 and -14.15 integrating in a 1:2 ratio, respectively, this presumably corresponding to the more thermally stable *mer* isomer (Figure 4-8). The peak at δ -14.15 compares with that at δ -16.00 for *trans*-[$4\text{NO}_2\text{ImH}$][$\text{RuCl}_4(5\text{NO}_2\text{Im})_2$] with mutually *trans* $5\text{NO}_2\text{Im}$ ligands.²⁷ This finding suggests that the proton signals for $5\text{NO}_2\text{Im}$ ligands *trans* to Cl are found downfield relative to those of mutually *trans* $5\text{NO}_2\text{Im}$ ligands. The IR spectra for the isolated solid and crystals of **40** were essentially the same. There are four strong, broad bands observed between 1350 and 1650 cm^{-1} , two of which originate from N-O stretching ($\nu_{\text{NO}_{\text{asym}}}$ 1525 and $\nu_{\text{NO}_{\text{sym}}}$ 1379 cm^{-1} ; cf. 1522 and 1381 cm^{-1} for *trans*-[PPh_4][$\text{RuCl}_4(5\text{NO}_2\text{Im})_2$]²⁷); specific bands to *mer*- and *fac*-isomers could not be identified. The remaining two bands 1480 and 1559 cm^{-1} likely correspond to stretching modes of the imidazole ring.

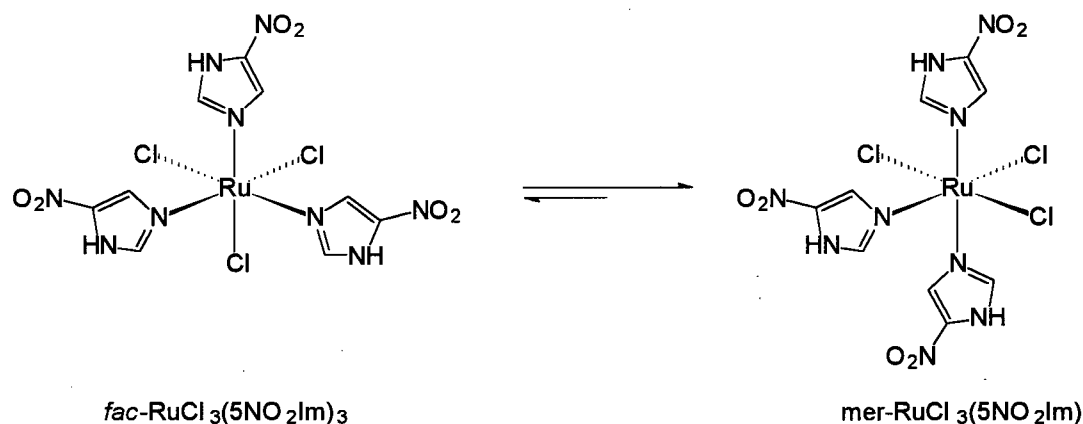


Figure 4-8: Geometrical isomerization of complex **40** in d_6 -dmso.

The reaction of $2\text{Me}5\text{NO}_2\text{Im}$ with $\text{RuCl}_3 \cdot 3\text{H}_2\text{O}$, similar to that of other reactions with imidazoles containing the sterically demanding 2Me -group (Sections 4.2.1.4 and 4.2.1.7) resulted in some quite remarkable, and not yet fully understood findings. As well as an orange Ru(III) product **41** (see below), two organic products were isolated using preparative TLC. The first band (highest R_f) gave a colourless oil which according to $\text{DCI}(+)$ MS was a ‘dimer’ formed by loss of two H-atoms from $2\text{Me}5\text{NO}_2\text{Im}$, but IR and NMR spectroscopies did not reveal its nature (Figure 4-9). The UV-Vis spectrum revealed a $\pi \rightarrow \pi^*$ band at 278 nm, slightly higher in energy than that

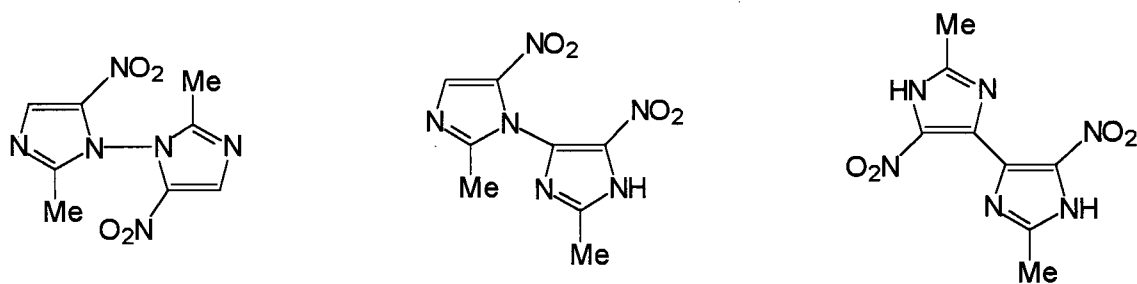


Figure 4-9: Possible configurations of a dimer formed from $2\text{Me}5\text{NO}_2\text{Im}$.

observed for $2\text{Me}5\text{NO}_2\text{Im}$ (300 nm). This dimer was unstable in solution and slowly became yellow at r.t. in CDCl_3 or MeOH ; higher temperatures resulted in instantaneous formation of the yellow species. The MS readout for the yellow species showed a parent mass of 438 suggesting even further conglomeration of the $2\text{Me}5\text{NO}_2\text{Im}$ ring system.

Complex **41**, like **40**, was air-sensitive. Its elemental analysis was significantly different from that expected for a composition $\text{RuCl}_3(2\text{Me}5\text{NO}_2\text{Im})_3$ in that the N was 3.65 % low. The IR spectrum (Figure 4-10) unveiled a possible reason for the discrepancy. A set of two bands at 2370 and 2337 cm^{-1} suggested the presence of free CO_2 (cf. 2360 and 2339 cm^{-1}) within the complex's lattice, and incorporation of 3 moles of CO_2 into the composition leads to an acceptable elemental analysis. The synthesis of **41** was repeated and the elemental analysis data were reproducible. When a KBr pellet of **41** was heated to $>200^\circ\text{C}$ for 5-10 s, the resulting IR spectrum revealed the loss of the bands corresponding to CO_2 , but also the intensities of the NO_2Im bands were decreased suggesting decomposition of the complex.

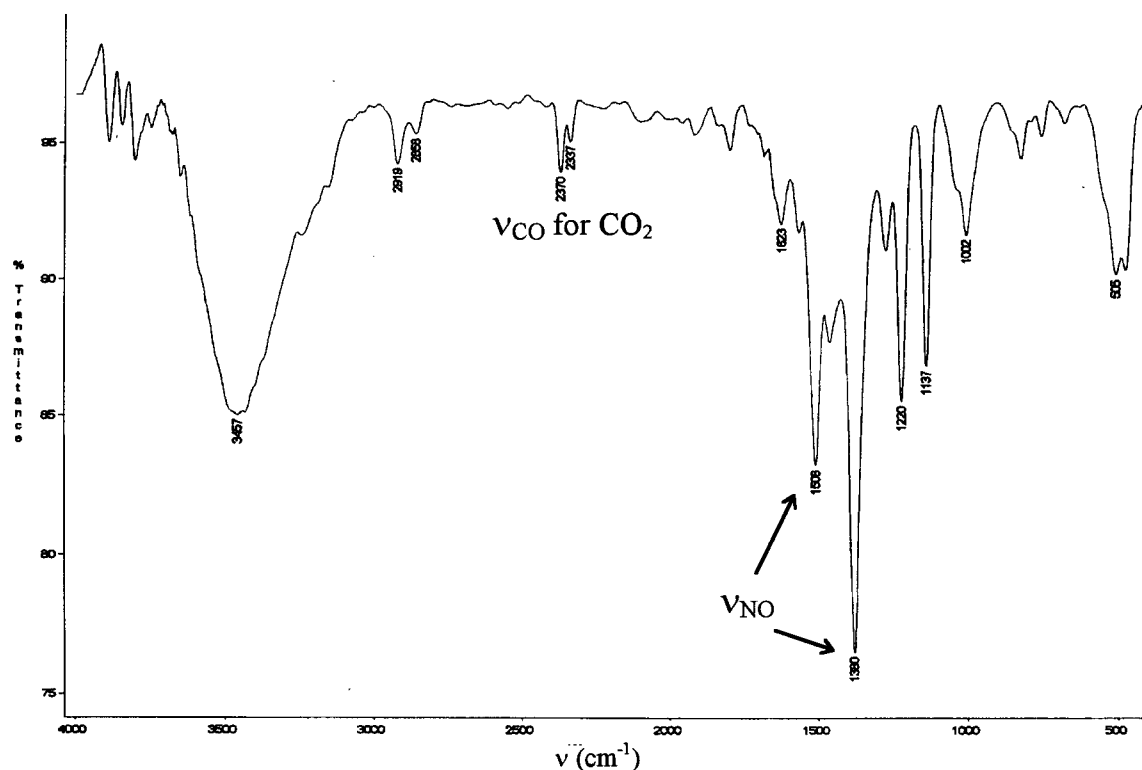


Figure 4-10: IR spectrum for the isolated, orange complex **41**.

The UV-Vis spectrum for **41** contained a band at 360 nm similar to those observed for **39** (368 nm) and **40** (350 nm), supporting coordination of a heterocyclic ligand (in this case nitroimidazole) to a Ru(III) centre.^{14,16,60} The ^1H NMR spectrum

(Figure 4-11) initially revealed the presence of two inequivalent 2Me5NO₂Im ligands in a 2:1 ratio, supporting a *mer* geometry. Analogous to *mer*-40, a downfield signal (δ 17.25) is observed for the H₄ proton of the ligand *trans* to Cl, with the corresponding 2Me peak at δ -5.05. The peaks matching the H₄ and 2Me protons for the mutually *trans* nitroimidazole ligands are observed at δ -7.90 and -3.95, respectively. After 6 days the spectrum contained only two signals (δ -3.85 and -8.65), comparable to the peaks observed for the mutually *trans* nitroimidazole ligands in the *mer* complex; the δ -5.05 and downfield peaks have disappeared. This spectrum may be that of a species formed by ligand dissociation (peaks corresponding to free 2Me5NO₂Im are observed in the δ 0 to 15 region after 6 d), for example *trans*-[RuCl₂(2Me5NO₂Im)₂](μ -Cl)₂.

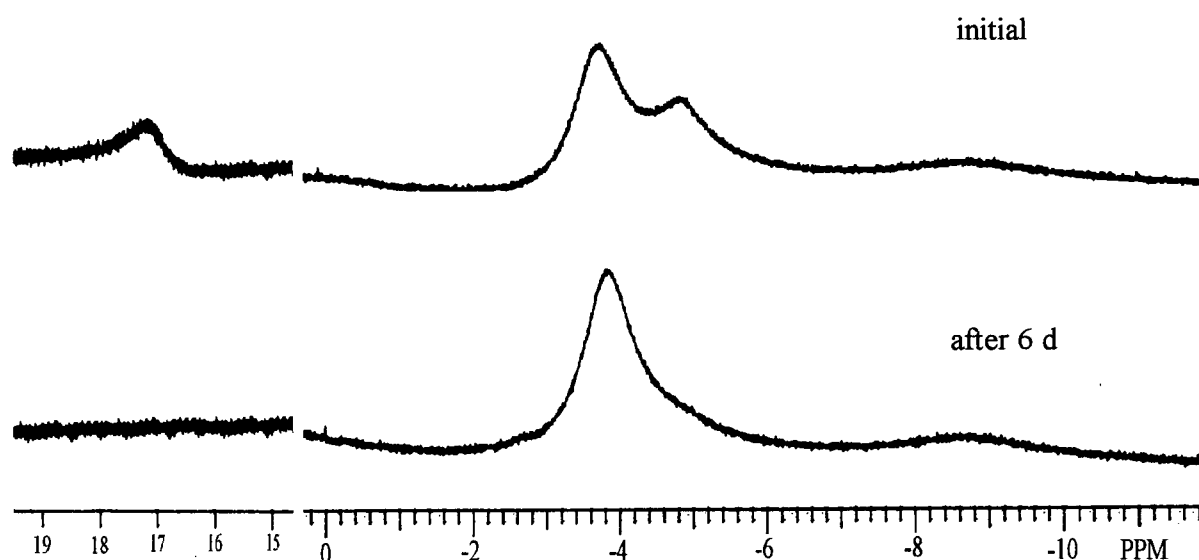


Figure 4-11: ¹H NMR spectra for complex **41** in CD₃OD (initial and after 6 d).

The reaction of RuCl₃•3H₂O with metronidazole, a 5-nitroimidazole containing a side-chain on N1, led to formation of complex **42**, again with RuCl₃L₃ composition and *mer*-geometry, elemental analysis revealing two associated H₂O molecules.

The reaction of $\text{RuCl}_3 \cdot 3\text{H}_2\text{O}$ with **SR2508** or **EF5**, $2\text{NO}_2\text{Im}$ compounds containing an N1 side-chain, gave isolated complexes of composition $\text{RuCl}_3(\text{L})_2(\text{EtOH}) \cdot 3\text{H}_2\text{O}$ (**43** and **44**), presumably because of the bulkier $2\text{NO}_2\text{Im}$ ligands. The EtOH is weakly bonded to the Ru(III) and was readily displaced by H_2O . For example, an initially blue solution of **43** turned purple over 8 h, from which $\text{RuCl}_3(\text{SR2508})_2(\text{H}_2\text{O}) \cdot 2\text{H}_2\text{O}$ was isolated. This exchange reaction was monitored by UV-Vis spectroscopy, peaks of **43** at 326 and 522 nm being replaced by those at 322 and 518 nm. The EtOH can also be removed under vacuum at 80 °C to give the 5-coordinate Ru(III) complex. This reversible process was demonstrated for **44**; dissolution of the 5-coordinate species in EtOH gave a green solution which after 1 h was purple with a peak at 530 nm, identical to that of an EtOH solution of **44**.

The solvolysis of the antitumour Ru(III) complex $[\text{RuCl}_4\text{Im}_2]^-$ at r.t. involves three successive aquation steps,⁴⁰ the first correlating well with the initial binding profile of the species to DNA.⁶¹ For the Ru(III) complex $[\text{RuCl}_4(5\text{NO}_2\text{Im})_2]^-$, the aquation reaction (in D_2O) is much slower, not being detected using ^1H NMR until after 3 days.²⁷ The solvolysis of complexes **43** and **44**, which lacked meaningful ^1H NMR signals, was conveniently followed by conductivity changes in H_2O . Complexes **43** and **44**, when compared to $[\text{RuCl}_4\text{Im}_2]^-$, have some relatively labile chloride ligands; for **44** the first and second aquation steps are complete in ~8 and 18 h, respectively, which compare with 22 h for the first aquation step of $[\text{RuCl}_4\text{Im}_2]^-$. Displacement of the final Cl^- ligand requires up to 120 h to go to completion, while the third aquation step for $[\text{RuCl}_4\text{Im}_2]^-$ is only 30 % complete after 8 months. These findings are consistent with the scheme shown in Figure 4-12 where a $2\text{NO}_2\text{Im}$ ligand leads to labilization of a *trans* chloride; the third Cl^- is more difficult to displace as it is *trans* to H_2O .

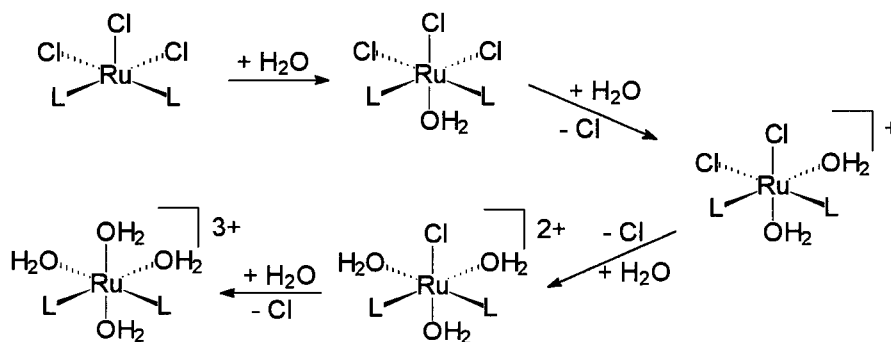


Figure 4-12: Successive aquation of **43** (L = **SR2508**) and **44** (L = **EF5**).

The trichloro Ru(III) complexes were also studied using Evans' NMR solution method to determine their paramagnetic susceptibility in solution.⁶² The position of a line in the ^1H NMR spectrum of a molecule depends on the bulk susceptibility of the medium in which the molecule is situated. Different resonance lines are obtained from residual solvent protons in solutions having different volume susceptibilities, with the line from "the more paramagnetic solution" lying at higher frequencies⁶³ (see Figure 4-13). The molar susceptibility (χ_M) and hence the effective magnetic moment (μ_{eff}) can be calculated from $\Delta\delta$ (Section 2.2.1, chapter 2).^{64,65} For all of the complexes tested the μ_{eff} values, typical of Ru(III) low spin centres with values higher than the calculated spin only value due to orbital contributions,⁶⁶ correspond to the presence of one unpaired electron.

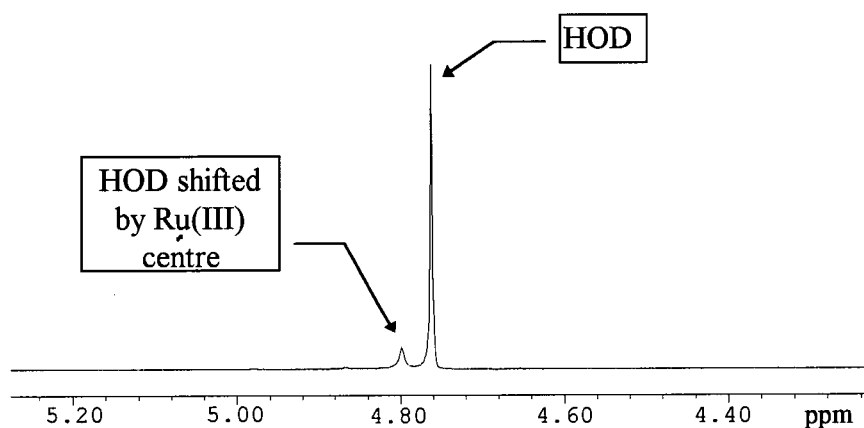


Figure 4-13: ^1H NMR (200 MHz) spectrum (Evans Method) of **43** (0.0032 g / mL D_2O , in a 0.1 mm capillary tube) referenced to the residual proton peak, HOD.

Ruthenium(II) dichloro nitroimidazole complexes were synthesized from “Ru blue” solutions, formed by reducing $\text{RuCl}_3 \cdot 3\text{H}_2\text{O}$ with H_2 , but only in one case was a pure product isolated, namely $\text{RuCl}_2(\text{metro})_4$ (**45**). The coordination of the metronidazole resulted in an increase in energy of the ligand $\pi \rightarrow \pi^*$ from 312 to 304 nm and the appearance of a band at 494 nm, typical of Ru(II) heterocyclic complexes.⁶⁷ The visible band is assigned as a MLCT band in which an electron from Ru(II) is transferred to an unoccupied orbital of the nitroimidazole, presumably the lowest lying π -antibonding orbital. The ^1H NMR spectrum of **45** contained broad signals, typical for nitroimidazole complexes even for a diamagnetic Ru(II) species. The assignments were made according to coupling observed in the 2D COSY spectrum, and the relative integrations of the peaks. The presence of only a single set of ligand peaks suggests a *trans* geometry for **45**.

4.3.3 Complexes Synthesized from *cis/trans*- $\text{RuCl}_2(\text{DMSO})_4$

Complexes of Ru(II) with a myriad of different ligands have been formed via *cis*- and *trans*- $\text{RuCl}_2(\text{DMSO})_4$ precursors.⁶⁸ Of note, complexes of the type $\text{RuCl}_2(\text{DMSO})_2(\text{NO}_2\text{Im})_2$ have been investigated, including their usefulness as hypoxic radiosensitizers.^{19,20} In this case, the metal binds to DNA by utilizing the strong binding affinity of Ru(II) for purine and pyrimidine bases,⁶⁹ and acts as a carrier for the nitroimidazole radiosensitizer whose local concentration at the DNA target is thus increased. Further investigation into the synthesis of these mixed-DMSO/nitroimidazole complexes during this work revealed that the reported isolated species⁴⁶ are actually a mixture of products,⁷⁰ whose composition is uncertain. For the reported, non-toxic complex $\text{RuCl}_2(\text{DMSO})_2(4\text{NO}_2\text{Im})_2$, a good sensitizer enhancement ratio ($\text{SER} = 1.6$) was obtained in hypoxic CHO cells; however, because of the uncertainty in the nature of the active species in aqueous solution, the conclusions are less definitive. In an attempt to avoid the non-selective reactivity of $\text{RuCl}_2(\text{DMSO})_4$ with nitroimidazoles, it was proposed to synthesize complexes with nitroimidazoles containing N1-diamine side-chains (*e.g.* the reduced form of compound **22**, chapter 3). It was thought that an amine-N might form a stable five-membered chelate ring and favour formation of a single product, while at the

same time introduce the requisite "electron-affinic" nitroimidazole moiety. Trial reactions with en were studied to probe the proposed coordination chemistry.

The reaction of one equivalent of en with *cis*-RuCl₂(DMSO)(DMSO)₃ resulted in the displacement of two DMSO ligands and formation of two *cis* isomers of RuCl₂(DMSO)₂(en), **46a** and **46b**, the product depending on the reaction time. The geometry of **46a** shown in Figure 4-14 is supported by observation of two $\nu_{\text{S-O}}$ bands in the IR spectrum (1068 and 1051 cm⁻¹), while the ¹H NMR spectrum reveals four distinct peaks for the en protons. The NH₂ *trans* to Cl is assumed to appear further downfield (δ 3.65) than that *trans* to DMSO (δ 3.04), while the adjacent CH₂ resonances appear at δ 3.47 and 2.61, respectively; the Me resonances of DMSO are considered to overlap at δ 3.28. For formation of **46a** (reaction time 45 min), presumably the more weakly held O-bound DMSO is displaced first⁷¹ followed by displacement of an adjacent S-bound DMSO to form the chelate ring. The stronger *trans* effect of DMSO (versus Cl) implies coordination of en such that one N-atom is *trans* to Cl while the other is *trans* to DMSO. A longer reaction time of 15 h allows for isolation of **46b** (Figure 4-14). The IR spectrum contains a single $\nu_{\text{S-O}}$ band, consistent with *trans* DMSO ligands, while the ¹H NMR spectrum contains single resonances for the NH₂ (δ 3.60) and CH₂ (δ 3.00) protons of en, now the structure having a plane of symmetry. The isomerization of **46a** to **46b** with time suggests that **46b** is the more thermally stable isomer; the preference for this geometry has been observed for other S- and N-donor ligand sets.⁶⁸

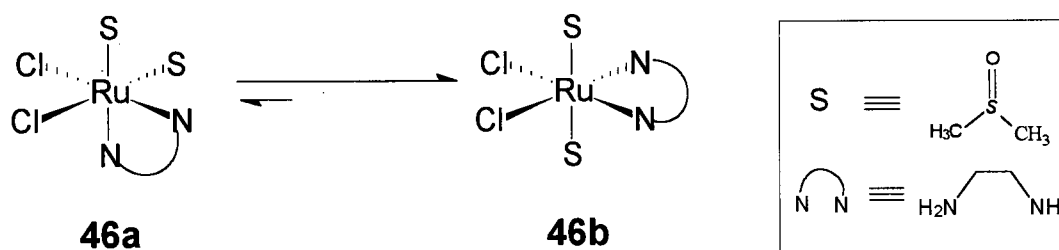


Figure 4-14: Isomerization of *cis*-RuCl₂(DMSO)₂(en) from **46a** to **46b**.

The reaction of en with *trans*-RuCl₂(DMSO)₄ yielded the single species *trans*-RuCl₂(DMSO)₂(en) (**47**). The IR spectrum displays two $\nu_{\text{S-O}}$ bands (1075 and 1059 cm⁻¹),

analogous to those of **46a**, supporting *cis* geometry for the DMSO ligands. The ^1H NMR spectrum, analogous to that of **46b**, has single resonances for the NH_2 (δ 4.20) and CH_2 (δ 2.90) protons of en due to symmetry.

The synthesis of a Ru(II)-DMSO/**EF5** complex was also attempted with the hope of isolating a complex analogous to $\text{RuCl}_2(\text{DMSO})_2(\text{SR2508})$, previously synthesized and characterized in our laboratory.⁴⁶ However, the reaction of one equivalent of **EF5** with *cis*- $\text{RuCl}_2(\text{DMSO})_4$ resulted in formation of a product analyzing as $\text{RuCl}_2(\text{DMSO})_2(\text{EF5})(\text{acetone})$ (**48**). The acetone is likely coordinated as it was not removed under vacuum at 80 °C, even though the complex melted under these conditions. Neither the ^1H NMR nor IR spectra identifies definitively the coordinated acetone because of overlap of peaks/bands. The $\nu_{\text{C=O}}$ IR band, thought to be that of **EF5**, does show a shoulder at 1703 cm^{-1} which may correspond to acetone coordinated to the strong π -donor Ru(II) ($\nu_{\text{C=O}}$ for free acetone is at 1715 cm^{-1}). **48** is unstable in acetone solution, as indicated by the appearance of peaks corresponding to free **EF5** in the ^1H NMR spectrum after 24 h; this behaviour is similar to that of the analogous TMSO complex, see Table 4.2, p.151.

4.3.4 Miscellaneous Ru Complexes

Because of our research group's ongoing interest in synthesizing Ru(II) complexes that contain a single bis(phosphine) ligand per metal and their use as catalysts for the hydrogenation of unsaturated organics,⁷²⁻⁷⁵ the synthesis of an **EF5** nitroimidazole derivative was attempted. Previous reports have shown that reaction of the N-donor ligands Im or NMeIm with $[\text{RuCl}_2(\text{dppb})]_2(\mu\text{-dppb})$ results in isolation of the monomeric complexes, $[\text{RuCl}(\text{dppb})\text{Im}_3]\text{Cl}$ ⁷² and *trans*- $\text{RuCl}_2(\text{dppb})(\text{NMeIm})_2$.⁷³ The reaction of $[\text{RuCl}_2(\text{dppb})]_2(\mu\text{-dppb})$ with **EF5** gave a brilliant blue solid which analyzed for $\text{RuCl}_2(\text{dppb})(\text{EF5})$. The ^{31}P NMR spectrum, however, revealed two AB patterns (labelled AB/CD) consistent with a Ru(II,II) dimer, $[\text{RuCl}(\text{dppb})(\text{EF5})]_2(\mu\text{-Cl})_2$ (**49**), with one **EF5** ligand *trans* to a terminal Cl and one *trans* to a bridging Cl (Figure 4-15). The ^2J coupling constants reveal *cis* P atoms,⁷⁶ nullifying the possibility of a bridging dppb ligand. The IR spectrum for **49** contains a $\nu_{\text{C=O}}$ band at 1709 with a shoulder at 1714 cm^{-1} , possibly

consistent with the presence of two inequivalent **EF5** ligands (*cf.* the $\nu_{\text{C=O}}$ value of 1689 cm^{-1} for free **EF5**). The asymmetric and symmetric $\nu_{\text{N-O}}$ bands, centered at 1479 and 1366 cm^{-1} , may also contain more than one band as shoulders are observed on both bands. The UV-Vis spectrum is similar to that of other Ru(II) phosphine/imidazole complexes,⁷² and shows a 236 nm band, matching a $\pi \rightarrow \pi^*$ transition for the phenyl groups of dppb, and peaks at 336 and 694 nm that could correspond to LMCT bands. The monomeric Im and NMeIm Ru(II)-dppb complexes^{72,73} noted above show absorptions at 350 and 340 nm , respectively, but neither contains a lower energy band at $\sim 700\text{ nm}$ which may be a property of the doubly-chloro-bridged, six-coordinate dimer. Other monomeric species have exhibited bands in the $675\text{--}680\text{ nm}$ range, but these are extremely low in intensity and have been assigned to d-d transitions.⁷³

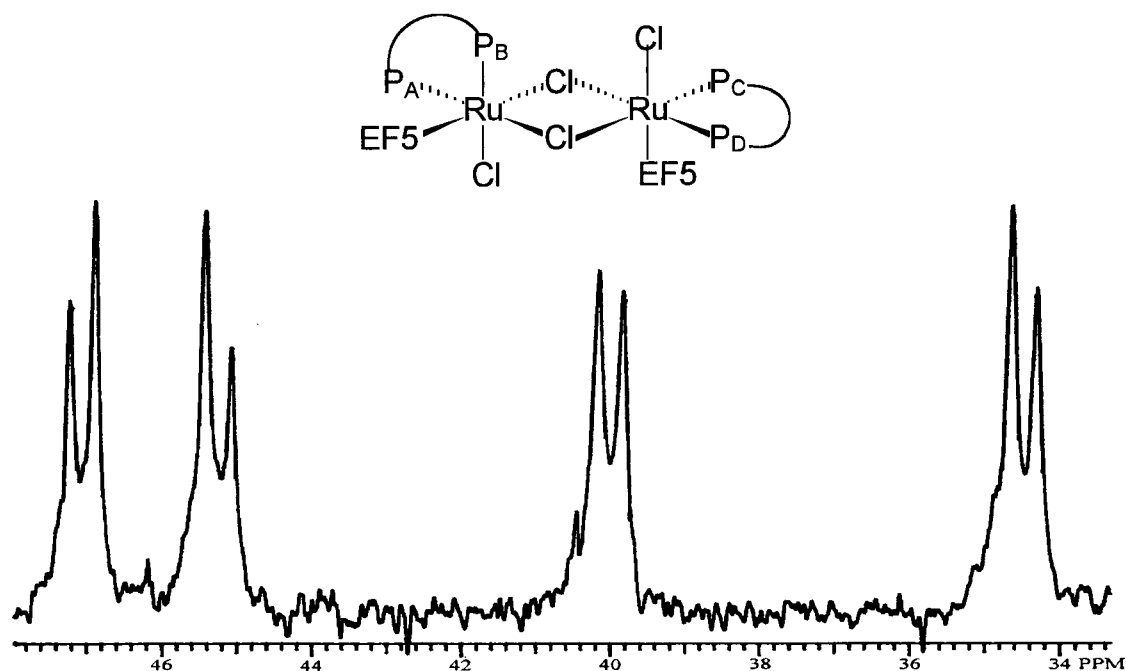


Figure 4-15: $^{31}\text{P}\{^1\text{H}\}$ NMR spectrum for complex **49**, with proposed structure.

The $^{31}\text{P}\{^1\text{H}\}$ NMR spectrum for **50**, a purple side-product formed along with **49**, suggests the presence of three magnetically inequivalent P atoms in a typical ABX pattern (Figure 4-16). This is the pattern expected for the bridging dppb precursor

$[\text{RuCl}_2(\text{dppb})]_2(\mu\text{-dppb})$, but because of low solubility of this complex its $^{31}\text{P}\{^1\text{H}\}$ spectrum has not been reported. An analogous complex, $[\text{RuCl}_2(\text{diop})]_2(\mu\text{-diop})$ (Figure 4-17), is soluble and gives a peak pattern (δ_X 68.3, δ_A 33.4, δ_B 18.7; $^2J_{AB} = 306$ Hz, $^2J_{AX} = 35.4$ Hz, $^2J_{BX} = 29.0$ Hz in CDCl_3 , -60°C)^{77,78} similar to that observed in Figure 4-16. The *cis* coupling constants ($^2J_{AX} = 33.2$ Hz, $^2J_{BX} = 30.6$ Hz) are similar to those of the diop complex while the *trans* coupling constant ($^2J_{AB} = 270$ Hz) is slightly lower.

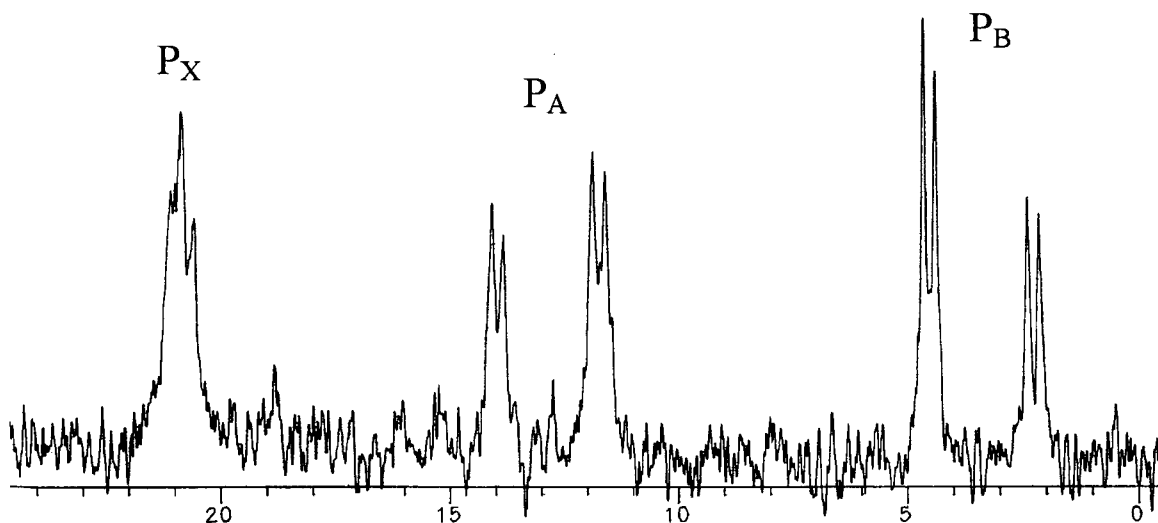


Figure 4-16: $^{31}\text{P}\{^1\text{H}\}$ NMR spectrum for the proposed $[\text{RuCl}_2(\text{dppb})(\text{EF5})]_2(\mu\text{-dppb})$ (**50**).

For **50**, the maximum chemical shift difference between peaks ($\delta_X - \delta_B$) is significantly less ($\Delta\delta$ 17.5) than for the diop species ($\Delta\delta$ 49.6), perhaps due to coordination of **EF5** at the vacant sixth site (Figure 4-17). The 2NO_2 -group on the imidazole ring will make **EF5** a much weaker base and hence a weaker coordinating ligand than Im or NMeIm which yield monomeric products.^{72,73} The strongly electron-withdrawing NO_2 -group may account for the significant upfield shift of the ^{31}P resonances (vs. the μ -diop complex). The only Ru-dppb complexes showing similar upfield shifts are monomeric and contain CO coordinated *trans* to a P-atom of dppb (for

cc-RuCl₂(CO)₂(dppb), δ_A 32.8, δ_X 6.9, $^2J_{AX} = 31.9$ Hz; and for *tc*-RuCl₂(CO)₂(dppb), δ 8.1).⁷⁹ The dimeric complex [RuCl₂(dppb)(CO)]₂(μ -dppb) has been synthesized in the solid state from [RuCl₂(dppb)]₂(μ -dppb), the incorporation of CO being confirmed by ν_{CO} at 1990 cm⁻¹.⁸⁰ In solution isomerization occurs shifting ν_{CO} to 1950 cm⁻¹, the CO group now probably being *trans* to Cl.⁸⁰ This implies that if the $^{31}\text{P}\{^1\text{H}\}$ NMR spectrum was

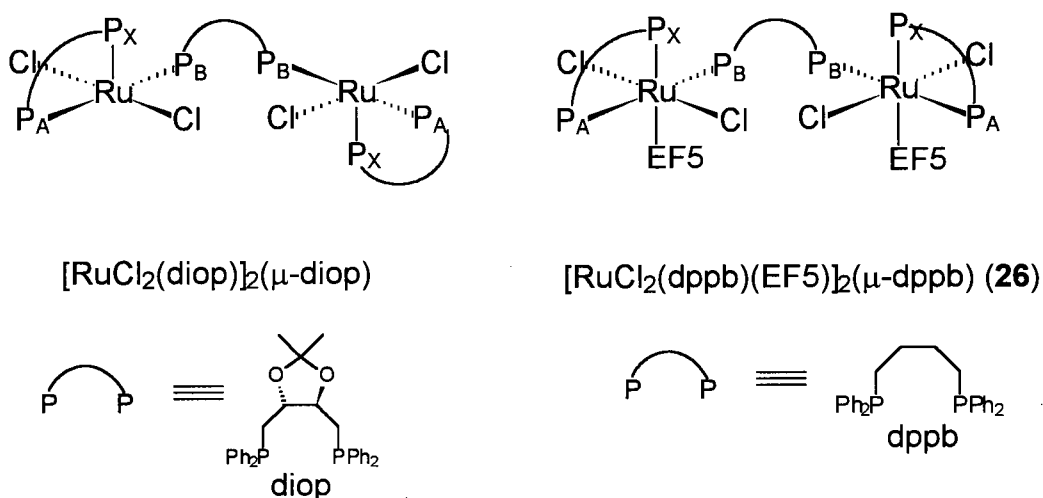


Figure 4-17: [RuCl₂(diop)]₂(μ -diop) and the proposed structure for **50**.

obtained in solution there would be no significant upfield shift of the P signal, as the CO ligands are no longer *trans* to P. The analogous dimeric diop CO complex (as shown above) has been isolated in the solid state, but in solution this breaks apart into two monomeric species.⁷⁸ The strong π -acceptor CO ligand removes electron density from the Ru(II) metal and hence from the *trans* Ru-P bond; this would lead to a longer Ru-P bond and an upfield shift of the $^{31}\text{P}\{^1\text{H}\}$ resonance.⁷³ The IR and $^{31}\text{P}\{^1\text{H}\}$ NMR data suggest that EF5 is acting as a strong π -acceptor ligand, analogous to a CO ligand.

In an attempt to synthesize *trans*-RuCl₂(MeCN)₄ from known literature methods^{11,81} the formation of the complexes *cis*-RuCl₂(MeCN)₄ (**51**) and *mer*-RuCl₃(MeCN)₃ (**52**) were discovered serendipitously. The reaction of RuCl₃•3H₂O in MeCN under 1 atm H₂ with Adam's catalyst over a 24 h period typically gives *trans*-RuCl₂(MeCN)₄ in high yield as a pure yellow solid. Prior to precipitation of the

yellow solid which is insoluble in MeCN, the reaction solution is orange; TLC analysis at this stage reveals the presence of two major orange bands which were isolated. Because of the reactivity and thermal instability of these orange species they were stored under N₂ at r.t.

Complex **51** has not been previously reported in the literature, likely due to its instability. This geometry presumably results from the substitution of one mutually *trans* Cl by MeCN, as the *trans* effect of Cl is greater than that of MeCN, with subsequent reduction to Ru(II) (see below).⁸² The IR spectrum of **51** reveals two $\nu_{\text{C}\equiv\text{N}}$ bands at 2322 and 2296 cm⁻¹ consistent with *cis* geometry (*cf.* values of 2320 and 2291 cm⁻¹ for [Ru(MeCN)₄(dppb)][PF₆]₂).¹¹ The *trans* complex has a single $\nu_{\text{C}\equiv\text{N}}$ band at 2278 cm⁻¹. The positive IR coordination shifts for $\nu_{\text{C}\equiv\text{N}}$ of N-bonded acetonitrile (*cf.* 2254 cm⁻¹ for free MeCN) imply a shortening of the C-N bond and is perhaps evidence against any π -backbonding component of the metal-ligand interaction.^{11,83} The ¹H NMR spectrum of **51** also supports a *cis*-Ru(II) complex as the Me peaks at δ 2.19 and 2.05 are well resolved and integrate closely to a 1:1 ratio, once again implying two magnetically inequivalent MeCN ligands. This species is unstable in solution and quickly isomerizes to the *trans* isomer (the thermodynamic product), as indicated by a colour change from orange to yellow and the appearance of a peak at δ 2.51 in the ¹H NMR spectrum. Unfortunately, an acceptable elemental analysis of **51** could not be obtained after repetitive attempts.

The synthesis and isolation of *mer*-RuCl₃(MeCN)₃ (**52**) were previously reported by Duff and Heath⁸⁴ by the reaction of [NBu₄][RuCl₄(MeCN)₂] with NaBF₄ in MeCN; however, only elemental analysis and UV-Vis data were reported. The *mer*-geometry was evidenced by the UV-Vis spectrum which was exemplary of C_{2v} MX₃ chromophores⁸⁵: a major band (414 nm) flanked by weak shoulders (292 and 482 nm) for **52** was analogous to that observed for *mer*-RuX₃(H₂O)₃ and the crystallographically characterized *mer*-RuCl₃(PhCN)₃ complex also contained a similar band distribution.⁸⁶ The X-ray structure for *mer*-RuCl₃(MeCN)₃ was obtained during this work (Figure 4-18), unequivocally proving the *mer*-geometry. The red-orange prismatic crystals crystallized

out in the orthorhombic primitive lattice with a space group of $Pbca$. The average Ru-Cl bond length for the mutually *trans* Cl atoms was 2.332 Å, while that for the Cl *trans* to MeCN was shorter (2.307 Å). These data are analogous to those for *mer*- $\text{RuCl}_3(\text{PhCN})_3$ except the Ru-Cl bond for Cl *trans* to PhCN was shorter (2.293 Å),⁸⁶ presumably because of the increased electron withdrawing ability of the phenyl group. Similarly, the Ru-N for MeCN *trans* to Cl (2.058 Å) is longer than for the two mutually *trans* MeCN ligands (average 2.014 Å). The observations concur with the *trans* influence of Cl being greater than that of MeCN.⁸⁶ Of interest, the structure contains one mole of CHCl_3 per molecule and contains H-bonds as shown in Figure 4-18.

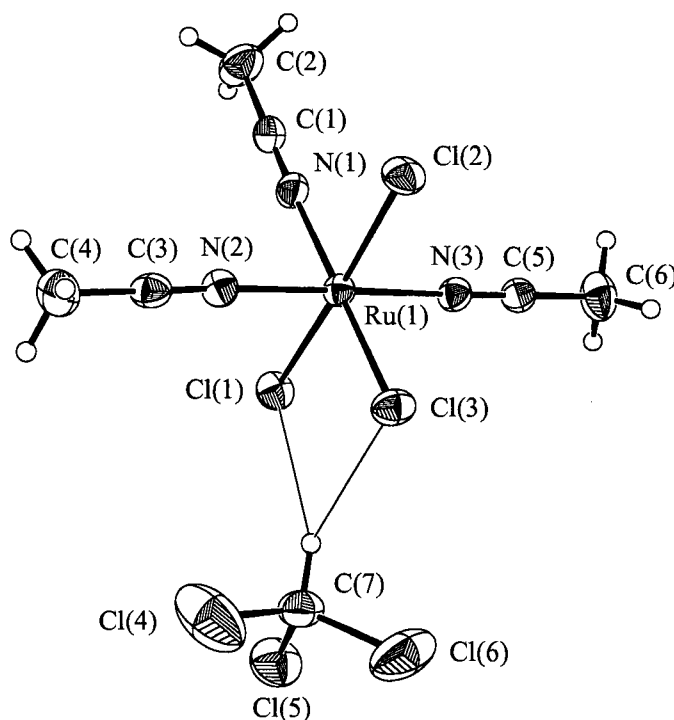


Figure 4-18: ORTEP view of *mer*- $\text{RuCl}_3(\text{MeCN})_3$ (**52**); 50% probability thermal ellipsoids are shown.

The IR spectrum of **52** contains three $\nu(\text{C}\equiv\text{N})$ bands at 2325, 2297 and 2235 cm^{-1} as predicted for *mer*- MX_3L_3 complexes.⁸⁷ All the C-N bonds are essentially the same length (avg. 1.122 Å), implying that the distribution of the IR bands is due to slightly different energies for the A_1 , B_1 and B_2 vibrations. The ^1H NMR spectrum for **52** containing broad isotropically shifted peaks is also consistent with a *mer*-Ru(III) complex. Peaks at δ 46.95 and -15.24 with an integral ratio of 1:2 correspond to two inequivalent MeCN ligands. The downfield shift of the peak for the MeCN *trans* to Cl is analogous to those observed for the 2Me protons of *mer*- $\text{RuCl}_3(2\text{Me}5\text{NO}_2\text{Im})_3$ (**41**), although the shift observed for **52** is significantly higher. Interestingly, after one week the ^1H NMR spectrum in CDCl_3 changed significantly: the δ 46.95 peak disappeared, that at δ -15.24 shifted to -15.47, while new peaks at δ 3.11 and 2.04 were present. The peak at δ -15.47 is likely due to the formation of the dimer $[\text{RuCl}_2(\text{MeCN})_2]_2(\mu\text{-Cl})_2$ as $\text{RuCl}_3(\text{RCN})_3$ complexes are prone to condensation in non-coordinating solvents.^{84,88} The sharp singlet at δ 2.04 (typical of Ru(II)) and the broad peak at δ 3.11 (typical of a paramagnetic species) likely correspond to disproportionation products of **52**, $\text{RuCl}_2(\text{MeCN})_4$ and $\text{RuCl}_4(\text{MeCN})_2$, respectively.

4.4 References

- 1 Clarke, M. J. *Metal Ions Biol. Syst.* **1980**, *11*, 231.
- 2 Keppler, B. K. *In Metal Complexes in Cancer Chemotherapy*; B. K. Keppler, Ed.; VCH, Weinheim, Germany, 1993, p. 429.
- 3 Clarke, M. J.; Bailey, V. M.; Doan, P. E.; Hiller, C. D.; LaChance-Galang, K. J.; Daghlial, H.; Mandal, S.; Bastos, C. M.; Lang, D. *Inorg. Chem.* **1996**, *35*, 4896.
- 4 McNamara, M.; Clarke, M. J. *Inorg. Chim. Acta* **1992**, *195*, 175.
- 5 Clarke, M. J.; Taube, H. *J. Am. Chem. Soc.* **1974**, *96*, 5413.
- 6 Hartmann, M.; Einhäuser, T. J.; Keppler, B. K. *J. Chem. Soc., Chem. Commun.* **1996**, 1741.
- 7 Ocain, T.D.; Bastos, C. M.; Gordon, K. A.; Granstein, R. D.; Jenson, J. C.; Jones, B.; McAuliffe, D. J.; Newcomb, J. R. *Transplant. Proc.* **1998**, *28*, 3032.
- 8 Clarke, M. J. *In Metal Complexes in Cancer Chemotherapy*; B. K. Keppler, Ed.; VCH, Weinheim, Germany, 1993, p. 179.
- 9 Marzilli, L.; Iwamoto, M.; Alessio, E.; Hansen, L.; Calligaris, M. *J. Am. Chem. Soc.* **1994**, *116*, 815.
- 10 Clarke, M. J. *Prog. Clin. Biochem. Med.* **1989**, *10*, 25.
- 11 Fogg, D. E.; Rettig, S. J.; James, B. R. *Can. J. Chem.* **1995**, *73*, 1084.
- 12 Keppler, B.K.; Wehe, D.; Endres, H.; Rupp, W. *Inorg. Chem.* **1987**, *26*, 844.
- 13 Ni Dhubhghaill, O. M.; Hagen, W. R.; Keppler, B. K.; Lipponer, K.-G.; Sadler, P. J. *J. Chem. Soc., Dalton Trans.* **1994**, 3306.
- 14 Keppler, B. K.; Rupp, W.; Juhl, U. M.; Endres, H.; Niebl, R.; Balzer, W. *Inorg. Chem.* **1987**, *26*, 4366.
- 15 Anderson, C.; Beauchamp, A. L. *Inorg. Chem.* **1995**, *34*, 6065.
- 16 Chatlas, J.; van Eldik, R.; Keppler, B. K. *Inorg. Chim. Acta* **1995**, 233, 59.
- 17 Clarke, M. J.; Bailey, V. M.; Doan, P. E.; Hiller, C. D.; LaChance-Galang, K. J.; Daghlial, H.; Mandal, S.; Bastos, C. M.; Lang, D. *Inorg. Chem.* **1996**, *35*, 4896.

- 18 Bastos, C. M.; Ocain, T. D. US Patent 5708022A (1998), through Chem. Abst. 128:123807 (1998).
- 19 Chan, P. K. L.; Chan, P. K. H.; Frost, D. C.; James, B. R.; Skov, K. A. *Can. J. Chem.* **1988**, *66*, 117.
- 20 Chan, P. K. L.; James, B. R.; Frost, D. C.; Chan, P. K. H.; Hu, H.-L.; Skov, K. A. *Can. J. Chem.* **1989**, *67*, 508.
- 21 Judd, R. J.; Cao, R.; Biner, M.; Armbruster, T.; Bürgi, H.-B.; Merbach, A. E.; Ludi, A. *Inorg. Chem.* **1995**, *34*, 5080.
- 22 Hallman, P. S.; Stephenson, T. A.; Wilkinson, G. *Inorg. Synth.* **1970**, *12*, 237.
- 23 Collman, J. P.; Gagne, R. R.; Halbert, T. R.; Marchon, J.-C.; Reed, C. A. *J. Am. Chem. Soc.* **1973**, *95*, 7868.
- 24 Chin, D.-H.; Balch, A. L.; La Mar, G. N. *J. Am. Chem. Soc.* **1980**, *102*, 1446.
- 25 Wilkins, R.G. Kinetics and Mechanism of Reactions of Transition Metal Complexes, 2nd Edn.; VGH, New York, 1991, Chpt.4.
- 26 Stynes, H. C.; Ibers, J. A. *Inorg. Chem.* **1971**, *10*, 2304.
- 27 Anderson, C.; Beauchamp, A. L. *Inorg. Chim. Acta* **1995**, *233*, 33.
- 28 Huheey, J. E.; Keiter, E.A.; Keiter, R. L. Inorganic Chemistry, 4th Edn.; Harper Collins, New York, 1993, p.433.
- 29 Sundberg, R. J.; Bryan, R. F.; Taylor, Jr., I. F.; Taube, H. *J. Am. Chem. Soc.* **1974**, *96*, 381.
- 30 Belani, R. M.; James, B. R.; Dolphin, D.; Rettig, S. J. *Can. J. Chem.* **1988**, *66*, 2072, and refs. therein.
- 31 Chatt, J.; Leigh, G. J.; Thankarajan, N. *J. Organomet. Chem.* **1970**, *25*, C77.
- 32 Camenzind, M. J.; James, B. R.; Dolphin, D. *J. Chem. Soc., Chem. Commun.* **1986**, 2008.
- 33 Porta, F.; Tollari, S.; Bianchi, C.; Recchia, S. *Inorg. Chim. Acta* **1996**, *24*, 79.
- 34 Evans, D. F. *J. Chem. Soc.* **1959**, 2003.
- 35 Geary, W. J. *Coord. Chem. Rev.* **1971**, *7*, 81.

-
- 36 Miles, M. G.; Doyle, G.; Cooney, R. P.; Tobias, R. S. *Spectrochim. Acta* **1969**, *25A*, 1515.
- 37 Otieno, T.; Rettig, S. J.; Thompson, R. C.; Trotter, J. *Can. J. Chem.* **1990**, *68*, 1901.
- 38 Adams, G. E.; Clarke, E. D.; Flockhart, I. R.; Jacobs, R. S.; Sehmi, D. S.; Stratford, I. J.; Wardman, P.; Watts, M. E.; Parrick, J.; Wallace, R. G.; Smithen, C. E. *Int. J. Radiat. Biol.* **1970**, *35*, 133.
- 39 Gilbert, J. D.; Rose, D.; Wilkinson, G. *J. Chem. Soc. (A)* **1970**, 2765.
- 40 Anderson, C.; Beauchamp, A. L. *Can. J. Chem.* **1995**, *73*, 471.
- 41 Burlinson, N. Personal communication.
- 42 Heijden, M.; van Vliet, P. M.; Haasnoot, J. G.; Reedijk, J. *J. Chem. Soc., Dalton Trans.* **1993**, 3675.
- 43 Misra, T. K.; Das, D.; Sinha, C.; Ghosh, P.; Pal, C. K. *Inorg. Chem.* **1998**, *37*, 1672.
- 44 Kober, E. M.; Meyer, T. J. *Inorg. Chem.* **1982**, *21*, 3967.
- 45 Decurtines, S.; Felix, F.; Ferguson, J.; Gudel, H. U.; Ludi, A. *J. Am. Chem. Soc.* **1980**, *102*, 4102.
- 46 Chan, P. K. L. Ph. D. Thesis, University of British Columbia, 1988.
- 47 Bora, T.; Devi, M; Gogoi, K. *Transition Met. Chem.* **1986**, *11*, 467.
- 48 Hartmann, M.; Einhäuser, T. J.; Keppler, B. K. *J. Chem. Soc., Chem. Commun.* **1996**, 1741.
- 49 Pubin, J. R.; Sabat, M.; Sundarliagam, M. *Nucleic Acid Res.* **1983**, *11*, 6571.
- 50 Kratz, F.; Keppler, B. K.; Messori, L.; Smith, C.; Baker, E. N. *Metal Based Drugs* **1994**, *1*, 169.
- 51 Smith, C. A.; Sutherland-Smith, A. J.; Keppler, B. K.; Kratz, F.; Baker, E. N. *J. Biol. Inorg. Chem.* **1996**, *1*, 424.
- 52 Farrell, N.; Carneiro, T. M. G.; Einstein, F. W. B.; Jones, T.; Skov, K. A. *Inorg. Chim. Acta* **1984**, *92*, 61.
- 53 Chan, P. K. L.; Skov, K. A.; James, B. R.; Farrell, N. P. *Int. J. Radiat. Oncol. Biol. Phys.* **1986**, *12*, 1059.

- 54 Goodgame, D. M. L.; Lawrence, A. S.; Slawin, A. M. Z.; Williams, D. J.; Stratford, I. *J. Inorg. Chim. Acta* **1986**, *125*, 143.
- 55 Brown, G. M.; Sutton, J. E.; Taube, H. *J. Am. Chem. Soc.* **1978**, *100*, 2767.
- 56 Hartmann, M.; Lipponer, K.-G.; Keppler, B. K. *Inorg. Chim. Acta* **1998**, *267*, 137.
- 57 Clarke, M. J.; Jansen, B.; Marx, K. A.; Kruger, R. *Inorg. Chim. Acta* **1986**, *124*, 13.
- 58 Germentia, S.; Alessio, E.; Todone, F. *Inorg. Chim. Acta* **1996**, *253*, 87.
- 59 Keppler, B. K.; Lipponer, K.-G.; Stenzel, B.; Kratz, F. *In Metal Complexes in Cancer Chemotherapy*; B. K. Keppler, Ed.; VCH, Weinham, Germany, 1993, p. 187.
- 60 Kralik, F.; Vrestal, J. *J. Collect. Czech. Chem. Commun.* **1960**, 1298.
- 61 Holler, E.; Schaller, W.; Keppler, B. *Arzneim.-Forsch. Drug Res.* **1991**, *41*, 1065.
- 62 Evans, D. F. *J. Chem. Soc.* **1959**, 2003.
- 63 Live, D. H.; Chan, S. I. *Anal. Chem.* **1970**, *42*, 791.
- 64 Evans, D. F.; Fazakerley, G. V.; Phillips, R. F. *J. Chem. Soc. (A)* **1971**, 1931.
- 65 Crawford, T. H.; Swanson, J. *J. Chem. Educ.* **1971**, *48*, 382.
- 66 Figgis, B. N. *Introduction to Ligand Fields*; Interscience Publishers, New York, 1966, p. 288.
- 67 Ford, P.; Rudd, D. F. P.; Gaunter, R.; Taube, H. *J. Am. Chem. Soc.* **1968**, *90*, 1187.
- 68 Evans, I. P.; Spencer, A.; Wilkinson, G. *J. Chem. Soc., Dalton Trans.* **1973**, 204.
- 69 Clarke, M. J. *In Chemistry and Biochemistry of Platinum, Gold and Other Chemotherapeutic Agents*; S. J. Lippard, Ed.; Am. Chem. Soc. Symposium Series, No. 209, Am. Chem. Soc., Washington, 1983, p. 279.
- 70 These experiments were performed with the help of Mr. Fei Gao.
- 71 Alessio, E.; Mestroni, G.; Nardin, G.; Attia, W. M.; Calligaris, M.; Sava, G.; Zorzet, S. *Inorg. Chem.* **1988**, *27*, 4099.
- 72 Batista, A. A.; Polato, E. A.; Queiroz, S. L.; Nascimento, O. R.; James, B. R.; Rettig, S. J. *Inorg. Chim. Acta* **1995**, *230*, 111.
- 73 Queiroz, S. L.; Batista, A. A.; Olivia, G.; Gambardella, M. T. doP.; Santos, R. H. A.; MacFarlane, K. S.; Rettig, S. J.; James, B. R. *Inorg. Chim. Acta* **1998**, *267*, 209.

-
- 74 Joshi, A. M.; Thorburn, I. S.; Rettig, S. J.; James, B. R. *Inorg. Chim. Acta* **1992**, 198-200, 283.
- 75 MacFarlane, K. S.; Thorburn, I. S.; Cyr, P. W.; Chau, D. E. K.-Y.; Rettig, S. J.; James, B. R. *Inorg. Chim. Acta* **1998**, 270, 130.
- 76 Jameson, C. J. In Phosphorus-31 NMR Spectroscopy in Spectrochemical Analysis; J. G. Verkade and L. D. Quin, Eds.; VCH, Weinheim, Germany, 1987, p. 226.
- 77 Cyr, P. Personal communication.
- 78 James, B. R.; McMillan, R. S.; Morris, R. H.; Wang, D. K. W. *Adv. Chem. Ser.* **1978**, 167, 122.
- 79 MacFarlane, K. S. Ph. D. Thesis, University of British Columbia, 1995.
- 80 Bressan, M.; Rigo, P. *Inorg. Chem.* **1975**, 14, 2286.
- 81 Newton, W. E.; Searles, J. E. *Inorg. Chim. Acta* **1973**, 7, 349.
- 82 Shriver, D. F.; Atkins, P. W.; Langford, C. H. *Inorganic Chemistry*; W. H. Freeman & Co., New York, 1990, p. 475.
- 83 Endres, H. In *Comprehensive Coordination Chemistry*, Vol. 2; G. Wilkinson, R. D. Gillard, and J. A. McCleverty, Eds.; Pergamon Press, Oxford, U. K., 1987, p. 261.
- 84 Duff, C. M.; Heath, G. A. *J. Chem. Soc., Dalton Trans.* **1991**, 2401.
- 85 Duff, C. M.; Heath, G. A. *Inorg. Chem.* **1991**, 30, 2528.
- 86 Duff, C. M.; Heath, G. A.; Willis, A. C. *Acta Cryst.* **1990**, C46, 2320.
- 87 Nakamoto, K. *Infrared Spectra of Inorganic and Coordination Compounds*; Wiley-Interscience, New York, 1970, p. 215.
- 88 Duff, C. M.; Heath, G. A.; Khoo, T. J. Unpublished results, quoted in ref. 83.

Chapter 5

Synthesis and Characterization of Ru(II) and Ru(III) β -Diketonate Imidazole Complexes

5.1 Introduction

Acetylacetonate (acac) and other β -diketonate compounds constitute a class of chelating ligands that has been widely employed with several different metals; their coordination chemistry with Ru(II) and Ru(III) has been widely studied,¹⁻⁷ with stable, six-membered chelate rings being formed. Variation of the substituents at the 1 and 5 positions of acac leads to numerous ligand possibilities.⁸⁻¹¹ Many research groups, including Shimizu's, which studied the electrochemical and chemical properties of tris(β -diketonato) ruthenate(II) and ruthenium(III) complexes,⁹⁻¹³ have studied the effects of the electronic properties of substituents on electrochemical properties.^{6,8,13-16} Patterson and Holm reported that the half-wave reduction potentials span a very large range from +0.726 V for Ru(hfac)₃ to -0.728 V for Ru(acac)₃ (vs. SCE).¹⁵ Substitution at the 3-position (for R₁(CO)CR₃(CO)R₅) results in an increase of E_{1/2} for electron-accepting substituents (e.g. Cl, Br) and a decrease of E_{1/2} for electron-donating substituents (e.g. CH₃).⁶

Typically, the synthesis of Ru tris(β -diketonato) complexes is performed by reacting the β -diketone with RuCl₃·3H₂O in H₂O:EtOH (1:2) (i.e. via a Ru "blue" intermediate)³ or in 10% aqueous HCl and Na₂CO₃.¹ However, for isolation of mixed-ligand β -diketonato complexes, this synthesis is limited, yielding only a small amount of a mixture of the tris and the mixed-ligand complexes which must be isolated chromatographically.⁷ The synthesis of tris(β -diketonato) complexes with asymmetric ligands (where R≠R' for R(CO)CH(CO)R') has also been reported, but a mixture of optical (*mer*- and *fac*-) isomers resulted, making subsequent purification difficult.¹⁷

In one instance, the mixed-ligand complexes Ru(hfac)₂(acac) and Ru(acac)₂(hfac) were prepared by refluxing Ru(hfac)₃ and Ru(acac)₃ in toluene for a minimum of 7 days, but neither complex was isolated as a pure species;¹⁵ however, Ru(acac)₂(hfac) was synthesized and isolated via a "Ru blue" route.¹⁰ Substitution of a β -diketonate ligand by two MeCN ligands in the presence of a strong acid, such as CF₃SO₃H, yields the bis-MeCN complex [Ru(β -diketonato)₂(MeCN)₂]

[CF₃SO₃] which is a useful intermediate for the synthesis of mixed-ligand, β -diketonato complexes.¹⁸⁻²⁰ Because the MeCN ligands are reasonably labile, the bis-MeCN complexes can be used for the synthesis of numerous bis-substituted bis- β -diketonato complexes.

The coordination chemistry of imidazoles is of interest because of their role in biological systems (*e.g.* in the active sites of metalloenzymes and metalloproteins, and in the pyrimidine bases of DNA). The imidazole moiety of histidine is the centre of attachment for metals such as Cu, Fe, and Zn in many biopolymers, and appears in various redox-active and metabolic enzymes, particularly those with Cu(II), Zn(II), Mn(II), or Fe(II) active centres.²¹ A study of the interaction between imidazoles and Ru centres gives insight on the effect of the imidazole moiety on the redox properties and stabilities of different ruthenium oxidation states. Also, the fact that Ru(acac)₃ is exceptionally soluble in aqueous solution ($\sim 0.5 \text{ mmol dm}^{-3}$ at 25 °C),¹³ while other tris-acac metal complexes are not, may prove of value for *in vitro* testing of newly synthesized, ionic acac/imidazole complexes.

5.2 Experimental

5.2.1 Ruthenium(III) Acetylacetonato Complexes

5.2.1.1 Ru(acac)₃ (**53**)

In a Schlenk tube, RuCl₃•3H₂O (4.00 g, 16.2 mmol) was dissolved in 20 mL EtOH and the solution stirred at 80 °C under a steady flow of H₂ for 4 h during which the mixture transformed from orange to dark blue (Ru "blue"). NaHCO₃ (4.61 g, 0.0549 mol) was added, followed by dropwise addition of acetylacetone (6.53 mL, 0.0549 mol). The mixture was stirred under 1 atm N₂ for 12 h resulting in a bright red solution. The solvent was removed under reduced pressure and the residue (dissolved in CH₂Cl₂) was loaded onto a silica gel column and eluted (CH₂Cl₂:MeOH, 50:1). The first band yielded **53** as a red, powdered solid (5.83 g, 90 %). Anal. calc. for C₁₅H₂₁O₆Ru: C, 45.22 ; H, 5.31; found: C, 45.07 ; H, 5.18. UV-Vis (MeOH): 212 (10.9), 270 (14.1), 346 (7.47), 506 (1.58). ¹H NMR (300 MHz, d₆-acetone): δ -7.11 (s, 6H, acac *Me*), -30.25 (s, 1H, acac-*H*). This procedure is adapted from a literature method,² and the spectroscopic data are in agreement with those reported in the literature.⁹

5.2.1.2 *cis*-[Ru(acac)₂(MeCN)₂][CF₃SO₃] (**54**)

In a 250 mL RBF, **53** (1.07 g, 2.68 mmol) was dissolved in 100 mL MeCN and the mixture stirred for 5 min at 65 °C to yield a bright red solution; CF₃SO₃H (300 µL, 3.39 mmol) was then added dropwise. Instantly, the solution became red-brown; a reflux condenser was attached and the mixture was refluxed for 1 h. After ~ 10 min the mixture was purple and at 1 h it was navy blue. The solvent was removed and the residue was dissolved in CH₂Cl₂ (~ 40 mL). Et₂O was then layered on top of the CH₂Cl₂ and the mixture stored at r.t. overnight, resulting in a dark blue crystalline solid which was isolated via filtration, washed with Et₂O (3 x 10 mL) and dried *in vacuo* (1.42 g, 96 %; *cf.* lit. yield of 70 %). Anal. calc. for C₁₅H₂₀N₂O₇SF₃Ru·H₂O: C, 31.85; H, 3.91; N, 3.98; found: C, 32.13; H, 3.87; N, 3.96. LR-MS [+LSIMS]: 382 (M⁺), 341 (M⁺ - MeCN), 300 (M⁺ - 2MeCN). IR (ν, cm⁻¹): 3469 (O-H); 3098, 2990, 2931 (C-H); 2326 (C≡N_{asym.}); 2296 (C≡N_{sym.}); 1524 (C=O); 1428, 1329, 1265, 1157, 1030, 939, 639. UV-Vis (MeOH): 214 (11.6), 282 (9.67), 318 (5.12), 552 (1.40). ¹H NMR (300 MHz, CDCl₃): δ 37.53 (br s, 6H, MeCN), -23.46 (s, 6H, acac Me), -27.22 (s, 6H, acac Me). ¹⁹F{¹H} NMR (188 MHz, CDCl₃): δ -1.89 (s, CF₃SO₃⁻). Conductivity for **54** (MeOH): Λ_M = 82.2 ohm⁻¹mol⁻¹cm². This procedure is adapted from a literature method used to synthesize the analogous perchlorate salt, and the spectroscopic data are in agreement with those reported.¹⁹

5.2.1.3 *cis*-[Ru(acac)₂(Im)₂][CF₃SO₃] (**55**)

In a Schlenk tube, **54** (0.162 g, 0.305 mmol) and Im (0.122 g, 1.79 mmol) were dissolved in 10 mL EtOH and the solution stirred at 75 °C under air. The reaction was monitored via TLC. After 1 h, the solution was red-brown and slowly progressed to a deep blood-red solution (~ 24 h). According to TLC (eluent CH₂Cl₂:MeOH, 20:1), there were several products with similar R_f values; after the solvent was removed, the product mixture as an acetone solution was loaded on the preparative TLC plate. Elution resulted in the appearance of 4 bands: pink, purple, orange and red (in order from highest to lowest R_f). The pink and red bands were the most concentrated and yielded a shiny burgundy-red solid (0.0230 g) and a deep red powdered solid (0.0725 g, 41 %), respectively. According to ¹H NMR and MS data the highest R_f band was actually the mono-substituted complex *cis*-[Ru(acac)₂(MeCN)(Im)][CF₃SO₃] (**57**), while the ¹H

NMR data for the red band showed a mixture of *cis*-[Ru(acac)₂(Im)₂][CF₃SO₃] (**55**) and *trans*-[Ru(acac)₂(Im)₂][CF₃SO₃] (**56**). This reaction was repeated as described above, but using a reaction time of 48 h. This resulted in formation of only **55** and a few minor side-products; neither **56** nor **57** was detected. From the second reaction, pure **55** was isolated as a bright red, powdered solid via preparative TLC (0.0778 g, 44 %). Red, block-like crystals suitable for X-ray analysis were grown from a MeOH/THF (1:1) solution layered with hexanes. Anal. calc. for C₁₇H₂₂N₄O₇SF₃Ru (**55**): C, 34.93; H, 3.79; N, 9.59; found: C, 35.27; H, 3.73; N, 9.41. LR-MS [+LSIMS]: (**55**) 436 (M⁺), 368 (M⁺ - Im), 300 (M⁺ - 2Im); (**57** + EtOH) 455 (M⁺), 368 (M⁺ - EtOH - MeCN), 300 (M⁺ - EtOH - MeCN - Im). UV-Vis (MeOH): (**55**) 214 (9.83), 282 (10.4), 330 (5.79), 524 (1.49); (**57**) 212 (9.79), 282 (10.4), 330 (5.91), 518 (1.69). ¹H NMR (300 MHz, d₆-acetone, **55**): δ 0.45 (s, 2H, Im-*H*₁), -0.55 (s, 2H, Im-*H*₅), -2.25 (s, 2H, Im-*H*₄), -16.25 (s, 6H, acac *Me*), -21.30 (s, 2H, Im-*H*₂), -21.75 (s, 6H, acac *Me*), -53.15 (br s, 2H, acac-*H*); (**56**) δ -3.00 (s, 2H, Im-*H*₁), -3.90 (s, 2H, Im-*H*₄), -4.35 (s, 2H, Im-*H*₅), -15.75 (s, 12H, acac *Me*), -18.90 (s, 2H, Im-*H*₂), -40.50 (br s, 2H, acac-*H*); (**57**) δ 45.35 (s, 3H, MeCN), 1.20 (s, 1H, Im-*H*₁), 0.00 (s, 1H, Im-*H*₅), -1.25 (s, 1H, Im-*H*₄), -14.65 (s, 3H, acac *Me*), -15.85 (s, 3H, acac *Me*), -18.60 (s, 1H, Im-*H*₂), -20.25 (s, 3H, acac *Me*), -22.50 (s, 3H, acac *Me*), -48.25 (br s, 1H, acac-*H*), -58.15 (br s, 1H, acac-*H*). ¹⁹F{¹H} NMR (188 MHz, d₆-acetone, **55**): δ -1.93 (s, CF₃SO₃⁻); (**57**) δ -1.97 (s, CF₃SO₃⁻). Conductivity for **55** (MeOH): Λ_M = 81.1 ohm⁻¹mol⁻¹cm².

5.2.1.4 *cis*-[Ru(acac)₂(NMeIm)₂][CF₃SO₃] (**58**)

In a Schlenk tube, **54** (0.157 g, 0.295 mmol) and NMeIm (50 μL, 0.627 mmol) were dissolved in 5 mL EtOH and the solution stirred at 75 °C for 16 h under air during which the mixture transformed from dark blue to a brilliant purple. Analysis of this solution by TLC showed the presence of two major products, and ~ 10 minor side-products. The solvent was removed, the mixture then loaded onto a preparative TLC plate and eluted (CH₂Cl₂:MeOH, 20:1). Two major bands, purple (higher R_f) and red were isolated, and yielded a dark purple powdered solid (0.0526 g, 29 %) and a red solid (0.0152 g, 8.4 %), respectively. According to MS and ¹H NMR data, the purple band isolated was the mono-substituted complex *cis*-[Ru(acac)₂(MeCN)(NMeIm)][CF₃SO₃] (**59**), while the red complex matched the formulation *cis*-[Ru(acac)₂(NMeIm)₂][CF₃SO₃] (**58**). The reaction was repeated using 10 equivalents of NMeIm and this resulted in

isolation of only complex **58** in a higher yield (54 %). Red, irregular shaped crystals suitable for X-ray analysis were grown in a MeOH/acetone (1:1) solution layered with hexanes.

Data for **58**: Anal. calc. for $C_{19}H_{26}N_4O_7SF_3Ru \cdot 0.5 H_2O$: C, 36.72; H, 4.38; N, 9.01; found: C, 36.67; H, 4.14; N, 8.89. LR-MS [+LSIMS]: 464 (M^+), 382 ($M^+ - NMeIm$), 300 ($M^+ - 2NMeIm$). UV-Vis (MeOH): 214 (14.3), 284 (14.3), 330 (7.96), 524 (2.14). 1H NMR (300 MHz, d_6 -acetone): δ 13.65 (s, 6H, Im- Me_1), -1.00 (s, 2H, Im- H_5), -3.35 (s, 2H, Im- H_4), -16.05 (s, 6H, acac Me), -18.55 (s, 2H, Im- H_2), -21.55 (s, 6H, acac Me), -52.50 (br s, 2H, acac- H). $^{19}F\{^1H\}$ NMR (188 MHz, d_6 -acetone): δ -1.70 (s, $CF_3SO_3^-$). Conductivity for **58** (MeOH): $\Lambda_M = 85.0 \text{ ohm}^{-1}\text{mol}^{-1}\text{cm}^2$.

Data for **59**: Anal. calc. for $C_{17}H_{23}N_3O_7SF_3Ru$: C, 32.93; H, 3.84; N, 6.40; found: C, 33.16; H, 3.85; N, 6.42. LR-MS [+LSIMS]: 423 (M^+), 382 ($M^+ - MeCN$), 300 ($M^+ - MeCN - NMeIm$). UV-Vis (MeOH): 212 (12.0), 286 (11.0), 320 (6.29), 540 (1.91). 1H NMR (300 MHz, d_6 -acetone): δ 19.74 (s, 3H, $MeCN$), 17.26 (s, 3H, Im- Me_1), -2.35 (s, 1H, Im- H_5), -4.14 (s, 1H, Im- H_4), -15.35 (s, 3H, acac Me), -16.95 (s, 3H, acac Me), -22.82 (s, 3H, acac Me), -23.10 (s, 3H, acac Me), -25.41 (s, 1H, Im- H_2), -53.72 (br s, 1H, acac- H), -66.16 (br s, 1H, acac- H). $^{19}F\{^1H\}$ NMR (188 MHz, d_6 -acetone): δ -1.86 (s, $CF_3SO_3^-$).

5.2.1.5 *cis*-[Ru(acac)₂(2MeIm)₂][CF₃SO₃] (**60**)

Complex **60** was synthesized in the same manner as **55**, but using **54** (0.201 g, 0.0379 mmol) and 2MeIm (0.185 g, 0.225 mmol). The mixture was stirred for 48 h. Two major bands, burgundy (higher R_f) and red, were isolated from the preparative TLC plate (CH_2Cl_2 :MeOH, 20:1) to yield a red-brown solid (**60**) (0.0351 g, 15 %) and a red solid (**61**) (0.0767 g, 33 %), respectively; total yield (48 %). The isolated complex **61**, *trans*-[Ru(acac)₂(2MeIm)₂][CF₃SO₃], was not completely pure as a small amount of **60** was also detected in the 1H NMR spectrum. Orange, prismatic crystals of **60** suitable for X-ray analysis were grown in an acetone/MeOH (1:1) solution layered with hexanes.

Data for **60**: Anal. calc. for $C_{19}H_{26}N_4O_7SF_3Ru \cdot H_2O$: C, 36.19; H, 4.47; N, 8.88; found: C, 36.05; H, 4.15; N, 8.56. LR-MS [+LSIMS]: 464 (M^+), 382 ($M^+ - 2MeIm$), 300 ($M^+ - 2(2MeIm)$). UV-Vis (MeOH): 216 (11.8), 282 (14.2), 330 (8.86), 518 (2.40). 1H NMR (300 MHz, d_6 -acetone): δ 43.50 (s, 6H, Im- Me_2), 5.15 (s, 2H, Im- H_4), -0.90 (s, 2H, Im- H_1), -5.30 (s,

2H, Im- H_5), -17.25 (s, 6H, acac Me), -23.30 (s, 6H, acac Me), -54.10 (br s, 2H, acac- H). $^{19}\text{F}\{^1\text{H}\}$ NMR (188 MHz, d_6 -acetone): δ -1.88 (s, CF_3SO_3^-). Conductivity for **60** (MeOH): $\Lambda_{\text{M}} = 88.4 \text{ ohm}^{-1}\text{mol}^{-1}\text{cm}^2$.

Data for **61**: UV-Vis (MeOH): 212 (11.6), 280 (9.43), 330 (6.62), 518 (1.84). ^1H NMR (300 MHz, d_6 -acetone): δ 50.30 (s, 6H, ImMe $_2$), 7.85 (s, 2H, Im H_4), -3.40 (s, 2H, Im H_1), -5.30 (s, 2H, Im H_5), -19.05 (s, 12H, acac Me), -55.20 (br s, 2H, acac- H). $^{19}\text{F}\{^1\text{H}\}$ NMR (188 MHz, d_6 -acetone): δ -2.05 (s, CF_3SO_3^-).

5.2.1.6 *cis*-[Ru(acac) $_2$ (5MeIm) $_2$][CF $_3$ SO $_3$] (**62**)

Complex **62** was synthesized in the same manner as **55**, but using **54** (0.203 g, 0.0382 mmol) and 4(5)MeIm (0.189 g, 0.231 mmol). The mixture was stirred for 48 h to yield a deep red solution. TLC revealed two red bands, one significantly more concentrated. The major product was isolated from the preparative TLC plate (CH_2Cl_2 :MeOH, 20:1) as a brilliant, shiny red solid (0.130 g, 55 %), predicted to be the *cis*-isomer, analogous to the major band (with a lower R_f) for **60**; however, the ^1H NMR spectrum (in d_6 -acetone) showed a myriad of peaks from +15 to -30 ppm, indicating that there could be a mixture of **62** and possibly a mixed 4MeIm/5MeIm complex (**63**) resulting from tautomerism of 4(5)MeIm in solution. Further attempts to isolate a single species using chromatographic methods were unsuccessful; however, elemental analysis of the isolated red solid indicated that only bis-substituted 4(5)MeIm complexes were present. Irregular-shaped, red crystals of **62** suitable for X-ray analysis were grown in an acetone/MeOH (1:1) solution layered with hexanes, and this made possible the assignment of peaks in the ^1H NMR spectrum of the original red solid. Anal. calc. for $\text{C}_{19}\text{H}_{26}\text{N}_4\text{O}_7\text{SF}_3\text{Ru}$: C, 37.26; H, 4.28; N, 9.15; found: C, 37.57; H, 4.39; N, 9.03. LR-MS [+LSIMS]: 464 (M^+), 382 ($\text{M}^+ - 5\text{MeIm}$), 300 ($\text{M}^+ - 2(5\text{MeIm})$). UV-Vis (MeOH): 212 (12.9), 282 (10.5), 330 (5.57), 518 (1.42). The ^1H NMR spectrum of the isolated solid revealed a mixture of **62** and **63** in an approximate ratio of 3.5 to 1, respectively. ^1H NMR (300 MHz, d_6 -acetone): δ (**62**) 7.55 (s, 6H, Im-Me $_5$), 1.95 (s, 2H, Im- H_1), -1.40 (s, 2H, Im- H_4), -15.50 (s, 6H, acac Me), -20.65 (s, 6H, acac Me), -26.90 (s, 2H, Im- H_2), -50.30 (br s, 2H, acac H); (**63**) 14.70 (s, 3H, Im-Me $_4$), 7.50 (s, 3H, Im-Me $_5$), 1.98 (s, 1H, Im- H_1), 1.10 (s, 1H, Im- H_1), -2.35 (s, 1H, Im- H_4), -2.65 (s, 1H, Im- H_5), -16.50 (s, 6H, acac Me), -22.50

(s, 6H, *acac Me*), -29.25 (br s, 2H, *Im-H₂*), -51.80 (br s, 2H, *acac-H*). $^{19}\text{F}\{^1\text{H}\}$ NMR (188 MHz, d_6 -acetone): δ -1.89 (s, CF_3SO_3^-). Conductivity for **62** (MeOH): $\Lambda_{\text{M}} = 77.0 \text{ ohm}^{-1}\text{mol}^{-1}\text{cm}^2$.

5.2.1.7 [Ru(*acac*)₂(2NO₂Im)₂][CF₃SO₃] (**64**)

In a Schlenk tube, 2NO₂Im (0.0466 g, 0.0412 mmol) was dissolved in warm EtOH (~5 mL) to yield a pale yellow solution. **54** (0.0733 g, 0.0138 mmol), dissolved in 5 mL EtOH, was added and the mixture was stirred at 65 °C for 24 h under air. During this time, the colour changed from dark navy blue to burgundy-purple. The solvent was removed and 20 mL CH₂Cl₂ were added resulting in a blue solid and a pink-purple filtrate. This mixture was sonicated for 5 min and the solid isolated via filtration. The blue precipitate was washed with warm CH₂Cl₂ (6 x 5 mL) in hopes of removing any unreacted 2NO₂Im; however, TLC analysis showed the presence of unreacted 2NO₂Im. The blue solid was then suspended in 10 mL EtOAc and the mixture heated to reflux for 10 min; this was followed by filtration and then washing the solid with boiling EtOAc (5 x 5 mL). The resulting colourless filtrate and washings tested positive for the presence of 2NO₂Im by TLC. The blue solid was then washed through the frit with MeOH and the solvent was removed to give a dark blue solid which, according to TLC (CH₂Cl₂:MeOH, 20:1), had an $R_f = 0$ and had no free 2NO₂Im present (0.0101 g, 11 %). Anal. calc. for C₁₇H₂₀N₆O₁₁SF₃Ru: C, 30.27; H, 2.99; N, 12.46; found: C, 30.20; H, 3.14; N, 12.22. LR-MS [+LSIMS]: 413 ($\text{M}^+ - 2\text{NO}_2\text{Im}$), 383 ($\text{M}^+ - 2\text{NO}_2\text{Im} - \text{NO}$), 300 ($\text{M}^+ - 2(2\text{NO}_2\text{Im})$). UV-Vis (MeOH): 210, 276 (sh), 346, ~ 660 (br). Of note, the poor solubility of this complex prevented its characterization by $^1\text{H}/^{19}\text{F}\{^1\text{H}\}$ NMR spectroscopy.

5.2.1.8 [Ru(*acac*)₂(SR2508)₂][CF₃SO₃] (**65**)

In a Schlenk tube, SR2508 (0.0456 g, 0.0214 mmol) was dissolved in acetone (~10 mL) to give a pale yellow solution; **54** (0.0572 g, 0.0108 mmol) was then added to yield a navy blue solution. The vessel was sealed and the contents stirred at 60 °C for 32 h, the final solution being reddish purple. The volume of the mixture was reduced to ~2 mL, then Et₂O was layered on top and the mixture was stored at 0 °C overnight. The resulting purple precipitate was isolated via filtration and washed with Et₂O (4 x 5 mL). Of note, the solid when exposed to air (after washing) became a dark purple gum-like material, indicating that it was extremely hygroscopic. TLC

analysis of the purple gum also revealed the presence of more than one product. The purple gum was washed through the frit with acetone and the solvent was removed. The solid on the inside walls of the flask was washed with CH_2Cl_2 , the contents were sonicated and then washed through a clean frit to give a purple solid and a dark burgundy filtrate. The solid was filtered off, washed with CH_2Cl_2 (6 x 5 mL), then rinsed with MeOH through the frit and the solvent removed to yield a purple solid; dried *in vacuo* at 80 °C for 48 h (0.0301 g, 32 %). Anal. calc. for $\text{C}_{25}\text{H}_{34}\text{N}_8\text{O}_{15}\text{SF}_3\text{Ru}\cdot 2\text{H}_2\text{O}$: C, 32.90; H, 4.20; N, 12.28; found: C, 32.68; H, 3.95; N, 12.53. LR-MS [+LSIMS]: 300 ($\text{M}^+ - 2(\text{SR2508})$). UV-Vis (MeOH): 212, 274, 530, 760.

The ^1H NMR spectrum for **65** was 'noisy' and contained a number of broad peaks in the range δ 2 to 9 which could not be definitively assigned. Interestingly, no large isotropic shifts for the proton signals (analogous to those of the corresponding MeIm complexes) were observed.

It is apparent in the MS of the $2\text{NO}_2\text{Im}$ complexes **64** and **65** that the major peak is $\text{Ru}(\text{acac})^{2+}$ at 300 while the parent peak is not observed, suggesting that nitroimidazoles form a weaker bond with Ru than do methylimidazoles or imidazole.

5.2.1.9 $[\text{Ru}(\text{acac})_2(\text{EF5})_2][\text{CF}_3\text{SO}_3]$ (**66**)

In a Schlenk tube, **EF5** (0.0723 g, 0.0239 mmol) and **54** (0.0634 g, 0.0120 mmol) were dissolved in acetone (10 mL), yielding a navy blue solution. The vessel was sealed (under 1 atm air) and stirred at 65 °C for 40 h during which the solution went through purple *en route* to a final burgundy colour. The solvent was removed and then the residue was dissolved in 3-5 mL CH_2Cl_2 . The now dark purple solution was then layered with Et_2O (~ 25 mL) and stored at r.t. overnight. The resulting purple precipitate was isolated via filtration, washed with Et_2O (3 x 10 mL) and then washed through the frit into a clean RBF with acetone; the solvent was removed under reduced pressure. CH_2Cl_2 (15 mL) was added and the mixture sonicated for 5 min; a dark purple precipitate was filtered off and washed with copious amounts of CH_2Cl_2 to yield a dark purple-blue powder (**66**) which was dried *in vacuo* (0.0316 g, 25 %). Anal. calc. for $\text{C}_{27}\text{H}_{28}\text{N}_8\text{O}_{13}\text{SF}_{13}\text{Ru}\cdot 4\text{H}_2\text{O}$: C, 28.83; H, 3.23; N, 9.96; found: C, 28.70; H, 2.93; N, 10.14. LR-MS [+LSIMS]: 379, 273; [-LSIMS] 785, 677, 571, 321, 299 ($\text{Ru}(\text{acac})_2$), 149 (CF_3SO_3^-). UV-Vis (MeOH): 212, 304, 544, 718. ^1H NMR (300 MHz, d_6 -acetone): δ 8.35 (br s, Im-*H*), 7.60 (br s, Im-*H*), 5.40 (s, $-\text{CH}_2\text{-CO}$), 4.15 (br m, $-\text{CH}_2\text{-CF}_2-$); peaks corresponding to the coordinated acac ligands are not seen in this

NMR spectrum even with a large sweep width (+60 \rightarrow -80 ppm). $^{19}\text{F}\{^1\text{H}\}$ NMR (188 MHz, d_6 -acetone): δ -2.00 (s, CF_3SO_3^-), -8.13 (s, $-\text{CF}_3$), -45.23 (s, $-\text{CF}_2-$). Conductivity for **66** (MeOH): $\Lambda_{\text{M}} = 79.2 \text{ ohm}^{-1}\text{mol}^{-1}\text{cm}^2$.

5.2.1.10 $[\text{Ru}(\text{acac})_2(\text{metro})_2][\text{CF}_3\text{SO}_3]$ (**67**)

In a Schlenk tube, metronidazole (0.0645 g, 0.0377 mmol) and **54** (0.100 g, 0.0188 mmol) were dissolved in EtOH (5 mL), yielding a navy blue solution. The mixture was stirred at 70 °C for 10 h when the solution turned red-purple and finally dark orange. TLC analysis (CH_2Cl_2 :MeOH, 20:1) revealed several products with the major one appearing as a dark orange band ($R_f = 0.80$). The solvent was removed and the mixture was purified via preparative TLC (eluted CH_2Cl_2 :MeOH, 20:1) to yield a dark orange solid. Analysis of this product by TLC revealed a second minor band with an R_f value similar to that of the desired product. A second preparative TLC (CH_2Cl_2 :MeOH, 10:1) resulted in separation of the major band which was washed from the silica gel with acetone and the solution then taken to dryness to yield a dark orange powder (0.0275 g, 19 %). Anal. calc. for $\text{C}_{23}\text{H}_{32}\text{N}_6\text{O}_{13}\text{SF}_3\text{Ru} \cdot 5\text{C}_3\text{H}_6\text{O}$: C, 40.17; H, 5.53; N, 7.21; found: C, 40.26; H, 5.19; N, 7.09. (N.B. When this complex was heated under vacuum, decomposition occurred and a satisfactory analysis could not be obtained.) LR-MS [+LSIMS]: 612 ($\text{M}^+ - \text{NO}$), 596 ($\text{M}^+ - \text{NO}_2$), 580 ($\text{M}^+ - \text{NO}_3$), 471 ($\text{M}^+ - \text{metro}$), 441 ($\text{M}^+ - \text{metro} - \text{NO}$), 300 ($\text{M}^+ - 2 \text{ metro}$). UV-Vis (CH_2Cl_2): 234, 284, 362. ^1H NMR (400 MHz, d_6 -acetone): δ 7.13 (br s, Im- Me_2), 2.92 (s, $-\text{OH}$), -0.44 (s, $-\text{CH}_2\text{OH}$), -2.15 (s, Im- CH_2-), -6.10 (s, acac Me), -8.27 (s, acac Me), -17.39 (s, Im- H_4), -30.45 (vbr s, acac- H); all peaks are broad and spectral integrations do not correlate well with the expected proton distributions; assignments were based on trends seen for a similar Ru(III) complex, $\text{RuCl}_3(\text{metro})_3$ (chapter 4, Section 4.2.2.4). $^{19}\text{F}\{^1\text{H}\}$ NMR (188 MHz, d_6 -acetone): δ -1.93 (s, CF_3SO_3^-).

5.2.1.11 Reaction of *cis*- $[\text{Ru}(\text{acac})_2(\text{MeCN})_2][\text{CF}_3\text{SO}_3]$ (**54**) with EtOH

Investigation of this reaction was warranted because of the number of side-products formed in each of the reactions where **54** was used as a precursor in EtOH (Sections 5.2.1.3-11). It is uncertain whether an accompanying *in situ* reduction of Ru(III) occurs or, for example, whether EtOH displaces coordinated MeCN. In a Schlenk tube, a solution of **54** (~ 100 mg) in 5

mL EtOH was refluxed for 48 h under air; the solution became red-purple. TLC analysis revealed several products (~ 10); there was only one major band (burgundy colour, $R_f = 0.70$) which resembled the high R_f band observed in some of the incomplete imidazole displacement reactions. The volume of the reaction mixture was reduced, and the mixture was then loaded onto a silica gel column and eluted ($\text{CH}_2\text{Cl}_2:\text{MeOH}$, 20:1). The separation of the bands was poor due to streaking, but the bands eluted in the following order: pink, yellow, yellow-brown, brown, orange, brown, orange-brown. The major band isolated from the column was orange, suggesting that the burgundy band observed on the TLC plate was composed of more than one species. The combined fractions were taken to dryness to yield an orange solid. ^1H NMR (300 MHz, d_6 -acetone): δ -2.22 (s, $\text{CH}_3\text{CH}_2\text{OH}$), -4.05 (s, $\text{CH}_3\text{CH}_2\text{OH}$), -4.76 (s, $\text{CH}_3\text{CH}_2\text{OH}$), -21.55 (s, acac Me), -24.85 (s, acac Me); the noisy spectrum gave non-meaningful integrations. Of note, the coupling between the protons on the coordinated EtOH is not observed, perhaps due to the effect of the paramagnetic Ru(III).

5.2.1.12 Reaction of *cis*-[Ru(acac)₂(MeCN)₂][CF₃SO₃] (**54**) with H₂O

This reaction was investigated in part to determine the effect that the presence of water might have on the outcome of the previously reported displacement reactions. Also, information on the behaviour of $[\text{Ru}(\text{acac})_2(\text{L})_2]^+$ complexes in aqueous (and biological) systems might be gleaned. **54** (~ 30 mg) was dissolved in 10 mL H₂O in a 25 mL RBF and the dark blue solution was stirred at r.t. for 24 h; TLC analysis of the still blue solution revealed several bands. After another 4 d (or 5 h at 75 °C), when the solution became dark red, UV-Vis analysis revealed that **54** had been completely consumed. In the first product isolation method, the mixture (~ 15 bands) was separated using preparative TLC ($\text{CH}_2\text{Cl}_2:\text{MeOH}$, 25:2). The major orange-red band was scraped from the plate, eluted from the silica gel with acetone, and the resulting solution was taken to dryness. In the second method, the solvent was removed from the initial reaction solution and the resulting residue was washed with Et₂O to give a red solid and a dark red solution. The Et₂O solution was decanted and the red solid was washed with CH_2Cl_2 to yield a bright orange/red precipitate. LR-MS [+LSIMS]: 359 (M^+ for $[\text{Ru}(\text{acac})_2(\text{MeCN})(\text{H}_2\text{O})]^+$), 300 ($M^+ - \text{MeCN} - \text{H}_2\text{O}$). UV-Vis (λ_{max} , nm): 206, 282, 332, 508. IR (ν , cm^{-1}): 3540 (O-H); 3026, 2923, 2851 (C-H); 1733; 1542, 1522 (C=O); 1273, 1172, 1034, 697, 640, 471, 419. ^1H NMR of isolated solid (300 MHz, d_6 -acetone):

δ 30.55 (br s, 3H, MeCN), -17.48 (s, 6H, acac Me), -18.05 (s, 1H, H₂O), -21.60 (s, 6H, acac Me), -25.75 (br d, 2H, HOD?), -53.30 (br s, 2H, acac H). *In situ* reaction of **54** in D₂O after 7 d at 80 °C: ¹H NMR (300 MHz, D₂O): -17.00 (s, acac Me), -20.75 (s, acac Me); ²H NMR (46 MHz, D₂O): -29.16 (br s, coordinated D₂O).

5.2.2 Ruthenium(II) 1,1,1,5,5,5-Hexafluoroacetylacetonate Complexes

5.2.2.1 [Na][Ru(hfac)₃] (**68**) and [Ru(hfac)(EtOH)₄][hfac] (**69**)

The synthesis of the potassium salt of Ru(hfac)₃⁻ was previously reported.⁹ Here a new synthetic route to the analogous sodium salt is reported. In a Schlenk tube, a solution of RuCl₃·3H₂O (4.015 g, 0.0162 mol) in 30 mL EtOH was stirred at 75 °C for 4 h under a steady stream of H₂. NaHCO₃ (4.615 g, 0.0549 mol) was added slowly to the resulting "Ru blue" solution, followed by addition of Hhfac (7.76 mL, 0.0549 mol). The reaction vessel was sealed under 1 atm N₂ and the mixture then stirred for 16 h at r.t. The final solution was purple-pink, and TLC analysis revealed one major product (pink band, **68**) and a minor product (green band, **69**). The solvent was removed, the mixture was then loaded onto a silica gel column (~ 150 mL silica) and eluted dropwise (CH₂Cl₂:MeOH, 20:1). The first minor, orange band was followed by the major purple-pink band. Because the pink band and a subsequent green band had similar R_f values, small fractions were collected. The appropriate fractions for the pink and for the green band were combined and taken to dryness, yielding purple-black (~ 8 g) and green-black solids (0.350 g), respectively. The purple-black solid was further purified via vacuum sublimation at 100 °C to give pure **68** (7.576 g, 65 %). Anal. calc. for C₁₅H₃O₆F₁₈RuNa: C, 24.18; H, 0.41; found: C, 24.07; H, 0.50. IR (ν, cm⁻¹) 1555 (C=O); 1526, 1447, 1333, 1265, 1221, 1150, 820, 698, 606. UV-Vis (MeOH): 210 (8.01), 236 (8.89), 290 (17.4), 490 (11.6), 528 (13.9). ¹H NMR (200 MHz, d₆-acetone): δ 6.19 (s, hfac-H). ¹⁹F{¹H} NMR (188 MHz, d₆-acetone): δ 2.18 (s, -CF₃). The spectroscopic data are in agreement with those reported in the literature.⁹

The purity of the green solid was checked by TLC, revealing a small amount of **68** present. The green solid was dissolved in acetone and then loaded onto a preparative TLC plate and eluted (CH₂Cl₂:MeOH, 15:1). The major green band was scraped from the plate and the complex was then washed from the silica gel with acetone. The washings were taken to dryness to

yield a green-black, powdered solid (0.223 g). The pure solid in d_6 -acetone revealed two signals in the ^1H NMR spectrum corresponding to two inequivalent hfac ligands which when combined with the MS data led to its formulation as $[\text{Ru}(\text{hfac})(\text{EtOH})_4][\text{hfac}]$. UV-Vis (MeOH): 232, 298, 384, 452, 748. LR-MS [+LSIMS]: 493 (M^+), 401 ($\text{M}^+ - 2\text{EtOH}$). HR-MS [+LSIMS] for $\text{C}_{13}\text{H}_{25}\text{O}_6\text{F}_6\text{Ru}$: 493.05988; found 493.05887. ^1H NMR (200 MHz, d_6 -acetone): δ 6.54 (s, 1H, hfac- $H_{(\text{coord.})}$), 6.46 (s, 2H, hfac- $H_{(\text{anion})}$), 3.61 (q, 8H, $-\text{CH}_2\text{-OH}$), 3.31 (s, 3H, $-\text{OH}$), 1.18 (t, 12H, CH_3 -). $^{19}\text{F}\{^1\text{H}\}$ NMR (188 MHz, d_6 -acetone): δ 2.66 (s, $-\text{CF}_3(\text{anion})$), 2.58 (s, $-\text{CF}_3(\text{coord.})$). A suitable elemental analysis for this complex could not be obtained presumably because of the labile EtOH ligands. Conductivity for **69** (MeOH): $\Lambda_{\text{M}} \sim 157 \text{ ohm}^{-1}\text{mol}^{-1}\text{cm}^2$.

5.2.2.2 $\text{Ru}(\text{hfac})_3$ (**70**)

This complex was synthesized according to a modified literature procedure.⁹ In a 250 mL RBF, **68** (1.05 g, 1.41 mmol) was suspended in an H_2O :benzene (200 mL, 1:1) to give a red-brown biphasic system. H_2O_2 (1 % aqueous) was added dropwise (total volume ~ 5 mL) with continuous stirring at r.t. for 2 h; the resulting aqueous phase was opaque, yellow-brown, while the organic layer was a deep red solution. The aqueous phase was separated and washed with benzene (2 x 40 mL). The organic washings were then transferred to a RBF and the benzene removed at r.t. under reduced pressure, to ensure that **70** did not sublime prematurely. The RBF was then fitted with a sublimation cold finger with a vacuum adapter, and the residue was heated to 60 °C. **70** sublimed as shiny, prismatic red crystals (0.776 g, 76 %). Anal. calc. for $\text{C}_{15}\text{H}_3\text{O}_6\text{F}_{18}\text{Ru}$: C, 24.95; H, 0.42; found: C, 25.07; H, 0.60. IR (ν , cm^{-1}): 1582 (C=O); 1539, 1421, 1348, 1266, 1210, 1149, 822, 698, 601. UV-Vis (MeOH): 216 (12.5), 274 (14.5), 376 (6.65), 524 (1.87). ^1H NMR (300 MHz, CDCl_3): δ -41.67 (s, hfac- H). $^{19}\text{F}\{^1\text{H}\}$ NMR (188 MHz, CDCl_3): δ -11.49 (s, $-\text{CF}_3$); not previously reported. The other spectroscopic data agree with those previously reported in the literature.⁹

5.2.2.3 *cis*- $\text{Ru}(\text{hfac})_2(\text{MeCN})_2$ (**71**)

In a 250 mL RBF, **68** (4.00 g, 5.54 mmol) was dissolved in 150 mL MeCN giving a purple-pink solution. The mixture, heated slowly during dropwise addition of $\text{CF}_3\text{SO}_3\text{H}$ (0.865 mL, 6.09 mmol), quickly turned red-brown, this being accompanied by much fuming. The RBF

was next fitted with a reflux condenser, and the solution was refluxed for 1 h in air during which the colour turned dark brown. TLC analysis revealed a number of side-products and a concentrated brown band ($R_f = 0.90$; $\text{CH}_2\text{Cl}_2\text{:MeOH}$, 50:1). The solvent was removed and the residue was dissolved in acetone (~ 50 mL); to this was added 25 mL of silica gel, and the resulting brown slurry was dried *in vacuo* overnight. (N.B. Silica gel is very fine and its evacuation into the vacuum line during the drying process can be prevented by the use of a Kim-Wipe® plug.) The dried silica gel-adsorbed complex mixture was then introduced onto a silica gel column filled with CH_2Cl_2 , and the column was eluted dropwise using CH_2Cl_2 . A bright red band of unreacted **68** eluted first, followed by a dark brown band which, following removal of solvent, yielded **71** as a shiny, brown solid (2.709 g, 95 %). Suitable crystals for X-ray analysis were obtained from slow evaporation of a concentrated MeOH solution of **71**. Anal. calc. for $\text{C}_{14}\text{H}_8\text{N}_2\text{O}_4\text{F}_{12}\text{Ru}$: C, 28.15; H, 1.35; N, 4.69; found: C, 28.35; H, 1.33; N, 4.62. LR-MS [+LSIMS]: 598 (M^+), 516 ($\text{M}^+ - 2\text{MeCN}$). IR (ν , cm^{-1}): 2357 ($\text{C}\equiv\text{N}_{\text{asym.}}$); 2285 ($\text{C}\equiv\text{N}_{\text{sym.}}$); 1576, 1546 ($\text{C}=\text{O}$); 1482, 1475, 1335, 1262, 1212, 1195, 1153, 1095, 798, 696. UV-Vis (MeOH): 218 (17.1), 286 (16.8), 418 (6.10), 470 (8.43). ^1H NMR (200 MHz, d_6 -acetone): δ 6.20 (s, 2H, *hfac-H*), 2.87 (s, 6H, *MeCN*). $^{19}\text{F}\{^1\text{H}\}$ NMR (188 MHz, d_6 -acetone): δ 0.98 (s, $-\text{CF}_3$), 0.38 (s, $-\text{CF}_3$).

Of note, **71** could also be synthesized from **70** in relatively high yield (75 %) using conditions identical to those above reported for the synthesis of **71** from **68**.

5.2.2.4 *cis*-Ru(*hfac*)₂(Im)₂ (**72**)

A solution of Im (0.162 g, 0.237 mmol) and **71** (0.190 g, 0.0317 mmol) in 10 mL EtOH was stirred under air at 75 °C in a Schlenk tube. After 6 h two products were apparent in the orange-brown solution by TLC. The colour became reddish-brown after 12 h; the reaction was stopped after 24 h when TLC analysis indicated complete consumption of **71**. The solvent was removed and the residue (dissolved in CH_2Cl_2) was loaded onto a silica gel column ($\text{CH}_2\text{Cl}_2\text{:MeOH}$, 25:1) and eluted dropwise; the first minor (brown) band yielded a red-brown solid (~ 10 mg) and was followed (after a minor pink band) by a major, red band. The red band was collected and the solvent was removed from the combined fractions to yield a bright red solid (0.0765 g, 37 %). Analytical data revealed that the red solid was the bis-imidazole complex (**72**), and that the red-brown solid was the mono-substituted complex *cis*-Ru(*hfac*)₂(Im)(MeCN) (**73**).

Data for **72**: Anal. calc. for $C_{16}H_{10}N_4O_4F_{12}Ru$: C, 29.51; H, 1.55; N, 8.60; found: C, 29.80; H, 1.48; N, 8.54. LR-MS [+LSIMS]: 652 (M^+), 584 ($M^+ - Im$), 516 ($M^+ - 2 Im$), 445 ($M^+ - hfac$). UV-Vis (MeOH): 212 (14.5), 244 (13.7), 288 (16.4), 452 (7.30), 542 (14.1). 1H NMR (200 MHz, d_6 -acetone): δ 11.92 (br s, 2H, Im- H_1), 7.67 (q, 2H, Im- H_2), 7.32 (p, 2H, Im- H_5), 6.85 (q, 2H, Im- H_4), 6.10 (s, 2H, hfacH). $^{19}F\{^1H\}$ NMR (188 MHz, d_6 -acetone): δ 1.80 (s, $-CF_3$), 1.78 (s, $-CF_3$).

Data for **73**: Anal. calc. for $C_{15}H_9N_3O_4F_{12}Ru$: C, 28.86; H, 1.45; N, 6.73; found: C, 28.65; H, 1.47; N, 6.46. LR-MS [+LSIMS]: 625 (M^+), 584 ($M^+ - MeCN$), 516 ($M^+ - MeCN - Im$), 418 ($M^+ - hfac$), 377 ($M^+ - hfac - MeCN$). UV-Vis (MeOH): 212 (5.39), 288 (4.28), 434 (1.74), 504 (2.76). 1H NMR (200 MHz, d_6 -acetone): δ 11.88 (br s, 1H, Im- H_1), 7.70 (d, 1H, Im- H_2), 7.32 (p, 1H, Im- H_5), 6.93 (q, 1H, Im- H_4), 6.12 (s, 1H, hfac-H), 6.07 (s, 1H, hfac-H), 2.70 (s, 3H, MeCN). $^{19}F\{^1H\}$ NMR (188 MHz, d_6 -acetone): δ 2.04, 1.95, 1.88, 1.60 (all peaks are singlets corresponding to magnetically inequivalent $-CF_3$ signals).

5.2.2.5 *cis*-Ru(hfac)₂(NMeIm)₂ (**74**)

In a Schlenk tube, a solution of NMeIm (100 μ L, 0.125 mmol) and **71** (0.167 g, 0.0280 mmol) in 10 mL EtOH was stirred under air at 75 °C for 24 h to give a brilliant purple colour. The solvent was removed, the residue loaded onto a silica gel column and eluted dropwise (CH_2Cl_2 :hexanes, 1:1). A bright pink band (possibly the the mono-substituted complex) preceded a purple band which was collected in a number of fractions. The fractions were combined and the solvent was removed to yield a dark purple solid (0.136 g, 72 %). Anal. calc. for $C_{18}H_{14}N_4O_4F_{12}Ru$: C, 31.82; H, 2.08; N, 8.25; found: C, 31.96; H, 1.98; N, 7.97. LR-MS [+LSIMS]: 680 (M^+), 598 ($M^+ - NMeIm$), 516 ($M^+ - 2NMeIm$), 473 ($M^+ - hfac$), 391 ($M^+ - NMeIm - hfac$). UV-Vis (MeOH): 214 (16.9), 244 (13.0), 288 (17.6), 450 (7.28), 542 (13.6). 1H NMR (200 MHz, d_6 -acetone): δ 7.54 (br t, 2H, Im- H_2), 7.20 (t, 2H, Im- H_5), 6.73 (t, 2H, Im- H_4), 6.02 (s, 2H, hfac-H), 3.83 (s, 6H, Im- Me_1). $^{19}F\{^1H\}$ NMR (188 MHz, d_6 -acetone): δ 1.92 (s, $-CF_3$), 1.82 (s, $-CF_3$).

5.2.2.6 [Ru(hfac)(NMeIm)₄][PF₆] (76)

In a Schlenk tube, **71** (0.143 g, 0.0240 mmol) was dissolved in neat NMeIm (~ 5 mL) and the solution stirred under air at 100 °C for 24 h; the mixture became a brilliant pink-purple colour. Because of the high b.p. of NMeIm (198 °C) the solution volume was reduced slowly (to ~ 2 mL) at high temperature under vacuum. The bright purple solution was then loaded onto a preparative TLC plate and eluted (CH₂Cl₂:MeOH, 10:1). The isolated band, after elution from the silica gel with acetone and then removal of solvent, yielded a purple gum. Some of the unreacted NMeIm was not removed in the first purification step, and so the purple gum was dissolved in a minimal volume of CH₂Cl₂ and then hexanes was added. A red-purple solid, believed to be impure [Ru(hfac)(NMeIm)₄][hfac] (**75**) was isolated via filtration and dried *in vacuo* (0.0622 g, 50%). Anal. calc. for C₂₆H₂₆N₈O₄F₁₂Ru: C, 37.02; H, 3.11; N, 13.28; found: C, 32.11; H, 1.96; N, 7.88. IR [KBr, ν (cm⁻¹): 3142, 2967, 2931 (C-H); 1674 (C=O_{free} hfac); 1533 (C=O_{coord.} hfac); 1328, 1258, 1200, 1148, 791, 663. ¹H NMR (200 MHz, d₆-acetone): δ 7.64 (s, 2H, Im-H₂), 7.49 (s, 2H, Im-H_{2'}), 7.27 (s, 2H, Im-H₅), 7.26 (s, 2H, Im-H_{5'}), 6.85 (s, 2H, Im-H₄), 6.70 (s, 2H, Im-H_{4'}), 6.07 (s, 1H, coord. hfac-H), 5.60 (s, 3H, free hfac-H), 3.83 (s, 6H, Im-Me₁), 3.82 (s, 6H, Im-Me_{1'}). ¹⁹F{¹H} NMR (188 MHz, d₆-acetone): δ 2.26 (s, -CF₃ coord. hfac), -0.89 (s, -CF₃ free hfac). The unsatisfactory analysis and the NMR results imply that free hfac anion is present in a > 1:1 ratio with the complex cation. Further attempts to purify this sample were unsuccessful, and so a different counter anion was introduced.

All of complex **75** (0.0622 g) was dissolved in 5 mL acetone to give a bright purple solution. NH₄PF₆ (large excess) was then added and the solution was stirred in air for 16 h at r.t., when the colour became bright pink. TLC analysis revealed two minor products and one major product; the major pink band (**76**), with a higher R_f than **75**, was isolated via preparative TLC as a dark pink solid (0.0831 g, 44 % from **71**). Anal. calc. for C₂₆H₂₆N₈O₄F₁₂Ru: C, 32.28; H, 3.22; N, 14.34; found: C, 32.55; H, 3.15; N, 14.16. LR-MS [+LSIMS]: 637 (M⁺), 555 (M⁺ - NMeIm), 473 (M⁺ - 2NMeIm), 391 (M⁺ - 3NMeIm). IR (ν , cm⁻¹): 3139, 2910, 2814, 2754 (C-H); 1535 (C=O); 1323, 1261, 1192, 1140, 1095, 841, 557. UV-Vis (MeOH): 214 (17.1), 252 (8.63), 284 (9.36), 532 (5.92). ¹H NMR (200 MHz, d₆-acetone): δ 7.62 (s, 2H, Im-H₂), 7.48 (s, 2H, Im-H_{2'}), 7.26 (s, 2H, Im-H₅), 7.25 (s, 2H, Im-H_{5'}), 6.86 (s, 2H, Im-H₄), 6.70 (s, 2H, Im-H_{4'}), 6.03 (s, 1H, hfac-H),

3.83 (s, 6H, Im-Me₁), 3.82 (s, 6H, Im-Me₁). ¹⁹F{¹H} NMR (188 MHz, d₆-acetone): δ 2.90 (d, ¹J_{PF} = 353 Hz, PF₆⁻), 0.12 (s, -CF₃). Conductivity for **76** (MeOH): Λ_M = 104.7 ohm⁻¹mol⁻¹cm².

5.2.2.7 *cis*-Ru(hfac)₂(2MeIm)₂ (**77**)

This synthesis was done to ascertain if the *trans* geometry would predominate with the more sterically demanding 2MeIm ligand. In a Schlenk tube, a brown solution of **71** (0.0976 g, 0.0163 mmol) and 2MeIm (0.0674 g, 0.0821 mmol) in 5 mL EtOH was stirred for 24 h under air at 75 °C. TLC analysis revealed 3 well separated products (CH₂Cl₂:hexanes, 1:1). The solvent was removed and the products were isolated separately using column chromatography (silica gel, CH₂Cl₂:hexanes, 1:1 → 2:1): the first (red) band yielded a dark red solid (0.0150 g) formulated as *cis*-Ru(hfac)₂(2MeIm)₂ (**77**); the second, minor (brown) band yielded a dark brown solid (0.0065 g), formulated as *cis*-Ru(hfac)₂(2MeIm)(MeCN) (**78**); and the third band (eluted with a higher % CH₂Cl₂) was isolated as a dark red solid (0.0760 g) formulated as *trans*-Ru(hfac)₂(2MeIm)₂ (**79**). The total yield of bis-substituted products as the two geometrical isomers, **77** + **79** was 0.0910 g, 82 %.

Data for **77**: Anal. calc. for C₁₈H₁₄N₄O₄F₁₂Ru: C, 31.82; H, 2.08; N, 8.25; found: C, 32.17; H, 2.03; N, 8.01. LR-MS [+LSIMS]: 680 (M⁺), 598 (M⁺ - 2MeIm), 516 (M⁺ - 2(2MeIm)), 473 (M⁺ - hfac), 391 (M⁺ - 2MeIm - hfac). IR (ν, cm⁻¹): 3336 (N-H); 3142 (C-H); 1540 (C=O); 1476, 1323, 1263, 1212, 1147, 801, 740, 693. UV-Vis (MeOH): 212 (15.1), 244 (10.9), 288 (14.3), 446 (6.01), 542 (13.2). ¹H NMR (200 MHz, d₆-acetone): δ 11.47 (br s, 1H, Im-H₁), 7.51 (s, 1H, Im-H₁), 7.23 (t, 1H, Im-H₅), 7.09 (s, 1H, Im-H₅), 6.73 (s, 1H, Im-H₄), 6.45 (s, 1H, Im-H₄), 5.98/5.99 (two overlapping s, 2H, hfac-H), 3.92 (s, 3H, Im-Me₂), 2.28 (s, 3H, Im-Me₂). ¹⁹F{¹H} NMR (188 MHz, d₆-acetone): δ 1.84, 1.79, 1.75, 1.65 (s, inequiv. -CF₃ groups on hfac).

Data for **78**: LR-MS [+LSIMS]: 639 (M⁺), 598 (M⁺ - MeCN), 516 (M⁺ - 2MeIm - MeCN), 432 (M⁺ - hfac), 391 (M⁺ - MeCN - hfac). ¹H NMR (200 MHz, d₆-acetone): δ 11.65 (br s, 1H, Im-H₁), 7.18 (q, 1H, Im-H₅), 6.66 (s, 1H, Im-H₄), 6.14 (s, 1H, hfac-H), 6.04 (s, 1H, hfac-H), 2.75 (s, 3H, MeCN), 2.51 (s, 3H, Im-Me₂). ¹⁹F{¹H} NMR (188 MHz, d₆-acetone): δ 2.03, 2.00, 1.81, 1.62 (s, inequiv. -CF₃ groups on hfac).

Data for **79**: Anal. calc. for C₁₈H₁₄N₄O₄F₁₂Ru: C, 31.82; H, 2.08; N, 8.25; found: C, 32.05; H, 2.04; N, 8.17. LR-MS [+LSIMS]: 680 (M⁺), 598 (M⁺ - 2MeIm), 516 (M⁺ - 2(2MeIm)),

473 ($M^+ - \text{hfac}$), 391 ($M^+ - 2\text{MeIm} - \text{hfac}$). IR (ν , cm^{-1}): 3299 (N-H); 3138 (C-H); 1574 (C=O); 1545, 1464, 1323, 1261, 1204, 1147, 806, 739, 693. UV-Vis (MeOH): 212 (15.3), 244 (11.4), 288 (13.6), 446 (6.64), 542 (14.1). ^1H NMR (200 MHz, d_6 -acetone): δ 11.43 (br s, 2H, Im- H_1), 7.10 (t, 2H, Im- H_5), 6.51 (s, 2H, Im- H_4), 5.98 (s, 2H, hfac- H), 2.17 (s, 6H, Im- Me_2). $^{19}\text{F}\{^1\text{H}\}$ NMR (188 MHz, d_6 -acetone): δ 1.79, 1.66 (s, inequiv. $-\text{CF}_3$ groups on hfac).

5.2.2.8 *cis*-Ru(hfac)₂(4MeIm)(5MeIm) (**80**)

In a Schlenk tube under air, a brown solution of **71** (0.116 g, 0.0195 mmol) and 4(5)MeIm (0.0868 g, 0.106 mmol) in 7 mL EtOH was stirred for 24 h at 75 °C. Analysis by TLC after ~ 2 h revealed partial formation of two products while after 20 h only one band was observed. The solvent was removed and the resulting residue was purified by flash chromatography on a silica gel column (CH_2Cl_2 :MeOH, 20:1) to yield a red-purple solid (0.112 g, 85 %). Anal. calc. for $\text{C}_{18}\text{H}_{14}\text{N}_4\text{O}_4\text{F}_{12}\text{Ru}$: C, 31.82; H, 2.08; N, 8.25; found: C, 32.06; H, 2.15; N, 8.04. LR-MS [$+\text{LSIMS}$]: 680 (M^+), 598 ($M^+ - 4(5)\text{MeIm}$), 516 ($M^+ - 2(4(5)\text{MeIm})$), 473 ($M^+ - \text{hfac}$), 391 ($M^+ - 4(5)\text{MeIm} - \text{hfac}$). UV-Vis (MeOH): 214 (15.5), 246 (10.6), 286 (13.6), 448 (6.27), 542 (12.8). The elemental analysis and MS data suggest that the isolated solid is a single species; however, the NMR data suggest that the solid is a mixture of **80** and *trans*-Ru(hfac)₂(4MeIm)(5MeIm) (**81**). ^1H NMR (300 MHz, d_6 -acetone): δ (**80**) 11.68 (br s, 2H, Im- H_1), 7.48/7.35 (s, 2H, Im- H_2), 7.07 (s, 1H, Im- H_5), 6.58 (s, 1H, Im- H_4), 6.04/6.02 (overlapping s, 2H, hfac- H), 2.28 (s, 3H, Im- Me_4), 1.88 (s, 3H, Im- Me_5); (**81**) 11.61 (br s, 2H, Im- H_1), 7.46/7.31 (s, 2H, Im- H_2), 7.02 (s, 1H, Im- H_5), 6.56 (s, 1H, Im- H_4), 6.02 (s, 2H, hfac- H), 2.25 (s, 3H, Im- Me_4), 1.86 (s, 3H, Im- Me_5). $^{19}\text{F}\{^1\text{H}\}$ NMR (188 MHz, d_6 -acetone): δ (**80**) 1.81, 1.76, 1.73, 1.64 (s, inequiv. $-\text{CF}_3$ groups on hfac); (**81**) 1.79, 1.56 (s, $-\text{CF}_3$).

5.2.2.9 Ru(hfac)₂(2NO₂Im)₂ (**82**)

In a Schlenk tube, 2NO₂Im (0.0336 g, 0.0297 mmol) was dissolved in EtOH at 70 °C, followed by the addition of **71** (0.0863 g, 0.0144 mmol) to give an orange-brown solution. The mixture was stirred at reflux in air for 24 h during which the solution became dark purple-blue. The solvent was removed and CH_2Cl_2 (~ 25 mL) was then added; the dark blue solid was sonicated from the walls of the tube and isolated via filtration. The solid was washed with CH_2Cl_2 until the

filtrate became clear; however, TLC analysis revealed the presence of unreacted 2NO₂Im. The residue was washed with hot ddH₂O (4 x 15 mL), followed by CH₂Cl₂ (2 x 10 mL) which yielded a pale brown filtrate; alternate washes with H₂O and CH₂Cl₂ were continued until the CH₂Cl₂ washings were no longer brown and the H₂O washings contained no free 2NO₂Im. The final blue-black solid was dried *in vacuo* at 80 °C for 5 d (0.0367 g, 34 %). Anal. calc. for C₁₆H₈N₆O₈F₁₂Ru•2NO₂Im: C, 26.71; H, 1.30; N, 14.16; found: C, 26.82; H, 1.48; N, 13.94. LR-MS [\pm LSIMS]: no signals observed in either spectrum. ¹H NMR (200 MHz, d₆-acetone): δ 13.21 (br s, Im-H₁), 7.47 & 7.31 (broad overlapping singlets, Im-H_{4&5}), 6.21 (br s, hfac-H). ¹⁹F{¹H} NMR (188 MHz, d₆-acetone): δ 2.10, -0.55 (s, inequiv. -CF₃ groups on hfac). [N.B. This synthesis was done on three separate occasions and each time the resulting product showed no free 2NO₂Im by TLC analysis, but one mole of 2NO₂Im was present for each elemental analysis performed. The integrations in the ¹H NMR spectrum may support the presence of three 2NO₂Im molecules, but do not discern the difference between coordinated and free 2NO₂Im as the free signal (δ 7.40 for ImH_{4/5}) would overlap with those observed for the isolated solid.]

5.2.2.10 Ru(hfac)₂(EF5)₂ (83)

In a Schlenk tube, a solution of **71** (0.0495 g, 0.00829 mmol) and **EF5** (0.0492 g, 0.0163 mmol) in 5 mL acetone was stirred at 60 °C for 50 h in air. By TLC analysis, the black-brown solution contained trace **71** and **EF5**. The solvent was removed, the residue suspended in 5 mL EtOH and the suspension stirred at 75 °C for an additional 18 h, yielding a red-purple solution. This was taken to dryness, CH₂Cl₂ (~ 20 mL) then added and the tube sonicated for 5 min to yield a burgundy solution and a dark blue precipitate, which was isolated. The solid was washed with warm CH₂Cl₂ (8 x 5 mL), until the washings became clear, and the solid was then dried *in vacuo* for 48 h (0.0123 g, 13 %). Anal. calc. for C₂₆H₁₆N₈O₁₀F₂₂Ru•3MeCN: C, 30.93; H, 2.03; N, 12.40; found: C, 31.18; H, 2.38; N, 12.05. LR-MS [\pm LSIMS]: 1208, 1167, 1125, 1085 and 977, 938, 897, 853 (each of these peak sets suggests the presence of 3 MeCN molecules associated with the isolated complex; however, the expected M⁺ peak at 1119 is not observed). ¹H NMR (200 MHz, d₆-acetone): δ 8.25 (br s, Im-H_{4&5}), 6.20 (br s, hfac-H), 5.30 (br s, Im-CH₂-), 4.15 (br m, -CH₂-CF₂-); all peaks are extremely broad and the spectrum is quite noisy. ¹⁹F{¹H} NMR (188 MHz, d₆-acetone): δ 1.73 (s, -CF₃ of hfac), -8.13 (s, -CF₃), -45.17 (s, -CF₂-).

5.2.2.11 Attempted Synthesis of Ru(hfac)₂(SR2508)₂ (84)

In a Schlenk tube, a solution of **71** (0.0645 g, 0.0108 mmol) and **SR2508** (0.0472 g, 0.0220 mmol) in 5 mL EtOH was stirred at 75 °C for 20 h in air. The resulting red-purple solution was taken to dryness. CH₂Cl₂ (~ 20 mL) was added to the residue and then the mixture was sonicated for 5 min to give a burgundy solution and a dark purple precipitate. The precipitate was collected and then washed with warm CH₂Cl₂ (10 x 5 mL) until the washings became clear. The purity of the solid was tested using TLC which revealed the presence of two pink bands, in addition to the purple product; all unreacted **SR2508** had been removed. The solid was then washed with Et₂O until the pink colour was no longer present in the filtrate. Again TLC showed that only one of the pink bands had been removed. The purple solid was then washed with cold acetone (3 x 5 mL), leaving only a dark blue-purple precipitate in the frit which was a single species by TLC (0.0281 g, 27 %). Anal. calc. for C₂₄H₂₂N₈O₁₂F₁₂Ru: C, 30.55; H, 2.35; N, 11.88; found: C, 35.82; H, 4.03; N, 17.64. LR-MS [+LSIMS]: 902, 761, 718, 677; peaks did not match the proposed formulation of the complex. This synthesis was repeated, but the same analysis and MS results were obtained.

5.2.3 Ruthenium(II) and (III) acac/hfac Complexes

5.2.3.1 Ru(acac)₂(hfac) (85)

In a Schlenk tube, **54** (2.45 g, 4.61 mmol) was dissolved in 30 mL EtOH. NaHCO₃ (0.433 g, 5.16 mmol) and Hhfac (725 µL, 5.12 mmol) were then added to the flask and the reaction mixture was heated to reflux under air (~80 °C). After 10 min, the mixture, originally navy blue, became brown and continued to change through pink to dark red after 1.5 h. The solvent was removed and the residue was loaded onto a silica gel column and eluted quickly (CH₂Cl₂:MeOH, 25:1) (by flash chromatography) to remove any low R_f side-products. The first band (dark red) yielded a solid which was dissolved in acetone and the solution transferred to a sublimation flask equipped with a cold finger and heated to 100 °C under vacuum; the dark red product, which sublimed onto the cold finger, was transferred to a sample vial and dried *in vacuo* at r.t. (1.75 g, 75 %). [N.B. **85** is hygroscopic and must be transferred quickly when handling in air. Because **85** sublimates at ~ 60 °C under vacuum, the removal of acetone solvate, prior to elemental analysis, was

not possible.] Anal. calc. for $C_{15}H_{15}O_6F_6Ru \cdot 0.5C_3H_6O$: C, 37.02; H, 3.39; found: C, 37.02; H, 3.26. UV-Vis (MeOH): 210 (13.4), 284 (13.6), 332 (6.43), 502 (2.38). 1H NMR (300 MHz, d_6 -acetone): δ -8.82 (s, 6H, acac *Me*), -9.01 (s, 6H, acac *Me*), -28.45 (s, 1H, hfac-*H*), -38.95 (s, 2H, acac-*H*). $^{19}F\{^1H\}$ NMR (188 MHz, d_6 -acetone): δ -9.71 (s, $-CF_3$).

5.2.3.2 [Na][Ru(hfac)₂(acac)] (86)

In a Schlenk tube, **71** (0.300 g, 0.502 mmol) was dissolved in 10 mL EtOH to give a dark brown solution. $NaHCO_3$ (0.0534 g, 0.636 mmol) and Hacac (60 μ L, 0.584 mmol) were added and the mixture was heated to reflux ($\sim 80^\circ C$) in air. The reaction was monitored using TLC as no colour change was observed; the concentration of **71** decreased while a new pink band appeared after ~ 2 h. After 7 h the solvent was removed under reduced pressure, and then CH_2Cl_2 (20 mL) was added. The mixture was sonicated for 5 min, yielding a dark purple solid, which was collected and washed with CH_2Cl_2 (3 x 10 mL); several minor bands were detected in the isolated solid by TLC. The solid was dissolved in acetone, loaded onto a silica gel column and eluted (CH_2Cl_2 :acetone, 20:1). A yellow-green band eluted first, followed by an orange-pink band. The eluent strength was increased to 20 % acetone which resulted in a pink band separating from the dark blue band which moved down the column very slowly. The eluent strength was again increased to 35 % acetone which eluted the dark blue band. The solvent was removed to yield a pink-purple solid (0.0986 g, 32 %). Anal. calc. for $C_{15}H_9O_6F_{12}Ru$: C, 28.27; H, 1.42; found: C, 28.06; H, 1.38. IR (ν , cm^{-1}): 1550, 1521 (C=O); 1466, 1391, 1323, 1264, 1198, 1146, 940, 808, 695. UV-Vis (MeOH): 210 (8.06), 248sh (11.1), 278 (18.2), 380 (2.01), 478 (7.59). 1H NMR (200 MHz, d_6 -acetone): δ 5.77 (s, 2H, hfac-*H*), 5.00 (s, 1H, acac-*H*), 1.86 (s, 6H, acac *Me*). $^{19}F\{^1H\}$ NMR (188 MHz, d_6 -acetone): δ 2.50 (s, $-CF_3$), 2.48 (s, $-CF_3$).

5.2.3.3 Ru(hfac)₂(acac) (87)

In a 100 mL RBF, **86** (0.0550 g, 0.0863 mmol) was suspended in an H_2O (20 mL): benzene (20 mL) mixture to give a dark purple biphasic system. This was stirred at r.t. in air, and H_2O_2 (1 % aqueous, 5 mL) was added dropwise, the mixture becoming green. The aqueous phase was pale yellow while the organic layer was dark green. After 1 h the organic phase was transferred to a RBF and the benzene removed via rotary evaporation at $20^\circ C$. The RBF was

equipped with a sublimation cold finger (with vacuum adapter) and heated to 60 °C; **87** sublimed onto the cold finger as a green-black solid (0.0423 g, 80 %). Anal. calc. for $C_{15}H_9O_6F_{12}Ru$: C, 29.33; H, 1.48; found: C, 28.99; H, 1.49. IR (ν , cm^{-1}): 1583, 1579 (C=O); 1553, 1520, 1436, 1344, 1264, 1207, 1152, 807, 699, 598. UV-Vis (MeOH): 248sh (11.1), 286 (19.2), 376 (8.25), 556 (1.67). 1H NMR (300 MHz, $CDCl_3$): δ -14.34 (s, 6H, acac Me), -31.82 (s, 1H, acac-H), -56.72 (s, 2H, hfac-H). $^{19}F\{^1H\}$ NMR (188 MHz, $CDCl_3$): δ -6.71 (s, $-CF_3$), -8.06 (s, $-CF_3$).

5.2.3.4 *cis*-Ru(acac)(hfac)(MeCN)₂ (**88**)

In a 25 mL RBF, **85** (0.159 g, 0.313 mmol) was dissolved in 10 mL MeCN and the mixture heated in air to 70 °C yielding a red solution to which CF_3SO_3H (44 μ L, 0.313 mmol) was then added.

Eluent (CH_2Cl_2 :MeOH, 20:1)

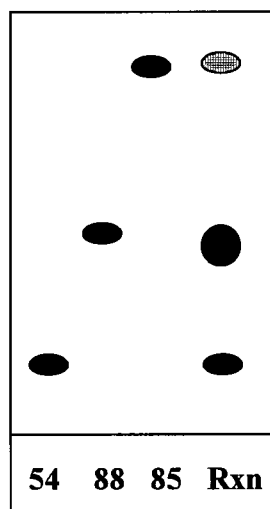


Figure 5-1: TLC analysis for the synthesis of **88** from **85**.

TLC analysis after 2 h (Figure 5-1) revealed that acac⁻ and hfac⁻ displaced products (**88**) and (**54**), respectively, were formed in equal amounts. The mixture was then purified using preparative TLC (CH_2Cl_2 :MeOH, 20:1); the band corresponding to **88** yielded a red-brown solid (0.0746 g, 49 %). Crystals suitable for X-ray analysis were obtained via slow evaporation of a concentrated MeOH solution of **88**. Anal. calc. for $C_{14}H_{14}N_2O_4F_6Ru$: C, 34.46; H, 2.88; N, 5.72; found: C, 34.38; H, 2.88; N, 5.42. IR (ν , cm^{-1}): 2993, 2930 (C-H); 2346 ($C\equiv N_{asym.}$); 2270 ($C\equiv N_{sym.}$); 1567, 1547 (C=O); 1406, 1261, 1200, 1147. UV-Vis (MeOH): 228 (15.8), 276 (14.1), 352 (4.07), 482 (4.67). 1H NMR (200 MHz, d_6 -acetone): δ 6.04 (s, 1H, hfac-H), 5.37 (s, 1H,

acac-*H*), 2.76 (s, 3H, MeCN), 2.69 (s, 3H, MeCN), 1.94 (s, 3H, acac Me), 1.93 (s, 3H, acac Me). $^{19}\text{F}\{^1\text{H}\}$ NMR (188 MHz, d_6 -acetone): δ 2.29 (s, $-\text{CF}_3$), 2.09 (s, $-\text{CF}_3$).

This reaction was repeated using a ratio of 1:40 for **85**: $\text{CF}_3\text{SO}_3\text{H}$ which yielded results different from those described above. The major product here was **54**, while only ~ 10 % of **88** was present, showing that the stoichiometry of the reactants was important in determining the reaction path (see Scheme 5-2, p. 223).

The synthesis of **88** was also attempted starting from either **86** or **87**, following the same reaction conditions as described above; however, only **71** was produced (see Scheme 5-3, p. 224).

5.2.3.5 *cis*-Ru(acac)(hfac)(Im)₂ (**89**)

In a Schlenk tube, **88** (0.0600 g, 0.123 mmol) and Im (0.0418 g, 0.615 mmol) were dissolved in 5 mL EtOH to give a brown solution. The tube was sealed under air and the mixture stirred at 75 °C for 24 h during which the colour changed to deep red. Analysis by TLC showed that all of **88** had reacted; there was a minor pink band, a dark purple band and a brown band ($R_f = 0$), which appeared to be in highest concentration. Purification via preparative TLC (CH_2Cl_2 :MeOH, 25:2) yielded a dark purple solid (**89**) (0.0121 g, 18 %). LR-MS [+LSIMS]: 1019 ($2\text{M}^+ - \text{Im}$), 951 ($2\text{M}^+ - 2\text{Im}$), 544 (M^+), 476 ($\text{M}^+ - \text{Im}$), 408 ($\text{M}^+ - 2\text{Im}$). HR-MS [+LSIMS] for $\text{C}_{16}\text{H}_{16}\text{O}_4\text{N}_4\text{F}_6\text{Ru}$: 544.01129; found 544.01153.

5.2.3.6 *cis*-Ru(acac)(hfac)(NMeIm)₂ (**90**)

In a Schlenk tube, to a solution of **88** (0.0599 g, 0.122 mmol) in 5 mL EtOH was added 12 drops of NMeIm (excess). The brown mixture was heated to 75 °C and the reaction monitored via TLC. After 2 h, a red-purple solution yielded red and purple bands; the solvent was then removed, and the residue loaded onto a preparative TLC plate and eluted (CH_2Cl_2 :MeOH, 20:1). The bands yielded red (0.0135 g, 21 %) and purple (0.0069 g, 10 %) solids, which were assigned as the mono-substituted product *cis*-Ru(acac)(hfac)(NMeIm)(MeCN) (**91**) and the bis-substituted product (**90**), respectively. Because of the low yield, the reaction was repeated in neat NMeIm which resulted in a dark purple solution after 1 h at 75 °C. The purple solid was isolated and purified as described previously with a final yield of 65 %.

Data for **90**: Anal. calc. for $C_{18}H_{20}N_4O_4F_6Ru$: C, 37.83; H, 3.53; N, 9.80; found: C, 37.90; H, 3.65; N, 9.86. LR-MS [+LSIMS]: 572 (M^+), 490 ($M^+ - NMeIm$), 408 ($M^+ - 2 NMeIm$). HR-MS [+LSIMS] for $C_{18}H_{20}N_4O_4F_6Ru$: 572.04258; found 572.04433. UV-Vis (MeOH): 278 (16.6), 380 (3.33), 564 (7.52). 1H NMR (200 MHz, d_6 -acetone): [Several overlapping peaks were observed and so the assignments were made according to integration ratios.] δ 6.15-6.60 (overlapping singlets, 6H, Im- $H_{2,4}$ & 5), 4.60 (s, 4H, hfac H + Im- Me_1), 4.29 (s, 4H, acac H + Im- Me_1), 0.70 (s, 3H, acac Me), 0.43 (s, 3H, acac Me). $^{19}F\{^1H\}$ NMR (188 MHz, d_6 -acetone): δ 0.86 (s, $-CF_3$), 0.73 (s, $-CF_3$).

Data for **91**: LR-MS [+LSIMS]: 531 (M^+), 490 ($M^+ - MeCN$), 408 ($M^+ - MeCN - NMeIm$). HR-MS [+LSIMS] for $C_{16}H_{17}N_3O_4F_6Ru$: 489.98949; found 489.99018. 1H NMR (200 MHz, d_6 -acetone): δ 7.69 (s, 1H, Im- H_2), 7.18 (s, 1H, Im- H_5), 6.88 (s, 1H, Im- H_4), 5.92 (s, 1H, hfac- H), 5.29 (s, 1H, acac- H), 3.83 (s, 3H, Im- Me_1), 2.59 (s, 3H, $MeCN$), 1.88 (s, 3H, acac Me), 1.85 (s, 3H, acac Me). $^{19}F\{^1H\}$ NMR (188 MHz, d_6 -acetone): δ 2.21 (s, $-CF_3$), 1.99 (s, $-CF_3$).

5.2.4 Cyclic Voltammetry of Ru(II) and Ru(III) β -diketonato Complexes

The cyclic voltammograms for the complexes reported in this chapter were obtained using the procedure described in chapter 2 (Section 2.2.6) with the cell depicted in Figure 2.3. The reduction potentials for the one-electron Ru(III/II) couple are reported in Table 5.1 versus the SCE. The listed conversion factor is detailed in chapter 2, Section 2.2.6.

Table 5.1: Summary of Ru(III/II) reduction potentials vs. SCE (mV).

Complex		FeCp ₂ E _{1/2} (avg.) vs. Pt	E _{1/2} (avg.) vs. Pt	Conversion Factor ²² (424 - E _{1/2} FeCp ₂)	E _{1/2} vs. SCE
Ru(hfac) ₃	70	262	559	+ 162	721
[Na][Ru(hfac) ₃]	68	268	562	+156	718
Ru(hfac) ₂ (acac)	87	247	112	+ 176	289
[Na][Ru(hfac) ₂ (acac)]	86	284	144	+140	284
<i>cis</i> -Ru(hfac) ₂ (MeCN) ₂	71	248	967	+ 176	1143
<i>cis</i> -Ru(hfac) ₂ (MeCN)(Im)	73	364	516	+ 60	576
<i>cis</i> -Ru(hfac) ₂ (Im) ₂	72	248	378	+ 176	554
<i>cis</i> -Ru(hfac) ₂ (NMeIm) ₂	74	251	373	+ 173	546
[Ru(hfac)(NMeIm) ₄][PF ₆]	76	250	301	+ 174	475
<i>cis</i> -Ru(hfac) ₂ (2MeIm) ₂	77	266	325	+ 158	483
<i>trans</i> -Ru(hfac) ₂ (2MeIm) ₂	79	228	256	+ 196	452
<i>cis</i> -Ru(hfac) ₂ (4MeIm)(5MeIm)	80	97	171	+ 327	498
Ru(acac) ₂ (hfac)	85	173	-483	+ 251	- 232
<i>cis</i> -Ru(hfac)(acac)(MeCN) ₂	88	276	396	+ 148	544
<i>cis</i> -Ru(hfac)(acac)(NMeIm) ₂	90	265	83	+ 159	242
Ru(acac) ₃	53	390	- 764	+ 34	- 730
<i>cis</i> -[Ru(acac) ₂ (MeCN) ₂][Tf]	54	367	-134	+ 57	-77
<i>cis</i> -[Ru(acac) ₂ (MeCN)(Im)][Tf]	57	294	- 548	+ 130	- 418
<i>cis</i> -[Ru(acac) ₂ (Im) ₂][Tf]	55	315	- 548	+ 109	- 439
<i>trans</i> -[Ru(acac) ₂ (Im) ₂][Tf]	56	318	- 571	+ 106	- 465
<i>cis</i> -[Ru(acac) ₂ (MeCN)(NMeIm)][Tf]	59	346	- 501	+ 78	- 423
<i>cis</i> -[Ru(acac) ₂ (NMeIm) ₂][Tf]	58	409	- 461	+ 15	- 446
<i>cis</i> -[Ru(acac) ₂ (2MeIm) ₂][Tf]	60	312	- 625	+ 112	- 513
<i>trans</i> -[Ru(acac) ₂ (2MeIm) ₂][Tf]	61	310	- 660	+ 114	- 546
<i>cis</i> -[Ru(acac) ₂ (5MeIm) ₂][Tf]	62	301	- 601	+ 123	- 478

5.3 Results and Discussion

5.3.1 Ruthenium tris(β -diketonato) complexes

Many series of Ru(III) tris(β -diketonato) complexes have been synthesized previously^{14,15} and they have been shown to act as catalysts in a number of organic reactions. For instance, Ru(acac)₃ effects the hydrogenation of nitroarenes to amines.²³ Although the synthesis of Ru(acac)₃ had been reported previously,^{2,13,24} the procedure in this thesis work used a "Ru blue" solution made by H₂-reduction of RuCl₃•3H₂O similar to that reported by Johnson and Everett, Jr.² No major side-products were formed in the synthesis and the resulting yield (90 %) was higher than those previously reported (70-80 %). Of note, addition of NaHCO₃ to acetylacetone leads to proton abstraction from the 3-carbon (*i.e.* the most acidic proton) yielding the negatively charged, strongly coordinating bidentate anionic ligand with de-localized charge (Figure 5-2, right hand resonance structure).

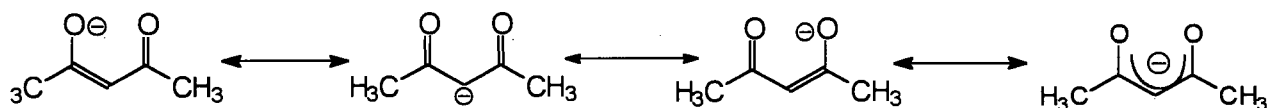
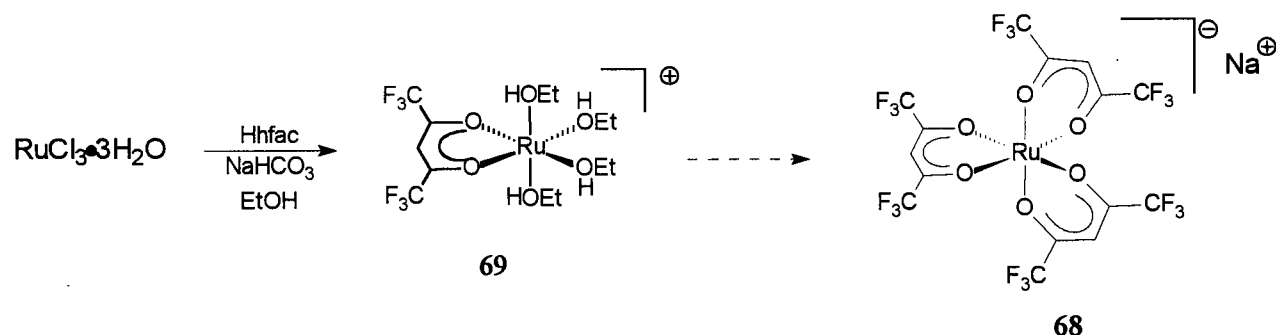


Figure 5-2: Resonance structures for acetylacetonate (acac[−]).

Owing to its high solubility in water (0.5 mmol dm^{−3} at 25 °C),¹³ Ru(acac)₃ seemed a possible precursor for the synthesis of imidazole complexes that could subsequently be tested *in vitro* in aqueous media. Attempts to substitute acac[−] with ligands such as imidazole and 2-nitroimidazole, however, were unsuccessful, the acac ligands remaining bound due to substitution inertness sometimes encountered with these Ru(III) d⁵ systems.

Synthesis of the Ru(III) complex Ru(hfac)₃ (**70**), containing the fluorinated analogue of acac[−] (hfac[−]), was more problematic. Treatment of RuCl₃•3H₂O with Hhfac and NaHCO₃ in EtOH generated mainly [Na][Ru(hfac)₃] (**68**); the accompanying reduction of Ru to the 2+ oxidation state⁹ is a consequence of the influence of the strongly electron-accepting ligand hfac on the Ru(III/II) reduction potential of some species (see Table 5.1). Of note, analysis of the reaction mixture via TLC also revealed several other products, one of those being a green complex

formulated as $[\text{Ru}(\text{hfac})(\text{EtOH})_4][\text{hfac}]$ (**69**) according to MS and ^1H and $^{19}\text{F}\{^1\text{H}\}$ NMR data. For example, in the ^1H NMR spectrum of **69** two hfac signals are observed at δ 6.54 and 6.46 which likely correspond to coordinated and free hfac, respectively (*cf.* for free hfac, δ 6.16) while the quartet at δ 3.61 is due to the CH_2 group of coordinated EtOH, also shifted downfield from the “uncoordinated” value (δ 3.48). Of note, the closer proximity of the CH_2 group to the Ru affects its chemical shift more than that of the methyl group (δ 1.18 vs. δ 1.15 for Me group of free EtOH); these shifts may be accounted for by the electron-withdrawing nature of the CF_3 groups on the hfac ligand. The integration of the signals at δ 6.54 and 3.61 gives a ratio of $\sim 1:8$, suggesting (as do the MS data) that four EtOH ligands are coordinated. Complex **69** may be an intermediate *en route* to **68**; the initial reduction is perhaps promoted by the presence of an hfac ligand. The displacement of the chloride ligands by EtOH, leading to formation of **69**, followed by successive displacement by, and coordination of, hfac gives species **68** (see Scheme 5-1); the formation of **68**, even with a large excess of hfac added, did not go to completion. Of note, **69** could be isolated only in 5-10 % yield despite several attempts to stop the reaction at its initial stages.



Scheme 5-1: Synthesis of $\text{Na}[\text{Ru}(\text{hfac})_3]$ (**68**) from $\text{RuCl}_3 \cdot 3\text{H}_2\text{O}$.

The H_2O_2 -oxidation of **68** to **70** followed that reported previously by Endo *et al.* who found **70** to be unstable, even under an N_2 atmosphere in the absence of light.⁹ The **70** isolated during this work was, however, found to be stable for long periods of time in air. An X-ray structure was obtained for **70** (Figure 5-3, Appendix I-11) which crystallized in the monoclinic space group $\text{P}2_1/\text{n}$. The Λ enantiomer is seen here, but both stereoisomers are present in the unit cell; the Δ isomer was illustrated for the X-ray structure of $\text{Ru}(\text{acac})_3$,³ which crystallized in the

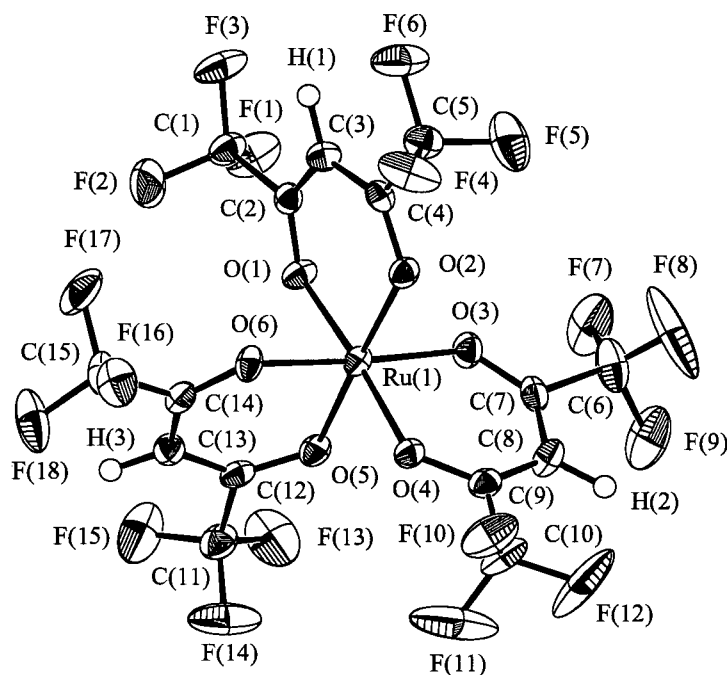


Figure 5-3: ORTEP view of $\text{Ru}(\text{hfac})_3$ (**70**); 50 % probability thermal ellipsoids are shown.

$P2_1/c$ space group. The average O-Ru-O bond angles were $\sim 90^\circ$ and the average Ru-O bond length for the hfac complex (1.99 Å) is essentially the same as that of the acac structure (2.00 Å), showing that the electron-withdrawing ability of the CF_3 groups has surprisingly little effect on the interaction of these β -diketonate ligands with Ru(III).

The mixed-ligand complexes containing both acac^- and hfac^- were isolated, but not without some difficulty. Patterson and Holm previously reported the synthesis of the mixed-ligand complexes $\text{Ru}(\text{acac})_2(\text{hfac})$ (**85**) and $\text{Ru}(\text{hfac})_2(\text{acac})$ (**87**), by refluxing $\text{Ru}(\text{acac})_3$ and $\text{Ru}(\text{hfac})_3$ (1:1) in toluene for 7 days,¹⁵ but the products were not isolated and purified; the reaction was only carried out to determine reduction potentials of the two *in situ* species **85** and **87**.¹⁵ High reaction temperatures and long reaction times were needed to ensure effective ligand exchange within the

strongly bound β -diketonates. **85** has been isolated, albeit in very low yield, from the "Ru blue" route.¹⁰ The "Ru blue" method²⁵ has also been applied for the synthesis of mixed-ligand complexes, within the series $\text{Ru}(\text{acac})_n(\text{bfa})_{3-n}$ (bfa = 4,4,4-trifluoro-1-phenyl-1,3-butanedione).⁷ However, a mixture of the homoleptic and mixed-ligand complexes result, and the yields are again low. The bis-MeCN complexes, *cis*- $[\text{Ru}(\text{acac})_2(\text{MeCN})_2][\text{CF}_3\text{SO}_3]$ (**54**) and *cis*- $\text{Ru}(\text{hfac})_2(\text{MeCN})_2$ (**71**) (see Section 5.3.2), were thus developed as synthetic precursors as they gave less complicated product mixtures in much higher yields.

Complex **85** was synthesized by treating **54** with one equiv. of Hhfac and base (NaHCO_3); the reaction proceeded rapidly giving a high yield (75 %), presumably because of the labile nitrile ligands and the entropically favoured chelate formation. Kobayashi *et al.* have synthesized **85** from the Ru(II) precursor $\text{Ru}(\text{acac})_2(\text{MeCN})_2$, but the isolated yield was only 32 %.¹⁸ There were several minor side-products in the synthesis from **54**, but **85** was easily purified by sublimation at 100 °C under vacuum. Elemental analysis indicated the presence of 0.5 mole equiv. of acetone, the solvent molecule likely trapped within the solid during the sublimation process (recall that the crude product was dissolved in a minimal amount of acetone prior to sublimation).

Synthesis of **87** required a two-step procedure: ligand substitution in **71** to form $[\text{Na}][\text{Ru}(\text{hfac})_2(\text{acac})]$ (**86**) followed by a Ru(II) \rightarrow Ru(III) oxidation step using H_2O_2 . The reaction to generate **86** required longer times than the synthesis of **85**, presumably due to the decreased affinity that the acac O-atoms have for the electron-rich Ru(II) versus the electron-deficient Ru(III) species; the yield of **86** (32 %) is also considerably lower than that for the synthesis of **85**. Again, there were a number of minor side-products in the synthesis of **86** as established by TLC: in addition to the product band (dark blue), a major orange-pink band was seen, but identification of the species was unsuccessful. The presence of two hfac ligands apparently enhances the stabilization of the Ru(II) oxidation state.⁵

Using the same reaction conditions for the transformation of **68** to **70**, H_2O_2 -oxidation of **86** proceeded quickly. This oxidation is more efficient than for the synthesis of **70** as the final aqueous phase was pale yellow, suggesting all of **86** had been oxidized and transferred to the

organic phase. The final green product (**87**), not previously isolated,¹⁰ was purified via sublimation and obtained in 80 % yield.

Comparison of the electronic spectra for the four complexes **53**, **70**, **85** and **87** (Table 5.2) reveals that there is an effect on the energy of the LMCT band when acac is successively displaced by hfac. The energy of the LMCT band in the 330 - 380 nm range, previously assigned by Satsu *et al.*,²⁶ increases slightly (for **85**) when one acac ligand is substituted by an hfac ligand in **53** and then decreases significantly when a second acac ligand is substituted (**87**). The substitution of a third hfac ligand (to give **70**) unexpectedly gives no change in the LMCT energy when compared with **87**. The band in the 270 - 286 nm region is assigned to the $\pi \rightarrow \pi^*$ transition of the

Table 5.2: Summary of UV-Vis data for complexes **53**, **70**, **85** and **87** in MeOH [λ_{max} ($\epsilon \times 10^{-3}$)].

Complex	$\pi \rightarrow \pi^*$ (singlet)	LMCT	$\pi \rightarrow \pi^*$ (triplet)
Ru(acac) ₃ 53	270 (14.1)	346 (7.7)	506 (1.58)
Ru(acac) ₂ (hfac) 85	284 (13.6)	332 (6.43)	502 (2.38)
Ru(hfac) ₂ (acac) 87	286 (19.2)	376 (8.25)	556 (1.67)
Ru(hfac) ₃ 70	274 (14.5)	376 (6.65)	524 (1.87)

ligand singlet states and varies little between complexes. The band in the 500-560 nm region is ascribed to the $\pi \rightarrow \pi^*$ transition of the excited triplet states that are configuration-interaction admixtures of the ligand;⁹ the energy of this transition also does not appear to follow a trend related to the number of hfac ligands.

The IR spectra of metal acetylacetonato complexes show a very strong, characteristic $\nu_{\text{C=O}}$ stretching mode near 1570 cm^{-1} .²⁷⁻²⁹ The $\nu_{\text{C=O}}$ and $\nu_{\text{C=C}}$ bands of Ru(III) β -diketonato complexes typically appear in the 1510-1620 and the 1420-1580 cm^{-1} regions, respectively, and are substituent dependent, the hfac complexes displaying higher values than the acac complexes. These shifts can be explained in terms of the electron-withdrawing CF_3 group, and the consequent strengthening of the C=O and C=C bonds. For example, for Ru(hfac)₂(acac) (**87**), the $\nu_{\text{C=O}}$ bands appear at 1583 and 1579 cm^{-1} corresponding to the hfac and acac ligands, respectively. Correspondingly, the Ru(II) complex [Na][Ru(hfac)₂(acac)] (**86**) has C=O bands at 1550 and 1521

cm^{-1} . The shift of the bands to lower energy is due to the lower oxidation state of the Ru metal. The higher $\nu_{\text{C=O}}$ for $\text{Ru}(\text{hfac})_3$ (**70**; 1582 cm^{-1}) (vs. its Ru(II) analogue, $[\text{Na}][\text{Ru}(\text{hfac})_3]$ (**68**; 1555 cm^{-1})) coincides with the value previously reported.⁹

An interesting characteristic of the Ru(III) complexes is their ^1H NMR spectra. Typically, Ru(III) complexes give very broad, poorly resolved signals as a result of rapid nuclear spin relaxation induced by the paramagnetism.² Those paramagnetic complexes which have shorter relaxation times are usually the species which give the best resolved NMR spectra; however, these species are not especially amenable to EPR studies.² The magnitude of the isotropic shift, the term used to include nuclear resonance shifts arising from Fermi hyperfine contact interactions or from electron-nuclear dipolar (pseudocontact) interactions in paramagnetic substances, will depend on both the imbalance of electron spin on the ligand due to spin transfer between metal and ligand and the orientation with respect to the ligand-field axis of the complex and its distance from the metal ion.³⁰ Table 5.3 summarizes the chemical shifts for the four tris(β -diketonato) complexes. The δ values for the Me signals of the coordinated acac ligands reveal an upfield shift (compared to a

Table 5.3: ^1H and $^{19}\text{F}\{^1\text{H}\}$ NMR data for the Ru(III) tris(β -diketonato) complexes.^a

Complex		$\delta_{\text{H Me (acac)}}$	$\delta_{\text{H CH (acac)}}$	$\delta_{\text{H CH (hfac)}}$	δ_{F}
$\text{Ru}(\text{acac})_3$	53	-7.11	-30.25	---	---
$\text{Ru}(\text{acac})_2(\text{hfac})$	85	-8.82, -9.01 ^b	-38.95 ^b	-28.45 ^b	-9.71 ^b
$\text{Ru}(\text{hfac})_2(\text{acac})$	87	-14.34	-56.72	-31.82	-6.71, -8.06
$\text{Ru}(\text{hfac})_3$	70	---	---	-41.67	-11.49

^a In CDCl_3 at r.t., unless stated otherwise.

^b In d_6 -acetone at r.t.

'diamagnetic value') due to interaction with the paramagnetic Ru(III) centre. The "stronger electron-withdrawing hfac ligand" shifts the Me signals further upfield, which may result from greater electron spin imbalance between the metal and ligand σ and π molecular orbitals, induced by the properties of the hfac ligand, which changes the local magnetic fields.² Of note, complexes

53 and **87** have one signal for the Me groups due to increased symmetry of these complexes. Complex **85** has two Me group signals, one from a moiety *trans* to the hfac⁻ ligand and one from a moiety *trans* to an acac⁻ ligand. The signals for the methine protons of acac and hfac exhibit very significant upfield shifts. Because the isotropic shift is dependent on the distance of the specific proton from the metal ion, one might expect the methine protons to have δ values similar to those of the CH₃ groups; however, the δ_{CH} signals appear much further upfield. This implies an electronic delocalization on the coordinated ligand across the methine proton, that produces an even greater electron spin imbalance between the ligand and the metal and hence a greater isotropic shift.² Again, the more hfac ligands that are coordinated, the greater the upfield shift. This effect is more pronounced for the acac methine signal as substitution of two acac ligands by hfac (from **53** to **87**) renders a chemical shift change of ~26 ppm, while the reverse (from **70** to **85**) produces a chemical shift change of ~13 ppm. A representative ¹H NMR spectrum illustrating the upfield shifts is shown in Figure 5-4 for complex **87**; δ assignments were made according to integral ratios.

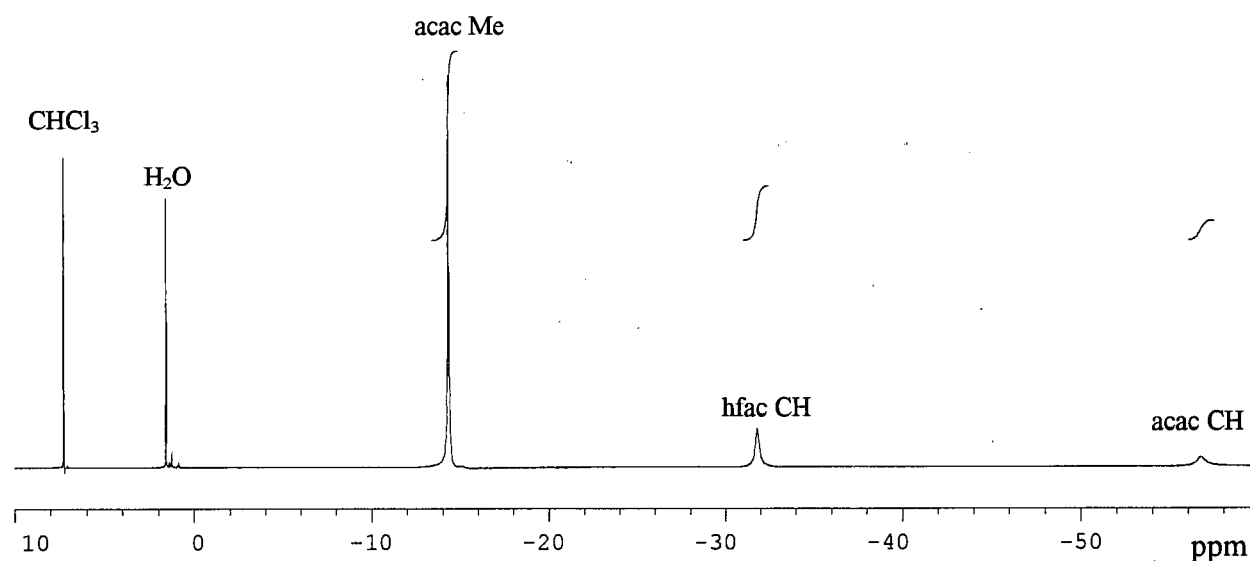


Figure 5-4: ¹H NMR spectrum of Ru(hfac)₂(acac) (**87**) in CDCl₃ at r.t.

Investigation of the ¹⁹F{¹H} NMR spectra for these complexes (Table 5.3) also demonstrates the effect of the electron-withdrawing CF₃ group. Complex **70**, with magnetically equivalent CF₃ groups, exhibited the greatest upfield fluorine signal (δ -11.49). Substitution of one

hfac by an acac resulted in a downfield shift for complex **87**; two signals are observed at δ -6.55 and -8.06, as for the Me proton signals of acac in **85**. The non-regular trend in δ_F with increasing (or decreasing) number of hfac ligands may result from a solvent effect (CDCl_3 vs. d_6 -acetone).

The successive displacement of acac by hfac ligands on Ru(III) had a marked effect on the reversible one-electron reduction potential of the metal centre. Patterson and Holm showed that the half-wave potentials of **53**, **85**, **87** and **70** in DMF solution at 25 °C were strongly influenced by the nature of the substituents.¹⁵ The potentials became more positive (increasing ease of reduction of the Ru(III) species) as the number of electron-withdrawing CF_3 substituents increases. Because these complexes possess similar octahedral geometries and a common redox-active centre, the mechanism of electron transfer should be the same, as is the case for a related series of organic molecules.^{15,31} For this thesis work, similar to literature data^{6,14,15}, the plot of $E_{1/2}$ versus the sum of the Hammett constants ($\Sigma \sigma_m$, calculated using the values given by Murov³²) affords a straight line (Figure 5-5). The agreement between the two sets of data is remarkable, yet not surprising as the relative permittivities of the two solvents are almost identical ($\epsilon_r(\text{MeCN}) = 38$

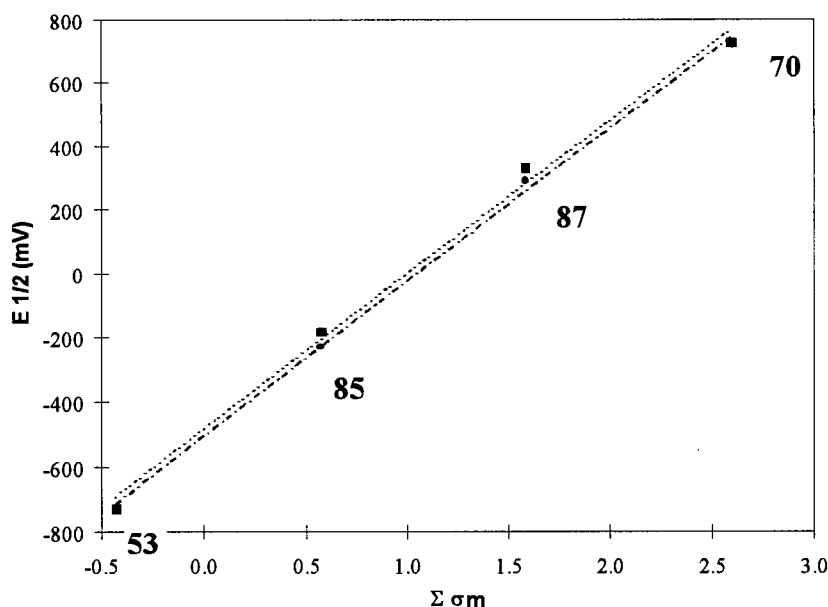


Figure 5-5: Relationship between $E_{1/2}$ and $\Sigma \sigma_m$ in 0.1 M TBAP at 25°C. ---●---, this work (CV data in MeCN); ---■---, Patterson and Holm (polarographic data in DMF).¹⁵

and ϵ_r (DMF) = 37 at 25 °C³³), if there is little specific solute-solvent interaction. This linear relationship was explained by Patterson and Holm qualitatively as follows. The d electrons for the d^5 , low-spin Ru(III) species are localized in the t_{2g} metal orbital,^{34,35} a d_π orbital which forms a π molecular orbital with a π ligand orbital. In the redox process the electron will be added to or subtracted from this molecular orbital. The Hammett constant is a measure of the electron-accepting character of the substituent which affects the energies of both the σ and π molecular orbitals.³⁶ The more electron-accepting is the substituent, the more stabilized is the reduced form with respect to the oxidized form, hence the more positive is $E_{1/2}$.

5.3.2 Bis-MeCN Complexes

Because of the substitution-inert nature of the Ru tris(β -diketonato) complexes, a more useful precursor for introduction of different mono- and bidentate ligands via ligand substitution was needed. Kobayashi *et al.* initially reported that bis(MeCN)bis(β -diketonato)ruthenium(II) complexes could be prepared by reducing the corresponding tris(β -diketonato)ruthenium(III) with zinc amalgam in an MeCN-EtOH-H₂O mixture, and that these bis-MeCN complexes were useful intermediates for the synthesis of mixed-ligand β -diketonato ruthenium(III) complexes.¹⁸ Kasahara *et al.* then reported the preparation of bis(MeCN)bis(β -diketonato)ruthenium(III) species through a ligand displacement reaction of tris(β -diketonato)ruthenium(III) complexes, induced by strong acid.¹⁹ Ru(acac)₃ has been shown to be stable under basic and neutral conditions, while introduction of acid leads to protonation of an acac ligand.³⁷

Treatment of Ru(acac)₃ with perchloric acid in MeCN has yielded the complex *cis*-[Ru(acac)₂(MeCN)₂][ClO₄].¹⁹ The HClO₄:Ru stoichiometry was determined by spectrophotometric titration to be 1:1, additional acid gave no further acac displacement. The corresponding reactions using H₂SO₄ or HCl were much slower, but qualitatively gave the same results,¹⁹ although excess acid was needed to force the reaction to completion. The difference may be explained by the larger K_a value of HClO₄ in MeCN.¹⁹ Of note, no corresponding substitution reaction was observed in dmso or DMF,¹⁹ both of which can coordinate to ruthenium(III).³⁸⁻⁴¹ Because HClO₄ is hazardous, triflic acid, which also has a large K_a , was used in this thesis work for the synthesis of the bis-MeCN complexes; during this work, the same synthesis was also reported in the literature.²⁰

Reaction of $\text{Ru}(\text{acac})_3$ with $\text{CF}_3\text{SO}_3\text{H}$ in MeCN was slow at r.t. (~ 5 h to completion); however, **54** was formed in 20 min at refluxing conditions. A reaction pathway similar to that proposed for the ligand exchange of $\text{Co}(\text{acac})_3$ ⁴²⁻⁴⁴ can be invoked (Figure 5-6).¹⁹ Proton attack at

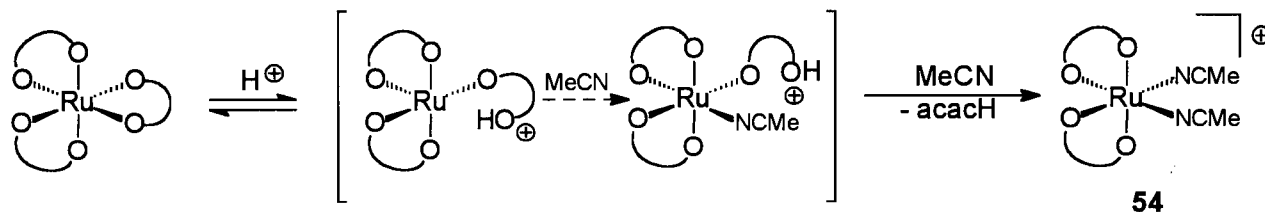


Figure 5-6: Proposed reaction mechanism for acid catalyzed displacement of acac (adapted from ref. 19).

an acac oxygen weakens the Ru-O bond and results in a 'dangling' monodentate acacH^+ intermediate. The vacant site will be occupied by the coordinating MeCN, and the dangling ligand will dissociate, allowing for a second MeCN molecule to coordinate. The 96 % yield was higher than for the perchlorate salt (81 %),¹⁹ and the method of complex isolation was more facile.

Complex **54** is assumed from the IR and ^1H NMR data to have *cis* geometry, in accordance with those reported for the perchlorate salt.¹⁹ The IR spectrum of free MeCN^{45,46} shows a strong ν_{CN} band at 2254 cm^{-1} and a weak combination band at 2290 cm^{-1} which derives its intensity from proximity to ν_{CN} . The IR spectrum for **54** has two medium intensity bands at 2326 and 2296 cm^{-1} corresponding to the asymmetric and symmetric ν_{CN} of coordinated MeCN (*cf.* 2324 and 2295 cm^{-1} for the perchlorate salt). A weak shoulder at 2288 cm^{-1} may correspond to the combination band derived from the accidental coincidence of δ_{CH_3} (symmetrical CH_3 deformation) and ν_{CC} (C-C stretch).⁴⁵ *Trans* coordinated MeCN ligands give only one IR active ν_{CN} band.⁴⁷ A few examples are seen where coordination of MeCN to Ru results in a shift of ν_{CN} to lower frequencies;⁴⁸ however, ν_{CN} generally shifts to higher frequencies. An increase in the ν_{CN} value implies a stronger C-N bond with coordination to Ru(III), suggesting that the $d\pi \rightarrow p\pi$ backbonding interaction is virtually non-existent for this complex.⁴⁹ Stabilization of the C-N bond in turn destabilizes the Ru-N bond, making the MeCN ligand labile for ligand substitution.

The ^1H NMR spectrum of **54** in CDCl_3 showed shifts analogous to those of the perchlorate salt reported by Kasahara *et al.*,¹⁹ except the methine proton signal was not observed

in the present work; the signal must be broadened into the baseline. The presence of two acac ligands, as for **53** and **85**, results in large isotopic shifts of the proton signals. Two signals were observed for the acac Me groups (δ -23.46 and -27.22), further supporting a *cis* geometry. The shifts of the Me signal for coordinated MeCN to lower field (δ +37.53) are opposite to those for the acac ligands, showing that the electron spin imbalance between metal and ligand originates from molecular orbitals different from those involved with the binding of acac.

The high reactivity of **54** is displayed when it is dissolved in either EtOH or H₂O (Sections 5.2.1.11, 5.2.1.12). The EtOH reaction, under reflux, yielded a number of products including one major one, an orange solid, its ¹H NMR data suggesting that both MeCN ligands had been displaced by two EtOH molecules. The ¹H assignments are tentative because of the poor resolution of the spectrum and the broadened peaks due to the effect of the paramagnetic Ru(III) centre; however, the reaction manifests the reactivity of the Ru-N bond and may rationalize why reactions of **54** with imidazoles in EtOH give many products and hence overall a quite low yield (see Section 5.3.3). Reaction of **54** with H₂O also yields a number of products; ¹H NMR data for the major one suggest that one MeCN ligand had been displaced, while there is still a signal in the δ +25 to +35 region typical of a coordinated MeCN. The MS spectrum (M^+ 359) also supports the formulation [Ru(acac)₂(MeCN)(H₂O)][Tf]. This study suggested that heating was required for removal of both MeCN ligands. Analysis of an *in situ* reaction of **54** with D₂O at 80°C by ¹H and ²H NMR revealed the formation of a D₂O complex which may be the bis-substituted complex [Ru(acac)₂(D₂O)₂][Tf] as there was no downfield ¹H peak for MeCN.

The reaction analogous to that for the synthesis of **54** was carried out with Ru(hfac)₃ to generate the bis-MeCN derivative. Analysis of the isolated product, however, revealed its composition to be Ru(hfac)₂(MeCN)₂ (**71**), implying an *in situ* reduction of Ru(III)→Ru(II). The electron-accepting CF₃ substituents of hfac stabilize the Ru(II) oxidation state, thus promoting reduction of the Ru(III) centre, presumably by residual H₂O (introduced by either the MeCN solvent or the hygroscopic CF₃SO₃H), upon removal of an hfac ligand in the presence of CF₃SO₃H. The geometry of **71** is *cis*, according to the IR, NMR and X-ray crystallographic data. The IR displays two ν_{CN} bands at 2357 and 2285 cm⁻¹ indicating even less $d\pi \rightarrow p\pi$ backbonding from Ru than in complex **54**; consistent with the presence of the electron-accepting CF₃ groups in

hfac. The ^1H NMR data were not useful for determining the geometry of the complex as only two singlets were observed at δ 6.20 and 2.87 corresponding to the hfac methine proton and Me of MeCN, respectively. The $^{19}\text{F}\{^1\text{H}\}$ NMR spectrum, however, showed signals at δ 0.98 and 0.38 for two inequivalent CF_3 groups on each coordinated hfac, supporting the *cis* formulation; the *trans* isomer would have revealed only one singlet. The X-ray structure (Figure 5-7) unequivocally proved the *cis* geometry. The complex, with close to 90° inter-ligand *cis* geometry at the Ru, crystallized in the monoclinic space group $\text{C}2/c$ with the four Ru-O distances averaging $2.038(2)$ Å and the two Ru-N distances averaging $2.011(2)$ Å (see Appendix I-12). The nitriles exhibit a slight

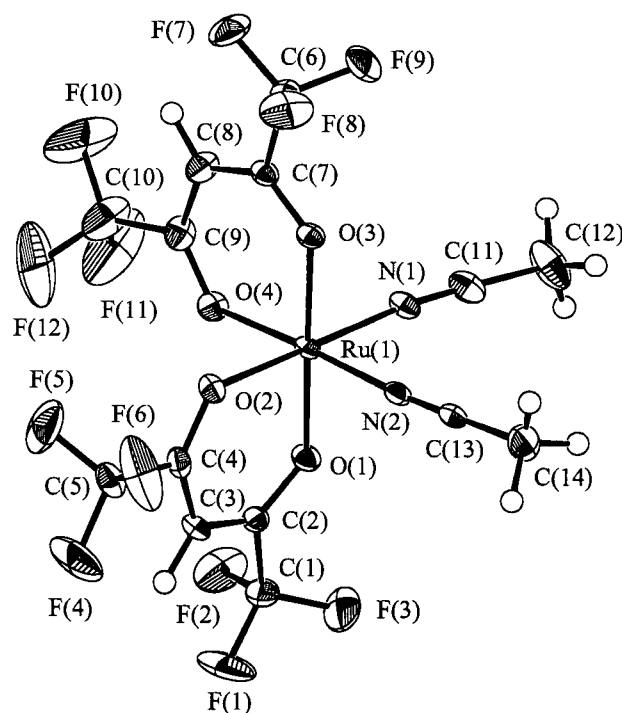
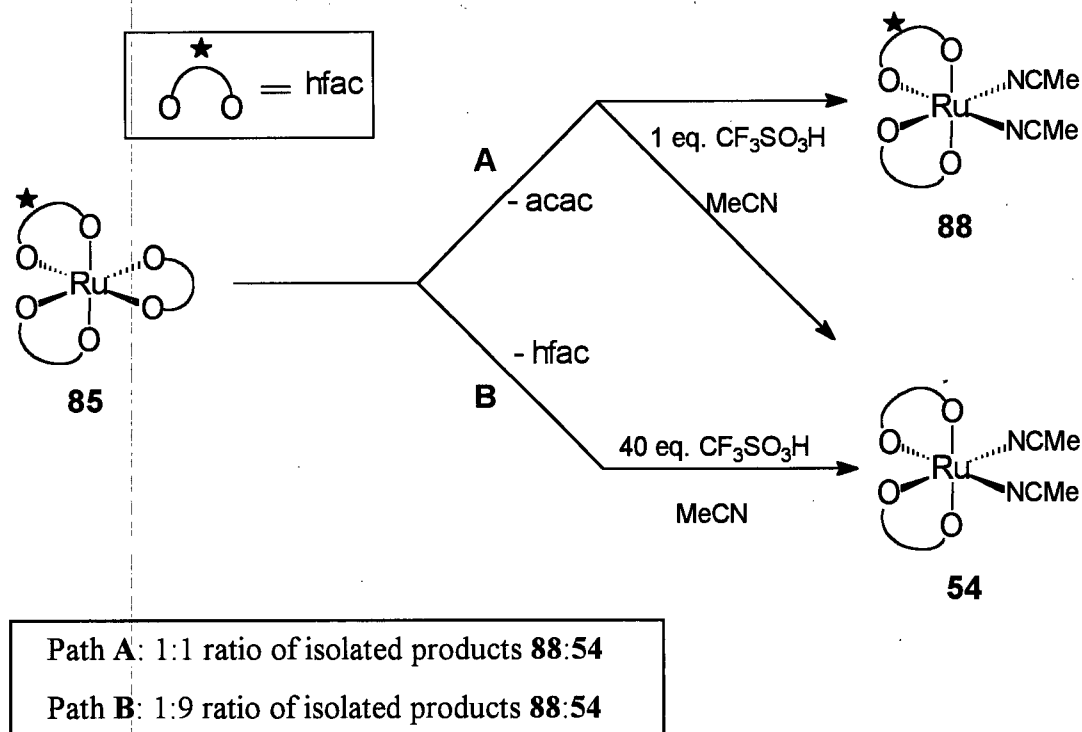


Figure 5-7: ORTEP view of *cis*- $\text{Ru}(\text{hfac})_2(\text{MeCN})_2$ (**71**); 50 % probability thermal ellipsoids are shown.

lengthening of the Ru-N bonds compared to those, for example in $\text{Ru}_2(\text{OH}_2)_2(\text{MeCN})_2(\mu\text{-O}_2\text{CC}_6\text{H}_4\text{-}p\text{-NO}_2)_4(\text{PPh}_3)_2$ (Ru-N 1.98 Å),⁵³ suggesting a relatively strong *trans* influence exerted

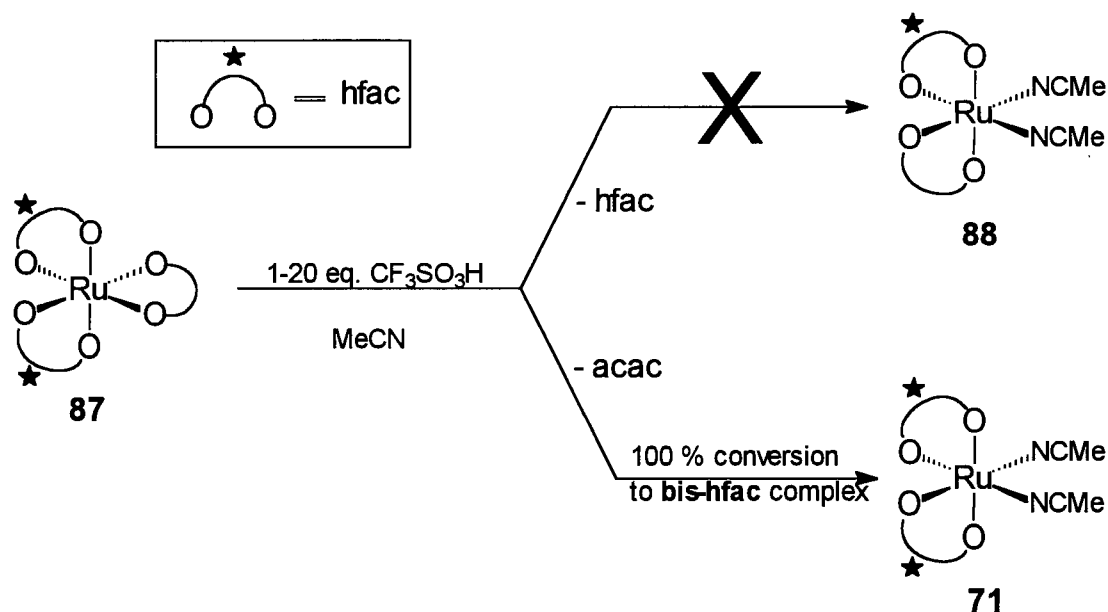
by the hfac ligand. Both Ru-N bonds are longer than 2.0 Å, the sum of the estimated single covalent radii,⁵⁰ implying little Ru(II)→N, dπ→pπ backbonding. The C-N bond lengths average 1.137(2) Å, slightly shorter than the value of 1.157 Å calculated for MeCN in the gas phase,⁵¹ as commonly observed in both transition metal⁴⁶ and main group⁵² nitrile complexes. Shortening of the C-N bond is also evidence against any π-backbonding in the metal-ligand interaction, which correlates well with the positive infrared shift of ν_{CN} for this complex.

Synthesis of the mixed-ligand (acac/hfac) bis-MeCN complex (**88**) was more involved than the synthesis of either **54** or **71**. As described in section 5.3.1, the mixed-ligand β-diketonato complexes **85** and **87** were synthesized from the bis-MeCN complexes **54** and **71** in the presence of Hhfac and Hacac, respectively; **87** was obtained from the oxidation of **86**. The synthesis of *cis*-Ru(acac)(hfac)(MeCN)₂ (**88**) (see below for *cis* formulation) was attempted from the two mixed-ligand precursors **85** and **87**, however, only one of the reactions was moderately successful (involving *in situ* reduction of Ru(III)→Ru(II)). Addition of one equivalent of triflic acid to an MeCN solution of **85** resulted in a rapid colour change, and comparison of isolated species with pure complexes revealed formation of **54** and **88** in approximately equal amounts (Scheme 5-2). Use of 40 equivalents of triflic acid resulted in a lower yield of **88**, thus displaying the acid



Scheme 5-2: Synthesis of *cis*-Ru(acac)(hfac)(MeCN)₂ (**88**) from Ru(acac)₂(hfac) (**85**).

dependence of the reaction. At stoichiometric acid concentrations there is no preference for reaction of acac^- or hfac^- with H^+ , but as the acid concentration is increased the hfac^- ligand is preferentially displaced. This observation is opposite to that reported by Kobayashi *et al.* where for a number of mixed β -diketonato complexes the more basic acac ligand is preferentially displaced.¹⁸ These workers also reported the synthesis of **88** by treatment of **85** with a refluxing mixture of EtOH, MeCN and H_2O (10:1:1) in the presence of zinc amalgam for 2 h. A brown solid was the major product isolated from this reaction (in addition to a small amount of an unidentified, yellow product), but the yield was 10 % lower than that observed in this thesis (49 %). If the observation holds for the reaction of other mixed-ligand complexes with triflic acid then one would expect hfac to be preferentially displaced from **87** to give **88** in high yields. However, the opposite case seems to prevail (Scheme 5-3); the amount of acid used had no effect as 100 % conversion to **71** was seen. This phenomenon may be rationalized by considering the strength of the Ru-O bond for acac



Scheme 5-3: Attempted synthesis of $\text{cis-Ru}(\text{acac})(\text{hfac})(\text{MeCN})_2$ (**88**) from $\text{Ru}(\text{hfac})_2(\text{acac})$ (**87**).

versus hfac and the different affinities of acac and hfac for H^+ . For example, in complex **87**, the preference for cleavage of a weaker Ru-O (*cf.* for **88**, $\text{Ru-O}_{\text{acac}}$ and $\text{Ru-O}_{\text{hfac}}$, 2.029(3) Å and 2.041(3) Å, respectively) appears to be exceeded by the preference that the stronger base (acac^-) has for H^+ . In complex **85**, on the other hand, the $\text{Ru-O}_{\text{acac}}$ bonds have either an acac^- or hfac^-

ligand *trans* to them. Consequently, at low acid concentrations, there will be no preference between the cleavage of a weaker Ru-O bond and the affinity for H⁺ of the stronger base acac⁻. As the acid concentration is increased, the propensity for Ru-O_{hfac} bond cleavage appears to outweigh the higher H⁺ affinity of acac⁻. Of note, attempts to synthesize **88** from the Ru(II) starting material [Na][Ru(hfac)₂(acac)] (**86**) were also unsuccessful.

The ¹H NMR spectrum of **88** supports a *cis* geometry, in accordance with data for the bis-MeCN complexes **54** and **71**. Thus, two signals for the coordinated MeCN ligands are observed (δ 2.76 and 2.69), illustrating different effects for the *trans* ligands. Again, the methine ¹H signal for hfac is further downfield than the corresponding signal for acac (δ 6.04 and 5.37, respectively) due to the electron-withdrawing property of the CF₃ substituents. The IR spectrum correspondingly shows two ν_{CN} bands at 2346 and 2270 cm⁻¹, in the range observed for **54** and **71** and indicating the presence of both acac and hfac. X-ray analysis of **88** (Figure 5-8) revealed crystallization in the triclinic space group $P\bar{1}$. Within essentially octahedral bonding at the metal, the average Ru-O bond distance is 2.029(3) Å for the acac ligand and 2.041(3) Å for the hfac ligand (see Appendix I-13), this difference reflecting the greater electron-withdrawing ability of hfac. The Ru-N(1) bond distance is 2.006(4) Å for MeCN *trans* to hfac while that of Ru-N(2) for MeCN *trans* to acac is 2.030(3) Å. This finding suggests that there is not a large *trans* influence on the bonding of these MeCN ligands with Ru. As in **71**, the C-N bond lengths (average 1.133(5) Å) are shorter than that of free MeCN (1.157 Å)⁵¹ and indicate zero π -backbonding in the ligand-metal interaction.

Comparison of UV-Vis spectra of the Ru(II) complexes **71** and **88** shows the effect of ligand substitution (hfac for acac) on the electronic properties (MLCT band) of these complexes. As the acac ligands are replaced by hfac ligands, the energy for the MLCT electronic transition decreases, λ_{max} shifting from 352 to 418 nm for **88** and **71**, respectively. The LMCT band for the Ru(III) species, **54**, was observed at 318 nm. An analogous trend, with respect to the LMCT bands, was also observed by Satsu *et al.*²⁶ for the tris(β -diketonato) Ru(III) complexes. The presence of the MeCN ligands also has a marked effect; for instance, substitution of an acac ligand by two MeCN ligands (**53** vs. **54**) results in a red shift of the LMCT band from 346 to 318 nm.

When an hfac ligand is substituted (**70** vs. **71**), however, a blue shift of the MLCT band is observed from 374 to 418 nm.

The Ru(III) \rightarrow Ru(II), $E_{1/2}$ reduction potentials for **54**, **88** and **71** are -77, +544 and +1143 mV (vs. SCE), respectively, and these values again demonstrate that the Ru(II) oxidation state is more stabilized with increasing number of hfac ligands. For the tris(β -diketonato) Ru(III) complexes, substitution of one acac by one hfac leads to an increase in $E_{1/2}$ by about +484 mV (see Figure 5-5, p. 218). The bis-MeCN complexes exhibit similar, but higher, increases in the $E_{1/2}$ values by about +610 mV. Coordination of MeCN also affects the Ru(III/II) reduction couple. Several literature examples show that coordination of MeCN to Ru results in a marked increase in the $E_{1/2}$ value.^{20,53,54} For example, with Ru(MeCN)₆²⁺ no oxidation to the Ru(MeCN)₆³⁺ species occurs in MeCN up to 2.5 V, and this is not unreasonable as a single MeCN ligand stabilizes the +2 oxidation state by ~ 0.4 V!⁵⁵ The *in situ* reduction that occurs during the syntheses of **71** and **88** from a Ru(III) precursor may be due to the presence of residual H₂O which could act as a reductant under such acidic conditions.

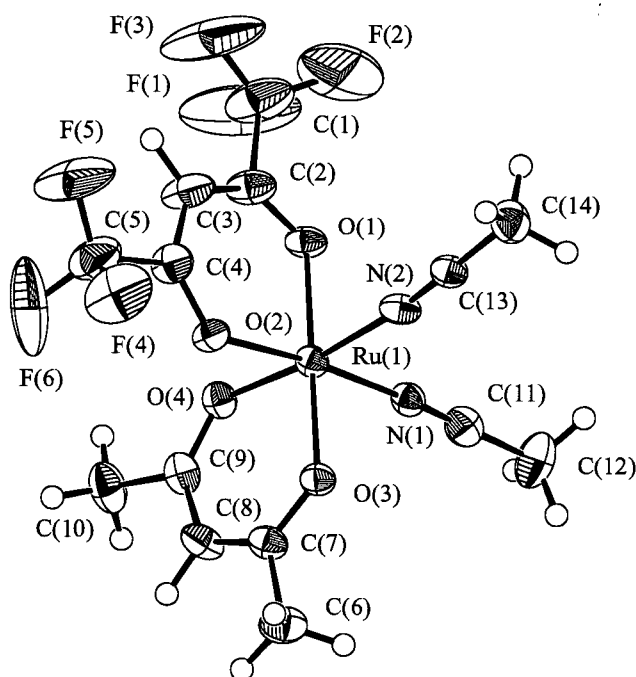


Figure 5-8: ORTEP view of *cis*-Ru(acac)(hfac)(MeCN)₂ (**88**); 50 % probability thermal ellipsoids.

5.3.3 Bis-imidazole Complexes

5.3.3.1 Bis(acetylacetonato)bis(imidazole)ruthenium(III) complexes

The Ru(III) bis-MeCN complex **54** has been shown previously to be a useful precursor for a number of complexes due to the lability of the Ru-N_{MeCN} bond.^{18,19} Furthermore, **54** is ionic which may be advantageous as the ultimate goal of this thesis work is to prepare water-soluble complexes for delivery of specific compounds to target areas within a cell. As indicated by reaction of **54** with EtOH and/or H₂O the MeCN ligands are extremely labile; excess of the desired imidazole was used in attempts to displace both MeCN ligands, but, in some cases, the reaction did not go to completion, and both the bis- and mono-substituted complexes were isolated. The

relatively low yields seen are also indicative of the reactivity of the Ru-N bond. Analysis of the reaction mixtures by TLC prior to complex isolation revealed that in most cases several minor side-products were formed. These side-products probably result from reaction of **54** with the solvent, including sometimes *in situ* reduction of Ru(III) to Ru(II), for example, in refluxing EtOH.

The imidazole and methyl-substituted imidazole derivatives (**55**, **58-63**) were isolated as red solids, with the only exception being the purple NMeIm complex **59**. Elemental analyses of the isolated complexes were generally satisfactory except for complexes **58** and **60**, which 'required' a half mole and a mole of H₂O, respectively, and were noticeably hygroscopic when exposed to the air for extended periods of time. The dark purple-blue solids (**64-66**) formed from coordination of 2-nitroimidazoles were also noticeably hygroscopic; the **SR2508** and **EF5** complexes (**65** and **66**, respectively) were shown to contain two and four molecules of hydration, respectively, according to elemental analyses. Attempts to dry these complexes at >100 °C under vacuum resulted in decomposition.

MS data for the Im and MeIm complexes are generally in agreement with the chemical formulation; an exception is complex **57**, initially formulated as *cis*-[Ru(acac)₂(MeCN)(Im)] [CF₃SO₃], which contains a solvated EtOH. The use of +LSIMS was the MS method of choice, but this only gives the mass of the cationic species. In general, the cationic parent mass peak is observed as well as two other peaks (of similar intensity) for successive loss of the imidazole ligands; no peaks are observed for the loss of the more strongly bound acac ligands. The MS data for the nitroimidazole complexes (**64-67**), on the other hand, were less definitive for purposes of identification; the signal intensities are extremely weak, the parent peak for the cation is not observed, and some of the peaks are unidentifiable. For example, for **64**, the (M⁺ - 2NO₂Im) peak is seen along with fragmentation patterns for loss of 2NO₂Im and NO species; for **65**, only a peak for Ru(acac)₂⁺ is observed and, for **66**, none of the peaks in the +LSIMS spectrum can be identified. This problem of obtaining useful MS data for Ru(III) nitroimidazole complexes is also found for the Ru(II) hfac-NO₂Im complexes studied in this thesis and for other Ru(II) DMSO-NO₂Im species reported previously.⁵⁶

The electronic spectra for the Im and MeIm complexes (**55-63**) reveal little difference in various transition energies with changes in the imidazole ligand. The band in the 212-214 nm

region corresponds to a $\pi \rightarrow \pi^*$ electronic transition within the imidazole ligand,⁵⁷ while that in the 280-284 nm region corresponds to the $\pi \rightarrow \pi^*$ transition for the acac ligand.²⁶ Because Ru(III) is relatively electron deficient, the two higher wavelength, lower energy bands (at ~ 330 and ~ 520 nm) are assigned as LMCT bands. Reported calculations on the electronic distribution of the imidazole ligand indicate that the transfer of electron density to a Ru(III) centre is predominantly σ -donating (86 %) with only minor π -donation (14 %).⁵⁸ As the π MOs are higher in energy than the σ MOs, the observed LMCT transitions will have mainly π -character; the observed intensity ratios ($\sim 1:7$) of the visible (518-524 nm) and the near-UV (330 nm) bands are in accordance with calculated coefficients at the imidazole N-donor site for the highest occupied (π_1 , HOMO) and the second highest occupied (π_2) molecular orbitals, and this leads to assignments for the two bands as $\pi_1 \rightarrow \text{Ru(d)}$ and $\pi_2 \rightarrow \text{Ru(d)}$ LMCT, respectively.^{58,59} Of note, these two LMCT bands may also overlap with the LMCT band originating from the acac ligand which has a similar transition energy.²⁶

¹H NMR spectroscopy was the most useful technique for characterization of the Ru(III) imidazole complexes, and provided not only an opportunity to study the isotropic shifts of the imidazole protons induced by the paramagnetic Ru(III) centre, but also permitted assignment of the coordination geometry. The chemical shifts for complexes **55-63** are summarized in Table 5.4. The broad ¹H NMR resonances were shifted significantly from those of the free ligand (see Table 5.5, p. 240); as for the Ru(III) β -diketonate complexes (Section 5.3.1).

In the initial synthesis of **55**, ¹H NMR analysis of the red solid isolated after 24 h revealed a mixture of *cis* and *trans* isomers. Assignments of the imidazole proton signals were made when just the *cis* isomer was isolated after 48 h; this implies that the *trans* isomer (**56**) is the kinetic product and the *cis* isomer (**55**) is the thermodynamic product and, consistent with this, ¹H NMR analysis of a d₆-acetone solution of the initial *cis/trans*-isomer mixture after 7 d revealed only signals corresponding to the *cis* isomer (Figure 5-9).

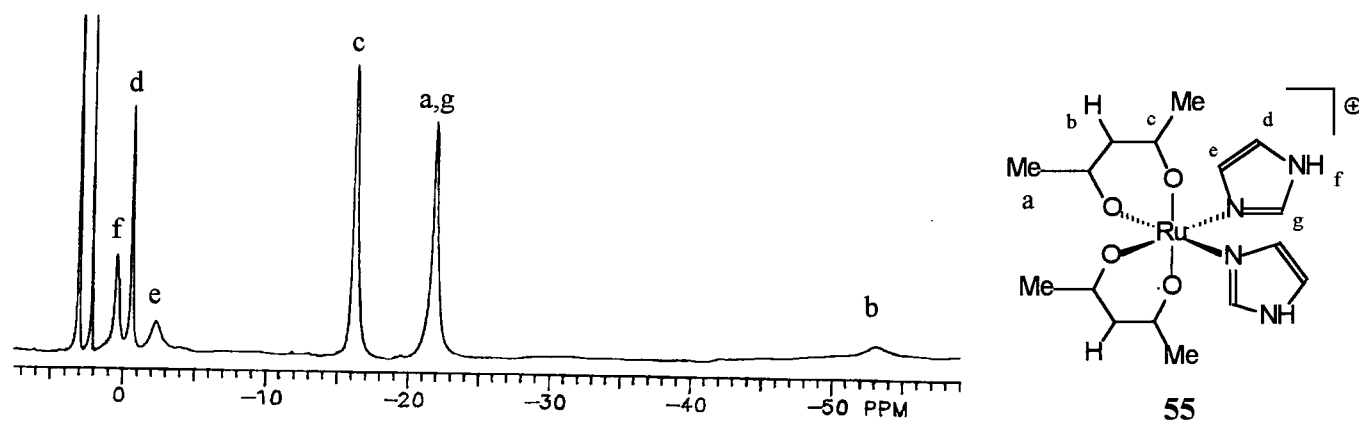


Figure 5-9: ^1H NMR spectrum of *cis*- $[\text{Ru}(\text{acac})_2(\text{Im})_2][\text{CF}_3\text{SO}_3]$ (**55**) in d_6 -acetone.

Peak assignments for **55** were made by comparison with data for other Ru(III) complexes containing the corresponding ligands. The acac methine proton signal is the very broad and most upfield signal (δ -53.15). The presence of two Me signals for the acac ligands supports *cis* coordination of the imidazoles, one Me being *trans* to an acac and the other *trans* to an imidazole. Of the imidazole protons, H_2 is most affected by the Ru(III), with the signal shifted upfield by ~28 ppm relative to that of free Im, and this shift is likely due to both the proximity of the proton to the Ru as well as it being saddled between the two imidazole N atoms. Assignments of the other protons on the imidazole ring remain tentative; however, the narrowest peak (d) can be assigned to H_5 , further removed from the paramagnetic centre, while the H_4 signal (e) is broadened because of closer proximity to the Ru.^{60,61}

The bis-NMeIm complex **58** is also *cis*, the ^1H shifts being similar to those of **55** except that substitution of the N(1) proton by a Me group results in observation of a downfield shifted Me proton signal at δ 13.65, peak f (Figure 5-10). This downfield shift is much smaller than that seen for **60** and **61** (δ 43.50 and 50.30, respectively) where the Me group is closer to the paramagnetic metal centre. It is not clear why in the complexes a downfield shift occurs for an NMe, 2Me (see below) or 4(5)Me group, whereas for an NH proton an upfield shift is seen; however, this trend is consistently seen as the Me signal for coordinated MeCN is also shifted downfield (see Section 5.3.2).

Table 5.4: NMR data for the Im and Melm complexes [Ru(acac)₂(L)₂][CF₃SO₃] in d₆-acetone at r.t.

Complex	¹ H NMR					¹⁹ F{ ¹ H} NMR	
	δ Me (acac)	δ acac H	δ Im Positions				
			1 (f)	2 (g)	4 (e)		5 (d)
55 <i>cis</i> -[Ru(acac) ₂ (Im) ₂][Tf]	-16.25, -21.75	-53.15	0.45	-21.30	-2.25	-0.55	-1.93
56 <i>trans</i> -[Ru(acac) ₂ (Im) ₂][Tf]	-15.75	-40.50	-3.00	-18.90	-3.90	-4.35	-1.97
58 <i>cis</i> -[Ru(acac) ₂ (NMeIm) ₂][Tf]	-16.05, -21.55	-52.50	13.65	-18.55	-3.35	-1.00	-1.70
60 <i>cis</i> -[Ru(acac) ₂ (2MeIm) ₂][Tf]	-17.25, -23.30	-54.10	-0.90	43.50	5.15	-5.30	-1.88
61 <i>trans</i> -[Ru(acac) ₂ (2MeIm) ₂][Tf]	-19.05	-55.20	-3.40	50.30	7.85	-5.30	-2.05
62 <i>cis</i> -[Ru(acac) ₂ (5MeIm) ₂][Tf]	-15.50, -20.65	-50.30	1.95	-26.90	-1.40	7.55	-1.89
63 <i>trans</i> -[Ru(acac) ₂ (4MeIm)(5MeIm)][Tf]	-16.50, -22.50	-51.80	1.98, 1.10	-29.25	-2.35, 14.70	7.50, -2.65	-1.89

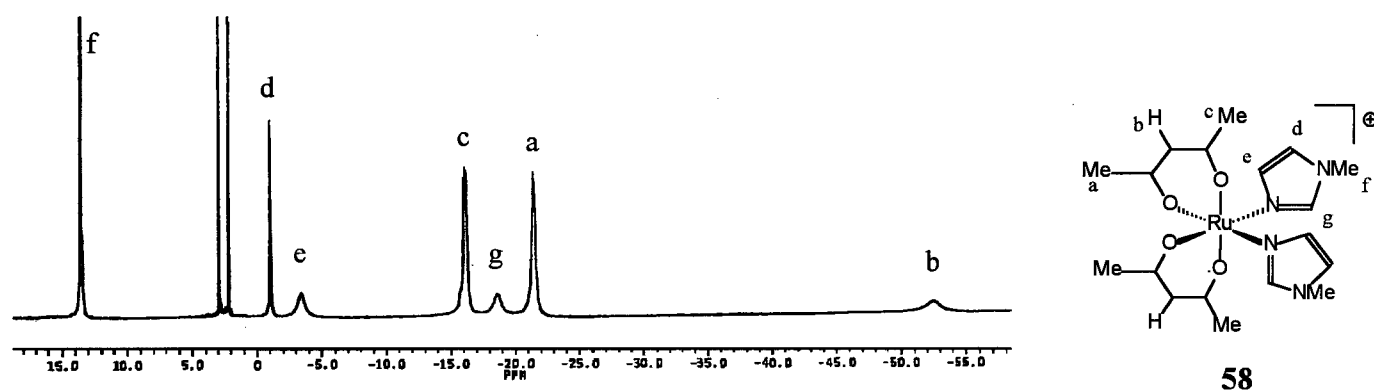


Figure 5-10: ^1H NMR spectrum of $\text{cis-}[\text{Ru}(\text{acac})_2(\text{NMeIm})_2][\text{CF}_3\text{SO}_3]$ (**58**) in d_6 -acetone.

Reaction of the more sterically demanding 2MeIm with **54** results in the formation of both the *cis* and *trans* isomers (**60** and **61**, respectively) in a 2:1 ratio. Comparison of the chemical shifts for **55** and **58** with the 2MeIm complex of the same geometry (**60**) (where the 2MeIm is presumably sterically hindered from rotating) reveals significantly different H_4 values while all the H_5 values are comparable. This is rationalized by considering that the lack of rotation has a negligible effect on H_5 , but significantly affects the paramagnetic field for both H_4 and H_2 .⁵⁷ For both **60** and **61**, the H_4 signal is shifted downfield relative to those seen for the other Ru(III) imidazole complexes, **55**, **56** and **58**. Previous literature descriptions for other Ru(III) imidazole complexes report two scenarios, H_5 being downfield from H_4 (e.g. $[\text{ImH}][\text{RuCl}_4(\text{Im})_2]$),^{62,63} or H_4 downfield from H_5 (e.g. $\text{cis-}[(\text{Im})_2(\text{NH}_3)_4\text{Ru}]\text{Br}_3$),⁶⁴ the trend observed clearly depends on the coordinated ligands. The Me signal for **60** and **61**, like that in **58**, is shifted downfield, the shift possibly being accentuated by the position of the Me group between the two nitrogen atoms of the imidazole ring. Of note, the ^1H NMR spectrum of **60** after 7 d at r.t. shows no peaks for the less sterically demanding *trans* isomer (**61**).

Isolation of a pure product from the reaction of **54** with 5MeIm was the most problematic in the syntheses of the bis-imidazole complexes. In its free, uncoordinated form, 5MeIm tautomerizes in solution to the 4MeIm species, and ^1H NMR spectra accordingly show averaged signals of the two rapidly equilibrating species. Upon coordination to a transition metal, the less sterically hindered 5Me tautomer is presumably preferred, although coordination of the

4Me tautomer has been observed previously by ^1H NMR spectroscopy;⁶⁴ there are examples of X-ray structures of Ru-5MeIm species in this thesis work, complexes **30** (chapter 4) and **62**, but there appears to be no reported structures of a Ru-4MeIm species. The ^1H NMR spectrum of the isolated red solid for the reaction described above showed signals for a mixture of the *cis* isomer of the bis-5MeIm complex (**62**) and a likely mixed *trans* 4MeIm/5MeIm species; definite assignments for the *cis* isomer were made after the ^1H NMR spectrum was obtained for a solution of the red crystals of pure **62**, and the signals for the mixed 4MeIm/5MeIm complex were inferred from the original spectrum by process of elimination (Table 5.4).

^1H NMR spectra of the nitroimidazole complexes **64-67** showed that the presence of the nitro group resulted in extremely broad peaks. In most cases, small isotropic shifts were seen for these complexes while, in the case of **64**, no peaks were observed. The ^1H NMR spectrum of **66** did not yield sufficient evidence that **EF5** had coordinated; however, the $^{19}\text{F}\{^1\text{H}\}$ NMR spectrum revealed two peaks for coordinated **EF5**. The reaction of **54** with the 5NO₂Im (metronidazole) yielded **67** for which assignable proton peaks were observed. This suggests that the proximity of the nitro group to the Ru(III) centre certainly affects the proton chemical shifts; in the case of **67**, large isotropic shifts are seen for the ^1H NMR signals, analogous to those found with the 'NO₂-free' imidazoles.

X-ray Crystal Structures of *cis*-[Ru(acac)L₂][CF₃SO₃] (L = Im or a MeIm)

Cis-[Ru(acac)₂(Im)₂][CF₃SO₃] (**55**) crystallized in the monoclinic space group C2/m, surprisingly with a solvent molecule of benzene; presumably this comes from the hexanes used to grow the crystal. The cation, whose structure is shown in Figure 5-11 (Appendix I-14), has C₂ symmetry while the triflate anion and benzene both have mirror (C_s) symmetry. The average Ru-O bond length is 1.998(2) Å for the mutually *trans* acac O-atoms and 2.007(2) Å for the acac oxygens *trans* to imidazole. These Ru-O bond lengths are comparable to those seen in the Ru(acac)₃ (average 2.00 Å)³ and are shorter than those of Ru(II) acac complexes (typically 2.06 Å)⁶⁵; see also Appendix I-13 for data on **88**. The average Ru-N bond length of 2.045(2) Å is comparable to that seen in [RuCl₅Im]²⁻ (2.044 Å),⁶⁶ suggesting that the chloro and acac ligands have similar *trans* influences. Ru(III) complexes having other nitrogen-containing ligands (*e.g.* 5MeIm, bipyridine) coordinated *trans* to the imidazole have longer Ru-N_{Im} bonds.^{67,68} Of interest,

in **55** H-bonding is seen between the Im H(1) (on N(2)) and two of the O-atoms of the triflate anion, resulting in short (2.06 Å) or longer (2.48 Å) interactions with the same imidazole. This interaction probably plays a key role in stabilizing the crystal.

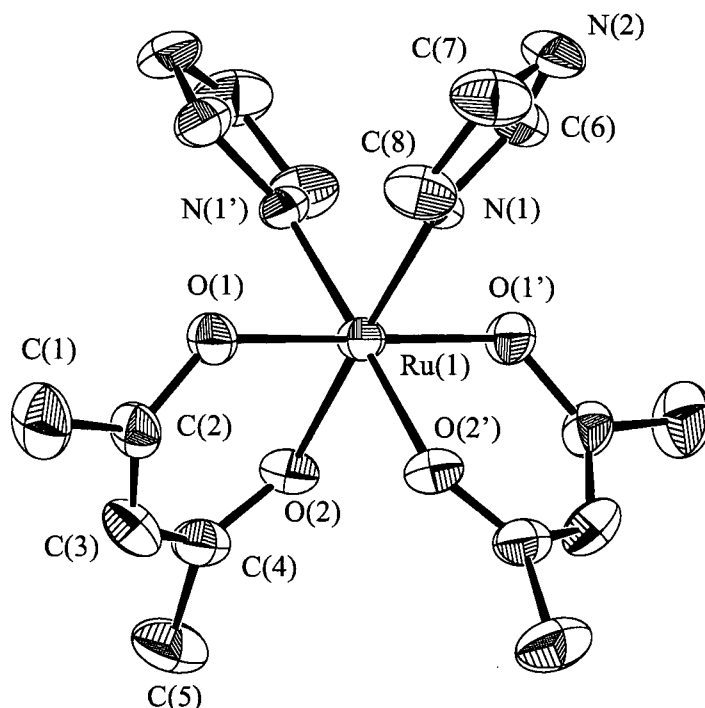


Figure 5-11: ORTEP view of the cation of *cis*-[Ru(acac)₂(Im)₂][Tf] (**55**); 50 % probability thermal ellipsoids are shown.

Cis-[Ru(acac)₂(NMeIm)₂][Tf] (**58**) crystallized in the monoclinic space group P2₁/c (Figure 5-12, Appendix I-15), and revealed an average Ru-O bond length of 2.012(2) Å, with little difference between those *trans* to acac (average 2.014 Å) vs. those *trans* to NMeIm (2.010 Å). The average Ru-N bond distance is 2.052(2) Å, which is slightly longer than that seen for the corresponding Im complex **55**; NMeIm is presumably a slightly stronger σ-donor. H-bonding interactions with triflate are also observed in **58**; for each triflate anion, only two of the O-atoms

are H-bonded, one with the Im proton on C(15) (2.25 Å) and the other with a proton of the NMe group (2.24 Å).

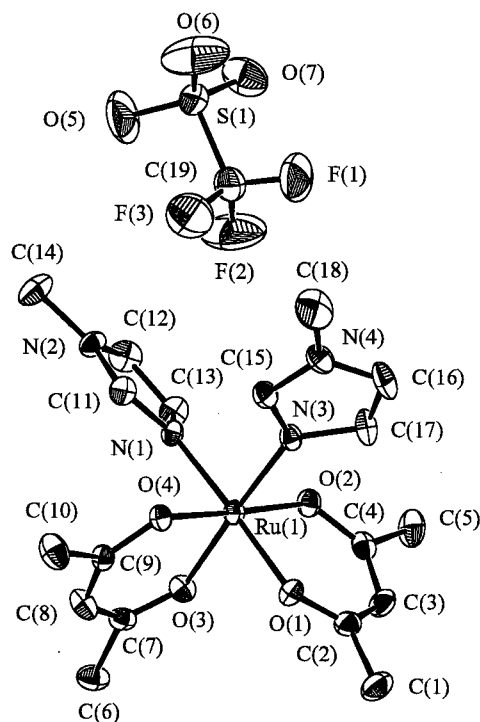


Figure 5-12: ORTEP view of *cis*-[Ru(acac)₂(NMeIm)₂][Tf] (**58**); 50 % probability thermal ellipsoids.

Analogous to **55**, *cis*-[Ru(acac)₂(2MeIm)₂][Tf] (**60**) crystallized in the monoclinic space group C2/m with 0.5 mole of hexane (from the hexanes solution used to grow the crystal). The cation (Figure 5-12, Appendix I-16) has C₂ symmetry, the triflate anion has mirror (C_s) symmetry, and the hexane although poorly resolved has C_{2h} symmetry. The average Ru-O bond length is 2.013(3) Å with little variation seen for different *trans* ligands. The average Ru-N bond is 2.060(3) Å, the longest seen for this series of *cis* acac-imidazole complexes (**55**, **58**, **60** and **62** (see below)) and is presumably due to the increased steric demand of the 2MeIm ligand. As with **55**, there are H-bonding interactions between the triflate and the imidazole, but in **60** all three O-atoms

of the triflate are involved; however, the O---H distances are now more similar (2.20 and 2.30 Å). There is also an intramolecular H-bonding interaction between the acac oxygen atom closest to the imidazole and a proton on the 2Me group.

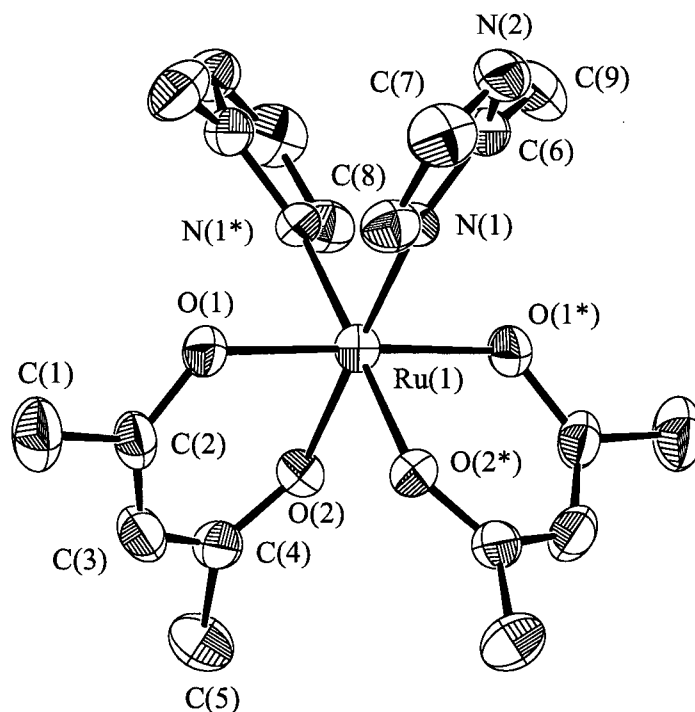


Figure 5-13: ORTEP view of the cation of *cis*-[Ru(acac)₂(2MeIm)₂][Tf] (**60**); 50 % probability thermal ellipsoids.

The final structure of this series was obtained for the bis-5MeIm complex **62** (Figure 5-14, Appendix I-17) which crystallized from a mixture of complexes that contained the mixed 4MeIm/5MeIm complex. Presumably because of the unfavourable steric interaction of a 4Me group, the bis-5MeIm complex was the major product. Complex **62** crystallized in the monoclinic space group *P2₁/n* with an average Ru-O bond length of 2.012(2) Å. The average Ru-N bond distance is 2.059(2) Å, similar to that of **60**, and H-bonding interactions between the triflate and

the imidazole are also prevalent in this structure. The H-bonds between the O-atoms of the triflate anion and the Im H(1) and H(2) (on N(2) and N(4), respectively) are much shorter (1.93 and 1.95 Å, respectively) than in the previous structures. Of note, there is also intramolecular H-bonding between the Im H(17) and H(22) (on C(11) and C(15), respectively) and the acac ligand O(1) (2.51 and 2.55 Å, respectively) as well as between the Im H(23) (on C(17)) and the acac ligand O(3) (2.54 Å).

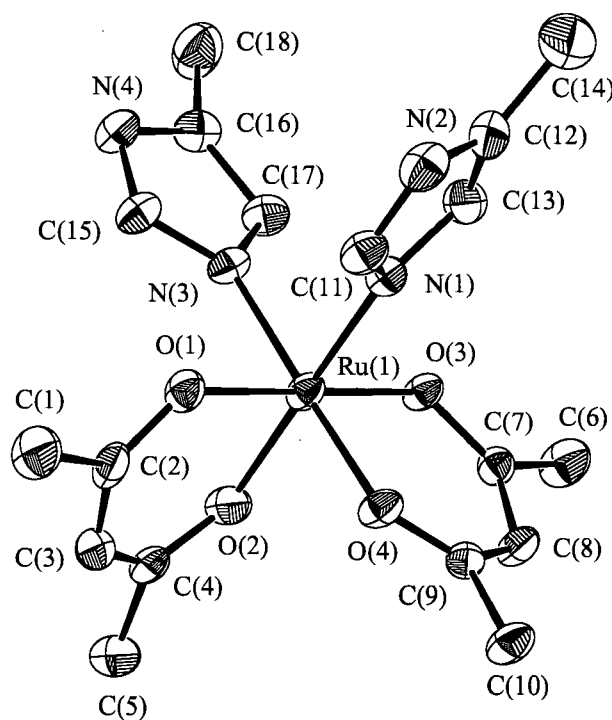


Figure 5-14: ORTEP view of the cation of *cis*-[Ru(acac)₂(5MeIm)₂][Tf] (**62**); 50 % probability thermal ellipsoids.

5.3.3.2 Bis(1,1,1,5,5,5-hexafluoroacetylacetonato)bis(imidazole)ruthenium(II) complexes

Cis-Ru(hfac)₂(MeCN)₂ (**71**) was synthesized from either Ru(hfac)₃ (**70**) or [Na][Ru(hfac)₃] (**68**), with little difference in yield or purity (Section 5.3.2). The two MeCN ligands of **71** are quite labile and the complex proved to be a useful precursor for the synthesis of bis-imidazole complexes **72**, **74**, **77** and **79-84**. Although these complexes were not soluble in H₂O, a comparison of their structural properties with those of the corresponding bis-acac complexes is useful. Presumably, because the MeCN ligands were bound stronger to the Ru(II) centre in **71** than to the Ru(III) in **54**, the number of side-products (according to TLC) was less and isolated product yields were much higher than for the acac analogues. In most cases, longer reaction times gave the bis-imidazole complex following formation of the mixed MeCN/imidazole product that was typically observed and sometimes isolated. The Ru(II)-O bond formed with the hfac ligand appears to be weaker than that in an acac analogue, as reaction with NMeIm resulted in displacement of both MeCN ligands and an hfac ligand from **71** to yield the cationic tetra-imidazole complex **75**; the associated hfac⁻ anion was exchanged with PF₆⁻ to yield **76**.

The *cis*-bis-Im (**72**) and *cis*- and *trans*-bis-2MeIm (**77** and **79**) complexes were isolated as deep red solids while the mixed 4MeIm/5MeIm complex was a red-purple solid isolated as a mixture of the *cis* and *trans* isomers, **80** and **81**. The tetra-substituted NMeIm complex was isolated as a pink-purple species. The neutral hfac complexes and the cationic complex **76** were air-stable and non-hygroscopic. The mixed MeCN/imidazole complexes were brown-orange and were only isolated for the Im and 2MeIm ligands (**73** and **78**). The nitroimidazole complexes (**82-84**) were more difficult to isolate as pure species than the MeIm complexes; for example, the data for the bis-EF5 complex (**83**) imply 3 moles of associated MeCN.

MS, EA and NMR data were used to distinguish between the mixed MeCN/imidazole and the bis-imidazole complexes. In the mass spectra the parent M⁺ peak is seen for both types of species, in addition to peaks corresponding to successive loss of the MeCN and/or imidazole ligands. The M⁺ - hfac peak is also observed for these complexes,⁶⁹ further supporting the notion (see Sections 5.3.1 and 5.3.2) that the hfac ligand is more weakly bound to the Ru(II) than acac is to the Ru(III) centre; the M⁺ - 2hfac peak is not observed. For **76**, the peaks corresponding to the successive loss of only three of the NMeIm ligands are the only ones observed. Again, the

nitroimidazole complexes do not give identifiable peaks in the mass spectra. The MS data for **83**, however, support the EA data for the presence of three 'associated' MeCN.

The electronic spectra for the $\text{Ru}(\text{hfac})_2(\text{L})_2$ complexes [$\text{L} = \text{Im}$, NMeIm , 2MeIm , $4(5)\text{MeIm}$] show little variation. Similar to data for the bis-acac complexes, absorption bands are observed in the 212-214 and 286-288 nm regions, corresponding to $\pi \rightarrow \pi^*$ transitions for the imidazole⁵⁷ and hfac²⁶ ligands, respectively. Another absorption band in the 244-246 nm region is observed that is absent in the bis-acac complexes, but is also present for **68** and **86**, anionic Ru(II) complexes that contain three and two hfac ligands, respectively, implying that this electronic transition is ligand dependent. The lower energy band observed in the 446-452 nm region for $\text{Ru}(\text{hfac})_2(\text{L})_2$ probably corresponds to a MLCT as Ru(II) is a good, ostensibly the best, metal π -donor.⁷⁰ This band is likely dependent on the coordination of both hfac ligands and is absent when only one hfac ligand is present (*i.e.* in complex **76**). The mixed ligand complex **73** shows this MLCT band, but with a higher transition energy (434 nm), perhaps related to the better π -acceptor ability of MeCN than imidazole. A charge-transfer band at 542 nm ($\epsilon > 13,000$) is typically observed for the bis-imidazole complexes, but in **73**, this band is absent and a lower intensity band ($\epsilon = 2760$) appears at 504 nm.

The NMR spectra for the diamagnetic Ru(II) species were much easier to interpret than those for the paramagnetic Ru(III) complexes (due to the absence of isotropic shifts), and provided good criteria for determining the composition of the complexes; the peaks were in the range 0 - 15 ppm. A summary of the shifts for the bis-imidazole complexes is presented in Table 5.5.

Synthesis of **72** revealed that the MeCN ligands of the precursor **71** are not easily displaced from Ru(II); there is a relatively low yield (37 %) and the mono-substituted product **73** is also isolated. The ^1H NMR spectra of **72** and **73** (Figure 5-15) show that the imidazole proton shifts are in part dependent on the proximity of the H-atoms to the Ru. For **72**, the H_1 signal, typically for an NH proton, appears furthest downfield (δ 11.92), and the H_2 signal comes at δ 7.67 (*cf.* δ 7.65 for the free ligand). One signal for each of H_4 and H_5 is observed (*cf.* the 'combined' single peak seen at δ 7.03 in the spectrum for the free ligand) and these are assigned according to their proximity to the Ru. The H_4 signal is shifted upfield to δ 6.85 while that of H_5 moved downfield to δ 7.32, these shifts being similar to those observed for the $[\text{Ru}(\text{Im})_6][\text{Tf}]_2$

Table 5.5 NMR data for the free imidazole ligands and their complexes Ru(hfac)₂(L)₂ in d₆-acetone at r. t.

Complex	¹ H NMR					¹⁹ F{ ¹ H} NMR
	δ hfac H	δ Im Positions				
		1	2	4	5	
<i>cis</i> -Ru(hfac) ₂ (Im) ₂ 72	6.10	11.92	7.67	6.85	7.32	1.78, 1.80
<i>cis</i> -Ru(hfac) ₂ (NMeIm) ₂ 74	6.02	3.83	7.54	6.73	7.20	1.82, 1.92
<i>cis</i> -Ru(hfac) ₂ (2MeIm) ₂ 77	5.98, 5.99	11.47, 7.51	2.28, 3.92	6.73, 6.45	7.09, 7.23	1.65, 1.75, 1.79, 1.84
<i>trans</i> -Ru(hfac) ₂ (2MeIm) ₂ 79	5.98	11.43	2.17	6.51	7.10	1.66, 1.79
<i>cis</i> -Ru(hfac) ₂ (4MeIm)(5MeIm) 80	6.02, 6.04	11.68	7.35, 7.48	6.58	7.07	1.64, 1.73, 1.76, 1.81
<i>trans</i> -Ru(hfac) ₂ (4MeIm)(5MeIm) 81	6.02	11.61	7.31, 7.46	6.56	7.02	1.56, 1.79
Im	---	12.04	7.65	7.03	7.03	---
NMeIm	---	3.70	7.48	6.90	7.04	---
2MeIm	---	11.65	2.26	6.85	6.85	---
4(5)5MeIm	---	11.93	7.52	6.73	2.16	---

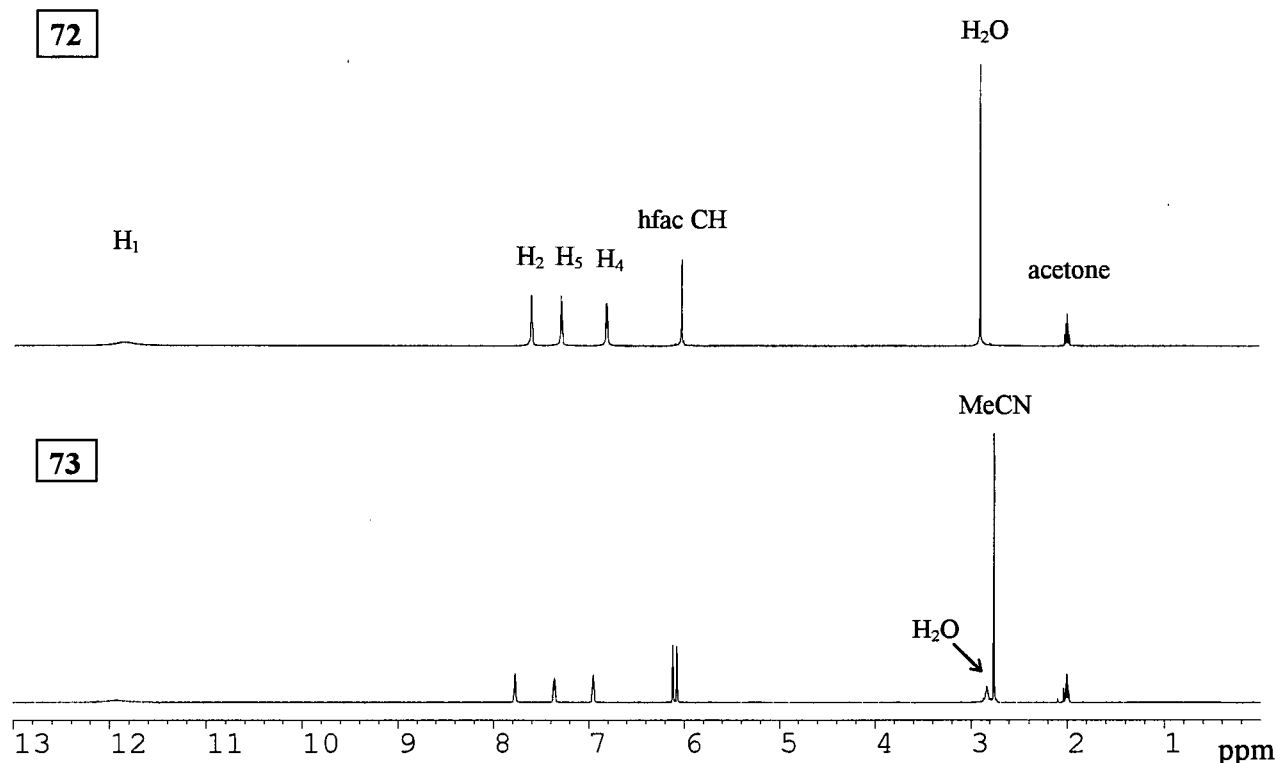


Figure 5-15: ^1H NMR spectra for complexes **72** and **73** in d_6 -acetone.

complex (see chapter 4, Section 4.2.1.1). The ^1H NMR spectrum for **73** reveals shifts for the Im protons similar to those for **72**; the hfac methine protons give two singlets, indicating magnetic inequivalence for the asymmetric, mixed-ligand *cis*-complex, and the peak at δ 2.70 confirms one MeCN ligand. The $^{19}\text{F}\{^1\text{H}\}$ NMR spectrum of **72** shows two singlets for the two different CF_3 groups, implying a *cis* configuration; for *trans* imidazoles only one singlet would be observed for magnetically equivalent CF_3 groups. The mixed ligand species **73**, however, gives rise to four signals for the four inequivalent CF_3 groups.

The bis-NMeIm complex (**74**) was the only species isolated from the reaction of NMeIm with **71**, implying that, as expected, NMeIm is a stronger coordinating ligand than Im. The proton shifts of the NMeIm ligand are similar to those seen for **72**, and the NMe signal at δ 3.83 is downfield from that of the free ligand (δ 3.65). Interestingly, this spectrum (as well as those for all the bis-hfac bis-imidazole complexes) exhibits fine structure for the H_2 , H_4 and H_5 signals; the ^1H NMR spectrum of the free ligand, conversely, reveals only singlets for these protons, but upon coordination of the ligand to the Ru centre, the signals for H_2 , H_4 , and H_5 appear as broad triplets (see Figure 5-16). This fine structure also depends on the number of coordinated hfac ligands, as

coupling is lost when one of the hfac ligands in complex **74** is replaced by two NMeIm ligands (complex **76**). The $^{19}\text{F}\{^1\text{H}\}$ NMR spectrum of **74** supports a *cis* geometric assignment as two singlets are observed. The signals for the two inequivalent CF_3 groups are more separated (0.10 ppm) than are those in **72** (0.02 ppm).

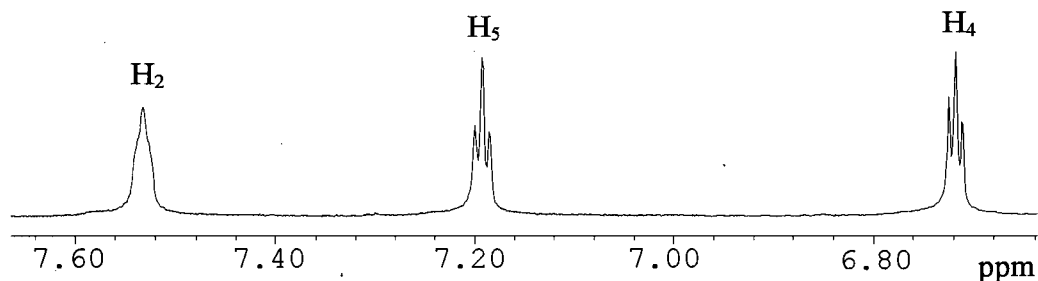


Figure 5-16: Proton signals for the coordinated NMeIm ligands of **74** in d_6 -acetone.

Reaction of **71** with neat NMeIm results in displacement of both MeCN ligands and an hfac ligand to generate the tetra-NMeIm complex $[\text{Ru}(\text{hfac})(\text{NMeIm})_4][\text{hfac}]$ (**75**), which is 'better stabilized' as the PF_6^- salt (**76**). The ^1H NMR spectrum reveals two sets of NMeIm proton signals, corresponding to those of the mutually *trans* NMeIm ligands and those *trans* to hfac. The ^1H NMR 2D COSY spectrum shows coupling between different protons within the two types of NMeIm ligand; the fine structure for this coupling, however, was not observed. It is inferred that the ^1H signals for the NMeIm ligands *trans* to hfac will appear further downfield than the corresponding ones for the mutually *trans* NMeIm ligands (Figure 5-17). The $^{19}\text{F}\{^1\text{H}\}$ NMR spectrum reveals one singlet and one doublet corresponding to the hfac ligand and the $^1J_{\text{PF}}$ coupling in PF_6^- , respectively.

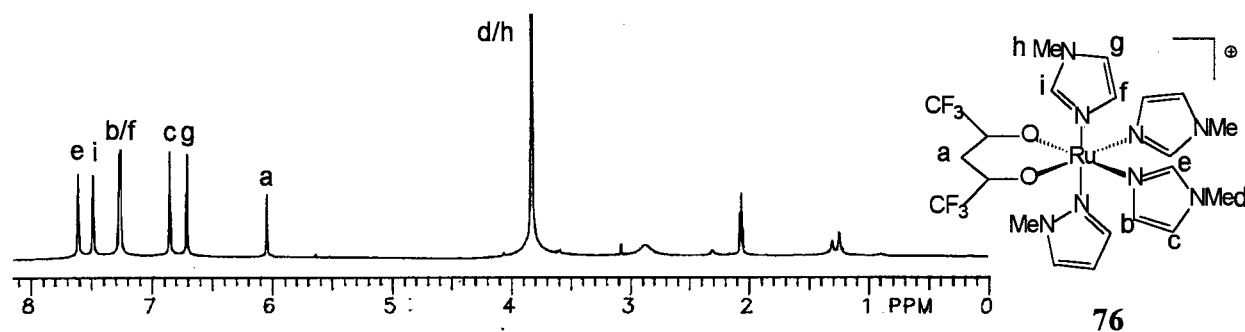


Figure 5-17: ^1H NMR spectrum of $[\text{Ru}(\text{hfac})(\text{NMeIm})_4][\text{PF}_6]$ (**76**) in d_6 -acetone.

Reaction of **71** with the more sterically demanding 2MeIm ligand results in the formation of both the *cis* (**77**) and *trans* (**79**) isomers of the bis-substituted complex, as well as a small amount of the mono-substituted *cis*-complex (**78**). Unlike the corresponding acac complexes **60** and **61**, the chromatographic separation of **77** and **79** was facile, and the ratio of the isolated yields suggests that the *trans* isomer is more stable (*cis* (**77**) : *trans* (**79**) = 1 : 5). The ^1H NMR spectrum of **77** (Figure 5-18) is different from those of the other two *cis* complexes, **72** and **74** in that the two 2MeIm ligands are magnetically inequivalent and give rise to different signals. The inequivalence of the 2MeIm ligands also affects the magnetic environment of the hfac ligands, and two methine proton signals are observed (δ 5.98 and 5.99). The H_1 signal for one of the 2MeIm

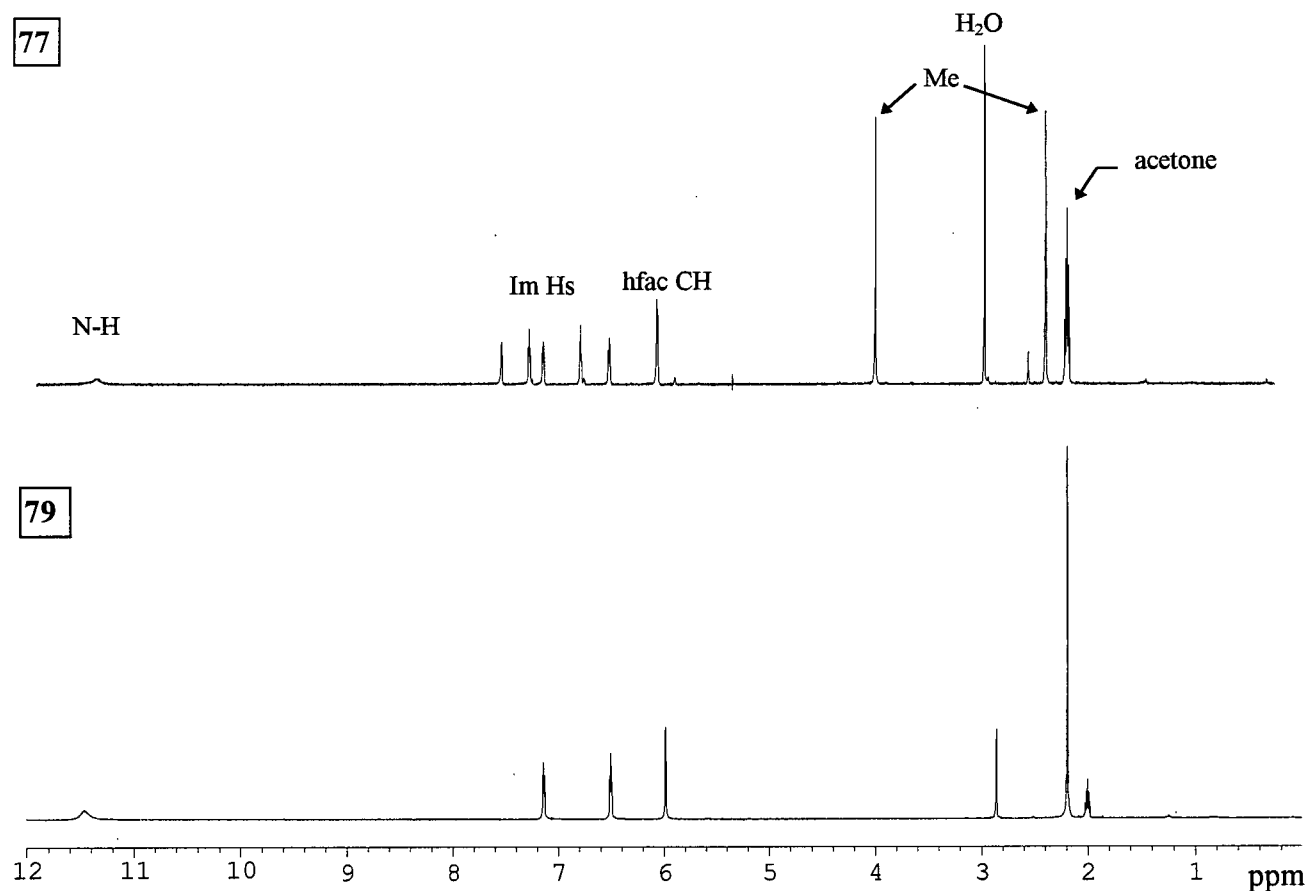


Figure 5-18: ^1H NMR spectra of *cis*- and *trans*- $\text{Ru}(\text{hfac})_2(2\text{MeIm})_2$ (**77** and **79**) in d_6 -acetone.

ligands is shifted ~ 4 ppm upfield relative to that of the other (δ 7.51 vs. 11.47); moreover, the two signals of the two Me groups are separated by 1.64 ppm. The H_4 and H_5 proton signals are not greatly shifted from those of the free ligand, however, one of the H_4 signals is considerably upfield (δ 6.45) relative to that of the free ligand (δ 6.85). These observations imply that one of the 2MeIm ligands strongly interacts (probably intramolecularly) with an hfac ligand; however, no X-ray structure data are available. The 1H NMR spectrum of **79** shows a single set of signals for the imidazole protons, and thus the *trans* configuration is assigned. The $^{19}F\{^1H\}$ NMR spectral characteristics are unusual. Instead of the expected two singlets for the *cis* isomer (**77**) (*cf.* data for **72** and **74**) four signals are seen, as observed for the mixed-ligand complex **73**. The variation in the δ_F values suggests interaction between the CF_3 groups and the 2MeIm ligands, which in turn affects the δ values of the proton signals. For **79**, unexpectedly two peaks are observed, implying that the CF_3 groups interact with the 2MeIm ligands.

Synthesis of the bis-5MeIm product was problematic because of the ability of the free ligand to tautomerize in solution. Further, the sterically demanding 4MeIm tautomer (as with 2MeIm) leads to formation of a *trans* isomer. The 1H NMR spectrum of the isolated complex (Figure 5-19) reveals the presence of not only *cis* and *trans* isomers (**80** and **81**), but also coordination of the two tautomeric forms of 5MeIm. The *cis* isomer has two inequivalent hfac ligands as shown by two different methine proton signals; the more symmetric *trans* isomer gives only one methine proton signal. The 4Me signals are assigned upfield relative to the 5Me signals because of the closer proximity of the 4Me to the Ru(II); two signals are observed for each moiety

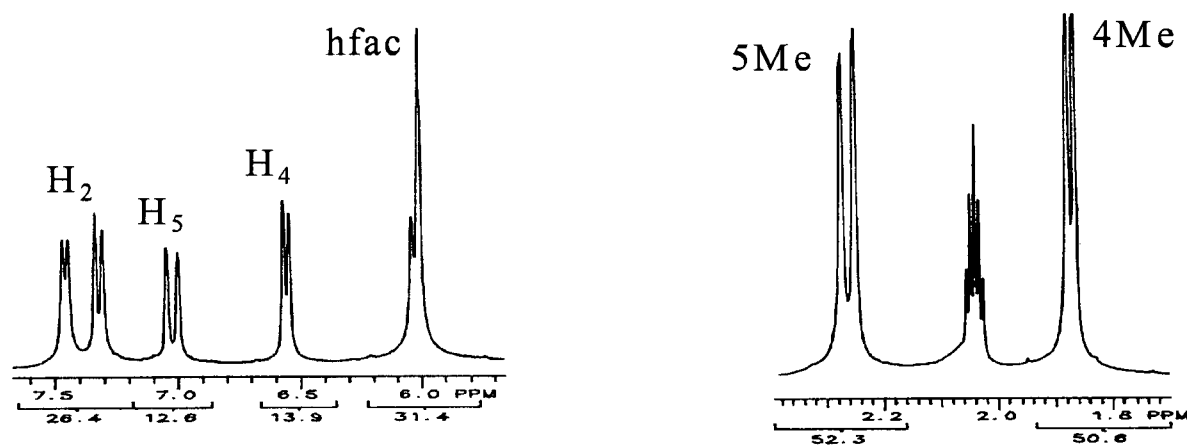


Figure 5-19: 1H NMR of the mixed-ligand complex $Ru(hfac)_2(4MeIm)(5MeIm)$ in d_6 -acetone.

because of the presence of the two geometrical isomers. Also, two H_4 and H_5 signals corresponding to the two isomers are seen in addition to four H_2 signals. As with complexes **77** and **79**, four and two signals, respectively, are observed in the $^{19}\text{F}\{^1\text{H}\}$ NMR spectrum for the mixture of **80** and **81**; the coordination of the two tautomers induces magnetic inequivalence of the CF_3 groups.

The nitroimidazole complexes were also analyzed using ^1H and $^{19}\text{F}\{^1\text{H}\}$ NMR spectroscopy, but the ^1H peaks are quite broad (*cf.* data for the bis-acac complexes, Section 5.3.3.1). Complex **82** exhibits coordination of $2\text{NO}_2\text{Im}$ in that the singlet for H_4 and H_5 of the free ligand is split into a pair of broad overlapping singlets. The two CF_3 signals seen at δ 2.10 and -0.55 in the $^{19}\text{F}\{^1\text{H}\}$ NMR spectrum suggest *cis* coordination of the two $2\text{NO}_2\text{Im}$ ligands; the large difference in the δ values suggests possible intramolecular interaction of the $2\text{NO}_2\text{Im}$ with two of the CF_3 groups. The ^1H NMR spectrum for **83** reveals insufficient information to confirm coordination of **EF5**; however, the $^{19}\text{F}\{^1\text{H}\}$ NMR spectrum shows three peaks with two corresponding to the side-chain of the **EF5** and the third consistent with the signal for four equivalent CF_3 groups, implying a *trans* geometry for the bis-**EF5** complex.

The Ru(II) bis-hfac complexes reported here have been generally well characterized, although attempts to grow crystals suitable for X-ray crystallographic analysis were unsuccessful. Of note, the Ru(III) bis-acac complexes readily crystallize, suggesting that another moiety, such as triflate, is needed to induce crystallization in the solid state; the observation of H-bonding interactions between the triflate anion and the imidazole ligands of the bis-acac complexes lends credence to this suggestion.

5.3.3.3 Cyclic Voltammetric Results for the Bis-imidazole Complexes

The cyclic voltammogram was obtained using a standard 3-electrode system (chapter 2, Figure 2.3) for most of the Ru(II) and Ru(III) β -diketonate complexes reported here, excluding only the NO_2Im complexes for which no suitable CV plot could be obtained. The working and counter electrodes were the standard Pt plates while the reference electrode was a Pt wire (and not the normal SCE or Ag/AgCl reference electrodes). The results obtained using this system were reproducible when the internal standard FeCp_2 was added to each sample. The $E_{1/2}$ value vs. the Pt

electrode was corrected against the internal standard, and the final reduction potential is reported vs. the SCE in Table 5.1 (p. 210).

The Ru(III) \rightarrow Ru(II) $E_{1/2}$ values for the $[\text{Ru}(\text{acac})_2(\text{L})_2][\text{Tf}]$ complexes ($\text{L} = \text{Im}$, NMeIm, 2MeIm, 5MeIm) are all negative, in agreement with the values reported for other bis-acac complexes,^{6,15} and are found in the range -439 to -546 mV. A comparison of the values for the *cis*-complexes reveals that substitution of the methyl group at different positions on the imidazole ring affects the potential, with the more sterically demanding 2MeIm decreasing the $E_{1/2}$ value. This decrease indicates relative stabilization of the Ru(III) oxidation state as the ligand becomes bulkier ($E_{1/2} \text{Im} > \text{NMeIm} > 5\text{MeIm} > 2\text{MeIm}$). In cases where both geometrical isomers were isolated (**55** and **56**, **60** and **61**, and **77** and **79**), the *cis* complex has a higher $E_{1/2}$ value (by ~ 30 mV) than the *trans* complex, an observation previously noted for other Ru systems.⁷¹⁻⁷³ The mixed MeCN/imidazole complexes (**57**, **59** and **73**) were found to have a higher $E_{1/2}$ value (by ~ 22 mV) than the corresponding bis-Im species, as the π -accepting MeCN stabilizes the Ru(II) oxidation state (see Section 5.3.2). Substitution of an acac by an hfac ligand further stabilizes the Ru(II) centre; for example, there is an increase in the $E_{1/2}$ value by +690 mV when one of the acac ligands on **58** is substituted by hfac to yield **90**, and another 600 mV when the second acac is replaced (**90** \rightarrow **74**). The increase in $E_{1/2}$ leads bis-imidazole complexes containing either an acac and an hfac ligand (**90**) or two hfac ligands (**72**, **74**, **77**, **79** and **80**) to be most readily isolated in the Ru(II) oxidation state.

The Ru(III) \rightarrow Ru(II) $E_{1/2}$ values for the $\text{Ru}(\text{hfac})_2(\text{L})_2$ complexes ($\text{L} = \text{Im}$, NMeIm, 2MeIm, 4(5)MeIm) are all positive, in agreement with the values reported for other bis-hfac complexes,¹⁰ and are found in the range 452 to 554 mV. Again, the same trend is observed for the $E_{1/2}$ values of the bis-imidazole complexes ($\text{Im} > \text{NMeIm} > 4(5)\text{MeIm} > 2\text{MeIm}$). For the complexes containing 2MeIm, the $E_{1/2}$ value of the *cis* isomer (**77**) is more positive than that of the *trans* isomer (**79**) (Figure 5-20), analogous to data seen for the bis-acac complexes.

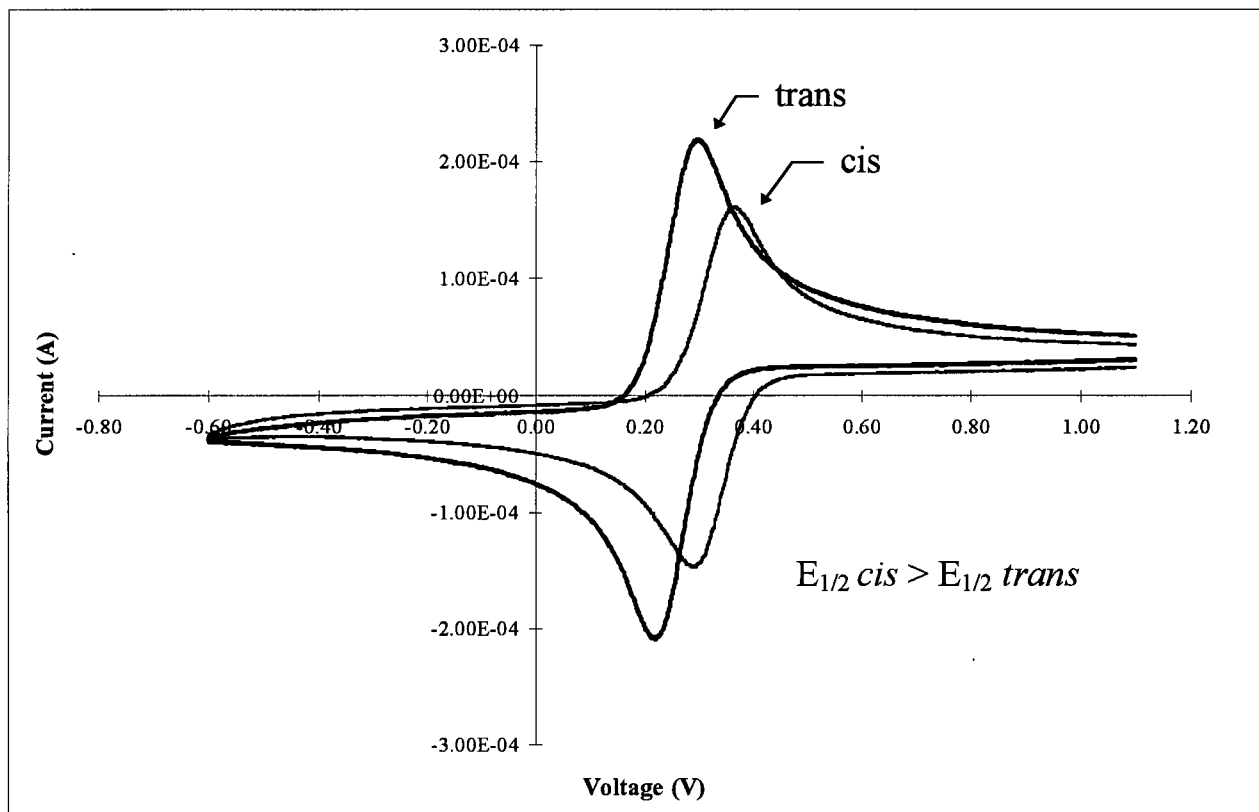


Figure 5-20: Cyclic voltammograms for *cis*- and *trans*- $\text{Ru}(\text{hfac})_2(2\text{MeIm})_2$ in 0.1 M Bu_4NClO_4 in MeCN.

5.4 References

- 1 Veening, H.; Bachman, W. E.; Wilkinson, D. M. *J. Gas Chromatog.* **1967**, 248.
- 2 Johnson, A.; Everett, Jr., G. W. *J. Am. Chem. Soc.* **1972**, 94, 1419.
- 3 Knowles, T. S.; Howells, M. E.; Howlin, B. J.; Smith, G. W. *Polyhedron* **1994**, 13, 2197.
- 4 Hiroaki, K.; Saito, K. *Bull. Chem. Soc. Jpn.* **1979**, 52, 3545.
- 5 Endo, A.; Shimizu, K.; Satô, G. P.; Mukaida, M. *Chem. Lett.* **1984**, 437.
- 6 Endo, A.; Shimizu, K.; Satô, G. P. *Chem. Lett.* **1985**, 581.
- 7 Hoshino, Y.; Yukawa, Y.; Endo, A.; Shimizu, K.; Satô, G. P. *Chem. Lett.* **1987**, 845.
- 8 Satsu, Y.; Endo, A.; Shimizu, K.; Satô, G. P.; Ono, K.; Watanabe, I.; Ikeda, S. *Chem. Lett.* **1986**, 585.
- 9 Endo, A.; Kajitani, M.; Mukaida, M.; Shimizu, K.; Satô, G. P. *Inorg. Chim. Acta* **1988**, 150, 25.
- 10 Hoshino, Y.; Yukawa, Y.; Maruyama, T.; Endo, A.; Shimizu, K.; Satô, G. P. *Inorg. Chim. Acta* **1990**, 174, 41.
- 11 Hoshino, Y.; Takahashi, R.; Shimizu, K.; Satô, G. P.; Aoki, K. *Inorg. Chem.* **1990**, 29, 4816.
- 12 Endo, A.; Hoshino, Y.; Hirakata, K.; Takeuchi, Y.; Shimizu, K.; Furushima, Y.; Ikeuchi, H.; Satô, G. P. *Bull. Chem. Soc. Jpn.* **1989**, 62, 709.
- 13 Endo, A.; Watanabe, M.; Hayashi, S.; Shimizu, K.; Satô, G. P. *Bull. Chem. Soc. Jpn.* **1978**, 51, 800.
- 14 Endo, A. *Bull. Chem. Soc. Jpn.* **1983**, 56, 2733.
- 15 Patterson, G.S.; Holm, R.H. *Inorg. Chem.* **1972**, 11, 2285.
- 16 Tang, J.; Shimizu, K.; Osteryoung, R.A. *Inorg. Chem.* **1992**, 31, 2328.
- 17 Kobayashi, K.; Satsu, Y.; Hoshino, Y.; Arai, S.; Hatakeyama, K.; Endo, A.; Shimizu, K.; Satô, G.P. *Bull. Chem. Soc. Jpn.* **1989**, 62, 3252.
- 18 Kobayashi, T.; Nishina, Y.; Shimizu, K.; Satô, G.P. *Chem. Lett.* **1988**, 1137.
- 19 Kasahara, Y.; Hoshino, Y.; Shimizu, K.; Satô, G.P. *Chem. Lett.* **1990**, 381.
- 20 Oomura, K.; Ooyama, D.; Satoh, Y.; Nagao, N.; Nagao, H.; Howell, F.S.; Mukaida, M. *Inorg. Chim. Acta* **1998**, 269, 342.
- 21 Elliott, M.G.; Shepherd, R.E. *Inorg. Chem.* **1987**, 26, 2067.
- 22 Connelly, N. G.; Geiger, W. E. *Chem. Rev.* **1996**, 96, 877.

- 23 Knifton, J. F. *J. Org. Chem.* **1976**, *41*, 1200.
- 24 Gmelins Handbuch der Anorganischen Chemie, 8th ed.; Ruthenium Ergänzungsband, Verlag Chemie, Weinheim, 1970, p. 468.
- 25 Endo, A.; Shimizu, K.; Satô, G. P.; Mukaida, M. *Chem. Lett.* **1985**, 1984.
- 26 Satsu, Y.; Endo, A.; Shimizu, K.; Satô, G. P.; Matsuzawa, H.; Kaizu, Y.; Kobayashi, H. *52nd Annual Meeting of the Chemical Society of Japan*, Kyoto, 1986, 4K05; through ref. 9.
- 27 Holtzclow, Jr., H. F.; Collman, J. P. *J. Am. Chem. Soc.* **1957**, *79*, 3318.
- 28 Nakamoto, K.; Morimoto, Y.; Martell, A. J. *Am. Chem. Soc.* **1961**, *83*, 4533.
- 29 Nakamoto, K. *Infrared and Raman Spectra of Inorganic and Coordination Compounds*, 3rd ed.; Wiley, New York, 1978.
- 30 Eaton, D. R.; Phillips, W. D. *Advan. Magn. Resonance* **1965**, *1*, 103.
- 31 Zuman, P. *Substituent Effects in Organic Polarography*; Plenum Press, New York, 1967.
- 32 Murov, S. L. *Handbook of Photochemistry*; Marcel Dekker, Inc., New York, 1973, Sec. 26.
- 33 Butler, J. N., *In Advances in Electrochemistry and Electrochemical Engineering*; P. Delahay and C. W. Tobias, Eds.; Interscience Publishers, New York, 1970, vol. 7, p. 82.
- 34 Mann, C. K.; Barnes, K. K. *Electrochemical Reactions in Non-aqueous Systems*; Marcel Dekker, New York, 1970, Ch. 13.
- 35 Olson, D. C.; Mayweg, V. P.; Schrauzer, G. N. *J. Am. Chem. Soc.* **1966**, *88*, 4876.
- 36 DeArmand, K.; Forste, L. S. *Spectrochim. Acta* **1963**, *19*, 1393.
- 37 Cargill Thompson, A. M. W.; Bardwell, D. A.; Jeffery, J. C.; Rees, L. H.; Ward, M. D. *J. Chem. Soc., Dalton Trans.* **1997**, 721.
- 38 Judd, R. J.; Cao, R.; Biner, M.; Armbruster, T.; Bürgi, H.-B.; Merbach, A. E.; Ludi, A. *Inorg. Chem.* **1995**, *34*, 5080.
- 39 James, B. R.; Ochiai, E.; Rempel, G. L. *Inorg. Nucl. Chem. Lett.* **1971**, *7*, 781.
- 40 Evans, I. P.; Spencer, A.; Wilkinson, G. *J. Chem. Soc., Dalton Trans.* **1973**, 204.
- 41 Bernhard, P.; Sargeson, A. M. *J. Chem. Soc., Chem. Commun.* **1985**, 1516.
- 42 Kido, H.; Saito, K. *Inorg. Chem.* **1977**, *16*, 397.
- 43 Saito, K.; Murakami, M. *Bull. Chem. Soc. Jpn.* **1972**, *45*, 2472.

-
- 44 Kido, H.; Saito, K. *Bull. Chem. Soc. Jpn.* **1979**, *52*, 3545.
- 45 Pace, E. L.; Noe, L. J. *J. Chem. Phys.* **1968**, *49*, 5317.
- 46 Endres, H. *In Comprehensive Coordination Chemistry*, Vol. 2; G. Wilkinson, R. D. Gillard, and J. A. McCleverty, Eds.; Pergamon Press, Oxford, U.K., 1987, p. 264.
- 47 Newton, W. E.; Searles, J. E. *Inorg. Chim. Acta* **1973**, *7*, 349.
- 48 Clarke, R. E.; Ford, P. C. *Inorg. Chem.* **1970**, *9*, 227.
- 49 Fogg, D. E.; Rettig, S. J.; James, B. R. *Can. J. Chem.* **1995**, *73*, 1084.
- 50 Rodgers, G. E. *Introduction to Coordination, Solid State, and Descriptive Inorganic Chemistry*; McGraw-Hill, New York, 1994, p. 164.
- 51 Costain, C. C. *J. Chem. Phys.* **1958**, *29*, 864.
- 52 Swanson, B.; Shriver, D. F.; Ibers, J. A. *Inorg. Chem.* **1969**, *8*, 2182.
- 53 Das, B. K.; Chakravarty, A. R. *Inorg. Chem.* **1991**, *30*, 4978.
- 54 DeGiovani, W. F.; Deronzier, A. *J. Chem. Soc., Chem. Commun.* **1992**, 1461.
- 55 Rapaport, I.; Helm, L.; Merbach, A. E.; Bernhard, P.; Ludi, A. *Inorg. Chem.* **1988**, *27*, 873.
- 56 Chan, P. K. L. Ph.D. Thesis, University of British Columbia, 1988.
- 57 LaChance-Galang, K. J.; Doan, P. E.; Clarke, M. J.; Rao, U.; Yamano, A.; Hoffman, B. M. *J. Am. Chem. Soc.* **1995**, *117*, 3529.
- 58 Krogh-Jespersen, K.; Westbrook, J. D.; Potenza, J. A.; Schugar, H. J. *J. Am. Chem. Soc.* **1987**, *109*, 7025.
- 59 Krogh-Jespersen, K.; Schugar, H. J. *Inorg. Chem.* **1984**, *23*, 4390.
- 60 Alessio, E.; Balducci, G.; Lutman, A.; Mestroni, G.; Calligaris, M.; Attia, W. M. *Inorg. Chim. Acta* **1993**, *203*, 205.
- 61 Toi, H.; La Mar, G. N.; Margalit, R.; Che, C. M.; Gray, H. B. *J. Am. Chem. Soc.* **1984**, *106*, 6213.
- 62 Anderson, C.; Beauchamp, A. L. *Inorg. Chem.* **1995**, *34*, 6065.
- 63 Anderson, C.; Beauchamp, A. L. *Can. J. Chem.* **1995**, *73*, 471.
- 64 Clarke, M. J.; Bailey, V. M.; Doan, P. E.; Hiller, C. D.; LaChance-Galang, K. J.; Daghlilian, H.; Mandal, S.; Bastos, C. M.; Lang, D. *Inorg. Chem.* **1996**, *35*, 4896.
- 65 Ernst, R. D.; Melendez, E.; Stahl, L. *Organometallics* **1991**, *10*, 3635.

- 66 Keppler, B. K.; Wehe, D.; Endres, H.; Rupp W. *Inorg. Chem.* **1987**, 26, 844.
- 67 Keppler, B. K.; Rupp, W.; Juhl, U. M.; Endres, H.; Niebl, R.; Balzer, W. *Inorg. Chem.* **1987**, 26, 4366.
- 68 Reddy, K. B.; Cho, M. P.; Wishart, J. F.; Emge, T. J.; Isied, S. S. *Inorg. Chem.* **1996**, 35, 7241.
- 69 Morris, M. L.; Koob, R. D. *Inorg. Chem.* **1983**, 22, 3502.
- 70 Richardson, D. E.; Walker, D. D.; Sutton, J. E.; Hodgson, K. O.; Taube, H. *Inorg. Chem* **1979**, 18, 2216.
- 71 Lever, A. B. P. *Inorg. Chem.* **1990**, 29, 1271.
- 72 Siebald, H. G. L.; Fabre, P.-L.; Dartiguenave, M.; Dartiguenave, Y.; Simard, M.; Beauchamp, A. L. *Polyhedron* **1996**, 15, 4221.
- 73 Queiroz, S. L.; Batista, A. A.; Oliva, G.; do P. Gambardella, M. T.; Santos, R. H. A.; MacFarlane, K. S.; Rettig, S. J.; James, B. R. *Inorg. Chim. Acta* **1998**, 267, 209.

Chapter 6

In Vitro Evaluation of Selected Nitroimidazoles and Ruthenium Nitroimidazole Complexes

6.1 Introduction

The rapid growth of some tumours can lead to a decrease in blood supply to various parts of the tumour resulting in regional hypoxia and necrosis. The diffusional barrier, which prevents oxygen from reaching the hypoxic regions of the tumour, can also prevent the diffusion of an agent to the targeted area¹ (see Section 1.2). The hypoxic cells have also been shown to be radioresistant,² a problem which can lead to treatment failure, thus making it essential to identify the presence of hypoxia in individual patients.

A number of groups have shown that the bioreductive activation of nitroimidazoles leads to binding (by formation of adducts to cellular macromolecules), a phenomenon which is maximal in the absence of oxygen.^{3,4} This compound binding has been used to measure hypoxia in a number of ways. Firstly, incorporation of radioactive atoms into the compound allow for the development of different types of radioactivity assays,⁵ including PET,⁶⁻⁸ while the presence of a fluorine-containing compound allow for the use of MRI.⁹⁻¹¹ Secondly, the antigenic properties of the compound-adducts allow for secondary detection by monoclonal antibodies.¹²⁻¹⁵ The latter technique is the one focused on in this project.

The effects that the variation of the side-chain, the type and number of halogens on the side-chain and the position of the nitro group on the imidazole ring, had on the MoAb's recognition were investigated. The toxicity, cell accumulation and DNA-binding of select Ru complexes were also examined, including possible radiosensitizing ability of two of these Ru complexes. The experiments within this chapter resulted from the collaboration between Prof. James at the Univ. of B.C. (synthesis of new compounds), Dr. Koch at the Univ. of Pennsylvania (supplier of monoclonal antibodies ELK3-51 and ELK5-A8 made by Dr. Lord) and Dr. Skov at the B.C. Cancer Research Centre (toxicity, accumulation, DNA-binding, radiosensitization and immunocyto-chemistry). The cell line

used for all experiments was mouse squamous cell carcinoma SCCVII because of past experience with this cell line which was known to be hypoxic in tumours and could be tested both *in vitro* (cells) and *in vivo* (tumour).

6.2 Experimental

6.2.1 Materials and Methods

6.2.1.1 Media

Eagle's minimum essential medium (GIBCO) formed the basis of the α -modified medium used for the maintenance and incubation of the SCCVII cells. (Of note, the following description of media $\alpha x/y$ refer to: $x = +$, with serum; $x = -$, without serum; $y = +$, with NaHCO_3 buffer; $y = -$, without NaHCO_3 buffer.) To make α -/- medium, one packet of α -medium powder and 10,000 units of penicillin/streptomycin antibiotic (GIBCO) were added to 10 L of ddH₂O and the solution was stirred for 2 h at r.t. Preparation of $\alpha+/+$ medium involved the addition of fetal bovine serum (GIBCO) to a final concentration of 10 % and NaHCO_3 (20 g / 10 L) to the α -/- solution before filtration. The pH was adjusted to 7.30 with 4 M $\text{NaOH}_{(\text{aq})}$. Preparation of $\alpha+/-$ medium was accomplished by adding 10 % (v/v) of fetal bovine serum to α -/- medium buffered with 10 mM HEPES. All media were stored at 4 °C.

6.2.1.2 General Solutions

PBS The phosphate buffered saline (PBS) solution was prepared by dissolving NaCl (160 g), KCl (4 g), Na_2HPO_4 (23 g) and KH_2PO_4 (4 g) in ddH₂O (20 L). The 10x PBS was made by dissolving the same salt quantities in 2 L ddH₂O.

'PBS' This solution was prepared by adding 0.25 % (v/v) 1.0 M NaN_3 (prepared by dissolving 0.65 g NaN_3 in 10 mL ddH₂O) and 0.25 % (v/v) 0.1 M Thimerosal (prepared by dissolving 0.41 g Thimerosal in 10 mL ddH₂O) to PBS. This solution was only used for the Ab binding experiments.

PBS^{tt} This solution is composed of 0.3 % Tween 20 in 'PBS' (1.5 mL per 500 mL PBS).

Paraformaldehyde (pF) This solution was prepared by adding 100 μL of 1 M NaOH to 60 mL ddH₂O and then heating the mixture to boiling. The mixture was then added to a slurry of 4 g paraformaldehyde (pF) in 30 mL ddH₂O, yielding a colourless solution. To the cool solution (at 0 °C) 10 mL of 10x PBS was added and then the mixture was filtered through a sterile 0.22 μm Millex[®] filter. The final step was to add 100 μL of 1 M HCl to the filtered solution. This solution was stored at 0 °C.

Ab Carrier This solution contains 1.5 % bovine serum albumin (BSA, 0.15 g) in 10 mL PBS^{tt}; the BSA is partially insoluble, and so the suspension is stirred for 1 h at 37 °C prior to use.

Blocking Solution A mixture containing 20 % (v/v) fresh skim milk and 5 % (v/v) mouse serum was added to Ab carrier. The treatment of the cells with this solution prior to the addition of Ab is necessary to prevent the Ab from binding to other sites within the cell other than those where the compound is present (*i.e.* this "blocks" non-specific activity of the Ab).

TE This mixture contains 10 mM tris(hydroxymethyl)aminomethane (T) and 1 mM ethylenediaminetetraacetic acid (E, which chelates many metal contaminants). These additives are important in forming a buffered solution of pH 8.0.

TNE This is a solution of TE containing 150 mM NaCl. The addition of NaCl at physiological concentration ensures that the cells are not hypertonic with respect to the external solution.

TNE* This solution was made by addition of the following components to 25 mL of TNE: 0.5 mL of 10 % sodium dodecylsulfate (SDS) used to solubilize the cytoplasmic and nuclear membranes, leading to the formation of micelles; 0.5 mL of RNase (5 mg of RNase A dissolved in 0.5 mL ddH₂O) which digests the majority of RNA within the cell; 0.5 mL of Proteinase K (5 mg in 0.5 mL ddH₂O), a standard digestion enzyme with general proteolytic activity which cleaves amino acid linkages, leading to the breakdown of proteins within the cell.

6.2.1.3 Cell Handling

All the work performed with the SCCVII cells was done using sterile techniques in order to avoid contamination. The cells were grown in medium and/or large tissue culture flasks, in α +/- medium, in a tray incubator (National, Inc.) at 37 °C containing an atmosphere of 5 % CO₂ to maintain physiological pH. The SCCVII cells exhibited a doubling time of ~14 h and so the cells were generally plated 2 days prior to the commencement of the experiment (area of flask: med = 75 cm²; large = 175 cm²). On the day of the experiment, the medium was poured off and the cells were rinsed with sterile PBS (2 x 10 mL), followed by the addition of 0.25 % trypsin in Hank's buffer. (The addition of trypsin releases the cells from the plastic by breaking down the protein coating on the cell membrane which otherwise causes the cell to adhere to the bottom of the flask.) The cells are then suspended in α +/-, spun down (800 rpm for 8 min) and resuspended in the appropriate volume to yield the desired cell concentration of 3 x 10⁶ cells/mL. The cell concentration (cells/mL) was determined using a "Coulter Cell Counter" from Coulter Electronics, Inc.

6.2.1.4 Preparation of Compound Solutions

Nitroimidazoles

All nitroimidazole compounds tested were prepared as 1 mM stock solutions. For the more hydrophobic species (*i.e.* those compounds containing a number of F-atoms on the side-chain) sonication was used to aid in the dissolution (SONIFIER Cell Disruptor W-350, output control = 4). The solutions were then filtered through 0.22 μ m filters into sterile tubes prior to experimental use. The exception was the tirapazamine derivative, TF5; here the solubility was extremely low, and the complex was stirred for 24 h at 37 °C prior to filtration. The concentration of TF5 was determined using UV-Vis spectroscopy by comparison of the absorbance values for the filtered mixture and a TF5 solution of known concentration in MeOH, assuming that the ϵ values for TF5 in PBS and MeOH are the same. The final TF5 concentration was determined to be 0.063 mM.

Ru Complexes

Attempts to make up a 1 mM solution of the selected Ru complexes were for the most part unsuccessful; only the SR2508 complexes ($\text{RuCl}_3(\text{SR2508})_2(\text{EtOH})$, $[\text{Ru}(\text{DMF})_4(\text{SR2508})_2][\text{Tf}]$ and $[\text{Ru}(\text{acac})_2(\text{SR2508})_2][\text{Tf}]$) and the DMSO complexes (*cis*- and *trans*- $\text{RuCl}_2(\text{DMSO})_2(\text{en})$) were soluble enough in PBS to give 1 mM solutions. For $\text{RuCl}_3(\text{SR2508})_2(\text{EtOH})$ the concentration could be increased to ~4 mM for radiosensitization experiments. The other suspensions of the complexes were all sonicated and stirred at 37 °C for 1 h prior to filtration. The EF5 complexes ($\text{RuCl}_3(\text{EF5})_2(\text{EtOH})$, $[\text{Ru}(\text{DMF})_2(\text{EtOH})_2(\text{EF5})_2][\text{Tf}]$ and $[\text{Ru}(\text{acac})_2(\text{EF5})_2][\text{Tf}]$) were quite insoluble; and so to obtain the maximum concentration, α +/- media was added to the complex/PBS slurry and the mixture was stirred for 2 h at 37 °C, followed by sonication and then filtration directly into the incubation flask. The concentrations of all of the Ru stock solutions were determined using AAS (see Section 6.2.2.1), following calibration using a Ru standard solution. The concentrations were first calculated as ng/mL of Ru and are reported in μM for the complex, after taking dilution factors into account.

6.2.1.5 Cell Incubation Procedures

The agent to be studied was typically made up with 1 mL of stock solution in 8 mL α +/- (for those complexes with limited solubility 2 mL in 7 mL α +/- was used) in a toxicity ('tox') flask fitted with a modified rubber stopper designed to introduce a flow of gas (through a syringe needle) and allow sampling (Figure 6-1). The tox vessels were shaken in a Labline Instruments "Orbit Shaker Bath", maintained at 37 °C in a warm room. Humidified air or N_2 (oxygen-free), for oxic and hypoxic conditions, respectively, was passed over the solutions for 1 h prior to adding the cells, and was maintained throughout the experiment. Approximately 3×10^6 cells were added to each of the vessels as suspensions in 1 mL of α +/- medium to give a total volume of 10 mL per vessel.

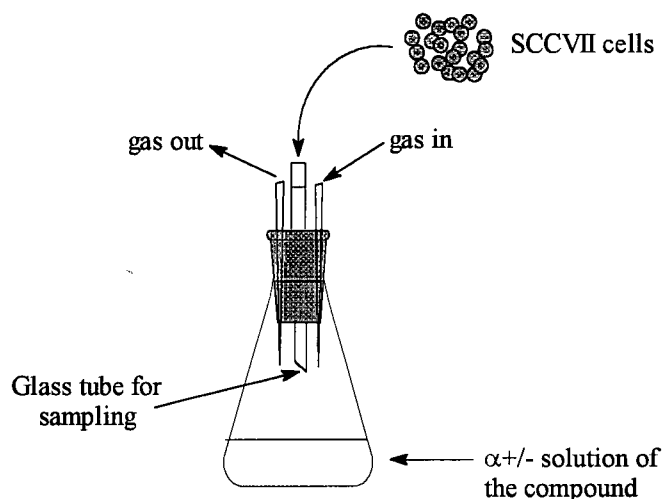


Figure 6-1: Diagram of 'tox' vessel used for the accumulation and toxicity experiments.

6.2.2 Instrumentation

6.2.2.1 Atomic Absorption Spectroscopy (AAS)

A Varian SpectrAA-300 Zeeman Atomic Absorption Spectrometer, controlled by a Compaq Deskpro 386s computer, was used to analyze for the presence of Ru in the cellular samples, including determination of the concentration of the Ru stock solutions. Instrument calibration was performed using Ru standards supplied by Sigma. This spectrometer uses a Ru hollow cathode lamp with a 10 mA current (Varian) as the source, with a λ_{max} of 349.9 nm. The samples were injected as 20 μL aliquots (single injections for stock solutions, double injections for cell digests and triple injections for DNA-binding samples); the samples were then dried (120 $^{\circ}\text{C}$ for 10 s), ashed (1100 $^{\circ}\text{C}$ for 10 s) and atomized (2800 $^{\circ}\text{C}$ for 1 s), using pyrolytic-coated partitioned graphite tubes (Varian). The corrections for background absorption were done using a technique, developed by Varian, based on the Zeeman effect.¹⁶ A re-slope calibration was performed after every fifth sample to ensure that buildup on the pyrolytic graphite surface did not cause significant variations in the background reference.

6.2.2.2 UV-Vis Spectroscopy

This technique was used for measuring the optical density (OD) of the DNA solutions (diluted 50-fold); an OD₂₆₀ of 1.0 is equivalent to a DNA concentration of 50 µg/mL.¹⁷ Measurements were made on a Cary 1E double-beam, single dispersion Czerny-Turner monochromator UV-Vis spectrometer. Each sample was scanned in the range 320 to 200 nm and the absorbancies at 260 and 280 nm were recorded for each sample.

6.2.2.3 Flow Cytometry (FCM)

The recognition of NO₂Im adducts by a monoclonal antibody (MoAb) was facilitated by a Cy3 tag on the MoAb using fluorescence detection. All measurements were performed on a Coulter Epics Elite fluorescence activated, cell-sorter equipped with a Coherent Inova 90 Ar laser. The ultrasonic vibrator splits the sample stream into droplets and each droplet is passed through the focused laser beam (those containing only one cell are analyzed). Although the Cy3 dye is optimally excited at 565 nm,¹⁸ an excitation wavelength of 510 nm was used and emission was collected using a 580-590 nm band pass filter. For each sample, the fluorescence of 10,000 cells was measured, gated on forward- and side-scatter signals. This technique was used for every MoAb experiment reported herein.

6.2.2.4 Image Cytometry (ICM)

Fluorescence microscopy procedures used to visualize the localization of nitroimidazoles and Ru-nitroimidazole complexes within the cells were adapted from those reported previously.¹⁵ This technique allows for the "quantitation" of the amount of Cy3-labeled MoAb and hence the amount of compound remaining within the cell. The cells (100 µL), isolated at the end of the MoAb procedure, were smeared on the surface of positively charged microscope slides and then allowed to air dry for 15 min at r.t. in the dark. The slides were subsequently rinsed with ddH₂O, patted dry with Kimwipes® and then 1-2 drops of mounting solution (10 % PBS^{tt} in glycerol) were added to the surface followed by a large cover-slip (carefully added on an angle to prevent the formation of air bubbles). The slides were stored in a humidified chamber at 4 °C.

The image cytometry device used for quantifying immunofluorescence signals was a fluorescence-adapted Cyto-Savant system. The microscope is equipped with an epi-fluorescence illumination attachment for Koehler illumination, and uses a 100 W Hg arc lamp with stabilized power supply. Images were captured by a 12-bit scientific CCD camera (MicroImager 1400, Xillix Technologies, Richmond, B.C.) mounted in the primary image plane. All measurements were made with a Nikon pan-apochromat 20X objective (NA = 0.75) and an additional 1.25X lens within the light path, giving overall magnification of 25X. Cy3 fluorescence was observed using a 510-560 nm excitation filter, a 580 nm dichroic mirror and a 590 nm high pass barrier filter. For the low fluorescence levels of oxidic samples, no light filter was required for the excitation source. However, in order to measure the hypoxic samples, either the 2X or the 4X filter was required to decrease the resulting fluorescence intensity into a measurable range. The integration (using the pulse frequency of the camera) and the gain could also be adjusted to account for the changes in intensity of the fluorescence signal. An acceptable intensity is determined by selecting a single cell, usually the brightest one in the field of view, on the slide and integrating its fluorescence intensity over the entire area of the cell. If the signal in the histogram does not exceed the preset threshold signal then the settings are used, otherwise they are adjusted accordingly.

For each slide, 100 cells were individually selected, making sure to select only cells which do not appear necrotic or apoptotic (Figure 6-2). The cell image was "grabbed", focused and the threshold was set to determine cell boundaries and the integrated optical intensity (IOI) of each; the sum of fluorescence intensity of all pixels within the cell was calculated. All IOI measurements were calibrated against a uniformly fluorescent field to remove illumination non-uniformities. Because of the limited availability of this apparatus within the Cancer Imaging Department at the BCCRC, only a few MoAb experiments were analyzed using this method.

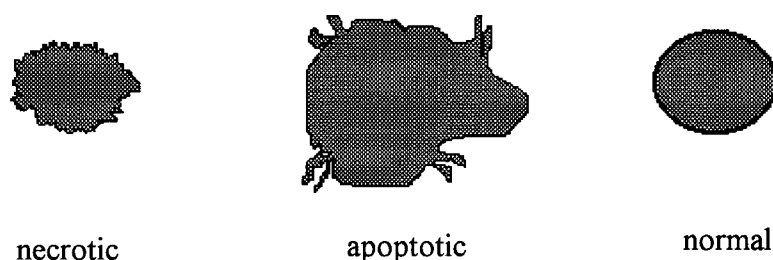


Figure 6-2: Different types of SCCVII cells observed on microscope slides.

6.2.3 Biological Assays

6.2.3.1 Toxicity Assays

The toxicity assays were performed under 1 atm of air or N₂ according to a standard protocol.¹⁹ In each case, the cells were sampled after a 3 h incubation period with the compound in α +/- media (Section 6.2.1.5). The 0.5 mL sample was diluted in α -/- medium (9 mL), and the mixtures were vortexed and centrifuged (8 min at 800 rpm). The supernatant was decanted and the cells were resuspended in α -/- medium (10 mL). At this point the concentration of the cells was determined by diluting 2 mL of the cell mixture in 10 mL PBS and then counted using the Coulter Counter.²⁰ Aliquots (10 and 100 μ L) from the cell suspensions were plated in duplicate into separate 5 cm Petri dishes which contained α +/+ medium (5 mL). The dishes were incubated for 1 week at 37 °C in air (5% CO₂), when the colonies were stained with methylene blue and counted. The toxicity is expressed in terms of the plating efficiency (PE = number of colonies / number of cells plated).

6.2.3.2 Cell Accumulation (Uptake) Assay

To determine whether an agent was adhering within and/or to the cells, the above incubations (Section 6.2.1.5) of SCCVII cells in the test solution under both oxic and hypoxic conditions were performed. After 3 h, the mixture was transferred to centrifuge tubes and the cells were pelleted (8 min at 800 rpm) and the supernatant discarded. The cells were washed twice with PBS (10 mL at 0 °C) to remove any unbound

complex and then resuspended in 7.5 mL PBS. At this point, the samples were vortexed and then separated into three portions into polypropylene tubes: 3 mL for the cell accumulation, 4 mL for the DNA-binding assay (Section 6.2.3.3) and the remaining 0.5 mL to determine the number of cells (200 μ L of the cell suspension in 20 mL PBS). For the accumulation assay portion, cells were pelleted, the supernatant poured off, and the cell pellet air-dried overnight at 37 °C. Concentrated HNO₃ (100 μ L) was then added to the cell pellet, and the acid mixture (yellow) was agitated and allowed to digest at 37 °C for 2 days. To the acid digested samples, ddH₂O (250 μ L) was added and then the mixtures were analyzed directly for Ru content using AAS. The accumulation results are expressed as ng Ru/10⁶ cells.

6.2.3.3 DNA-binding Assay (Isolation of DNA from SCCVII Cells)

The 4 mL sample obtained from the cell accumulation assay (section 6.2.3.2) was pelleted, the supernatant poured off, and 1 mL TNE* was added while vortexing. The samples were stored at 37 °C overnight to ensure the cells were solubilized. The following day each sample was sonicated for ~ 8 s and then extracted with washes (2 x 1 mL) of TNE-equilibrated phenol. Once the sample was vortexed after the addition of the phenol, the samples were centrifuged (5 min at 1000 rpm) to ensure that the layer separation was well-defined. The samples were then washed (2 x 1 mL) with 4 % *iso*-amyl alcohol in CHCl₃. The DNA was precipitated by adding 99.5 % EtOH (2 mL) and cooling the solution to -20 °C for 2 h. The precipitated DNA was pelleted by centrifugation (45 min at 3000 rpm, 4 °C), the supernatant discarded, and the pelleted DNA air-dried. The dried DNA was then hydrated in 200 μ L of TE and analyzed for Ru content using AAS (Section 6.3.4); the amount of Ru bound was normalized to the amount of DNA present which was determined by measuring the optical density (OD) of the re-hydrolyzed DNA solutions (dilution: 20 μ L + 980 μ L TE) at 260 nm.

6.2.3.4 Radiosensitizing Assays

The radiosensitizing assays were based on literature procedures.¹⁹ A sterile solution of the agent of interest (1 mL) was added to α +/- medium (8 mL) in a glass

"duck" irradiation vessel, and the mixture was stirred magnetically. The "ducks" were kept at 37 °C and humidified N₂ was passed over the solutions for ~1 h. Then 3 x 10⁶ cells (suspended in 1 mL of α +/- medium) were added to each of the vessels, and the mixtures were stirred for 3 h at constant temperature and N₂-flow.

The "ducks" were then immersed in ice and then one duck at a time in ice (oxic samples followed by hypoxic samples) was set up on the arm of the X-ray machine with stirring and then irradiated with an X-ray source (Phillips, 250 kV, 0.5 mm Cu) (see Figure 6-3). The X-ray source was calibrated using a Precision Electrometer (Victoreen, Model 500). The doses given for the oxic samples (0, 0.5, 1, 2, 4, 6 and 8 Gy) were different from those for the hypoxic samples (0, 1, 2, 5, 10, 15, 20 and 25 Gy); 0.5 mL was removed after each dose increment except following the greatest dose, when 1.0 mL was sampled from the "duck". The zero-dose sample (0.5 mL) was removed from the "duck" prior to irradiation. For the hypoxic samples, N₂-flow was continued and precautions were taken to eliminate air contamination during sampling which would sensitize the cells to radiation. Each 0.5 or 1.0 mL was diluted in α -/- medium (9 mL), and the mixtures were vortexed and centrifuged; the supernatant was decanted and the cells were resuspended in α -/- medium (10 mL). The plating, cell counting, incubation and colony counting followed procedures described in Sections 6.2.1.5 and 6.2.3.1, but the aliquots for plating were 25, 25, 50/200, 100/500, 200/1000, 1000 and 2000 μ L for the 0, 0.5, 1, 2, 4, 6 and 8 Gy samples (oxic), respectively, and 15, 15, 15/50, 20/100, 50/200, 100/500, 200/1000, 500/2000 μ L for the 0, 1, 2, 5, 10, 15, 20 and 25 Gy samples (hypoxic), respectively.

The results of the experiment are expressed in a dose-response curve by plotting the log of the surviving fraction [SF = (PE at dose D) / (PE at zero dose)] as a function of dose (in Gy). The effectiveness of a sensitizer is expressed by its sensitizer enhancement ratio defined here as SER = (dose at 0.01 SF for control) / (dose at 0.01 SF for "drug").

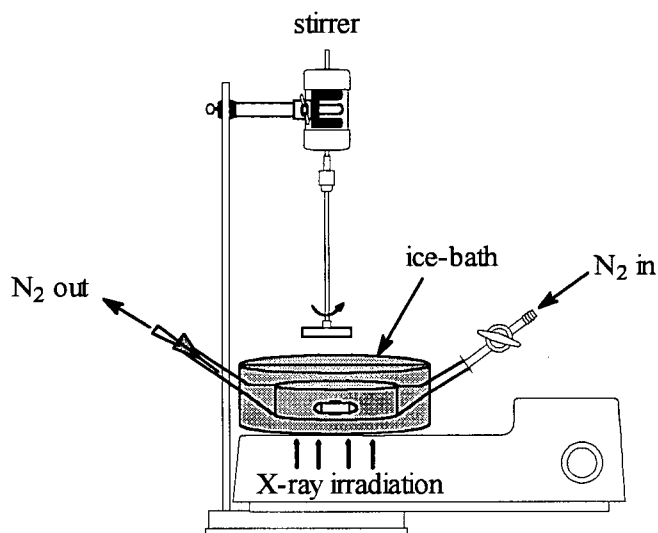


Figure 6-3: Setup used for irradiation of the "ducks" in the radiosensitization assay.

6.2.3.5 Monoclonal Antibody Assay¹³ (see Figure 6-4)

As described in the cell incubation procedures above (Section 6.2.1.5), the compounds were incubated with SCCVII cells at 37 °C for 3 h under both oxic (air) and hypoxic (N₂) conditions. Once the incubation was complete, the cell suspensions were put on ice, transferred to centrifuge tubes (15 mL) and the cells were pelleted by centrifugation (8 min at 1200 rpm). The cells were washed three times with cold, sterile 'PBS' (7 mL each, one wash = resuspension in cold 'PBS' by vortexing, followed by centrifugation and then decanting of the supernatant). After the final wash, the pellet was briefly vortexed to disturb the pellet and then 3 mL of pF was added to each vial dropwise with continuous vortexing. The samples were rotated at 4 °C for 1 h, and then spun down and washed twice with 'PBS'. Following removal of the final supernatant, the cells were resuspended in 1 mL 'PBS' and then transferred to Eppendorf tubes. These were spun down, the supernatant removed and 100 µL of blocking solution was added to each sample. The tubes were rotated at 4 °C for 5 h. Then 1 mL 'PBS' was added to the Eppendorf tubes with gentle mixing. The samples were spun down and the supernatant was carefully removed using a 1000 µL micropipettor. This was followed by the addition

of 100 μL of the MoAb (either ELK3-51 or ELK5-A8; 1:20 dilution in Ab carrier). These samples were then covered with Al foil and rotated at 4 °C overnight (~ 10 h). It is important to note that the intensity of the fluorescence for the Cy3-labeled MoAbs will fade if exposed to light, so all MoAb work was done in a dark-room.

The following morning, the samples were spun down and the MoAb solution was removed from each. One mL of PBS^{tt} was added with gentle vortexing to disperse the pellet and then the tube was rotated at 4 °C for 40 min. This procedure was repeated two additional times. After the final spin down, the cells were resuspended in 400 μL PBS^{tt} and 2 x 100 μL were used for the preparation of the microscope slides (supplied by ICM); the remaining 200 μL were diluted with 1 mL of 1 % pF and then submitted for flow cytometry. The stability of the fluorescent signal was excellent when stored in pF at 4 °C with no degradation of fluorescent signal for up to 3 weeks.¹³

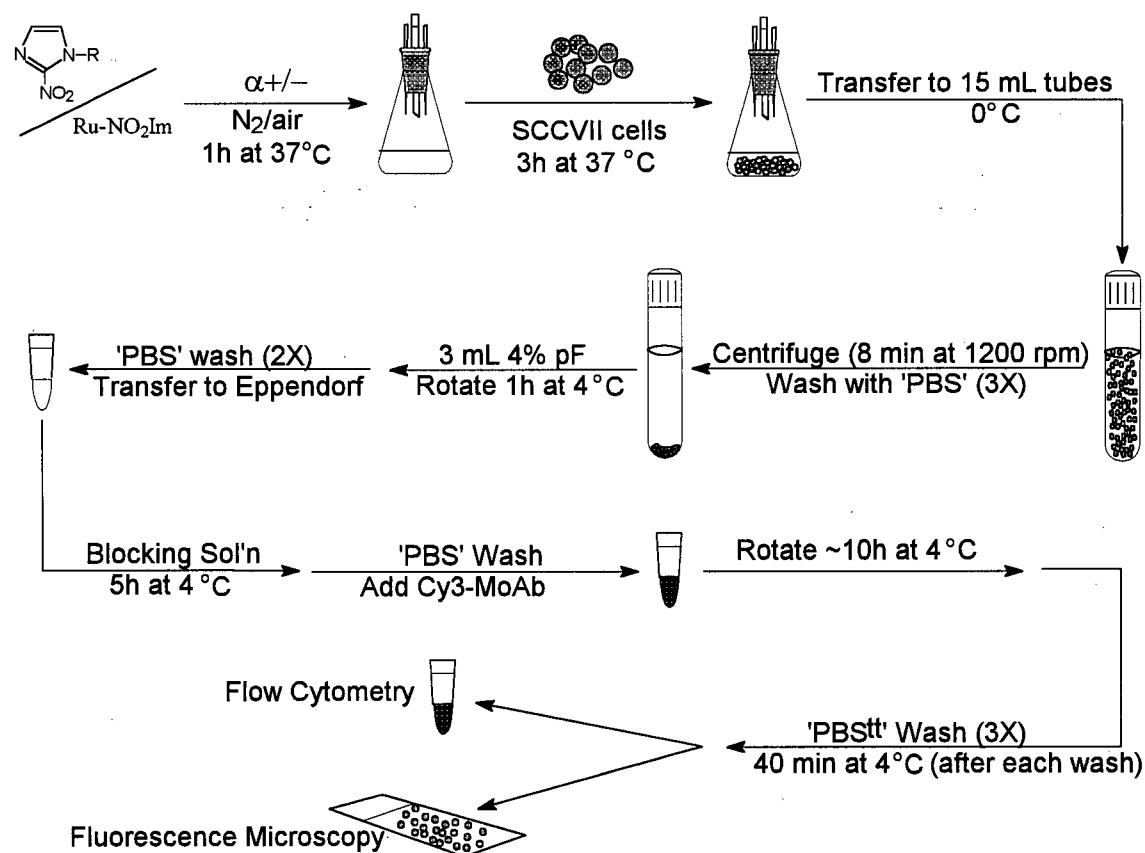


Figure 6-4: Pictorial summary of the *in vitro* MoAb assay.

6.3 Results and Discussion

6.3.1 Compound Solubility

Analysis of selected nitroimidazoles and Ru complexes was performed *in vitro*. For the most part the nitroimidazoles were soluble in PBS, but in some cases the Ru complexes had limited solubility and thus limited the ease of comparing complexes at the same concentrations. A summary of the compound concentrations used for the experiments performed in this chapter is listed in Table 6.1 and should be referred to for the data presented in the following sections. The synthesis and characterization of the nitroimidazoles are reported in Chapter 3, while those of the Ru complexes appear in chapters 4 and 5.

Table 6.1: Actual compound concentrations used for *in vitro* experiments.

Sample	Concentration (μM)
EF5, RevEF5, MF5, 2M4NF5, EF4Br, EF3, EF3(-1), EF2Br, E=F2, EF1, EF1(-1), EC11, EBr1, EPrA, EIAA, cycF3, IF5	100
SR2508	600 ^a
TF5	0.63
RuCl ₃ (EF5) ₂ (EtOH) 44	44.3 ^{b,c} ; 60.6 ^a
[Ru(DMF) ₂ (EtOH) ₂ (EF5) ₂][Tf] ₃ 38	47.4
[Ru(acac) ₂ (EF5) ₂][Tf]	22.0
RuCl ₃ (SR2508) ₂ (EtOH) 43	100, 206, 412 ^{b,c} ; 308 ^a
[Ru(DMF) ₄ (SR2508) ₂][Tf] ₃ 37	100
[Ru(acac) ₂ (SR2508) ₂][Tf] 65	50.1
<i>cis</i> -[Ru(acac) ₂ (Im) ₂][Tf] 55	87.8
<i>cis</i> -[Ru(acac) ₂ (NMeIm) ₂][Tf] 58	82.4
[Ru(Im) ₆][Tf] ₂ 28	37.8
[Ru(NMeIm) ₆][Tf] ₂ 29	50.8
<i>cis</i> -RuCl ₂ (DMSO)(en) 46	100
<i>trans</i> -RuCl ₂ (DMSO)(en) 47	100

a = radiosensitizing assay; b = toxicity assay; c = cell accumulation assay

For the compounds which had an initial concentration $<100\ \mu\text{M}$, the results were normalized (*i.e.* multiplied by a conversion factor, $100/\text{actual concentration}$) so that the data could be easily compared within a given series of compounds. This was done assuming a linear response for cell accumulation and DNA-binding over the concentration range up to and including $100\ \mu\text{M}$. The toxicity (determined by plating efficiency), however, was not normalized and is a result of the original compound concentration.

6.3.2 Toxicity

6.3.2.1 Nitroimidazoles

The toxicity of the selected compounds in SCCVII cells was measured as plating efficiency (PE) after a 3 h incubation at $37\ ^\circ\text{C}$. In general, the nitroimidazoles tested at $100\ \mu\text{M}$ were non-toxic in air and in N_2 , a typical result observed for other 2-nitroimidazoles tested *in vitro* at similar concentrations (*e.g.* misonidazole (miso), **SR2508**, metronidazole).²¹ However, at higher concentrations, 2-nitroimidazoles such as misonidazole have significant toxicity, particularly in the absence of O_2 . Although there was no hypoxia-selective cytotoxicity (HSC) at only $100\ \mu\text{M}$, there was hypoxia-selective binding (see Section 6.3.6), suggesting that there may be HSC at higher concentrations (to be tested in future). The only nitroimidazole to exhibit HSC (a difference in PE from oxic to hypoxic conditions) was **cycF3** which showed a 50 % decrease in PE in hypoxic cells. As this was the only $2\text{NO}_2\text{Im}$ that contained a cyclic side-chain, the hypoxic cytotoxicity may perhaps be attributed to this composition; the presence of an SO_2 group is only observed for **cycF3** and may also attribute to the cytotoxic selectivity at low O_2 concentrations. Even though large single doses are tolerated and pharmacological evidence has shown that, in most cases, tumour penetration is good, clinical studies have revealed that the $2\text{NO}_2\text{Im}$ s previously tested (*e.g.* miso, **SR2508**) induce acute peripheral neuropathy in patients, particularly when administered in multiple dose regimens.^{22,23} The new compounds tested may prove to be useful, non-toxic alternatives *in vivo* as the parent compound of this series, **EF5**, has been shown to have no significant side-effects at high and cumulative doses.²⁴ The results for some of the $2\text{NO}_2\text{Im}$ s are presented in Figure 6-5.

EF5 and **EF3** show moderate toxicity when compared to the control, but show no difference in toxicity, within experimental error, between oxic and hypoxic conditions. **IF5** is extremely toxic under both oxic and hypoxic conditions (PE ~ 0 at 100 μM), as expected for the species containing a labile C-I bond in which the I is readily displaced by any nucleophilic groups (*e.g.* thiols, acids, alcohols) contained on or within the cell. The **TF5** compound, a pentafluorinated derivative of SR4233, exhibits the greatest

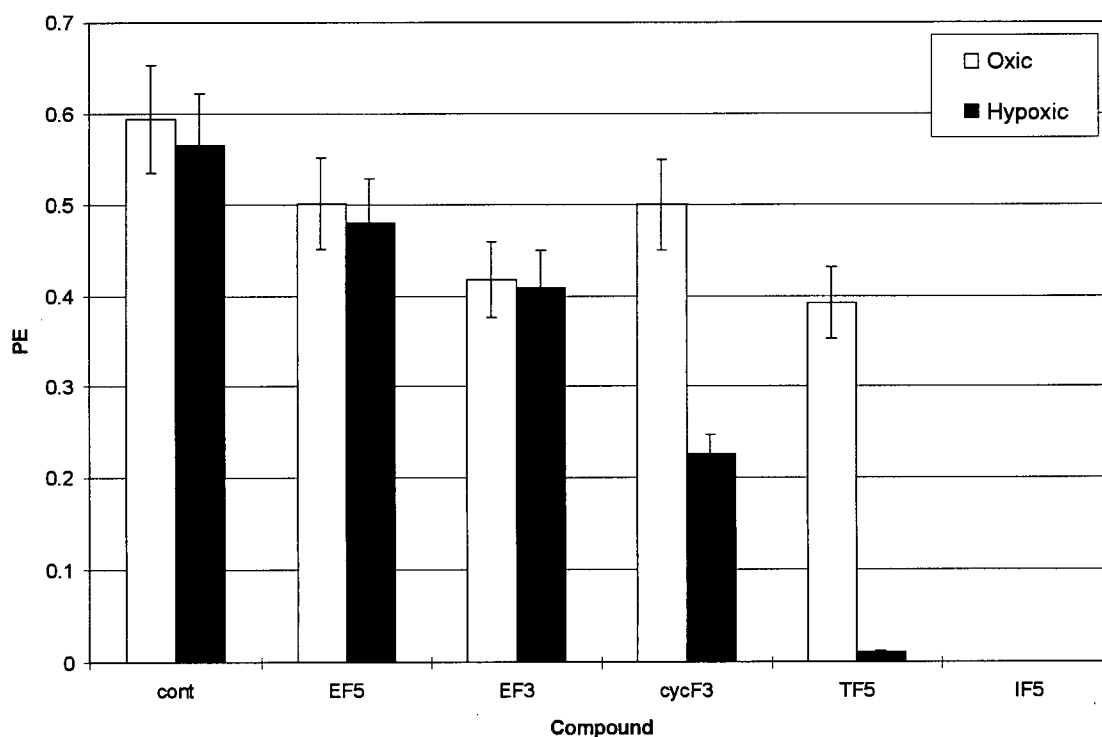


Figure 6-5: Comparison of toxicity for selected compounds (at 100 μM except for **TF5**) in oxic and hypoxic SCCVII cells (incubated for 3 h); average of 2 or 3 experiments. (The plating efficiencies for the other 2NO₂Ims, which also show little oxic/hypoxic variability, reported in Table II-1, Appendix II.)

hypoxia-selective cytotoxicity (Hypoxic Cytotoxic Ratio (HCR) ~ 35) of the compounds tested, analogous to that of the parent compound, SR4233,²⁵ which has been reported to exhibit HCR values of 75-200 for rodent and 15-50 for human cells *in vitro*.²⁶ Interestingly, a comparison of the hypoxic cytotoxicity of **TF5** in SCCVII (mouse) cells with SR4233 in V79-WNRE (Chinese hamster) cells revealed a large difference in the

compound concentration required to obtain the same cytotoxicity. The hypoxic surviving fraction for **TF5** at a concentration of 0.63 μM was 0.020 (this study), while the concentration of SR4233 required to obtain the same surviving fraction was 36 μM .²⁷ This hypoxic selectivity is occurring at extremely low **TF5** concentrations, suggesting that either **TF5** is a more potent hypoxic-selective cytotoxin or the addition of the fluorinated side-chain increases uptake of the compound into the cell or alters the reduction potential to cause a significant biological effect. The toxicity of SR4233 in SCCVII cells must be measured in the future to substantiate this hypothesis.

6.3.2.2 Ruthenium Complexes

The Ru complexes, like the nitroimidazoles, typically showed no significant toxicity towards SCCVII cells at the concentrations tested. This behaviour is different from that observed for the Pt nitroimidazole complexes which are cytotoxic even at relatively low concentrations.^{28,29} *cis*-PtCl₂(NH₃)(**EF5**) was significantly more toxic than any of the Ru(III) bis-**EF5** complexes (3 h under N₂; PE = 0.004 at 100 μM and ~ 0.5 at 22 - 60 μM , respectively).^{15,30} This suggests the potential use of Ru complexes as non-toxic alternatives to the toxic Pt complexes, for delivery of the radiosensitizing nitroimidazoles to their site of action, the DNA.³¹⁻³³ There was little difference seen for the samples exposed to oxic versus hypoxic conditions with the exception of a few complexes which did not contain nitroimidazoles (Table 6.2). The bis-acac complexes containing two imidazole ligands (Im or NMeIm) both exhibited hypoxia-selective toxicity, with about half the PE in hypoxia. These results were unexpected, especially when the complexes containing the 2NO₂Im ligands ([Ru(acac)₂(L)₂]**Tf**, where L = **EF5** or **SR2508**) were both shown to be relatively non-toxic under air and N₂. These results are even more bizarre when the accumulation data are taken into account (Section 6.3.3) as they show that the cells treated with *cis*-[Ru(acac)₂(Im)₂]**Tf** and *cis*-[Ru(acac)₂(NMeIm)₂]**Tf** have virtually no Ru content, suggesting that if any of the complex was taken up by the cell it did not remain within the cell after several washings. It is possible that the hypoxic reducing environment leads to reduction of the Ru(III) complex³⁴ and subsequent release of the imidazole ligand may induce cytotoxicity within the cells, although this is purely

speculation. Further experiments, including incubation of the cells with imidazole ligands alone, may help elucidate why these complexes are hypoxia cytotoxins. Of note, only a single experiment was performed for most of the values reported and so the PE values of these complexes require substantiation.

Table 6.2: Aerobic and hypoxic toxicity data (PE at 3 h) of Ru complexes in SCCVII cells. (See Table 6.1 for complex concentrations.)

Compound	PE (oxic)	PE (hypoxic)
control ($\pm 15\%$)	0.67	0.55
$\text{RuCl}_3(\text{EF5})_2(\text{EtOH})$	0.75	0.58
$[\text{Ru}(\text{DMF})_2(\text{EtOH})_2(\text{EF5})_2][\text{Tf}]_3$	0.61	0.58
$[\text{Ru}(\text{acac})_2(\text{EF5})_2][\text{Tf}]$	0.54	0.48
$\text{RuCl}_3(\text{SR2508})_2(\text{EtOH})$	0.61	0.60
$[\text{Ru}(\text{DMF})_4(\text{SR2508})_2][\text{Tf}]_3$	0.61	0.46
$[\text{Ru}(\text{acac})_2(\text{SR2508})_2][\text{Tf}]$	0.47	0.48
<i>cis</i> - $[\text{Ru}(\text{acac})_2(\text{Im})_2][\text{Tf}]$	0.59	0.33
<i>cis</i> - $[\text{Ru}(\text{acac})_2(\text{NMeIm})_2][\text{Tf}]$	0.63	0.30
$[\text{Ru}(\text{Im})_6][\text{Tf}]_2$	0.57	0.42
$[\text{Ru}(\text{NMeIm})_6][\text{Tf}]_2$	0.53	0.33
<i>cis</i> - $\text{RuCl}_2(\text{DMSO})(\text{en})$	0.56	0.40
<i>trans</i> - $\text{RuCl}_2(\text{DMSO})(\text{en})$	0.52	0.45

6.3.3 Cellular Accumulation of Ru Complexes

These experiments were performed to determine if the Ru complexes, treated under oxic and hypoxic conditions in SCCVII cells, were adhering to the cells. AAS was used to determine the amount of Ru bound to cellular macromolecules and thus does not reflect initial uptake of the complex. The results indicate the total amount of Ru (expressed as ng Ru/ 10^6 cells) present in the whole cell. No attempt was made to

determine the relative amounts of Ru in various cellular components (*e.g.* membranes, nuclei and proteins).

A large variability in accumulation was observed in SCCVII cells (Table 6.3): the Ru-**EF5** complexes exhibit significant accumulation while most of the other complexes do not accumulate within the cells. The lower hydrophilicity of **EF5**, compared with that of **SR2508**, may explain the difference observed between analogous complexes of these two nitroimidazoles. The binding of Ru within the cell does, however, depend on the presence of nitroimidazole ligands. Both the **EF5** and **SR2508** Ru-acac complexes show significant cellular accumulation whereas the Im and NMeIm complexes do not accumulate. This may also imply that the reduction of the nitro group, and not a direct interaction of Ru itself, is responsible for the binding of the complex within the cell.

Table 6.3: Accumulation of Ru complexes (normalized to 100 μM) in SCCVII cells incubated for 3 h; expressed as ng Ru/ 10^6 cells ($\pm 5\%$).

Compound	Oxic Ru (ng/ 10^6 cells)	Hypoxic Ru (ng/ 10^6 cells)
control	0.1	0.0
RuCl₃(EF5)₂(EtOH)	59.1	164.8^a
[Ru(DMF)₂(EtOH)₂(EF5)₂][Tf]₃	55.4	37.1
[Ru(acac)₂(EF5)₂][Tf]	76.3	57.8
RuCl ₃ (SR2508) ₂ (EtOH)	6.6	3.5
[Ru(DMF) ₄ (SR2508) ₂][Tf] ₃	2.8	4.2
[Ru(acac) ₂ (SR2508) ₂][Tf]	21.1	25.9
<i>cis</i> -[Ru(acac) ₂ (Im) ₂][Tf]	0.4	0.8
<i>cis</i> -[Ru(acac) ₂ (NMeIm) ₂][Tf]	0.4	0.5
[Ru(Im) ₆][Tf] ₂	15.6	10.6
[Ru(NMeIm) ₆][Tf] ₂	4.6	1.7
<i>cis</i> -RuCl ₂ (DMSO)(en)	4.4	3.2
<i>trans</i> -RuCl ₂ (DMSO)(en)	2.6	1.2

^a This result may not be a true indication of the actual accumulation under hypoxic conditions because the sample was used for the accumulation assay following irradiation up to 25 Gy.

A comparison of the accumulation values with those reported by Yapp *et al.* for a number of Ru(II) sulfoxide complexes reveals that on average the en-sulfoxide complexes (Table 6.3) exhibit less whole cell accumulation. Yapp *et al.* report complexes typically having values on the order of 60-100 ng Ru/10⁶ cells with no selectivity for hypoxic conditions over air.^{35,36} The *cis*- and *trans*-RuCl₂(DMSO)₄ complex-treated cells were determined to contain 36 and 91 ng Ru/10⁶ cells, respectively,³⁶ while cells treated with the analogous complexes with two DMSO ligands substituted by en contained only 3.2 and 1.2 ng Ru/10⁶ cells (Table 6.3). This shows the importance that a simple ligand substitution can have on the biological properties of the complex. Yapp *et al.* also noted that the Ru(II) sulfoxide complexes could be separated into two categories according to their kinetics over a 6h period: the first showed generally linear accumulation increasing steadily with time, while the second reached a plateau after 3 h; as results here are reported for only one time point, more details (including different time and concentration points) should be obtained for a true comparison of results, and should be done for the more prominent agents, in particular [Ru(acac)₂(EF5)₂][Tf] because of its potential as a hypoxia imaging agent.

The accumulation of RuCl₃(SR2508)₂(EtOH) was determined at three different concentrations and found to be concentration dependent with no marked difference between oxic and hypoxic conditions (Figure 6-6).

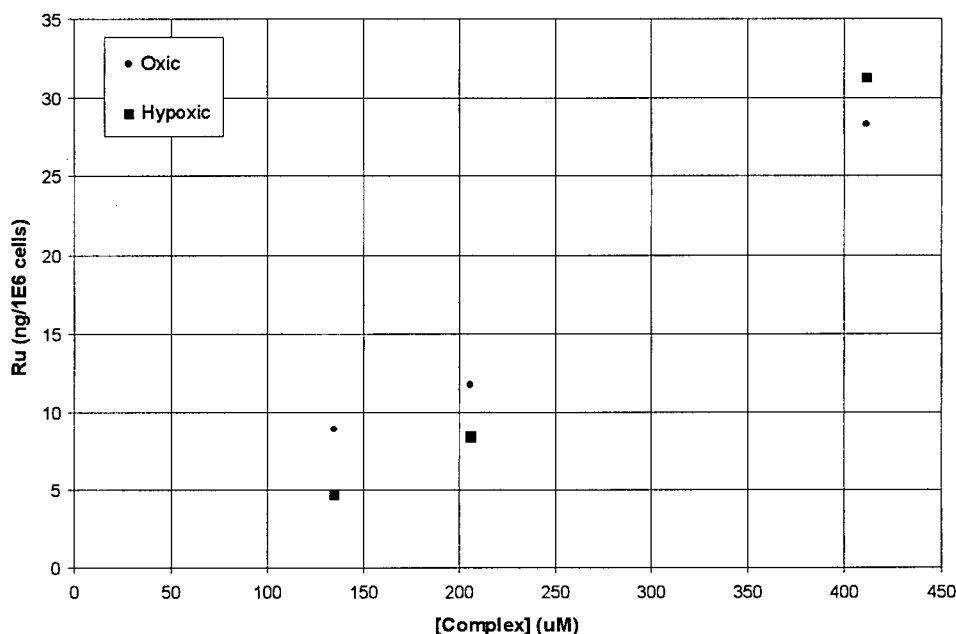


Figure 6-6: Accumulation data for $\text{RuCl}_3(\text{SR2508})_2(\text{EtOH})$ in SCCVII cells after a 3 h incubation; reported as ng Ru/ 10^6 cells ($\pm 5\%$).

6.3.4 DNA-binding by Ru Complexes

The purpose of this experiment was to examine whether the complexes reach the nuclei and bind to the DNA. The results (Table 6.4) indicate that the **EF5** and **SR2508** complexes bind to the DNA, isolated from SCCVII cells, at higher levels than do the other non-nitroimidazole complexes. A comparison of these data with the accumulation results reveals that a high accumulation level usually results in a high DNA-binding level. A comparison of Ru content per mg DNA against the whole cell accumulation data revealed that $\text{RuCl}_3(\text{SR2508})_2(\text{EtOH})$, which had ~ 16 ng Ru/mg DNA, had the highest DNA to cell Ru binding ratio and hence affinity for DNA. An increase in the concentration of the complex also showed a significant increase in the DNA-binding level (Figure 6-7), similar to the results seen from the accumulation data (Figure 6-6). Once again, the hypoxic value for $\text{RuCl}_3(\text{EF5})_2(\text{EtOH})$ was significantly higher than for the oxic sample, suggesting that the high radiation dose used with this sample may have increased the permeability of the

membranes leading to an increase in the concentration of the complex within the cell and nucleus.

Table 6.4: Amount of Ru bound to DNA extracted from SCCVII cells after 3 h exposure to complex (normalized to 100 μ M; ng Ru/mg DNA (\pm 5 %)).

Compound	Oxic ng Ru/mg DNA	Hypoxic ng Ru/mg DNA
control	2.2	0.4
RuCl₃(EF5)₂(EtOH)	0.4	19.4
[Ru(DMF)₂(EtOH)₂(EF5)₂][Tf]₃	8.9	13.3
[Ru(acac)₂(EF5)₂][Tf]	19.9	23.1
RuCl₃(SR2508)₂(EtOH)	20.7	16.4
[Ru(DMF) ₄ (SR2508) ₂][Tf] ₃	1.4	4.1
[Ru(acac) ₂ (SR2508) ₂][Tf]	4.3	8.5
<i>cis</i> -[Ru(acac) ₂ (Im) ₂][Tf]	1.3	1.0
<i>cis</i> -[Ru(acac) ₂ (NMeIm) ₂][Tf]	1.1	4.4
[Ru(Im) ₆][Tf] ₂	2.2	0.0
[Ru(NMeIm) ₆][Tf] ₂	2.0	0.0
<i>cis</i> -RuCl ₂ (DMSO)(en)	2.2	2.6
<i>trans</i> -RuCl ₂ (DMSO)(en)	0.6	1.7

A comparison of the amount of Ru bound to DNA after incubation with *cis*- and *trans*-RuCl₂(DMSO)₂ shows that several values in Table 6.4 are significantly higher. Yapp *et al.* report the highest DNA-binding values to be in the range 1.2-1.7 ng Ru/mg DNA³⁵ while values in Table 6.4 range from 4-23 ng Ru/mg DNA (hypoxia). For the two DMSO complexes (*cis*- and *trans*-RuCl₂(DMSO)₂(en)), values similar to those reported by Yapp *et al.* were observed under hypoxic conditions (2.6 and 1.7 ng Ru/mg DNA, respectively). The high levels of Ru binding to DNA suggest that further investigation (using radiosensitization and damaged DNA precipitation assays) of the Ru-nitroimidazole complexes is warranted.

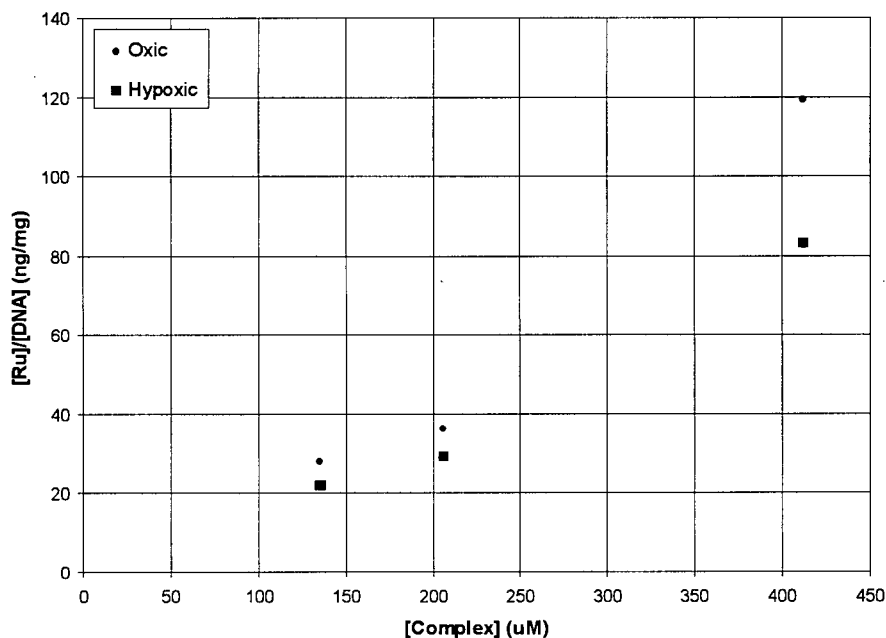


Figure 6-7: DNA-binding data for $\text{RuCl}_3(\text{SR2508})_2(\text{EtOH})$ in SCCVII cells after a 3 h incubation; reported as ng Ru/mg DNA ($\pm 5\%$).

6.3.5 Radiosensitization

The high DNA-binding of $\text{RuCl}_3(\text{SR2508})_2(\text{EtOH})$ prompted the preliminary investigation of this complex's ability to radiosensitize under hypoxic conditions. The analogous **EF5** complex was also studied and the results were compared with the radiosensitizing ability of the ligands themselves. The results are presented in Figure 6-8, and show that the $\text{Ru-NO}_2\text{Im}$ complexes do not radiosensitize hypoxic SCCVII cells at the concentrations tested. The slight deviations from the control curve are not significant. The **EF5** complex actually shows some radioprotection; it has a consistently higher surviving fraction than the control. This cell line appears to be quite radioresistant, similar to the V79 and CHO cell lines which have been used extensively to study the radiosensitizing properties of **SR2508**.^{37,38} For CHO cells, the surviving fraction (SF) at 25 Gy is typically 0.02 for non-treated (control) cells, comparable to an SF = 0.028 observed for SCCVII cells; however, for CHO cells treated with 400 μM **SR2508** a SF = 0.002 was observed,³⁹ approximately 100 times greater than that observed here for a 600 μM solution, SF =

0.00002. This increased radiosensitivity is not likely accounted for by the higher concentration of **SR2508** used in this experiment. Further radiosensitizing experiments, in other cell lines (*e.g.* CHO cells) and at varying concentrations, should be performed with these Ru **SR2508** and **EF5** complexes before any definite conclusions can be made.

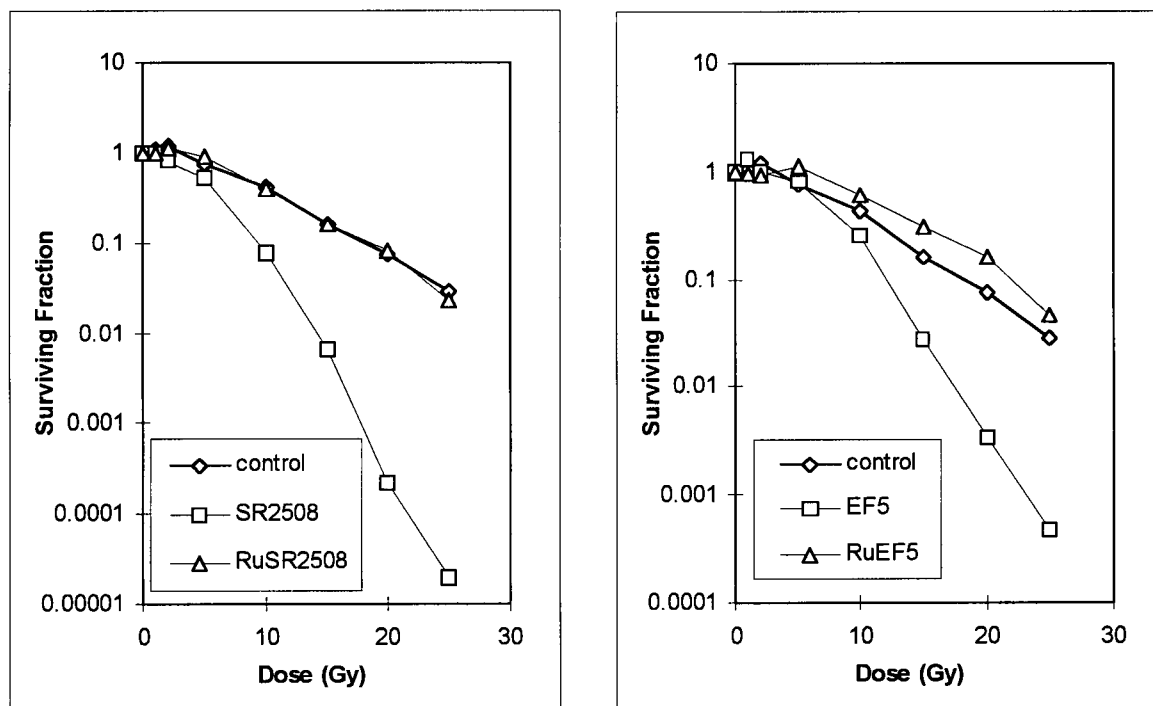


Figure 6-8: Radiosensitization by **SR2508** (600 μM) and **EF5** (150 μM) and lack thereof by their Ru complexes $\text{RuCl}_3(\text{SR2508})_2(\text{EtOH})$ (308 μM) and $\text{RuCl}_3(\text{EF5})_2(\text{EtOH})$ (60.6 μM); after 3 h pre-incubation with hypoxic SCCVII cells.

Extrapolation of the surviving fraction curve to a value of 0.01 (the level used to determine the SER) gave a dose of 28.5 Gy. Calculation of the SER values for **SR2508** and **EF5** gave 2.0 and 1.6, respectively. The slightly lower SER value for **EF5** shows that its efficacy may be greater than **SR2508** as its concentration is one quarter that of **SR2508**; however, these compounds need to be tested at equivalent concentrations to confirm this suggestion. Others have shown that the SER value for **SR2508** increases with an increase in concentration³⁷ which may also hold for **EF5**. This finding, coupled with the fact that **EF5** is extremely non-toxic and shows consistent uptake and binding in a number

of different cell lines,²⁴ suggests that **EF5** might be appropriate for use as a radiosensitizer in the clinic.

6.3.6 Nitroimidazole Adduct Recognition using Monoclonal Antibodies

It was postulated by Koch that a fluorine-containing derivative of etanidazole (**SR2508**) would, like the parent compound, have limited nonoxygen-dependent variations in binding, while allowing the detection techniques offered by the fluorine atoms (*e.g.* PET, MRI and immunocytochemistry).⁴⁰ The initial report supported this concept. The five F-atoms of **EF5** substantially decrease the hydrophilicity of the compound, compared to etanidazole, thus causing a greatly decreased proportion of acid-soluble adducts which are lost during typical histological processing because of their low molecular weights.⁴⁰ Lord *et al.* reasoned that the pentafluorinated side-chain of **EF5** "might be sufficiently non-physiological as to allow the formation of highly specific antibodies,"¹² analogous to the studies of Raleigh *et al.* using polyclonal antibodies for the detection of CCI-103F.⁴¹ The first MoAb developed for **EF5** (by Dr. Edith Lord, University of Rochester), ELK2-4, had a high affinity for the **EF5** adduct and based on equilibrium dialysis experiments the affinity was on the order of 10^6 for the parent compound and 5 to 10 times higher for protein adducts of **EF5**.¹² Thereafter a more specific MoAb, ELK3-51, was developed and was used to determine the oxygen dependence of bioreductive metabolism-induced binding of **EF5** after whole cell permeabilization and fixing.¹² The detection of the antibody adduct was made possible by conjugation of the fluorescent dye, Cy3 (Figure 6-9),¹⁸ with the secondary protein amines of the MoAb yielding a dye/protein ratio of about 4.

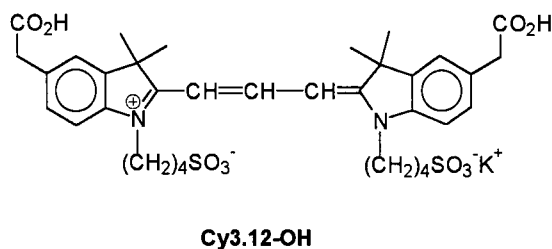


Figure 6-9: The indocarbocyanine fluorescent dye Cy3.

Previous studies by Koch *et al.* have clearly demonstrated the oxygen dependency for binding of **EF5**.^{12,13} This dependence was the same using assays based on either radioactive compound (¹⁴C-labeled at the Im-C₂ position) uptake or immuno-histochemical staining (Figure 6-10). The dynamic range of binding by **EF5**, as measured by radioactive compound uptake, was large (up to 100 in rodent cell lines^{13,15} and 50 in human cell lines²⁴) and compared well with the values obtained for the antibody assay showing that ELK3-51 had very high sensitivity and specificity.

Using standard ELISA techniques, several nitroaromatic compounds were tested by Koch's group for their ability to competitively inhibit the binding of the first generation MoAb, ELK2-4, to **EF5**-bovine serum albumin adsorbed to the ELISA plates. The data obtained suggested that the only compound to effectively inhibit binding was **EF5** itself, although CCI-103F did show some reactivity, albeit at a 100-fold higher concentration than **EF5**.¹² This clearly indicated the specificity of the MoAb, but at the

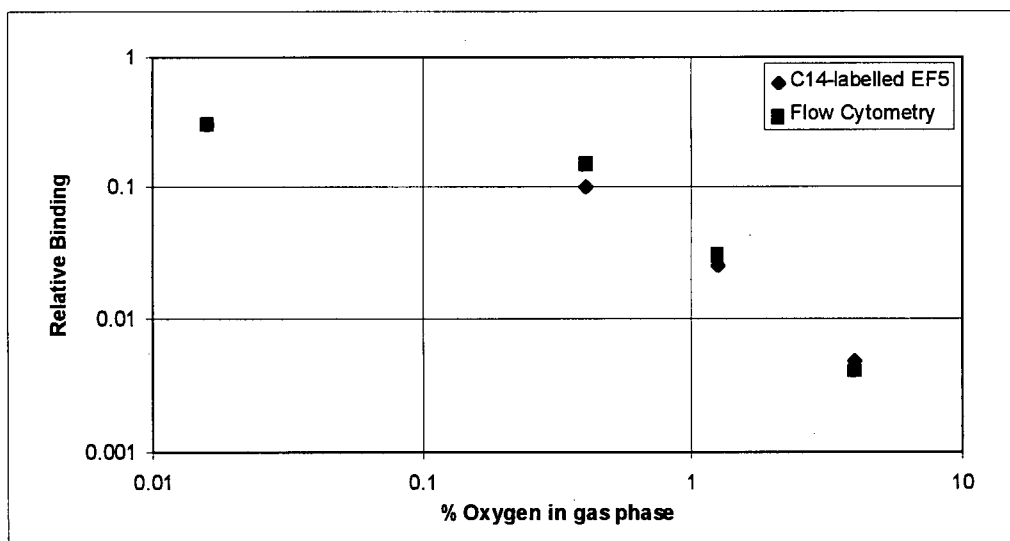


Figure 6-10: Direct comparison of relative median fluorescence intensity and radioactive compound uptake for 9L cells incubated with 100 μ M **EF5** for 3 h at indicated oxygen partial pressures (adapted from ref. 13).

same time suggested that the similarity of the side-chains for **EF5** and CCI-103F (both contain CF₃ groups) may be the determinant for interaction at the recognition site of the antibody. For this reason, the recognition by the MoAb, ELK3-51, of adducts formed by some newly synthesized analogues of **EF5** was studied (see Chapter 3). This approach

was extended to ELK5-A8, a new, highly specific MoAb, made against radiochemically produced adducts of **EF3**.

6.3.6.1 Recognition of NO₂Im Adducts by ELK3-51

For ELK3-51, the relative mean fluorescence intensity for SCCVII cells incubated with 100 μ M of the nitroimidazole compound for 3 h was determined under both oxic and hypoxic conditions using flow and image cytometry. Because of the reproducibility of the signal obtained for **EF5** from one experiment to another, this was used as the reference from which all other experimental values were normalized. A comparison of the hypoxic flow cytometry data with those for the oxic samples reveals that the dynamic range of binding by **EF5** for this cell line was at least 65 (comparable to the value obtained by Matthews *et al.* of ~ 70 for the same cell line¹⁵), with an average of 90 (slightly higher than observed for 9L and WNRE cell lines¹³). The results obtained for the cells treated with compound under hypoxic conditions are summarized in Figure 6-11 (*cf.* oxic results in Table II-2). The other 2NO₂Im compounds had dynamic ranges with limits of 50 for **EF2Br** down to one for **cycF3**. Although **IF5** has a higher fluorescence intensity than **EF5** in hypoxia, its value is virtually identical to that in air, reinforcing the idea that reduction of the nitro moiety on the imidazole ring, especially at the 2-position, is essential for hypoxic selectivity.⁴² The observation that the ELK3-51 readily binds to **IF5** does, however, suggest that the binding site of the antibody is not specific for the reduced nitroimidazole, but more importantly is specific for the composition of the side-chain. It is possible that the amount of **IF5** remaining within the cell may be higher than that of **EF5** (given equal initial concentrations) because of the lability of the C-I bond promotes binding to multiple species within the cell. The other fluorinated 2NO₂Im compounds also have significant fluorescence intensities suggesting that the binding of the antibody may not be as specific as suggested initially.¹³ The non-fluorinated compounds (**EPrA** and **EIAA**; see Sections 3.2.2.16 and 3.2.2.17, respectively) are also readily bound by ELK3-51, implying that the binding pocket is dependent on the size and length/composition of the side-chain. **CycF3** and **RevEF5** are the only two 2NO₂Im compounds which have different side-chains and do not have a hypoxic fluorescence signal greater than that of the background.

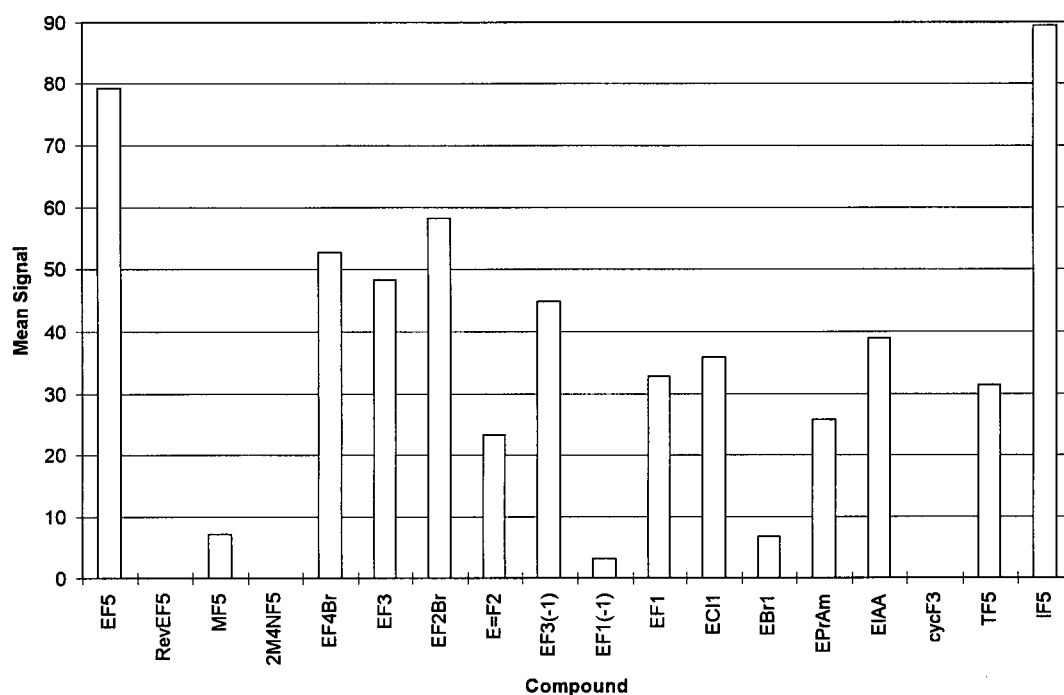


Figure 6-11: Relative mean fluorescence intensity for SCCVII cells incubated with 100 μ M compound for 3 h under N₂ and then treated with ELK3-51 (Cy3); determined using flow cytometry (average of 2 or 3 expts.; \pm 10 %). (The oxid data are reported in Table II-2, Appendix II.)

An additional important determining factor is the one-electron reduction potential of the nitroimidazoles (Tables 3.2-3.4, Chapter 3). According to Figure 6-12, the log of the fluorescence signal is perhaps proportional to the reduction potential of the compound: the higher the reduction potential, the higher the fluorescence signal. Because the reduction potential of the nitro group determines the amount of compound which could potentially form macromolecular adducts within the cell, the concentration of compound will conform to the trend $E_{1/2} \text{ 2NO}_2 > 5\text{NO}_2 > 4\text{NO}_2$.⁴² The data follow this trend as **EF5** has a much higher value than **MF5**, and **2M4NF5** gives no signal as the reduction potential of the nitro moiety is outside the reducing range existing within the hypoxic cells.⁴³ The observation that the signal for **EBr1** ($E_{1/2} = -1038$ mV) is significantly less than the values for **EF1** ($E_{1/2} = -1037$ mV) and **EC11** ($E_{1/2} = -1036$ mV), however, is not easily explained. Their one-electron reduction potentials are the same and the chain-length and

composition are identical with the only variable being the terminal halogen. This suggests that the decreased electronegativity of the Br-atom (versus the F- and Cl-atoms) must result in decreased affinity of the antibody's binding pocket for the nitroimidazole. One explanation for the decreased fluorescence of **EBr1** is that the C-Br bond is more labile than the C-Cl or C-F bonds and in aqueous solution this leads to the formation of elimination and cyclization products⁴⁴ (also see chapter 3, Section 3.2.1.2) which are not likely to be recognized/bound by the incoming MoAb. Of note, **EBr1** is the only compound that significantly deviates from the linear regression line of the plot (Figure 6-12), also suggesting that **EBr1** is different from the other halogenated nitroimidazoles. Hence, one may conclude from these results that the reduction potential determines the amount of compound retained within the cell (via adduct formation of the reduced nitro species)⁴⁵, while the composition of the side-chain affects the recognition and/or binding of the monoclonal antibody, ELK3-51 and thus the intensity of the fluorescent signal observed.

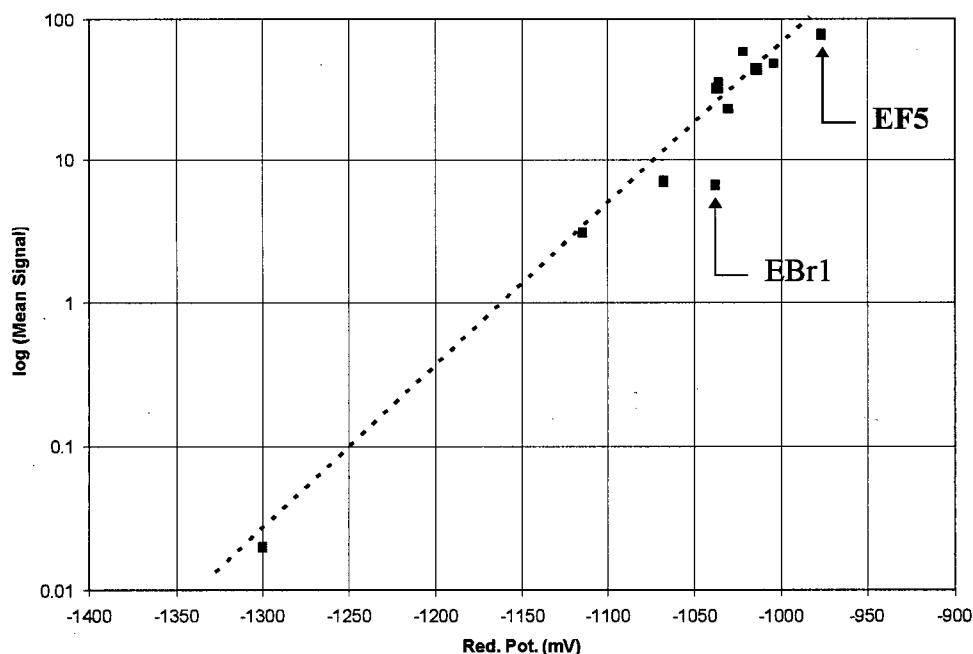


Figure 6-12: Log of mean fluorescence signal determined by flow cytometry versus the compound's reduction potential (determined by CV; Chapter 3, Section 3.2.8). See Table II-3, Appendix II.

A comparison of the image cytometry results (Figure 6-13) with the flow cytometry results (Figure 6-11) reveals an excellent correlation between the two techniques for quantification of fluorescence, as shown previously.¹⁵ Once again the oxic fluorescent signals for all compounds tested were extremely low, yielding a significant dynamic range for those compounds with positive hypoxic signals; for example **EF5** had a dynamic range of ~ 80 . The advantage of this finding is that image cytometry can be used to quantitatively assess the degree of hypoxia within a given tumour using simple biopsy techniques. Evans *et al.* have shown the distribution of cellular oxygenation within individual rat tumours (9L epigastric) using this **EF5**-binding technique, the major advantage being the ability to distinguish variation in binding over cell-cell distances.⁴⁶

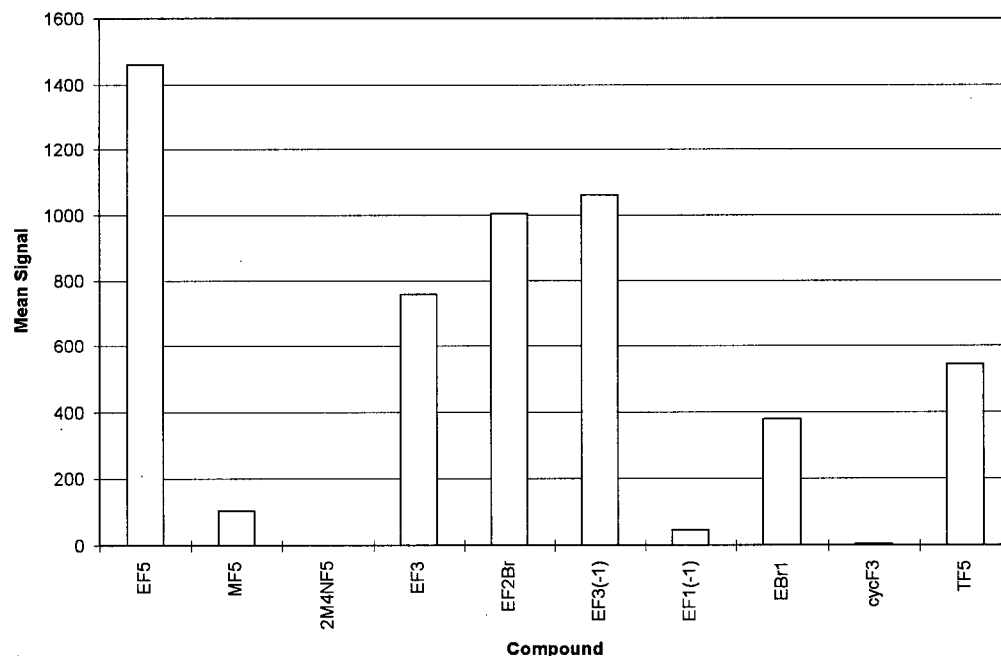


Figure 6-13: Relative mean fluorescence intensity for SCCVII cells incubated with 100 μ M compound for 3 h under N_2 and then treated with ELK3-51; determined using image cytometry (data from 2 expts.; $\pm 10\%$). (The oxic data are reported in Table II-4, Appendix II.)

Indirect measures of 9L tumour hypoxia, using [3H]miso, suggested that the 9L tumour contained few hypoxic cells,⁴⁷ but the **EF5**-binding immunohistochemical fluorescence technique suggests extensive hypoxia with significant inter- and intratumour variability.

This finding likely accounts for the radiation resistance of the 9L epigastric tumours and shows the usefulness of this technique as a probe to determine hypoxia and suggest the type of therapy required. The recent evidence that hypoxic tumours are more "aggressive" than other relatively well-oxygenated tumours^{48,49} also emphasizes "more than ever the need to be able to assess which patients have these hypoxia containing tumours, regardless of whether hypoxia is a cause or an effect of this aggressiveness".⁵⁰

The non-toxic Ru-EF5 complexes were also evaluated in SCCVII cells following hypoxic treatment and immunocytochemical procedures using ELK3-51. As the recognition of the EF5 was originally believed to be at the end of its side-chain it was postulated that the ELK3-51 would be able to recognize EF5, even if it remained coordinated to the Ru centre within the cell. Others have suggested that Ru(III) complexes are "prodrugs" of their active Ru(II) counterparts³⁴ which readily bind to molecules within the cell (*e.g.* DNA bases, amino acids). The lack of oxygen in hypoxic cells will promote the reduction of Ru(III) to Ru(II) which, aside from increased binding within the cell, may also promote release of the nitroimidazole and hence promote delivery of the compound into the cell.

The mean fluorescence values for the Ru-bisEF5 complexes, $\text{RuCl}_3(\text{EF5})_2$ (EtOH), $[\text{Ru}(\text{DMF})_2(\text{EtOH})_2(\text{EF5})_2][\text{Tf}]_3$ and $[\text{Ru}(\text{acac})_2(\text{EF5})_2][\text{Tf}]$ (abbreviated as RuClF5, RuDF5 and RuAcF5, respectively) were normalized according to EF5 on a molar basis (Figure 6-14). Analysis revealed that the singly charged cationic $[\text{Ru}(\text{acac})_2(\text{EF5})_2]^+$ species gives a signal ~ 4 times higher than EF5 itself. One major difference between this complex and the other Ru-EF5 complexes is its net charge; the RuDF5 complex has a 3+ charge while the RuClF5 complex has up to a 3+ charge from the successive displacement of Cl^- by H_2O (see Section 4.2.2.6). Previous studies with Al(III), Fe(III), Ga(III) and In(III) complexes containing a highly flexible hexadentate N4O2 Schiff-base phenolic ligand have shown that the modestly lipophilic monocationic complexes are readily transported across the membrane, due to the enhanced mitochondrial transmembrane potentials in tumour cells.⁵¹ Although this example is not directly related to the work here, it does support the ability of the monocationic complex to be transported into the cell. The cell-uptake data (Table 6.3) reveal that the Ru content per cell is higher for the bis-acac

species than the other complexes, suggesting that it remains bound within the cell. This result implies that the higher fluorescence value observed for the original bis-acac complex is for the intact species (with **EF5** bound, with or without reduction of the metal) which forms a stable interaction within the cell. This effect is not likely to be from the delivery of **EF5** into the cell followed by subsequent **EF5** release upon reduction of Ru(III) to Ru(II). Previous results have shown that **EF5** itself readily crosses the cell membrane; the **EF5** concentration within hypoxic cells increases with an increased **EF5** stock solution introduced to the cells prior to incubations.¹² The RuAcF5 complex does, however, accumulate in the cell (Table 6.3) and more importantly binds to DNA (Table 6.4), suggesting that the **EF5** remains bound to the Ru centre. This finding may prove useful

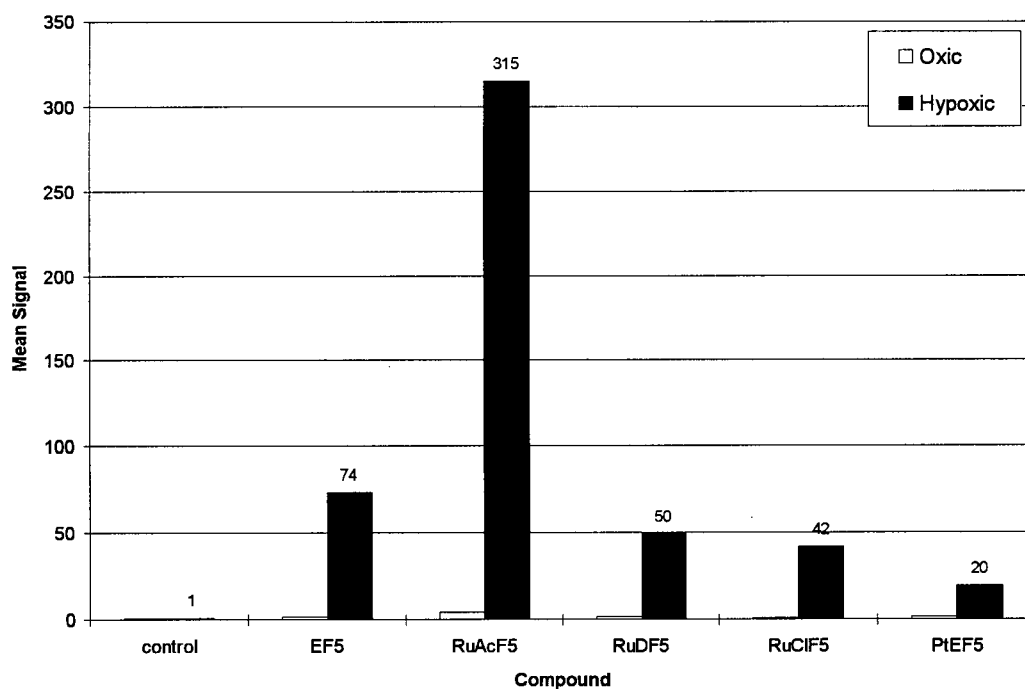


Figure 6-14: Relative mean fluorescence intensity for SCCVII cells incubated with compound for 3 h under N₂ and treated with ELK3-51; determined using flow cytometry (data for Ru complexes from 2 experiments; $\pm 10\%$). All values are normalized for **EF5** content (100 μ M). The *cis*-PtCl₂(NH₃)(**EF5**) (PtEF5) results were obtained from ref. 13.

in future as a lower compound concentration, using the Ru complex, can be administered to obtain the same effect as **EF5** itself, although the limited solubility of the Ru complex

may be a factor. Of note, the PtEF5 complex (*cis*-PtCl₂(NH₃)(EF5)) gives a signal approximately one quarter that of EF5, which in conjunction with its cytotoxicity does not make it a useful candidate for hypoxia-imaging, although PtEF5 is useful in redistributing the signal, with higher localization of the Pt complex in the nucleus using confocal microscopy.¹⁵ This is presumably due to targeting the nitroimidazole to the DNA, also the intended target of Ru.

6.3.6.2 Recognition of NO₂Im Adducts by ELK5-A8

Experiments with ELK5-A8 were initiated to obtain valuable information about the properties of the binding site of this antibody which is more specific than ELK3-51.²⁴ Only selected nitroimidazoles were tested because of the limited amount of ELK5-A8. The fluorescent data for this MoAb were quantitated using flow cytometry only. A summary of these findings can be seen in Figure 6-15. These results show that ELK5-A8 has a much higher specificity for the compound from which it was generated (EF3) than ELK3-51 has for EF5, as previously suggested.²⁴ These data also show that the nature of the binding pocket of the antibody is extremely dependent on the length of the side-chain. For example, a comparison of the fluorescence values for EF3 and EF3(-1) shows that the compound with one less CH₂ group, EF3(-1), is not bound by the antibody, although their similar reduction potentials (Table 3.2) suggest a similar extent of enzymatic reduction within the cell. It is apparent that the side-chain must contain a 3-carbon segment after the amide NH in order to be bound by the antibody. The composition of the side-chain also determines the level of compound interaction with the antibody. The mean fluorescence signal for EF5 is approximately one tenth that of EF3, presumably because of larger F-atoms on the second C atom from the terminal end which must interfere with ELK5-A8 binding. The low signal observed for EIAA, which contains a terminal isopropyl group with similar steric size to that of a CF₃ group,^{52,53} implies that the binding at the recognition site of the antibody is dependent more on the electronic composition of the terminal species than its steric bulk, although sterics are definitely important (EIAA has a

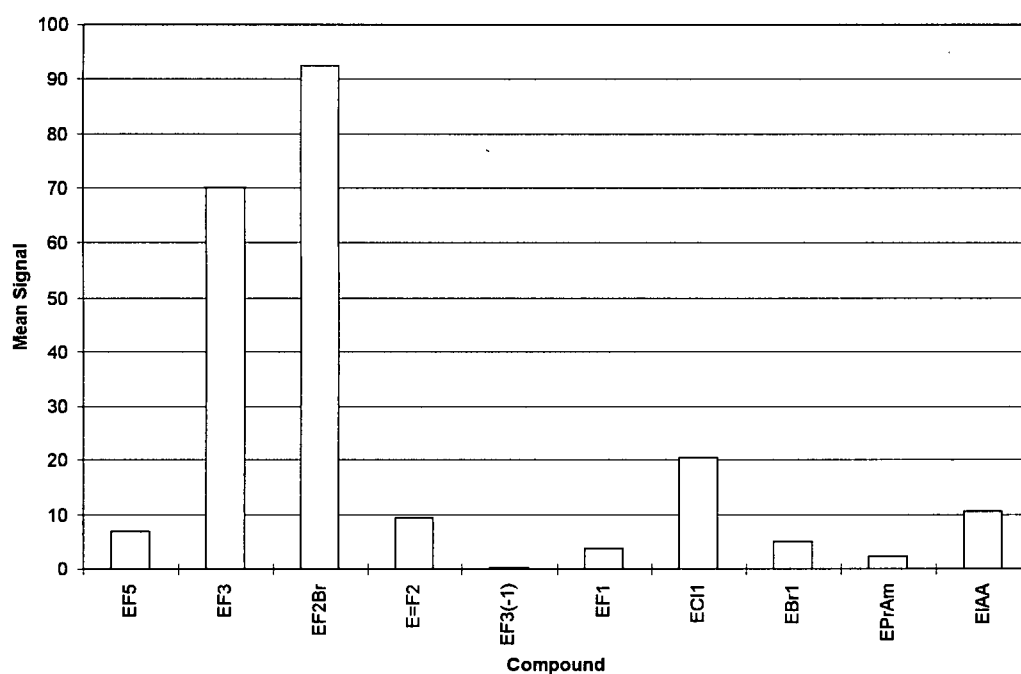


Figure 6-15: Relative mean fluorescence intensity for SCCVII cells incubated with 100 μ M compound for 3 h under N_2 and treated with ELK5-A8; determined using flow cytometry. (The oxid data are reported in Table II-5, Appendix II.)

mean fluorescence higher than that of **EF5**). Finally, the observation that **EF2Br** gives a higher signal than **EF3** itself is difficult to explain as their reduction potentials are virtually identical (-1022 and -1024 mV, respectively). Coupled with the findings presented in Section 3.2.1.2, displaying the lability of the C-Br bond, the increased signal for **EF2Br** may be due to a chemical reaction (*e.g.* cleavage of the C-Br bond) within the antibody's binding site, leading to a strong compound-antibody interaction. These findings lead to a simplified although speculative picture of the ELK5-A8 recognition/binding site (Figure 6-16).

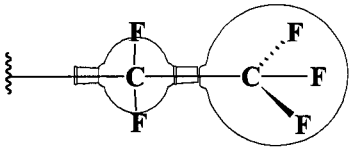
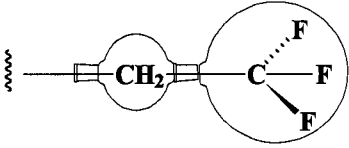
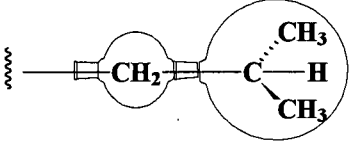
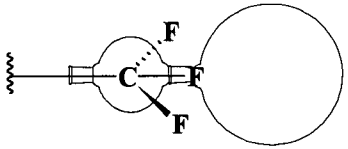
		<u>Mean Signal</u>
	EF5 - limited by CF ₂ group adjacent to CF ₃ group.	7
	EF3 - both binding pockets fit side-chain, hence strong interaction with MoAb	70
	EIAA - same size sterically as EF3; limited by electronic interactions within large pocket	11
	EF3(-1) - binding extremely limited by length of side-chain	0

Figure 6-16: Proposed recognition sites for the ELK5-A8 MoAb.

6.4 Refereneces

- 1 Moulder, J. E.; Rockwell, S. C. *Int. J. Radiat. Oncol. Biol. Phys.* **1984**, *10*, 695.
- 2 Bush, R. S.; Jenkin, R. D. T.; Allt, W. E. C.; Beale, F. A.; Bean, H. A.; Dembo, A. J.; Pringle, J. F. *Br. J. Cancer* **1978**, *37*, 255.
- 3 Chapman, J. D. *New Eng. J. of Med.* **1979**, *301*, 1429.
- 4 Koch, C. J.; Stobbe, C. C.; Baer, K. A. *Int. J. Rad. Oncol. Biol. Phys.* **1984**, *10*, 1327.
- 5 Parliament, M. B.; Chapman, J. D.; Urtasun, R. C.; McEwan, A. J.; Golberg, L.; Mercer, J. R.; Mannan, R. H.; Wiebe, L. I. *Br. J. Cancer* **1992**, *65*, 90.
- 6 Rasey, J. S.; Grunbaum, Z.; Magee, S.; Nelson, N. J.; Olive, P. L.; Durand, R. E.; Krohn, K. A. *Radiat. Res.* **1987**, *111*, 292.
- 7 Koh, W. J.; Rasey, J. S.; Evans, M. L.; Grierson, J. R.; Lewellen, T. K.; Graham, M. M.; Krohn, K. A.; Griffen, T. W. *Int. J. Radiat. Oncol. Biol. Phys.* **1992**, *22*, 199.
- 8 Kachur, A. V.; Evans, S. M.; Shiue, C.-Y.; Dolbier, Jr., W. R.; Li, A.-R.; Roche, A.; Skov, K. A.; Baird, I. R.; James, B. R.; Koch, C. J. *Appl. Rad. Isot.* (submitted Oct., 1998).
- 9 Raleigh, J. A.; Franko, A. J.; Treiber, E. O.; Lunt, J. A.; Allen, P. S. *Int. J. Radiat. Oncol. Biol. Phys.* **1984**, *10*, 1337.
- 10 Aboagye, E. O.; Lewis, A. D.; Johnson, A.; Workman, P.; Tracy, M.; Huxham, I. M. *Br. J. Cancer* **1995**, *73*, 312.
- 11 Siemann, D. W.; Inglis, B. A.; Cranston, B. A.; Lord, E. M.; Koch, C. J. *10th International Conference on Chemical Modifiers of Cancer Treatment*, Clearwater, Florida, Jan. 28-31, 1998, Abstract p. 43.
- 12 Lord, E. M.; Harwell, L.; Koch, C. J. *Cancer Res.* **1993**, *53*, 5271.
- 13 Koch, C. J.; Evans, S. M.; Lord, E. M. *Br. J. Cancer* **1995**, *72*, 869.
- 14 Woods, M. L.; Koch, C. J.; Lord, E. M. *Int. J. Radiat. Oncol. Biol. Phys.* **1996**, *34*, 93.

- 15 Matthews, J.; Adomat, H.; Farrell, N.; King, P.; Koch, C.; Lord, E.; Palcic, B.; Poulin, N.; Sangulin, J.; Skov, K. *Br. J. Cancer* **1996**, *74*, S200.
- 16 Brodie, K. Furnace Atomization. *In* Analytical Methods for Graphite Tube Atomizers; E. Rothery, Ed.; Varian Techtron Pty. Ltd., Mulgrave, Australia, Sept., 1988.
- 17 Matthews, J. B. M. Sc. Thesis, University of British Columbia, 1992.
- 18 Southwick, P. L.; Ernst, L. A.; Tauriello, E. W.; Parker, S. R.; Mujumdar, R. B.; Mujumdar, S. R.; Clever, H. A.; Waggoner, A. S. *Cytometry* **1990**, *11*, 418.
- 19 Moore, B. A.; Palcic, B.; Skarsgard, L. D. *Radiat. Res.* **1976**, *67*, 459.
- 20 The reading obtained for the coulter counter is for the number of cells in 0.5 mL. The actual number of cells in the original suspension can be calculated by multiplying the Coulter Counter value by 12, the dilution factor, to give a value of cells/mL.
- 21 Jenkins, T.C. *In* The Chemistry of Antitumour Agents; D. E. V. Wilman, Ed.; Blackie and Son Ltd., Glasgow, 1990, p. 343.
- 22 Dische, S.; Saunders, M. I.; Lee, M. E.; Adams, G. E.; Flockhart, I. R. *Br. J. Cancer* **1977**, *35*, 567.
- 23 Coleman, C. N.; Urtasun, R. C.; Wasserman, T. H.; Hancock, S.; Harris, J. W.; Halsey, J.; Hirst, K. V. *Int. J. Radiat. Oncol. Biol. Phys.* **1984**, *10*, 1749.
- 24 Koch, C. J. Personal communication.
- 25 Wardman, P.; Priyadarsini, K. I.; Dennis, M. F.; Everett, S. A.; Naylor, M. A.; Patel, K. B.; Stratford, I. J.; Stratford, M. R. L.; Tracy, M. *Br. J. Cancer* **1996**, *74*, S70.
- 26 Zeeman, E. M.; Brown, J. M.; Lemmon, M. J.; Hirst, V. K.; Lee, W. W. *Int. J. Radiat. Biol. Oncol. Phys.* **1986**, *12*, 1239.
- 27 Skarsgard, L. D.; Vinczan, A.; Skwarchuk, M. W.; Chaplin, D. J. *Int. J. Radiat. Oncol. Biol. Phys.* **1994**, *29*, 363.
- 28 Skov, K. A.; Adomat, H.; Conway, D. C.; Farrell, N. P. *Chemico-Biol. Inter.* **1987**, *62*, 117.

- 29 Skov, K. A.; Adomat, H.; Doedee, M.; Farrell, N. P. *Anticancer Drug Design* **1994**, *9*, 103 (and references therein).
- 30 Adomat, H.; Skov, K. A.; Farrell, N. P. Unpublished results.
- 31 Chan, P. K. L.; Skov, K. A.; Farrell, N. P.; James, B. R. *Int. J. Radiat. Oncol. Biol. Phys.* **1986**, *12*, 1059.
- 32 Chan, P. K. L.; Skov, K. A.; James, B. R. *Int. J. Radiat. Biol.* **1987**, *52*, 49.
- 33 Clarke, M. J. *In Inorganic Chemistry, Biology and Medicine*; A. E. Martell, Ed.; Am. Chem. Soc., Washington, D. C., 1979, p. 157.
- 34 Clarke, M. J. *In Progress in Clinical Biochemistry and Medicine*; Springer-Verlag, Berlin, 1989, p. 25.
- 35 Yapp, D. T. T. Ph. D. Thesis, University of British Columbia, 1991.
- 36 Yapp, D. T. T.; Rettig, S. J.; James, B. R.; Skov, K. A. *Inorg. Chem.* **1997**, *36*, 5635.
- 37 Skov, K. A.; Koch, C. J.; Marples, B. *Rad. Oncol. Invest.* **1994**, *2*, 164.
- 38 Skov, K. A.; MacPhail, S. *Int. J. Radiat. Oncol. Biol. Phys.* **1994**, *29*, 87.
- 39 Adomat, H.; Skov, K. A. Unpublished results.
- 40 Born, J. L.; Smith, B. R.; Harper, N.; Koch, C. J. *Biochem. Pharmacol.* **1992**, *43*, 1337.
- 41 Raleigh, J. A.; Miller, G. G.; Franko, A. J.; Koch, C. J.; Fuciarelli, A. F.; Kelly, D. A. *Br. J. Cancer* **1987**, *56*, 395.
- 42 Adams, G. E.; Stratford, I. J.; Wallace, R. G.; Wardman, P.; Watts, M. E. *J. Natl. Cancer Inst.* **1980**, *64*, 555.
- 43 Wardman, P. *Environ. Health Perspec.* **1985**, *64*, 309.
- 44 Kachur, A. V.; Koch, C. J. Unpublished results.
- 45 Adams, G. E.; Clarke, E. D.; Flockhart, I. R.; Jacobs, R. S.; Sehmi, D. S.; Stratford, I. J.; Wardman, P.; Watts, M. E.; Parrick, J.; Wallace, R. G.; Smithen, C. E. *Int. J. Radiat. Biol.* **1979**, *35*, 133.
- 46 Evans, S. M.; Joiner, B.; Jenkins, W. T.; Laughlin, K. M.; Lord, E. M.; Koch, C. J. *Br. J. Cancer* **1995**, *72*, 875.

- 47 Franko, A. J.; Koch, C. J.; Boisvert, D. P. J. *Cancer Res.* **1992**, *52*, 1.
- 48 Brizel, D. M.; Scully, S. P.; Harrelson, J. M.; Layfield, L. J.; Bean, J. M.; Prosnitz, L. R.; Dewhirst, M. W. *Cancer Res.* **1996**, *56*, 941.
- 49 Höckel, M.; Schlenger, K.; Aral, B.; Mitze, M.; Schäffer, U.; Vaupel, P. *Cancer Res.* **1996**, *56*, 4509.
- 50 Skov, K. A. British Columbia Cancer Research Centre, 1998; from a report on the importance of hypoxia.
- 51 Sharma, V.; Crankshaw, C. L.; Piwnica-Worms, D. *J. Med. Chem.* **1996**, *18*, 3483.
- 52 Hagan, D. O.; Rzepa, H. S. *J. Chem. Soc., Chem. Commun.* **1997**, 645.
- 53 Bott, G.; Field, L. D.; Sternhell, S. *J. Am. Chem. Soc.* **1980**, *102*, 5618.

Chapter 7

Conclusions and Recommendations for Future Work

7.1 General Remarks

This chapter is intended to highlight the successful projects within this thesis and includes a summary of the most significant results obtained for each specific area of synthetic chemistry studied (Chapters 3 to 5). The less successful experiments will also be considered, including suggestions on how syntheses may be improved. New ideas and suggestions for future work are also included throughout this chapter. Finally, general conclusions are made regarding the use of halogenated nitroimidazoles and their Ru complexes as potential hypoxia-imaging agents (Chapter 6).

7.2 Halogenated Nitroimidazoles (Chapter 3)

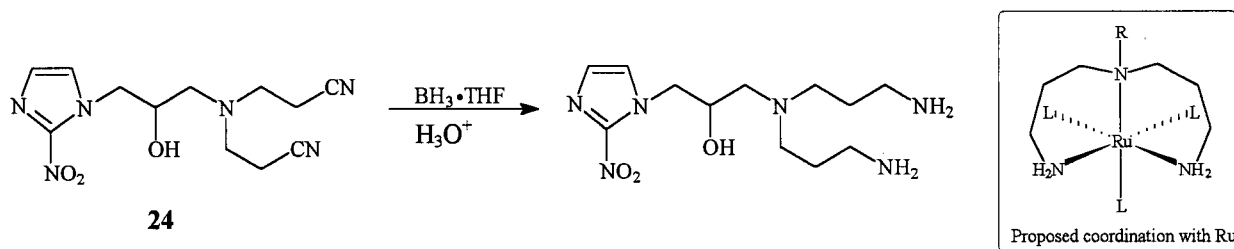
One aim of this work was to synthesize a large amount of **EF5** and study its coordination chemistry with Ru (Chapters 4 and 5); however, because of interest in the interaction of the monoclonal antibody (ELK3-51) with **EF5** (Chapter 6), presumably via binding with the side-chain, the synthesis of analogous nitroimidazoles was investigated. The coupling of an N1 acid-containing, nitroimidazole derivative with an amine hydrohalide resulted in formation of an amide linkage, typically in high yield. The only nitroimidazole compound synthesized which could not be isolated in >15 % yield was **EF1**. This was likely due to the extremely hygroscopic nature of $\text{H}_2\text{NCH}_2\text{CH}_2\text{CH}_2\text{F}\cdot\text{HCl}$, and this complication could likely be remedied by weighing and mixing reactants in an inert atmosphere glove box. Ensuring that the THF, NMM and iBuClFrm are 'absolutely' H_2O free would also restrict the preferential formation of hydrolysis products.

The $2\text{NO}_2\text{Im}$ compounds were the most widely investigated species in Chapter 3 because of their higher $E_{1/2}$ values when compared to those of the $2\text{Me}_5\text{NO}_2$ - and $2\text{Me}_4\text{NO}_2\text{Im}$ compounds. The $2\text{Me}_5\text{NO}_2$ - (M series) and $2\text{Me}_4\text{NO}_2\text{Im}$ ($2\text{M}_4\text{N}$ series) analogues of the E series ($2\text{NO}_2\text{Im}$) could be easily synthesized but, because they are not easily reduced *in vitro/vivo*, even

under hypoxic conditions, there appears to be no need to pursue these compounds (unless their coordination chemistry warrants it).

The coupling of iodoacetic acid with $\text{H}_2\text{NCH}_2\text{CF}_2\text{CF}_3 \cdot \text{HCl}$ to yield **IF5** proved to be a useful method¹ for the synthesis of **EF5** in higher yields than previously reported. The ease of purification of **IF5** and **ClIF5** by sublimation, and thus avoiding tedious chromatography, was another major advantage for generating the amide linkage prior to introduction of the NO_2Im moiety. This approach could conceivably be used to synthesize all of the NO_2Im compounds reported in this thesis and, for that matter, would be useful for the introduction of new side-chains onto a wide range of heterocycles. This approach would avoid the sometimes difficult synthesis and isolation of the $\text{NO}_2\text{Im}/\text{acid}$ species. Of note, because of the lability of the C-Br bond, syntheses of the monobromo derivatives of **IF5** (e.g. **IBr**) are not effective.

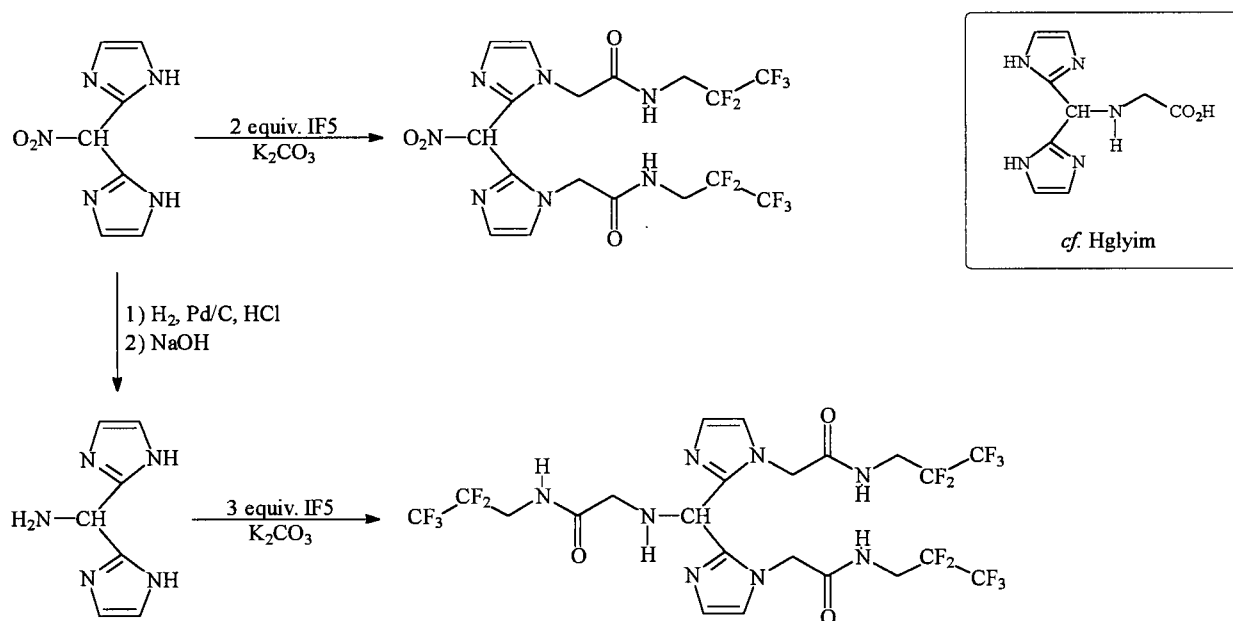
Because of the decreased coordinating ability of NO_2Im versus Im, the introduction of a chelating moiety into the side-chain might facilitate a more stable interaction with Ru. The synthesis of the bis-nitrile species (**24**) was intended to test this hypothesis. Reduction of the nitrile groups to their corresponding amines with $\text{BH}_3 \cdot \text{THF}$ ² with non-reduction of the nitro group would yield a tridentate ligand analogous to dien (Scheme 7-1); however, the limited availability of **RSU1111** curtailed attempts of this reaction. The position of the nitroimidazole moiety on the outer edge of the ligand (not directly bound to Ru) may contribute significantly to the radiosensitizing properties of the proposed complex.



Scheme 7-1: Proposed reduction of bis-CN compound (**24**) with $\text{BH}_3 \cdot \text{THF}$.

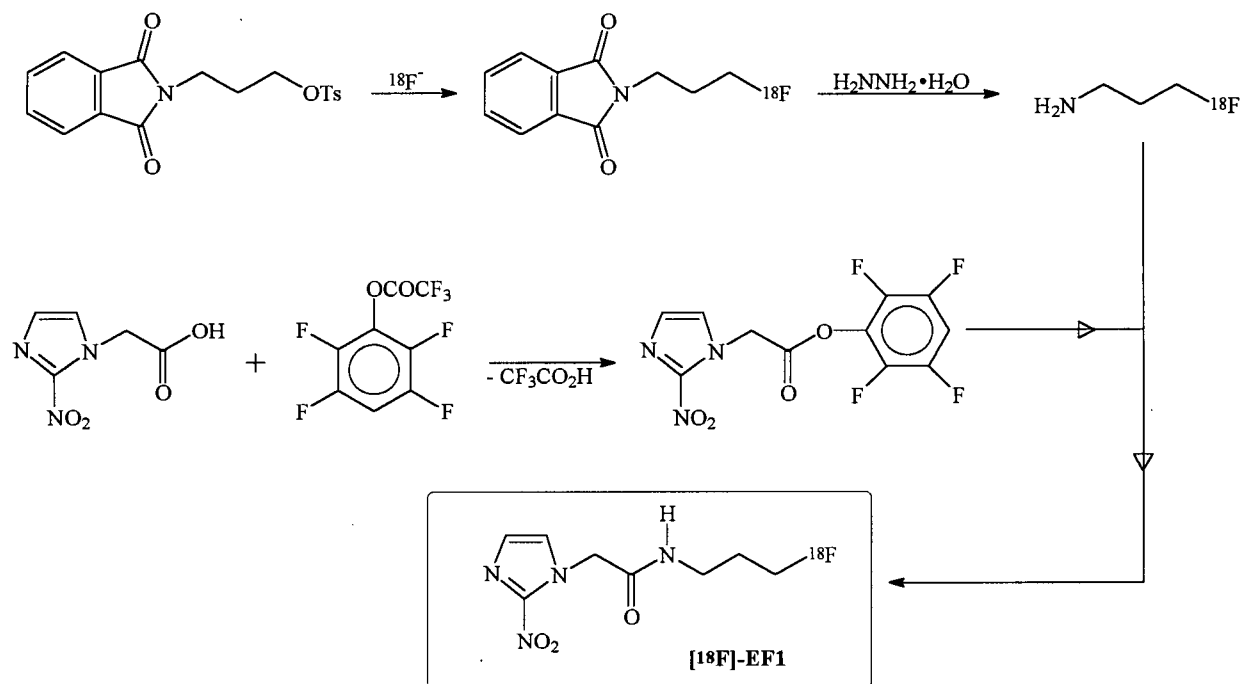
The discovery that only the $-\text{CH}_2\text{CF}_2\text{CF}_3$ group (in **IF5**) was required for recognition by the MoAb ELK3-51, and not the entire nitroimidazole compound (**EF5**) (Chapter 6), led to ideas for the synthesis of other interesting ligands which could potentially form a stronger interaction

with Ru than does **EF5**. These potentially new ligands are analogous to Hglyim, previously synthesized by Campbell *et al.*³ (using a modified method reported by Joseph *et al.*⁴), and which is known to form dinuclear Cu(II) compounds.³ Again, these ligands could form stable chelate rings with Ru and would allow for the introduction of up to three $-\text{CH}_2\text{CF}_2\text{CF}_3$ units (Scheme 7-2).



Scheme 7-2: Proposed synthesis of ligands containing two or three $-\text{CH}_2\text{CF}_2\text{CF}_3$ units.

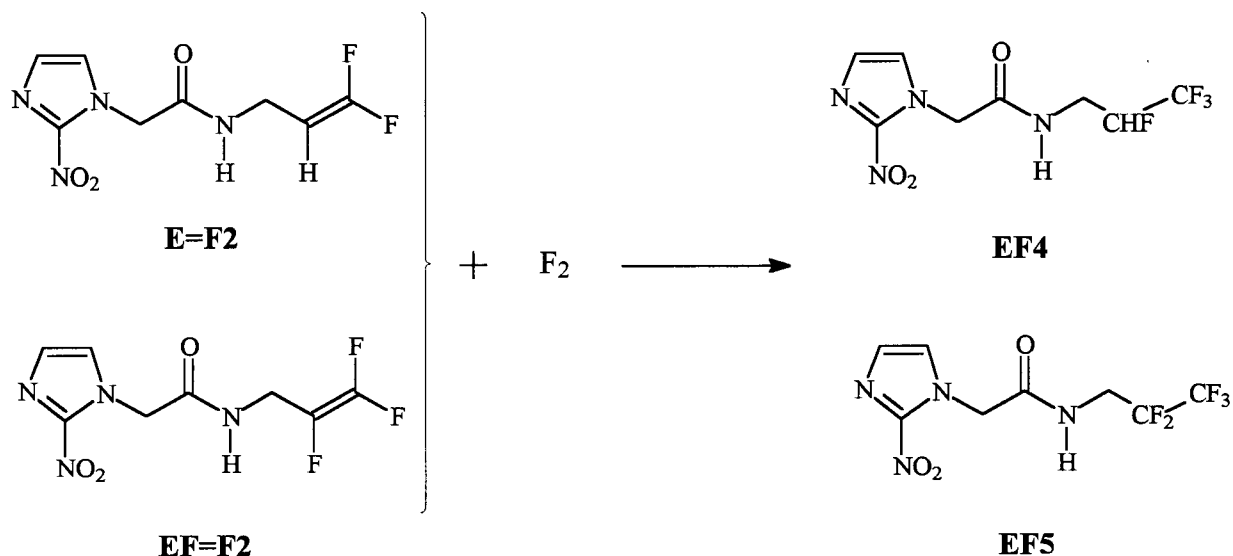
The goal of synthesizing an ^{18}F -labeled nitroimidazole for use in PET imaging of hypoxic tumours was not realized during this thesis work, although some of the negative results suggest the need for alternate synthetic pathways. For example, the synthesis of fluorinated nitroimidazoles via exchange of F^- with other halogens in the side-chain was, for the most part, unsuccessful because of the reactivity of the 2NO_2 group which was easily displaced by F^- . However, a synthesis of ^{18}F -fluoroetanidazole recently reported by Tewson, avoids the problem of the labile nitro group by introducing an ^{18}F -atom onto the amine prior to coupling with the nitroimidazole.⁵ A method analogous to that of Tewson seems plausible for synthesis of ^{18}F -**EF1** in higher yields than previously reported (Scheme 7-3).⁶



Scheme 7-3: Proposed synthesis of [^{18}F]-EF1 similar to that used by Tewson to synthesize [^{18}F]-fluoroetanidazole.

Another alternate route for the introduction of ^{18}F could be via addition of [^{18}F] F_2 across an alkene double bond.⁷ The advantages of this approach are that F_2 does not displace the nitro group on the imidazole and that ^{18}F activity ($T_{1/2} \sim 110$ min) is not lost over the course of subsequent chemical reactions. The elimination of HBr from EF2Br gave the difluoro alkene $\text{E}=\text{F}_2$ which could conceivably form [^{18}F]-EF4 when reacted with [^{18}F] F_2 (Scheme 7-4). If successful, this reaction should also be attempted with $\text{EF}=\text{F}_2$ (whose synthesis is currently being developed by Prof. Dolbier's group) which would yield the analogous [^{18}F]-EF5 species.

The final suggestion for introduction of ^{18}F into a $2\text{NO}_2\text{Im}$ species stems from a report by Rozen *et al.* which describes the transformation of carbonyl to CF_2 using BrF_3 .⁸ The reaction of EF5 with BrF_3 could give a species akin to 12 (see p. 68), and this would remedy the problem of F-addition but, at the same time, may alter the compound's lipophilicity to an extent that it may no longer be useful as a non-toxic, hypoxia-imaging agent.



Scheme 7-4: Possible F_2 addition to fluoroalkenes to yield **EF4** and **EF5**.

7.3 Ruthenium Imidazole Complexes (Chapter 4)

Synthesis and isolation of a variety of Ru(II) and Ru(III) imidazole and nitroimidazole complexes were generally successful. The initial goal was to obtain a water-soluble Ru(III)-**EF5** complex which could be used for either hypoxia-imaging or radiosensitization. To achieve this, the coordination chemistry of Im and its Me-substituted derivatives with Ru was investigated to determine whether reaction with the less basic nitroimidazoles was possible. Once a general reaction scheme was developed for the imidazoles, reaction with the nitroimidazoles was performed. In general, the nitroimidazole complexes were significantly more difficult to characterize than their imidazole analogues because of their low solubility in most organic solvents, their noisy ^1H NMR spectra and their hygroscopic nature.

The Ru(III) complex $[\text{Ru}(\text{DMF})_6][\text{CF}_3\text{SO}_3]_3$ was a useful synthetic precursor because of the weakly coordinated DMF ligands. Interestingly, all Im/ NO_2Im complexes synthesized from this complex were isolated as Ru(II) species as a result of the *in situ* reduction of Ru(III). The oxidation of the isolated Ru(II) complexes should be investigated to determine if the corresponding Ru(III) complexes can be generated, as these are potentially more useful biologically. Of note, the number of ligands coordinated to Ru(II) was found to be related to the

steric bulk of the ligand; however, it is not obvious why the $[\text{Ru}(\text{2NO}_2\text{Im})_6][\text{CF}_3\text{SO}_3]_2$ could be synthesized while the analogous 2MeIm complex could not.

The use of $\text{RuCl}_3 \cdot 3\text{H}_2\text{O}$ as a direct synthetic precursor has, for the most part, not been studied because of its ill-defined composition. However, the addition of Im or NO_2Im to an EtOH solution of $\text{RuCl}_3 \cdot 3\text{H}_2\text{O}$ typically yields complexes of the type RuCl_3L_3 ($\text{L} = \text{Im}$ or NO_2Im), unless the NO_2Im species has a bulky side-chain which leads to isolation of $\text{RuCl}_3\text{L}_2(\text{EtOH})$ (e.g. $\text{L} = \text{SR2508}$, **EF5**) complexes. This work paved the way for the synthesis of a new series of Ru(III) trichloro complexes containing the new, halogenated nitroimidazoles reported in Chapter 3.

The synthesis of Ru-phosphine-Im complexes by past members of the group^{9,10} prompted the synthesis of analogous NO_2Im complexes. The isolation of $[\text{RuCl}(\text{dppb})(\text{EF5})]_2(\mu\text{-Cl})_2$ revealed that the NO_2Im complexes exhibit coordination chemistry different from that of Im and its Me-derivatives, and so the reaction of the other halogenated nitroimidazoles with $\text{Ru}_2\text{Cl}_4(\text{dppb})_2(\mu\text{-dppb})$ should be investigated. Preliminary reactions of several **2M4NX(-1)** with $\text{RuCl}_2(\text{PPh}_3)_3$ have recently been examined¹¹ and were determined to yield ionic complexes of composition $[\text{RuCl}(\text{PPh}_3)_2\text{L}]\text{Cl}$ ($\text{L} = \text{2M4NX(-1)}$; $\text{X} = \text{F3}$ (see Figure 7-1), F, Cl), prompting further investigation of similar monomeric Ru(II) complexes.

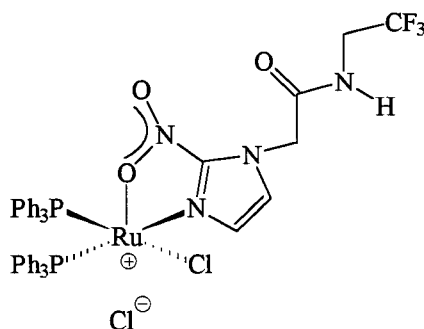


Figure 7-1: Proposed coordination geometry of $[\text{RuCl}(\text{PPh}_3)_2(\text{2M4NF3(-1)})]\text{Cl}$.

The aqueous chemistry of all the complexes reported in Chapter 4 (except **43** and **44**) was not examined, but should be investigated. Determination of the composition of the species in aqueous solution would be invaluable for potentially understanding the action of the complexes *in vitro/vivo*. The electrochemistry of the NO_2Im complexes should also be examined.

7.4 Ruthenium β -Diketonate Imidazole Complexes (Chapter 5)

The precursors *cis*-[Ru(acac)₂(MeCN)₂][CF₃SO₃], *cis*-Ru(hfac)₂(MeCN)₂ and *cis*-Ru(acac)(hfac)(MeCN)₂ were useful for the synthesis of several bis-Im and bis-NO₂Im complexes. The Im and MeIm complexes were generally easy to isolate because no side-products, other than the mono-substituted complexes, were observed. Conversely, synthesis of the NO₂Im complexes resulted in numerous side-products, the major product being isolated only in lower yields. The isolation and characterization of the other minor products, by performing the reaction on a larger (gram) scale, may give insight as to why the reactions with NO₂Im are typically not clean.

Of all the Ru-EF5 complexes synthesized throughout this work, [Ru(acac)₂(EF5)₂][CF₃SO₃] was determined to be the most biologically useful species as it gave a fluorescent signal four times that of EF5 in hypoxia (determined via MoAb assay, Chapter 6). This result suggests that the non-toxic acac complexes may be useful hypoxia-imaging agents. The synthesis and isolation of the complexes [Ru(acac)₂(L)₂][CF₃SO₃] (L = **ImF5**, **MF5**, **2M4NF5**), with subsequent testing by way of the MoAb assay, would be useful in determining if the fluorescent signal obtained is directly due to binding of the MoAb with the pentafluorinated side-chain, regardless of the position and/or presence of a nitro group on the imidazole ring.

The ability to regulate the Ru(III/II) reduction potential by varying the nature of the substituents R, R' and R" on the β -diketonate ligand (RC(O)CR'C(O)CR") allows one to synthesize a Ru(III) complex with a specific $E_{1/2}$. This may be especially useful in determining if a specific Ru(III) complex, a potential prodrug to its more active Ru(II) species, will be reduced under hypoxic conditions. By alteration of the R, R' and R" substituents on the acac ligands within [Ru(acac)₂(EF5)₂][CF₃SO₃], the $E_{1/2}$ could be increased to a level which could yield a higher fluorescence value.

The bis-hfac Im and MeIm complexes were all isolated as Ru(II) species and were not characterized by single crystal X-ray analysis, while for the Ru(III) bis-acac Im and MeIm complexes X-ray structures were determined. The inability to grow single crystals of the bis-hfac complexes may be due to the properties of the hfac ligand or the oxidation state of the Ru. The oxidation of the bis-hfac complexes with H₂O₂ in the presence of CF₃SO₃⁻ should give the

analogous Ru(III) triflate complexes, which may or may not be stable, but may yield single crystals.

7.5 *In Vitro* Evaluation of Nitroimidazoles and their Ru Complexes

In general, the 2-, 4- and 5-nitroimidazoles and Ru Im and NO₂Im complexes showed little *in vitro* toxicity toward SCCVII cells treated under either oxic or hypoxic conditions. The concentrations of the compounds tested were typically quite low ($\leq 100 \mu\text{M}$), and this would explain their absence of cytotoxicity; tests with higher concentration intervals (*e.g.* 100, 500, 1000 and 2000 μM) should be carried out to determine if these compounds are then toxic. The Ru complexes should also be tested at high doses, although their solubility typically limits the maximum concentration obtainable in aqueous solution.

The accumulation of the Ru complexes revealed a large variability in SCCVII cells. The Ru-EF5 complexes typically exhibited significant accumulation, while most of the other complexes did not appear to accumulate. This result is likely due to the lower hydrophilicity of EF5 which may facilitate transport of the Ru complex into the cell; however, this assay cannot determine whether the complex is within the cell or simply adhering to proteins on the outer membrane. The synthesis and testing of other fluorinated-2NO₂Im Ru(III) complexes should be studied to determine if the cellular accumulation is dependent on a specific ligand (such as EF5), or on the type (composition) of ligand present.

The result of DNA-binding reinforces the trend observed for the accumulation studies that the Ru-EF5 complexes exhibit the highest values of all complexes tested. These high DNA-binding values also lend support for the transport, either by active transport or passive diffusion, of the Ru-EF5 complexes into the cell. Interestingly, the only other complex to exhibit significant DNA-binding was RuCl₃(SR2508)₂(EtOH). SR2508 is also a 2NO₂Im species, suggesting that the coordination of the 2NO₂Im ligands to Ru(III) plays a key role in DNA-binding. This is likely due to the potentially increased $E_{1/2}$ value of these complexes in comparison to those of the analogous nitro-free complexes. The synthesis, isolation and subsequent biological testing (DNA-binding assay) of RuCl₃(ImF5)₂(EtOH) should be done to substantiate this hypothesis; if the levels of Ru associated with the DNA are found to be significantly lower for this complex then the binding will be related to the presence of the nitro moiety in the imidazole ligand.

Preliminary investigation of $\text{RuCl}_3(\text{EF5})_2(\text{EtOH})$ and $\text{RuCl}_3(\text{SR2508})_2(\text{EtOH})$ as potential hypoxia-selective radiosensitizers revealed no activity. However, **EF5** was determined to be a potentially useful radiosensitizer as it had a modest sensitivity enhancement ratio (SER) value (1.6). The radiosensitizing ability of **EF5** must be tested at several concentrations before any conclusions can be made as to its potential use in the clinic. The other halogenated nitroimidazoles (chapter 3) should also be screened for their potential as radiosensitizers.

A comparison of the MoAb assays for ELK3-51 and ELK5-A8 with the same set of nitroimidazoles revealed significant differences between the two MoAbs. As determined from the fluorescence values in hypoxia, the binding pocket of ELK3-51 was dependent on both the size and length of the N1 side-chain on $2\text{NO}_2\text{Im}$, while the log of the fluorescence was perhaps directly proportional to the reduction potential of the compound. ELK5-A8 had much higher specificity and was determined to bind only to compounds with a specific length and terminal group composition; no dependence on reduction potential was observed. The excellent correlation of image (ICM) and flow cytometry data suggests the potential use of ICM in quantitatively assessing the degree of hypoxia within a given tumour.

A summary of the most significant results obtained from the *in vitro* assays performed at the BCCRC are recorded in Table 7.1.

Table 7.1: Summary of most significant *in vitro* assay results obtained during this thesis work.

Compound	Toxicity (PE)		Cell Accum. Ru (ng/10 ⁶ cells)		DNA-binding ng Ru/mg DNA		ELK3-51 (FCM) Mean Signal		ELK5-A8 (FCM) Mean Signal	
	Oxic	Hypoxic	Oxic	Hypoxic	Oxic	Hypoxic	Oxic	Hypoxic	Oxic	Hypoxic
EF5	0.50	0.48					0.8	79.2	0.4	7.0
EF3	0.42	0.41					1.2	48.4	0.6	70.2
EF3(-1)							1.0	44.9	0.3	0.2
EF2Br							1.2	58.4	0.8	92.5
EC11							1.5	35.7	0.4	20.5
MF5							0.2	7.2		
RuCl₃(EF5)₂(EtOH)	0.75	0.58	59.1	164.8	0.4	19.4	2.0	42		
[Ru(DMF)₂(EtOH)₂(EF5)₂]Tf₃	0.61	0.58	55.4	37.1	8.9	13.3	2.7	50		
[Ru(acac)₂(EF5)₂]Tf	0.54	0.48	76.3	57.8	19.9	23.1	8.6	315		
RuCl₃(SR2508)₂(EtOH)	0.61	0.60	6.6	3.5	20.7	16.4				

7.6 References

- ¹ Baird, I. R.; Skov, K. A.; James, B. R.; Rettig, S. J.; Koch, C. J. *Synth. Commun.* **1998**, 28, 3701.
- ² Fortier, D. G.; McAuley, A. *Inorg. Chem.* **1989**, 28, 655.
- ³ Campbell, C. J.; Driessen, W. L.; Reedijk, J.; Smeets, W.; Spek, A. L. *J. Chem. Soc., Dalton Trans.* **1998**, 2703.
- ⁴ Joseph, M.; Leigh, T.; Swain, M. L. *Synthesis* **1977**, 459.
- ⁵ Tewson, T. J. *Nucl. Med. Biol.* **1997**, 24, 755.
- ⁶ Kachur, A. V.; Evans, S. M.; Shiue, C.-Y.; Dolbier, Jr., W. R.; Li A.-R.; Roche, A.; Skov, K. A.; Baird, I. R.; James, B. R.; Koch, C. J. *Appl. Rad. Isot.* submitted.
- ⁷ Rozen, S. *In The chemistry of halides, pseudo-halides and azides*; S. Patai and Z. Rappoport, Eds.; Wiley, Chichester, UK, 1995, p. 629.
- ⁸ Rozen, S.; Mishani, E.; Bar-Haim, A. *J. Org. Chem.* **1994**, 59, 2918.
- ⁹ Batista, A. A.; Polato, E. A.; Queiroz, S. L.; Nascimento, O. R.; James, B. R.; Rettig, S. J. *Inorg. Chim. Acta* **1995**, 230, 111.
- ¹⁰ Quieroz, S. L.; Batista, A. A.; Olivia, G.; Gambardella, M. T. doP.; Santos, R. H. A.; MacFarlane, K. S.; Rettig, S. J.; James, B. R. *Inorg. Chim. Acta* **1998**, 267, 209.
- ¹¹ Syntheses performed by Mr. Fei Gao, visiting scientist from Shanxi University, P.R. of China.

Appendix I

X-ray Data

Appendix I-1 X-ray data for EF5

Table I-1.1 Experimental details for EF5

Formula	C ₈ H ₇ F ₅ N ₄ O ₃
fw	302.16
Crystal system	Monoclinic
Space group	<i>Pc</i> (No. 7)
<i>a</i> , Å	4.9116(7)
<i>b</i> , Å	10.1627(5)
<i>c</i> , Å	11.6029(7)
α , °	—
β , °	95.189(9)
γ , °	—
<i>V</i> , Å ³	576.79(9)
<i>Z</i>	2
ρ_{calc} , g/cm ³	1.740
<i>F</i> (000)	304
μ , cm ⁻¹	16.73
Crystal size, mm	0.05 × 0.20 × 0.40
Transmission factors	0.86-1.00
Scan type	ω -2 θ
Scan range, deg in ω	1.05 + 0.20 tan θ
Scan speed, deg/min	16 (up to 9 scans)
Data collected	—
2 θ_{max} deg	155
Crystal decay, %	2.09
Total reflections	1402
Unique reflections	1265
<i>R</i> _{merge}	0.026
No. with $I \geq 3\sigma(I)$	1081
No. of variables	208
<i>R</i> (<i>F</i>) ($I \geq 3\sigma(I)$)	0.026
<i>R</i> _w (<i>F</i>) ($I \geq 3\sigma(I)$)	0.022
<i>R</i> (<i>F</i> ²) (all data)	—
<i>R</i> _w (<i>F</i> ²) (all data)	—
gof	0.73
Max Δ/σ (final cycle)	0.002
Residual density e/Å ³	-0.12 to 0.10

Table I-1.2 Atomic coordinates and $B_{\text{iso}}/B_{\text{eq}}$ for EF5

atom	x	y	z	B_{eq}
F(1)	0.2251	-0.0166(2)	0.4659	5.84(5)
F(2)	-0.1905(6)	0.0362(2)	0.4056(3)	5.50(5)
F(3)	-0.0859(6)	-0.0095(2)	0.1859(2)	6.96(6)
F(4)	0.3305(6)	-0.0553(2)	0.2387(3)	6.96(6)
F(5)	0.0069(7)	-0.1726(2)	0.2965(3)	7.83(7)
O(1)	0.5183(6)	0.3407(2)	0.4946(3)	4.79(5)
O(2)	0.4893(7)	0.3659(3)	0.7908(3)	7.12(8)
O(3)	0.8590(7)	0.4748(3)	0.8326(2)	5.79(6)
N(1)	0.3276(6)	0.5459(2)	0.6183(2)	3.27(5)
N(2)	0.6766(7)	0.6703(3)	0.6881(3)	4.18(6)
N(3)	0.0934(6)	0.2622(2)	0.4489(3)	3.72(5)
N(4)	0.6367(7)	0.4603(3)	0.7794(3)	4.18(6)
C(1)	0.5500(7)	0.5585(3)	0.6957(3)	3.28(5)
C(2)	0.5297(9)	0.7333(3)	0.5997(4)	4.83(8)
C(3)	0.3175(8)	0.6592(3)	0.5566(3)	4.28(7)
C(4)	0.1495(8)	0.4337(3)	0.5896(3)	3.63(6)
C(5)	0.2760(7)	0.3413(3)	0.5060(3)	3.18(6)
C(6)	0.1605(7)	0.1775(3)	0.3571(3)	3.51(6)
C(7)	0.0714(8)	0.0387(3)	0.3769(3)	3.65(6)
C(8)	0.0827(9)	-0.0514(3)	0.2735(4)	4.63(8)

Table I-1.3 Bond lengths (Å) for EF5

atom	atom	distance
F(1)	C(7)	1.345(4)
F(3)	C(8)	1.322(4)
F(5)	C(8)	1.321(4)
O(2)	N(4)	1.217(3)
N(1)	C(1)	1.356(3)
N(1)	C(4)	1.457(4)
N(2)	C(2)	1.360(4)
N(3)	C(6)	1.431(4)
C(2)	C(3)	1.344(5)
C(6)	C(7)	1.501(4)

atom	atom	distance
F(2)	C(7)	1.358(3)
F(4)	C(8)	1.317(4)
O(1)	C(5)	1.209(3)
O(3)	N(4)	1.214(3)
N(1)	C(3)	1.354(4)
N(2)	C(1)	1.302(4)
N(3)	C(5)	1.335(3)
N(4)	C(1)	1.430(4)
C(4)	C(5)	1.523(4)
C(7)	C(8)	1.514(4)

Table I-1.4 Bond angles (°) for EF5

atom	atom	atom	angle
C(1)	N(1)	C(3)	105.0(2)
C(3)	N(1)	C(4)	123.5(2)
C(5)	N(3)	C(6)	122.8(2)
O(2)	N(4)	C(1)	118.7(2)
N(1)	C(1)	N(2)	113.5(3)
N(2)	C(1)	N(4)	122.7(3)
N(1)	C(3)	C(2)	106.9(3)
O(1)	C(5)	N(3)	124.5(3)
N(3)	C(5)	C(4)	113.1(2)
F(1)	C(7)	F(2)	106.4(3)
F(1)	C(7)	C(8)	107.3(2)
F(2)	C(7)	C(8)	106.7(2)
F(3)	C(8)	F(4)	107.8(3)
F(3)	C(8)	C(7)	110.4(3)
F(4)	C(8)	C(7)	111.2(3)

atom	atom	atom	angle
C(1)	N(1)	C(4)	131.0(3)
C(1)	N(2)	C(2)	103.8(3)
O(2)	N(4)	O(3)	123.8(3)
O(3)	N(4)	C(1)	117.4(3)
N(1)	C(1)	N(4)	123.8(3)
N(2)	C(2)	C(3)	110.9(3)
N(1)	C(4)	C(5)	110.9(2)
O(1)	C(5)	C(4)	122.3(2)
N(3)	C(6)	C(7)	111.2(2)
F(1)	C(7)	C(6)	111.0(3)
F(2)	C(7)	C(6)	110.5(2)
C(6)	C(7)	C(8)	114.5(2)
F(3)	C(8)	F(5)	106.7(3)
F(4)	C(8)	F(5)	108.6(3)
F(5)	C(8)	C(7)	111.9(3)

Appendix I-2 X-ray data for EF2Br•0.5 H₂O

Table I-2.1 Experimental details for EF2Br•0.5 H₂O

Formula	C ₈ H ₁₀ BrF ₂ N ₄ O _{3.50}
fw	336.09
Crystal system	Monoclinic
Space group	<i>P</i> 2 ₁ / <i>n</i> (No. 14)
<i>a</i> , Å	5.1203(6)
<i>b</i> , Å	17.3444(3)
<i>c</i> , Å	13.4033(6)
α , °	—
β , °	101.1438(9)
γ , °	—
<i>V</i> , Å ³	1167.9(2)
<i>Z</i>	4
ρ_{calc} , g/cm ³	1.911
<i>F</i> (000)	668
μ , cm ⁻¹	35.70
Crystal size, mm	0.40 × 0.08 × 0.05
Transmission factors	0.87-1.00
Scan type	ϕ , ω sweeps
Scan range, deg in ω	0.5
Scan speed, deg/min	—
Data collected	462 frames, 75 s/frame
$2\theta_{max}$, deg	61
Crystal decay, %	—
Total reflections	10761
Unique reflections	3080
<i>R</i> _{merge}	0.044
No. with $I \geq 3\sigma(I)$	1498
No. of variables	172
<i>R</i> (<i>F</i>) ($I \geq 3\sigma(I)$)	0.035
<i>R</i> _w (<i>F</i>) ($I \geq 3\sigma(I)$)	0.031
<i>R</i> (<i>F</i> ²) (all data)	—
<i>R</i> _w (<i>F</i> ²) (all data)	—
gof	1.18
Max Δ/σ (final cycle)	0.00
Residual density e/Å ³	-1.49 to 1.54

Table I-2.2 Atomic coordinates and $B_{\text{iso}}/B_{\text{eq}}$ for **EF2Br•0.5 H₂O**

atom	x	y	z	B_{eq}	occ
Br(1)	0.36706(11)	0.43247(4)	0.08749(5)	2.982(10)	0.50
F(1)	0.0513(6)	0.4948(2)	0.2034(3)	3.76(6)	
F(2)	0.1815(6)	0.3782(2)	0.2453(3)	3.97(7)	
O(1)	0.5915(6)	0.6114(2)	0.4783(2)	1.89(6)	
O(2)	0.7908(6)	0.8587(2)	0.5753(3)	2.24(6)	
O(3)	0.6535(6)	0.7877(2)	0.4418(2)	1.69(6)	
O(4)	0.055(2)	0.5181(8)	0.4888(13)	10.0(4)	
N(1)	0.2680(6)	0.7222(2)	0.5341(3)	0.89(6)	
N(2)	0.4559(7)	0.7843(2)	0.6771(3)	1.30(7)	
N(3)	0.3950(7)	0.6176(2)	0.3112(3)	1.15(6)	
N(4)	0.6446(7)	0.8094(2)	0.5288(3)	1.36(7)	
C(1)	0.4560(8)	0.7736(3)	0.5794(4)	1.00(7)	
C(2)	0.2543(8)	0.7373(3)	0.6959(4)	1.35(8)	
C(3)	0.1371(8)	0.6989(3)	0.6088(4)	1.32(8)	
C(4)	0.2075(8)	0.6949(3)	0.4290(3)	1.17(8)	
C(5)	0.4187(9)	0.6367(3)	0.4090(4)	1.14(8)	
C(6)	0.5701(8)	0.5602(3)	0.2801(3)	1.21(7)	
C(7)	0.4877(10)	0.4778(3)	0.2975(4)	1.64(8)	
C(8)	0.2689(9)	0.4466(3)	0.2179(4)	1.91(9)	
H(1)	0.2684	0.6407	0.2636	1.4	
H(2)	0.2015	0.7318	0.7621	1.6	
H(3)	-0.0108	0.6622	0.6017	1.6	
H(4)	0.0327	0.6698	0.4162	1.4	
H(5)	0.2045	0.7389	0.3830	1.4	
H(6)	0.5692	0.5669	0.2075	1.4	
H(7)	0.7506	0.5685	0.3190	1.4	
H(8)	0.6439	0.4446	0.3006	2.0	
H(9)	0.4289	0.4760	0.3629	2.0	

Table I-2.3 Bond lengths (Å) for **EF2Br•0.5 H₂O**

atom	atom	distance
Br(1)	C(8)	1.936(3)
F(1)	C(8)	1.363(4)
F(2)	C(8)	1.343(4)
O(1)	C(5)	1.234(4)
O(2)	N(4)	1.230(3)
O(3)	N(4)	1.236(3)
C(4)	C(5)	1.535(4)
C(6)	C(7)	1.523(4)
C(7)	C(8)	1.489(5)

atom	atom	distance
N(1)	C(1)	1.360(4)
N(1)	C(3)	1.362(4)
N(1)	C(4)	1.459(4)
N(2)	C(1)	1.314(4)
N(2)	C(2)	1.366(4)
N(3)	C(5)	1.326(4)
N(3)	C(6)	1.457(4)
N(4)	C(1)	1.435(4)
C(2)	C(3)	1.372(4)

Table I-2.4 Bond angles (°) for **EF2Br•0.5 H₂O**

atom	atom	atom	angle
C(1)	N(1)	C(3)	105.0(3)
C(1)	N(1)	C(4)	130.1(3)
C(3)	N(1)	C(4)	125.0(3)
C(1)	N(2)	C(2)	104.2(3)
C(5)	N(3)	C(6)	120.5(3)
O(2)	N(4)	O(3)	124.7(3)
O(2)	N(4)	C(1)	117.2(3)
O(3)	N(4)	C(1)	118.1(3)
N(1)	C(1)	N(2)	113.7(3)
N(1)	C(1)	N(4)	123.3(3)
N(2)	C(1)	N(4)	123.0(3)
N(2)	C(2)	C(3)	110.0(3)
N(1)	C(3)	C(2)	107.1(3)

atom	atom	atom	angle
N(1)	C(4)	C(5)	111.4(3)
O(1)	C(5)	N(3)	124.5(3)
O(1)	C(5)	C(4)	121.5(3)
N(3)	C(5)	C(4)	113.9(3)
N(3)	C(6)	C(7)	113.1(3)
C(6)	C(7)	C(8)	115.4(3)
Br(1)	C(8)	F(1)	107.1(2)
Br(1)	C(8)	F(2)	106.7(2)
Br(1)	C(8)	C(7)	113.3(2)
F(1)	C(8)	F(2)	106.9(3)
F(1)	C(8)	C(7)	110.9(3)
F(2)	C(8)	C(7)	111.7(3)

Appendix I-3 X-ray data for MF5

Table I-3.1 Experimental details for MF5

Formula	C ₉ H ₉ F ₅ N ₄ O ₃
fw	316.19
Crystal system	Monoclinic
Space group	<i>P</i> 2 ₁ / <i>c</i> (No. 14)
<i>a</i> , Å	8.227(1)
<i>b</i> , Å	12.323(2)
<i>c</i> , Å	12.5380(6)
α , °	—
β , °	98.546(6)
γ , °	—
<i>V</i> , Å ³	1257.0(2)
<i>Z</i>	4
ρ_{calc} , g/cm ³	1.671
<i>F</i> (000)	640
μ , cm ⁻¹	15.64
Crystal size, mm	0.05 × 0.25 × 0.40
Transmission factors	0.60-0.74
Scan type	ω -2 θ
Scan range, deg in ω	1.15 + 0.20 tan θ
Scan speed, deg/min	16 (up to 9 scans)
Data collected	—
2 θ_{max} , deg	155
Crystal decay, %	—
Total reflections	2869
Unique reflections	2676
<i>R</i> _{merge}	0.024
No. with $I \geq 3\sigma(I)$	1758
No. of variables	227
<i>R</i> (<i>F</i>) ($I \geq 3\sigma(I)$)	0.039
<i>R</i> _w (<i>F</i>) ($I \geq 3\sigma(I)$)	0.039
<i>R</i> (<i>F</i> ²) (all data)	—
<i>R</i> _w (<i>F</i> ²) (all data)	—
gof	2.37
Max Δ/σ (final cycle)	0.0008
Residual density e/Å ³	-0.23 to 0.18

Table I-3.2 Atomic coordinates and $B_{\text{iso}}/B_{\text{eq}}$ for MF5

atom	x	y	z	B_{eq}
F(1)	0.5177(2)	0.4407(1)	0.1586(1)	6.94(5)
F(2)	0.7242(2)	0.3335(2)	0.1470(1)	6.80
F(3)	0.3306(2)	0.3290(2)	0.0065(1)	8.06(6)
F(4)	0.5117(3)	0.2061(2)	0.0071(1)	7.38(6)
F(5)	0.5607(2)	0.3662(2)	-0.0421(1)	7.62(6)
O(1)	0.2812(2)	0.1043(1)	0.1682(1)	4.40(4)
O(2)	0.0088(2)	0.2538(2)	0.0202(2)	5.26(5)
O(3)	-0.1498(2)	0.1544(2)	-0.0923(1)	5.48(5)
N(1)	-0.0438(2)	0.1176(1)	0.1896(1)	2.95(4)
N(2)	0.3408(2)	0.2701(2)	0.2410(2)	3.32(5)
N(3)	-0.1927(2)	-0.0333(2)	0.1744(2)	3.65(4)
N(4)	-0.0810(2)	0.1747(2)	-0.0015(2)	3.65(5)
C(1)	-0.0583(5)	0.0140(3)	0.3593(2)	4.64(7)
C(2)	-0.0987(3)	0.0319(2)	0.2411(2)	3.19(5)
C(3)	0.0683(3)	0.2009(2)	0.2390(2)	3.28(5)
C(4)	-0.1976(3)	0.0106(2)	0.0748(2)	3.54(5)
C(5)	-0.1066(3)	0.1023(2)	0.0826(2)	3.06(5)
C(6)	0.2398(3)	0.1859(2)	0.2113(2)	3.06(5)
C(7)	0.5123(3)	0.2660(2)	0.2306(2)	3.98(6)
C(8)	0.5587(3)	0.3367(2)	0.1424(2)	4.27(6)
C(9)	0.4882(4)	0.3095(3)	0.0274(2)	5.04(8)

Table I-3.3 Bond lengths (\AA) for MF5

atom	atom	distance
F(1)	C(8)	1.347(3)
F(3)	C(9)	1.306(3)
F(5)	C(9)	1.326(3)
O(2)	N(4)	1.229(3)
N(1)	C(2)	1.351(3)
N(1)	C(5)	1.377(3)
N(2)	C(7)	1.437(3)
N(3)	C(4)	1.356(3)
C(1)	C(2)	1.486(3)
C(4)	C(5)	1.351(3)
C(8)	C(9)	1.509(4)

atom	atom	distance
F(2)	C(8)	1.354(3)
F(4)	C(9)	1.320(3)
O(1)	C(6)	1.214(3)
O(3)	N(4)	1.220(2)
N(1)	C(3)	1.455(3)
N(2)	C(6)	1.347(3)
N(3)	C(2)	1.323(3)
N(4)	C(5)	1.420(3)
C(3)	C(6)	1.514(3)
C(7)	C(8)	1.502(4)

Table I-3.4 Bond angles ($^\circ$) for MF5

atom	atom	atom	angle
C(2)	N(1)	C(3)	125.7(2)
C(3)	N(1)	C(5)	129.3(2)
C(2)	N(3)	C(4)	106.0(2)
O(2)	N(4)	C(5)	119.0(2)
N(1)	C(2)	N(3)	112.1(2)
N(3)	C(2)	C(1)	124.3(2)
N(3)	C(4)	C(5)	109.1(2)
N(1)	C(5)	C(4)	108.0(2)
O(1)	C(6)	N(2)	124.0(2)
N(2)	C(6)	C(3)	113.6(2)
F(1)	C(8)	F(2)	107.1(2)
F(1)	C(8)	C(9)	106.6(2)
F(2)	C(8)	C(9)	106.0(2)
F(3)	C(9)	F(4)	107.9(3)
F(3)	C(9)	C(8)	112.3(2)
F(4)	C(9)	C(8)	110.6(2)

atom	atom	atom	angle
C(2)	N(1)	C(5)	104.8(2)
C(6)	N(2)	C(7)	121.4(2)
O(2)	N(4)	O(3)	123.3(2)
O(3)	N(4)	C(5)	117.7(2)
N(1)	C(2)	C(1)	123.5(2)
N(1)	C(3)	C(6)	111.7(2)
N(1)	C(5)	N(4)	124.2(2)
N(4)	C(5)	C(4)	127.8(2)
O(1)	C(6)	C(3)	122.4(2)
N(2)	C(7)	C(8)	114.0(2)
F(1)	C(8)	C(7)	110.1(2)
F(2)	C(8)	C(7)	108.4(2)
C(7)	C(8)	C(9)	118.1(2)
F(3)	C(9)	F(5)	107.6(2)
F(4)	C(9)	F(5)	106.8(2)
F(5)	C(9)	C(8)	111.4(3)

Appendix I-4 X-ray data for 2M4NF5

Table I-4.1 Experimental details for 2M4NF5

Formula	C ₁₀ H ₁₁ F ₅ N ₄ O ₃
fw	330.21
Crystal system	Monoclinic
Space group	<i>P</i> 2 ₁ / <i>n</i> (No. 14)
<i>a</i> , Å	6.563(1)
<i>b</i> , Å	15.3005(9)
<i>c</i> , Å	13.7582(8)
α , °	—
β , °	97.854(8)
γ , °	—
<i>V</i> , Å ³	1368.7(3)
<i>Z</i>	4
ρ_{calc} , g/cm ³	1.602
<i>F</i> (000)	672
μ , cm ⁻¹	14.63
Crystal size, mm	0.20 × 0.25 × 0.45
Transmission factors	0.91-1.00
Scan type	ω -2 θ
Scan range, deg in ω	1.05 + 0.20 tan θ
Scan speed, deg/min	32 (up to 9 scans)
Data collected	—
2 θ_{max} deg	155
Crystal decay, %	1.27
Total reflections	3207
Unique reflections	2943
<i>R</i> _{merge}	0.020
No. with $I \geq 3\sigma(I)$	2004
No. of variables	276
<i>R</i> (<i>F</i>) ($I \geq 3\sigma(I)$)	0.039
<i>R</i> _w (<i>F</i>) ($I \geq 3\sigma(I)$)	0.035
<i>R</i> (<i>F</i> ²) (all data)	—
<i>R</i> _w (<i>F</i> ²) (all data)	—
gof	0.93
Max Δ/σ (final cycle)	0.02
Residual density e/Å ³	-0.15 to 0.17

Table I-4.2 Atomic coordinates and $B_{\text{iso}}/B_{\text{eq}}$ for **2M4NF5**

atom	x	y	z	B{eq}	occ.
F(1)	0.4155(8)	0.0487(3)	0.1329(3)	6.3(1)	0.50
F(1a)	0.294(1)	0.0461(4)	0.0874(4)	11.8(2)	0.50
F(2)	0.518(2)	-0.0298(8)	0.2387(8)	11.1(3)	0.50
F(2a)	0.165(1)	-0.0796(5)	0.0410(4)	11.2(2)	0.50
F(3)	0.336(1)	-0.1729(4)	0.1268(4)	10.8(2)	0.50
F(3a)	0.3934(10)	-0.1572(4)	0.1898(5)	10.4(2)	0.50
F(4)	0.272(1)	-0.0851(5)	0.0131(4)	9.7(2)	0.50
F(4a)	0.505(1)	-0.0448(6)	0.2491(4)	6.1(1)	0.50
F(5)	0.569(3)	-0.0985(8)	0.075(1)	9.3(3)	0.50
F(5a)	0.574(3)	-0.089(1)	0.100(1)	12.3(4)	0.50
O(1)	0.1894(3)	-0.04304(9)	0.3941(1)	4.56(4)	
O(2)	-0.0270(3)	0.2616(1)	0.7822(1)	7.03(6)	
O(3)	0.2095(3)	0.3595(1)	0.8134(1)	5.97(5)	
N(1)	0.3250(3)	0.1762(1)	0.5799(1)	3.94(4)	
N(2)	0.4152(3)	0.2946(1)	0.6679(1)	3.82(4)	
N(3)	0.1261(3)	0.0469(1)	0.2641(1)	4.40(5)	
N(4)	0.1341(3)	0.2966(1)	0.7673(1)	4.81(5)	
C(1)	0.4655(3)	0.2422(1)	0.5988(2)	3.79(5)	
C(2)	0.2389(3)	0.2598(1)	0.6924(1)	3.83(5)	
C(3)	0.1787(3)	0.1872(1)	0.6398(2)	4.18(5)	
C(4)	0.6463(4)	0.2524(2)	0.5467(2)	5.11(6)	
C(5)	0.3297(4)	0.1027(1)	0.5107(2)	4.64(5)	
C(6)	0.1603(4)	0.1098(1)	0.4260(2)	4.32(5)	
C(7)	0.1604(3)	0.0307(1)	0.3606(2)	3.63(5)	
C(8)	0.146(2)	-0.023(1)	0.2018(8)	4.3(2)	0.50
C(8a)	0.081(2)	-0.020(1)	0.1835(10)	4.9(2)	0.50
C(9)	0.3596(10)	-0.0270(4)	0.1699(4)	3.8(1)	0.50
C(9a)	0.240(1)	-0.0317(4)	0.1217(5)	6.3(2)	0.50
C(10)	0.389(1)	-0.0994(4)	0.0956(5)	5.7(2)	0.50
C(10a)	0.432(1)	-0.0766(6)	0.1616(8)	7.2(3)	0.50

Table I-4.3 Bond lengths (Å) for **2M4NF5**

atom	atom	distance
F(1)	C(9)	1.337(7)
F(2)	C(9)	1.31(1)
F(3)	C(10)	1.270(8)
F(4)	C(10)	1.301(10)
F(5)	C(10)	1.25(2)
O(1)	C(7)	1.224(2)
O(3)	N(4)	1.219(2)
N(1)	C(3)	1.358(3)
N(2)	C(1)	1.320(3)
N(3)	C(7)	1.339(3)
N(3)	C(8a)	1.51(1)
C(1)	C(4)	1.476(3)
C(5)	C(6)	1.500(3)
C(8)	C(9)	1.53(2)
C(9)	C(10)	1.538(7)

atom	atom	distance
F(1a)	C(9a)	1.347(8)
F(2a)	C(9a)	1.365(9)
F(3a)	C(10a)	1.329(10)
F(4a)	C(10a)	1.32(1)
F(5a)	C(10a)	1.35(2)
O(2)	N(4)	1.227(3)
N(1)	C(1)	1.369(3)
N(1)	C(5)	1.475(3)
N(2)	C(2)	1.357(3)
N(3)	C(8)	1.39(2)
N(4)	C(2)	1.431(3)
C(2)	C(3)	1.355(3)
C(6)	C(7)	1.509(3)
C(8a)	C(9a)	1.45(2)
C(9a)	C(10a)	1.48(1)

Table I-4.4 Bond angles (°)for 2M4NF5

atom	atom	atom	angle
C(1)	N(1)	C(3)	107.9(2)
C(3)	N(1)	C(5)	124.4(2)
C(7)	N(3)	C(8)	117.0(5)
O(2)	N(4)	O(3)	123.7(2)
O(3)	N(4)	C(2)	118.9(2)
N(1)	C(1)	C(4)	123.5(2)
N(2)	C(2)	N(4)	122.3(2)
N(4)	C(2)	C(3)	125.0(2)
N(1)	C(5)	C(6)	111.5(2)
O(1)	C(7)	N(3)	122.7(2)
N(3)	C(7)	C(6)	115.4(2)
N(3)	C(8a)	C(9a)	115(1)
F(1)	C(9)	C(8)	112.6(8)
F(2)	C(9)	C(8)	117.7(7)
C(8)	C(9)	C(10)	115.2(7)
F(1a)	C(9a)	C(8a)	110.0(8)
F(2a)	C(9a)	C(8a)	109.5(8)
C(8a)	C(9a)	C(10a)	119.3(7)
F(3)	C(10)	F(5)	113.5(9)
F(4)	C(10)	F(5)	105(1)
F(5)	C(10)	C(9)	110.3(9)
F(3a)	C(10a)	F(5a)	103.2(10)
F(4a)	C(10a)	F(5a)	115(1)
F(5a)	C(10a)	C(9a)	117(1)

atom	atom	atom	angle
C(1)	N(1)	C(5)	127.7(2)
C(1)	N(2)	C(2)	104.2(2)
C(7)	N(3)	C(8a)	126.4(6)
O(2)	N(4)	C(2)	117.3(2)
N(1)	C(1)	N(2)	110.9(2)
N(2)	C(1)	C(4)	125.6(2)
N(2)	C(2)	C(3)	112.7(2)
N(1)	C(3)	C(2)	104.3(2)
C(5)	C(6)	C(7)	110.2(2)
O(1)	C(7)	C(6)	121.8(2)
N(3)	C(8)	C(9)	112.2(9)
F(1)	C(9)	F(2)	94.0(7)
F(1)	C(9)	C(10)	107.8(5)
F(2)	C(9)	C(10)	107.3(7)
F(1a)	C(9a)	F(2a)	105.9(6)
F(1a)	C(9a)	C(10a)	106.7(8)
F(2a)	C(9a)	C(10a)	104.5(6)
F(3)	C(10)	F(4)	106.6(7)
F(3)	C(10)	C(9)	110.3(6)
F(4)	C(10)	C(9)	110.2(6)
F(3a)	C(10a)	F(4a)	97.8(8)
F(3a)	C(10a)	C(9a)	110.6(7)
F(4a)	C(10a)	C(9a)	110.4(8)

Appendix I-5 X-ray data for 2M4NF1(-1)

Table I-5.1 Experimental details for 2M4NF1(-1)

Formula	C ₉ H ₁₃ FN ₄ O ₃
fw	244.23
Crystal system	Monoclinic
Space group	<i>P</i> 2 ₁ / <i>n</i> (No. 7)
<i>a</i> , Å	4.488(1)
<i>b</i> , Å	13.314(1)
<i>c</i> , Å	18.7599(9)
α , °	—
β , °	94.83(1)
γ , °	—
<i>V</i> , Å ³	1116.9(3)
<i>Z</i>	4
ρ_{calc} , g/cm ³	1.452
<i>F</i> (000)	512
μ , cm ⁻¹	10.48
Crystal size, mm	0.07 × 0.15 × 0.45
Transmission factors	0.93-1.00
Scan type	ω -2 θ
Scan range, deg in ω	1.05 + 0.20 tan θ
Scan speed, deg/min	32 (up to 9 scans)
Data collected	—
2 θ_{max} , deg	155
Crystal decay, %	—
Total reflections	2688
Unique reflections	2372
<i>R</i> _{merge}	0.015
No. with $I \geq 3\sigma(I)$	1542
No. of variables	159
<i>R</i> (<i>F</i>) ($I \geq 3\sigma(I)$)	0.048
<i>R</i> _w (<i>F</i>) ($I \geq 3\sigma(I)$)	0.046
<i>R</i> (<i>F</i> ²) (all data)	—
<i>R</i> _w (<i>F</i> ²) (all data)	—
gof	0.72
Max Δ/σ (final cycle)	0.0002
Residual density e/Å ³	-0.21 to 0.19

Table I-5.2 Atomic coordinates and $B_{\text{iso}}/B_{\text{eq}}$ for 2M4NF1(-1)

atom	x	y	z	B{eq}
F(1)	0.6429(6)	0.0536(2)	0.4458(1)	8.14(7)
O(1)	0.6837(6)	0.3841(2)	0.4876(1)	5.83(6)
O(2)	-0.3414(5)	0.8101(2)	0.2528(1)	5.13(6)
O(3)	-0.2479(6)	0.8031(2)	0.3676(1)	5.40(6)
N(1)	0.3025(5)	0.5721(2)	0.3206(1)	3.10(5)
N(2)	0.0231(5)	0.6497(2)	0.2343(1)	3.26(5)
N(3)	0.6927(6)	0.2612(2)	0.4072(1)	3.57(6)
N(4)	-0.2131(6)	0.7731(2)	0.3068(1)	3.72(6)
C(1)	0.2173(6)	0.5766(2)	0.2483(1)	3.13(6)
C(2)	-0.0134(6)	0.6913(2)	0.2994(1)	3.08(6)
C(3)	0.1548(6)	0.6453(2)	0.3533(1)	3.29(6)
C(4)	0.3278(8)	0.5065(2)	0.1955(2)	4.15(7)
C(5)	0.5157(6)	0.5020(2)	0.3577(2)	3.52(6)
C(6)	0.3720(7)	0.4057(2)	0.3801(2)	3.82(7)
C(7)	0.5951(7)	0.3483(2)	0.4297(1)	3.41(6)
C(8)	0.9147(7)	0.2026(2)	0.4498(2)	4.01(7)
C(9)	0.7796(9)	0.1235(3)	0.4927(2)	5.04(9)

Table I-5.3 Bond lengths (Å) for 2M4NF1(-1)

atom	atom	distance
F(1)	C(9)	1.386(4)
O(2)	N(4)	1.225(3)
N(1)	C(1)	1.379(3)
N(1)	C(5)	1.468(3)
N(2)	C(2)	1.363(3)
N(3)	C(8)	1.451(4)
C(1)	C(4)	1.477(4)
C(5)	C(6)	1.511(4)
C(8)	C(9)	1.486(5)

atom	atom	distance
O(1)	C(7)	1.222(3)
O(3)	N(4)	1.231(3)
N(1)	C(3)	1.355(4)
N(2)	C(1)	1.318(3)
N(3)	C(7)	1.322(4)
N(4)	C(2)	1.425(4)
C(2)	C(3)	1.357(4)
C(6)	C(7)	1.515(4)

Table I-5.4 Bond angles (°) for 2M4NF1(-1)

atom	atom	atom	angle
C(1)	N(1)	C(3)	107.9(2)
C(3)	N(1)	C(5)	124.6(2)
C(7)	N(3)	C(8)	121.8(2)
O(2)	N(4)	C(2)	118.8(3)
N(1)	C(1)	N(2)	110.7(3)
N(2)	C(1)	C(4)	125.8(2)
N(2)	C(2)	C(3)	112.6(3)
N(1)	C(3)	C(2)	104.5(2)
C(5)	C(6)	C(7)	108.9(2)
O(1)	C(7)	C(6)	119.9(3)
N(3)	C(8)	C(9)	112.8(3)

atom	atom	atom	angle
C(1)	N(1)	C(5)	127.5(2)
C(1)	N(2)	C(2)	104.4(2)
O(2)	N(4)	O(3)	123.2(3)
O(3)	N(4)	C(2)	117.9(2)
N(1)	C(1)	C(4)	123.5(2)
N(2)	C(2)	N(4)	121.5(2)
N(4)	C(2)	C(3)	125.9(3)
N(1)	C(5)	C(6)	113.2(2)
O(1)	C(7)	N(3)	122.3(3)
N(3)	C(7)	C(6)	117.8(2)
F(1)	C(9)	C(8)	108.1(3)

Appendix I-6 X-ray data for cycF3

Table I-6.1 Experimental details for cycF3

Formula	C ₈ H ₇ F ₃ N ₄ O ₅ S
fw	328.22
Crystal system	Triclinic
Space group	$P\bar{1}$ (No. 2)
a , Å	7.8016(7)
b , Å	11.278(1)
c , Å	7.4946(7)
α , °	107.804(9)
β , °	95.295(8)
γ , °	100.682(9)
V , Å ³	609.1(1)
Z	2
ρ_{calc} , g/cm ³	1.790
$F(000)$	332
μ , cm ⁻¹	30.89
Crystal size, mm	0.17 × 0.30 × 0.40
Transmission factors	0.74-1.00
Scan type	ω -2 θ
Scan range, deg in ω	1.20 + 0.20 tan θ
Scan speed, deg/min	32 (up to 9 scans)
Data collected	—
2 θ_{max} , deg	155.3
Crystal decay, %	—
Total reflections	2689
Unique reflections	2492
R_{merge}	0.019
No. with $I \geq 3\sigma(I)$	2011
No. of variables	272
$R(F)$ ($I \geq 3\sigma(I)$)	0.042
$R_w(F)$ ($I \geq 3\sigma(I)$)	0.037
$R(F^2)$ (all data)	—
$R_w(F^2)$ (all data)	—
gof	1.19
Max Δ/σ (final cycle)	0.006
Residual density e/Å ³	-0.17 to 0.16

Table I-6.2 Atomic coordinates and B_{iso}/B_{eq} for cycF3

atom	x	y	z	B{eq}	occ
S(1a)	0.8481(1)	0.1401(1)	0.3027(2)	4.10(3)	0.549(3)
S(1b)	0.6939(2)	0.0155(2)	0.3375(3)	4.89(4)	0.451
F(1a)	0.742(1)	-0.076(1)	0.348(2)	9.2(2)	0.549
F(1b)	1.004(2)	0.117(1)	0.281(2)	7.2(2)	0.451
F(2a)	0.555(2)	-0.026(1)	0.188(2)	7.9(2)	0.549
F(2b)	0.787(2)	0.162(2)	0.139(2)	9.3(4)	0.451
F(3a)	0.767(2)	-0.0857(6)	0.059(2)	12.5(3)	0.549
F(3b)	0.829(2)	-0.0273(9)	0.035(1)	11.0(2)	0.451
O(1)	0.6364(2)	0.3160(2)	0.7110(2)	4.73(4)	
O(2)	0.4403(3)	0.3282(3)	0.0681(3)	8.31(7)	
O(3)	0.1952(3)	0.3822(2)	0.0186(3)	7.37(6)	
O(4a)	0.795(2)	0.192(1)	0.164(2)	5.2(1)	0.549
O(4b)	0.513(2)	-0.026(2)	0.229(4)	6.6(2)	0.451
O(5a)	1.022(2)	0.126(1)	0.346(1)	6.1(2)	0.549
O(5b)	0.782(2)	-0.073(2)	0.402(2)	7.1(2)	0.451
N(1)	0.3798(2)	0.3381(2)	0.4350(3)	4.17(4)	
N(2)	0.1731(2)	0.4446(2)	0.3905(3)	4.77(5)	
N(3a)	0.7824(5)	0.2059(4)	0.4973(6)	3.94(9)	0.549
N(3b)	0.7092(7)	0.1468(5)	0.5120(7)	4.4(1)	0.451
N(4)	0.3084(3)	0.3615(2)	0.1209(3)	5.40(6)	
C(1)	0.2855(3)	0.3802(3)	0.3133(3)	4.16(5)	
C(2)	0.1947(3)	0.4454(3)	0.5721(4)	5.23(7)	
C(3)	0.3181(3)	0.3804(3)	0.6023(3)	4.81(6)	
C(4)	0.5031(4)	0.2593(3)	0.3940(3)	5.98(7)	
C(5)	0.6203(4)	0.2536(3)	0.5265(3)	5.60(7)	
C(6)	0.8518(5)	0.1963(4)	0.6870(4)	6.08(8)	
C(7)	0.8007(3)	0.3112(3)	0.8103(3)	5.31(7)	
C(8a)	0.7194(10)	-0.0252(6)	0.212(1)	6.8(2)	0.549
C(8b)	0.838(1)	0.0700(8)	0.188(1)	6.1(2)	0.451

Table I-6.3 Bond lengths (Å) for cycF3

atom	atom	distance
S(1a)	O(4a)	1.40(2)
S(1a)	N(3a)	1.599(4)
S(1b)	O(4b)	1.48(2)
S(1b)	N(3b)	1.625(6)
F(1a)	C(8a)	1.32(1)
F(2a)	C(8a)	1.28(1)
F(3a)	C(8a)	1.27(1)
O(1)	C(5)	1.327(3)
O(2)	N(4)	1.218(3)
N(1)	C(1)	1.367(3)
N(1)	C(4)	1.419(3)
N(2)	C(2)	1.352(3)
N(3a)	C(6)	1.516(5)
N(3b)	C(6)	1.524(6)
C(2)	C(3)	1.356(3)
C(6)	C(7)	1.490(4)

atom	atom	distance
S(1a)	O(5a)	1.42(1)
S(1a)	C(8a)	1.830(7)
S(1b)	O(5b)	1.47(1)
S(1b)	C(8b)	1.819(8)
F(1b)	C(8b)	1.34(2)
F(2b)	C(8b)	1.31(2)
F(3b)	C(8b)	1.31(1)
O(1)	C(7)	1.440(3)
O(3)	N(4)	1.218(3)
N(1)	C(3)	1.365(3)
N(2)	C(1)	1.304(3)
N(3a)	C(5)	1.473(4)
N(3b)	C(5)	1.479(5)
N(4)	C(1)	1.425(3)
C(4)	C(5)	1.312(3)

Table I-6.4 Bond angles (°) for cycF3

atom	atom	atom	angle
O(4a)	S(1a)	O(5a)	124.0(7)
O(4a)	S(1a)	C(8a)	103.3(6)
O(5a)	S(1a)	C(8a)	103.1(6)
O(4b)	S(1b)	O(5b)	122(1)
O(4b)	S(1b)	C(8b)	106.7(9)
O(5b)	S(1b)	C(8b)	104.3(7)
C(5)	O(1)	C(7)	110.7(2)
C(1)	N(1)	C(4)	128.1(2)
C(1)	N(2)	C(2)	103.9(2)
S(1a)	N(3a)	C(6)	123.9(3)
S(1b)	N(3b)	C(5)	130.4(4)
C(5)	N(3b)	C(6)	104.4(4)
O(2)	N(4)	C(1)	118.9(2)
N(1)	C(1)	N(2)	113.9(2)
N(2)	C(1)	N(4)	121.5(2)
N(1)	C(3)	C(2)	106.7(2)
O(1)	C(5)	N(3b)	105.6(3)
O(1)	C(5)	C(4)	125.5(2)
N(3a)	C(5)	C(4)	126.2(3)
N(3a)	C(6)	C(7)	97.5(2)
S(1a)	C(8a)	F(1a)	107.3(6)
S(1a)	C(8a)	F(3a)	110.2(7)
F(1a)	C(8a)	F(3a)	112.9(9)
S(1b)	C(8b)	F(1b)	110.5(7)
S(1b)	C(8b)	F(3b)	107.6(7)
F(1b)	C(8b)	F(3b)	111.8(10)

atom	atom	atom	angle
O(4a)	S(1a)	N(3a)	110.4(4)
O(5a)	S(1a)	N(3a)	108.3(4)
N(3a)	S(1a)	C(8a)	106.1(4)
O(4b)	S(1b)	N(3b)	109.2(8)
O(5b)	S(1b)	N(3b)	110.3(6)
N(3b)	S(1b)	C(8b)	101.9(4)
C(1)	N(1)	C(3)	104.3(2)
C(3)	N(1)	C(4)	127.4(2)
S(1a)	N(3a)	C(5)	129.0(3)
C(5)	N(3a)	C(6)	105.1(3)
S(1b)	N(3b)	C(6)	124.2(3)
O(2)	N(4)	O(3)	123.5(2)
O(3)	N(4)	C(1)	117.6(2)
N(1)	C(1)	N(4)	124.6(2)
N(2)	C(2)	C(3)	111.3(2)
N(1)	C(4)	C(5)	122.3(2)
O(1)	C(5)	N(3a)	106.6(2)
N(3b)	C(5)	C(4)	125.5(3)
N(3b)	C(6)	C(7)	103.8(3)
O(1)	C(7)	C(6)	105.3(2)
S(1a)	C(8a)	F(2a)	109.5(8)
F(1a)	C(8a)	F(2a)	105(1)
F(2a)	C(8a)	F(3a)	111(1)
S(1b)	C(8b)	F(2b)	110.7(8)
F(1b)	C(8b)	F(2b)	107(1)
F(2b)	C(8b)	F(3b)	109(1)

Appendix I-7 X-ray data for [Ru(Im)₆][CF₃SO₃]₂

Table I-7.1 Experimental details for [Ru(Im)₆][CF₃SO₃]₂

Formula	C ₂₀ H ₂₄ F ₆ N ₁₂ O ₆ RuS ₂
fw	807.67
Crystal system	Triclinic
Space group	$P\bar{1}$ (No. 2)
<i>a</i> , Å	7.4010(6)
<i>b</i> , Å	9.9846(15)
<i>c</i> , Å	11.275(2)
α , °	113.469(5)
β , °	92.419(2)
γ , °	94.737(2)
<i>V</i> , Å ³	759.1(2)
<i>Z</i>	1
ρ_{calc} , g/cm ³	1.767
<i>F</i> (000)	406
μ , cm ⁻¹	7.49
Crystal size, mm	0.20 × 0.30 × 0.45
Transmission factors	0.87-1.00 ^c
Scan type	ϕ , ω sweeps
Scan range, deg in ω	0.5
Scan speed, deg/min	—
Data collected	462 frames, 40 s/frame
$2\theta_{max}$, deg	60.1
Crystal decay, %	—
Total reflections	7056
Unique reflections	3451
<i>R</i> _{merge}	0.033
No. with $I \geq 3\sigma(I)$	2883
No. of variables	215
<i>R</i> (<i>F</i>) ($I \geq 3\sigma(I)$)	0.029
<i>R</i> _w (<i>F</i>) ($I \geq 3\sigma(I)$)	0.027
<i>R</i> (<i>F</i> ²) (all data)	0.050
<i>R</i> _w (<i>F</i> ²) (all data)	0.055
gof	1.34
Max Δ/σ (final cycle)	0.0005
Residual density e/Å ³	-0.79 to 0.84

Table I-7.2 Atomic coordinates and $B_{\text{iso}}/B_{\text{eq}}$ for $[\text{Ru}(\text{Im})_6][\text{CF}_3\text{SO}_3]_2$

atom	x	y	z	B_{eq}
Ru(1)	0.50000	0.50000	0.50000	1.235(6)
S(1)	0.19005(7)	0.21625(7)	0.91424(6)	2.120(14)
F(1)	0.4885(2)	0.1445(2)	0.9942(2)	3.66(4)
F(2)	0.5242(2)	0.2327(2)	0.8517(2)	4.85(5)
F(3)	0.3976(3)	0.0135(3)	0.7969(2)	5.91(6)
O(1)	0.1255(2)	0.2036(2)	0.7878(2)	2.91(4)
O(2)	0.0917(2)	0.1169(2)	0.9590(2)	3.44(5)
O(3)	0.2307(2)	0.3644(2)	1.0103(2)	3.00(4)
N(1)	0.6451(2)	0.3574(2)	0.5536(2)	1.51(4)
N(2)	0.8337(3)	0.2726(3)	0.6562(2)	2.58(5)
N(3)	0.3026(2)	0.3239(2)	0.3962(2)	1.44(4)
N(4)	0.1474(3)	0.1354(3)	0.2378(2)	2.40(5)
N(5)	0.6399(2)	0.4505(2)	0.3323(2)	1.48(4)
N(6)	0.7406(3)	0.4527(3)	0.1512(2)	2.74(5)
C(1)	0.7822(3)	0.3920(3)	0.6434(3)	2.33(6)
C(2)	0.7263(3)	0.1538(3)	0.5701(3)	2.71(6)
C(3)	0.6097(3)	0.2068(3)	0.5069(3)	2.26(6)
C(4)	0.2784(3)	0.2473(3)	0.2698(2)	2.07(5)
C(5)	0.0814(3)	0.1393(3)	0.3499(3)	2.19(6)
C(6)	0.1766(3)	0.2537(3)	0.4471(2)	1.99(5)
C(7)	0.6319(3)	0.5123(3)	0.2471(3)	2.46(6)
C(8)	0.8250(3)	0.3478(3)	0.1764(2)	2.31(6)
C(9)	0.7602(3)	0.3487(3)	0.2874(2)	2.21(6)
C(10)	0.4104(4)	0.1481(3)	0.8878(3)	2.83(6)

Table I-7.3 Bond lengths (Å) for $[\text{Ru}(\text{Im})_6][\text{CF}_3\text{SO}_3]_2$

atom	atom	distance	atom	atom	distance
Ru(1)	N(1)	2.105(2)	Ru(1)	N(3)	2.095(2)
Ru(1)	N(5)	2.098(2)	S(1)	O(1)	1.437(2)
S(1)	O(2)	1.442(2)	S(1)	O(3)	1.440(2)
S(1)	C(10)	1.810(3)	F(1)	C(10)	1.325(3)
F(2)	C(10)	1.332(3)	F(3)	C(10)	1.319(3)
N(1)	C(1)	1.323(3)	N(1)	C(3)	1.378(3)
N(2)	C(1)	1.340(3)	N(2)	C(2)	1.357(4)
N(3)	C(4)	1.318(3)	N(3)	C(6)	1.396(3)
N(4)	C(4)	1.337(3)	N(4)	C(5)	1.362(3)
N(5)	C(7)	1.334(3)	N(5)	C(9)	1.364(3)
N(6)	C(7)	1.346(3)	N(6)	C(8)	1.378(3)
C(2)	C(3)	1.362(3)	C(5)	C(6)	1.344(4)
C(8)	C(9)	1.355(3)			

Table I-7.4 Bond angles (°) for $[\text{Ru}(\text{Im})_6][\text{CF}_3\text{SO}_3]_2$

atom	atom	atom	angle	atom	atom	atom	angle
N(1)	Ru(1)	N(1)*	180.0	N(1)	Ru(1)	N(3)	89.19(7)
N(1)	Ru(1)	N(3)*	90.81(7)	N(1)	Ru(1)	N(5)	90.72(7)
N(1)	Ru(1)	N(5)*	89.28(7)	N(3)	Ru(1)	N(3)*	180.0
N(3)	Ru(1)	N(5)	89.48(7)	N(3)	Ru(1)	N(5)*	90.52(7)
N(5)	Ru(1)	N(5)*	180.0	O(1)	S(1)	O(2)	114.65(11)
O(1)	S(1)	O(3)	115.10(12)	O(1)	S(1)	C(10)	103.04(12)
O(2)	S(1)	O(3)	114.75(12)	O(2)	S(1)	C(10)	103.19(13)
O(3)	S(1)	C(10)	103.83(12)	Ru(1)	N(1)	C(1)	128.0(2)
Ru(1)	N(1)	C(3)	126.81(15)	C(1)	N(1)	C(3)	105.1(2)
C(1)	N(2)	C(2)	107.8(2)	Ru(1)	N(3)	C(4)	128.16(15)
Ru(1)	N(3)	C(6)	127.20(15)	C(4)	N(3)	C(6)	104.5(2)
C(4)	N(4)	C(5)	107.4(2)	Ru(1)	N(5)	C(7)	127.60(15)
Ru(1)	N(5)	C(9)	127.27(15)	C(7)	N(5)	C(9)	105.1(2)
C(7)	N(6)	C(8)	107.4(2)	N(1)	C(1)	N(2)	111.4(2)
N(2)	C(2)	C(3)	106.0(2)	N(1)	C(3)	C(2)	109.7(2)
N(3)	C(4)	N(4)	112.0(2)	N(4)	C(5)	C(6)	106.6(2)
N(3)	C(6)	C(5)	109.6(2)	N(5)	C(7)	N(6)	111.1(2)
N(6)	C(8)	C(9)	105.5(2)	N(5)	C(9)	C(8)	110.9(2)
S(1)	C(10)	F(1)	111.8(2)	S(1)	C(10)	F(2)	111.5(2)
S(1)	C(10)	F(3)	111.5(2)	F(1)	C(10)	F(2)	106.9(2)
F(1)	C(10)	F(3)	107.1(2)	F(2)	C(10)	F(3)	107.8(2)

Appendix I-8 X-ray data for [Ru(NMeIm)₆][CF₃SO₃]₂

Table I-8.1 Experimental details for [Ru(NMeIm)₆][CF₃SO₃]₂

Formula	C ₂₆ H ₃₆ F ₆ N ₁₂ O ₆ RuS ₂
fw	891.83
Crystal system	Trigonal
Space group	$P\bar{3}$ (No. 147)
<i>a</i> , Å	11.558(2)
<i>b</i> , Å	11.558(2)
<i>c</i> , Å	8.109(3)
α , °	90
β , °	90
γ , °	120
<i>V</i> , Å ³	938.1(4)
<i>Z</i>	1 1
ρ_{calc} , g/cm ³	1.579
<i>F</i> (000)	454
μ , cm ⁻¹	6.15
Crystal size, mm	0.38 × 0.45 × 0.50
Transmission factors	0.94-1.00
Scan type	ω -2 θ
Scan range, deg in ω	1.15 + 0.35 tan θ
Scan speed, deg/min	32 (up to 9 scans)
Data collected	$\pm h$, $\pm k$, $\pm l$
2 θ_{max} , deg	60.0
Crystal decay, %	5.6
Total reflections	2078
Unique reflections	1830
<i>R</i> _{merge}	0.048
No. with $I \geq 3\sigma(I)$	1215
No. of variables	135
<i>R</i> (<i>F</i>) ($I \geq 3\sigma(I)$)	0.035
<i>R</i> _w (<i>F</i>) ($I \geq 3\sigma(I)$)	0.031
<i>R</i> (<i>F</i> ²) (all data)	—
<i>R</i> _w (<i>F</i> ²) (all data)	—
gof	1.91
Max Δ/σ (final cycle)	0.01
Residual density e/Å ³	-0.19 to 0.78

Table I-8.2 Atomic coordinates and $B_{\text{iso}}/B_{\text{eq}}$ for $[\text{Ru}(\text{NMeIm})_6][\text{CF}_3\text{SO}_3]_2$

atom	x	y	z	B_{eq}	occ
Ru(1)	0.0000	0.0000	0.0000	4.013(6)	0.167
S(1)	0.628(2)	0.2857(9)	0.2615(8)	10.3(3)	0.333
F(1)	0.533(2)	0.349(4)	0.083(4)	15.6(9)	0.300
F(2)	0.590(6)	0.208(4)	0.055(5)	22.0(14)	0.250
F(3)	0.686(3)	0.516(2)	0.250(6)	17.1(9)	0.250
F(4)	0.577(8)	0.373(8)	0.376(5)	19.1(18)	0.200
O(1)	0.559(2)	0.278(5)	0.162(2)	24.5(14)	0.333
O(2)	0.733(4)	0.284(6)	0.360(4)	17.7(11)	0.333
O(3)	0.504(2)	0.287(5)	0.262(5)	18.3(12)	0.333
N(1)	0.0974(2)	0.1708(2)	0.1494(2)	4.54(5)	
N(2)	0.2507(3)	0.3619(2)	0.2552(3)	6.54(7)	
C(1)	0.2197(3)	0.2707(3)	0.1352(4)	6.56(8)	
C(2)	0.1418(4)	0.3185(3)	0.3504(3)	6.87(9)	
C(3)	0.0492(3)	0.2020(3)	0.2851(4)	6.65(8)	
C(4)	0.3793(4)	0.4870(4)	0.2776(6)	11.44(13)	
C(5)	0.710(5)	0.252(5)	0.053(6)	9.4(8)	0.220
C(6)	0.6667	0.3333	0.12(2)	27.8(17)	0.110

Table I-8.3 Bond lengths (Å) for $[\text{Ru}(\text{NMeIm})_6][\text{CF}_3\text{SO}_3]_2$

atom	atom	distance
Ru(1)	N(1)	2.100(2)
N(1)	C(3)	1.361(3)
N(2)	C(2)	1.342(4)
C(2)	C(3)	1.341(4)

atom	atom	distance
N(1)	C(1)	1.308(3)
N(2)	C(1)	1.345(3)
N(2)	C(4)	1.477(4)

Table I-8.4 Bond angles (°) for $[\text{Ru}(\text{NMeIm})_6][\text{CF}_3\text{SO}_3]_2$

atom	atom	atom	angle
N(1)	Ru(1)	N(1a)	90.05(7)
N(1)	Ru(1)	N(1c)	89.95(7)
Ru(1)	N(1)	C(3)	128.1(2)
C(1)	N(2)	C(2)	106.9(2)
C(2)	N(2)	C(4)	126.3(3)
N(2)	C(2)	C(3)	106.1(3)

atom	atom	atom	angle
N(1)	Ru(1)	N(1b)	180.0
Ru(1)	N(1)	C(1)	127.8(2)
C(1)	N(1)	C(3)	104.0(2)
C(1)	N(2)	C(4)	126.8(3)
N(1)	C(1)	N(2)	112.0(3)
N(1)	C(3)	C(2)	111.0(3)

Appendix I-9 X-ray data for [Ru(5MeIm)₆][CF₃SO₃]₂

Table I-9.1 Experimental details for [Ru(5MeIm)₆][CF₃SO₃]₂

Formula	C ₂₆ H ₃₆ F ₆ N ₁₂ O ₆ RuS ₂
fw	891.83
Crystal system	Trigonal
Space group	$R\bar{3}$ (No. 148)
<i>a</i> , Å	12.6547(4)
<i>b</i> , Å	12.6547(4)
<i>c</i> , Å	20.4078(12)
α , °	90
β , °	90
γ , °	120
<i>V</i> , Å ³	2830.3(2)
<i>Z</i>	3
ρ_{calc} , g/cm ³	1.570
<i>F</i> (000)	1362
μ , cm ⁻¹	6.11
Crystal size, mm	0.10 × 0.20 × 0.25
Transmission factors	0.74-1.00
Scan type	ϕ , ω sweeps
Scan range, deg in ω	0.5
Scan speed, deg/min	—
Data collected	462 frames, 75 s/frame
$2\theta_{max}$, deg	60.0
Crystal decay, %	—
Total reflections	8224
Unique reflections	1744
<i>R</i> _{merge}	0.032
No. with $I \geq 3\sigma(I)$	1071
No. of variables	81
<i>R</i> (<i>F</i>) ($I \geq 3\sigma(I)$)	0.034
<i>R</i> _w (<i>F</i>) ($I \geq 3\sigma(I)$)	0.028
<i>R</i> (<i>F</i> ²) (all data)	0.061
<i>R</i> _w (<i>F</i> ²) (all data)	0.058
gof	1.12
Max Δ/σ (final cycle)	0.0001
Residual density e/Å ³	-1.22 to 1.92

Table I-9.2 Atomic coordinates and $B_{\text{iso}}/B_{\text{eq}}$ for $[\text{Ru}(\text{5MeIm})_6][\text{CF}_3\text{SO}_3]_2$

atom	x	y	z	B_{eq}	occ
Ru(1)	0.00000	0.00000	0.00000	1.834(7)	0.17
S(1)	-0.33333	0.33333	0.03331(7)	2.51(2)	0.33
F(1)	-0.4460(2)	0.2642(3)	-0.07733(12)	9.81(9)	
O(1)	-0.3899(2)	0.2058(2)	0.05007(11)	4.02(6)	
N(1)	0.0306(2)	0.1511(2)	-0.05623(10)	1.92(5)	
N(2)	0.0764(2)	0.3384(2)	-0.07995(12)	2.59(5)	
C(1)	0.0856(2)	0.2660(2)	-0.03460(13)	2.46(6)	
C(2)	0.0153(2)	0.2693(2)	-0.13355(13)	2.29(6)	
C(3)	-0.0115(2)	0.1539(2)	-0.11780(13)	2.13(6)	
C(4)	-0.0120(3)	0.3201(3)	-0.1920(2)	3.25(8)	
C(5)	-0.3333	0.3333	-0.0546(4)	5.41(11)	0.33
H(1)	0.1060	0.4200	-0.0757	3.1	
H(2)	0.1265	0.2936	0.0079	3.0	
H(3)	-0.0549	0.0827	-0.1465	2.6	
H(4)	0.0644	0.3836	-0.2114	3.9	
H(5)	-0.0624	0.3555	-0.1793	3.9	
H(6)	-0.0562	0.2550	-0.2241	3.9	

Table I-9.3 Bond lengths (\AA) for $[\text{Ru}(\text{5MeIm})_6][\text{CF}_3\text{SO}_3]_2$

atom	atom	distance
Ru(1)	N(1)	2.093(2)
S(1)	C(5)	1.794(7)
N(1)	C(1)	1.335(3)
N(2)	C(1)	1.347(3)
C(2)	C(3)	1.362(3)

atom	atom	distance
S(1)	O(1)	1.442(2)
F(1)	C(5)	1.329(3)
N(1)	C(3)	1.372(3)
N(2)	C(2)	1.372(3)
C(2)	C(4)	1.476(4)

Table I-9.4 Bond angles ($^\circ$) for $[\text{Ru}(\text{5MeIm})_6][\text{CF}_3\text{SO}_3]_2$

atom	atom	atom	angle
N(1)	Ru(1)	N(1a)	92.81(8)
N(1)	Ru(1)	N(1c)	87.19(8)
O(1)	S(1)	C(5)	103.72(10)
Ru(1)	N(1)	C(3)	129.0(2)
C(1)	N(2)	C(2)	109.1(2)
N(2)	C(2)	C(3)	104.7(2)
C(3)	C(2)	C(4)	132.2(3)
S(1)	C(5)	F(1)	110.4(3)

atom	atom	atom	angle
N(1)	Ru(1)	N(1b)	180.0
O(1)	S(1)	O(1d)	114.56(8)
Ru(1)	N(1)	C(1)	124.9(2)
C(1)	N(1)	C(3)	105.8(2)
N(1)	C(1)	N(2)	109.8(2)
N(2)	C(2)	C(4)	123.1(2)
N(1)	C(3)	C(2)	110.6(2)
F(1)	C(5)	F(1d)	108.5(3)

Appendix I-10 X-ray data for *mer*-RuCl₃(MeCN)₃•CHCl₃

Table I-10.1 Experimental details for *mer*-RuCl₃(MeCN)₃•CHCl₃

Formula	C ₇ H ₁₀ Cl ₆ N ₃ Ru
fw	449.96
Crystal system	Orthorhombic
Space group	<i>Pbca</i> (No. 61)
<i>a</i> , Å	14.906(2)
<i>b</i> , Å	19.562(2)
<i>c</i> , Å	11.411(2)
α , °	—
β , °	—
γ , °	—
<i>V</i> , Å ³	3327.4(7)
<i>Z</i>	8
ρ_{calc} , g/cm ³	1.796
<i>F</i> (000)	1752
μ , cm ⁻¹	18.87
Crystal size, mm	0.30 × 0.30 × 0.40
Transmission factors	0.92-1.00
Scan type	ω -2 θ
Scan range, deg in ω	1.05 + 0.35 tan θ
Scan speed, deg/min	32
Data collected	—
2 θ_{max} deg	70
Crystal decay, %	—
Total reflections	8039
Unique reflections	—
<i>R</i> _{merge}	—
No. with $I \geq 3\sigma(I)$	2714
No. of variables	154
<i>R</i> (<i>F</i>) ($I \geq 3\sigma(I)$)	0.039
<i>R</i> _w (<i>F</i>) ($I \geq 3\sigma(I)$)	0.036
<i>R</i> (<i>F</i> ²) (all data)	—
<i>R</i> _w (<i>F</i> ²) (all data)	—
gof	1.74
Max Δ/σ (final cycle)	0.0007
Residual density e/Å ³	-0.66 to 0.85

Table I-10.2 Atomic coordinates and $B_{\text{iso}}/B_{\text{eq}}$ for *mer*- $\text{RuCl}_3(\text{MeCN})_3 \cdot \text{CHCl}_3$

atom	x	y	z	B{eq}
Ru(1)	0.17615(2)	0.42894(2)	0.49157(3)	2.776(7)
Cl(1)	0.04099(8)	0.38728(7)	0.56701(11)	3.88(3)
Cl(2)	0.30595(8)	0.48117(7)	0.42224(12)	4.42(3)
Cl(3)	0.20784(9)	0.32747(7)	0.39713(12)	4.21(3)
Cl(4)	0.11179(15)	0.17468(13)	0.5937(2)	11.90(9)
Cl(5)	-0.06848(11)	0.20027(9)	0.5203(2)	6.77(5)
Cl(6)	0.06654(14)	0.17957(11)	0.3488(2)	10.26(7)
N(1)	0.1488(3)	0.5195(2)	0.5762(3)	3.51(10)
N(2)	0.2396(3)	0.3945(2)	0.6356(4)	3.42(10)
N(3)	0.1118(3)	0.4620(2)	0.3471(3)	3.28(9)
C(1)	0.1378(4)	0.5702(3)	0.6202(4)	3.88(12)
C(2)	0.1208(4)	0.6354(3)	0.6758(5)	5.9(2)
C(3)	0.2719(3)	0.3734(3)	0.7164(5)	3.82(13)
C(4)	0.3136(4)	0.3468(3)	0.8228(5)	5.9(2)
C(5)	0.0773(3)	0.4811(3)	0.2660(4)	3.47(11)
C(6)	0.0313(4)	0.5062(3)	0.1618(5)	5.4(2)
C(7)	0.0460(4)	0.2111(3)	0.4880(5)	4.98(14)

Table I-10.3 Bond lengths (Å) for *mer*- $\text{RuCl}_3(\text{MeCN})_3 \cdot \text{CHCl}_3$

atom	atom	distance
Ru(1)	Cl(1)	2.3376(13)
Ru(1)	Cl(3)	2.3073(13)
Ru(1)	N(2)	2.013(4)
Cl(4)	C(7)	1.709(6)
Cl(6)	C(7)	1.731(6)
N(2)	C(3)	1.119(6)
C(1)	C(2)	1.447(7)
C(5)	C(6)	1.457(7)

atom	atom	distance
Ru(1)	Cl(2)	2.3267(13)
Ru(1)	N(1)	2.058(4)
Ru(1)	N(3)	2.014(4)
Cl(5)	C(7)	1.759(5)
N(1)	C(1)	1.125(6)
N(3)	C(5)	1.123(5)
C(3)	C(4)	1.460(7)

Table I-10.4 Bond angles (°) for *mer*- $\text{RuCl}_3(\text{MeCN})_3 \cdot \text{CHCl}_3$

atom	atom	atom	angle
Cl(1)	Ru(1)	Cl(2)	174.29(5)
Cl(1)	Ru(1)	N(1)	87.50(12)
Cl(1)	Ru(1)	N(3)	90.16(11)
Cl(2)	Ru(1)	N(1)	86.93(12)
Cl(2)	Ru(1)	N(3)	88.68(11)
Cl(3)	Ru(1)	N(2)	89.86(12)
N(1)	Ru(1)	N(2)	89.86(15)
N(2)	Ru(1)	N(3)	179.1(2)
Ru(1)	N(2)	C(3)	176.9(4)
N(1)	C(1)	C(2)	178.2(6)
N(3)	C(5)	C(6)	179.2(5)
Cl(4)	C(7)	Cl(6)	113.5(3)

atom	atom	atom	angle
Cl(1)	Ru(1)	Cl(3)	92.78(5)
Cl(1)	Ru(1)	N(2)	89.30(11)
Cl(2)	Ru(1)	Cl(3)	92.79(5)
Cl(2)	Ru(1)	N(2)	91.93(12)
Cl(3)	Ru(1)	N(1)	179.60(12)
Cl(3)	Ru(1)	N(3)	89.50(12)
N(1)	Ru(1)	N(3)	90.79(15)
Ru(1)	N(1)	C(1)	176.4(4)
Ru(1)	N(3)	C(5)	178.7(4)
N(2)	C(3)	C(4)	179.0(6)
Cl(4)	C(7)	Cl(5)	111.0(3)
Cl(5)	C(7)	Cl(6)	108.7(3)

Appendix I-11 X-ray data for Ru(hfac)₃

Table I-11.1 Experimental details for Ru(hfac)₃

Formula	C ₁₅ H ₃ F ₁₈ O ₆ Ru
fw	722.23
Crystal system	Monoclinic
Space group	<i>P</i> 2 ₁ / <i>n</i> (No. 14)
<i>a</i> , Å	8.7781(4)
<i>b</i> , Å	13.0760(11)
<i>c</i> , Å	19.1857(5)
α , °	—
β , °	92.2275(5)
γ , °	—
<i>V</i> , Å ³	2200.5(2)
<i>Z</i>	4
ρ_{calc} , g/cm ³	2.180
<i>F</i> (000)	1388
μ , cm ⁻¹	8.97
Crystal size, mm	0.25 × 0.25 × 0.07
Transmission factors	0.80-1.00
Scan type	ϕ , ω sweeps
Scan range, deg in ω	0.5
Scan speed, deg/min	—
Data collected	462 frames, 16 s/frame
$2\theta_{max}$, deg	61
Crystal decay, %	—
Total reflections	20189
Unique reflections	5883
<i>R</i> _{merge}	0.039
No. with $I \geq 3\sigma(I)$	3416
No. of variables	389
<i>R</i> (<i>F</i>) ($I \geq 3\sigma(I)$)	0.036
<i>R</i> _w (<i>F</i>) ($I \geq 3\sigma(I)$)	0.028
<i>R</i> (<i>F</i> ²) (all data)	0.063
<i>R</i> _w (<i>F</i> ²) (all data)	0.061
gof	1.34
Max Δ/σ (final cycle)	0.007
Residual density e/Å ³	-1.43 to 1.22

Table I-11.2 Atomic coordinates and $B_{\text{iso}}/B_{\text{eq}}$ for $\text{Ru}(\text{hfac})_3$

atom	x	y	z	B_{eq}	occ
Ru(1)	0.47142(3)	0.51053(2)	0.227564(15)	1.748(5)	
F(1)	0.4268(2)	0.83468(15)	0.32557(12)	3.97(6)	
F(2)	0.5454(3)	0.7439(2)	0.40285(12)	5.14(7)	
F(3)	0.6673(2)	0.85231(14)	0.34254(12)	3.74(6)	
F(4)	0.9754(2)	0.55083(15)	0.16592(13)	4.29(6)	
F(5)	0.8538(3)	0.6459(2)	0.09299(12)	4.99(7)	
F(6)	0.9753(2)	0.7118(2)	0.17944(13)	4.52(6)	
F(7)	0.1954(14)	0.6787(7)	0.0561(5)	6.0(2)	0.59(2)
F(7a)	0.159(2)	0.657(2)	0.0530(10)	10.5(6)	0.41
F(8)	0.3296(15)	0.602(2)	-0.0187(7)	8.5(5)	0.59
F(8a)	0.3702(12)	0.6675(12)	0.0184(11)	6.6(3)	0.41
F(9)	0.1151(10)	0.5490(6)	0.0081(7)	5.6(2)	0.59
F(9a)	0.227(5)	0.5520(8)	-0.0224(8)	10.5(7)	0.41
F(10)	0.5636(2)	0.20879(15)	0.10617(13)	4.32(6)	
F(11)	0.3435(3)	0.1850(2)	0.1437(2)	8.29(10)	
F(12)	0.3711(4)	0.2238(2)	0.0388(2)	8.33(10)	
F(13)	-0.0024(2)	0.4753(2)	0.31532(13)	5.38(7)	
F(14)	0.0698(2)	0.3273(2)	0.34603(15)	5.77(7)	
F(15)	0.0801(2)	0.4506(2)	0.41828(13)	6.01(8)	
F(16)	0.7611(2)	0.3579(2)	0.40578(11)	3.42(5)	
F(17)	0.7195(2)	0.5095(2)	0.44183(11)	4.42(6)	
F(18)	0.5939(2)	0.3827(2)	0.48218(12)	5.00(7)	
O(1)	0.4656(2)	0.64111(15)	0.27960(12)	2.04(5)	
O(2)	0.6666(2)	0.54635(15)	0.18299(11)	1.90(5)	
O(3)	0.3569(2)	0.5736(2)	0.14549(12)	2.26(5)	
O(4)	0.4743(2)	0.37309(15)	0.18088(12)	2.03(5)	
O(5)	0.2725(2)	0.47438(15)	0.26934(12)	1.98(5)	
O(6)	0.5926(2)	0.4562(2)	0.30892(11)	1.93(5)	
C(1)	0.5551(4)	0.7852(3)	0.3394(2)	2.49(9)	
C(2)	0.5794(4)	0.7000(2)	0.2860(2)	1.83(7)	
C(3)	0.7155(4)	0.6968(2)	0.2514(2)	2.03(8)	
C(4)	0.7450(4)	0.6230(2)	0.2018(2)	1.82(7)	
C(5)	0.8920(4)	0.6319(3)	0.1609(2)	2.57(9)	
C(6)	0.2492(6)	0.5944(4)	0.0333(2)	3.86(12)	
C(7)	0.3201(4)	0.5243(3)	0.0911(2)	2.17(8)	
C(8)	0.3377(4)	0.4225(3)	0.0756(2)	2.65(9)	
C(9)	0.4121(3)	0.3546(2)	0.1213(2)	2.02(8)	
C(10)	0.4230(5)	0.2419(3)	0.1017(2)	3.50(10)	
C(11)	0.0995(4)	0.4256(3)	0.3531(2)	2.77(9)	
C(12)	0.2626(4)	0.4476(2)	0.3319(2)	1.96(7)	
C(13)	0.3811(4)	0.4326(2)	0.3819(2)	2.11(8)	
C(14)	0.5326(4)	0.4379(2)	0.3664(2)	1.97(7)	
C(15)	0.6542(4)	0.4211(3)	0.4249(2)	2.71(9)	
H(1)	0.7934	0.7486	0.2624	2.4	
H(2)	0.2965	0.3968	0.0307	3.2	
H(3)	0.3549	0.4175	0.4300	2.5	

Table I-11.3 Bond lengths (\AA) for $\text{Ru}(\text{hfac})_3$

atom	atom	distance	atom	atom	distance
Ru(1)	O(1)	1.980(2)	F(12)	C(10)	1.295(4)
Ru(1)	O(2)	2.000(2)	F(13)	C(11)	1.303(4)
Ru(1)	O(3)	2.012(2)	F(14)	C(11)	1.318(4)
Ru(1)	O(4)	2.009(2)	F(15)	C(11)	1.310(4)
Ru(1)	O(5)	2.006(2)	F(16)	C(15)	1.313(4)
Ru(1)	O(6)	1.986(2)	F(17)	C(15)	1.326(4)
F(1)	C(1)	1.318(4)	F(18)	C(15)	1.336(4)
F(2)	C(1)	1.337(4)	O(1)	C(2)	1.263(3)
F(3)	C(1)	1.319(4)	O(2)	C(4)	1.261(3)
F(4)	C(5)	1.290(4)	O(3)	C(7)	1.258(4)
F(5)	C(5)	1.346(4)	O(4)	C(9)	1.270(4)
F(6)	C(5)	1.316(4)	O(5)	C(12)	1.256(4)
F(7)	F(7a)	0.42(3)	O(6)	C(14)	1.264(4)
F(7)	F(8a)	1.73(1)	C(1)	C(2)	1.535(4)
F(7)	C(6)	1.283(9)	C(2)	C(3)	1.389(4)

F(7a)	F(9)	1.70(3)
F(7a)	C(6)	1.21(2)
F(8a)	F(8)	1.16(1)
F(8a)	C(6)	1.46(1)
F(8)	F(9a)	1.11(2)
F(8)	C(6)	1.248(7)
F(9a)	F(9)	1.16(3)
F(9a)	C(6)	1.21(1)
F(9)	C(6)	1.388(8)
F(10)	C(10)	1.307(4)
F(11)	C(10)	1.317(5)

C(3)	C(4)	1.387(4)
C(4)	C(5)	1.540(5)
C(6)	C(7)	1.551(5)
C(7)	C(8)	1.374(4)
C(8)	C(9)	1.393(4)
C(9)	C(10)	1.526(5)
C(11)	C(12)	1.531(5)
C(12)	C(13)	1.402(4)
C(13)	C(14)	1.376(4)
C(14)	C(15)	1.534(4)

Table I-11.4 Bond angles (°) for Ru(hfac)₃

atom	atom	atom	angle
O(1)	Ru(1)	O(2)	93.05(8)
O(1)	Ru(1)	O(3)	91.11(9)
O(1)	Ru(1)	O(4)	176.08(9)
O(1)	Ru(1)	O(5)	87.80(8)
O(1)	Ru(1)	O(6)	86.32(9)
O(2)	Ru(1)	O(3)	88.83(9)
O(2)	Ru(1)	O(4)	89.60(8)
O(2)	Ru(1)	O(5)	178.23(9)
O(2)	Ru(1)	O(6)	88.76(9)
O(3)	Ru(1)	O(4)	91.85(9)
O(3)	Ru(1)	O(5)	89.60(9)
O(3)	Ru(1)	O(6)	176.37(9)
O(4)	Ru(1)	O(5)	89.63(9)
O(4)	Ru(1)	O(6)	90.85(8)
O(5)	Ru(1)	O(6)	92.84(9)
Ru(1)	O(1)	C(2)	122.6(2)
Ru(1)	O(2)	C(4)	122.1(2)
Ru(1)	O(3)	C(7)	122.9(2)
Ru(1)	O(4)	C(9)	124.0(2)
Ru(1)	O(5)	C(12)	122.7(2)
Ru(1)	O(6)	C(14)	121.7(2)
F(4)	C(5)	F(5)	107.6(3)
F(4)	C(5)	F(6)	109.0(3)
F(4)	C(5)	C(4)	112.6(3)
F(5)	C(5)	F(6)	105.6(3)
F(5)	C(5)	C(4)	108.8(3)
F(6)	C(5)	C(4)	113.0(3)
F(7)	C(6)	F(8)	115.8(10)
F(7)	C(6)	F(9)	99.7(6)
F(7)	C(6)	C(7)	114.0(6)
F(7a)	C(6)	F(8a)	95.8(11)
F(7a)	C(6)	F(9a)	120.2(13)
F(7a)	C(6)	C(7)	115.3(9)
F(8)	C(6)	F(9)	104.7(8)
F(8)	C(6)	C(7)	113.2(5)
F(8a)	C(6)	F(9a)	102.7(13)
F(8a)	C(6)	C(7)	104.5(6)
F(9)	C(6)	C(7)	107.9(5)
F(9a)	C(6)	C(7)	113.9(7)
F(10)	C(10)	F(11)	107.1(4)
F(10)	C(10)	F(12)	107.3(4)
F(10)	C(10)	C(9)	111.8(3)

atom	atom	atom	angle
F(1)	C(1)	F(2)	107.3(3)
F(1)	C(1)	F(3)	108.2(3)
F(1)	C(1)	C(2)	111.2(3)
F(2)	C(1)	F(3)	107.6(3)
F(2)	C(1)	C(2)	109.3(3)
F(3)	C(1)	C(2)	113.0(3)
O(1)	C(2)	C(1)	112.2(3)
O(1)	C(2)	C(3)	128.9(3)
C(1)	C(2)	C(3)	119.0(3)
C(2)	C(3)	C(4)	122.4(3)
O(2)	C(4)	C(3)	129.4(3)
O(2)	C(4)	C(5)	111.9(3)
C(3)	C(4)	C(5)	118.7(3)
O(3)	C(7)	C(6)	111.9(3)
O(3)	C(7)	C(8)	130.4(3)
C(6)	C(7)	C(8)	117.6(3)
C(7)	C(8)	C(9)	122.3(3)
O(4)	C(9)	C(8)	128.3(3)
O(4)	C(9)	C(10)	112.1(3)
C(8)	C(9)	C(10)	119.5(3)
F(11)	C(10)	F(12)	107.0(3)
F(11)	C(10)	C(9)	110.8(4)
F(12)	C(10)	C(9)	112.6(3)
F(13)	C(11)	F(14)	107.5(3)
F(13)	C(11)	F(15)	107.1(3)
F(13)	C(11)	C(12)	112.8(3)
F(14)	C(11)	F(15)	108.0(3)
F(14)	C(11)	C(12)	109.9(3)
F(15)	C(11)	C(12)	111.4(3)
O(5)	C(12)	C(11)	114.0(3)
O(5)	C(12)	C(13)	128.1(3)
C(11)	C(12)	C(13)	117.9(3)
C(12)	C(13)	C(14)	122.9(3)
O(6)	C(14)	C(13)	129.6(3)
O(6)	C(14)	C(15)	111.4(3)
F(16)	C(15)	F(17)	108.1(3)
F(16)	C(15)	C(14)	111.8(3)
F(17)	C(15)	C(14)	109.6(3)
C(13)	C(14)	C(15)	119.1(3)
F(16)	C(15)	F(18)	107.7(3)
F(17)	C(15)	F(18)	107.9(3)
F(18)	C(15)	C(14)	111.7(3)

Appendix I-12 X-ray data for Ru(hfac)₂(MeCN)₂

Table I-12.1 Experimental details for Ru(hfac)₂(MeCN)₂

Formula	C ₁₄ H ₈ F ₁₂ N ₂ O ₄ Ru
fw	597.28
Crystal system	Monoclinic
Space group	C2/c (No. 15)
<i>a</i> , Å	25.731(4)
<i>b</i> , Å	8.8332(13)
<i>c</i> , Å	18.1955(4)
α , °	—
β , °	93.3395(6)
γ , °	—
<i>V</i> , Å ³	4128.5(7)
<i>Z</i>	8
ρ_{calc} , g/cm ³	1.922
<i>F</i> (000)	2320
μ , cm ⁻¹	8.90
Crystal size, mm	0.25 × 0.35 × 0.40
Transmission factors	0.82-1.00
Scan type	ϕ , ω sweeps
Scan range, deg in ω	0.5
Scan speed, deg/min	—
Data collected	462 frames, 45 s/frame
$2\theta_{max}$, deg	60.1
Crystal decay, %	—
Total reflections	19530
Unique reflections	5100
<i>R</i> _{merge}	0.047
No. with $I \geq 3\sigma(I)$	5100
No. of variables	325
<i>R</i> (<i>F</i>) ($I \geq 3\sigma(I)$)	0.035
<i>R</i> _w (<i>F</i>) ($I \geq 3\sigma(I)$)	0.052
<i>R</i> (<i>F</i> ²) (all data)	—
<i>R</i> _w (<i>F</i> ²) (all data)	—
gof	1.23
Max Δ/σ (final cycle)	0.01
Residual density e/Å ³	-1.19 to 1.18

Table I-12.2 Atomic coordinates and $B_{\text{iso}}/B_{\text{eq}}$ for $\text{Ru}(\text{hfac})_2(\text{MeCN})_2$

atom	x	y	z	B_{eq}	occ
Ru(1)	0.117317(7)	0.08910(2)	0.180137(9)	1.139(6)	
F(1)	0.09616(9)	-0.4694(2)	0.27965(12)	4.77(6)	
F(2)	0.16861(10)	-0.4176(2)	0.23531(11)	4.27(6)	
F(3)	0.14916(10)	-0.3197(2)	0.33702(9)	4.57(5)	
F(4)	-0.03090(8)	-0.3111(2)	0.11089(11)	5.05(6)	
F(5)	-0.00757(9)	-0.1691(3)	0.02583(9)	5.10(6)	
F(6)	-0.05149(9)	-0.0805(2)	0.11131(14)	5.46(6)	
F(7)	0.12310(8)	0.4963(2)	-0.03331(8)	3.36(4)	
F(8)	0.06129(8)	0.5104(2)	0.04013(9)	3.72(5)	
F(9)	0.13844(10)	0.5722(2)	0.07789(11)	3.83(5)	
F(10)	0.2069(6)	0.054(2)	-0.0731(7)	8.4(4)	0.50
F(10a)	0.1884(6)	0.025(2)	-0.0831(6)	7.3(3)	0.50
F(11)	0.2276(5)	-0.1038(13)	0.0057(5)	8.1(3)	0.50
F(11a)	0.2465(4)	-0.0193(11)	0.0083(7)	7.8(3)	0.50
F(12)	0.1555(4)	-0.1276(12)	-0.0461(6)	9.3(3)	0.50
F(12a)	0.1831(5)	-0.1624(7)	-0.0169(6)	7.7(3)	0.50
O(1)	0.13423(7)	-0.1058(2)	0.23605(9)	1.60(4)	
O(2)	0.05185(7)	0.0009(2)	0.12815(8)	1.51(4)	
O(3)	0.10304(7)	0.2867(2)	0.12462(8)	1.41(4)	
O(4)	0.15802(7)	-0.0017(2)	0.09778(9)	1.68(4)	
N(1)	0.18032(9)	0.1845(2)	0.23242(11)	1.60(4)	
N(2)	0.07570(8)	0.1686(2)	0.26171(10)	1.49(4)	
C(1)	0.12963(12)	-0.3577(3)	0.27183(14)	2.27(6)	
C(2)	0.10631(10)	-0.2225(3)	0.22884(12)	1.55(5)	
C(3)	0.05953(11)	-0.2422(3)	0.18688(13)	1.75(5)	
C(4)	0.03673(10)	-0.1319(3)	0.14080(13)	1.55(5)	
C(5)	-0.01368(11)	-0.1720(3)	0.09705(14)	2.08(6)	
C(6)	0.11061(12)	0.4731(3)	0.03616(13)	2.10(6)	
C(7)	0.12169(10)	0.3115(3)	0.06287(13)	1.41(5)	
C(8)	0.14984(11)	0.2164(3)	0.01946(13)	2.05(6)	
C(9)	0.16416(12)	0.0702(3)	0.03864(14)	1.97(6)	
C(10)	0.1927(2)	-0.0240(4)	-0.0173(2)	4.20(10)	
C(11)	0.21031(11)	0.2445(3)	0.26948(15)	2.27(6)	
C(12)	0.24757(13)	0.3242(4)	0.3197(2)	3.71(8)	
C(13)	0.05440(10)	0.2211(3)	0.30914(13)	1.75(5)	
C(14)	0.02774(13)	0.2902(4)	0.36895(15)	3.04(7)	

Table I-12.3 Bond lengths (\AA) for $\text{Ru}(\text{hfac})_2(\text{MeCN})_2$

atom	atom	distance	atom	atom	distance
Ru(1)	O(1)	2.034(2)	Ru(1)	O(2)	2.038(2)
Ru(1)	O(3)	2.040(2)	Ru(1)	O(4)	2.042(2)
Ru(1)	N(1)	2.016(2)	Ru(1)	N(2)	2.007(2)
F(1)	C(1)	1.323(4)	F(2)	C(1)	1.344(4)
F(3)	C(1)	1.305(3)	F(4)	C(5)	1.336(3)
F(5)	C(5)	1.314(3)	F(6)	C(5)	1.302(4)
F(7)	C(6)	1.338(3)	F(8)	C(6)	1.317(3)
F(9)	C(6)	1.339(3)	F(10)	C(10)	1.296(13)
F(10a)	C(10)	1.272(10)	F(11)	C(10)	1.196(9)
F(11a)	C(10)	1.436(11)	F(12)	C(10)	1.403(11)
F(12a)	C(10)	1.247(9)	O(1)	C(2)	1.259(3)
O(2)	C(4)	1.261(3)	O(3)	C(7)	1.266(3)
O(4)	C(9)	1.267(3)	N(1)	C(11)	1.127(3)
N(2)	C(13)	1.147(3)	C(1)	C(2)	1.531(3)
C(2)	C(3)	1.398(4)	C(3)	C(4)	1.393(3)
C(4)	C(5)	1.523(4)	C(6)	C(7)	1.529(3)
C(7)	C(8)	1.386(4)	C(8)	C(9)	1.382(4)
C(9)	C(10)	1.535(4)	C(11)	C(12)	1.466(4)
C(13)	C(14)	1.454(4)			

Table I-12.4 Bond angles (°) for Ru(hfac)₂(MeCN)₂

atom	atom	atom	angle
O(1)	Ru(1)	O(2)	93.19(7)
O(1)	Ru(1)	O(4)	86.03(7)
O(1)	Ru(1)	N(2)	91.94(7)
O(2)	Ru(1)	O(4)	87.40(7)
O(2)	Ru(1)	N(2)	90.84(7)
O(3)	Ru(1)	N(1)	89.59(7)
O(4)	Ru(1)	N(1)	94.46(8)
N(1)	Ru(1)	N(2)	87.36(8)
Ru(1)	O(2)	C(4)	121.76(15)
Ru(1)	O(4)	C(9)	121.4(2)
Ru(1)	N(2)	C(13)	175.5(2)
F(1)	C(1)	F(3)	108.2(2)
F(2)	C(1)	F(3)	107.0(3)
F(3)	C(1)	C(2)	112.5(2)
O(1)	C(2)	C(3)	128.8(2)
C(2)	C(3)	C(4)	124.1(2)
O(2)	C(4)	C(5)	112.5(2)
F(4)	C(5)	F(5)	105.3(2)
F(4)	C(5)	C(4)	113.4(2)
F(5)	C(5)	C(4)	111.3(2)
F(7)	C(6)	F(8)	107.4(2)
F(7)	C(6)	C(7)	113.1(2)
F(8)	C(6)	C(7)	112.3(2)
O(3)	C(7)	C(6)	111.7(2)
C(6)	C(7)	C(8)	118.6(2)
O(4)	C(9)	C(8)	129.6(2)
C(8)	C(9)	C(10)	118.0(2)
F(10)	C(10)	F(12)	105.7(10)
F(10a)	C(10)	F(11a)	109.0(9)
F(10a)	C(10)	C(9)	114.9(6)
F(11)	C(10)	C(9)	117.7(5)
F(11a)	C(10)	C(9)	105.0(5)
F(12a)	C(10)	C(9)	115.1(4)
N(2)	C(13)	C(14)	179.0(3)

atom	atom	atom	angle
O(1)	Ru(1)	O(3)	177.98(7)
O(1)	Ru(1)	N(1)	88.55(8)
O(2)	Ru(1)	O(3)	88.70(7)
O(2)	Ru(1)	N(1)	177.54(7)
O(3)	Ru(1)	O(4)	93.33(7)
O(3)	Ru(1)	N(2)	88.76(7)
O(4)	Ru(1)	N(2)	177.24(7)
Ru(1)	O(1)	C(2)	122.5(2)
Ru(1)	O(3)	C(7)	121.36(15)
Ru(1)	N(1)	C(11)	169.3(2)
F(1)	C(1)	F(2)	105.6(2)
F(1)	C(1)	C(2)	113.5(3)
F(2)	C(1)	C(2)	109.6(2)
O(1)	C(2)	C(1)	112.4(2)
C(1)	C(2)	C(3)	118.8(2)
O(2)	C(4)	C(3)	129.6(2)
C(3)	C(4)	C(5)	117.9(2)
F(4)	C(5)	F(6)	105.9(3)
F(5)	C(5)	F(6)	108.6(3)
F(6)	C(5)	C(4)	112.0(2)
F(7)	C(6)	F(9)	106.6(2)
F(8)	C(6)	F(9)	106.9(2)
F(9)	C(6)	C(7)	110.3(2)
O(3)	C(7)	C(8)	129.7(2)
C(7)	C(8)	C(9)	124.3(2)
O(4)	C(9)	C(10)	112.3(2)
F(10)	C(10)	F(11)	110.3(10)
F(10)	C(10)	C(9)	113.6(7)
F(10a)	C(10)	F(12a)	109.4(9)
F(11)	C(10)	F(12)	103.2(7)
F(11a)	C(10)	F(12a)	102.4(7)
F(12)	C(10)	C(9)	105.0(5)
N(1)	C(11)	C(12)	177.6(3)

Appendix I-13 X-ray data for Ru(acac)(hfac)(MeCN)₂

Table I-13.1 Experimental details for Ru(acac)(hfac)(MeCN)₂

Formula	C ₁₄ H ₁₄ F ₆ N ₂ O ₄ Ru
fw	489.34
Crystal system	Triclinic
Space group	P $\bar{1}$ (No. 2)
<i>a</i> , Å	7.6812(9)
<i>b</i> , Å	10.680(2)
<i>c</i> , Å	12.578(2)
α , °	88.062(6)
β , °	83.874(3)
γ , °	69.5898(15)
<i>V</i> , Å ³	961.5(2)
<i>Z</i>	2
ρ_{calc} , g/cm ³	1.690
<i>F</i> (000)	484
μ , cm ⁻¹	8.92
Crystal size, mm	0.45 × 0.35 × 0.10
Transmission factors	0.83-1.00
Scan type	ϕ , ω sweeps
Scan range, deg in ω	0.5
Scan speed, deg/min	—
Data collected	462 frames, 30 s/frame
$2\theta_{max}$, deg	60.1
Crystal decay, %	—
Total reflections	9023
Unique reflections	4382
<i>R</i> _{merge}	0.037
No. with $I \geq 3\sigma(I)$	4363
No. of variables	256
<i>R</i> (<i>F</i>) ($I \geq 3\sigma(I)$)	0.068
<i>R</i> _w (<i>F</i>) ($I \geq 3\sigma(I)$)	0.089
<i>R</i> (<i>F</i> ²) (all data)	—
<i>R</i> _w (<i>F</i> ²) (all data)	—
gof	1.25
Max Δ/σ (final cycle)	0.00
Residual density e/Å ³	-0.92 to 0.97

Table I-13.2 Atomic coordinates and $B_{\text{iso}}/B_{\text{eq}}$ for $\text{Ru}(\text{acac})(\text{hfac})(\text{MeCN})_2$

atom	x	y	z	$B\{\text{eq}\}$	occ
Ru(1)	0.20695(5)	0.14390(4)	0.25742(3)	1.987(8)	
F(1)	0.2765(10)	0.4950(6)	0.0344(3)	12.7(2)	
F(2)	0.4682(9)	0.4651(7)	0.1417(5)	13.6(2)	
F(3)	0.2210(9)	0.6248(5)	0.1610(4)	11.7(2)	
F(4)	-0.2279(8)	0.4349(6)	0.5051(4)	6.46(15)	0.75
F(5)	-0.2249(9)	0.6083(6)	0.4250(7)	10.3(2)	0.75
F(6)	-0.3732(10)	0.4815(11)	0.3666(7)	9.8(3)	0.75
F(7)	-0.212(4)	0.504(3)	0.493(2)	10.7(8)	0.25
F(8)	-0.316(3)	0.604(2)	0.3479(13)	6.6(4)	0.25
F(9)	-0.352(4)	0.452(3)	0.401(2)	5.8(5)	0.25
O(1)	0.2894(4)	0.2882(3)	0.1782(2)	2.54(7)	
O(2)	-0.0114(4)	0.2787(3)	0.3448(2)	2.35(7)	
O(3)	0.1259(4)	0.0012(3)	0.3374(2)	2.23(7)	
O(4)	0.0328(4)	0.1643(3)	0.1430(2)	2.33(7)	
N(1)	0.4089(5)	-0.0015(4)	0.1730(3)	2.21(8)	
N(2)	0.3827(5)	0.1435(4)	0.3672(3)	2.31(9)	
C(1)	0.2898(12)	0.5021(7)	0.1350(6)	6.1(2)	
C(2)	0.2025(8)	0.4100(5)	0.1988(4)	3.23(12)	
C(3)	0.0495(8)	0.4706(5)	0.2689(4)	4.00(14)	
C(4)	-0.0464(7)	0.4019(5)	0.3349(4)	3.16(12)	
C(5)	-0.2231(10)	0.4873(7)	0.4052(6)	5.3(2)	
C(6)	-0.0418(7)	-0.1433(5)	0.3796(4)	3.56(13)	
C(7)	-0.0040(6)	-0.0354(5)	0.3117(3)	2.42(10)	
C(8)	-0.1094(7)	0.0144(5)	0.2241(3)	3.03(12)	
C(9)	-0.0874(6)	0.1072(5)	0.1475(3)	2.75(11)	
C(10)	-0.2189(7)	0.1455(6)	0.0585(4)	3.70(13)	
C(11)	0.5206(7)	-0.0910(5)	0.1307(4)	2.88(12)	
C(12)	0.6639(8)	-0.2044(6)	0.0769(4)	4.36(14)	
C(13)	0.4872(6)	0.1527(5)	0.4201(3)	2.31(10)	
C(14)	0.6205(7)	0.1689(5)	0.4864(4)	3.65(13)	

Table I-13.3 Bond lengths (Å) for $\text{Ru}(\text{acac})(\text{hfac})(\text{MeCN})_2$

atom	atom	distance	atom	atom	distance
Ru(1)	O(1)	2.053(3)	Ru(1)	O(2)	2.030(3)
Ru(1)	O(3)	2.036(3)	Ru(1)	O(4)	2.023(3)
Ru(1)	N(1)	2.006(4)	Ru(1)	N(2)	2.030(3)
F(1)	C(1)	1.288(8)	F(2)	C(1)	1.298(9)
F(3)	C(1)	1.269(8)	F(4)	C(5)	1.360(9)
F(5)	C(5)	1.319(8)	F(6)	C(5)	1.319(11)
F(7)	C(5)	1.14(3)	F(8)	C(5)	1.41(2)
F(9)	C(5)	1.18(3)	O(1)	C(2)	1.259(6)
O(2)	C(4)	1.253(6)	O(3)	C(7)	1.266(4)
O(4)	C(9)	1.268(5)	N(1)	C(11)	1.140(6)
N(2)	C(13)	1.127(4)	C(1)	C(2)	1.534(7)
C(2)	C(3)	1.365(7)	C(3)	C(4)	1.406(6)
C(4)	C(5)	1.546(7)	C(6)	C(7)	1.502(6)
C(7)	C(8)	1.415(6)	C(8)	C(9)	1.399(6)
C(9)	C(10)	1.537(6)	C(11)	C(12)	1.451(7)
C(13)	C(14)	1.445(5)			

Table I-13.4 Bond angles (°) for Ru(acac)(hfac)(MeCN)₂

atom	atom	atom	angle
O(1)	Ru(1)	O(2)	93.59(12)
O(1)	Ru(1)	O(4)	87.03(11)
O(1)	Ru(1)	N(2)	86.98(12)
O(2)	Ru(1)	O(4)	86.99(11)
O(2)	Ru(1)	N(2)	91.31(13)
O(3)	Ru(1)	N(1)	88.82(13)
O(4)	Ru(1)	N(1)	90.89(12)
N(1)	Ru(1)	N(2)	91.33(14)
Ru(1)	O(2)	C(4)	121.7(3)
Ru(1)	O(4)	C(9)	123.1(3)
Ru(1)	N(2)	C(13)	172.0(3)
F(1)	C(1)	F(3)	107.1(7)
F(2)	C(1)	F(3)	106.7(7)
F(3)	C(1)	C(2)	115.6(6)
O(1)	C(2)	C(3)	130.7(5)
C(2)	C(3)	C(4)	124.2(5)
O(2)	C(4)	C(5)	113.6(4)
F(4)	C(5)	F(5)	102.1(7)
F(4)	C(5)	C(4)	110.6(6)
F(5)	C(5)	C(4)	113.4(5)
F(7)	C(5)	F(8)	115.3(18)
F(7)	C(5)	C(4)	119.1(17)
F(8)	C(5)	C(4)	108.6(9)
O(3)	C(7)	C(6)	115.7(4)

atom	atom	atom	angle
O(1)	Ru(1)	O(3)	179.45(11)
O(1)	Ru(1)	N(1)	91.40(14)
O(2)	Ru(1)	O(3)	86.20(12)
O(2)	Ru(1)	N(1)	174.46(14)
O(3)	Ru(1)	O(4)	93.48(11)
O(3)	Ru(1)	N(2)	92.51(12)
O(4)	Ru(1)	N(2)	173.66(14)
Ru(1)	O(1)	C(2)	120.5(3)
Ru(1)	O(3)	C(7)	123.6(3)
Ru(1)	N(1)	C(11)	174.6(4)
F(1)	C(1)	F(2)	104.1(7)
F(1)	C(1)	C(2)	110.7(6)
F(2)	C(1)	C(2)	111.9(6)
O(1)	C(2)	C(1)	112.8(5)
C(1)	C(2)	C(3)	116.5(5)
O(2)	C(4)	C(3)	129.3(5)
C(3)	C(4)	C(5)	117.1(5)
F(4)	C(5)	F(6)	104.6(8)
F(5)	C(5)	F(6)	115.8(8)
F(6)	C(5)	C(4)	109.7(6)
F(7)	C(5)	F(9)	107.7(20)
F(8)	C(5)	F(9)	89.0(15)
F(9)	C(5)	C(4)	113.3(14)
O(3)	C(7)	C(8)	125.3(4)

Appendix I-14 X-ray data for [Ru(acac)₂(Im)₂][CF₃SO₃]•benzene

Table I-14.1 Experimental details for [Ru(acac)₂(Im)₂][CF₃SO₃]•benzene

Formula	C ₂₃ H ₂₈ F ₃ N ₄ O ₇ RuS
fw	662.62
Crystal system	Monoclinic
Space group	C2/m (No. 12)
<i>a</i> , Å	13.718(2)
<i>b</i> , Å	24.495(3)
<i>c</i> , Å	10.0987(15)
α, °	—
β, °	125.414(11)
γ, °	—
<i>V</i> , Å ³	2765.5(8)
<i>Z</i>	4
ρ_{calc} , g/cm ³	1.591
<i>F</i> (000)	1348
μ , cm ⁻¹	7.11
Crystal size, mm	0.35 × 0.35 × 0.35
Transmission factors	0.84-1.00
Scan type	φ, ω sweeps
Scan range, deg in ω	0.5
Scan speed, deg/min	—
Data collected	462 frames, 5 s/frame
2θ _{max} , deg	60.1
Crystal decay, %	—
Total reflections	12567
Unique reflections	3680
<i>R</i> _{merge}	0.045
No. with <i>I</i> ≥ 3σ(<i>I</i>)	2273
No. of variables	183
<i>R</i> (<i>F</i>) (<i>I</i> ≥ 3σ(<i>I</i>))	0.038
<i>R</i> _w (<i>F</i>) (<i>I</i> ≥ 3σ(<i>I</i>))	0.034
<i>R</i> (<i>F</i> ²) (all data)	—
<i>R</i> _w (<i>F</i> ²) (all data)	—
gof	1.34
Max Δ/σ (final cycle)	0.0004
Residual density e/Å ³	-0.43 to 0.46

Table I-14.2 Atomic coordinates and B_{iso}/B_{eq} for $[Ru(acac)_2(Im)_2][CF_3SO_3] \cdot benzene$

atom	x	y	z	B{eq}	occ
Ru(1)	0.50000	0.264670(13)	0.00000	2.071(7)	0.50
S(1)	0.32461(8)	0.5000	0.38111(13)	2.62(2)	0.50
F(1)	0.0967(2)	0.5000	0.2642(4)	5.14(7)	0.50
F(2)	0.1375(2)	0.45640(8)	0.1194(3)	5.60(5)	
O(1)	0.67111(14)	0.26496(8)	0.1919(2)	2.62(4)	
O(2)	0.45660(15)	0.20621(7)	0.0966(2)	2.58(4)	
O(3)	0.3840(2)	0.5000	0.3029(4)	3.44(7)	0.50
O(4)	0.3374(2)	0.45017(8)	0.4660(3)	4.09(5)	
N(1)	0.5417(2)	0.32347(8)	-0.1033(3)	2.28(5)	
N(2)	0.5259(3)	0.39147(10)	-0.2539(3)	3.99(7)	
C(1)	0.8529(3)	0.22885(14)	0.4118(4)	4.39(8)	
C(2)	0.7190(2)	0.22472(11)	0.2920(4)	2.79(6)	
C(3)	0.6575(3)	0.18137(12)	0.2983(4)	3.30(7)	
C(4)	0.5346(3)	0.17474(11)	0.2111(4)	2.82(7)	
C(5)	0.4821(3)	0.12909(13)	0.2536(5)	4.49(9)	
C(6)	0.4692(3)	0.36147(12)	-0.2084(4)	3.15(7)	
C(7)	0.6402(3)	0.37209(13)	-0.1748(5)	4.30(9)	
C(8)	0.6498(3)	0.33028(12)	-0.0818(4)	3.49(8)	
C(9)	0.1663(4)	0.5000	0.2119(6)	3.21(10)	0.50
C(10)	0.3276(8)	0.4756(2)	-0.1187(10)	19.2(3)	
C(11)	0.2515(7)	0.4439(3)	-0.2312(11)	12.4(3)	
C(12)	0.1763(6)	0.4734(2)	-0.3407(9)	14.9(2)	

Table I-14.3 Bond lengths (Å) for $[Ru(acac)_2(Im)_2][CF_3SO_3] \cdot benzene$

atom	atom	distance
Ru(1)	O(1)	1.9982(15)
Ru(1)	N(1)	2.045(2)
S(1)	O(4)	1.443(2)
F(1)	C(9)	1.332(5)
O(1)	C(2)	1.287(3)
N(1)	C(6)	1.326(3)
N(2)	C(6)	1.331(4)
C(1)	C(2)	1.508(4)
C(3)	C(4)	1.387(4)
C(7)	C(8)	1.343(4)
C(10)	C(11)	1.268(8)
C(12)	C(12)''	1.301(12)

atom	atom	distance
Ru(1)	O(2)	2.007(2)
S(1)	O(3)	1.426(3)
S(1)	C(9)	1.826(4)
F(2)	C(9)	1.320(3)
O(2)	C(4)	1.282(3)
N(1)	C(8)	1.379(3)
N(2)	C(7)	1.367(4)
C(2)	C(3)	1.380(4)
C(4)	C(5)	1.520(4)
C(10)	C(10)''	1.196(11)
C(11)	C(12)	1.220(8)

Table I-14.4 Bond angles (°) for $[Ru(acac)_2(Im)_2][CF_3SO_3] \cdot benzene$

atom	atom	atom	angle
O(1)	Ru(1)	O(1)'	179.59(11)
O(1)	Ru(1)	O(2)'	87.78(8)
O(1)	Ru(1)	N(1)'	91.23(8)
O(2)	Ru(1)	N(1)	178.74(9)
O(2)	Ru(1)	N(1)	90.30(8)
O(3)	S(1)	O(4)	114.68(11)
O(3)	S(1)	C(9)	103.5(2)
O(4)	S(1)	C(9)	103.00(12)
Ru(1)	O(2)	C(4)	122.7(2)
Ru(1)	N(1)	C(8)	126.7(2)
C(6)	N(2)	C(7)	107.9(3)
O(1)	C(2)	C(3)	125.4(2)
C(2)	C(3)	C(4)	127.7(3)
O(2)	C(4)	C(5)	114.3(3)
N(1)	C(6)	N(2)	110.3(3)
N(1)	C(8)	C(7)	108.7(3)
S(1)	C(9)	F(2)	111.6(2)
F(1)	C(9)	F(2)	107.0(3)
F(2)	C(9)	F(2)	108.0(4)
C(10)	C(11)	C(12)	105.9(7)

atom	atom	atom	angle
O(1)	Ru(1)	O(2)	92.51(8)
O(1)	Ru(1)	N(1)	88.49(8)
O(2)	Ru(1)	O(2)'	88.98(11)
O(2)	Ru(1)	N(1)'	90.30(8)
N(1)	Ru(1)	N(1)'	90.43(12)
O(3)	S(1)	O(4)''	114.68(11)
O(4)	S(1)	O(4)''	115.6(2)
Ru(1)	O(1)	C(2)	122.5(2)
Ru(1)	N(1)	C(6)	127.0(2)
C(6)	N(1)	C(8)	106.3(3)
O(1)	C(2)	C(1)	114.1(3)
C(1)	C(2)	C(3)	120.5(3)
O(2)	C(4)	C(3)	125.1(3)
C(3)	C(4)	C(5)	120.5(3)
N(2)	C(7)	C(8)	106.8(3)
S(1)	C(9)	F(1)	111.5(3)
S(1)	C(9)	F(2)	111.6(2)
F(1)	C(9)	F(2)	107.0(3)
C(10)''	C(10)	C(11)	127.7(5)
C(11)	C(12)	C(12)''	126.4(5)

Appendix I-15 X-ray data for [Ru(acac)₂(NMeIm)₂][CF₃SO₃]

Table I-15.1 Experimental details for [Ru(acac)₂(NMeIm)₂][CF₃SO₃]

Formula	C ₁₉ H ₂₆ F ₃ N ₄ O ₇ RuS
fw	612.56
Crystal system	Monoclinic
Space group	P2 ₁ /c (No. 14)
<i>a</i> , Å	13.9470(10)
<i>b</i> , Å	12.107(2)
<i>c</i> , Å	15.1402(5)
α , °	—
β , °	104.3087(6)
γ , °	—
<i>V</i> , Å ³	2477.3(3)
<i>Z</i>	4
ρ_{calc} , g/cm ³	1.642
<i>F</i> (000)	1244
μ , cm ⁻¹	7.86
Crystal size, mm	0.45 × 0.40 × 0.30
Transmission factors	0.66-1.00
Scan type	ϕ , ω sweeps
Scan range, deg in ω	0.5
Scan speed, deg/min	—
Data collected	462 frames, 10 s/frame
$2\theta_{max}$, deg	60.1
Crystal decay, %	—
Total reflections	22815
Unique reflections	6032
<i>R</i> _{merge}	0.030
No. with $I \geq 3\sigma(I)$	4116
No. of variables	317
<i>R</i> (<i>F</i>) ($I \geq 3\sigma(I)$)	0.031
<i>R</i> _w (<i>F</i>) ($I \geq 3\sigma(I)$)	0.025
<i>R</i> (<i>F</i> ²) (all data)	—
<i>R</i> _w (<i>F</i> ²) (all data)	—
gof	1.49
Max Δ/σ (final cycle)	0.0002
Residual density e/Å ³	-0.87 to 1.12

Table I-15.2 Atomic coordinates and $B_{\text{iso}}/B_{\text{eq}}$ for $[\text{Ru}(\text{acac})_2(\text{NMeIm})_2][\text{CF}_3\text{SO}_3]$

atom	x	y	z	$B\{\text{eq}\}$
Ru(1)	0.145231(13)	0.18848(2)	0.353382(14)	1.364(4)
S(1)	0.41433(5)	0.70278(7)	0.59074(5)	2.83(2)
F(1)	0.3172(2)	0.6691(2)	0.42288(15)	8.12(7)
F(2)	0.27565(14)	0.5634(2)	0.5203(2)	8.20(8)
F(3)	0.40667(14)	0.5355(2)	0.47986(15)	6.24(6)
O(1)	0.08057(10)	0.12056(14)	0.23211(11)	1.79(4)
O(2)	0.02005(10)	0.26934(14)	0.35908(12)	1.80(4)
O(3)	0.09713(11)	0.05951(14)	0.41432(12)	1.73(4)
O(4)	0.27204(10)	0.11399(14)	0.34764(11)	1.49(4)
O(5)	0.4464(2)	0.6291(2)	0.6650(2)	8.02(9)
O(6)	0.49010(15)	0.7507(2)	0.5558(2)	7.06(8)
O(7)	0.33968(15)	0.7786(2)	0.6002(2)	4.57(6)
N(1)	0.21487(13)	0.2525(2)	0.47752(14)	1.46(5)
N(2)	0.33079(13)	0.3103(2)	0.59483(13)	1.87(5)
N(3)	0.18920(13)	0.3204(2)	0.28695(13)	1.57(4)
N(4)	0.27819(15)	0.4321(2)	0.2254(2)	2.42(5)
C(1)	-0.0443(2)	0.0615(3)	0.1074(2)	2.78(7)
C(2)	-0.0121(2)	0.1267(2)	0.1934(2)	2.00(6)
C(3)	-0.0811(2)	0.1895(3)	0.2254(2)	2.15(6)
C(4)	-0.0633(2)	0.2571(2)	0.3015(2)	1.81(6)
C(5)	-0.1462(2)	0.3254(3)	0.3205(2)	2.70(7)
C(6)	0.0983(2)	-0.1195(2)	0.4777(2)	2.39(6)
C(7)	0.1479(2)	-0.0288(2)	0.4361(2)	1.72(6)
C(8)	0.2420(2)	-0.0485(2)	0.4238(2)	2.25(6)
C(9)	0.2979(2)	0.0186(2)	0.3816(2)	1.61(6)
C(10)	0.3975(2)	-0.0200(2)	0.3720(2)	2.76(7)
C(11)	0.3115(2)	0.2648(2)	0.5109(2)	1.86(6)
C(12)	0.2416(2)	0.3289(2)	0.6158(2)	2.32(6)
C(13)	0.1710(2)	0.2915(2)	0.5429(2)	2.01(6)
C(14)	0.4289(2)	0.3351(3)	0.6534(2)	3.13(7)
C(15)	0.2801(2)	0.3485(2)	0.2837(2)	2.10(6)
C(16)	0.1800(2)	0.4578(3)	0.1889(2)	2.89(7)
C(17)	0.1264(2)	0.3911(2)	0.2275(2)	2.39(7)
C(18)	0.3630(2)	0.4834(3)	0.2014(3)	4.93(10)
C(19)	0.3510(2)	0.6139(3)	0.4995(2)	3.47(8)

Table I-15.3 Bond lengths (\AA) for $[\text{Ru}(\text{acac})_2(\text{NMeIm})_2][\text{CF}_3\text{SO}_3]$

atom	atom	distance	atom	atom	distance
Ru(1)	O(1)	2.010(2)	Ru(1)	O(2)	2.0220(15)
Ru(1)	O(3)	2.011(2)	Ru(1)	O(4)	2.0063(15)
Ru(1)	N(1)	2.043(2)	Ru(1)	N(3)	2.060(2)
S(1)	O(5)	1.418(3)	S(1)	O(6)	1.418(2)
S(1)	O(7)	1.422(2)	S(1)	C(19)	1.800(3)
F(1)	C(19)	1.321(4)	F(2)	C(19)	1.320(4)
F(3)	C(19)	1.307(3)	O(1)	C(2)	1.282(3)
O(2)	C(4)	1.277(3)	O(3)	C(7)	1.281(3)
O(4)	C(9)	1.279(3)	N(1)	C(11)	1.326(3)
N(1)	C(13)	1.371(3)	N(2)	C(11)	1.350(3)
N(2)	C(12)	1.376(3)	N(2)	C(14)	1.466(3)
N(3)	C(15)	1.325(3)	N(3)	C(17)	1.385(3)
N(4)	C(15)	1.339(3)	N(4)	C(16)	1.380(3)
N(4)	C(18)	1.459(4)	C(1)	C(2)	1.493(4)
C(2)	C(3)	1.403(4)	C(3)	C(4)	1.385(4)
C(4)	C(5)	1.506(3)	C(6)	C(7)	1.515(4)
C(7)	C(8)	1.391(3)	C(8)	C(9)	1.386(4)
C(9)	C(10)	1.506(3)	C(12)	C(13)	1.362(3)
C(16)	C(17)	1.331(4)			

Table I-15.4 Bond angles (°)for **[Ru(acac)₂(NMeIm)₂][CF₃SO₃]**

atom	atom	atom	angle
O(1)	Ru(1)	O(2)	92.28(6)
O(1)	Ru(1)	O(4)	88.73(6)
O(1)	Ru(1)	N(3)	89.53(7)
O(2)	Ru(1)	O(4)	177.75(7)
O(2)	Ru(1)	N(3)	90.56(7)
O(3)	Ru(1)	N(1)	90.52(8)
O(4)	Ru(1)	N(1)	89.23(7)
N(1)	Ru(1)	N(3)	91.37(8)
O(5)	S(1)	O(7)	114.9(2)
O(6)	S(1)	O(7)	113.9(2)
O(7)	S(1)	C(19)	103.35(13)
Ru(1)	O(2)	C(4)	124.4(2)
Ru(1)	O(4)	C(9)	123.5(2)
Ru(1)	N(1)	C(13)	126.86(15)
C(11)	N(2)	C(12)	107.7(2)
C(12)	N(2)	C(14)	126.0(2)
Ru(1)	N(3)	C(17)	125.4(2)
C(15)	N(4)	C(16)	106.9(2)
C(16)	N(4)	C(18)	126.1(3)
O(1)	C(2)	C(3)	125.0(2)
C(2)	C(3)	C(4)	127.6(2)
O(2)	C(4)	C(5)	114.7(2)
O(3)	C(7)	C(6)	115.6(2)
C(6)	C(7)	C(8)	118.4(2)
O(4)	C(9)	C(8)	125.4(2)
C(8)	C(9)	C(10)	120.0(2)
N(2)	C(12)	C(13)	105.8(2)
N(3)	C(15)	N(4)	110.8(2)
N(3)	C(17)	C(16)	109.1(2)
S(1)	C(19)	F(2)	111.3(3)
F(1)	C(19)	F(2)	108.1(3)
F(2)	C(19)	F(3)	105.7(3)

atom	atom	atom	angle
O(1)	Ru(1)	O(3)	88.64(7)
O(1)	Ru(1)	N(1)	177.74(7)
O(2)	Ru(1)	O(3)	88.10(7)
O(2)	Ru(1)	N(1)	89.79(7)
O(3)	Ru(1)	O(4)	93.93(7)
O(3)	Ru(1)	N(3)	177.68(7)
O(4)	Ru(1)	N(3)	87.45(7)
O(5)	S(1)	O(6)	115.8(2)
O(5)	S(1)	C(19)	103.3(2)
O(6)	S(1)	C(19)	103.1(2)
Ru(1)	O(1)	C(2)	124.6(2)
Ru(1)	O(3)	C(7)	122.73(15)
Ru(1)	N(1)	C(11)	126.9(2)
C(11)	N(1)	C(13)	106.2(2)
C(11)	N(2)	C(14)	126.3(2)
Ru(1)	N(3)	C(15)	128.3(2)
C(15)	N(3)	C(17)	105.9(2)
C(15)	N(4)	C(18)	126.9(2)
O(1)	C(2)	C(1)	114.8(2)
C(1)	C(2)	C(3)	120.2(2)
O(2)	C(4)	C(3)	125.6(2)
C(3)	C(4)	C(5)	119.7(2)
O(3)	C(7)	C(8)	126.1(2)
C(7)	C(8)	C(9)	128.2(3)
O(4)	C(9)	C(10)	114.6(2)
N(1)	C(11)	N(2)	110.6(2)
N(1)	C(13)	C(12)	109.7(2)
N(4)	C(16)	C(17)	107.2(2)
S(1)	C(19)	F(1)	111.9(2)
S(1)	C(19)	F(3)	113.8(2)
F(1)	C(19)	F(3)	105.7(3)

Appendix I-16 X-ray data for [Ru(acac)₂(2MeIm)₂][CF₃SO₃] \cdot 0.5 hexane

Table I-16.1 Experimental details for [Ru(acac)₂(2MeIm)₂][CF₃SO₃] \cdot 0.5 hexane

Formula	C ₂₂ H ₃₃ F ₃ N ₄ O ₇ RuS
fw	655.65
Crystal system	Monoclinic
Space group	C2/m (No. 2)
<i>a</i> , Å	14.484(2)
<i>b</i> , Å	24.559(4)
<i>c</i> , Å	10.3079(14)
α , °	—
β , °	129.152(7)
γ , °	—
<i>V</i> , Å ³	2843.5(8)
<i>Z</i>	4
ρ_{calc} , g/cm ³	1.531
<i>F</i> (000)	1344
μ , cm ⁻¹	6.90
Crystal size, mm	0.35 \times 0.20 \times 0.10
Transmission factors	0.77-1.00
Scan type	ϕ , ω sweeps
Scan range, deg in ω	0.5
Scan speed, deg/min	—
Data collected	462 frames, 30 s/frame
$2\theta_{max}$, deg	60.1
Crystal decay, %	—
Total reflections	12984
Unique reflections	3537
<i>R</i> _{merge}	0.052
No. with $I \geq 3\sigma(I)$	1674
No. of variables	178
<i>R</i> (<i>F</i>) ($I \geq 3\sigma(I)$)	0.047
<i>R</i> _w (<i>F</i>) ($I \geq 3\sigma(I)$)	0.038
<i>R</i> (<i>F</i> ²) (all data)	—
<i>R</i> _w (<i>F</i> ²) (all data)	—
gof	1.37
Max Δ/σ (final cycle)	0.003
Residual density e/Å ³	-2.28 to 1.67

Table I-16.2 Atomic coordinates and $B_{\text{iso}}/B_{\text{eq}}$ for $[\text{Ru}(\text{acac})_2(2\text{MeIm})_2][\text{CF}_3\text{SO}_3] \cdot 0.5$ hexane

atom	x	y	z	B_{eq}	occ
Ru(1)	0.5000	0.26701(2)	0.0000	2.608(11)	0.50
S(1)	0.33063(13)	0.5000	0.3720(2)	3.11(4)	0.50
F(1)	0.1095(3)	0.5000	0.2576(5)	7.05(14)	0.50
F(2)	0.1362(2)	0.45703(13)	0.1034(3)	6.42(8)	
O(1)	0.6736(2)	0.26563(12)	0.2017(3)	2.74(6)	
O(2)	0.4606(2)	0.20879(11)	0.0959(3)	2.74(7)	
O(3)	0.3807(3)	0.5000	0.2890(5)	4.16(11)	0.50
O(4)	0.3498(3)	0.4508(2)	0.4584(4)	6.90(10)	
N(1)	0.5414(3)	0.32506(14)	-0.1004(3)	2.53(8)	
N(2)	0.5417(4)	0.3942(2)	-0.2333(4)	3.61(10)	
C(1)	0.8550(4)	0.2269(2)	0.4245(4)	4.50(12)	
C(2)	0.7217(3)	0.2241(2)	0.2995(4)	3.02(10)	
C(3)	0.6614(4)	0.1807(2)	0.3016(5)	3.55(11)	
C(4)	0.5376(4)	0.1754(2)	0.2087(5)	3.13(11)	
C(5)	0.4865(4)	0.1302(2)	0.2444(5)	4.89(13)	
C(6)	0.4803(4)	0.3681(2)	-0.1953(5)	3.06(11)	
C(7)	0.6455(5)	0.3664(2)	-0.1610(6)	4.28(14)	
C(8)	0.6457(4)	0.3242(2)	-0.0803(5)	3.35(11)	
C(9)	0.3639(4)	0.3872(2)	-0.2499(5)	4.12(12)	
C(10)	0.1707(6)	0.5000	0.2037(8)	3.7(2)	0.50
C(11)	0.2494(11)	0.5000	-0.1310(12)	9.7(4)	0.50
C(12)	0.163(2)	0.5189(14)	-0.309(3)	20.4(9)	0.50
C(13)	0.0501(13)	0.5000	-0.4160(14)	14.4(5)	0.50

Table I-16.3 Bond lengths (Å) for $[\text{Ru}(\text{acac})_2(2\text{MeIm})_2][\text{CF}_3\text{SO}_3] \cdot 0.5$ hexane

atom	atom	distance	atom	atom	distance
Ru(1)	O(1)	2.011(2)	Ru(1)	O(2)	2.015(3)
Ru(1)	N(1)	2.060(3)	S(1)	O(3)	1.429(4)
S(1)	O(4)	1.420(3)	S(1)	C(10)	1.817(6)
F(1)	C(10)	1.311(7)	F(2)	C(10)	1.334(4)
O(1)	C(2)	1.286(5)	O(2)	C(4)	1.277(5)
N(1)	C(6)	1.329(5)	N(1)	C(8)	1.389(5)
N(2)	C(6)	1.341(5)	N(2)	C(7)	1.367(6)
C(1)	C(2)	1.501(5)	C(2)	C(3)	1.387(6)
C(3)	C(4)	1.408(6)	C(4)	C(5)	1.504(6)
C(6)	C(9)	1.477(6)	C(7)	C(8)	1.328(6)
C(11)	C(12)	1.50(2)	C(12)	C(13)	1.35(2)
C(13)	C(13)*	1.39(2)			

Table I-16.4 Bond angles (°) for $[\text{Ru}(\text{acac})_2(2\text{MeIm})_2][\text{CF}_3\text{SO}_3] \cdot 0.5$ hexane

atom	atom	atom	angle	atom	atom	atom	angle
O(1)	Ru(1)	O(1)'	178.1(2)	O(1)	Ru(1)	O(2)	92.15(10)
O(1)	Ru(1)	O(2)'	86.48(10)	O(1)	Ru(1)	N(1)	87.75(11)
O(1)	Ru(1)	N(1)'	93.59(11)	O(2)	Ru(1)	O(2)'	89.6(2)
O(2)	Ru(1)	N(1)	178.58(13)	O(2)	Ru(1)	N(1)'	88.97(11)
N(1)	Ru(1)	N(1)'	92.4(2)	O(3)	S(1)	O(4)	113.8(2)
O(3)	S(1)	O(4)''	113.8(2)	O(3)	S(1)	C(10)	104.6(3)
O(4)	S(1)	O(4)''	116.5(3)	O(4)	S(1)	C(10)	103.0(2)
Ru(1)	O(1)	C(2)	121.9(3)	Ru(1)	O(2)	C(4)	123.2(3)
Ru(1)	N(1)	C(6)	130.6(3)	Ru(1)	N(1)	C(8)	123.3(3)
C(6)	N(1)	C(8)	106.1(4)	C(6)	N(2)	C(7)	107.8(4)
O(1)	C(2)	C(1)	113.8(4)	O(1)	C(2)	C(3)	126.0(4)
C(1)	C(2)	C(3)	120.2(4)	C(2)	C(3)	C(4)	127.2(4)
O(2)	C(4)	C(3)	124.5(4)	O(2)	C(4)	C(5)	114.5(4)
C(3)	C(4)	C(5)	120.9(4)	N(1)	C(6)	N(2)	109.9(4)
N(1)	C(6)	C(9)	127.1(4)	N(2)	C(6)	C(9)	123.0(4)
N(2)	C(7)	C(8)	107.3(4)	N(1)	C(8)	C(7)	108.9(4)
S(1)	C(10)	F(1)	113.0(4)	S(1)	C(10)	F(2)	111.6(3)
F(1)	C(10)	F(2)	107.8(4)	F(2)	C(10)	F(2)''	104.5(5)
C(11)	C(12)	C(13)	122.7(22)	C(12)	C(13)	C(13)*	142.2(20)

Appendix I-17 X-ray data for [Ru(acac)₂(5MeIm)₂][CF₃SO₃]

Table I-17.1 Experimental details for [Ru(acac)₂(5MeIm)₂][CF₃SO₃]

Formula	C ₁₉ H ₂₆ F ₃ N ₄ O ₇ RuS
fw	612.56
Crystal system	Monoclinic
Space group	P2 ₁ /n (No. 14)
<i>a</i> , Å	11.7804(4)
<i>b</i> , Å	13.5270(13)
<i>c</i> , Å	16.6914(3)
α , °	—
β , °	110.0051(4)
γ , °	—
<i>V</i> , Å ³	2499.3(2)
<i>Z</i>	4
ρ_{calc} , g/cm ³	1.628
<i>F</i> (000)	1244
μ , cm ⁻¹	7.79
Crystal size, mm	0.20 × 0.30 × 0.40
Transmission factors	0.87-1.00
Scan type	ϕ , ω sweeps
Scan range, deg in ω	0.5
Scan speed, deg/min	—
Data collected	462 frames, 18 s/frame
$2\theta_{max}$, deg	60.1
Crystal decay, %	—
Total reflections	21822
Unique reflections	6636
<i>R</i> _{merge}	0.029
No. with $I \geq 3\sigma(I)$	4013
No. of variables	316
<i>R</i> (<i>F</i>) ($I \geq 3\sigma(I)$)	0.062
<i>R</i> _w (<i>F</i>) ($I \geq 3\sigma(I)$)	0.066
<i>R</i> (<i>F</i> ²) (all data)	—
<i>R</i> _w (<i>F</i> ²) (all data)	—
gof	1.33
Max Δ/σ (final cycle)	0.0007
Residual density e/Å ³	-1.13 to 1.19

Table I-17.2 Atomic coordinates and $B_{\text{iso}}/B_{\text{eq}}$ for $[\text{Ru}(\text{acac})_2(5\text{MeIm})_2][\text{CF}_3\text{SO}_3]$

atom	x	y	z	$B\{\text{eq}\}$
Ru(1)	0.18350(2)	0.15219(2)	0.12579(2)	1.766(5)
S(1)	0.74488(7)	0.32692(6)	0.13762(5)	2.40(2)
F(1)	0.5952(2)	0.3660(2)	-0.01593(13)	5.21(6)
F(2)	0.5101(2)	0.3258(2)	0.07413(15)	6.08(7)
F(3)	0.5889(2)	0.4685(2)	0.07899(14)	5.18(6)
O(1)	0.1170(2)	0.02417(15)	0.15211(12)	2.16(5)
O(2)	0.1406(2)	0.2248(2)	0.21678(13)	2.31(5)
O(3)	0.2522(2)	0.28047(14)	0.10296(12)	1.79(5)
O(4)	0.0187(2)	0.18126(15)	0.04024(13)	2.05(5)
O(5)	0.7391(2)	0.3521(2)	0.21873(14)	4.29(7)
O(6)	0.8328(2)	0.3809(2)	0.11330(13)	3.02(6)
O(7)	0.7395(2)	0.2243(2)	0.1184(2)	4.86(7)
N(1)	0.2279(2)	0.0805(2)	0.03259(15)	1.88(6)
N(2)	0.2396(2)	-0.0372(2)	-0.0539(2)	2.79(7)
N(3)	0.3533(2)	0.1150(2)	0.20968(15)	1.88(6)
N(4)	0.5029(2)	0.0290(2)	0.2949(2)	2.65(7)
C(1)	-0.0004(3)	-0.0840(3)	0.1999(2)	3.39(9)
C(2)	0.0474(3)	0.0183(3)	0.1966(2)	2.55(8)
C(3)	0.0199(3)	0.0960(3)	0.2413(2)	2.57(8)
C(4)	0.0660(3)	0.1908(3)	0.2510(2)	2.28(7)
C(5)	0.0352(3)	0.2636(3)	0.3087(2)	3.21(9)
C(6)	0.2526(3)	0.4476(2)	0.0636(2)	2.91(8)
C(7)	0.1877(3)	0.3521(2)	0.0616(2)	1.81(6)
C(8)	0.0638(3)	0.3461(3)	0.0132(2)	2.16(7)
C(9)	-0.0105(3)	0.2639(2)	0.0022(2)	1.82(7)
C(10)	-0.1372(3)	0.2685(3)	-0.0611(2)	2.54(7)
C(11)	0.1845(3)	-0.0063(2)	-0.0001(2)	2.44(8)
C(12)	0.3212(3)	0.0342(3)	-0.0567(2)	2.73(8)
C(13)	0.3142(3)	0.1059(2)	-0.0032(2)	2.48(8)
C(14)	0.3995(4)	0.0243(3)	-0.1102(3)	4.73(11)
C(15)	0.3833(3)	0.0295(3)	0.2515(2)	2.45(8)
C(16)	0.5511(3)	0.1170(2)	0.2803(2)	2.23(7)
C(17)	0.4564(3)	0.1693(2)	0.2270(2)	2.26(7)
C(18)	0.6815(3)	0.1399(3)	0.3196(2)	3.80(9)
C(19)	0.6030(3)	0.3745(3)	0.0650(2)	3.17(9)
H(1)	0.2255	-0.0952	-0.0833	3.4
H(2)	0.5449	-0.0213	0.3283	3.2
H(3)	0.0673	-0.1296	0.2243	4.1
H(4)	-0.0515	-0.0836	0.2356	4.1
H(5)	-0.0482	-0.1055	0.1422	4.1
H(6)	-0.0392	0.0818	0.2691	3.1
H(7)	-0.0237	0.2339	0.3312	3.9
H(8)	0.1086	0.2808	0.3562	3.9
H(9)	0.0007	0.3234	0.2764	3.9
H(10)	0.2011	0.4922	0.0200	3.5
H(11)	0.2717	0.4781	0.1199	3.5
H(12)	0.3276	0.4350	0.0522	3.5
H(13)	0.0258	0.4067	-0.0160	2.6
H(14)	-0.1510	0.2124	-0.1003	3.0
H(15)	-0.1481	0.3304	-0.0934	3.0
H(16)	-0.1950	0.2659	-0.0306	3.0
H(17)	0.1212	-0.0428	0.0131	2.9
H(18)	0.3625	0.1666	0.0087	3.0
H(19)	0.3515	0.0376	-0.1699	5.7
H(20)	0.4322	-0.0429	-0.1049	5.7
H(21)	0.4661	0.0719	-0.0908	5.7
H(22)	0.3272	-0.0243	0.2508	2.9
H(23)	0.4615	0.2355	0.2047	2.7
H(24)	0.7280	0.0961	0.2956	4.6
H(25)	0.6958	0.2088	0.3077	4.6
H(26)	0.7069	0.1298	0.3813	4.6

Table I-17.3 Bond lengths (Å) for [Ru(acac)₂(5MeIm)₂][CF₃SO₃]

atom	atom	distance
Ru(1)	O(1)	2.010(2)
Ru(1)	O(3)	2.006(2)
Ru(1)	N(1)	2.047(2)
S(1)	O(5)	1.420(2)
S(1)	O(7)	1.421(3)
F(1)	C(19)	1.327(4)
F(3)	C(19)	1.313(4)
O(2)	C(4)	1.286(3)
O(4)	C(9)	1.273(3)
N(1)	C(13)	1.388(3)
N(2)	C(12)	1.375(4)
N(3)	C(17)	1.363(4)
N(4)	C(16)	1.376(4)
C(2)	C(3)	1.390(4)
C(4)	C(5)	1.506(4)
C(7)	C(8)	1.409(4)
C(9)	C(10)	1.506(4)
C(12)	C(14)	1.493(4)
C(16)	C(18)	1.482(4)

atom	atom	distance
Ru(1)	O(2)	2.013(2)
Ru(1)	O(4)	2.017(2)
Ru(1)	N(3)	2.073(2)
S(1)	O(6)	1.434(2)
S(1)	C(19)	1.814(4)
F(2)	C(19)	1.330(4)
O(1)	C(2)	1.284(3)
O(3)	C(7)	1.279(3)
N(1)	C(11)	1.322(4)
N(2)	C(11)	1.342(4)
N(3)	C(15)	1.335(4)
N(4)	C(15)	1.346(4)
C(1)	C(2)	1.502(4)
C(3)	C(4)	1.380(4)
C(6)	C(7)	1.496(4)
C(8)	C(9)	1.388(4)
C(12)	C(13)	1.339(4)
C(16)	C(17)	1.363(4)

Table I-17.4 Bond angles (°) for [Ru(acac)₂(5MeIm)₂][CF₃SO₃]

atom	atom	atom	angle
O(1)	Ru(1)	O(2)	92.20(8)
O(1)	Ru(1)	O(4)	88.29(8)
O(1)	Ru(1)	N(3)	90.06(9)
O(2)	Ru(1)	O(4)	90.55(8)
O(2)	Ru(1)	N(3)	92.42(8)
O(3)	Ru(1)	N(1)	92.32(8)
O(4)	Ru(1)	N(1)	89.34(9)
N(1)	Ru(1)	N(3)	87.71(9)
O(5)	S(1)	O(7)	115.9(2)
O(6)	S(1)	O(7)	114.42(14)
O(7)	S(1)	C(19)	103.7(2)
Ru(1)	O(2)	C(4)	123.2(2)
Ru(1)	O(4)	C(9)	123.7(2)
Ru(1)	N(1)	C(13)	128.8(2)
C(11)	N(2)	C(12)	107.9(3)
Ru(1)	N(3)	C(17)	126.6(2)
C(15)	N(4)	C(16)	108.7(3)
O(1)	C(2)	C(3)	125.1(3)
C(2)	C(3)	C(4)	127.7(3)
O(2)	C(4)	C(5)	113.6(3)
O(3)	C(7)	C(6)	115.9(3)
C(6)	C(7)	C(8)	119.0(3)
O(4)	C(9)	C(8)	126.0(3)
C(8)	C(9)	C(10)	119.2(3)
N(2)	C(12)	C(13)	106.4(3)
C(13)	C(12)	C(14)	130.9(3)
N(3)	C(15)	N(4)	109.1(3)
N(4)	C(16)	C(18)	122.1(3)
N(3)	C(17)	C(16)	109.3(3)
S(1)	C(19)	F(2)	110.7(3)
F(1)	C(19)	F(2)	107.5(3)
F(2)	C(19)	F(3)	107.5(3)

atom	atom	atom	angle
O(1)	Ru(1)	O(3)	178.43(8)
O(1)	Ru(1)	N(1)	88.74(9)
O(2)	Ru(1)	O(3)	86.74(8)
O(2)	Ru(1)	N(1)	179.05(9)
O(3)	Ru(1)	O(4)	92.88(8)
O(3)	Ru(1)	N(3)	88.82(9)
O(4)	Ru(1)	N(3)	176.65(9)
O(5)	S(1)	O(6)	114.97(15)
O(5)	S(1)	C(19)	102.60(15)
O(6)	S(1)	C(19)	102.70(15)
Ru(1)	O(1)	C(2)	123.6(2)
Ru(1)	O(3)	C(7)	123.7(2)
Ru(1)	N(1)	C(11)	124.8(2)
C(11)	N(1)	C(13)	106.2(3)
Ru(1)	N(3)	C(15)	125.8(2)
C(15)	N(3)	C(17)	107.4(3)
O(1)	C(2)	C(1)	113.6(3)
C(1)	C(2)	C(3)	121.2(3)
O(2)	C(4)	C(3)	125.5(3)
C(3)	C(4)	C(5)	120.8(3)
O(3)	C(7)	C(8)	125.1(3)
C(7)	C(8)	C(9)	127.2(3)
O(4)	C(9)	C(10)	114.8(3)
N(1)	C(11)	N(2)	110.2(3)
N(2)	C(12)	C(14)	122.7(3)
N(1)	C(13)	C(12)	109.2(3)
N(4)	C(16)	C(17)	105.6(3)
C(17)	C(16)	C(18)	132.3(3)
S(1)	C(19)	F(1)	112.1(2)
S(1)	C(19)	F(3)	111.6(3)
F(1)	C(19)	F(3)	107.2(3)

Appendix II

Miscellaneous Biological Data

Table II- 1: Toxicity (PE \pm 10 %) for selected compounds (at 100 μ M) in oxic and hypoxic SCCVII cells (incubated for 3 h).

Compound	PE (oxic)	PE (hypoxic)
cont	0.59	0.56
EF5	0.50	0.48
RevEF5	0.57	0.58
EF3	0.42	0.41
E=F2	0.49	0.52
EF1(-1)	0.30	0.34
EF1	0.49	0.49
EC11	0.53	0.58
EBr1	0.49	0.53
EPrA	0.48	0.54
cycF3	0.50	0.23
TF5	0.39	0.01
IF5	0	0

Table II- 2: Relative mean fluorescence intensity for SCCVII cells incubated with 100 μ M drug for 3 h under N₂ and then treated with ELK3-51 (Cy3); determined using flow cytometry (average of 2 or 3 expts.; \pm 10 %).

Compound	Mean Signal (oxic)	Mean Signal (hypoxic)
EF5	0.8	79.2
RevEF5	0.0	0.0
MF5	0.2	7.2
2M4NF5	0.0	0.0
EF4Br	1.6	52.7
EF3	1.2	48.4
EF2Br	1.2	58.4
E=F2	1.1	23.2
EF3(-1)	1.0	44.9
EF1(-1)	0.4	3.1
EF1	1.3	32.6
EC11	1.5	35.7
EBr1	1.0	6.7
EPrA	1.2	25.8
EIAA	0.8	38.8
cycF3	0.0	0.1
TF5	0.1	31.2
IF5	93.9	89.4

Table II- 3: Log of mean fluorescence signal determined by flow cytometry and the compound reduction potential (determined by CV vs. SCE).

Compound	log (Mean Sig.) (hypoxic)	E _{1/2} (mV)
EF5	79.2	-977
MF5	7.2	-1068
2M4NF5	0.0	-1300
EF3	48.4	-1024
EF2Br	58.4	-1022
E=F2	23.2	-1031
EF3(-1)	44.9	-1015
EF1(-1)	3.1	-1115
EF1	32.6	-1037
EC11	35.7	-1036
EBr1	6.7	-1038

Table II- 4: Relative mean fluorescence intensity for SCCVII cells incubated with 100μM drug for 3 h under N₂ and then treated with ELK3-51; determined using image cytometry (data from 2 expts.; ± 10 %).

Compound	Mean Signal (oxic)	Mean Signal (Hypoxic)
EF5	14.7	1461.0
MF5	3.9	103.9
2M4NF5	0.1	0.1
EF3	2.4	758.4
EF2Br	6.8	1002.9
EF3(-1)	5.4	1059.5
EF1(-1)	7.1	45.1
EBr1	6.8	380.3
cycF3	2.3	3.1
TF5	2.5	543.4

Table II- 5: Relative mean fluorescence intensity for SCCVII cells incubated with 100μM drug for 3 h under N₂ and treated with ELK5-A8; determined using flow cytometry.

Compound	Mean Signal (Oxic)	Mean Signal (Hypoxic)
EF5	0.4	7.0
EF3	0.6	70.2
EF2Br	0.8	92.5
E=F2	0.4	9.5
EF3(-1)	0.3	0.2
EF1	0.4	3.8
EC11	0.4	20.5
EBr1	0.4	5.0
EPrAm	0.3	2.3
EIAA	0.3	10.6